CARBONATE FACIES, DEPOSITIONAL SEQUENCES AND TECTONOSTRATIGRAPHY OF THE PALAEOGENE MALTA PLATFORM

GATT, PETER,A

DEPARTMENT OF EARTH SCIENCES
UNIVERSITY OF DURHAM

CARBONATE FACIES, DEPOSITIONAL SEQUENCES AND TECTONOSTRATIGRAPHY OF THE PALAEOGENE MALTA PLATFORM

Peter A. Gatt

A thesis submitted in partial fulfilment of the requirements for the degree of
Doctor of Philosophy at the
University of Durham

UNIVERSITAS DUNELMENSIS

2012

DECLARATION

No part of this thesis has previously been submitted for a degree at this or any other university. The work described in this thesis is entirely that of the author, except where reference is made to previously published or unpublished work.

Peter A. Gatt

Department of Earth Sciences
University of Durham
Durham
United Kingdom

March 2012

ABSTRACT

The break-up of Pangaea and the Late Mesozoic global sea-level rise drowned many Tethyan carbonate platforms although the resilient Malta Platform aggraded >4 km of carbonates along the North African passive margin where it was isolated from continental siliciclastics. Carbonate sedimentation was terminated by extensive Late Cretaceous to Early Paleogene depositional hiatuses, but renewed during the Oligocene, when basinward carbonate progradation began to drape over the >350 km long, cusp-shaped escarpment along the eastern margin of the isolated platform.

This study sub-divides the Oligocene sediments of Malta into eight facies associations. The facies consist of carbonate grains of coral, coralline red algae and large benthic foraminifera which dominated sediments of the Late Rupelian to early Chattian, mid-Chattian and late Chattian, respectively. These successive carbonate factories produced the photozoan-heterozoan-photozoan triplet of carbonate grain associations which, when dated by benthic foraminiferal biozonation, correlates to the succession of carbonate grain associations in other Mediterranean carbonate platforms.

The sedimentary triplet reflects abrupt changes in carbonate ecosystems that coincide with the last three of six surfaces that extend >80 km around Malta. The surfaces show evidence of the influence of meteoric water and pedogenic processes recognised by diagenetic features and isotopic excursions. These sequence boundaries sub-divide the succession into seven depositional sequences that reflect global third-order cyclic sea-level falls produced by glaciations with a periodicity of 1.2 Ma triggered by low-amplitude obliquity variations of the Earth's axis combined with orbital eccentricity cycles.

The periodic growth of the Antarctic ice-sheet during the Oligocene also affected Tethyan climate by shifting low latitude climate belts northwards. It is suggested that increased aridity over North Africa had reduced nutrient flux to the Tethys and favoured photozoan carbonate biota over the Malta Platform and other Tethyan carbonate platforms. The stepwise decrease in oxygen isotope ratio by the mid-

Chattian reflects Antarctic deglaciation that increased both precipitation over North Africa and nutrient flux in the Tethys, favouring heterozoan ecosystems.

The mid-Chattian transgressive heterozoan carbonates draped over structured bathymetry of an antecedent extensional regime that produced rotated fault-blocks. Highstand shedding of coralline red algae resulted in large clinoforms prograding into partly filled NNE trending half-graben (<10 km-wide) in the Maltese Islands whereas block rotation involving deep, *en echelon* listric faults formed escarpments along the platform margin. The escarpments were initially onlapped by syntectonic early Palaeogene sediments and later downlapped by prograding complexes. The central platform zone developed as a >50 km-wide basin by lithospheric sagging over a failed Mesozoic rift.

The late Chattian climatic optimum was reflected by a further decrease in the oxygen isotope ratio and aridity over North Africa and favoured a return to the photozoan association during the last phase of the Oligocene sedimentary triplet. Lepidocyclinids flourished in inner to mid-platform environments forming banks although the rate of accumulation of these hydrodynamic foraminifera did not keep up with sea-level rise. The shift to increased trophic resources by the end Oligocene terminated shallow marine carbonate sedimentation which resulted in the drowning of the Malta Platform.

ACKNOWLEDGEMENTS

The research work in this thesis was partly funded by the Malta Government Scholarship Scheme (grant number MGSS PHD 2008-15) and supported by the Malta Council for Science and Technology. I am grateful to BP for a conference travel fund awarded in 2009 for best presentation during Research in Progress Day and for providing well data in support of my research. TGS-Nopec is thanked for giving me access to their seismic data and Total for providing well data. Durham University acknowledges support of this research project by Landmark® Graphics Corporation via the Landmark University Grant Program.

My sincere gratitude goes to my supervisor Prof Jon Gluyas for his support, patience and encouragement. Dr Keith Gerdes (Shell) and Drs. Dave Harper, Mark Allen and Richard Davies (University of Durham) are also thanked for useful discussions and support. Dave Sales is thanked for making thin sections for me. The postgrad and postdoc community at the Department especially my colleagues Alan Roberts, Steve Richardson (now at BP), Colin Sergeant and Peter Holt are thanked for their friendship.

Finally, my gratitude goes to my brother, Louis, and my niece Christina and her two adorable children Michaela and Nicholas, for their support and encouragement throughout the three years I spent away from home.

TABLE OF CONTENTS

Chapter 1 Introduction and Datasets *page*

1.1 INTRODUCTION 2

1.2 RATIONALE OF STUDY 2

1.2.2 The study area 3

1.2.3 Previous studies 5

1.3. THESIS AIMS 6

1.4 DATASET AND METHODOLOGY 7

1.5 NOMENCLATURE AND ABBREVIATIONS 10

1.5.2 Formation names 10

1.5.3 Carbonate buildups 10

1.5.4 Time scale 11

1.5.5 Biota 11

1.5.6 Abbreviations and units 11

1.6 LAYOUT OF THESIS 11

Chapter 2 Meso-Cenozoic palaeogeography, geology and tectonic history of the Central Mediterranean

2.1 INTRODUCTION 15

2.1.2. Tectonic sub-divisions of the Central Mediterranean 15

2.2 CENTRAL MEDITERRANEAN TECTONOSTRATIGRAPHY 20

2.2.2 Late Palaeozoic 21

2.2.3 Mesozoic 22

2.2.4 Cenozoic 32

2.3 SUMMARY 44

Chapter 3 Facies analysis of the Oligocene carbonates of the Malta Platform

3.1 INTRODUCTION 46

3.2 METHODS AND MATERIALS 48

3.3 FACIES ASSOCIATIONS 49

3.3.1 Facies Association I: Bryozoan-echinoid-bivalve wackestone/mudstone 51

3.3.2 Facies Association II: Coralline Red Algal Limestone 55

3.3.3 Facies Association III: Large benthic foraminiferal limestone 64

3.3.4 Facies Association IV: Coral limestone 78

3.3.5 Facies Association V: Imperforate foraminiferal wackestone/packstone 83

3.3.6 Facies Association VI: Red argillaceous carbonates 90
3.3.7 Facies Association VII: Gypsum facies 94
3.4 DISCUSSION 95
3.4.1 Palaeoclimatic setting 95
3.4.2 Ecological relationships and trophic level 97
3.4.3 Recognition of carbonate platform type from facies 101
3.5 SUMMARY 104

Chapter 4 Diagenesis and carbonate reservoir porosity of the Palaeogene Malta Platform

4.1 INTRODUCTION 106
4.1.2 Diagenesis 107
4.1.3 Stable isotopes 109
4.2 METHODS 111
4.3 DIAGENETIC ENVIRONMENTS IN THE MALTA PLATFORM 113
4.3.1 Diagenetic surfaces identified by isotopic values and cement 113
4.3.2 Diagenesis in facies associations 119
4.3.3 Diagenetic indicators of palaeo-oxygenation 128
4.3.4 Diagenesis in Mesozoic to early Palaeogene carbonates 129
4.3.5 Burial stress and diagenesis 134
4.4. DIAGENETIC HISTORY AND POROSITY DEVELOPMENT 137
4.5. SUMMARY 140

Chapter 5 Stratigraphy of the Malta Platform (part 1): Sequence Stratigraphy

5.1 INTRODUCTION 142
5.2 METHODS AND DATASETS 142
5.3 INTRODUCTION TO SEQUENCE STRATIGRAPHY 143
5.4 PALAEOGENE Cyclostratigraphy and sequence development in malta 148
5.4.2 Major stratigraphic surfaces 148
5.4.3 Sediment packages 152
5.5 PALAEOGENE Depositional Sequences 156
5.5.2 Depositional Sequences 1a and 1b 158
5.5.3 Depositional Sequence 2 160
5.5.4 Depositional Sequence 3 160
5.5.5 Depositional Sequence 4 166
5.5.6 Depositional Sequence 5 179
5.5.7 Depositional Sequence 6 192

Chapter 5 Stratigraphy of the Malta Platform (part 2): Chronostratigraphy

5.6 INTRODUCTION 199
5.7 BIOSTRATIGRAPHICAL FRAMEWORK 199
5.7.2 Eocene 204
5.7.3 Oligocene 205
5.8 STRONTIUM ISOTOPE DATING 206
5.9 ASTROCHRONOLOGY 208
5.10 DISCUSSION 211
5.10.2 Third-order sea-level cycles 211
5.10.3 Fourth-order sea-level cycles 215
5.10.4 Fifth-order sea-level cycles 216
5.10.5 Sea-level cycles and controls on sedimentary cycles 217
5.10.6 Constructing the relative sea-level curve 220
5.10.7 Correlation to regional sequence boundaries 226
5.10.8 Malta Platform sequences and global third-order cycles 228
5.11 SUMMARY 230

Chapter 6 Tectonostratigraphic development of the Malta Platform

6.1 INTRODUCTION 232
6.2 METHODS and MATERIALS 235
6.3 Regional tectonostratigraphy 236
6.4 SEISMIC STRATIGRAPHY OF THE MALTA PLATFORM 242
6.4.1 Seismic facies of megasequence II 252
6.4.2 Seismic facies and outcrops of megasequence III 253
6.5 GEOTECTONIC SUBDIVISION OF THE MALTA PLATFORM 255
6.5.2 Platform interior zone 256
6.5.3 Central Malta Platform Basin (CMPB) 279
6.5.4 Escarpment zone 288
6.6 DISCUSSION 300
6.6.2 Stratigraphy 300
6.6.3 Tectonics 301
6.7 SUMMARY 306

Chapter 7 Environmental controls on Palaeogene carbonate sedimentation

7.1 PREAMBLE 309

7.1.1 Global ice volume, sea-level and oxygen isotopes 309

7.2.2 Global climate belts 310

7.1.3 Carbonate ecosystems 313

7.2 CLIMATIC CONTROLS ON FACIES IN PALAEOGENE MEDITERRANEAN SUBTROPICAL CARBONATE PLATFORMS 316

Chapter 8 Dicscussion and Conclusions

8.1 INTRODUCTION 346

8.2 KEY FINDINGS AND THEIR IMPLICATIONS 347

8.2.2 Stratigraphy 349

8.2.3 Carbonate platform model 349

8.2.4 Tectonics 351

8.3 TECTONOSTRATIGRAPHIC PLATFORM EVOLUTION 353

Tectonostratigraphic Phase 1 356

Tectonostratigraphic Phase 2 356

Tectonostratigraphic Phase 3 357

Tectonostratigraphic Phase 4 358

Tectonostratigraphic Phase 5 360

Tectonostratigraphic Phase 6 361

8.4 FUTURE WORK 361

8.5 CONCLUSIONS 362

APPENDICES

APPENDIX I 364

APPENDIX II 366

APPENDIX III 384

APPENDIX IV 394

APPENDIX V 397

REFERENCES 408

LIST OF FIGURES

Chapter 1

Figure 1.1. Location of the relatively intact Oligocene carbonate platforms 3
Figure 1.2. Location of the Malta Platform 4
Figure 1.3. Stratigraphic nomenclature of Maltese formations and members 6
Figure 1.4. Map of the Maltese Islands..... 8
Figure 1.5. Data acquired in this study and hierarchy level of resolution of analysis. 9

Chapter 2

Figure 2.1. The main tectonic units of the Central Mediterranean..... 16
Figure 2.2. Bathymetry of the Central Mediterranean. 18
Figure 2.3. Late Permian palaeogeography. 22
Figure 2.4. Norian (Late Triassic) palaeogeography. 23
Figure 2.5. Panormide Platform 25
Figure 2.6. Logs from Central Mediterranean 26
Figure 2.7. Carbonate platforms and basins since the Jurassic..... 28
Figure 2.8. Trapanese Platform. 29
Figure 2.9. Maastrichtian (Late Cretaceous- 70 Ma) palaeogeography. 30
Figure 2.10. Palaeogeography of the Central Mediterranean during the Cretaceous. 32
Figure 2.11. Palaeogeography of the world during the Early Oligocene..... 33
Figure 2.12. Reconstructions of Oligocene tectonics. 34
Figure 2.13. Position of Maltese Islands. 35
Figure 2.14. Facies map of the Early Eocene Metlaoui Group..... 37
Figure 2.15. Oligocene Formations in the Central Mediterranean. 39
Figure 2.16. Plio-Quaternary tectonic setting. 40
Figure 2.17. Neogene stratigraphy of the Maltese Islands 43

Chapter 3

Figure 3.1. FA I: Map showing geographical distribution facies.. 54
Figure 3.2. Depositional model for FA I: 54
Figure 3. 3. FA IIa: algal debris-foraminiferal grainstone (FA IIa-ii) at locality 5 58
Figure 3.4. FA II at locality 3: the rhodalgal biostrome. 60
Figure 3.5. FA IIb: Locality 6: rhodolith rudstone pavement. 61
Figure 3.6. Percent contents of rhodoliths, LBF and micrite 64
Figure 3.7. diagram from Beavington-Penney (2004); diagram from Aigner (1985). 68
Figure 3.8. FA III: top: facies map; bottom: Photograph of topmost locality 3 70
Figure 3.9. Facies IIIa: Locality 3..... 71
Figure 3.10. Facies IIIb at locality G..... 73
Figure 3.11. Facies IIIc at locality 12 74
Figure 3.12. Facies IVa: tabular coral biostrome 80
Figure 3.13. Facies IVb: dome-shaped coral patch reefs. 81
Figure 3.14. Model of coral framestone buildup morphology). 82

Figure 3.15. Macrofauna in FA V: siphonal tubes of Kuphus, Crustacean (crab). 84
Figure 3.16. FA V at locality 5: Mosta quarry showing facies succession 86
Figure 3.17. FA VI: locality 5: (1) rhodolith bed; (2) facies VIa 91
Figure 3.18. Facies VIb: Locality H: Inaccessible cliffed coast of western Gozo.. 93
Figure 3.19. Migration of North Africa and Malta. 96
Figure 3.20. Diagram showing relationship between depth and nutrient level 100
Figure 3.21. Common depositional depth range of carbonate biotas. 103

Chapter 4

Figure 4.1. Diagenetic environments along a carbonate platform 107
Figure 4.2. (a) The global deep sea oxygen isotope curve 110
Figure 4.3. Porosity classification by Choquette & Pray (1970). 112
Figure 4.4. Stratigraphy in outcrop and levels affected by diagenetic processes.. 114
Figure 4.5. Isotope values of bulk rock samples from localities 115
Figure 4.6. Photograph of sampled localities 1. 118
Figure 4.7. Facies association II. 124
Figure 4.8. FA III.. 124
Figure 4.9. Coral framestone/rudstone: 125
Figure 4.10. Facies Va at localities 9 and 14. 127
Figure 4.11. Facies VI 127
Figure 4.12. Locality 3 showing bed with orange colour 129
Figure 4.13. Lithology of wells. 130
Figure 4.14. Photomicrograph showing dolomite, gypsum and fibrous anhydrite. 132
Figure 4.15. Circular, <300 m-wide solution collapse features. 133
Figure 4.16. Lithostatic and hydrostatic gradients. 135
Figure 4. 17. Uniaxial compressive strength of Lower Coralline Limestone 136
Figure 4. 18. Range of porosity in different facies in outcrop. 137
Figure 4.19. Paragenetic sequence of the diagenetic features. 138
Figure 4.20. Comparison of outcrop and subsurface porosity. 139

Chapter 5

Figure 5.1. Astronomical variables 145
Figure 5.2. Geometries of parasequence sets 147
Figure 5. 3. Correlation of well logs to outcrops. 151
Figure 5.4. Composite log based on photographs and logs 154
Figure 5.5. Uninterpreted and interpreted cliff section 155
Figure 5.6. Generalised lithological log of Aqualta well and gamma ray log. 159
Figure 5.7. Photomicrographs and stratigraphy of cycle S3 161
Figure 5. 8. Outcrops of SbCH2 163
Figure 5.9. Outcrops, log and photomicrographs of top of sequence 3 164
Figure 5.10. Sequence boundaries SbCH2 and SbCH3 167
Figure 5. 11. Locality 5. Sequence boundary SbCH3 168
Figure 5.12. Locality 6: SbCH3 169
Figure 5.13. Photograph of cliff coast showing cross bedding truncated by SbCH3. 169
Figure 5.14. Forced regressive wedge systems tract (FRWST) 171

Figure 5.15. Parasequence sets A and B. 174
Figure 5.16. S4 highstand systems tract sediments. 175
Figure 5.17. Patch reefs and S3 and S4 175
Figure 5.18. Generalised stratigraphy of depositional sequence 4..... 177
Figure 5.19. Cartoon showing transgressive and lowstand systems tracts 179
Figure 5.20. Generalised stratigraphic log of depositional sequence 5..... 180
Figure 5.21. Sequence 5 181
Figure 5. 22. SbCH4 182
Figure 5.23. Sequence 5; Lowstand systems tract at locality 3 and H 183
Figure 5.24. Horizontal topsets that thicken from locality H to A..... 184
Figure 5.25. Cross-section from the planar topsets at locality 5 185
Figure 5.26. Cliff coast of SW Malta 185
Figure 5.27. Uninterpreted cliff coast around locality 14. 186
Figure 5.28. Mass transport (MT) events at localities 7 and C..... 187
Figure 5.29. Locality 5: transgressive systems tract 189
Figure 5.30. Locality A: the lowstand prograding wedge 189
Figure 5.31. West-east model showing the different types of clinoforms bedding 191
Figure 5.32. Logs of inaccessible locality G 193
Figure 5.33. The transgressive systems tract sediments. 196
Figure 5.34. Depositional model of sequence 6.. 197
Figure 5.35. Schematic log the Lower Coralline Limestone Formation in Naxxar-2 well.. .. 201
Figure 5.36. Data based on thin sections and hand specimens. 202
Figure 5.37. Generalised stratigraphic log of the Lower Coralline Limestone Formation . . 203
Figure 5.38.Generalised log of Lower Coralline Limestone Formation. 205
Figure 5.39. Photomicrograph shows Lepidocyclina Nephrolepidina 206
Figure 5.40. $^{87}Sr/^{86}Sr$ isotopes ratios of marine carbonates through time. 206
Figure 5.41. Locality 5: point sampled for strontium isotope value..... 208
Figure 5.42. Long-term obliquity cycles based on Laskar *et al.* (2004) 210
Figure 5.43. Chronostratigraphic chart.. 213
Figure 5.44. Stratigraphy of localities 5 and 14 217
Figure 5.45. Bar graph showing thickness of sequences 3 to 6 219
Figure 5.46. The third-order sea-level curve based on the four sequences in outcrop.. 223
Figure 5.47. Sea-level cycle and sedimentation. 224
Figure 5.48. Third-order relative sea-level curve for Malta. 225
Figure 5.49. Correlation chart of outcrops and wells in Italy, Malta and Libya 227
Figure 5.50. Part of global chart of coastal onlap 228
Figure 5.51. Comparison of sea-level curves for Malta and NE America 229

Chapter 6

Figure 6.1. Basic geometries in carbonates 234
Figure 6.2. MSC01 and MB01 grids. 237
Figure 6.3. Generalised cross-sections across two geotectonic settings..... 238
Figure 6.4. Burial history diagram based on well data from three carbonate platforms 239
Figure 6.5. Foraminiferal data from the Naxxar-2 well, Aqualta well and outcrops. 240
Figure 6.6. Lithology and formation names based on outcrops and well logs. 241

Figure 6.7. Stratigraphy and tectonics of the Malta Platform 243
Figure 6.8. Seismic cross-section of Malta Platform 245
Figure 6.9. Logs of wells that penetrate megasequences I to IV. 247
Figure 6.10. Calibration between Naxxar-2 well* and seismic line MSC01 311..... 249
Figure 6.11. Seismic interpretation of megasequence II and III 253
Figure 6.12. Lowstand and highstand systems tracts of rimmed shelf..... 255
Figure 6.13. Geotectonic sub-divisions of the Malta Platform..... 257
Figure 6.15. Sequence stratigraphic model. 259
Figure 6.16. Seismic lines 311 and 312 combined. 261
Figure 6.17. Stratigraphic logs showing thickness of Oligocene sediments 262
Figure 6.18. Schematic cross-section of the Maltese Islands along southern cliffed coast 264
Figure 6. 19. Uninterpreted section of cliffed coast.. 265
Figure 6.20. Interpreted section based on Figure 6.11 265
Figure 6.21. Location map of cross-sections and seismic line in Figure 6.20..... 266
Figure 6.22. Isopach map of the Globigerina Limestone Formation. 267
Figure 6.23. Location of dipping beds shown 269
Figure 6.24. The Naxxar half-graben described in Figure 6.17..... 271
Figure 6.25. Development of carbonate sequences along antecedent topography. 273
Figure 6.26. Composite model from Burchette & Wright (1992) 275
Figure 6.27. Deformation of sediments and formation of monoclines. 277
Figure 6.28. The extent and position of CMPB 280
Figure 6.29 Location of seismic sections shown in Figure 6.13..... 280
Figure 6.30 The western margin of the CMPB penetrated by the Aqualta well..... 283
Figure 6.31. Reflectors B, C, P and K are labelled along the Central Malta Platform Basin. 283
Figure 6.32. Interpretation of seismic line 106 that 287
Figure 6.33. Comparison of the Malta and Medina escarpments..... 289
Figure 6.34. Megasequence IV thins out towards the Malta Escarpment.. 292
Figure 6.35. Terraces 1 and 2 buried under megasequence IV and III 293
Figure 6.36. Uninterpreted seismic line from inset in Figure 6.35 295
Figure 6.37. Eastern end of seismic line 303 along the Medina Escarpment. 298
Figure 6.38. Change in geometry of Phases C and D along terrace 2..... 298
Figure 6.39. Tectonostratigraphic model of the Pelagian Block..... 301
Figure 6.40. Model of megasequence III sediments across a west-east transect 302
Figure 6.41. Rates of lithospheric subsidence in different tectonic settings..... 302
Figure 6.42. The Naxxar and Marsaxlokk basins across Malta 303
Figure 6.43. Progradation in Great Bahama Bank and progradation in Naxxar Basin..... 304
Figure 6.44 Prograding complexes along the escarpment zone..... 306

Chapter 7

Figure 7.1. Duration of ice-sheets and important climatic events 311
Figure 7.2. Climate belts and how they change in size and meridional position the ITCZ . 311
Figure 7.3. Changing position of thermal equator and ITCZ 312
Figure 7.4. World map of summer chlorophyll concentration 315
Figure 7.5. SW-NE cross-section; Field localities in the Maltese Islands..... 321
Figure 7.6. Stratigraphic distribution of biotas and correlation of well and outcrop data . 326

Figure 7.7. Shifts in carbonate ecosystems from photozoan to heterozoan 328
Figure 7.8. Chart showing climate-controlled Oligocene carbonate sedimentation 330
Figure 7.9. Correlation of carbonate platforms in the Central Mediterranean..... 330
Figure 7.10. Climate-sediment interaction model. 337
Figure 7.11. Model showing shifts in the ITCZ 344

Chapter 8
Figure 8.1. Lithofacies maps for the Cretaceous: Published and this thesis 351
Figure 8.2 Genralised cross section of Malta Platform 352
Figure 8.3. Generalised cross-section across the Sirt Rise..... 353
Figure 8.4. Tectonostratigraphic chart..... 354
Figure 8.5. Tectonostratigraphic phase IV in Malta..... 359

LIST OF TABLES

Chapter 1
Table 1-1. Classification of limestone. 7
Table 1-2. 11

Chapter 2
Table 2-1. Mesozoic Formations of the Central Mediterranean..... 23
Table 2-2. Cenozoic Formation names of the Central Mediterranean region. 35

Chapter 3
Table 3-1. Facies associations classified by grain type. 48
Table 3-2. Facies associations, facies and sub-facies recorded in outcrop..... 50
Table 3-3. The relative abundance of the facies associations 51
Table 3-4. Facies Association I: facies sub-divisions. 51
Table 3- 5. Coralline algae recorded in the Lower Coralline Limestone Formation. 56
Table 3-6. Facies association II: facies sub-divisions. 57
Table 3-7. LBF identified in thin sections of FA III belong to only suborder Rotaliina. 66
Table 3-8. Facies association III: facies sub-divisions. 67
Table 3-9. Oligocene corals found in Malta 79
Table 3- 10. Facies in facies association IV. 79
Table 3-11. Foraminiferal biota in FA V. 85
Table 3-12. Facies association V: facies sub-divisions. 85
Table 3-13. Facies association VI: facies sub-division. 90
Table 3- 14. Facies associations and grain associations..... 98
Table 3-15. Facies associations compared to facies zones of Wilson (1975). 102

Chapter 4
Table 4-1. Isotopic values for samples from locality 14..... 116

Chapter 5

Table 5-1. Sequence stratigraphic units produced by orders of sea-level cycles 144
Table 5-2. Depositional sequences of the Lower Coralline Limestone Formation. 150
Table 5-3. The four major sequence boundaries in outcrop 150
Table 5-4. Hierarchy of sequences and depositional environments..... 153
Table 5-5. Thickness of depositional sequences across the Malta Platform 157
Table 5-6. Thickness of depositional sequences 1a and 1b. 158
Table 5-7. Thickness of depositional sequence 2. 160
Table 5-8. Thickness of depositional sequence 3. 161
Table 5-9. Thickness of depositional sequence 4. 167
Table 5-10. Thickness of depositional sequence 5. 180
Table 5-11. Thickness of depositional sequence 6. 192
Table 5-12. Main foraniniferal assemblages in depositional sequences that crop out. 200
Table 5-13 Controls on sedimentary cycles..... 222

Chapter 6

Table 6-1. General stratigraphy of the Malta Platform 246
Table 6-2. The TWT depth of formations listed in Table 6-1. 249
Table 6-3. List of wells located on the platform interior. 257
Table 6-4. Summary of depositional sequences and facies 258
Table 6-5. Reflectors along the CMPB.. 279

Chapter 7

Table 7-1. Location and name of Oligocene formations referred to in text..... 319
Table 7-2. Biota and range of depositional depth. 330

Chapter 8

Table 8-1. Key findings of this thesis..... 347
Table 8-2. New lithostratigraphy of the Lower Coralline limestone Formation 350
Table 8-3. Stratigraphic subdivisions of the Malta Platform. 353

Chapter 1

Introduction and Datasets

1.1 INTRODUCTION 2

1.2 RATIONALE OF STUDY 2

1.2.2 The study area 3

1.2.3 Previous studies 5

1.3. THESIS AIMS 6

1.4 DATASET AND METHODOLOGY 7

1.5 NOMENCLATURE AND ABBREVIATIONS 10

1.5.2 Formation names 10

1.5.3 Carbonate buildups 10

1.5.4 Time scale 11

1.5.5 Biota 11

1.5.6 Abbreviations and units 11

1.6 LAYOUT OF THESIS 11

1.1 INTRODUCTION

This study focuses on the development of the isolated Palaeogene Malta Carbonate Platform that aggraded along offshore North Africa at the southern margin of the Tethys seaway. The Malta Platform is a poorly understood carbonate platform despite its potential for hydrocarbon reservoirs. This study investigates facies, diagenesis, stratigraphy, climatic controls and tectonostratigraphy with emphasis on the Oligocene Lower Coralline Limestone Formation which forms the backbone of the geology of the Maltese Islands. The study presents the description and interpretation of data derived from outcrops, seismic imaging and 6 exploration wells which are synthesized in a tectonostratigraphic model of the Malta Platform through the Meso-Cenozoic.

1.2 RATIONALE OF STUDY

This study presents a comprehensive analysis of the Malta Platform by examining data at different scales in order to attempt a holistic understanding of the carbonate platform. Reference is also made to other carbonate platforms along the Tethys seaway especially when discussing processes affecting the entire region such as tectonic and climatic controls.

The study also presents new findings on the stratigraphic and tectonic development of the Malta Platform that are relevant to hydrocarbon exploration. The exploration target has mostly been the Mesozoic carbonate reservoirs. Nevertheless, all the 12 exploratory wells drilled since the 1950s in the under-explored Malta Platform are unproductive. This contrasts with Tunisia and Libya where the Palaeogene is productive. This thesis offers insights into Palaeogene geology of the Malta Platform, an area that may in future prove to have hydrocarbon potential.

1.2.2 The study area

The Malta Platform was selected for detailed study due to five critical elements:

1. Many Tethyan carbonate platforms located between the Gondwanan and Eurasian continents were either upthrusted or overthrusted and extensively deformed when incorporated into orogenic wedges during the Neogene continental collision. Tethyan carbonate platforms that have partly escaped underthrusting are found in either the Mediterranean or Southeast Asia (Wilson & Bosence, 1997) (Figure 1.1). The Malta Platform developed on buoyant lithosphere (Jongsma *et. al.*, 1985) that escaped downthrusting by continental collision >100 km north of Malta. Most of this study focuses on the relatively less tectonically deformed area extending from the Maltese Islands to the Malta Escarpment.

Figure 1.1. Location of the relatively intact Oligocene carbonate platforms (orange circles) including the Malta Platform (red dot) and the collision zone (red line) formed by the convergence of India and Arabia with Asia where Cenozoic carbonate platforms were subducted or intensely deformed.

2. The Malta Platform is centrally located between the eastern and western Mediterranean Basins which makes it representative of other Mediterranean carbonate platforms (Figure 1.2).

3. The Malta Platform forms part/borders three productive petroleum provinces in the Central Mediterranean (Klett, 2001). The Pelagian and Sirt Basin provinces in Libya and Tunisia comprise productive Palaeogene carbonate reservoirs.
4. The Malta Platform has been an isolated carbonate platform and free of siliciclastics for a large part of its history. Since carbonate ecosystems are very sensitive environmental indicators, the Maltese carbonate succession provides a relatively complete record of environmental change in the western Tethys Ocean.
5. The Maltese Islands (Malta, Gozo, Comino islands) form the only emerged part of the Malta Platform and include well-exposed and accessible carbonate successions.

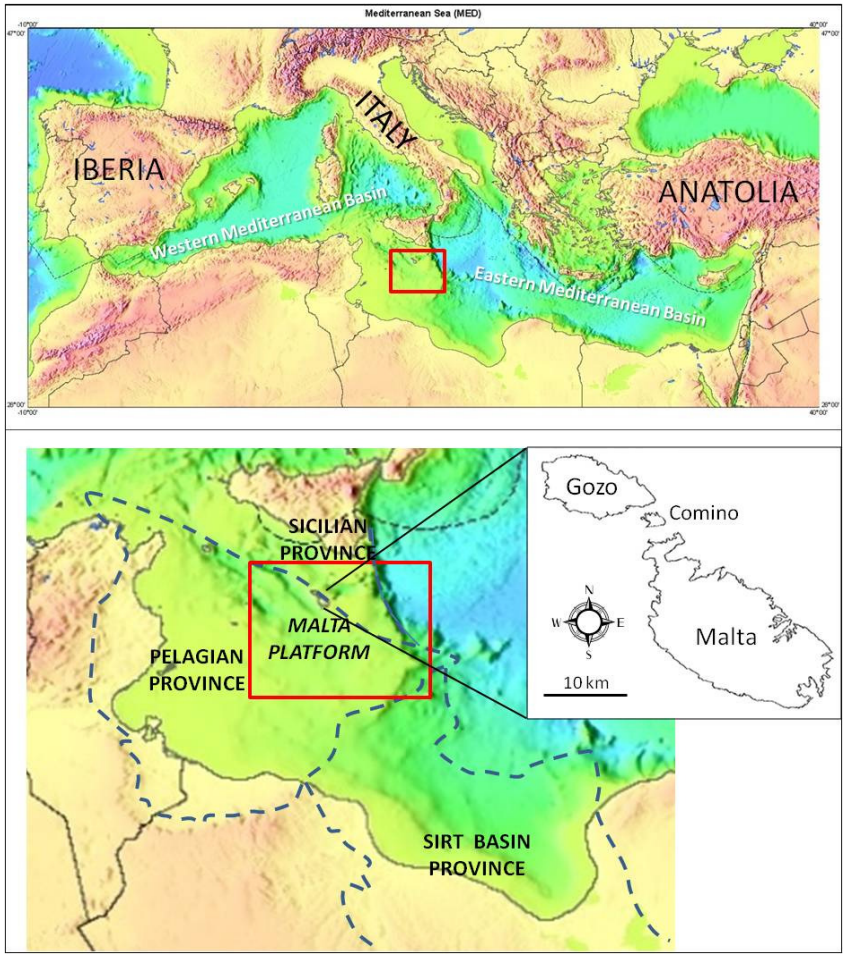

Figure 1.2. Location of the Malta Platform (red rectangle) relative to three petroleum provinces (Klett, 2001) and location of the Maltese Islands.

1.2.3 Previous studies

The Oligo-Miocene geology of the Maltese Islands has been the subject of studies since the early 19th century. The stratigraphic nomenclature for the Maltese Islands was established by Murray (1890) who was the first to use the name 'Lower Coralline Limestone' for the oldest formation in Malta (Figure 1.3). Felix (1973) used benthic foraminifera to date the Lower Coralline Limestone as Chattian whereas Pedley (1978) sub-divided the formation into four members. Bennett (1980) made changes to the stratigraphic sub-divisions, although the work of Pedley *et al.*, (1976) became the basis for mapping of formations and members. Diagenetic studies by Knoerich & Mutti (2006) include the chemostratigraphy (oxygen and carbon stable isotopes) of an Oligocene outcrop in Gozo.

The Palaeogene structural history of Malta remains hitherto poorly studied compared to the better known Late Neogene to Quaternary tectonics which have been the focus of a number of studies, e.g., Illies, 1981; Reuther & Eisbacher, 1985; Jongsma *et al.*, 1985. Dart *et al.*, (1993) consider Malta to be tectonically quiescent during the Oligocene although Gatt (2005) describes neptunian dykes and faults in the uppermost Oligocene. Pedley (1987) refers to a structural high over west Malta, a reflection of older regional N-S lineaments (Pedley, 1990). Buxton & Pedley (1989) and Brandano *et al.* (2009) propose facies models which suggest that the Lower Coralline Limestone was deposited along a carbonate ramp facing east, but Bosence (2005) classifies the Cenozoic Malta Platform as a fault-block platform.

The overlying hemipelagic Miocene sediments are not the focus of this study but have attracted considerable interest. The Globigerina Limestone Formation was formally subdivided into three Members by Rizzo (1932) on the basis of phosphorite beds, later named C_0 bed by Gatt (2005) and the ubiquitous C_1 and C_2 beds of Pedley (1978). These hiatal surfaces are discussed by Rehfeld & Janssen (1995) and Gruszczynski *et al.* (2008) and dated by Föllmi *et al.* (2008). The nannoplankton biostratigraphy published by Mazzei (1985) and the stratigraphy became the focus of climatic studies (Jacobs *et al.*, 1996; John *et al.*, 2003) and astrochronology (Abels *et al.*, 2005; Hilgen *et al.*, 2008).

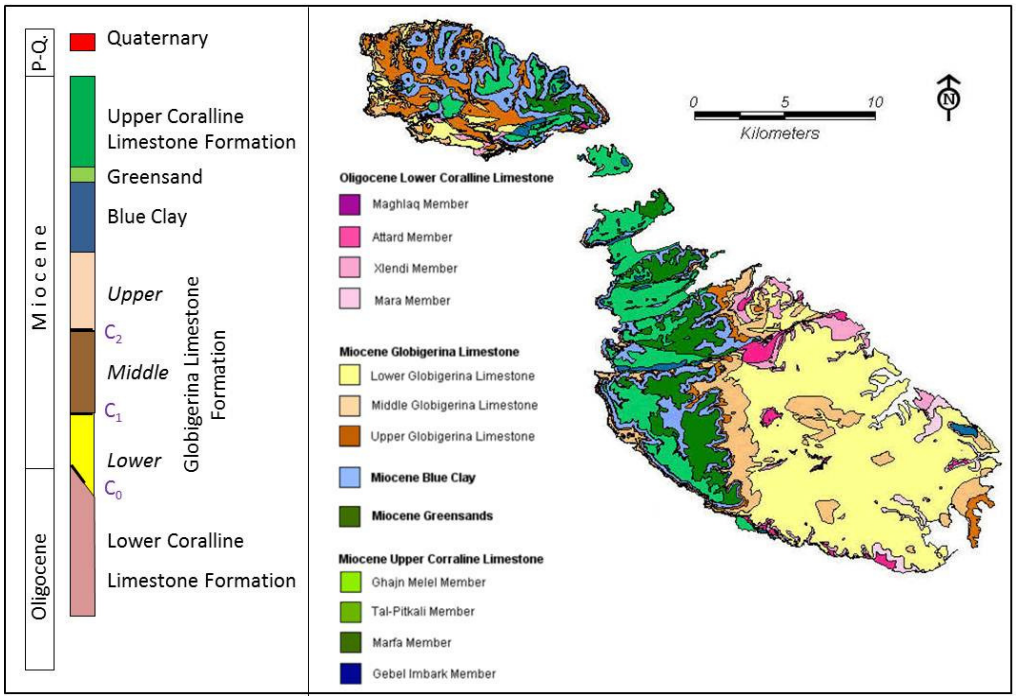

Figure 1.3. Stratigraphic nomenclature of Maltese formations and members based on Murray (1890), Rizzo (1932), Pedley *et al.* (1976) and Pedley (1978). Each formation is colour coded. The geological map was published by the British Geological Survey for the Malta Government.

1.3. THESIS AIMS

- To analyse Palaeogene facies and biotas of the Malta Platform and present a new and comprehensive lithostratigraphy of the Oligocene Lower Coralline Limestone Formation.
- To constrain the lithostratigraphy of the Malta Platform within a biostratigraphic and sequence stratigraphic framework in order to discuss links between the timing of relative sea-level change in the Malta Platform and cyclic global glacio-eustasy influenced by rhythmic astronomical controls on the Earth's climate.
- To determine the impact of tectonism on carbonate sedimentation in the Malta Platform. The depositional environments of facies in Oligocene outcrops are linked to structural controls and integrated to offshore seismic data. The overall aim is to provide insights on carbonate platform geotectonic setting.

- To evaluate the possible role of evaporites in thin-skinned extension in the Malta Platform.
- To discuss the dramatic vertical changes in carbonate facies in Malta and enquire whether these represent lateral shifts in contiguous facies along a carbonate platform *sensu* Walther's Law or, reflect regional environmental changes that periodically modified carbonate ecosystems?
- To hypothesize on a relationship between climate change and carbonate ecosystems in the Malta Platform and Tethyan carbonate platforms and enquire how climate change may have affected the geometry of sediment packages in the field and imaged in seismic.

1.4 DATASET AND METHODOLOGY

The sources of geophysical and geological data and methods include:

- Field work involved detailed facies description and analysis, and high resolution stratigraphy based on logging of 15 outcrop localities and two cores in the Maltese Islands (listed in Appendix I) mapped in Figure 1.4. The texture of outcrops are described using the classification of Dunham (1962) with additional terms from Embry & Klovan (1971) shown in Table 1-1. Stratigraphic logs of localities are shown in Appendix II.

<table>
<tr><td colspan="4">DEPOSITIONAL</td><td colspan="5">BIOLOGICAL</td></tr>
<tr><td colspan="4"><10% of grains >2 mm</td><td colspan="2">>10% of grains >2 mm</td><td rowspan="2">baffling by organisms</td><td rowspan="2">encrusting organisms</td><td rowspan="2">rigid framework organisms</td></tr>
<tr><td colspan="3">Contains lime mud (<0.02 mm)</td><td>No lime mud</td><td rowspan="3">Matrix supported</td><td rowspan="3">>2 mm component supported</td></tr>
<tr><td colspan="2">Mud supported</td><td rowspan="2" colspan="2">Grain supported</td></tr>
<tr><td><10% grains (<2 mm)</td><td>>10 % grains</td></tr>
<tr><td>mudstone</td><td>wackestone</td><td>packstone</td><td>grainstone</td><td>floatstone</td><td>rudstone</td><td>bafflestone</td><td>boundstone</td><td>framestone</td></tr>
</table>

Table 1-1. Classification of limestone based on Dunham (1962) and Embry & Klovan (1971).

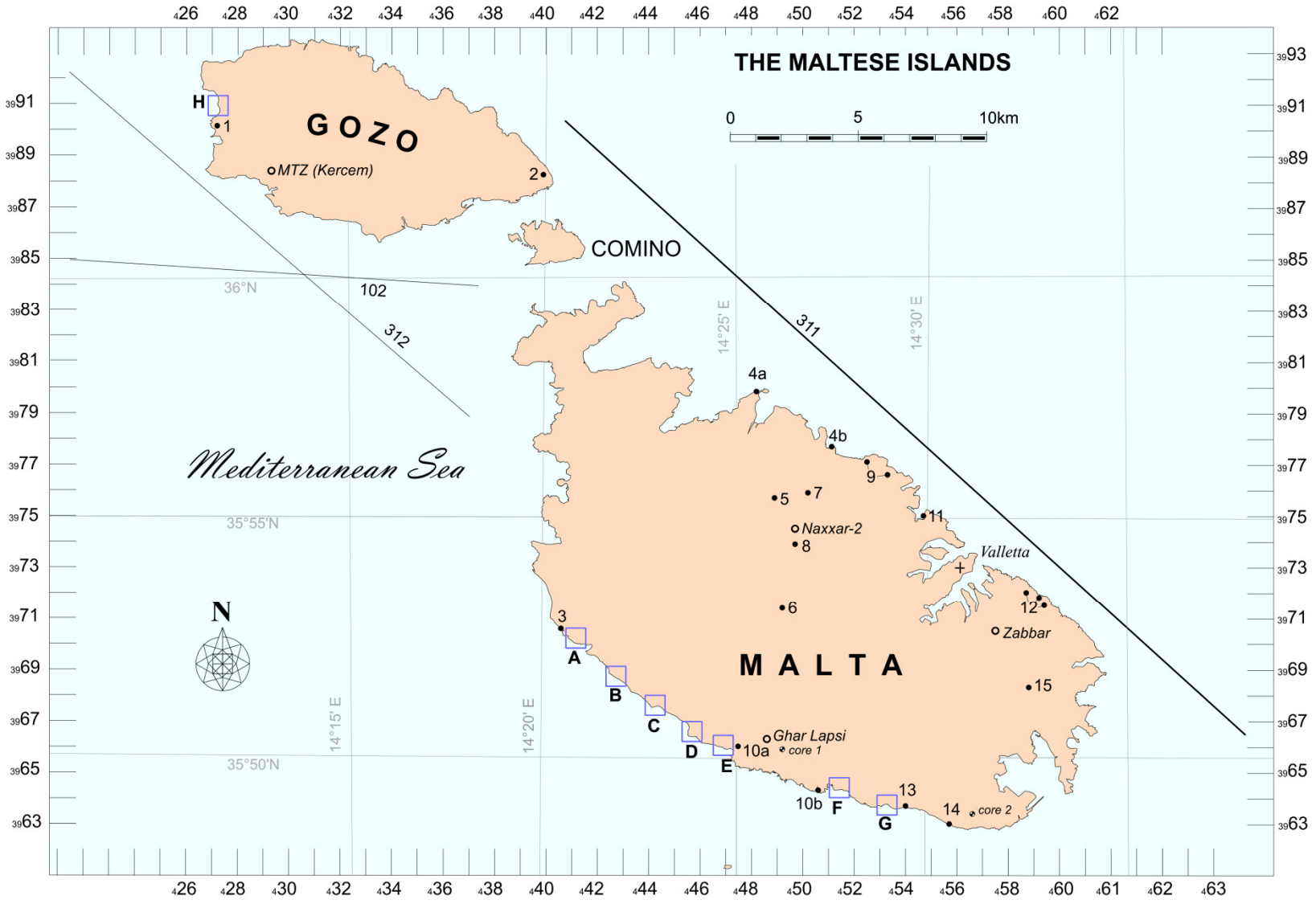

Figure 1.4. Map of the Maltese Islands. Black dots mark the logged localities 1 to 15. The southern coastal area forms the inaccessible cliff of Malta which is here sub-divided in localities A to G (in squares) and H in western Gozo. The Naxxar-2, MTZ and Zabbar exploration wells marked as open circles. The numbered offshore lines are seismic lines.

- Six exploration wells listed in Appendix I. Detailed logs are not available for the Medina Bank-1 well. The MTZ well data is limited to the lower 6 to 8 km
- Over 100 polished thin sections from outcrops in the Maltese Islands prepared in the laboratories of the University of Reading and the Earth Science labs at Durham University. The thin sections were examined petrographically and classified according to the limestone classification scheme of Dunham (1962). The thin sections were assessed for micropalaeontology shown in Appendix III.
- Photomontage of over 200 photographs of the southern cliffed coast of Malta and western cliffed coast of Gozo taken from a boat that cruised the *circa* 20 km length of Malta's southern cliffed coast (shown in Appendix IV). The coast is sub-divided into areas labelled A to G in Malta and H in Gozo (Figure 1.4) and cliffed localities photographed of and shown in Appendix V.
- Loose 2-D grid of offshore seismic lines shot by TGS-Nopec.

Figure 1.5 shows the hierarchical flowchart starting from data sources that were applied in the compilation and writing of this thesis.

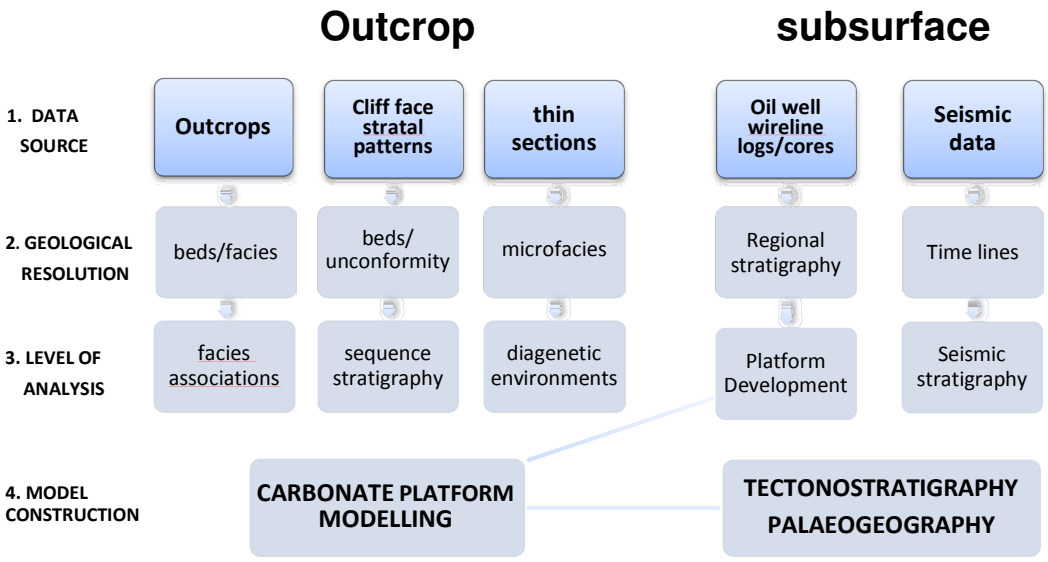

Figure 1.5. Data acquired in this study and hierarchy level of resolution of analysis.

1.5 NOMENCLATURE AND ABBREVIATIONS

1.5.2 Formation names

The formation names of the Oligo-Miocene succession in the Maltese Islands shown in Figure 1.3 do not refer to the type locality according to the conventions of the International Stratigraphic Guide (Salvador, 1994). For the sake of continuity, this thesis maintains the current practice of using established stratigraphical nomenclature although the sub-divisions of the Lower Coralline Limestone Formation have been modified and updated.

1.5.3 Carbonate buildups

'Carbonate platform': a term generally used for a thick sequence of mostly shallow-water carbonates (Tucker & Wright, 1990). Carbonate platforms develop along a variety of tectonic settings (Bosence, 2005) where the increase in accommodation space was sufficient to promote carbonate aggradation. They show particular characteristics on both the regional scale and the geological time scale and develop particular morphologies that can be modelled (Read, 1985) and have a remarkable longevity, although they will eventually drown (Schlager, 1999).

'*Malta Platform*': used in this study to describe a carbonate platform that has existed since the Mesozoic as a feature that was distinct from surrounding basins and nearby, well-documented carbonate platforms, e.g., Hyblean Platform in SE Sicily. The term does not refer to the present Malta-Ragusa Platform which forms a bathymetric feature <200 m deep.

'*Biostrome*': a horizontally bedded stratum of fossilized remains of sedentary organisms. In this study this term is used with reference to rhodalgal or coral buildups.

'*Patch reef*': small (10-20 m across) features, roughly equant in plan view and may have reached sea level, although this is not necessarily so. In this study this term is used with reference to coral and coralgal buildups that are <10 m high.

1.5.4 Time scale

Subdivision of geological record is based on the International Stratigraphic Code (Gradstein *et al*., 2004), e.g., the Oligocene Epoch begins at 33.9 Ma and ends at 23.03 Ma.

1.5.5 Biota

The nomenclature of carbonate-secreting biota used in this thesis follows the International Code of Zoological Nomenclature (Ride *et al*., 2000). Suborders are designated by the suffix '-ina' or '-ines', superfamilies by '-oidea' and families by the suffix '-idae'.

1.5.6 Abbreviations and units

SI units, symbols and abbreviation of words used in this study shown in **Error! Reference source not found.**.

SI units and symbols		Stratigraphy/biota	
km	kilometre	Ch	Chattian bounding surface
m	metre	CH	Chattian depositional sequence
Ma	million years	RU	Rupelian depositional sequence
kyr	thousand years	HST	Highstand Systems Tract
ρ	density	TST	Transgressive Systems Tract
φ	porosity	LBF	Large benthic foraminifera

Table 1-2

1.6 LAYOUT OF THESIS

This thesis contains a large amount of new data on the Malta Platform. This data is presented in chapters 2 to 8. Each chapter contains a summary section at the beginning which presents the major findings within the specified field of inquiry. The final chapter is on overall discussion of the preceding chapters and a conclusion that addresses the aims of this thesis. Details of the layout of this thesis are given here:

Chapter 1. Thesis introduction

The chapter is an overview of the aims of this thesis and the rationale for selecting the geographical area of study. The database and methodology are briefly reviewed, although more detail is presented in the relevant chapters.

Chapter 2. Meso-Cenozoic palaeogeography, geology and tectonic history of the Malta Platform

This chapter summarizes the tectonic and stratigraphic development of the western Tethys (Mediterranean) in the context of the current state of research and debate. The chapter describes the main structural elements and how they evolved through time and reviews the stratigraphy.

Chapter 3. Facies analysis of the Oligocene carbonates of the Malta Platform

This chapter introduces the Palaeogene facies of the Malta Platform and gives details on biotas and geographical spread of facies. The depositional environment of each facies is discussed and the carbonate ecosystems that produced the sediments are evaluated in terms of palaeoenvironmental controls.

Chapter 4. Diagenesis and carbonate reservoir porosity of the Palaeogene Malta Platform

This chapter provides a brief introduction to carbonate diagenesis and describes the main diagenetic features in the Palaeogene and Mesozoic carbonates of the Malta Platform. Data derived from carbonate textures, fabrics and cement, oxygen and carbon isotopes, cathodoluminescence and rock colour. The reservoir quality of the carbonates is reviewed briefly.

Chapter 5. Palaeogene stratigraphy of the Malta Platform

This chapter is sub-divided into two parts: Part 1 places for the first time, the Lower Coralline Limestone Formation in a sequence stratigraphic framework. Depositional sequences are described in terms of relative sea-level change; Part 2 dates the Palaeogene succession using large benthic foraminiferal biozones, strontium isotope dating and fine-tunes dating to the predominant astronomical cyclic forcing. The relative sea-level curve is compared to global eustasy.

Chapter 6. Tectonostratigraphic development of the Malta Platform

This chapter discusses the creation of accommodation space by tectonism deduced from seismic imaging. High amplitude and laterally persistent seismic reflectors are tied to well stratigraphy in order to determine the geometry of large scale sequences. The Malta Platform is sub-divided into geotectonic zones showing particular tectonic regime and features.

Chapter 7. Environmental controls on Palaeogene carbonate sedimentation

This chapter provides a brief introduction to environmental factors controlled by climate. The chapter comprises a paper accepted for publication in *Petroleum Geoscience*. Over 95% of the manuscript is my own work. Gluyas contributed to manuscript editing advice. The hypothesis presented in the paper is that Palaeogene carbonate facies in Malta and the Central Mediterranean were controlled by climate change over North Africa. This chapter provides insights to mechanisms of long-term climate change and its effect on carbonate ecosystems.

Chapter 8. Discussion and conclusions

This chapter provides an overall discussion on the development of the Malta Platform during successive tectonostratigraphic phases. The new data and interpretations are compared to previous publications and the new findings are summarized in the conclusions.

Chapter 2

Meso-Cenozoic palaeogeography, geology and tectonic history of the Central Mediterranean

2.1 INTRODUCTION 15

2.1.2. Tectonic sub-divisions of the Central Mediterranean 15

2.2 CENTRAL MEDITERRANEAN TECTONOSTRATIGRAPHY 20

2.2.2 Late Palaeozoic 21

2.2.3 Mesozoic 22

2.2.4 Cenozoic 32

2.3 SUMMARY 44

2.1 INTRODUCTION

This chapter presents a geotectonic overview of the Central Mediterranean and the Malta Platform. The geological complexity of the region has resulted in the development of diverse and sometimes debatable interpretations by researchers, especially in the understanding of the regional tectonics. The objectives of this chapter are to: (1) describe the geotectonic sub-divisions of the Central Mediterranean, (2) review the tectonics and sediments of the Central Mediterranean, and, (3) describe the Cenozoic stratigraphy of the Malta Platform.

2.1.2. Tectonic sub-divisions of the Central Mediterranean

The Central Mediteranean region is dominated by a central tectonic subunit of the African continent called the Pelagian Block (Burollet *et al.*, 1978). It forms part of the four main geotectonic units of the region which are the Pelagian Block, Adria Block (Apulian Platform), Ionian Crust and Calabrian Arc (Figure 2.1).

The Central Mediteranean shows diverse topographies as a result of two processes: (i) development of orogenic thrust belts and (ii) basins, which can be subdivided into: (a) older basins consisting of remnants of the Neotethys oceanic crust, e.g., the Ionian Basin (Ben-Avraham *et al.*, 2006), which are being subducted under the Calabrian and Hellenic arcs (Dewey *et al.*, 1973) and, (b) newer (post-Miocene) basins formed by crustal or back-arc extension, e.g., the Pantelleria Rift (Strait of Sicily) and Vavilov Basin (Tyrrhenian Sea).

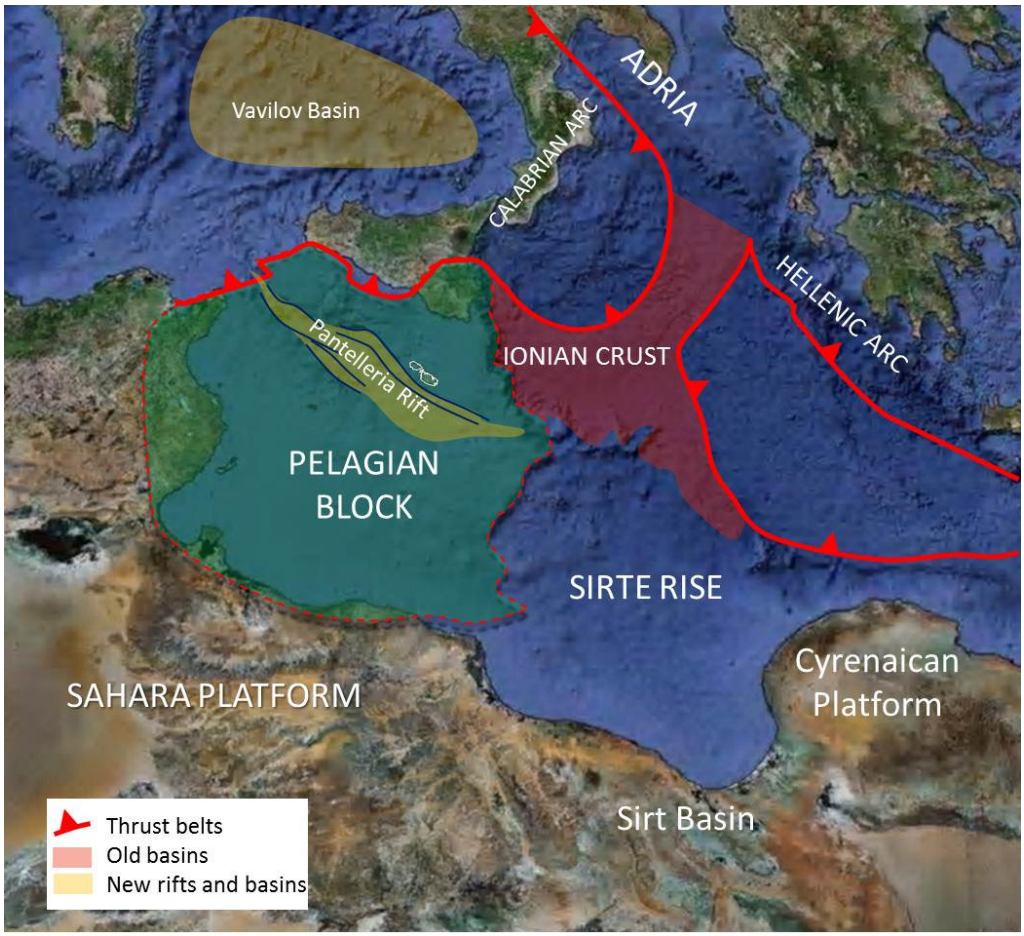

Figure 2.1. The main tectonic units of the Central Mediterranean: 1, Pelagian Block; 2, Ionian crust; 3, Adria; 4, Calabrian Arc. Based on Burollet *et al.* (1978) and Finetti (1982).

i. **Pelagian Block**: Part of the African crust on which the Malta Platform and other carbonate platforms aggraded. Seismic velocities indicate that the crust of the Pelagian Block is continental and forms a mostly submerged ~500 km-wide promontory of the North African continental crust. The margins of the Pelagian Block are bound by the N-S axis in eastern Tunisia (*circa* 9˚50'E) in the west (Burollet, 1967) and the Malta Escarpment in the east which coincides with the eastern margin of SE Sicily and the Malta Platform (*circa* 16˚E). The southern and northern the margins comprise the Nefusa uplift in NW Libya (32˚30'N) and to the north, the Sicilian thrust belt (37˚30'N). Although underlain by continental crust, Bouguer gravity anomalies are positive over large areas in the north which point to a zone of stretched, thinner crust below the Strait of Sicily and the

Medina Channel (Figure 2.2) where gravity values are between 50 and 100 mgal (Jongsma *et al.*, 1985). The stretched crust marks the extent of the Pantelleria Rift which bisects from the NE to the SW the northern part of the Pelagian Block and reaches a depth of >1000 m. Palaeomagnetic and hotspot studies to show that the kinematic motion of the Pelagian Block is coherent with the rest of Africa (Rosenbaum *et al.*, 2004).

The Malta Platform is located in the northeast corner of the Pelagian Block, along the eastern part which is relatively tectonically undeformed. This carbonate platform is penetrated by 12 offshore and onshore wells over a <200 km area from west to east (Figure 2.2). Lithospheric stretching and compression affected the Malta Platform and surrounding areas creating the following shelf areas that are presently <200m deep: (i) The Malta-Ragusa Platform where the Oligo-Miocene succession emerges in SE Sicily and the Maltese Islands; (ii) Adventure Bank along the western margin of the Malta Platform that developed by Cenozoic foreland deformation which produced a folded belt involving the carbonate platform sediments and Oligocene siliciclastics until it foundered below sea-level as a result of extension along the Pantelleria Rift (Corti *et al.*, 2006); (iii) Medina Bank that consists of the same rock formations exposed in Malta and was separated from the Malta by Plio-Quaternary wrenching (Jongsma *et al.*, 1987), (iv) Lampedusa Platform that extends from Tunisia and, (v) the Melita Bank.

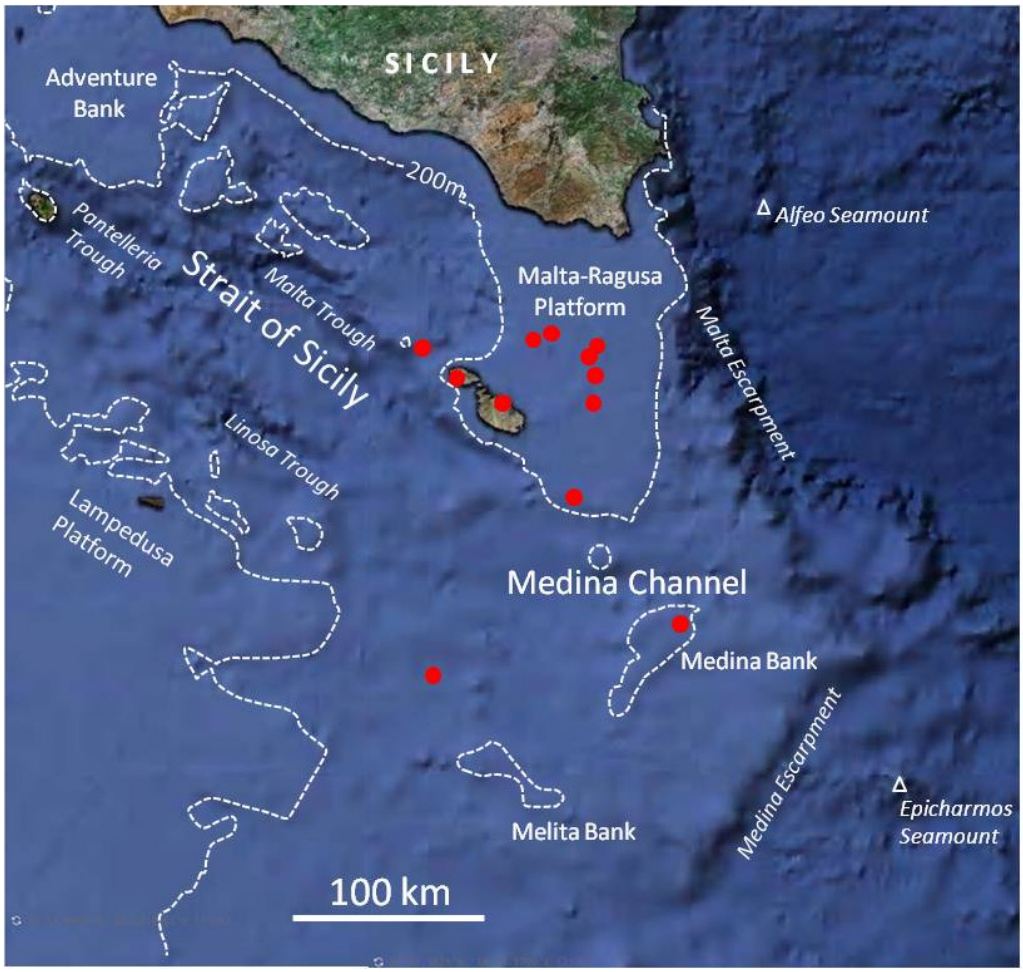

Figure 2.2. Bathymetry of the Central Mediterranean. Dashed white line is the 200 m isobaths. Red dots mark location of wells penetrating the Malta Platform. Two wells are on onshore Maltese Islands.

ii. **Adria Block**: The earliest documented unit which forms the backbone of the Italian Peninsula and has long been described as an emergent area (Suess, 1883). Dewey *et al.* (1973) considered Adria to comprise of two microplates: Apulia in the south and Carnia in the north which had split from Gondwana together with the Cimmerian archipelago of landmasses, although other researchers considered it to be a single landmass (Finetti, 2004). Subsequent Cenozoic continental collision has deformed its Mesozoic margin by orogenic belts that now encircle most of the Adriatic Sea (Channell *et al.*, 1979).

iii. **Ionian lithosphere**: Located between the Pelagian Block and Adria and is entirely submerged. The nature of this crust remains debatable because it has never been sampled in view of the fact that the seabed is >3000 m deep and the basement lies buried under kilometre-thick sediments (Finetti, 1982). This debate has implications on the origin of the Malta Escarpment and the overall tectonics of the adjacent Pelagian Block. Reuther & Eisbacher (1985) consider the Ionian crust to be *'greatly attenuated continental and/or oceanic crust'* which concurs with the two prevalent, but conflicting interpretations:

a. Many researchers (e.g., Finetti, 1982; Rosenbaum *et al.*, 2004; Ben-Avraham & Ginsburg, 1990) consider the Ionian crust to be relatively thick oceanic lithosphere. This is supported by Bouguer gravity anomalies which are all >100 mgal over the Ionian crust (Jongsma *et al.*, 1985). Catalano *et al.* (2001) also suggested crustal spreading along a central Ionian oceanic ridge, presently buried under thick sediments, and the development of two conjugate passive continental margins preserved along the Apulian escarpment to the northeast and the Malta Escarpment (Pelagian Block) to the southwest. Considerable amounts of Mesozoic volcanic extrusives and magmatic intrusives are reported along the latter margin by Finetti (1982) and Pedley *et al.* (1993).

b. Farrugia & Panza (1981) and Panza (1987) used seismological data to infer an attenuated Ionian continental lithosphere. This view is supported by the discovery of dinosaur tracks in central Apulia (Nicosia *et al.*, 2000) which would involve overland theropod migration from the nearby African continental landmass. Bosellini (2002) concluded that Adria is a promontory separated from the Pelagian Block by stretched continental lithosphere which formed a semi-enclosed basin surrounded by shallow-water carbonate banks discovered by Escarmed (1982) in the Medina seamounts area of the Ionian Basin.

The controversy on the nature of the Ionian crust extends to disagreement on its age: Ben-Avraham & Ginsburg (1990) and Catalano *et al.*, (1991) considered it

to be of Permian age; Finetti (1982) described it as Triassic; Roberston & Grasso (1995) as Mid-Jurassic and Dercourt *et al.* (1986) as Cretaceous. Recent work by Bevan *et al.* (2010) supports an Early Cretaceous rifting of the Ionian crust resulting in the formation of an oceanic crust. The rifting happened at the same time as the development of the onshore Sirt Rift in Libya.

iv. **Calabrian Arc**: Calabria and the northeast tip of Sicily form the Calabrian-Peloritan Arc which consists mainly of Palaeozoic crystalline-metamorphic rock of Eurasian origin (Sartori, 2003). The magmatic arc (that includes the Corso-Sardinian Block) began rotating rapidly towards the east about 45 Ma (Carminati & Doglioni, 2004) by rapid roll-back subduction of the Ligurian and Ionian crust (Malinverno & Ryan, 1986). This generated back-arc basins that produced the Tyrrhenian Sea. The advancing orogenic belt produced thrust sheets over most of Sicily and the northern margin of the Pelagian Block (Catalano *et al.*, 1993).

2.2 CENTRAL MEDITERRANEAN TECTONOSTRATIGRAPHY

Dewey *et al.* (1973) made an early attempt at introducing the plate tectonic model to the Mediterranean by describing the motion of Africa relative to Europe. Plate motion started with divergence during the Permian, but switched to convergence by the Late Cretaceous along the following steps:

i. Northward rifting of the Cimmerian terranes (e.g., Anatolia, Iran, Afghanistan) which split from northern Gondwana, resulting in the gradual consumption of the Palaeotethys oceanic crust under the Eurasian plate (Stampfli & Borel, 2001). In the Mediterranean area, Apulia rifted from the Bay of Sirt (N Libya) whereas the Greek autochthon left the margins of Egypt and the Levant, leaving the northward projecting promontory of Cyrenaica (Bosworth *et al.*, 2008).

ii. The Mesozoic opening of Neotethys and the development of continental passive margin environments along northern Gondwana. Several Triassic to Early Cretaceous E-W basins developed along a seaway that extended from Tunisia to Syria.
iii. The relative motion between Africa and Eurasia changed at *circa* 84 Ma to dextral convergence. The compression resulted in the inversion of Early Cretaceous E-W basins by the Cyrenaican indenter (Bosworth *et al.*, 2008).
iv. The migration of magmatic arcs (Calabria) from along the margin of Eurasia, triggered by the northward subduction of Palaeotethys and later Neotethys crust.

The complexity of the region's tectonostratigraphic development is discussed through geological time:

2.2.2 Late Palaeozoic

During the Late Carboniferous, continental collision of Gondwana and Laurasia produced the Pangaea supercontinent (Figure 2.3) whereas in the east, the intervening Palaeotethys was being rapidly consumed by northward subduction and rifting of the Cimmerian terranes which split from northern Gondwana, resulting in the gradual consumption of the Palaeotethys oceanic crust under the Eurasian plate (Stampfli & Borel, 2001).

Permo-Triassic E-W rifting resulted in the opening of the Neotethys Ocean and the flooding of the Eastern Mediterranean. Ziegler (1992) suggests that this trend was largely superimposed on the axes of the Hercynian fold belt. The rifting is generally accepted to be linked with the opening of the Central Atlantic which created a divergent/transform boundary across Pangaea that passed through the Strait of Gibraltar to Sicily, widening farther east between Adria and Cyrenaica (NE Libya) (Stampfli & Borel, 2001). This implies that Adria moved northwards as a microplate independently of the Pelagian Block and Africa, as proposed by Stampfli & Mosar, (1999).

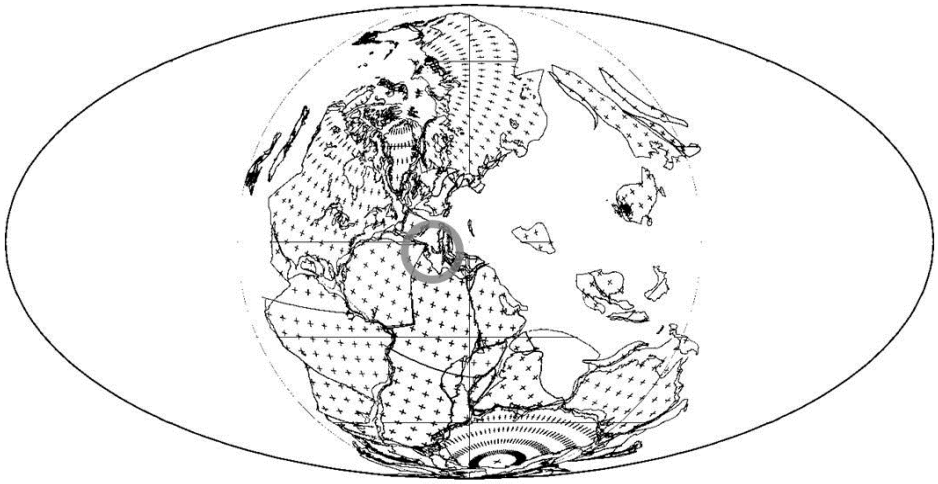

Figure 2.3. Late Permian palaeogeography showing supercontinent Pangaea (Lawver *et al.*, 2004). Grey circle marks location of Malta Platform.

The only Permian outcrops in the Pelagian Block are found in NW Libya, S Tunisia and W Sicily. Offshore, Permian sediments pass northeastwards to deep-marine mudrocks, estimated to be >2000m thick over the Lampedusa/Medina Bank area and thicken northwards to >3500m over Adventure Bank (Finetti, 1982) where they are bound by the tectonic imbricates from Neogene thrusting of W Sicily that include outcrops of the Permian Lercara Formation. Catalano *et al.* (1991) described these Sicilian imbricates as comprising; (i) flysch sediments consisting of micaceous quartz wackestone alternating with silty shales and sandstones; (ii) Clayey complex bearing olistoliths of reef slope limestone; (iii) Red Clay Unit with ostracods, sponge spicules and very few conodonts. These basinal sediments indicate a persistent deep-water seaway surrounded by shallow water which remained an open marine environment and did not desiccate under the arid climatic conditions as in the case of the Zechstein Basin in northern Europe.

2.2.3 Mesozoic

The Mesozoic was dominated by the evolution of the Neotethys as a result of continental divergence that broke up Gondwana (Roberston & Grasso, 1995) (Figure 2.4). The Pelagian Block became the sinking passive continental margin (Jongsma *et al.*, 1985) accompanied by rifting that caused the drowning of carbonate platforms (Bernoulli & Jenkyns, 1974). Mesozoic formations are listed in Table 2-1.

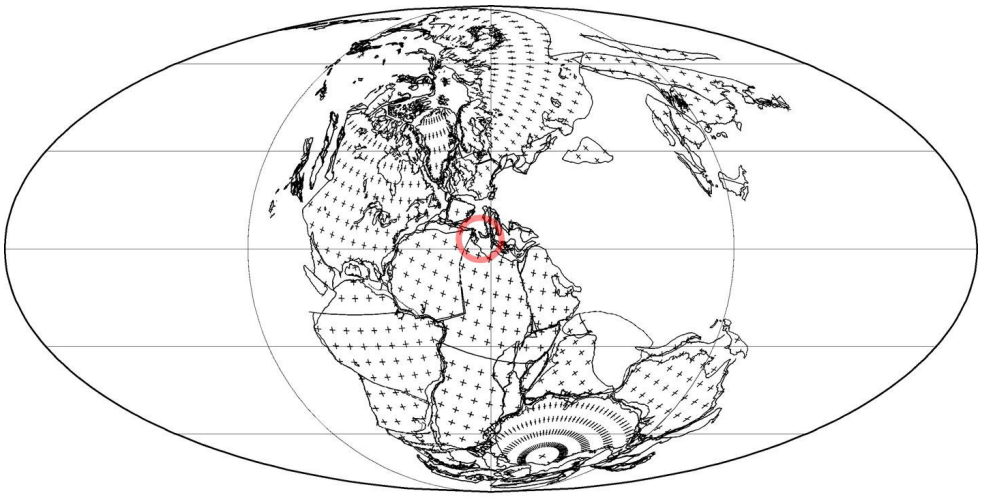

Figure 2.4. Norian (Late Triassic) palaeogeography (Lawver *et al.*, 2004). Red circle shows location of Malta Platform.

	Tunisia	**Malta**		**SE Sicily**	**Libya**
Cretaceous	Abiod *Aleg*	Naxxar Group		Amerillo	Rachmat
	Fahdene *Sidi Kralif*			*Hybla*	Nubian
Jurassic	Nara	Hurd Bank Group	Siracusa/Inici	Buccheri	
	Krachoua	Kerċem Group		*Streppenosa*	Bir el Ghnam
Triassic				Sciacca/Gela	Azizia

Table 2-1. Mesozoic formations of the Central Mediterranean. Italics indicate siliciclastic formations.

Mesozoic crustal thinning and intra-continental rifting occurred in two phases according to D'Argenio & Alvarez (1980):

i. Triassic intra-continental rifting during which oceanic crust was not produced.

ii. Jurassic-Cretaceous rifting resulting in seafloor spreading. The segmentation of the continental crust in the Central Mediterranean created several large carbonate platforms. Grasso *et al.* (1999) consider this extensional activity to

have migrated southwards towards Lampedusa Platform, bringing a progressive retreat of the African passive margin by hundreds of kilometres.

However, the palaeogeography of some of the rifting is contested. Ziegler (1992) suggested that the Triassic opening of the western Tethys followed a northerly position, between northern Adria and Europe, *contra* Stamplfi & Borel (2001) and Finetti (2004). Ophiolites along the external zones of Europe and Adria point to a former oceanic crust developing during Jurassic extension (Bortolotti, 2005). This implies that Adria remained an African promontory, as inferred earlier by Dercourt (1972), which counters the theory that the Ionian Basin is oceanic crust.

2.2.3.i Triassic

Early publications on Mesozoic Tethyan sedimentation, e.g., Hsü (1971) and Bernoulli & Jenkyns (1974), point to thick and widespread Triassic carbonate platform sediments on a subsiding crystalline continental basement. Much of the Central Mediterranean consisted of a shallow marine carbonate platform surrounded by continental areas. In the south, the Early Permian rifting of the NW-SE-trending Jeffara Basin (offshore Tripolitania) was filled by quartzo-feldspathic alluvial Triassic redbeds (Kurrush Formation) (Muttoni *et al.*, 2001). The northern Tethyan area of Adria was dominated by Norian-Rhaetian peritidal carbonate sediments of the Dolomia Principale (Southern Alps) and Hauptdolomit (northern Alps) where a succession of upward-shallowing cycles is preserved (Goldhammer *et al.*, 1990). The main builders of these Dachstein Limestone reefs were corals and sponges with a highly diversified flora and fauna. Farther south, Adria (Apulia) and Tuscany were dominated by the Burano Anhydrite (Bosellini, 2004).

In SE Sicily, well data and outcrops of tectonic imbricates over evaporitic décollements in W Sicily show the development of Norian-Rhaetian carbonate platforms. The carbonate platforms are characterised by Lofer cycles composed of stromatolitic dolomites and sabkha evaporites passing to sponge-tabulozoan reefs and backreef deposits (Figure 2.5), terminated in W Sicily by subaerial exposure

from block tilting that produced widespread karstification and bauxitic horizons (Di Stefano, 1990). In the Malta Platform, thick successions of Triassic shallow marine carbonates and evaporites are penetrated by the Madonna taz-Zejt (MTZ) well in Gozo Island (Figure 2.6).

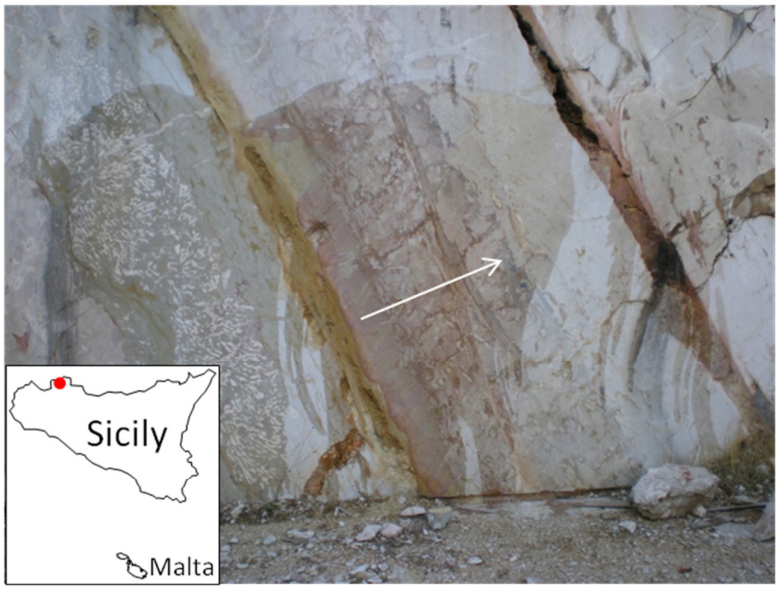

Figure 2.5. Panormide Platform: Contrada Cocuccio quarry along the Palermo mountains showing shallowing upward (arrow) peritidal/subtidal, 1.5 to 2 m-thick cycles with coral beds (Upper Triassic).

Farther south and along the continental margin of North Africa, *circa* 350 m of Triassic continental clastics to shallow-marine sediments had accumulated. These are exposed in outcrops in NW Libya and S Tunisia where they overlie the post-Hercynian unconformity (Bishop, 1975). The sediments thicken and extend offshore to the MTZ well in Gozo (Figure 2.6) where red beds penetrated at a depth of ~4.5 to 7 km inter-finger the carbonates. Three Late Triassic-Early Jurassic formations (Kerċem Group in Table 2-1) are identified in the area around the Malta Platform:

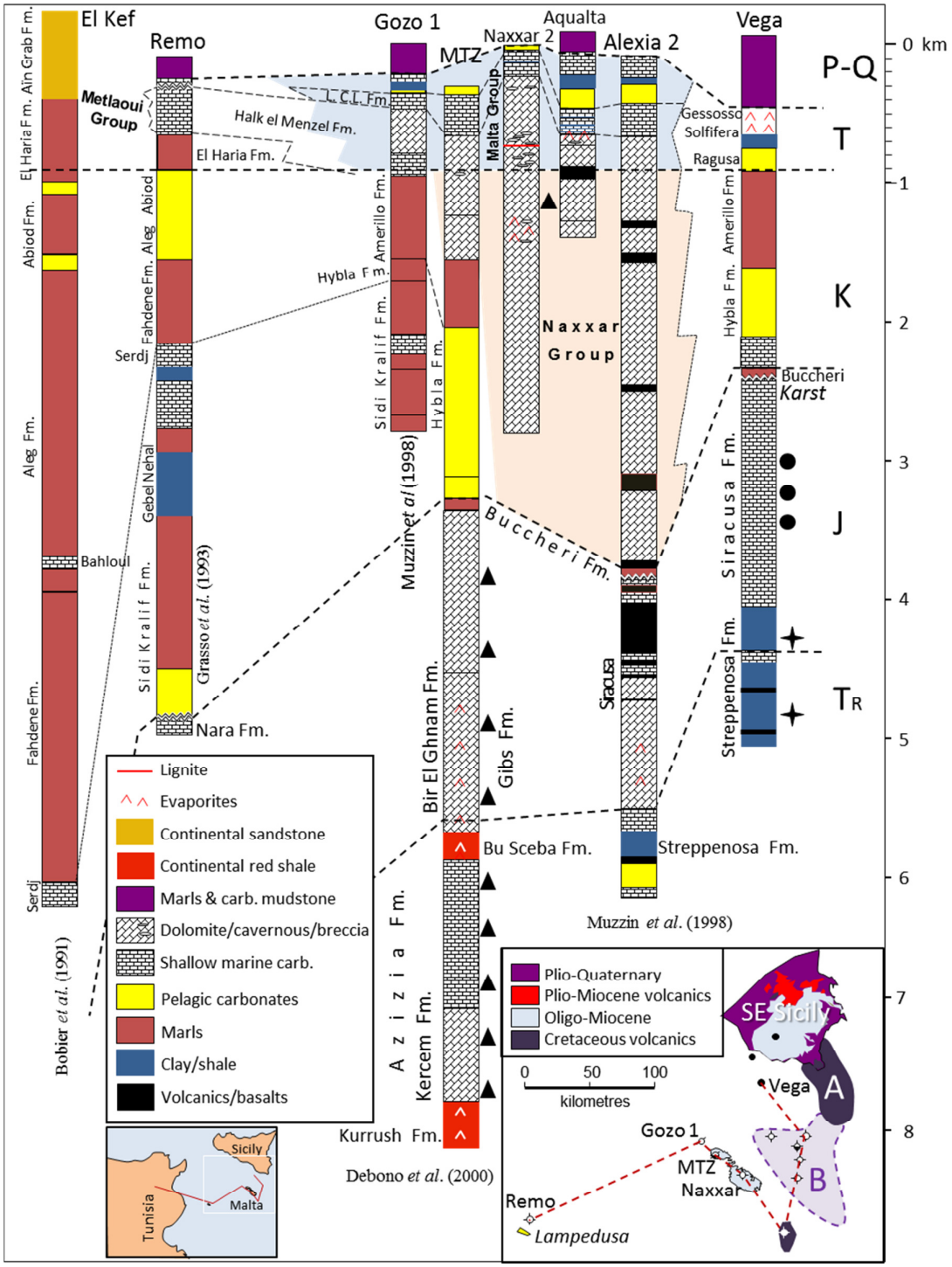

Figure 2.6. Logs from Central Mediterranean hung from Cenzoic-Cretaceous boundary (see Table 2-1). Map shows location of wells in SE Sicily through Malta to Lampedusa. A: Cretaceous offshore volcanic area; B. Approximate extent of Jurassic volcanic area.

(i) Dolomite with anhydrite of the Gibs Formation underlain by varicoloured, cross-bedded, marginal marine to braidplain and eolian sandstones of the Norian-Rhaetian Bu Sceba Formation; (ii) Carnian age carbonate platform sediments of the Kercem Formation showing a northerly increase in thickness from 120 m in NW Libya (Azizia Fm.) to 1581 m in the Malta Platform. Sediments comprise an upper member of oolitic-bioclastic packstone/grainstone with minor quartzose siltstone over a lower dolomitized member with rare anhydrite (Debono *et al.*, 2000); (iii) the quartzo-feldspathic redbeds of the Kurrush Formation. The siliciclastic sediments are alluvial, derived from highlands farther south, locally thinning over highs (e.g., Nefusa uplift) and thickening over the Jeffara Basin (Bishop, 1975).

This succession reflects changing palaeoclimatic conditions which show that N Libya drifted northwards from the equator to the arid subtropics and by Upper Triassic times, as confirmed by palaeomagnetic data, had crossed the humid subtropical boundary (Muttoni *et al.* 2001).

2.2.3.ii Jurassic

The crustal extension that began by the end of the Upper Triassic intensified in the mid- to Late Jurassic (Finetti, 1982). Extension and break-up of the Triassic carbonate platform produced five carbonate platforms on the Pelagian Block: Panormide Platform, Trapanese Platform, Saccense Platform, Hyblean Platform and Malta Platform, shown in Figure 2.7. Small segments of these carbonate platforms are exposed in W Sicily (Figure 2.8) which are bear similarities to the Malta Platform Jurassic sediments that are entirely subsurface. The carbonate platforms began drowning during the Jurassic and by the Pliensbachian had become pelagic platforms capped with condensed sediments e.g., pisolitic ironstones, red lime mudstones with ammonites (Ammonitico Rosso) (Bernouilli & Jenkyns, 1974). The exceptions to this regional drowned succession are the long-lived peri-Adriatic carbonate platforms that accumulated 7 km of sediment and the Malta Platform which accumulated ~6km of carbonates. However, some areas e.g., the Vega well area in offshore SE Sicily (Figure 2.6), remained bathymetric highs and accumulated algal packstone/grainstone of the Siracusa Formation during regressions and became

periodically emergent and karstified (Schramm & Livraga, 1986) until block faulting resulted in drowning (Ronco *et al.*, 1990).

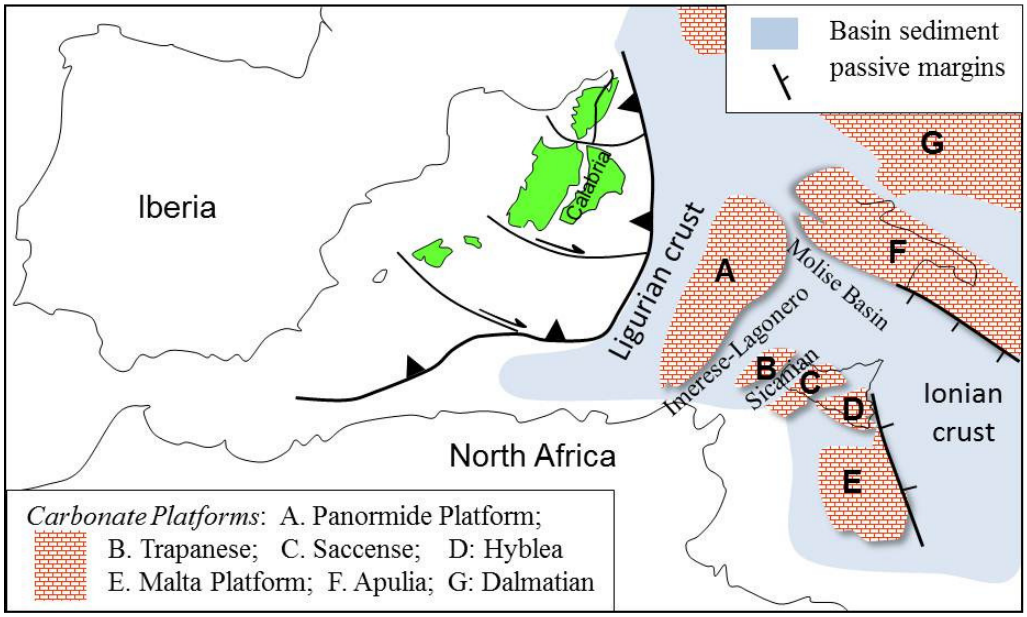

Figure 2.7. Carbonate platforms and basins since the Jurassic crustal extension (partly based on Dewey *et al.* 1989, Rosenbaum & Lister, 2004 and this study). Green shading: Corso-Sardinian Block and Calabrian Arc which began to rotate eastward in an anticlockwise direction during the Oligocene.

The rifted carbonate platforms were juxtaposed to the subsiding Sicanian and Imerese-Lagonero Basins that were partly filled by re-sedimented dolomitic limestone and ~430m of Norian-Rhaetian cherty limestone dominated by the pelagic halobid bivalve (Halobia Limestone) (Muttoni *et al.*, 2004). These directly overlie the Permian Lercara Formation, while contemporary sediments in Greece and Turkey are associated with ophiolites. In SE Sicily the Ragusa Basin began to develop as a pull-apart feature (D'Argenio & Horvath, 1984). Well data (Figure 2.6) shows that the Upper Triassic carbonate platform in SE Sicily (Gela Formation) and the northeast Malta Platform (penetrated by the base of Alexia well) subsided rapidly along the Ragusa Basin. As a result, the basin was filled with 3000 m of Rhaetian-Hettangian black shales and euxinic carbonates of the Noto Formation (Upper Triassic) and Liassic Streppenosa Formation (Antonelli *et al.*, 1988).

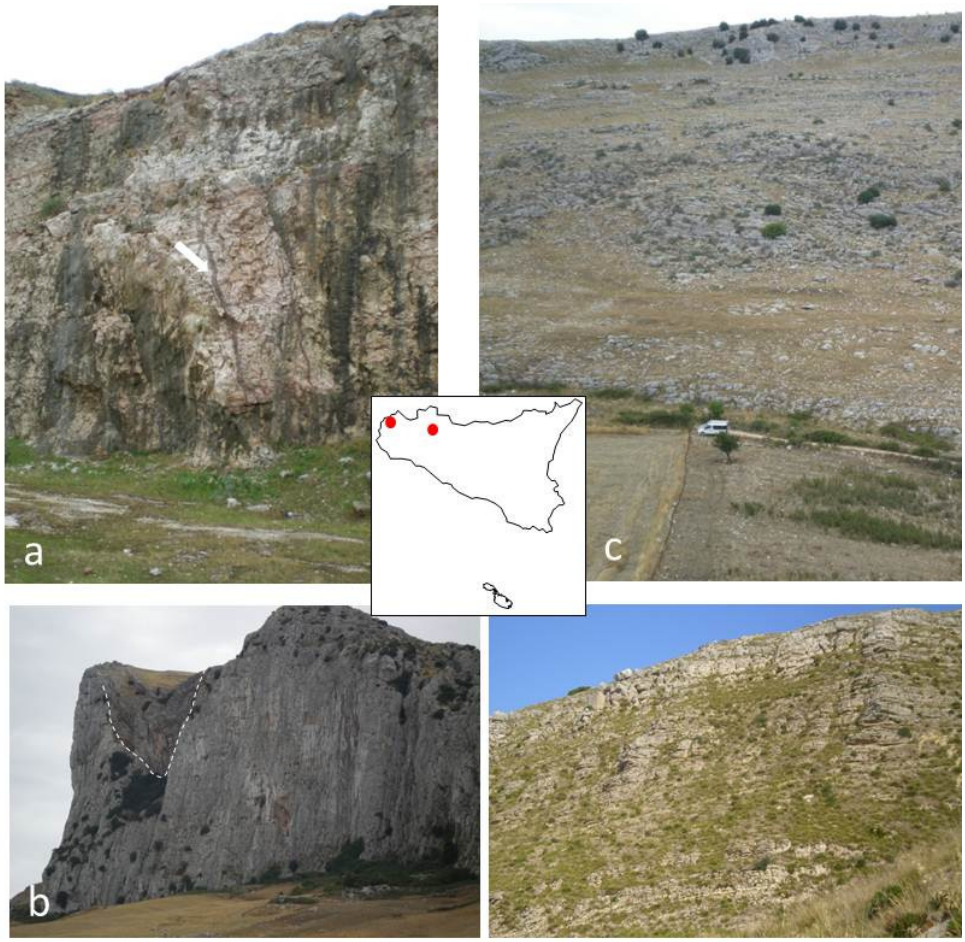

Figure 2.8. Trapanese Platform: (a) The Late Triassic to early Liassic Bahamian-type carbonate platform was drowned by the Early Jurassic and capped by Fe-Mn crusts. Rifting created neptunian dykes (marked by white arrow) and palaeofaults which are exposed at Rocca Busambra in Western Sicily and overlain by pelagic carbonates (Basilone, 2009); (b) Pizzo Nicolosi: The Jurassic platform is characterised by shallow marine/peritidal carbonates of the Inici Formation capped with pelagic Scaglia Formation (Cretaceous) carbonates that fills a depression (above dashed line).

2.2.3.iii Cretaceous

During the Cretaceous, 20% of the continental area was flooded as the sea level was 100-200 m higher than present, resulting in large and widespread carbonate platforms along the wide submerged Tethyan continental margins (Toni Simo *et al.*, 1993). Continental rifting created a wide west-east seaway between Gondwana and Eurasia (Figure 2.9) that produced carbonate ramps along the submerged Saharan

Platform and offshore isolated carbonate platforms that aggraded to several kilometres in thickness.

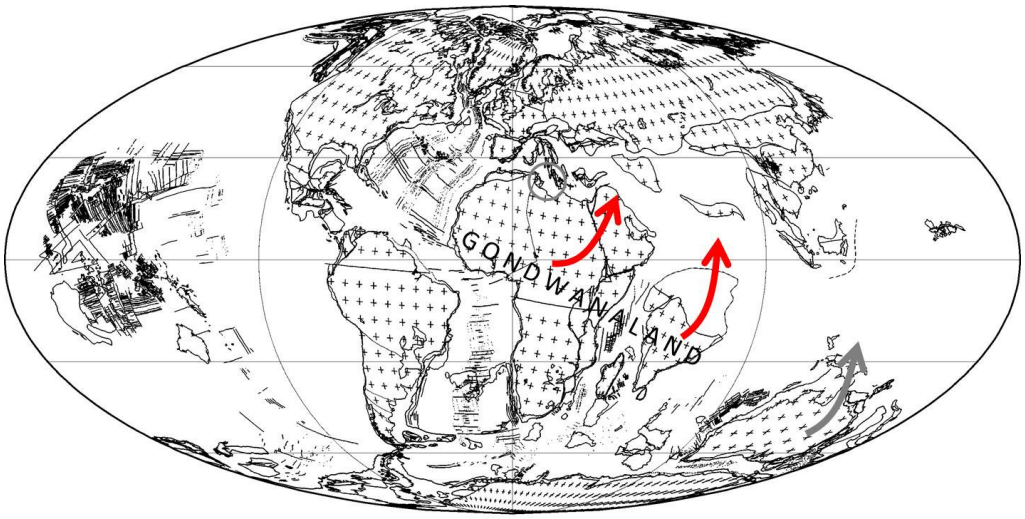

Figure 2.9. Maastrichtian (Late Cretaceous- 70 Ma) palaeogeography. Arrows show direction of movement of Gonwanaland. Base map from (Lawver *et al.*, 2004)

The Cretaceous sea-level rise caused carbonate platforms on the Pelagian Block to aggrade along two depositional settings:

i. Continent-fringing carbonate ramps along the Saharan Platform. These platforms formed two shallowing-upward sequences (Camoin, 1993): 1. The Turonian Bahloul pelagic carbonates and Fahdene marls that pass up ramp to the Bireno limestone and Beida evaporites (Table 2-1); 2. The Coniacian Douleb (carbonate) Formation that passes basinwards to the Aleg marls. These carbonate platforms were gradually drowned by the collapse of the Saharan margin and transgressed by the Campanian Abiod Formation (Camoin, 1993). The deep water marls, shales and carbonates together with the succeeding Abiod Formation reached an overall thickness of >5 km in the Tunisian Trough (Bobier *et al.*, 1991) and extended eastwards over the subsiding Lampedusa Shelf, Adventure Bank (Antonelli *et al.* 1988) and Melita Graben (Bishop & Debono, 1996), thinning significantly eastwards towards Gozo Island where equivalent Sicilian facies of the Hybla and Amerillo (Scaglia) Formations extend towards SE Sicily.

ii. Isolated carbonate platforms that had developed in the central part of the Pelagian Block, e.g., Malta Platform, Isis Reef, Limoncello and Chianti carbonate reefs and the Lampedusa reef. These platforms were surrounded by pelagic carbonates and marls (Figure 2.10). On these platforms, rudists replaced corals in importance and became the main reef builders by baffling sediments, producing low relief build-ups that favoured the development of ramps.

Well data shows that the Malta Platform extended between the Malta Escarpment and Malta Island where >1800 m of Cretaceous dolomite are recorded in the Naxxar-2 (Figure 2.6) and Aqualta well. The Cretaceous sediments include *Cuneolina*, *Inoceramus* fragments and miliolidae. These sediments suggest a shallow marine platform environment that was dolomitised. The margins of the Cretaceous Malta Platform were rimmed by reefal buildups seen in seismic along the Malta Escarpment on the east (Pedley *et al.*, 1993) and about 100 km to the SW of Malta.

The Lampedusa Shelf and the other platforms west of Malta were drowned by Barremian to Aptian marls. The basin areas between the isolated carbonate platforms showed high organic productivity which resulted in accumulations of organic-rich marls, shales and carbonates by the Early Cretaceous over most areas in the northern Pelagian Block. Basin subsidence in this area was driven by extension that produced NW-SE-trending normal faults, followed by post-rift thermal subsidence and widespread deep-marine environment when the Fahdene formation was deposited. The equivalent sediments of the Hybla formation were deposited over Sicily and Gozo (Grasso *et al.*, 1999).

The beginning of continental convergence during the Late Cretaceous resulted in compressive structures, uplift and erosion (Grasso *et al.*, 1993). Several examples of tectonic inversion in the Central Mediterranean are found in the Lampedusa area and offshore eastern Tunisia (Sebei *et al.*, 2007).

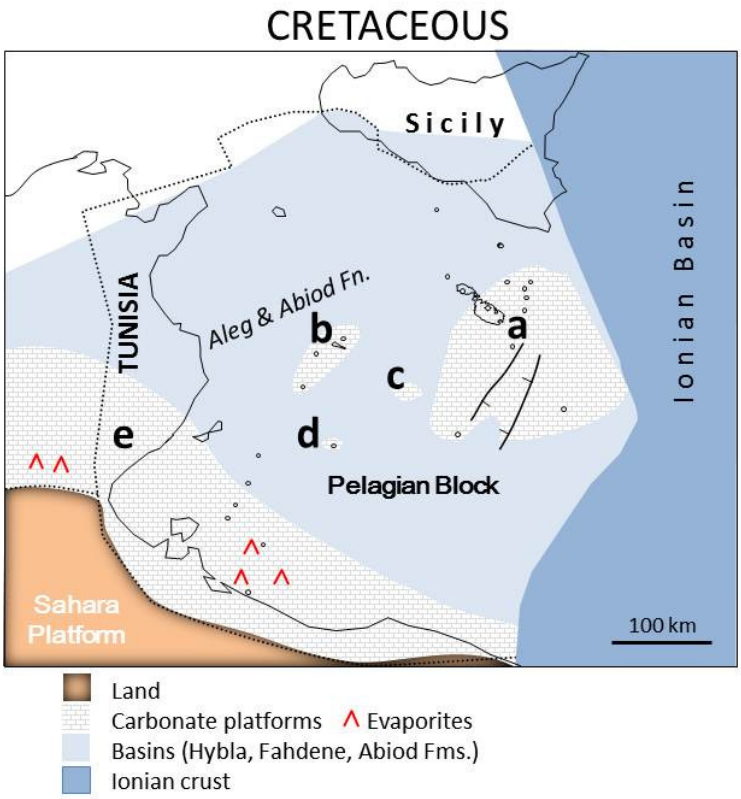

Figure 2.10. Palaeogeography of the Central Mediterranean during the Cretaceous. Isolated carbonate buildups include: a. Malta Platform, b. Lampedusa Platform, c. Limoncello and Chianti reef, d. Isis Platform and, e. carbonate platform attached to the Saharan Platform. Partly based on Bishop & Debono (1996); Grasso *et al.*, (1993), Camoin (1993) and seismic and well data.

2.2.4 Cenozoic

The Cenozoic marks the change from the Cretaceous and Early Palaeogene global greenhouse conditions (climatic optimum reached in Early Eocene) to the Plio-Pleistocene icehouse (Read, 1998). The intervening Oligo-Miocene was a transitional period when the Antarctic ice-sheets began to develop and sea-level varied by ten to tens of metres. As sea levels dropped after the Cretaceous highstand, large islands began to emerge in the southern Pelagian Block. Despite falling temperature and sea-level, carbonate platforms continued to develop along continental margins (Figure 2.11).

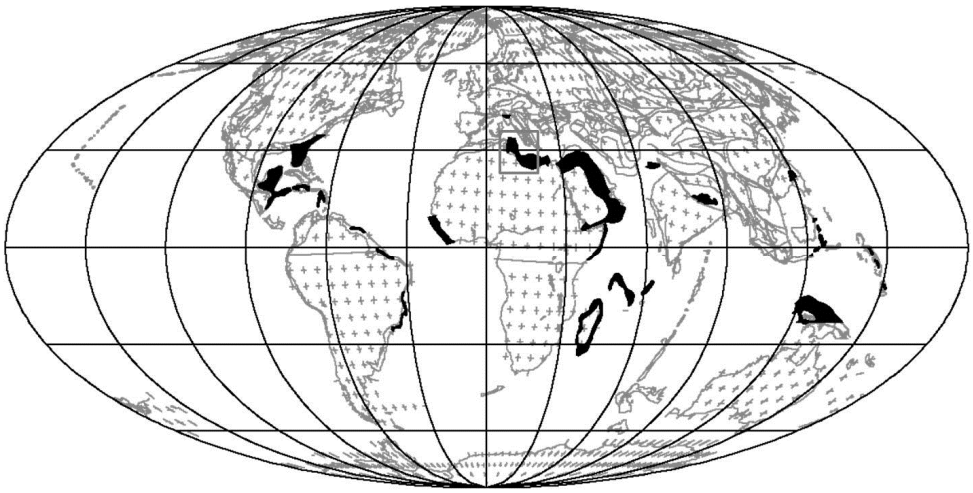

Figure 2.11. Palaeogeography of the Early Oligocene (30 M). Areas shaded black represent carbonate platforms.

The Central Mediterranean was characterised by a number of carbonate platforms that aggraded since the Mesozoic (Figure 2.7) flanked by two oceanic crusts: the Ligurian crust to the west and the Ionian crust to the east (Dewey *et al.*, 1989). However, different interpretations exist regarding the connectivity of the Ligurian and Ionian oceanic crusts: Rosenbaum *et al.* (2002) propose that the two oceanic crusts were separated by a landbridge whereas Catalano *et al.*(2001) suggests that the two oceans were connected (Figure 2.12).

Plate movement was dominated by two processes affecting the Mediterranean during the Cenozoic:

1. Convergence of the African and Eurasian plates which had started since the Late Cretaceous and resulted in inversion tectonics. The Malta Platform migrated northward with the rest of the African plate (Figure 2.13).

2. The rapid anti-clockwise rotation of a number of microcontinents that include the Calabrian-Peloritan Arc followed by the Corso-Sardinian massif (shown in Figure 2.7) as a result of the subduction rollback of the Ligurian crust (Rosenbaum *et al.*, 2002; Sartori, 2003). These orogens began to load and flex the northern margin of

the Pelagian Block by thrust sheets since the Oligocene (Guarnieri *et al.*, 2002) and by the Plio-Quaternary had downthrusted the northern margins of the African (Patacca & Scandone, 2004) which included carbonate platforms that had developed since the Mesozoic, e.g., Panormide Platform and also began to subduct the Ionian crust.

During these two coexisting tectonic movements affecting the eastern and central Mediterranean, >500 m of carbonates accumulated over the Hyblean Platform (SE Sicily) and *circa* 1 km of carbonates/marls of the Cenozoic Malta Group accumulated over the Malta Platform (Table 2-2). In contrast, the western Mediterranean was dominated by continental fluvial siliciclastics of North African origin (e.g., Fortuna Formation) with Numidian flysch accumulating in the depocentre (Thomas *et al.*, 2010).

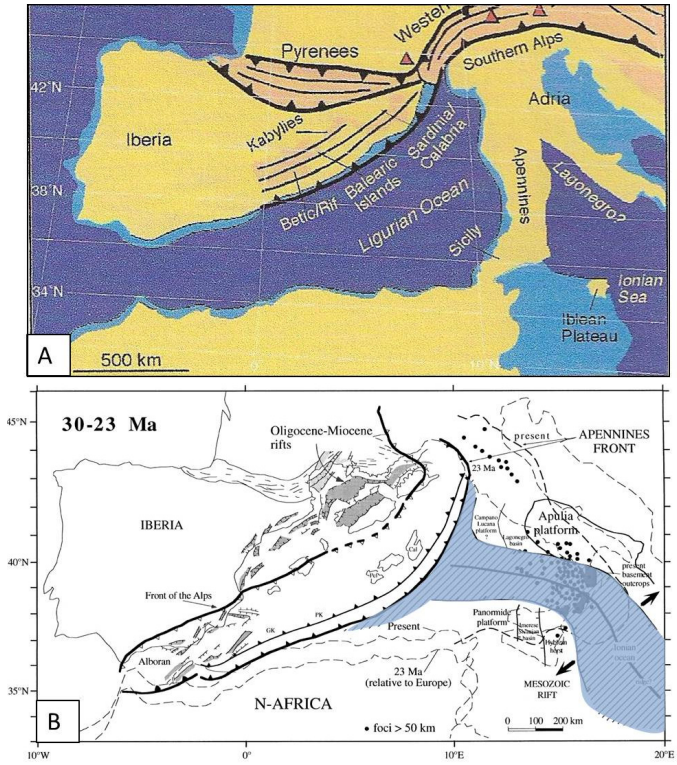

Figure 2.12. Reconstructions of Oligocene tectonics from: A. Rosenbaum *et al.* (2002) (figure 11) showing a N-S landbridge subdividing oceanic crust; B. Catalano *et al.* (2001) showing Ionian oceanic crust (blue shading) between the Pelagian Block and Apulia Platform.

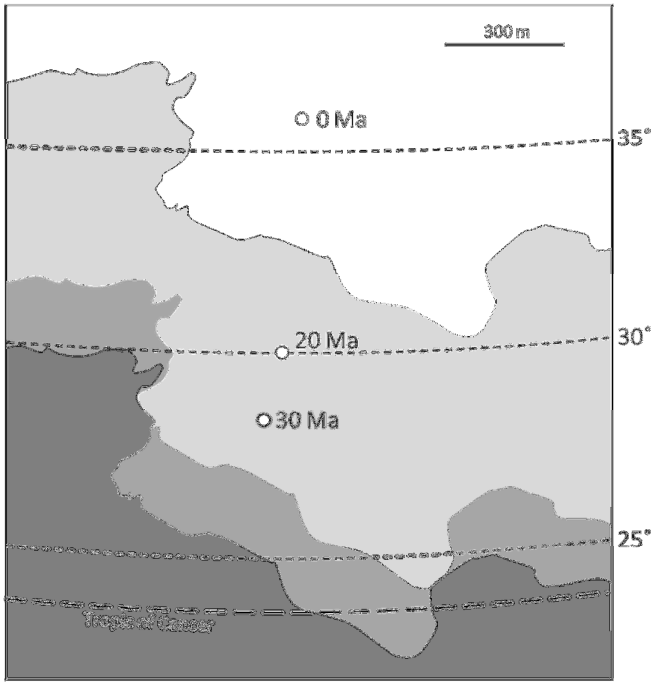

Figure 2.13. Open circles represents position of Maltese Islands. Shaded areas are the Tunisian/Libyan coast from the Oligocene (dark grey) to present shown in light grey (based on Schettino & Scotese, 2005).

	Tunisia		Malta Platform		SE Sicily	W Sirt Basin E	
Quaternary					*Trubi*		
Miocene	Melquart		Malta Group	Upper Coralline	Gessosso-Solfifiera	Marada	
	Remla			*Blue Clay*	*Tellaro*		
	Ketatna	*Fortuna*		Globigerina	Ragusa		
Oligocene				Lower Coralline		Bu Hashish	Diba / Arida
Eocene	*Souar*			Halk el Menzel/ Metlaoui Group		Gialo	
	Metlaoui Group						
Paleocene	*El Haria*					*Kheir/Hagfa*	

Table 2-2. Cenozoic Formation names of the Central Mediterranean region. Italics indicate siliciclastics sediments, other Formations are carbonates whereas green lettering indicates evaporites. Grey shading indicates prolonged depositional hiatus.

2.2.4.i Palaeogene

The continuation of the long-term Cretaceous marine transgression to the early Cenozoic resulted in the deposition of Palaeocene marine shales of the El Haria Formation over Tunisia (Bishop, 1975) and the Lampedusa Shelf (Grasso *et al.* 1993), whereas Palaeocene sediments on the Malta Platform are mostly absent. Well data and outcrops from the Central Mediterranean show that the Palaeogene includes two major regional depositional hiatuses:

i. A major hiatus separates the Paleocene from the Eocene. Paleocene sediments are missing in Tunisia and northern Libya where a long depositional hiatus of >10 Ma separates the top Cretaceous from the base of the Eocene (Jorry, 2004). The widespread depositional hiatus marks the emergence of Jeffara Island and Kasserine Island in south and central Tunisia respectively (Figure 2.14),
ii. A second regional hiatus separates the Eocene from the Oligocene sediments. This regional hiatus is marked by the deposition of evaporites in W. Egypt and Cyrenaica (Gerdes *et al.*, 2010).

Carbonate sediments were dominated by *Nummulites* that became the main carbonate factory of the Eocene and thrived over palaeohighs close to, or above fair-weather wave base from where they were exported in large quantities to the mid-ramp where they form thick units (Beavington-Penney *et al.*, 2005). Nummulitic banks are reported in the following areas:

i. The neritic environment of North Africa where carbonate ramp sediments accumulated, e.g., along eastern Tunisia the early Eocene Metlaoui Group was deposited along ramps that became emergent along with evaporite deposition (Aïn Merhotta Fm.), passing seaward to two main facies belt that comprised the inner ramp coquinoid facies (with shales) to nummulitic facies (El Garia Fm.) and the outer ramp globigerinid facies of the Bou Dabbous Formation (Beavington-Penney *et al.*, 2005).

ii. The Pelagian Islands (Lampedusa Platform) to the Malta Platform. These mid- to late Eocene shallow marine carbonates have been named the Halk el Menzel Formation by Bismuth & Bonnefous (1981) and developed offshore of North Africa where the continental siliciclastic input was negligble. This Formation comprises three successive facies: (a) the top carbonates include miliolids, Peneroplidae, coral and dascycladacean algae that Bismuth & Bonnefous (1981) claim to merge with the base of the Oligocene Lower Coralline Limestone over the Malta Platform, (b) Marine platform sediments with *Nummulites* and *Discocylcina* and, (c) crystalline dolomites. It is not clear how much of this Formation overlaps with the underlying Naxxar Group and the succeeding Lower Coralline Limestone Formation over the Malta Platform.

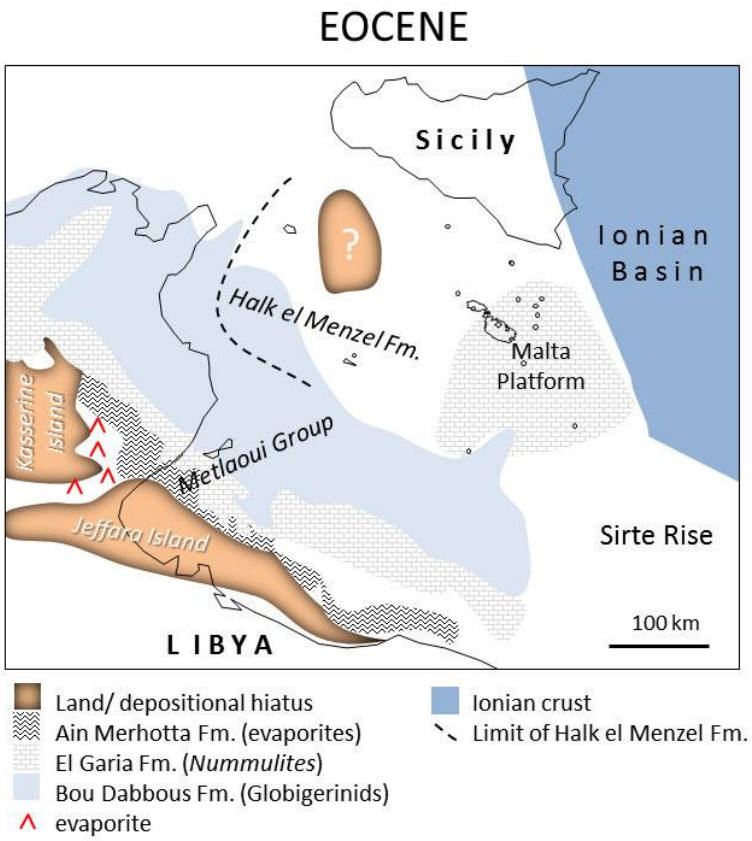

Figure 2.14. Facies map of the Early Eocene Metlaoui Group and middle to late Eocene Halk el Menzel Formation. The Metlaoui Group is succeeded by the marly Souar Formation that is penecontemporaneous with the upper Halk el Menzel Formation. Map based on Beavington-Penney *et al.* (2005) and Bismuth & Bonnefous (1981) and Malta outcrops and seismic data.

Late Palaeogene carbonates have been modelled by Buxton & Pedley (1989) that propose a facies model for the typical Oligo-Miocene ramp for the Central Mediterranean comprising nine facies, including lagoonal sediments, grainstone barrier, coralline algal rhodolith pavement and larger benthic foraminiferal carbonates. These facies can be found in parts of two platforms developed in the Central Mediterranean (Figure 2.15):

1. Hyblean Platform: platform carbonates were deposited along a ramp which became distally-steepened westwards (Pedley & Grasso, 1992) towards the Ragusa Basin. This basin accumulated outer ramp pelagic carbonates of the Ragusa Formation with phosphorite deposited along a N-S palaeohigh over Scicli in SE Sicily (Pedley, 1987), later becoming erosional in the upper Miocene. Towards the east, sediments become more condensed within a mid-ramp environment (Monti Climiti Formation). Inner ramp sediments are mostly absent and consist of coarse-grained packstones dominated by coralline algae, echinoids and large benthic foraminifer (*Lepidocyclina* and *Amphistegina*) (Pedley *et al.*, 1998). The ramp became emergent along the present SE coast of Sicily.

2. Malta Platform: The top ~120m of the Oligocene Lower Coralline Limestone Formation exposed in the Maltese Islands have been described by Felix (1973) and Pedley (1987). This formation extends offshore to the entire Malta Platform where it is penetrated by all Maltese wells over a 200 km-wide area.

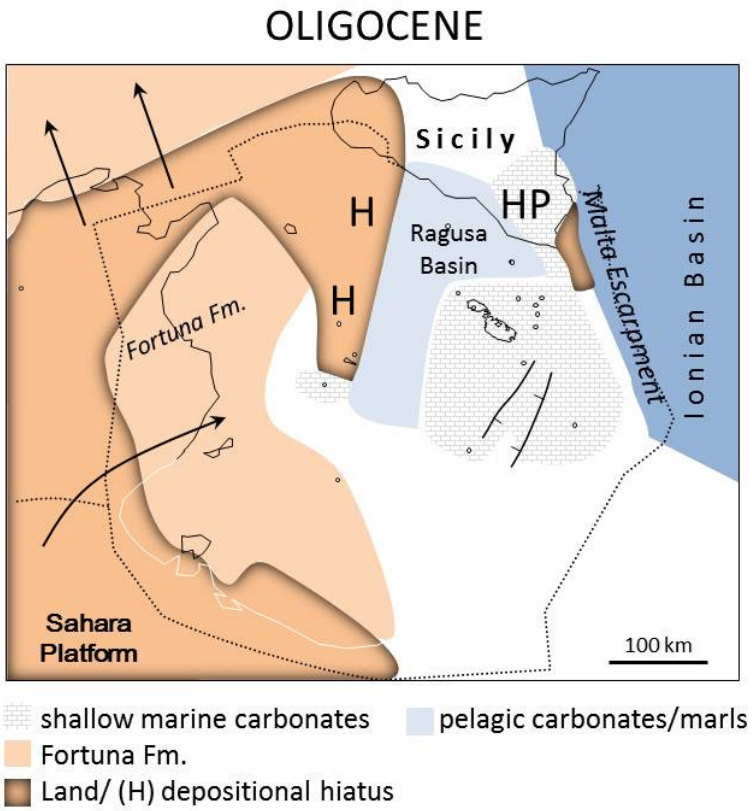

Figure 2.15. Oligocene Formations in the Central Mediterranean partly based on Antonelli *et. al.* (1988) and Bishop (1975) and offshore oil wells Malta. Arrows show direction of transport of fluvial clastics. HP is the Hyblean Platform.

2.2.4.ii Neogene

Despite continental plate convergence and microcontinent convergence with the African Plate, the Early Miocene is marked by the drowning of the Malta Platform and the deposition of hemipelagic sediments whereas lithospheric extension in the Pelagian Block continued throughout the Neogene. Extension resulted in the development of deep grabens in the Central Mediterranean and faulting that dissects Oligo-Miocene outcrops in SE Sicily and the Maltese Islands (Illies, 1981). Butler *et al.,* (1992) concluded that 'lithospheric extension continues throughout the African

foreland with no direct connection with orogenic loading'. Two processes affected the Pelagian Block:

1. Convergence of the African and Eurasian Plates accompanied by foreland crustal flexure as a result of loading from the Sicilian-Maghrebian thrust belt. Variations in the crustal structure of the northern African plate margin resulted in the segmentation of the African crust into three parts labelled a to c in Figure 2.16 separated by strike-slip faults perpendicular to the collision zone (Reuther *et al.*, 1993). Foreland downthrusting was greater in the Ionian Basin and Gela Basin relative to the Adventure Bank and Hyblean Platform. The Gela Basin was flexed downwards to form an 800m deep basin with >2km of sediments loaded by the Gela nappe (Butler *et al.,* 1992). Where continental crust is thicker as in the case of the Hyblean Plateau and Adventure Bank (a and c in Figure 2.16), the segments form two indenters in the orogen (Ben Avraham *et al.*, 1995).

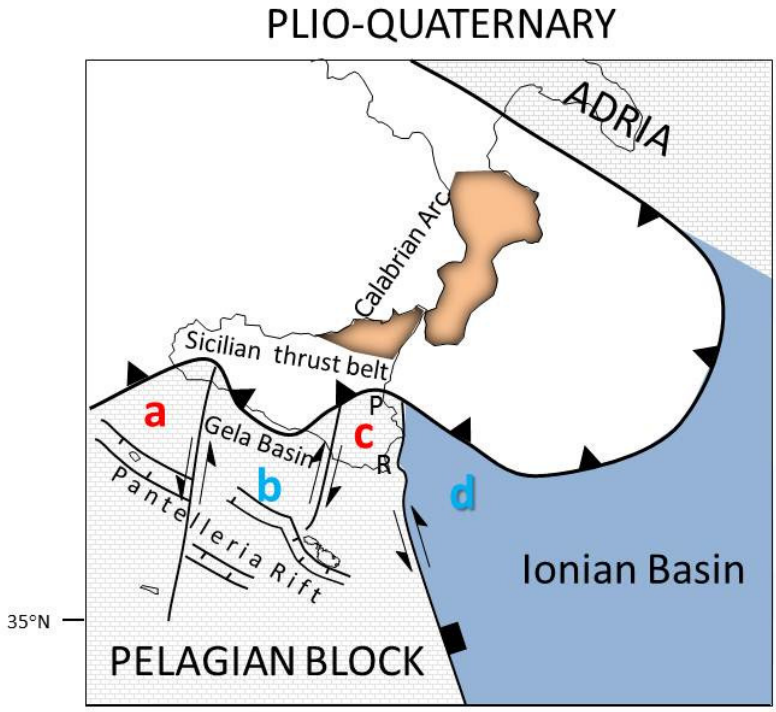

Figure 2.16. Plio-Quaternary tectonic setting. The Adventure Bank and Hyblean Plateau indenters labelled a and c in red; Gela Basin and Ionian Basin flexed foreland basins b and d in blue; P is the location of the Pleistocene carbonate ramp; R is the area of raised beaches.

2. The Plio-Quaternary Pantelleria Rift that developed orthogonal to the Maghrebian-Sicilian accretionary prism between W Sicily and N Tunisia. The Pantelleria Rift is subparallel to the orogen in Sicily and shows graben subsidence of 2 km which is considered to be the result of 1-2 km extension (Winnock, 1981). Two kinematic model have been suggested to explain the rift zone:
   (i) The ridge-push/slab-pull mechanism: slab-pull produced N-S extension in the African foreland. The remarkable symmetry of grabens in the Pantelleria Rift suggests extension by pure shear *sensu* (McKenzie, 1978; Ben-Avraham *et al.*, 2006). However, variable spreading rates along the Pantelleria Rift has segmented the foreland area along N-S trending transform faults (Argnani, 1990; Pedley & Grasso, 1992). The N-S stretching of the foreland area also produced the contemporaneous NE and SW-trending faults in the Maltese Islands (Dart *et al.*, 1993).
   (ii) Pull-apart basins: Reuther & Eisbacher (1985) and Jongsma *et al.* (1985) proposed an E-W dextral shear zone from the Medina Ridge to the Strait of Sicily resulting in pull-apart basins that formed the Pantelleria Rift. This implies a counter-clockwise rotation of SE Sicily (Hyblean Plateau) relative to Africa in Pliocene-Recent time (Rosenbaum & Lister, 2004). Since the Ragusa-Malta Platform segment (indenter C in Figure 2.16) resisted underthrusting it must have deformed to accommodate stress generated by the oblique collision of Africa and Europe. East-west dextral strike-slip faults and NE trending normal faults in the Maltese Islands and offshore accommodated this stress that produced tearing and the formation of the North Gozo Graben (Gardiner *et al.*, 1995).

These two coexisting processes of underthrusting by plate convergence and rifting (Pantelleria Rift) resulted in foreland volcanism that is more pronounced towards the hinterland, e.g., the calderas of Pantelleria Island. The opening of the Pantelleria Rift resulted in the foundering of the Malta Platform and the flooding of the Strait of Sicily (Corti *et al.*, 2006).

The Neogene is also marked by environmental factors that affected sedimentation (Figure 2.17):

1. Climatic change: A Neogene warm phase that peaked in the late mid-Miocene (15-17 Ma) (Zachos *et al.*, 2001). This Miocene climatic optimum coincides with what is claimed to be the Monterey Event (13-17.5 Ma) when $\delta^{13}C$ values in sediments increased by up to 1.5‰ as a result of greater carbon burial with the concomitant CO_2 sequestration that precipitated a global cooling event from the mid-Miocene to the Pliocene. The early to mid-Miocene warm phase was punctuated by brief glaciations identified by Miller (1991) on the basis of the $\delta^{18}O$ record and named Mi events. A tentative correlation of these global climatic events to Maltese lithostratigraphy is based on dating of outcrops using $^{87}Sr/^{86}Sr$ isotope (Föllmi *et al.*, 2008) and nannofossils (Mazzei, 1985) (Figure 2.17). The glaciations affected sedimentation at the formation level, e.g., The Mi-1 glacial event (23.5 Ma) closely corresponds to the termination of the Lower Globigerina Limestone Member and the deposition of a ubiquitous phosphate bed dated by Föllmi *et al.* (2008), whereas the Mi-3 Event (13.8 Ma) marks an increase in terrigenous influx from continental areas (John *et al.*, 2003) and the beginning of Blue Clay sedimentation (Hilgen *et al.*, 2008).

2. Change in palaeocurrents and palaeogeography: Closure of the eastern seaway by the Early Miocene (Stille *et al.*, 1996) brought a reversal in marine currents over Mediterranean carbonate platforms, from westerly-directed currents during the deposition of the Lower Coralline Limestone Formation in the Maltese Islands (Gatt, 2005), to easterly currents during the deposition of the Globigerina Limestone at the beginning of the Miocene (Pedley, 1987).

3. Change in nutrient levels: The succeeding global cooling during the mid-Miocene was marked by an increase in continental weathering and an increase in marine nutrient levels resulting in the deposition of phosphates and organic carbon (Föllmi *et al.*, 2005). The Monterey Event coincides with the deposition of mid-Miocene phosphorite beds in the Maltese Islands and SE Sicily. Carbone

et al. (1987) considered these regionally-widespread phosphorite conglomerates as having been eroded from along the slope and platform margin environments and transported eastward by sea currents over the regional submarine sill (drowned Hyblean and Malta Platforms) extending from SE Sicily to Malta, where hemipelagic sediments accumulated. Phosphorite sedimentation and transport was accentuated during marine shoaling events (Gruszczynski *et al.*, 2008).

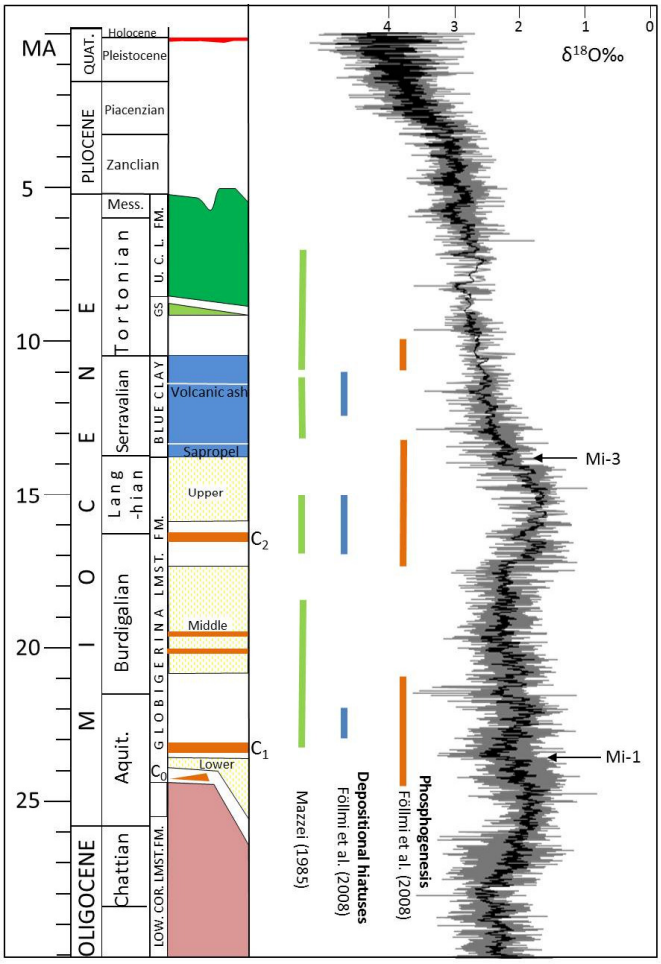

Figure 2.17. Neogene stratigraphy of the Maltese Islands and depositional hiatuses according to Föllmi *et al.* (2008) and Mazzei (1985) compared to the global oxygen isotope curve (Zachos *et al.*, 2008). The C_0 to C_2 beds are levels of phosphorites and Mi-3 isotopic event marks beginning of the Blue Clay Formation.

2.3 SUMMARY

The Mediterranean region was affected by a prolonged phase of plate divergence beginning in the Permian. The extensional regime dissected the widespread Triassic shallow marine carbonate platform into several platforms that began to drown by Jurassic time, when the Malta Platform became part of the North African passive margin. During the Cretaceous global transgression, carbonate sediments continued to accumulate on the Malta Platform which remained isolated from North Africa even when plate motion reversed to convergence by the Late Cretaceous. Palaeogene pure carbonates and evaporites were shielded from African continental siliciclastics until the Malta Platform drowned during the Miocene and was draped by pelagic carbonates and marls. Extension along the foreland caused by collision with the eastward migrating Calabrian Arc created NW-SE rifting south of Malta that resulted in the foundering of the present Malta Platform to 200 m below sea-level and emergence of the Maltese Islands along uplifted graben margin.

Chapter 3

Facies analysis of the Oligocene carbonates of the Malta Platform

3.1 INTRODUCTION 46

3.2 METHODS AND MATERIALS 48

3.3 FACIES ASSOCIATIONS 49

3.3.1 Facies Association I: Bryozoan-echinoid-bivalve wackestone to mudstone 51

3.3.2 Facies Association II: Coralline Red Algal Limestone 55

3.3.3 Facies Association III: Large benthic foraminiferal limestone 65

3.3.4 Facies Association IV: Coral limestone 78

3.3.5 Facies Association V: Imperforate foraminiferal wackestone/packstone 83

3.3.6 Facies Association VI: Red argillaceous carbonates 90

3.3.7 Facies Association VII: Gypsum facies 94

3.4 DISCUSSION 95

3.4.1 Palaeoclimatic setting 95

3.4.2 Ecological relationships and trophic level 97

3.4.3 Recognition of carbonate platform type from facies 101

3.5 SUMMARY 104

3.1 INTRODUCTION

This chapter describes the <120 m-thick carbonate facies, biotas and sedimentary structures of Oligocene age exposed in the Maltese Islands as well as the >100 m subsurface facies data derived from exploratory wells in the Malta Platform. The Oligocene outcrops of the Maltese Islands consist of the Lower Coralline Limestone Formation which is predominantly a limestone of high purity (>95% $CaCO_3$ in Gatt, 1992) with its top surface along the inter-formational boundary with the overlying hemipelagic Globigerina Limestone Formation (Murray, 1890; Felix, 1973; Pedley, 1978; Gatt, 2005; Föllmi *et al.*, 2008). Works preceding this study do not identify the subsurface basal boundary of this formation with the underlying Eocene carbonates penetrated by exploratory wells.

Deposition of the Lower Coralline Limestone Formation was along a carbonate platform affected by two fundamental hydrodynamic boundaries: the fair-weather wave-base (FWWB) which is the depth at which waves normally affect the sea bottom and the storm wave base (SWB) which is the depth of water affected during storms. The two hydrodynamic barriers sub-divide carbonate platforms into the inner, mid- and outer sections (Burchette & Wright, 1992). The depth of FWWB and SWB is approximately <20 m and >40 m respectively and considered to have been shallower in the semi-enclosed western Tethys relative to open oceans where greater fetch results in higher waves.

The formation comprises a large number of facies that are stacked vertically and show lateral variations. A *facies* is defined as a body of rock with specified characteristics that reflect a particular depositional environment (Reading, 1996). Carbonate facies are composed of micrite which can be inorganically precipitated or organically produced and skeletal grain associations. Skeletal components are the product of ancient carbonate ecosystems that reflect temperature, salinity, light intensity, oxygen, and water energy conditions (Pomar *et al.*, 2004; Carannante *et al.*, 1988; Hallock & Schlager, 1986; Pomar *et al.*, 2004). These factors make carbonate organisms and their ecological relationships valuable environmental indicators that can throw light on past environmental conditions and depositional

environment. Facies have been classified by the dominant type of skeletal grain associations (Table 3-1) (Nelson, 1988; Carannante *et al.*, 1988; Lees & Buller, 1972) that reflect the trophic level of the ancient ecosystems and its dependency on light for energy *sensu* James (1997). Modern examples of skeletal grain associations are typically constrained by latitude and depth, although there are notable exceptions that reflect the impact of nutrient level on carbonates (Westphal *et al.*, 2010). The temperature-dependent controls produce distinct associations of skeletal grains that reflect particular environmental parameters which are fundamental in identifying depositional environments in modern and ancient carbonates:

i. The tropical carbonate factory (sea temperature >20˚C) dominated by autotrophic chlorozoan and foramol carbonate biotas found in modern environments between latitudes 30°N and 30°S. During the Oligocene this carbonate factory extended to 40˚ in both hemispheres (Kiessling *et al.*, 2000). Environments tend to be poor in nutrients (oligotrophic) and organisms are dependent on light for food. Trophic level tends to be skewed towards photo-autotrophic organisms and heterotrophic organisms with autotrophic symbionts, e.g., calcareous green algae, hermatypic corals, certain foraminiferans, and certain molluscs.

ii. Temperate to cold marine environments (and deep-water tropical areas) that can be nutrient rich. The heterotrophic organisms include non-symbiotic molluscs and foraminifers, bryozoans, barnacles, and red algae which are classified as bryomol, rhodalgal and foramol carbonates. However, the foramol facies that consists of accumulations of large benthic foraminiferans (LBF) can also occur in tropical environments (Wilson & Vecsei, 2005).

iii. The mud-mound factory that grows by abiotic and biotic precipitation of carbonate in higher nutrient environment and low oxygen conditions.

Grain association	*Constituent grains in Malta*	*Facies Associations*	*Light-related* James (1997)
Bryomol Nelson (1988)	Bryozoans, bivalve molluscs, echinoderms, benthic foraminiferans	I	Heterozoan
Rhodalgal Carannante *et al.*, 1988	Crustose coralline red algae, bryozoans, LBF, bivalves, echinoderms	II	
Foramol	LBF, molluscs, bryozoans, echinoderms	III	Photozoan
Chlorozoan Lees & Buller (1972)	Calcareous green algae, zooxanthellate corals, LBF, geniculate coralline algae, branching coralline algae, molluscs	IV, V	

Table 3-1. Facies associations in Malta classified by grain type and light dependency.

Skeletal grains produced by carbonate-secreting genera provide valuable insights on ancient ecological conditions. However, sediment accumulation is slow relative to the life span of an organism so that carbonate fossil assemblages actually reflect composites spanning millennia (Kidwell & Bosence, 1991).

The objectives of this chapter are: (1) the synthesis of facies data into facies associations and the description of their depositional environment, and (2) to hypothesize on the type of carbonate platform and to relate its development to prevailing environmental conditions during the Oligocene.

3.2 METHODS AND MATERIALS

Eighteen sections in 15 localities in the Maltese Islands were measured, logged and sampled (location map in chapter 1, figure 1.4). Facies have been enumerated and the logs of the localities showing successive facies are shown in Appendix II. Outcrop data is supplemented by shallow borehole cores. Subsurface data is from exploration wells that penetrate the entire Lower Coralline Limestone Formation. Details on biostratigraphy are derived from cored sections shown in Appendix III-29 for Naxxar-2 and Zabbar-1 wells whereas biostratigraphy of the offshore Aqualta well is derived mainly from well cuttings.

3.3 FACIES ASSOCIATIONS

Groups of facies are combined in *facies associations* when they occur next to one another within the same depositional environment. The Lower Coralline Limestone Formation is sub-divided into seven depositional facies associations (FA) on the basis of constituent carbonate grains (see Table 3-1). The facies associations are enumerated by successive Roman numerals I to VII which reflect the transition from deep (below storm wave base) through shallow marine to subaerial depositional environments that reflects the numeration of facies zones along a carbonate platform of Wilson (1975) (see Table 3-15). Each facies association comprises a number of facies enumerated by the FA number followed by the lowercase letter representing the facies, whereas sub-facies carry the hyphenated suffix i or ii, e.g., facies IIIa-i. The facies characteristics are summarised in Table 3-2.

Overall stratigraphy and relative thicknesses of the lithofacies associations in outcrop and subsurface are shown in
Table 3-3. The upper *circa* 120 m of pure carbonates is dominated by coarse-grained bioclastic coralline algae and large benthic foraminiferans (FA II and III) with few thin horizons of slightly argillaceous limestone (FA VI) whereas the lowermost outcrops and the underlying 130 to 300 m of subsurface sediments are mostly fine-grained and consist of miliolids in a micritic matrix (FA V) and marls. Some of these limestones were altered to dolomite.

Carbonate plat. setting	*skeletal assemblage*	*Facies Association*	*Facies*	*Main biota*	*Palaeo -depth*
	subaerial	**VII**	gypsum		+ 0
	subaerial	**VI** Red argillaceous carbonates	a. Laminar packstone	*Kuphus,* miliolids	+ 0
	subaerial	**VI** Red argillaceous carbonates	b. Thin bedded to laminar limestone/palaeosol	Miliolids, *Microcodium*	>+2
Restricted plat. interior	chlorozoan	**V** Foraminiferal wackestone/pack-stone limestone	a. Miliolid-algal sand packstone and grainstone	Miliolids, geniculate coralline algae	<10
	chlorozoan	**V** Foraminiferal wackestone/pack-stone limestone	b. Miliolid wackestone and packstone	Miliolids, *Peneroplis*, *Kuphus*,	<5
	chlorozoan	**V** Foraminiferal wackestone/pack-stone limestone	c. Marl-miliolid wackestone	Miliolids, Globigerinids	>20
	chlorozoan	**IV** Coral limestone	a. Coral biostrome rudstone/ framestone	Coral, miliolids, coralline red algal debris	<10
Sand shoal of platform margin	chlorozoan	**IV** Coral limestone	b. Coral Patch Reef /rudstone	Coral, coralline algae	<20
	foramol	**III** Large benthic foraminiferal limestone	a. LBF ferruginous grainstone	LBF, bryozoans	<3
	foramol	**III** Large benthic foraminiferal limestone	b. Cross-bedded LBF packstone and grainstone	LBF, echinoids, bryozoans LBF, coralline algae	5 to 10
	foramol	**III** Large benthic foraminiferal limestone	c. *Lepidocyclina* packstone	LBF	>40
Slope	rhodalgal	**II** Coralline red algal limestone	a. Algal Sand packstone and grainstone	Corallinoidae (geniculate algae) Echinoids,Miliolids, LBF	<20
Slope	rhodalgal	**II** Coralline red algal limestone	b. Rhodolith boundstone	Melobesioideae, Sporolithoideae, echinoids, Rotaliids	20 to 40
Slope	Bryomol	**I** Micrite-echinoid limestone	a. *Scutella* packstone and wackestone	Echinoids, bryozoans	<20
Slope	Bryomol	**I** Micrite-echinoid limestone	b. Phosphorite packstone	Solitary coral, *Pecten*	>30
Open shelf	Bryomol	**I** Micrite-echinoid limestone	c. Echinoid wackestone and mudstone	*Prionocidaris,* bryozoans	>40
Open shelf	Bryomol	GLOBIGERINA LIMESTONE FORMATION			>70

Table 3-2. Facies associations, facies and sub-facies recorded in outcrop. The facies association show a general deepening trend down the table. Estimated depositional depths shown in the column on the right are explained in the text (depth in metres). Colour coding of Facies Associations is applied in Appendix II.

Facies	Dominant grain	Percent of formation	log
FA I	Echinoids, planktonic foram.	4%	FA II
FA III	Large benthic foraminifera	4-6 %	
FA II	Coralline red algae	<47 %	50%
FA IV	Coral	1 %	FA V
FA V	Micrite	>47 %	

Table 3-3. The average relative abundance of the facies associations in the Lower Coralline Limestone Formation based on well data (see Fig. 5.3 on p.151) and outcrops (see Appendix II-4). The facies are listed in the same stacking order as they commonly occur in outcrop. The generalised log shows relative thickness of the facies associations as a percentage of the entire formation thickness.

3.3.1 Facies Association I: Bryozoan-echinoid-bivalve wackestone to mudstone

Three micrite-rich facies (Table 3-4) cap the entire formation and are transitional to the overlying hemipelagic Globigerina Limestone which is characterised by >30% micrite content. The facies are distributed in geographical zones characterised by particular depth and current activity:

FA	Facies	biota	depositional depth (m)
I	a. *Scutella* packstn., wackstn.	Echinoids, bryozoans	<20
	b. Allochthonous phosphorite bed	Solitary coral, *Pecten*	>30
	c. Echinoid wackstn., packstn.	*Prionocidaris* (spines)	>40
	Globigerina Limestone Formation		

Table 3-4. Facies Association I: facies sub-divisions.

a. ***Scutella* packstone to wackestone**: thick accumulations occur in eastern Gozo (locality 2) and western Malta (between localities 9 and 11) along the uppermost Lower Coralline Limestone Formation. The packstone are dominated by the echinoid *Scutella subrotunda* (Challis, 1979) that are

entirely preserved in locality 1 at the base of the overlying Globigerina Limestone, becoming fragmented between localities 4 and 11. The latter locality consists of very coarse-grained bioclastic packstone with oysters attached to hardground surfaces.

b. **Phosphorite packstone**: Phosphorites in Malta form two brown coloured, <1 m thick ubiquitous beds (C_1 and C_2 beds) within the Globigerina Limestone Formation and several other discontinuous beds, e.g., Carbone *et al.* (1987) and Föllmi *et al.* (2008). A less known phosphorite sporadically caps the Lower Coralline Limestone Formation and is named C_0 bed (Gatt, 2005). The <1 m-thick, allochthonous dark-brown phosphorite C_0 bed is recorded at localities 4a and 11 and comprises well-preserved solitary corals, disarticulated *Pecten*, reworked fish and shark teeth. The phosphorite drapes over minor faults (<1 m offset) and fills <1 m-deep neptunian dykes at locality 11. Pteropods that are common in phosphorite beds C_1 and C_2 (Rehfeld & Janssen, 1995) are absent in the C_0 phosphorite bed (Janssen, *pers. comm.*).

c. **Echinoid-bryozoan wackestone**: In eastern Malta (localities 12 to 15) the <5m-thick succession of wackestones and mudstones includes disarticulated plates and <5cm-long spines of the echinoid *Prionocidaris*. The measured orientation of the disarticulated spines generally trends to the SSW and SW (Figure 3.1b). The succeeding wacke- mudstone beds include bryozoan fragments and framestone of *Cellepora* and *Sertella*, terminating with a pavement of disarticulated bivalves of *Pecten* and *Ostrea* that marks the boundary between the Lower Coralline and the succeeding hemipelagic lower member of the Globigerina Limestone Formation.

FA I: Interpretation

The three facies are characterised by the concentration of bioclasts and condensation of sediments. These characteristics reflect the rapid drop in the sedimentation rate over the Malta Platform, amplified by the effect of current activity. The main current direction flowing in the western Tethys during the Oligocene is thought to have been

directed towards the west (Frost, 1981). These current-swept sediments mark the initial drowning of the carbonate platform that was eventually draped with hemipelagic sediments.

The geographical distribution of the facies in FA I reflects the antecedent bathymetry of the drowned carbonate platform. Western Malta is characterised by early cementation, hardgrounds and coarse-grained bioclastic accumulations (facies Ia). The abundant accumulation of scutellid echinoids reflects both their gregarious nature and very high density populations as well as their high diameter/thickness ratio and low density which made these echinoids hydrodynamically mobile (Nebelsick & Kroh, 2002). The concentration of clypeasteroids suggests low amplitude bioclastic shoals in high energy environments within the fair-weather wave base (FWWB) that migrated over a palaeohigh in western Malta.

Current flow along the flanks of the palaeohigh produced local upwelling that resulted in the precipitation of phosphorite (facies Ib) within the oxygen minimum zone. The westerly current then transported the phosphorite from deeper areas found further east where solitary corals and bryomol faunal elements (bryozoans and echinoids) of facies Ic thrived. The entirely non-photic biota of facies Ic and the predominantly micritic sediments suggests environments below the storm wave base where lime mud accumulated. Unlike the other two facies, bioclasts were not directly affected by surface flow but were prone to weak currents that rearranged autochthonous accumulations. The preferential orientation of *Prionocidaris* spines below storm wave base suggests current flow that was parallel to the contours of the outer platform. This may implicate a geostrophic current produced by the west to east pressure gradient as a result of pressure buildup by the mainly westerly directed surface currents along the shallower parts of the platform, balanced by the Coriolis force acting in the opposite direction. The combination of these two forces resulted in a current flow that oriented the spines in a SSW direction (Figure 3.2).

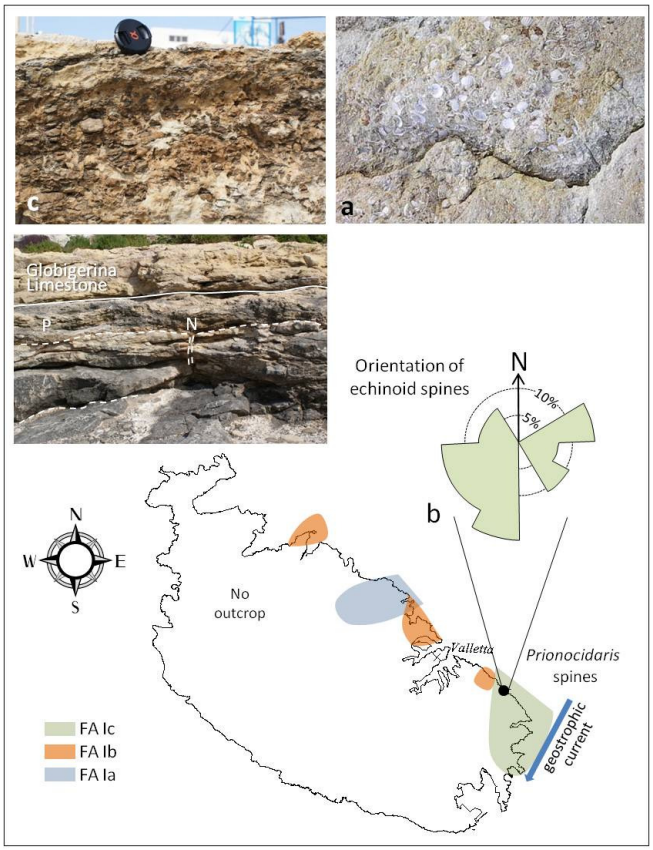

Figure 3.1. FA I: Map showing geographical distribution facies. (a) Pectinid pavement at locality 12; (b) Rose diagram showing SSW preferential orientation of disarticulated echinoid spines of facies Ic in locality 12; (c) Locality 11: hardgrounds (white dashed line) and phosphorite bed C_0 comprising phosphatised solitary coral, *Pecten* and bivalves, underlying the Globigerina Limestone Formation. Phosphorite (P) fills a small neptunian dyke (N) that cuts the hardground surface.

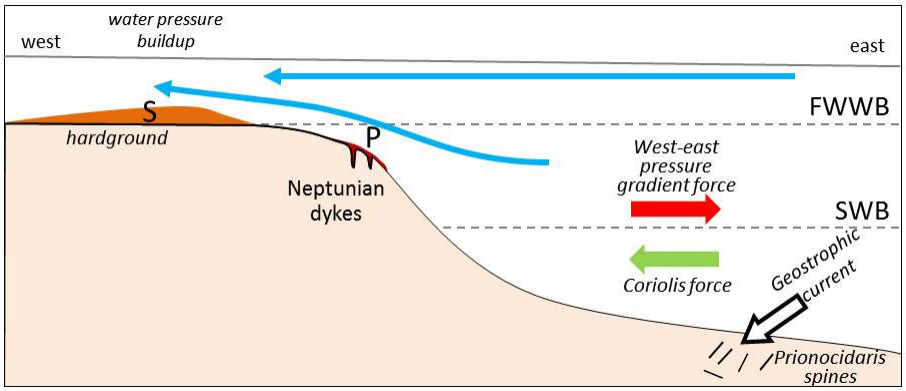

Figure 3.2. Depositional model for FA I: westerly sea currents (blue arrows) produced a pressure buildup on palaeohigh in west Malta (locality 3) and Gozo where hardgrounds and facies Ia accumulated (S, *Scutella* echinoids); facies Ib developed along the slope areas (P, Phosphorite) affected by tectonic extension, whereas facies Ic accumulated in the deeper part of the platform. The geostrophic current is perpendicular to the page and preferentially oriented the disarticulated echinoid spines in facies Ic.

3.3.2 Facies Association II: Coralline Red Algal Limestone

Coralline red algal facies make up >50% of the thickness of most of the studied outcrops and form massive beds exposed along the southern cliffed coast of Malta where this facies association thickens to >50 m between localities B and D but thins to <35 m at locality A. Although coralline red algae (CRA) can occupy a wide range of habitats from intertidal pools to deep sea (Steneck, 1986), their taxonomy and growth form throw light on depositional environment. Coralline red algal families and subfamilies are recognised in thin section by certain characteristics described by Aguirre *et al.* (2000) (see Appendix III-24):

- Sporolithaceae: crustose corallines that can have a lumpy growth form that is susceptible to breakage. This family is identified by sporangial chambers that are grouped in sori.
- Melobesioideae: may show fructose growth form liable to breakage. Genera have multipore sporangial conceptacles.
- Lithophylloideae and Mastophoroideaea: difficult to distinguish and are grouped together on the basis of uniporate sporangial conceptacles
- Corallinoideae: geniculate corallines are composed of calcified segments (intergenicula) connected by non-calcified genicula which decay on death, resulting in the disarticulation of segments (see Appendix III-22).

Corallines can occur in a broad range of water depth from intertidal to 250 m (Wray, 1977) and can withstand abrasion in turbulent conditions because each cell wall is calcified. The Order Corallines appears in the early Cretaceous and occupied different environments throughout the Cenozoic cooling (Aguirre *et al.*, 2000). The diversity of coralline families and subfamilies has changed through time: the number of Sporolithaceans species decreased through the Phanerozoic whereas the Corallinaceae (Melobesoideae, Lithophylloideae and Mastophoroideae) have increased especially through the Cenozoic. Sporolithaceans prefer warm, deep tropical environments and their decrease reflects Cenozoic global cooling (Aguirre *et al.*, 2000).

Several authors have identified coralline algal taxa in Maltese Oligocene outcrops, e.g., Bennett (1980) and Brandano *et al.* (2009). On the basis of thin sections in this study and published works, twelve genera of corallines have been identified in FA II shown in Table 3- 5.

Order	Family	subfamily	Genera
Corallinales Silva & Johansen 1986	Sporolithaceae Verheij 1993	Sporolithoideae	*Sporolithon* Heydrich 1897 *(formerly Archaeolithothamnion)*
	Hapalidiaceae Gray 1864	Melobesioideae Bizzozero 1885	*Mesophyllum* M. Lemoine 1928 *Phymatolithon* Foslie 1898 *Melobesia* *Lithothamnion*
	Corallinaceae Lamouroux 1812	Corallinoideae Foslie 1908	*Corallina* *Jania*
		Lithophylloideae Setchell 1943	*Lithophyllum* *Lithoporella* *Lithothamnium*
		Mastophoroideae Setchell 1943	*Spongites* *Neogoniolithon*
Peyssonneliales	Peyssonneliaceae		*Polystrata* Heydrich 1905

Table 3- 5. Coralline algae recorded in the Lower Coralline Limestone Formation (see Appendix III-23 and 24).

FA II: facies description

Although their taxonomy is not based on morphology, coralline facies can be broadly sub-divided on the basis of the two predominant growth forms seen in outcrop (Table 3-6): geniculate corallines and crustose corallines that can be branched, segmented or thin and leafy (Steneck, 1986). These forms can be identified in the field and used for facies analysis. Crustose corallines can coat grains to produce rhodoliths that are unattached nodules with morphologies described by Bosence (1983). Nebelsick & Bassi (2000) recognise five classes of coralline morphology based on both growth form and taphonomy (see Appendix III-22):

1. Bioerosion: endolithic borings in coralline algae caused by herbivory that can occur on relatively stationary or fixed coralline growths.
2. Encrustation: crustose forms that coat surfaces or grains to form rhodoliths.

3. Disarticulation: the post-mortem disarticulation of segments of geniculate coralline algae as a result of the decay of non-calcified genicula connecting segments.
4. Fragmentation: the breakage of protuberances, fructose fragments and thallial segments of crust.
5. Abrasion: the rounding of coralline fragments as a result of significant transport.

FA	Facies	Sub-facies	biota	Water depth (m)
II	a. algal sand pack. & grainstone	i. algal debris packstone	Corallinoidae (geniculate algae) miliolids	<-20
		ii. algal debris grainstone		
	b. rhodolith boundstone	i. rhodolith floatstone	Melobesioideae Sporolithoideae Echinoids Rotaliids	20 -40
		ii. rhodolith rudstone		

Table 3-6. Facies association II: facies sub-divisions.

a. Algal sand packstone & grainstone (FA IIa)

Medium to coarse-grained algal debris of geniculate Corallinoideae with accessory grains of echinoid debris, molluscs, gastropods and the foraminiferan *Austrotrillina* sp., *Peneroplis* sp., *Spirolina* sp., *Amphistegina* and more rarely *Lepidocyclina* and *Miogypsinoides complanatus.* The lithology generally has a pale yellow colour and is sub-divided on the basis of carbonate texture (Figure 3. 3):

i. Algal debris packstone: consist of coralline algae (*circa* 50% of bulk rock) comprising well-preserved geniculate coralline algae and fragmented crustose coralline algae. Accessory grains include micrite (average 9%), echinoids (9%) and foraminiferans (20%) which vary in abundance: the triloculine imperforate *Austrotrillina* in locality 5 to the large benthic foraminiferan *Amphistegina* in locality 6.

ii. Algal debris grainstone: same constituent grains as facies IIa-i but show less well-preserved geniculate algae and lack micrite. Sediments are well-bedded and

may show cross-bedding, e.g., at locality 5, 1 metre-thick sporadic lenses of cross-bedded algal and foraminiferal debris and *circa* 10 m of low-angle cross-beds along the southern cliffed coast of Malta at locality B (see Appendix V-30). The grains consist of well-sorted and sub-rounded geniculate and crustose coralline algae. In some cases, the internal structure of the grains is poorly preserved because of intense micritisation by boring endolithic algae. Associated with this facies are ellipsoidal rhodoliths and the large gastropod *Stombus costatus* that forms dense >1m-thick accumulations at locality 13.

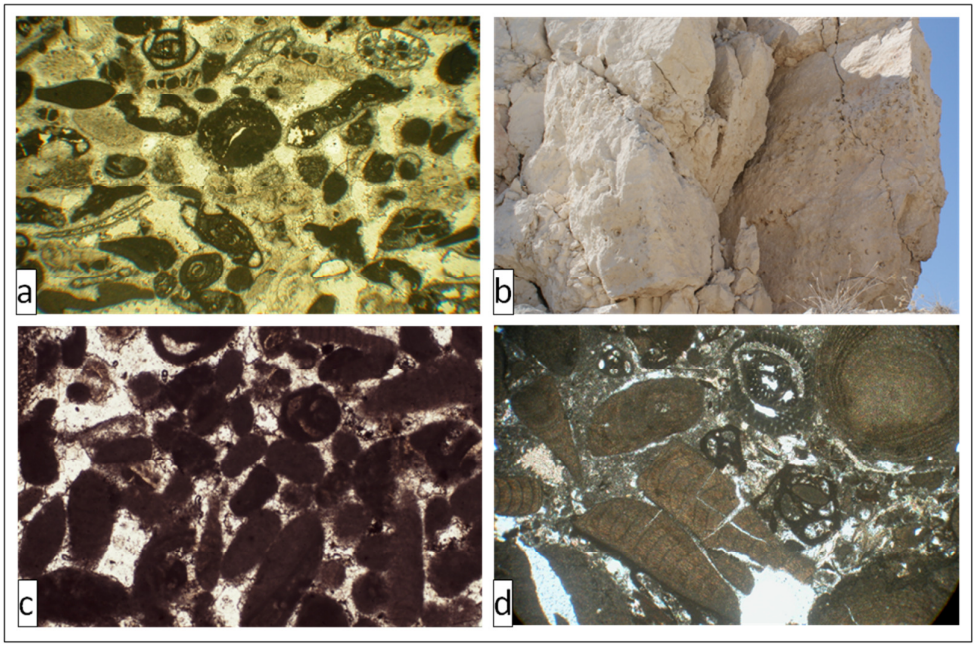

Figure 3. 3. FA IIa: algal debris-foraminiferal grainstone (FA IIa-ii) at locality 5 showing equant calcite cement; (b) Locality 13: 1 m-thick bed rich in moulds of *Strombus costatus* gastropods (diameter 10 cm) within facies IIa packstone/grainstone; (c) intensely micritised algal debris cemented by blocky equant calcite cement; (d) locality 5: geniculate algae associated with rounded crustose algae, miliolids and echinoid fragments (FA IIa-i).

b. Rhodolith boundstone (FA IIb)

The non-geniculate (crustose) coralline algal facies form a bright white, thickly bedded rhodalgal biostrome that outcrops in most of the studied localities and reaches *circa* 50 m in thickness along the cliffed southern coast of Malta (localities B to D), thinning to <25 m between and in localities 3 and A (Figure 3.4). The bulk of the sediments consist of crustose coralline families/subfamilies Sporolithaceae, Mesobesoideae and Mastophoroideae (see Appendix III-24). The crustose forms

produced free-living rhodoliths that coat grains, laminar crusts on hard substrate and rarely branching frameworks. Coralline algae have calcified cell walls that can withstand abrasion over unstable substrate, consequently rhodolith morphology is an indicator of the level of hydrodynamic energy (Bosence, 1983). Accessory bioclastic material forms the coarse matrix in which rhodoliths are preserved. The matrix in facies IIb includes echinoid clasts (>5%) whereas low diversity large benthic foraminiferan genera (*Amphistegina* and *Operculina*) constitute <10% of the rock. In the topmost rhodolithic biostrome, *Operculina* becomes abundant (Figure 3.4). The rhodolith biostrome comprises two lithofacies:

i. *Rhodolith floatstone*: The most widespread and voluminous facies in the rhodalgal biostrome forms thick to very thick, massive beds. Rhodoliths comprise <20% of the rock and consist mostly of laminar ellipsoidal forms with a diameter of *circa* 2 to 5 cm in a coarse-grained matrix of coralline red algal debris, echinoid clasts, foraminiferans and micrite. Variations to this include rhodolith size of up to 9 cm diameter in locality 6 and columnar rhodoliths in the lower part of locality 14.

ii. *Rhodolith-supported rudstone*: well-sorted spheroidal, densely packed laminar rhodoliths with a diameter of <2 cm to *circa* 5 cm that constitute *circa* 50% of the rock, the rest being a packstone matrix of coarse-grained highly fragmented coarse algal debris including geniculate red algae, *Amphistegina*, *Borelis* and echinoid bioclasts (Figure 3.5). The rudstone forms <2 m thick pavements bounded at the top by a planar truncation surface or deep scours. A rhodolith rudstone pavement marks the base of the rhodalgal biostrome at localities 5 and 14 and is ubiquitous along its top boundary (localities 3, 9, 10b and 12) where LBF increase significantly (<50%). Rhodolith rudstone pavements are also interbedded within rhodolith floatstone beds in the rhodalgal biostrome at locality 3 and 6 whereas below the rhodalgal biostrome they interfinger with beds of coral or geniculate algal sands at locality 5.

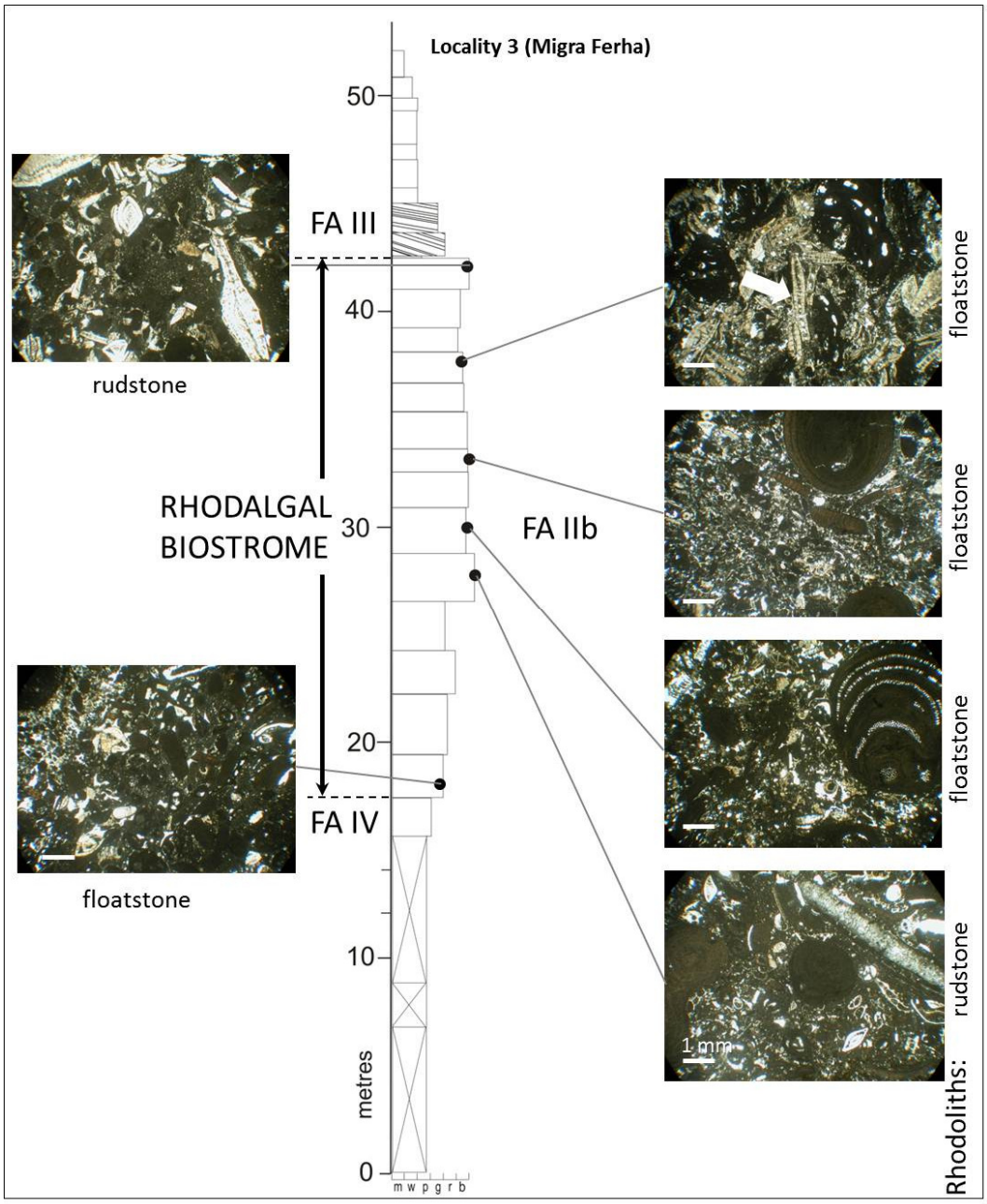

Figure 3.4. FA II at locality 3: the rhodalgal biostrome is bounded at the top by a rhodolith rudstone pavement. Photomicrographs show texture and grains of microfacies at different levels (horizontal scale bar = 1 mm). Each photomicrograph is labelled according to facies texture seen in the field. White arrow indicates *Operculina*.

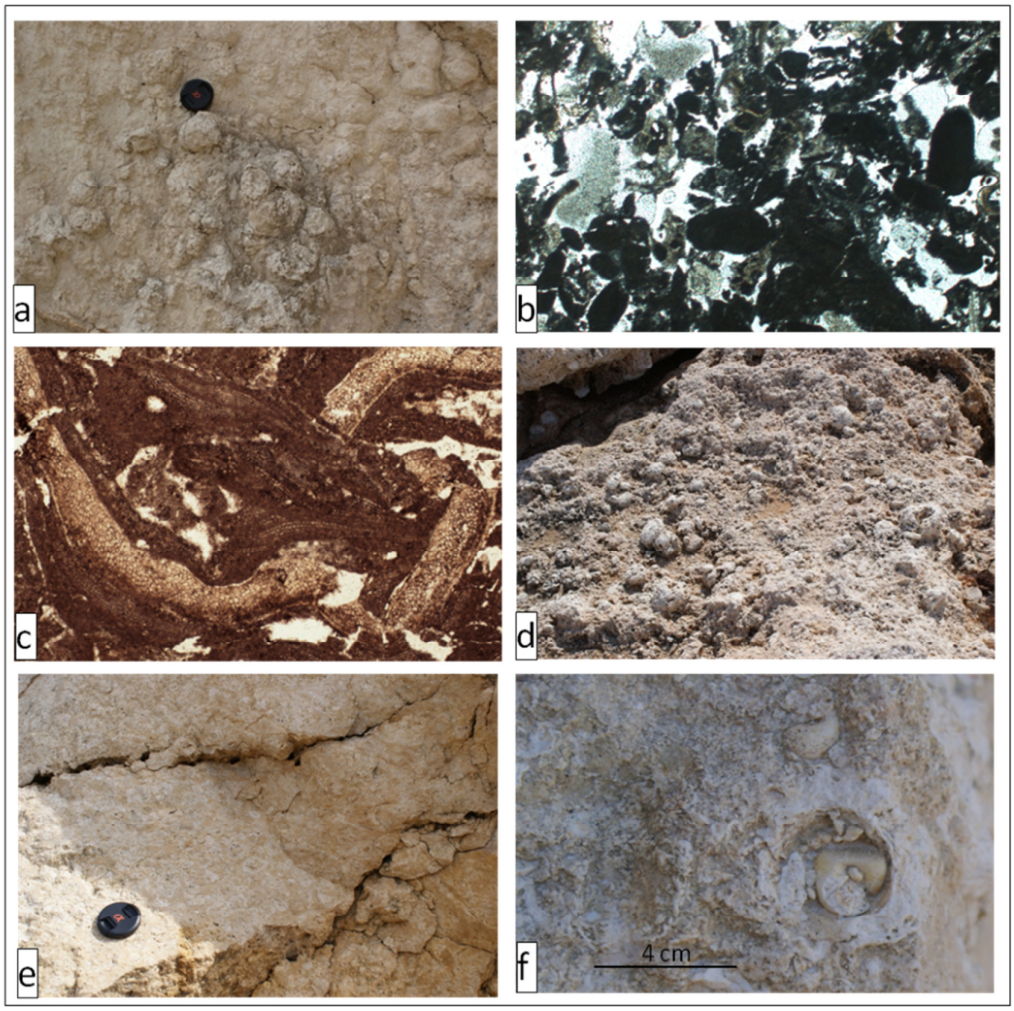

Figure 3.5. FA IIb: (a) Locality 6: rhodolith rudstone pavement interbedded with rhodolith floatstone beds. The size of the well-rounded rhodoliths is >5 cm diameter; (b) Photomicrograph of matrix of same bed shows rounded crustose algal debris and echinoid clasts showing syntaxial cement; (c) photomicrograph of cross section through rhodolith in locality 14 showing damaged crustose coralline algae; (d) Rhodolith rudstone pavement along topmost rhodalgal biostrome at locality 9 showing 3 to 5 cm wide rhodoliths exposed by differential erosion, within a very coarse-grained matrix; (e) rhodolith rudstone bed at locality 3. Rhodoliths are typically <2 cm wide, well-rounded and well-sorted; (f) cross-section of crustose rhodolith coating a gastropod (mould) in locality 8.

FA II: Interpretation

The estimated palaeodepths and palaeoenvironments of the facies that make up FA II show significant variations.

Facies IIa (Algal sand packstone & grainstone): Geniculate coralline algae are known to be abundant in high wave energy habitats of 10 m depth and usually extend over a range from the intertidal zone to a depth of 20 m (Wray, 1977). The intense micrization of algal grains along some beds points to euphotic conditions associated with shallow marine environments (<3 m deep). The algal sand is interpreted to have formed stable to mobile sand sheets deposited in the exposed part of the inner platform at depths of <20 m.

In less agitated areas, the stable sand sheet may have supported sea-grass and algal mats grazed upon by the large gastropod *Strombus costatus* in environments similar to modern shallow marine sea-grass meadows in the Bahamas (Bathurst, 1975) whereas the algal grainstone comprising rounded and well-sorted geniculate coralline algae is interpreted to have been deposited in a higher energy environment where micrite was winnowed. Brandano *et al.* (2009) studied an area located about 1 km west of locality 5 which shows sediments that correspond to facies IIa, interbedded with coral and rhodolith beds and suggested a depositional depth of 7 to 14 m based on test shape of *Amphistegina*.

Facies IIb (Rhodolith boundstone): The free-living rhodoliths were produced in response to unstable substrate where the mud fraction had been partly winnowed. The rhodolith floatstone was produced where current flow was sufficiently strong to occasionally overturn the rhodoliths. In cases of infrequent overturning in deeper water and baffling by sea grass in shallow water rhodoliths developed ellipsoidal shape and columnar forms seen in locality 14. The bulk of the rhodolith floatstone facies is found in the in the extensive and thick rhodalgal biostrome where sediments resemble those of other Cenozoic rhodolith rudstone or floatstone which are associated with marine transgressive events (Nalin *et al.*, 2008). Sea-level change affected the abundance of coralline algal species in locality 3: during falling sea-level the Melobesioidae became more common whereas highstand of sea-level favoured the slow growing Sporolithacean species that prefer warm water and are presently found in deeper water in modern tropical environments (Aguirre *et al.*, 2000).

The decline or absence of geniculate algae in the rhodalgal biostrome (facies IIb-i) suggests relatively deeper (>20 m) water than that of the depositional environment of facies IIa. The large benthic foraminiferans in the rhodolith floatstone facies include thin, plate-like *Operculina complanata* which is associated with the lower part of the photic zone in Oligocene sediments (Bassi *et al.*, 2007) and is presently found in tropical environments at 30 to 50 m depth in the Solomon Islands (Hughes, 1977). The other common LBF is *Amphistegina* that is known to live in a wide range of photic environments although dependent on algal-symbiosis. In deeper water, *Amphistegina* may have survived on food as an additional source of energy as recorded in modern examples (Hohenegger *et al.*, 1999). On the basis of large benthic foraminiferal species and the decline of geniculate algae, the rhodolith floatstone in the rhodalgal biostrome is interpreted to have been deposited within a range of 20 m to 40 m water depth.

The depositional depth of FA IIb would correspond to the mid-platform environment between the FWWB and the SWB. However, the spherical shape of rhodoliths seen in facies IIb-i point to the deeper limit being above the storm wave base (SWB) where there is some winnowing of fine. Although rhodoliths can tolerate a wide range of light they are susceptible to burial by fine sediments (Wilson *et al.*, 2004) so that depths below the storm wave base are disadvantageous to slow growing rhodoliths. This is reflected by the absence or scarcity of rhodoliths when the percentage of micrite in whole rock exceeds 40% in the Lower Coralline Limestone (Figure 3.6).

The compact laminar structure of rhodoliths in the rhodolith-supported rudstone (FA IIb-ii) suggests frequent overturning. The morphology and texture reflect higher hydrodynamic energy level (Bosence, 1983) relative to the rhodolith floatstone facies and resulted in more winnowing of lime mud. Moderately turbulent conditions are represented by the smaller sized rhodoliths that result from frequent breakage of rhodoliths with a diameter larger than 2 cm that resulted in the well-sorted rudstone. Bassi & Nebelsick (2010) describe Oligocene rhodolith pavements in northeast Italy from below the FWWB, where rhodoliths are larger and less sorted than those seen in Maltese outcrops. The depositional environment of the rhodolith rudstone is

interpreted to be close to the FWWB (<20 m) because of the rudstone is well sorted and includes geniculate algae. This facies covered large parts of the exposed inner platform and extended to the mid-platform environment dominated by rhodolith floatstone whenever sea-level dropped and hydrodynamic energy levels increased.

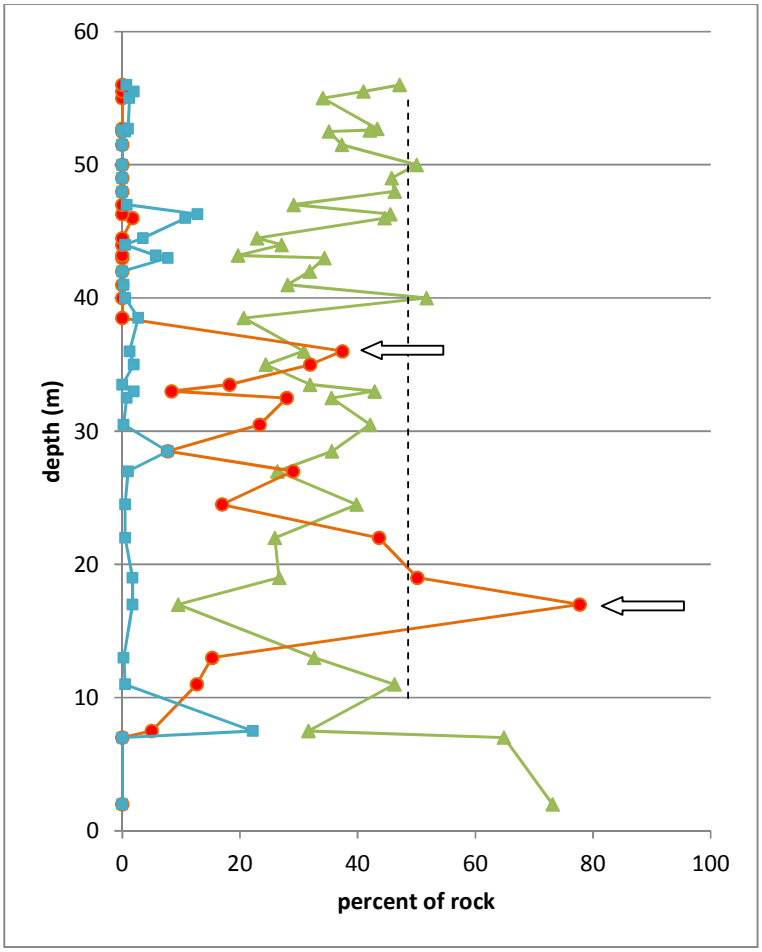

Figure 3.6. Percent contents of rhodoliths, LBF and micrite as percent of whole rock at locality 1 (raw data from Knoerich & Mutti (2003). The dashed line at 40% shows the approximate minimum level of micrite below which rhodoliths become abundant. Peak occurrence of rhodoliths (●) marked by open arrows is inversely related to micrite content (▲) in the rock. The abundance of LBF (■) is inversely related to both rhodoliths and micrite content.

3.3.3 Facies Association III: Large benthic foraminiferal limestone

Large benthic foraminiferans (LBF) are present throughout most outcrops of Lower Coralline Limestone Formation in the Maltese Islands but become highly concentrated and abundant in the top part of the formation, immediately above the rhodalgal biostrome. Facies association III comprises a number of facies dominated by LBF although it is not ubiquitous and varies considerably in thickness and texture from west to east. Over east Malta, FA III thickens to *circa* 30 m but thins to <3 m both westward and eastward where only 2 to 3 beds are preserved. The facies is missing or removed by erosion at localities 5, 7, 8 13, 14 and 15.

The LBF facies consist mainly of perforated large benthic foraminiferans of the Order Rotaliina (Table 3-7) with a volume that commonly exceeds 3 mm^3 and may include rare miliolines. The LBF can reach these large sizes as a result of symbiotic associations with unicellular algae, rhodophyte, diatom or dinoflagellate, e.g., in *Amphistegina* the symbionts are diatoms that live in blue light at depths of 0-130 m (BouDagher-Fadel, 2008). The symbionts hosted in chamberlets use light to provide the foraminiferans with nourishment in water which is poor in nutrients (Hallock & Glenn, 1986). It has been suggested that the wavelength of light required by specific symbionts is related to the depth of habitat of foraminiferans (BouDagher-Fadel, 2008).

More flattened tests result in greater surface area affected by light which permits a wider depth range close to the limits of endosymbionts (Hallock & Glenn, 1986). The increase in the diameter/thickness (D/T) ratio of the test is indicative of the change in test shape with increasing depth (Hallock & Glenn, 1986; Beavington-Penney *et al.*, 2005) in clear water. However, the size of LBF is also related to its life cycle which includes both sexual and asexual reproduction that produces smaller A-forms and larger B-forms, respectively, e.g., the asexually-produced (smaller) megalospheric A-forms arise when environmental conditions are optimal for growth and rapid multiplication in order to fill a favourable niche (Racey, 2001).

Suborder	Superfamily	Genera	
Rotaliina	Nummulitoidea	*Grzybowskia* Bieda 1950	
		Heterostegina D'Orbigny 1826	
		Spiroclypeus Douvillé 1905	
		Operculina D'Orbigny 1826	
	Asterigerinoidea	*Amphistegina* d'Orbigny 1826	
		Eulepidina Douvillé 1905	
		Lepidocyclina	*Lepidocyclina* Gümbel 1870
			Nephrolepidina Douvillé 1911
	Rotalioidea	*Miogypsinoides* Yabe & Hanzawa 1928	

Table 3-7. The LBF identified in thin sections of FA III belong to only suborder Rotaliina, although throughout Palaeogene sediments, three suborders of LBF persisted from the Mesozoic: Textulariina, Miliolina and Rotaliina (see Appendix III-25).

FA III: Taphonomy

The LBF show a number of taphonomic and physiological characteristics that are diagnostic of depositional environment (Figure 3.7):

a. Degree of sorting: Taphonomic processes have an effect on the bimodal sizes resulting from different reproductive strategies of LBF that produce A-forms and B-forms. Aigner (1985) identifies four common biofabrics that reflect increasing levels of hydrodynamic energy levels. In lower energy environments there is a mix of larger and smaller LBF, whereas in higher energy environments the accumulation may consist entirely of B-forms after the selective removal of smaller A-forms, resulting in a residual lag.
b. Degree of fragmentation: Large benthic foraminiferans (e.g., Nummulitids) are extremely resistant to abrasion so that fragmentation is the result of long transport times and reworking. The Beavington-Penney Taphonomic Scale (BPTS in Figure 3.7) (Beavington-Penney, 2004) categorizes the scale of damage resulting from transportation of the LBF as following; intact test (level 0) indicates an *in situ* test, whereas highly fragmented tests (level 3) are the result of significant transportation over several kilometres.

FA III description

Three facies are identified on the basis of significant variations in micrite content, LBF size and sedimentary structures shown in Table 3-8. The three facies have particular geographical distribution shown in Figure 3.8.

FA	Facies	Sub-facies	biota	BPTS	depth (m)
III	a. ferruginous LBF grainstone	i. iron-rich LBF packstones	LBF, bryozoans	3	<3
		ii. micrite-rich LBF packstones		2	
	b. Cross-bedded LBF pack./grainstone	i. LBF packstone/wackestone	LBF, echinoids, bryozoans	2	5 to 10
		ii. LBF packstone to grainstone		2	
		iii.LBF grainstone	LBF, CRA	2-3	
	c. *Lepidocyclina* packstone	i. Large *Lepidocyclina* packstone	LBF	0-1	>40
		ii. foraminiferal wackestone		0	

Table 3-8. Facies association III: facies sub-divisions.

a. Ferruginous LBF grainstone (FA IIIa)

This facies is restricted to western Malta (Figure 3.8) where its present base outcrops at about 45 m asl at locality 3 and 1 m asl at locality 4b. In locality 3, four distinct beds are recorded above the basal contact with the terminal rhodolith rudstone bed of FA II. The facies consists of two sub-facies:

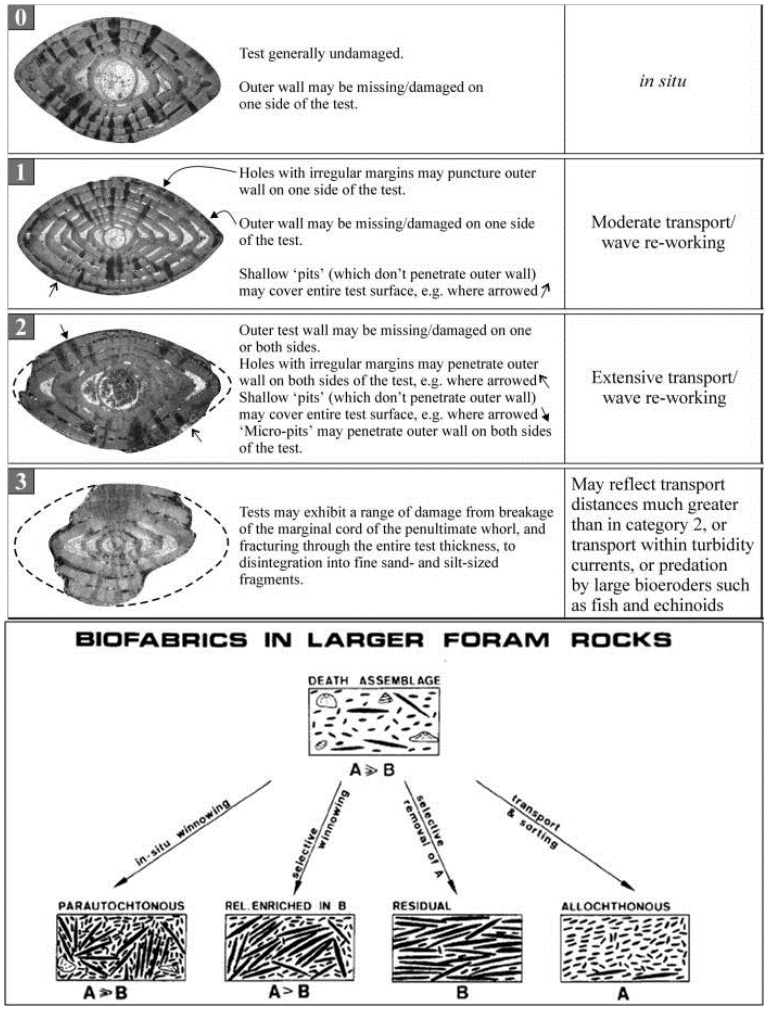

Figure 3.7. Top diagram reproduced from Beavington-Penney (2004) and shows the level of fragmentation of LBF (BPTS 0 to 3) as a result of transportation. Damage can also be inflicted by bioeroders; Bottom diagram reproduced from Aigner (1985) showing taphonomic changes to LBF assemblage with increasing current flow and the effect on the occurrence of A-form or B-form LBF.

i. Iron-rich facies comprising two beds of highly fragmented LBF packstones: Bed 1 is orange-brown and is <5 cm-thick (Figure 3.9-ii). It directly overlies the bright white rhodolith rudstone bed. In thin section the LBF genera are diverse and highly fragmented (BPTS = 3) and have most of their outer test wall missing, although rimmed by fibrous spar cement with some pore space filled by an orange-coloured fine-grained matrix. A bored flat hardground separates this bed from the succeeding <2 m-thick Bed 2 showing low angle cross-beds of packstone/grainstone (>90% LBF). The intragranular spaces of the fragmented

tests of *Lepidocyclina*, *Operculina* and *Spiroclypeus* are partly filled with glauconite. The hardground extends to locality 4b which is overlain by a bed of highly fragmented LBF that correlates to Bed 2 in locality 3.

ii. Micrite to clay-rich LBF packstones: The succeeding Bed 3 shows faintly cross-bedded 1 m-thick bed of *Operculina* and *Lepidocyclina*. The topmost Bed 4 consists of two facies: *Bed 4a;* An olive green basal bed that forms a <6 m-wide lens. Texture is fine-grained and includes *Operculina*. The bed has a friable nature and overlies the second hardground. A bed with *Operculina* is also recorded in locality 4b; *Bed 4b;* A coarse-grained LBF packstone of fragmented LBF. The top part of the bed is bored suggesting that a third hardground terminates this bed.

b. Large cross-bedded LBF packstone/grainstone (FA IIIb)*:*

Large cross-bedding is exposed along the coast of eastern Malta (localities 10b, G and 12) where the base of the facies <3 m above present sea-level (asl) and along the western cliffed of Gozo about 45 m asl. The maximum thickness of this facies is 30 m along the southern cliffed coast of Malta at locality G and thins northwards to <5m at locality 12, thinning farther to <3 m west of locality D. The entire facies is exposed at locality 10b (Figure 3.10) where it consists of:

i. Top section (<10 m thick) of low angle cross-bedding characterised by an increase in micrite content to (>50% of rock volume) and echinoids. LBF are less abundant and the abraded forms suggest transportation.

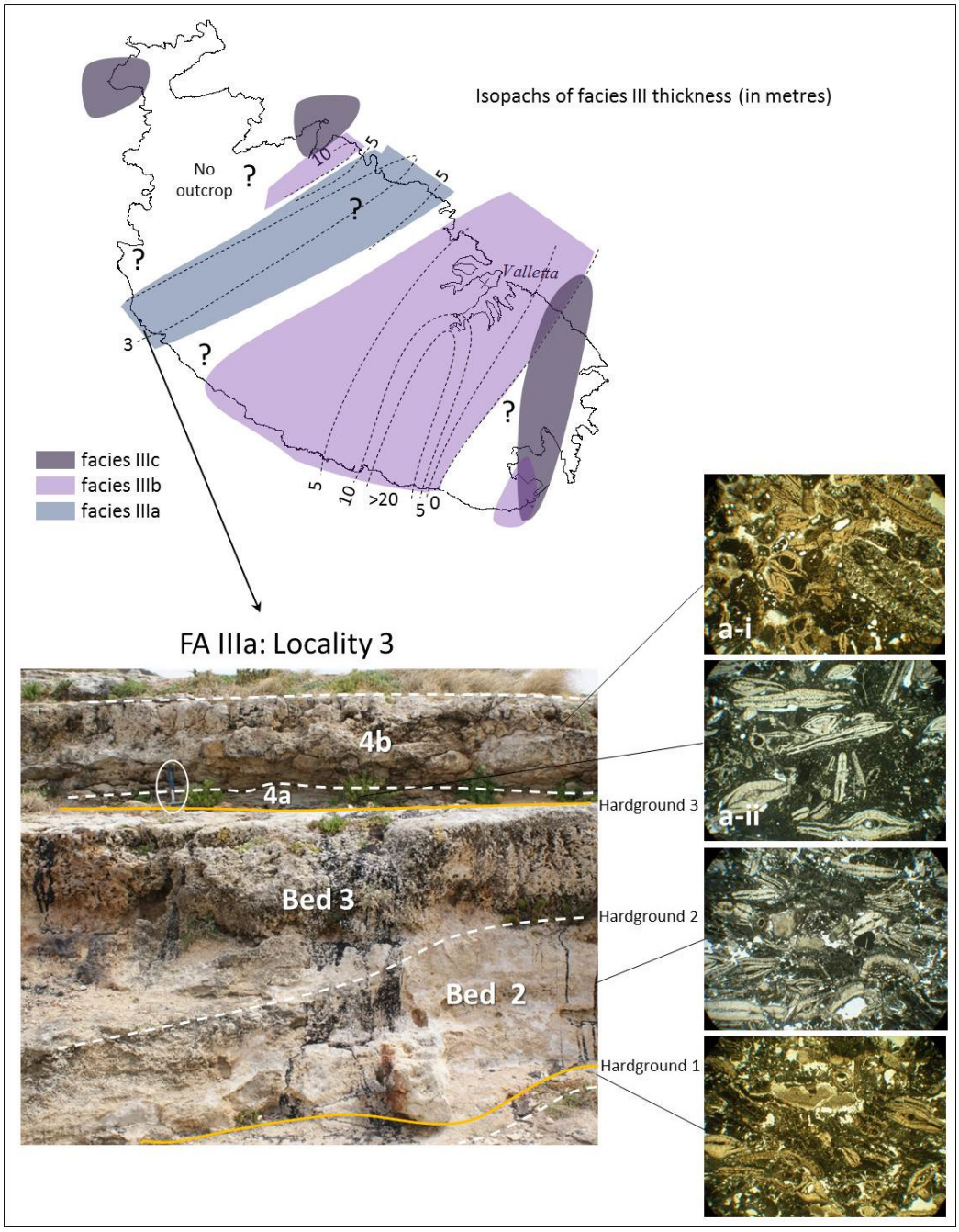

Figure 3.8. FA III: *top:* facies map; *bottom*: Photograph of topmost locality 3 showing the four beds of FA IIIa described in text (hammer in circle for scale). Photomicrographs of the four main beds show highly fragmented LBF. The black streaks are seeping hydrocarbon from bed 4a, although its source is unknown.

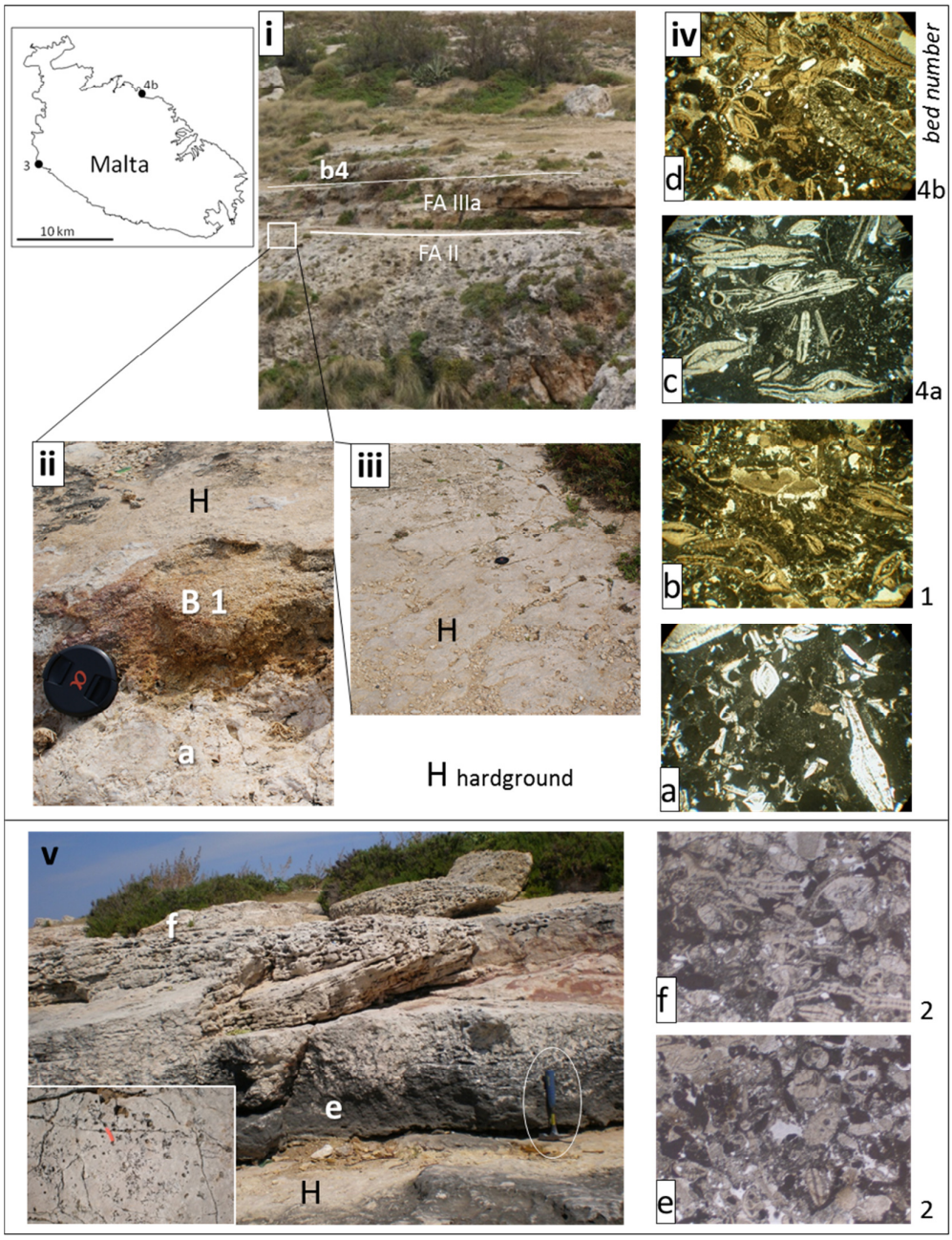

Figure 3.9. Facies IIIa: **Locality 3**: (i) overview of the beds; (ii) Photo of succession from rhodolith pavement (topmost bed of rhodalgal biostrome) through Bed 1, marked B1, showing distinct orange-brown colour capped by the first hardground surface H (*camera cap 5 cm for scale*); (iii) Surface of H showing <1 cm wide borings; (iv) a. Photomicrograph of rhodolith rudstone pavement showing coralline algae and LBF; b. Photomicrograph of Bed 1 showing highly fragmented LBF; c. Photomicrograph of Bed 4a olive green lensoid body showing *Operculina* and *Amphistegina* in a fine-grained matrix; d. Photomicrograph of Bed 4b showing fragmented LBF and bryozoans. **Locality 4b**: (v) Photo of cross-bedded sediments over hardground (H) shown in plan view right bottom inset (*hammer for scale*). Photomicrographs: e. lowermost bed showing highly fragmented LBF; f. top bed showing an increase in *Operculina* and less fragmentation (equivalent to c in locality 3).

ii. Middle section (<20 m thick) exposed at the cliffed locality G comprises up to ten <3 m thick sets of trough cross-bedding that can be correlated to the coarse to very coarse-grained (1000 to 1500 μm) LBF and coralline algal debris grainstone to packstone at the accessible locality 10b. The subcritical angular foresets are mostly inclined at 5˚ to 22˚ towards the west with some beds showing oppositely dipping foresets. Set boundaries are erosional and generally truncate the top part of the foresets. Cross-bedding along one bed shows foresets with dark-coloured muddy drapes that suggest deposition during slack water when tidal current reversed, whereas the overlying <2 m bed shows forests dipping in the opposite direction. The contrary orientation of foresets could be the result of tidal current reversal or it may have been produced by bioclastic dunes migrating in different directions. The fragmented LBF that make up this facies have an isopachous calcite rim reflecting a marine depositional environment.

iii. Basal <1 m thick bed of LBF grainstone showing planar cross-bedding that drapes over 10 m-wide scooped shaped erosional surface disconformably cut into the underlying rhodolithic sediments. The sediments include very rounded coralline red algal debris, possibly reworked from the underlying FA II that become increasingly enriched in LBF including *Amphistegina, Lepidocyclina* and *Borelis,* as well as geniculate coralline algae farther up.

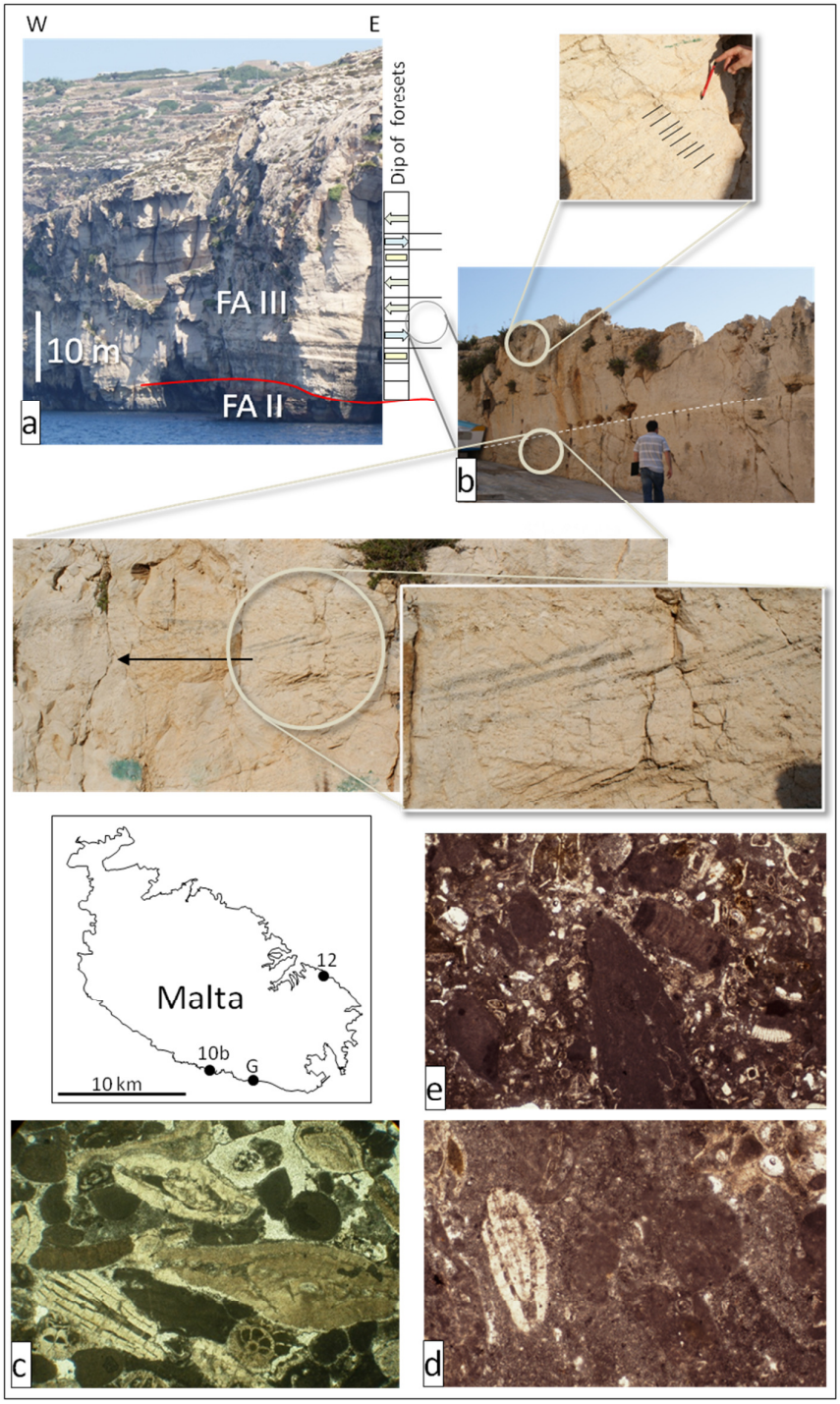

Figure 3.10. Facies IIIb at locality G: (a) cliffed coast showing 30 m of large cross-bedding. Cosets show foresets dipping westwards and a few dipping eastward; (b) Facies IIIb at locality 10b: Large cross-bedded coarse-grained LBF grainstone. Insets; (top) regular succession of thin and thick beds. (bottom) some foresets are muddy (dark colour) and may reflect tidal controls*; Photomicrographs*: (c) Fragmented LBF and coralline algae (crustose and geniculate); (d) Upper part of facies IIIb showing fragmented LBF in a micritic matrix; (e) topmost of facies IIIb showing algal grains in a matrix of highly fragmented bioclasts with planktonic foraminiferans. Map shows locations where facies IIIb is recorded.

c. Lepidocyclina *limestone*

This facies is found at localities 12 (where it overlies facies IIIb) and 15, locality 4a and is recorded in cores east of locality 14. The facies consists of <2 m thick beds of wackestones that alternate with thick beds of Lepidocyclinids packstones. The latter beds are characterised by sorted dense accumulations of *Lepidocylcina* sized 50 mm to 90 mm diameter that show sub-horizontal to edgewise imbrication in a micritic matrix (Figure 3.11 a,b). The diameter/thickness (D/T) ratio is mostly >8 whereas the less common *Amphistegina* has a diameter of <2 mm. In the western locality 4 the facies forms the terminal bed of the Lower Coralline Limestone outcropping just above sea-level and consists of accumulations of large *Lepidocyclina* showing some imbrication. A hardgound overlain by a pectenid pavement and a thin phosphorite bed caps the top of these LBF packstones.

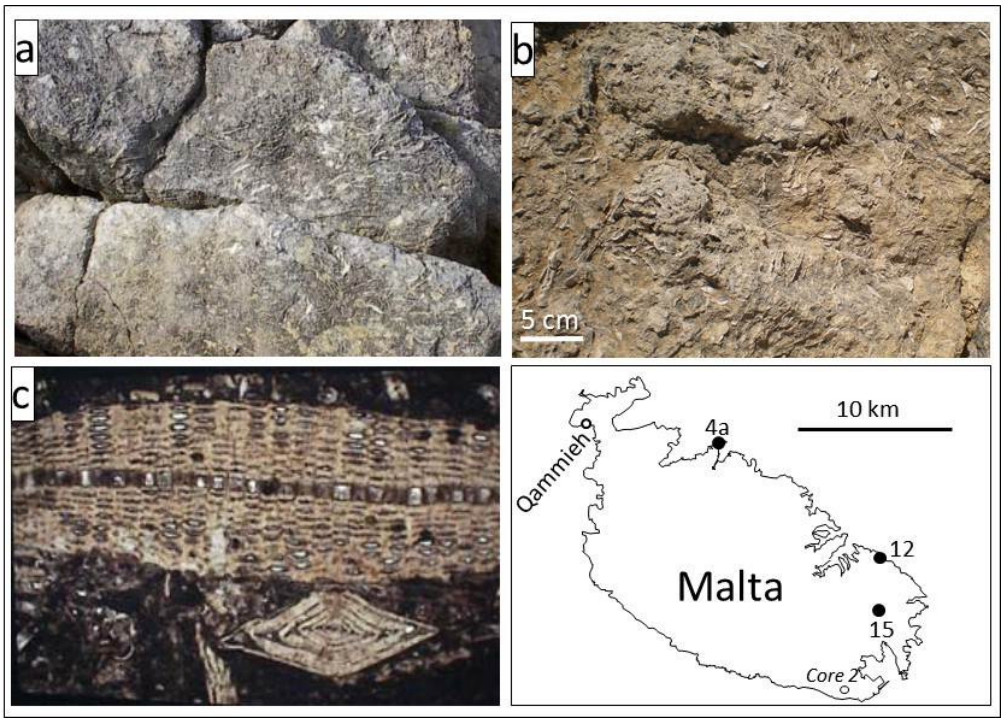

Figure 3.11. Facies IIIc at locality 12: (a) Large (9 cm) *Lepidocyclina* packstone showing imbrication; (b) *Lepidocyclina* packstone bed at Qammieh; (c) Photomicrograph of large *Lepidocyclina* and *Amphistegina* (locality 12). Map shows localities where facies IIIc is recorded in outcrops.

FA III: Interpretation

The distribution of LBF species in modern reef environments is related to particular ranges of depth which can be used as a proxy for Cenozoic palaeodepths (Hallock & Glenn, 1986). Many LBF thrive in oligotrophic environments (Pomar, 2001) and need light to produce food from symbiotic algae. The LBF assemblages also reflect changing environmental conditions in the Tethys. During the warm Eocene the Nummulitoidea (*Nummulites*) were the dominant carbonate producers (BouDagher-Fadel, 2008) although by the Early Oligocene conditions became cooler which favoured miliolids in shallow oxic environments (Hallock *et al.*, 1991). During the succeeding interval, *Lepidocyclina* invaded habitats in the inner- and mid-platform environments (Buxton & Pedley, 1989) during the return to warmer seas.

This facies association reflects large variations in accumulation rates because LBF are susceptible to transportation (Beavington-Penney, Wright, & Racey, 2005). This accounts for the remarkable differences in facies thickness (2 m to 30 m), variable foraminifer size and texture of LBF in FA III. These variations can be related to antecedent bathymetry that resulted in thinning and condensation of this facies over palaeohighs, e.g., over western Malta (localities 3 to 4b). Strong currents resulted in transportation and sorting of LBF and the skewed distribution of LBF sizes into two modal sizes of <5 mm and 50 mm in shoal or bank deposits:

1. *Ferruginous LBF grainstone* (facies IIIa)

The highly fragmented lepidocyclinids and nummulitids bioclasts in west Malta (localities 3 to 4b) are interpreted as condensed beds deposited over a palaeohigh where the accumulation rate was low and the level of reworking was high. These Oligocene beds are analogous to the condensed beds of Eocene *Nummulites* deposited across palaeohighs in Tunisia (Beavington-Penney *et al.*, 2005). Depths of <3 m resulted in current flushing and early seabed cementation producing hardgrounds that were bored by *lithophaga* and later eroded to a flat surface by corrasion from migrating bioclastic accumulations. The top boundary of the 5 cm-thick orange facies (facies IIIbi) forms the lowest of these planar hardground surface

that extends eastwards to locality 9 where it is capped by cross-bedded LBF (facies IIIb). The fragmented LBF are rimmed by fibrous calcite cement that suggests early marine cementation with some of the remaining pore space later filled with orange fine-grained sediment. The orange-coloured matrix points to oxidation of iron-rich minerals (glauconite) in shallow marine environment within the euphotic zone. The gradual decrease in test fragmentation in successive beds above the lowest hardground and the increase in planktonic foraminiferans and fine-grained matrix suggests gradual deepening.

2. *Cross-bedded LBF packstone & grainstone* (facies IIIb):

The <30 m-thick cross-bedded, fragmented LBF that extend over 5 km in eastern Malta suggests a low to moderate amplitude, high energy bioclastic shoal. The shoal is seen in cross-section along the southern cliffed coast of Malta (locality G in Figure 3.10) which suggests a NE-SW orientation. Storms and high velocity currents produced the large basal undulating erosional scours into the underlying FA II sediments and the erosional nature of the overlying coset boundaries. In this facies, B-forms >10 mm are completely absent. This suggests that either a large test size was not advantageous, or that all larger LBF were selectively winnowed.

The fibrous calcite cement and geniculate coralline algae (30% of the grains in some localities) is associated with marine environment <20 m deep (Wray, 1977). The intense micritisation of some of the coralline algae along the lower beds of the shoal suggests deposition within the euphotic environment whereas the miliolid foraminiferans *Borelis* is associated with unvegetated carbonate sand shoal (Brasier, 1995). The shoal was also influenced by tidal currents and may have been dissected by tidal channels. Davies (1976) interprets the cross-bedded sediments in western Gozo as having been deposited in very shallow (0 to 5 m) depth under strong westerly currents.

Facies IIIb is the Oligocene equivalent of the Eocene nummulitid LBF accumulations in the Tethys described by Racey (2001), although sedimentary structures are well-defined in Maltese LBF accumulations. The detection of cross-

bedding relies on the presence of subtle granulomentric contrasts. In facies IIIb, LBF from different rotalid superfamilies with different densities and sizes produced graded sediment packages along subaqueous dune foresets, hence preserving cross-bedding. This contrast with Eocene *Nummulites* of different sizes but the same hydrodynamic behaviour which resulted in a heterometric grain assemblage (Jorry *et al.*, 2006).

3. Lepidocyclina *packstone* (facies IIIc):

The upper part of the formation in northeast Malta consists of low-amplitude (1-2 m) foraminiferal banks of very large *Lepidocyclina* that developed in deeper water relative to the underlying facies IIIa. Flat, wide LBF similar to facies IIIc are reported in oligophotic environments at a depth of 70 m (Hallock & Pomar, 2008). Oligocene large *Lepidocyclina* are also known to have thrived at depths of 30 to 60 m (Bosellini *et al.*, 1987). The occurrence of *Lepidocyclina* in such outer mid-platform environment reflects their expansion from the reefal environment into deeper habitats during the Oligocene with the decline of Nummulitidae by the Eocene that left a vacant niche that was occupied by the Asterigerinoidea *(Lepidocyclina* and *Amphistegina*) (Buxton & Pedley, 1989).

In the deeper environment oligotrophic mid-platform environment, the large size (D/T> 6) of *Lepidocyclina* increases surface area relative to test volume permitting more algal symbionts to be exposed to weak light (Racey, 2001) thereby maximise the use of light by algal symbionts that provide energy to the host. The stressed environments characterised by low temperature or insufficient food or light also favoured the larger B-forms allowing for mixing of the gene pool by sexual reproduction, although individuals grow more slowly and mature at larger sizes (Hallock & Glenn, 1986).

According to Aigner (1985), an accumulation of LBF dominated by the larger B-forms represents a residual accumulation where the smaller A-forms were selectively winnowed. At locality 12, the smaller A-forms of *Lepidocyclina* are absent, although smaller tests of *Amphistegina* are common. This suggests that the LBF assemblage

was either a residual accumulation where the smaller *Lepidocyclina* was winnowed away or, an autochthonous assemblage where smaller A-forms were unable to survive in deeper water (low light) conditions. The large (90 mm), thin and unbroken *Lepidocyclina* (broken by post-depositional compaction) suggests little post-mortem transport. However, the dense accumulation of edgewise-oriented foraminiferans also suggests strong winnowing of fines under oscillatory currents. Such oscillatory currents are associated with deepening of the storm wave-base (*circa* 40 m) into the outer platform muddy sediments. Therefore, the LBF facies are interpreted to have been deposited in the mesophotic zone in clear water at depths of >40 m (*circa* 50 m). When the storm wave base shifted to this deeper environment, they were occasionally reworked by storms into a foraminiferal bank along the outer mid-platform environment. The paucity of planktonic foraminiferans precludes depths >50 m.

3.3.4 Facies Association IV: Coral limestone

The coral facies are associated with geniculate and crustose algae as well as bivalves and miliolid foraminiferans. All corals in outcrop were composed of aragonite that has been leached especially under the influence of meteoric water. Only their internal structure is preserved as moulds.

Coral facies taxa

Corals reached the acme of genera number during the Early Oligocene (Bosellini & Perrin, 2008). The Order Scleractinia is sub-divided in 5 sub-orders, three of which are found in the Maltese Oligocene sediments. Despite the relatively small volumetric size of the coral facies within the Lower Coralline Limestone, 24 coral genera are reported by Chaix & Saint-Martin (1994) in the western localities of 5 and 6 shown in Table 3-9. These coral genera in Malta include those presently found in the Atlantic (e.g., *Porites* and *Acropora*) and in the Indo-Pacific (e.g., *Goniopora*, *Stylophora* and *Astreopora*) which supports the view that the western Tethys was still connected to the major oceans during the Oligocene.

Order	Suborder	family	genera
Scleractinia	Astrocoeniina	Astrocoeniinae	Stylocoenia[3]
		Pocilloporidae	Stylophora[2]
		Acroporidae	Acropora[1]
			Astreopora[2]
	Fungiina	Siderastreidae	Siderastrea[3]
		Poritidae	Goniopora[2]
			Porites[1]
			Dictyaraea[3]
			Alveopora[2]
	Faviina	Faviidae	Favites[2]
			Meandrina[1]
			Montastrea[1]
			Antiguastrea[3]
			Caulastrea[2]

Table 3-9. The above Oligocene corals found in Malta are also found in the: 1 Carribean; 2 Indo-Pacific; 3 Tethyan (Mediterranean to Pacific).

Coral facies description

Corals are common in the lower part of outcrops of the Lower Coralline Limestone Formation and occur locally close to the top part of the formation. Corals comprise two main facies (Table 3- 10).

FA	Facies	Sub-facies	biota	Water depth (m)
IV	a. Coral Biostrome rudstone/framestone	i. Dense framestone to boundstone	Coral, miliolids, coralline red algal debris	<10
		ii. solitary framestone in packstones		
	b. Coral Patch Reef / rudstone	Coral framestone	Coral, coralline algae	<20

Table 3- 10. Facies in facies association IV.

a. Coral biostrome rudstone/framestone:

Coral biostromes cap the terminal beds of FA V in western localities 3, 5, 6 and 9. Two varieties are observed (Figure 3.12):

i. Tabular, <2 m-thick biostromes characterised by thickets of high coral framework density. The coral biostromes have a tabular shape, abruptly truncated by either rhodolithic limestone (FA II) or algal-miliolid fine sand limestone. Dominant coral species are *Porites* with branching and organ-pipe growth form and *Stylophora*. Microbiota includes *Borelis* which is associated with unvegetated shoal environments (Brasier, 1995).

ii. Sporadic, solitary dome-shaped coral heads in locality 6 that cap FA II. At locality 13 the coral is inter-bedded with rhodolith beds a few metres below the base of FA III.

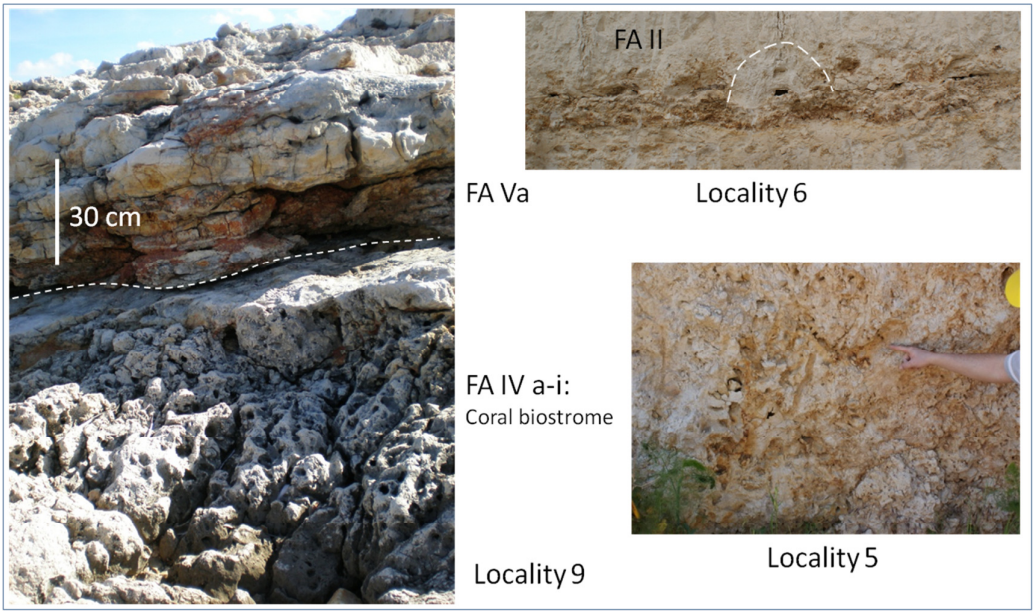

Figure 3.12. Facies IVa: Left: <1 m thick tabular coral biostrome with sharp erosional boundaries (facies IVa-i); Right. facies IVa-ii: leached dome-shaped coral (30 cm base). Void migration has resulted in vertical cracks above the coral. Coral biostrome at locality 5 is at the same stratigraphic level as that in locality 6 but much thicker and include 'organ-pipe' *Porites* (pointed by finger).

b. Coral patch reef rudstone

Metre-wide, dome-shaped coral patch reefs occur sporadically at two levels:

i. At locality 5 within FA V, sporadic metre-wide coral patch reefs often overlie fining upwards foraminiferal packstone beds with an undulating base. The beds are differentially compacted by the weight of the overlying patch reef.

ii. A <5 m-thick band of sporadic coral patch reefs in FA IIa, a few metres above the top of FA V (Figure 3.13) that extends through central and eastern localities (localities B to 14). These patch reefs are associated with coralline algae and may have formed coralgal constructions, although the coral is entirely leached. The patch reefs seen along the inaccessible southern cliffed coast of Malta show a gradual increase in the width of the base of the patch reefs from <3 m to 10 m over a distance of 5 km from locality A to locality D, and decreases to <3m from locality D to the accessible locality 14. The underlying algal sand limestones are differentially compacted underneath the patch reefs whereas the surface of the reefs were later draped and buried by laminar algal debris beds.

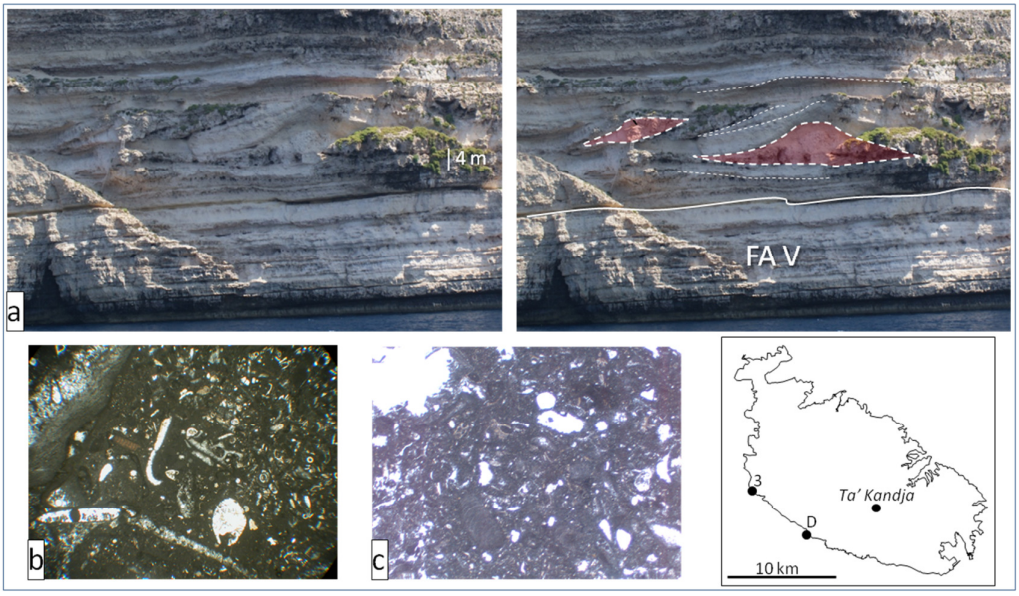

Figure 3.13. Facies IVb: (a) uninterpreted photo of base locality D; (right) interpreted photo: dome-shaped coral patch reefs (shaded red) height *circa* 5 m. Dashed lines show bedding deformed by differential compaction beneath the larger patch reef whereas overlying beds of algal debris drape over the patch reef. A smaller patch reef later colonised the west flank of the larger patch reef which acted as a barrier to algal sands that buried the larger patch reef; *Photomicrographs:* (b) locality 3 showing geniculate red algae, *Borelis* and *Stylophora* coral; (c) Ta' Kandja (water gallery) showing geniculate red algae.

FA IV: Interpretation

Algal symbionts in scleractinian zooxanthellate coral make them susceptible to environmental stress caused by algal overgrowth, temperature shock, and salinity stress (Hallock, 2000). Although depth does not affect coral growth, it controls light intensity, temperature and hydrodynamic energy level that influences coral growth (Perrin *et al.*, 1995). Oligocene corals did not build up to sea-level and may have even survived within the oligophotic zone (Pomar & Hallock, 2007) unlike Late Miocene to modern corals that require euphotic conditions for algal symbiosis within depths of <10 m (Schlager, 1981). Significantly, the Maltese Oligocene outcrops do not show any development of large reefal buildups.

The effect of depth is reflected in the change in the morphology of coral constructions and coral cover from shallow to deeper environment: tabular coral biostrome constructions in western Malta are characterised by extensive lateral coral cover. In central Malta coral cover decreases and grades laterally eastwards to <3 m-wide patch reefs (facies IVb-ii) east of locality B. The coral biostromes in western Malta at localities 3, 5 and 9, (facies IVa-i), especially those with branching *Porites* are interpreted to have been deposited in relatively high hydrodynamic energy levels similar to those found in Miocene reefs in Mallorca (Perrin *et al.*, 1995). Regular regression and storms resulted in the truncation of the coral build-ups and smoothened planar surfaces produced by migrating dunes.

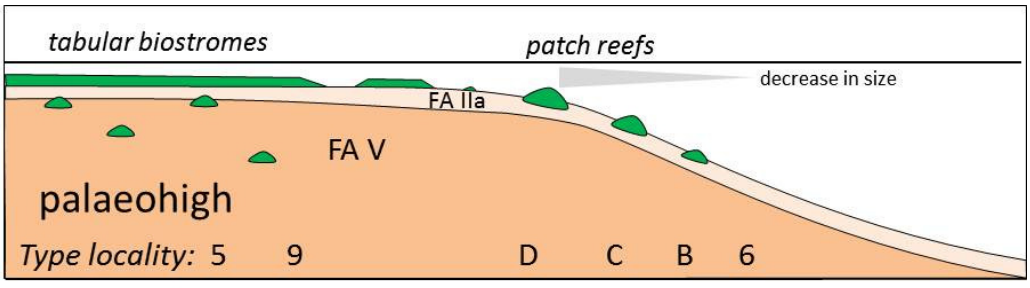

Figure 3.14. Model of coral framestone buildup morphology: Small coral patch reefs in FA V succeeded by coral build-ups that become disjointed and smaller with increasing palaeodepth (localities D, C, B and 6, respectively) whereas morphologies become more planar horizontal and continuous with increasing hydrodynamic energy level over palaeohighs (localities 3, 5 and 9).

The patch reefs in central-east Malta are characterised by upward aggradation which could be related to a decrease of light penetration along the seabed associated with deeper water environments. Sediment accumulation rates may have also been higher which forced the patch reefs to aggrade in order to keep up with sedimentation, until they were buried by coralline algal debris. The increase in patch reef size from locality B to D suggests higher levels of light penetration that can be associated with shallowing.

The coral patch reefs in the lower >30 m of locality 5 (facies IVb-i) are interpreted as deposited in shallow (<5 m deep) marine environment that was relatively restricted. These patch reefs have a flatter morphology relative to those found between localities B to D. This suggests that the coral patch reefs were not limited by the level of light but by the high sedimentation rate of mud in FA V.

3.3.5 Facies Association V: Imperforate foraminiferal wackestone/packstone

The maximum thickness in outcrop (<30 m) is found in the lower half of locality 5 and extends along the base (<10 m) of the southwest cliffed coast of Malta and the base of the cliffed coast of western Gozo. In the subsurface, cores and well cuttings (see Appendix III-29) from the Zabbar well show that FA V is 140 m thick which is more than half the thickness of the entire Lower Coralline Limestone Formation (FA I to VI), whereas in central Malta the thickness of FA V is 300 m (Naxxar-2 well), or about two-thirds of the entire Formation.

FA V taxa

The typical macrofauna includes the Teredinid bivalve *Kuphus* (Zammit-Maempel, 1993) which is sparse to abundant in this micrite-dominated facies. Only the <20 cm-long calcitic siphonal tube of the bivalve is preserved in near life position or fragmented (Figure 3.15a) and was later filled with lime mud and miliolines, whereas the aragonitic bivalve is leached. Further down this facies is a horizon of abundant, well-preserved tests of crabs in coral floatstone at locality 5. The crab tests intact with chelae suggest rapid burial in muddy environment.

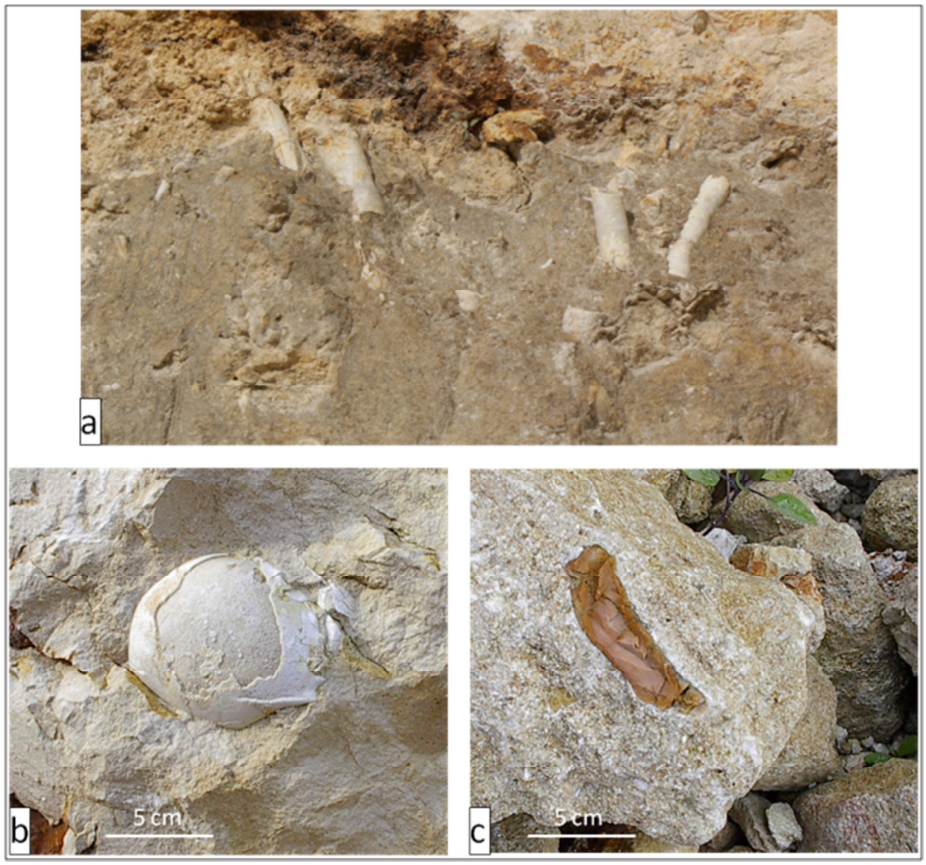

Figure 3.15. Macrofauna in FA V: (a) siphonal tubes of Kuphus; (b) Crustacean (crab) associated with coral rudstone; (c) Very rare mammalian (Sirenian?) bone fragment in coarse-grained sediment.

The taxonomic identification from thin section shows that the microfauna is dominated by small benthic foraminiferans (SBF) listed in Table 3-11. The foraminifera include *Praerhapydionina* that lived in soft seabed surface in very shallow water associated with lime-mud platform interiors, whereas *Austrotrillina* accompanied with miliolids lived under slightly higher energy conditions in the platform interior (Geel, 2000). *Peneroplis* is known to be an epiphytic foraminiferans associated with sea grass environments. Larger rotalid foraminiferans are generally absent in FA V except for *Rotalia viennoti* found in the top beds of FA V (facies Va).

Suborder	Superfamily	Genera
Miliolina	Alveolinoidea	*Borelis* de Monfort 1808
		Alveolina oblonga
	Milioloidea	*Austrotrillina* Parr 1942
	Soritoidea	*Peneroplis* de Monfort 1808
		Archaias de Monfort 1808
		Praerhapydionina Van Vessem 1943
Rotaliidae		*Rotalia viennoti*

Table 3-11. Foraminiferal biota in FA V.

FA V description

Three facies are identified in the field and in the subsurface listed in Table 3-12 and shown in Figure 3.16:

FA	Facies	Sub-facies	biota	Water depth (m)
V	a. miliolid-algal sand limestone		Miliolids, geniculate coralline algae	<-10
	b. miliolid limestone	i. *Kuphus* mudstone beds	Miliolids, *Peneroplis*, *Kuphus*, corals	<-5
		ii. *Peneroplis* packstone beds		
		iii. Coral rudstone beds		
	c. Marly-miliolid limestone		Miliolids, Globigerinids	-20 to -40

Table 3-12. Facies association V: facies sub-divisions.

a. Miliolid-algal sand limestone

This facies comprises the uppermost <15 m of FA V that outcrops at locality 5 and a few metres above present sea-level in localities 1 and 9. A characteristic of this facies is the thinly bedded (10 to <15 cm) and pale orange-coloured limestone along the interface between FA V and FA II. The packstone to grainstone consist of fine-grained, rounded and well-sorted geniculate algal debris and miliolids, which suggest that this facies is a hybrid of FA V and FA II.

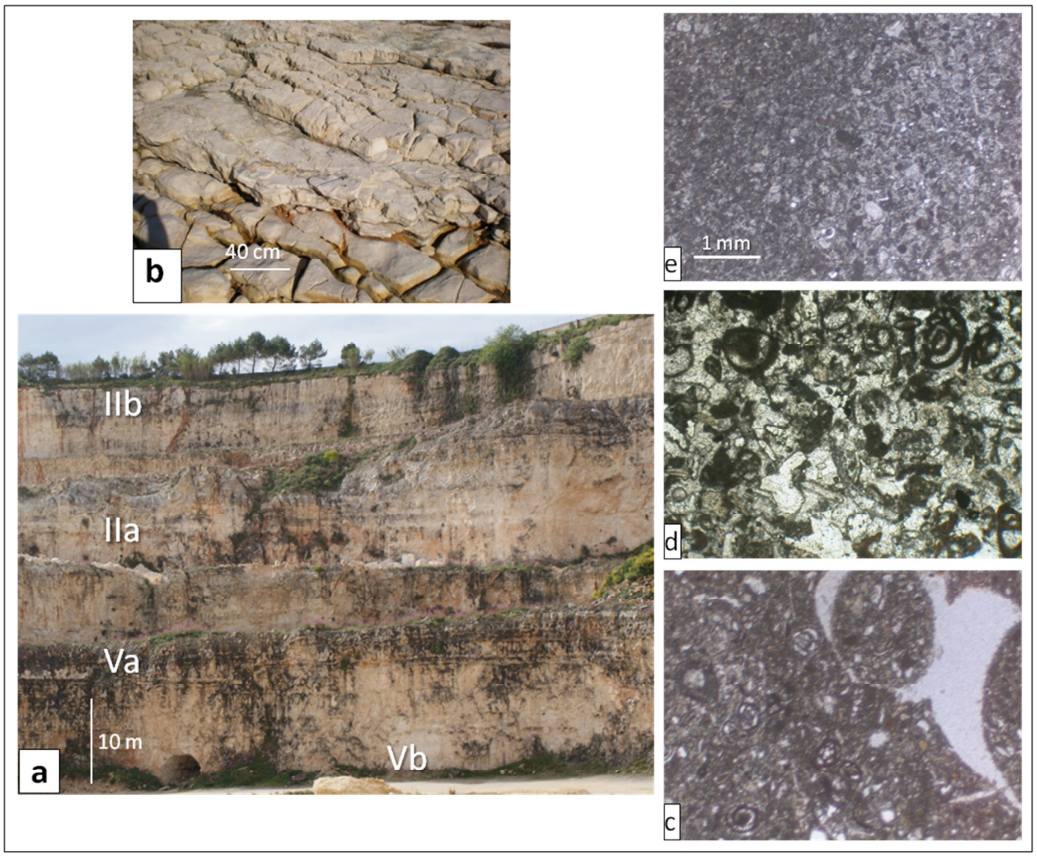

Figure 3.16. FA V at locality 5: (a) Mosta quarry showing facies succession; (b) locality 9 showing facies Vb characterised by thin bedding that consists of miliolids and geniculate algae; Photomicrographs: (c) Facies Vb: coral rudstone showing miliolids and leached bioclasts. The bed includes crab tests; (d) Miliolid packstone showing leached bioclasts and blocky equant cement; (e) Locality 9: facies Va consisting of fine miliolid and algal debris sand.

b. Miliolid limestone

This facies is differentiated from the overlying facies Va by the absence of geniculate algae (Figure 3.16). The lower <30 m at locality 5 consist of massive, white to pale yellow wackestone to packstone beds rich in imperforate foraminiferans, bivalves and coral. This facies comprises sub-facies that consist of beds having moderate to dense accumulations of *Kuphus* (facies V b-i), beds rich in the epiphytic foraminiferan *Peneroplis* (facies Vb-ii) and horizons with well-

preserved tests of crustaceans (crabs). This facies also outcrops along the southern cliffed coast of Malta from localities B to D. Well data from Zabbar and Ghar Lapsi wells show that below sea-level this micrite and miliolid-rich facies reaches a thickness of 36.5 m and overlies another similar succession that is about 39 m thick.

Sedimentary structures are rarely present or had been obliterated. The fine-grained succession is interrupted by four distinct wedge-shaped beds (facies Vb-iii) at intervals of 6, 3 and 2 m. These <2 m-thick beds of coarse-grained foraminiferal packstone include gastropods and articulated bivalves. The beds taper towards the west and were later colonised by corals that form a layer of rudstone or patch reefs, occasional draped with a thin mudstone bed.

d. Marly-miliolid limestone

Facies Vc is entirely below present sea-level. Well data from Zabbar and Ghar Lapsi wells show that in the subsurface this fine-grained unit is about 60 m and thickens to 200 m in the Naxxar-2 well (see Appendix III-29). Miliolids are common along with planktonic globigerinid foraminiferans. The limestone is described as marly in well logs and is at times dolomitised.

FA V: Interpretation

The abundance of micrite, shallow marine biota and overall absence of sedimentary structures suggests a low energy environment that was intensely bioturbated. This facies association is interpreted as shallowing upward to less restricted conditions:
Shallowest subtidal (facies Vb-i): The common occurrence of miliolids (*Austrotrillina* and *Quinqueloculina*) in some beds suggests subhaline to hypersaline conditions that are usually found in restricted environments at depths of 0 to 5 m (Geel, 2000). These muddy sediments were also intensely burrowed by soft-body organisms including the Teredinid bivalve *Kuphus melitensis* which is known to burrow muddy lagoonal and intertidal environments (Bennett, 1980) and interpreted as indicative of shallow marine, warm environment in the Oligocene of Malta and Greece (Wieland-Schuster *et al.*, 2004). In the Oligocene of Oman, *Kuphus* is

associated with the shallowest part of the subtidal zone, and as in Malta, it forms dense accumulations of siphonal tubes (Reuter *et al.*, 2008). It is also recorded in similar platform interior environments in the Eocene of Egypt (Racey, 2001), whereas Holocene *Kuphus* genera are found in mangrove swamps.

Shallow subtidal (facies Vb-ii): This facies has an abundance of micrite. The micrite could be of biogenic origin produced by bioerosion (e.g., crustaceans) of coral and disarticulation of rooted algae as well as abiogenic precipitation of lime mud possibly as a result of removal of CO_2 in warm shallow water. Lime mud and bacteria were also favourable for the growth of mats of microalgae which were grazed upon by large gastropods e.g., *Strombus*.

The occurrence of the epiphytic soritid foraminiferan *Peneroplis* suggests a platform interior environment that was covered with extensive sea-grass meadows. Although evidence of seagrass is lost during early burial its occurrence is implied from indirect sources such as epiphytic foraminiferans. The dominant Oligocene seagrass was *Cymodocea* that baffled sediment whereas its rhizomes stabilised the sandy to muddy surface (Brasier, 1975). The environments produced by seagrass can result in the eutrophication of sediment substrate which is unfavourable for coral growth. Significantly, extensive coral reefs did not develop in FA V.

Although muddy environments could be the result of low hydrodynamic energy conditions, organisms are needed to stabilise the lime mud and contribute to its aggradation. The spread of seagrasses in the Oligocene may have been critical for lime mud accumulation in the euphotic zone. Brandano *et al.* (2009) suggest that the spread of seagrass-dominated communities commenced in the Late Oligocene. However, the Maltese outcrops and well logs show the accumulation of many tens of metres of lime mud (FA V) during the Early Oligocene (Rupelian).

Strong storm events can generate 'blowouts' in grass covered areas (Wanless, 1981). The low energy environment of facies Vb was occasionally affected by high energy events that produced discrete beds of coarser sediments. The wedge-shaped packstones (facies Vb-iii) within the micritic sediments at locality 5 are interpreted

to be deposited by storms that tracked over the carbonate platform from east to west. The decreasing separation of these storm beds up the succession indicates either an increase in storm frequency or a change to more open marine conditions that exposed the Malta Platform to storm activity. The metre-wide patch reefs occur especially where the seabed was scoured during storms events that ripped-up sea grass and created new surfaces that could be colonised by coral. However, much of the transported material was autochthonous and originated from the platform interior which points to an environment that remained relatively restricted.

Shallow, open marine (facies Va): frequent storm events culminated in the hybrid facies Va at the top of this facies association. This facies heralds a major transgression resulting in the accumulation of increasing amounts of geniculate red coralline algae (FA II), sometimes well-rounded, that were washed over the lagoonal area. The increase in hydrodynamic energy level suggests more open marine conditions that were <10 m deep.

Deeper subtidal facies (facies Vc): the base of FA V is recorded in Naxxar-2, Zabbar and Aqualta wells and consists of argillaceous limestone that includes planktonic foraminiferans and the detrivore foram *Bolivina*. This benthic foraminiferan is commonly found in Oligocene argillaceous limestone in Libya (Imam & Galmed, 2000). The clay fraction and the occurrence of *Bolivina* suggest shallow basinal environment created by antecedent deep bathymetry over central Malta (see chapter 6). This palaeolow received an influx of planktonic foraminiferans as well as miliolids possibly resedimented from nearby shallower areas where facies Vb was being deposited. Further up the Naxxar-2 well cuttings log, planktonic foraminiferans become very rare and sediments include abundant accumulations of miliolids and *Praerhapydionina* as well as dasycladalean algae in Aqualta well. The microbiota suggests a change to shallow marine, muddy lagoon-type of conditions (facies Vb) that outcrop in Malta.

3.3.6 Facies Association VI: Red argillaceous carbonates

This facies association is characterised by additional fine-grained siliciclastics and palaeosol-related biota. The facies is recorded in outcrop and in the subsurface Naxxar-2 well and the offshore Aqualta well. In outcrop, FA VI is found in hitherto unrecorded outcrops <10 m above sea-level at locality A and as thin beds that inter-finger other facies in locality 5. The two facies are listed in Table 3-13.

FA	Facies	biota	Water depth (m)
VI	a. Laminar Limestone	*Kuphus,* miliolids (bivalve intraclasts)	+0
	b. Thinly-bedded to laminar limestone/palaeosol	*Microcodium*	> +2

Table 3-13. Facies association VI: facies sub-division (see Appendix III-29).

Bedding in FA VI is characterised by laminar structures and laminar bedding (Figure 3.17) that is distinguished by its reddish-brown colour in outcrop that contrasts with the white to pale yellow coloured carbonates that dominate this formation. This facies association is found at two levels in outcrop:

a. Facies VIa: pale red to yellow-coloured, <0.5 m-thick micritic beds inter-bedded with FA II, IV and V in the mid- and lower sections of localities 5 and 6. These laminar micrites are parallel to the undulating and irregular palaeotopography of the underlying bed. The sediments include bivalves and pelagic foraminifera and were later penetrated by siphonal tubes of the bivalve *Kuphus* from the overlying facies Vb-i beds. In thin section, lighter laminae alternate with darker laminae which tend to show seam-like voids produced during thin section making that removes unconsolidated fine material and organic matter. The crushed skeletal material, especially tube-like structures point to significant vertical shortening indicating little early cementation occurred before significant compaction. Darker strands may be clay-rich and organic-rich that inhibited early calcite cementation. When seen by scanning electron microscopy (Hitachi SU-70), the micrite consists of 0.05µm calcite crystals that could be coccoliths. The EDX analysis confirms the presence of aluminosilicates, although the principal mineral is calcite.

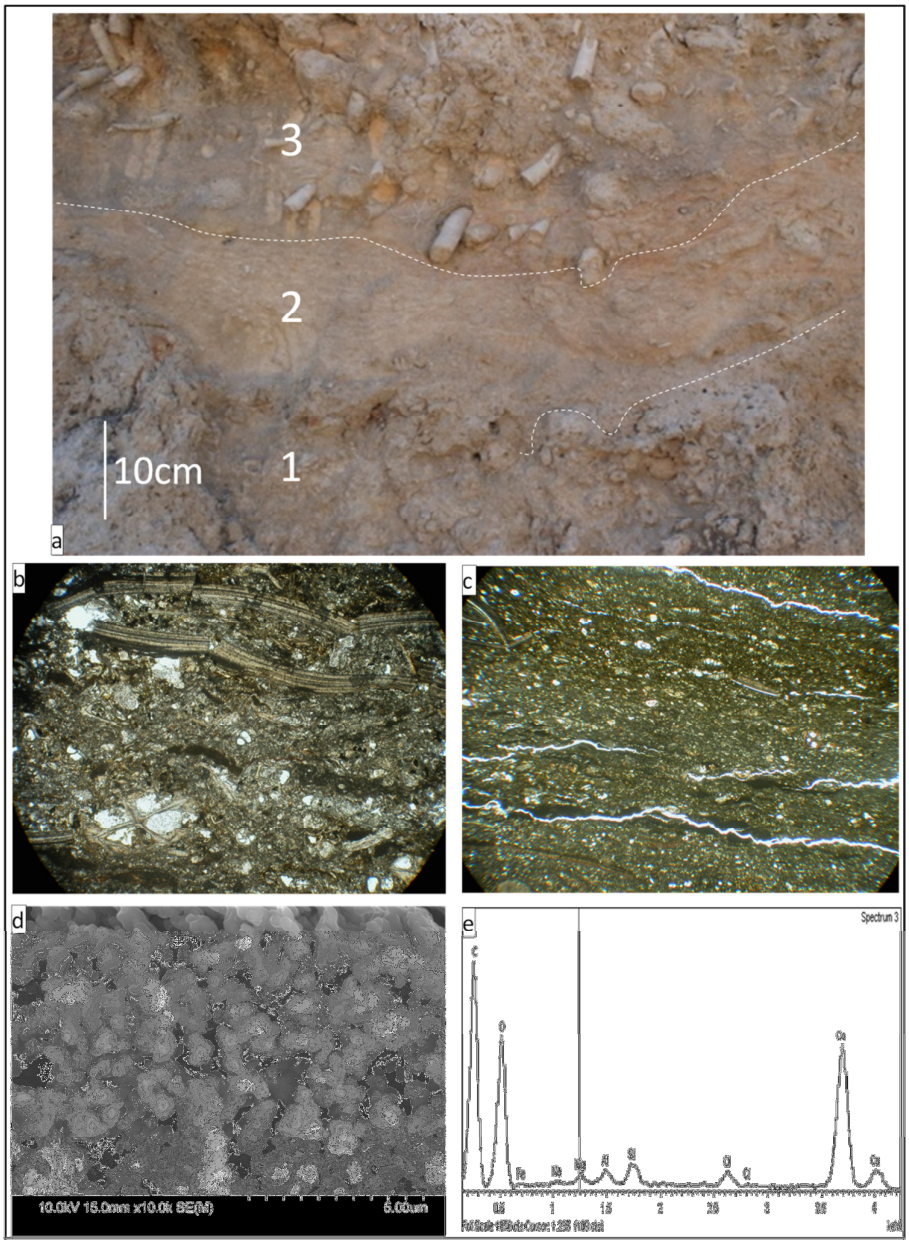

Figure 3.17. FA VI: locality 5: (a) (1) rhodolith bed; (2) facies VIa showing a light orange-brown coloration. The laminar sediments fill topographic lows in the underlying bed; (3) micritic bed intensely burrowed by *Kuphus*. Laminae are less well-defined and the bed shows disturbance; Photomicrographs: (b) crushed tube-like structures (juvenile *Kuphus*) suggesting significant compaction; (c) Locality 6: bedding consisting of dark and lighter laminae showing horizontal voids; (d) SEM photo showing calcite crystals that could be coccoliths; (e) EDX elemental analysis of sample of FA VI matrix under SEM from locality 5 showing abundant $CaCO_3$ and some aluminosilicates.

b. Facies VIb: The lower level is found at two geographical areas (Figure 3.18): (1) about >10 m of pale reddish-brown sediments at locality A along the base of the inaccessible cliffed coast of western Malta and, (2) about <1 m of pale reddish limestone at locality H along the inaccessible base of the cliffed coast of western Gozo and the base of localities 1 and 2. This facies is distinguished by its reddish-brown hue and thinly-bedded to laminar structure. The fine-grained bright reddish material may occupy interstitial spaces within white limestone or has been reworked into the carbonate which gives a pale reddish-brown hue to the rock. Between localities B and D the reddish beds are absent although the topmost <1 m thick bed over facies Va has been differentially eroded and forms a deep groove along the cliff face traceable for several kilometres. A <6 m thick clay bed is also recorded in the upper part of Naxxar-2 well about 140 m below the top of the Lower Coralline Limestone Formation. In the Aqualta well *Microcodium* is recorded from well cuttings at four levels at intervals of 30 to 60 m within the carbonates.

FA VI: Interpretation

Facies VIa

The red to yellow beds in localities 5 and 6 include shallow marine fauna (miliolids) and were burrowed by *Kuphus*. The *in situ* fauna suggest a depositional environment similar to a lagoon although paradoxically the sediments include an influx of pelagic marine fauna (pelagic foraminiferans and micrite). In thin sections, dark thin laminae alternate within lighter fine-grained material could be dissolution seams with insoluble residue (clay) concentrated along them (Tucker & Wright, 1990).

The red colour could be the result of ferric iron oxide that was transported into the lagoon in an otherwise purely carbonate succession. A source of reddish clay in such shallow marine environments could be terra rossa soil which usually accumulates as a residue by the weathering of limestone in exposed carbonate platforms (Goldhammer & Elmore, 1984). A possible mechanism that can explain the paradoxical faunal assemblage is storm activity which deposits pelagic fauna from the open sea and erodes terra rossa along the coast. These processes suggest subaerial conditions with pedogenesis along an unrecorded emergent area from where run-off water brought an influx of clay into the peritidal environment.

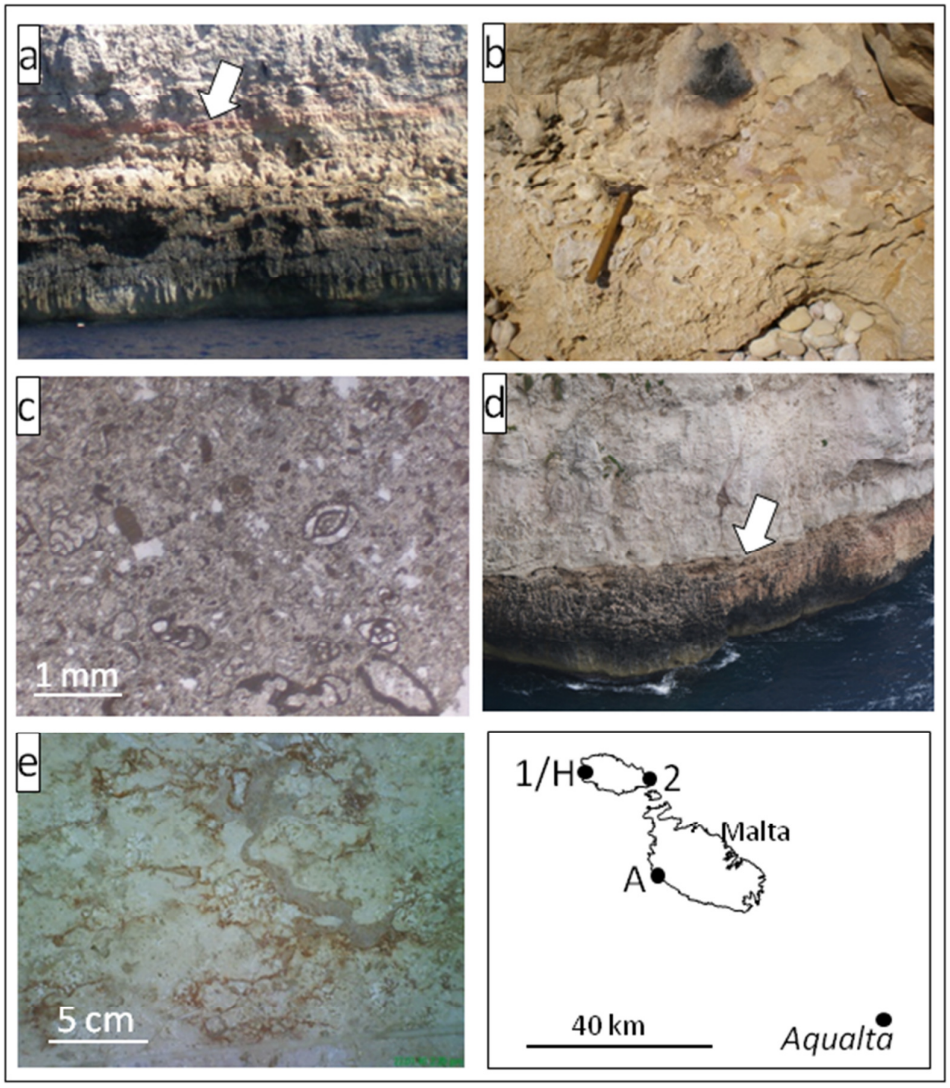

Figure 3.18. Facies VIb: (a) Locality H: Inaccessible cliffed coast of western Gozo. White arrows point to top reddish horizon which is *circa* 10 m above sea level; (b) Locality 1: photo of facies VIb at 2 m asl showing reddish hue (*hammer for scale*) (c) Photomicrograph of sample taken from the base accessible locality 1. Grains include miliolids and rounded coralline algae; (d) Locality A: inaccessible base of cliff where this facies reaches a thickness of >5 m; (e) Slab section from base of locality 2 showing reddish clay in interstitial spaces within the limestone. Location map of outcrops and Aqualta well where four levels of *Microcodium* are recorded from well cuttings.

Facies VIb

The beds at the base of the sea cliff at locality A are inaccessible and therefore, any interpretation is highly speculative. However, the facies is accessible at locality 1 where it shows sediments typical of shallow marine environments. Locality 1 shows

carbonate sediments indicative of shallow marine environment that may have received an influx of reddish clay from an adjacent emergent area. The reddish clay may be derived from erosion of terra rossa (chromic luvisols) that forms by the insoluble accumulation of clay over limestone. The soil residuum indicates subaerial exposure for a significant period of time when extensive limestone leaching results in the accumulation of insoluble residues such as clay and iron sesquioxides that impart a bright red coloration to the soil. The same process is responsible for the formation of the bright red-brown *terra rossa* soil over the Lower Coralline Limestone following the Plio-Quaternary emergence of the Maltese Islands which may be analogous to the reddish clay seen in the Oligocene outcrops.

The pedogenic origin of this facies is consistent with *Microcodium* in the Aqualta well. *Microcodium* is indicative of calcrete formation during subaerial exposure that results in the calcification of rhizoliths (Klappa, 1978). Throughout the Phanerozoic, laminar calcretes of biogenic origin consist of rhizoliths that form centimetre to decicentimetre thick horizons with gentle undulations (Wright *et al.*, 1978). This is similar to what is seen along the cliff coast at locality A.

Several metres of limestone need to be weathered to produce a thin layer of terra rossa whereas calcrete is mainly accretionary. The occurrence of terra rossa over the Maltese Islands and calcrete over the Aqualta suggests a period of exposure that was prolonged over the Maltese Islands. Both calcrete and terra rossa are associated with limestone parent rock, consequently a continental origin for the reddish clay is excluded.

3.3.7 Facies Association VII: Gypsum facies

The Aqualta, Naxxar-1 and Zabbar wells record less than metre-thick gypsum or anhydrite (Aqualta well) beds at the base of the Oligocene associated with dolomite or marls. The gypsum associated with dolomite in the Aqualta well suggests that the evaporites could have been deposited in an environment similar to a peritidal sabkha under the influence of an arid climate (Moore, 2001). The extensive evaporite horizon is here interpreted to mark the boundary between the Oligocene and Eocene

in the Malta Platform above which evaporites are absent in the Lower Coralline Limestone Formation. Evaporite beds also mark the Oligocene-Eocene boundary within the Qatrani formation of northern Egypt (Rasmussen *et al.*, 1992) which suggest that extensive evaporite deposits were precipitated during an arid episode affecting the Mediterranean region. The widespread evaporite along the Oligocene-Eocene boundary corresponds to the global oxygen isotope excursion (Zachos *et al.*, 2001) produced by the expansion of the Antarctic ice-sheet (DeConto *et al.*, 2008) that resulted in the first significant glacio-eustatic fall in sea-level during the Cenozoic

3.4 DISCUSSION

The three main skeletal biotas (coralline red algae, coral and LBF) that contributed to the aggradation of the Lower Coralline Limestone Formation show an increase in species diversity and geographical radiation during the Palaeogene. The Early Oligocene marks the beginning of global cooling that coincides with the acme in the number of coral genera (Bosellini & Perrin, 2008), the decline of Nummulites and the spread of coralline red algae that replaced corals by the early Miocene as trophic level increased (Halfar & Mutti, 2005). These changes reflect the palaeoclimatic setting and changing ecological and trophic conditions through time.

3.4.1 Palaeoclimatic setting

The palaeoclimatic setting of the Lower Coralline Limestone described in previous works is contradictory. The mean Oligocene sea temperature of the Mediterranean is estimated as <20°C by the 'energy hypothesis' applied to zooxanthellate coral (Bosellini & Perrin, 2007). Knoerich & Mutti (2003) concluded that the Maltese Oligocene carbonates were deposited in non-tropical setting whereas Brandano *et al.* (2009) suggest a tropical setting. In both cases, the conclusions reached were based on the study of one outcrop which is insufficient for an overall understanding of palaeoclimatic conditions. In this thesis, sampling is over a wider geographical and

chronological extent. The following arguments show that the Lower Coralline Limestone Formation was deposited in a tropical depositional setting:

i. The palaeolatitude of Malta during the Oligocene was about 27˚ to 29˚N based on works of Dercourt *et al.* (2000) and Schettino & Scotese (2005) (Figure 3.19). This latitude is within the meridional range of modern tropical carbonate factories (Schlager, 2003). This is especially so for the Oligocene when global temperature was higher so that coral expanded to higher latitudes relative to the present. Oligocene coral reefs are recorded at even higher latitudes relative to Malta, e.g., in Apulia (Bosellini, 2006) and Aquitaine Basin (Cahuzac & Chaix, 1996).

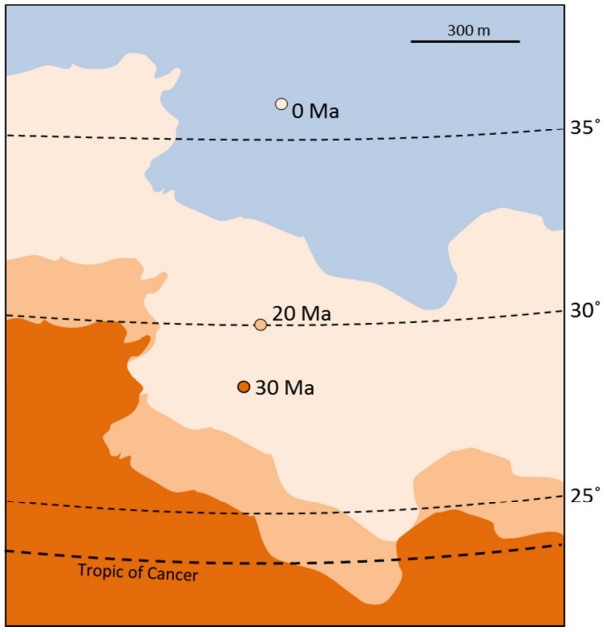

Figure 3.19. Migration of North Africa and Malta: Circle represents position of Maltese Islands from 30 Ma to present (based on Schettino & Scotese, 2005).

ii. Although >80% of the <120 m-thick succession exposed along the southern cliffed coast of Malta and the cliffed coast of western Gozo consist of the rhodalgal biostrome (facies IIb) with skeletal grains associated with non-tropical, cool-water carbonate factories, the occurrence of scleractinian coral and gastropod Strombidae mostly below the rhodalgal biostrome suggests a tropical carbonate factory. The foramol facies (FA III) above the rhodalgal

biostrome also reflects a tropical setting similar to other foramol assemblages in low latitudes described by (Wilson & Vecsei, 2005).

iii. The occurrence of Sporolithaceans in the rhodalgal biostrome (FA IIb) suggests warm environments albeit in deeper water (Aguirre *et al.*, 2000).

iv. The 'energy hypothesis' of Bosellini & Perrin (2007) is actually based on Lower Chattian coral reefs and is too low relative to palaeotemperature indicators in Upper Chattian outcrops of Malta. These indicators include the LBF *Amphistegina* found in FA II and FA III, which in modern environments is known to reproduce only when the temperature is above 25˚C (Adams *et al.*, 1990).

3.4.2 Ecological relationships and trophic level

The biolimiting nutrients phosphates and nitrates control the trophic structure of ecosystems. Consequently, subtropical carbonate ecosystems are either adapted to low nutrient oligotrophic environments or to conditions influenced by a high nutrient flux mesotrophic (Brasier, 1995). The carbonate grain assemblage in modern and ancient sediments reflects trophic level, especially the dependency on light as a source of food. James (1997) classifies carbonate ecosystems into the phototrophic *photozoan* association that thrive in low nutrient environments and low light to light-independent *heterozoan* association found in meso- to eutrophic environments. Biotas in the photozoan association typically show high species diversity, larger body size, slower growth rate ('K-strategy') relative to heterozoan biotas (Brasier, 1995). This is especially the case in LBF and corals (Hallock & Schlager, 1986; Hallock & Glenn, 1986).

Previous works, e.g., Knoerich & Mutti (2003) and Brandano *et al.* (2009) based on the study of only one location in Gozo and Malta respectively, have classified the Lower Coralline Limestone as being entirely heterozoan. This does not reflect the biotas observed in the large number of localities analysed in this study. Table 3-14 shows the classification of facies associations on the basis of trophic level.

Trophic level	*Grain association*	*Facies Association*
	non-marine	**VII:** gypsum
		VI: Red marly carbonates
PHOTOZOAN	chlorozoan	**V** Foraminiferal wackestone/packstone limestone
		IV Coral framestone
	foramol	**III** Large benthic foraminiferal limestone
HETEROZOAN	rhodalgal	**II** Coralline red algal limestone
	bryomol	**I** Micrite-echinoid limestone

Table 3- 14. Facies associations and grain associations.

The Lower Coralline Limestone Formation shows successive changes from photozoan to heterozoan associations which reflects sea-level and nutrient level change. The facies association are described in terms of trophic level:

FA I: the dominance of herbivores and filter-feeders (echinoids, bryozoans and molluscs) and the absence of phototrophic organisms, e.g., coral (except solitary coral) and LBF suggest a heterozoan association adapted to mesotrophic conditions and low light levels. The accumulation of phosphorite suggests an increase in nutrient levels resulting in eutrophic conditions.

FA II: The dominance of coralline red algae in the rhodalgal biostrome and the absence of coral, accompanied by the decline of LBF genera suggest that conditions were not advantageous for phototrophic organisms during the deposition of this facies. Coralline red algae in modern tropical environments are generally associated with mesotrophic environments and do not develop under shallow water, oligotrophic conditions (Halfar *et al.*, 2004). In modern heterozoan carbonate ecosystems the fouling of corallines by fleshy algae can cause stress, although the area occupied by fleshy algae can be significantly reduced by the activity of herbivores such as echinoids. There is an association between coralline algae and echinoids which reduces fouling and allows coralline algae to thrive in modern environments (Steneck, 1986). The FA II carbonate grain association dominated by coralline algae invariably includes echinoid bioclasts which suggests a symbiotic relationship between rhodoliths and echinoids that allowed coralline algae to flourish in otherwise stressed mesotrophic environment.

In mesotrophic environments, the depth of light penetration is reduced as a result of abundant planktonic algae. Coralline red algae are restricted to those parts of the seabed reached by light so that the occurrence of abundant planktonic algae decreases the depth limit of the rhodalgal facies IIb dramatically. The suggested maximum depositional depth of 40 m is within a proximal mid-platform setting where there is sufficient light and current velocity to winnow mud that would otherwise bury slow-growing rhodoliths.

Present day rhodoliths in the transparent, oligotrophic water of the Mediterranean are found at depths of 50 to 100 m and include *Amphistegina* re-sedimented from maerl and sea grass environments in shallower water (Carannante *et al.*, 1988). Around present day Malta, rhodoliths are also found at these depths (Gatt, 2007), mostly within 51 to 91 m (Sciberras *et al.*, 2009). Figure 3.20 shows the relationship between light penetration and nutrient level and the range of depth of modern rhodoliths in Malta along the seabed where light penetration in moderately oligotrophic environments is reduced to around 4% at depth of 90 m (Hallock, 1988). When the modern depth range of rhodoliths is transposed to the photic parameters of mesotrophic environments, the depth range reduces to <40 m if

rhodoliths are to receive the same level of light as extant examples. Rhodolith growth in water deeper than 40 m within mesotrophic environments would have been unlikely.

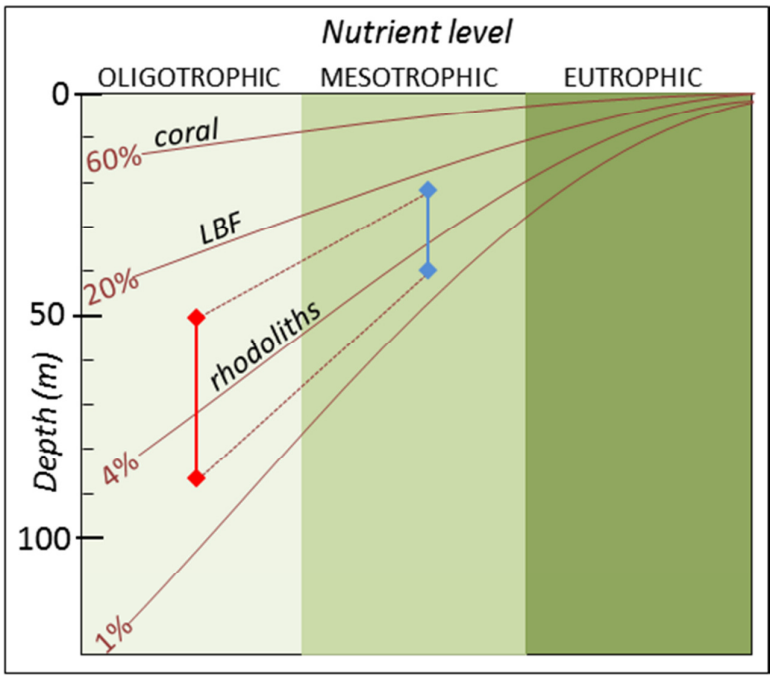

Figure 3.20. Diagram showing relationship between depth, light (curves show penetration of % of midday light intensity) and nutrient level (partly based on Hallock, 1988). Vertical red bars shows depth range of modern rhodoliths in oligotrophic conditions around Malta from which the depth of Oligocene rhodoliths of FA IIb in mesotrophic conditions is tentatively extrapolated (blue vertical bar). Coral growth is mostly found in oligotrophic environments where 60% of midday light reaches the seabed at 15 m depth.

FA III and IV: Corals and large benthic foraminiferans share similar environmental parameters. Most reefal zooxanthellate corals are found at depths of <15 m (Schlager, 1981) within the euphotic zone where midday light penetration reaches 60% (Hallock, 1988) (Figure 3.20). Light is essential to algal symbionts hosted by coral that provide them with energy. The survival of coral is also linked to competitors such as fleshy algae which can displace coral. Fleshy algae and planktonic algae increase in density with increased nutrient level and in so doing reduce light reaching the seabed. As a result, coral growth is mainly restricted to nutrient deficient environments and transparent water (Hallock & Schlager, 1986). Large benthic foraminiferans that host symbionts also require light for survival.

Phototrophic organisms like coral and LBF produce a photozoan grain association in the geological record that reflects oligotrophic environments.

FA V: The occurrence of small coral patch reefs is indicative of organisms that relied on photosymbiosis in shallow marine, oligotrophic environments. However, miliolids are common in this facies and not thought to be symbiont-bearing but generally considered as evidence for restricted lagoonal or relatively nutrient-rich environments (Geel, 2000). Nutrient level may have been locally elevated within the lagoonal setting as a result of seagrass accumulation and decay. This is reflected by the colonization by small coral patch reefs of storm bed surfaces cleared of seagrass in locality 5. Therefore, the sea is considered to have been oligotrophic with localised high level of nutrients in restricted, very shallow marine areas.

3.4.3 Recognition of carbonate platform type from facies

Carbonate platform morphology may vary from rimmed shelf to ramp depending on several factors that influence platform geometry including antecedent topography, synsedimentary tectonics, prevailing currents and carbonate framework builders (Read, 1985; Tucker & Wright, 1990; Bosence, 2005). The seven facies associations are compared to the nine standard facies zones of Wilson (1975) which were intended to describe rimmed platforms. The Malta Platform shows a reduced number of facies shown in (Table 3-15) deposited across four broad depositional belts: (1) inner-platform facies comprising peritidal mud (FA VI) or gypsum (FA VII) and the subtidal massive foraminiferal wackestone/packstone (FA V), coral rudstone and framestone (FA IV); (2) the exposed inner platform environment where high energy banks and shoals (FA III) developed; (3) the mid-platform facies dominated by coralline red algal rhodolithic boundstone (FA II) and; (4) the outer platform, molluscan and bryozoan mudstone/wackestone (FA I).

Facies Association	Facies Zone *sensu* Wilson (1975)		Carbonate Platform setting	Microfacies & sediments
I	**FZ 2** below SWB		Open sea shelf	Carbonate (skeletal wackestone), minor plankton
IIb	above FWWB	**FZ 4**	Slope	Pure carbonates, mud to rubble, floatstone, slumping
IIa/III		**FZ 6**	Sand shoal of platform margins	Clean lime sands, well-preserved cross-bedding
IV		**FZ 7**	Platform interior	Lime mud, sand, biostromes, shallow water benthos
V				
VI		**FZ 8**	Restricted platform interior	Lime mud, early diagenetic cement, terrigenous influx

Table 3-15. Facies associations compared to facies zones of Wilson (1975).

Many organisms can only survive within certain depositional depth range that reflects environmental parameters related to light and temperature. The depositional depth of biota within facies is shown graphically in Figure 3.21 along the log scale for depth in relation to depositional environments from inner to outer platform.

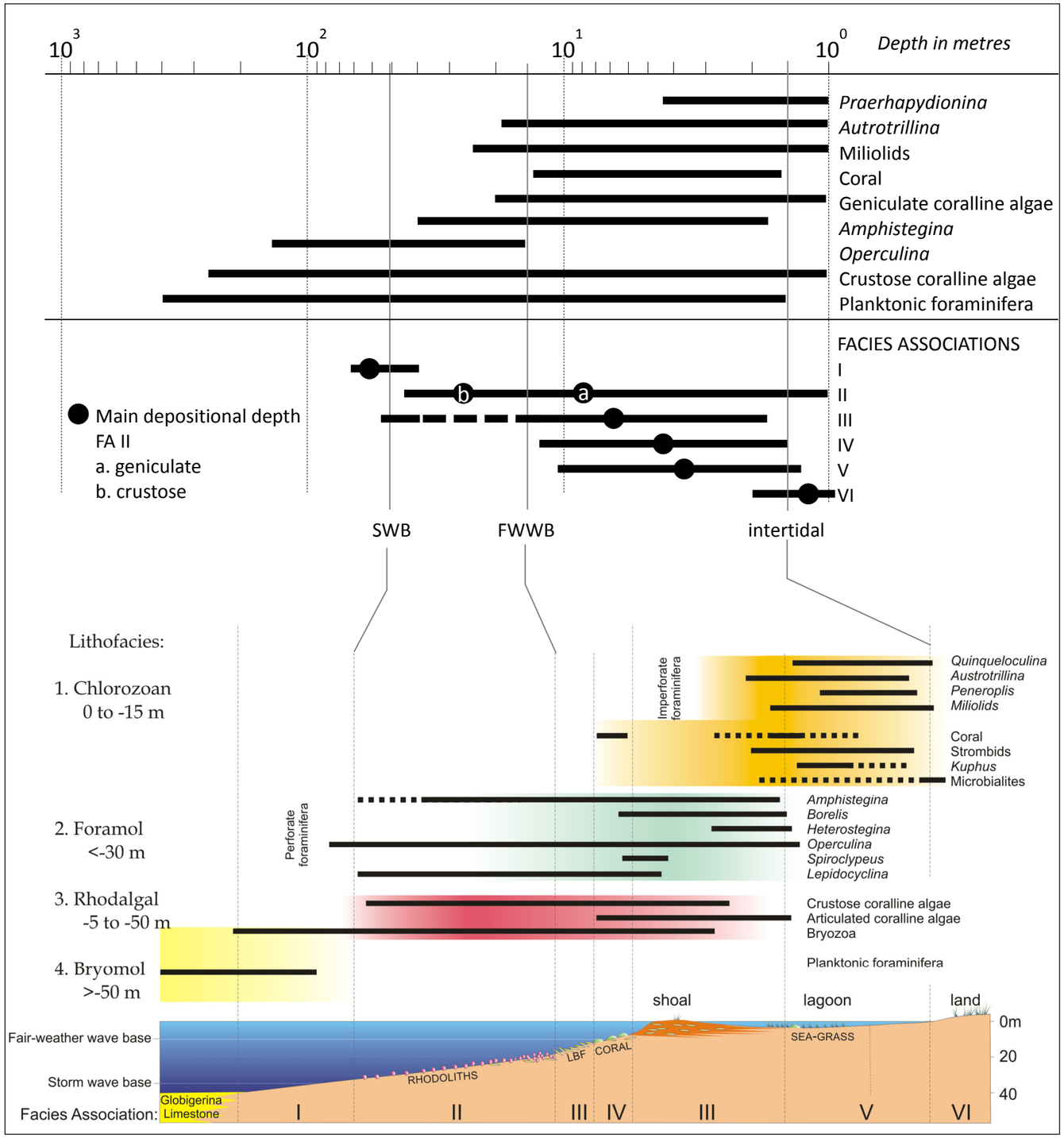

Figure 3.1. Common depositional depth range of carbonate biotas (depth in log scale): Miliolid foraminiferans (Geel, 2000), coral reefs (Schlager, 1981) and coralline algae (Wray, 1977;Bosence, 1983) compared to facies associations in the Lower Coralline Limestone of Malta and their depth relative to estimated fair-weather wave base (FWWB) and storm wave base (SWB). The platform model is a hypothetical representation of the carbonate platform.

3.5 SUMMARY

Seven facies associations (FA) are identified in the Oligocene carbonates of the Lower Coralline Limestone Formation. The three main carbonate grain producers are coralline red algae, large benthic foraminifera and coral. The FA generally form a succession starting with micrite-dominated wackestone to packstone associated with restricted, inner platform (lagoonal) environments, succeeded by packstone and boundstone textures produced by coralline algal sand sheets and a ubiquitous <60 m thick rhodalgal biostrome, terminated by packstone to grainstone produced by coarse-grained, high energy foraminiferal shoal/bank, which was later draped by deep marine micritic pelagic limestones. The depositional setting is that of an isolated carbonate platform free from the influx of continental siliciclastics, influenced by periodic emergence and palaeosol formation. Despite the isolation of the Malta Platform, its carbonate ecosystems were modified by varying levels of biolimiting nutrients ad relative sea-level. This is reflected in changes in the trophic level of successive carbonate ecosystems that alternate between photozoan and heterozoan carbonate grain associations.

Chapter 4

Diagenesis and carbonate reservoir porosity of the Palaeogene Malta Platform

4.1 INTRODUCTION 106
4.1.2 Diagenesis 107
4.1.3 Stable isotopes 109
4.2 METHODS 111
4.3 DIAGENETIC ENVIRONMENTS IN THE MALTA PLATFORM 113
4.3.1 Diagenetic surfaces identified by isotopic values and cement 113
4.3.2 Diagenesis in facies associations 119
4.3.3 Diagenetic indicators of palaeo-oxygenation 128
4.3.4 Diagenesis in Mesozoic to early Palaeogene carbonates 129
4.3.5 Burial stress and diagenesis 134
4.4. DIAGENETIC HISTORY AND POROSIT DEVELOPMENT 137
4.5. SUMMARY 140

4.1 INTRODUCTION

This chapter is a comprehensive description and interpretation of porosity and diagenetic features recognised in petrographic thin-sections of the Lower Coralline Limestone Formation. The relative time relationships (paragenetic sequence) of events that have affected sediments and porosity evolution are discussed in the context of carbonate platform development. The objectives of this chapter are to analyse porosity development in the Malta Platform using stable isotopes and diagenesis in order to: (1) identify surfaces that show particular diagenetic and stable isotope characteristics which are different from the rest of the succession, (2) shed light on depositional environments during the deposition of facies associations and (3) analyse the effect of diagenesis on carbonate reservoir potential.

Sedimentation and lithification in carbonate platforms consists of two consecutive and partly over-lapping stages that ultimately control the amount and type of porosity (φ). Primary porosity forms during the first stage and is partly controlled by taphonomy which encompasses the death and accumulation of carbonate-secreting organisms and their post-mortem modification along the seafloor (Kidwell & Bosence, 1991). The process partly depends on the level of palaeo-oxygenation, although all sediment pore water will eventually become anoxic (Allison, *et al.*, 1995) and seawater chemistry that influences the type of carbonate grain. Secular changes in seawater chemistry, principally pCO_2 and the Mg:Ca ratio affected hypercalcifying organisms. During the Early Palaeogene, the main hypercalcifying organisms were large benthic foraminifera (LBF) formed of low magnesium calcite (LMC). The increase in the global Mg:Ca ratio of seawater during the Oligocene favoured scleractinian corals formed of metastable aragonite and high magnesium calcite (HMC) coralline red algae (Stanley & Hardie, 1998). Coralline algae, LBF and coral are the main carbonate producers in the Lower Coralline Limestone Formation.

The second stage encompasses diagenesis. It begins at the seafloor and continues during burial and includes occlusion of primary porosity by mineral precipitation as

well as possible increases in porosity caused by grain and cement dissolution. Meteoric water may cause dissolution during this stage. Porosity development in the Malta Platform can be understood by evaluating two processes:

4.1.2 Diagenesis

Diagenesis encompasses the processes that affect sediments after deposition until metamorphism, reviewed in Bathurst (1975), Tucker & Wright (1990) and Moore (2001). It is one of the fundamental controls on carbonate reservoir porosity and includes six major processes: cementation, microbial micritisation, neomorphism, dissolution, compaction and dolomitization (Tucker & Wright, 1990). Diagenetic processes occur in different environments: the near-surface meteoric, marine and burial environments shown in Figure 4.1.

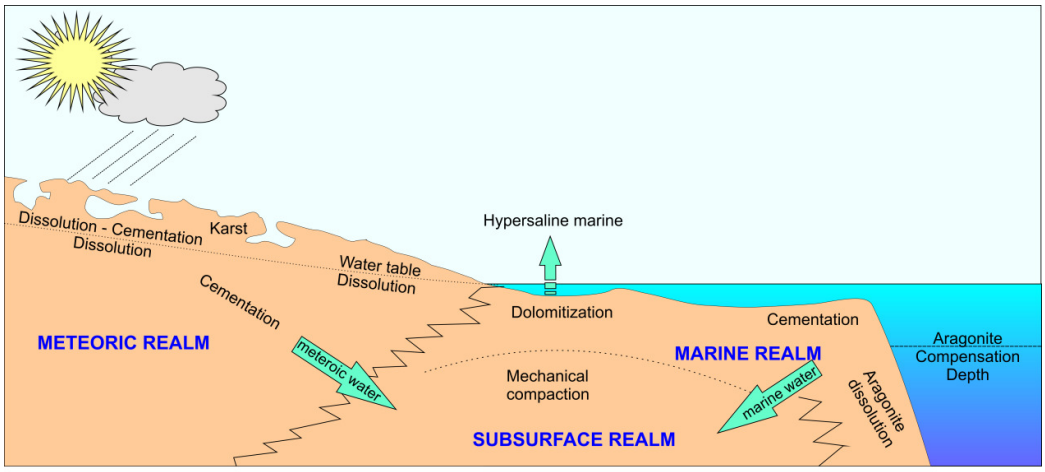

Figure 4.1. Diagenetic environments along a carbonate platform (from Moore, 2001).

There are a number of tools that can be used to determine diagenetic environment (Moore, 2001):

- The morphology of calcite cement crystals and their distribution
- Compaction of grains
- Micritization by biological borers.
- Stable isotopes of carbon and oxygen.
- Trace element geochemistry (Fe and Mn) using cathodoluminescence microscope.

Cement types identified in the Lower Coralline Limestone include fibrous, bladed, epitaxial and blocky calcite cements. Seawater chemistry determines whether marine cements precipitate as either fibrous crystals or microspar (micrite). However, in environments that were dominated by lime mud, it is impossible to resolve marine cement (micrite) from the original lime mud. Although fibrous cements may form under variable levels of Mg, the Mg^{2+} ions in seawater are thought to poison the calcite lattice and inhibit growth on all faces except the c-axis producing acicular cement (Tucker & Wright, 1990).

4.1.2.1 Meteoric diagenesis

The meteoric environment comprises the zone of sediment or rock affected by undersaturated meteoric freshwater within the vadose and phreatic zones. The phreatic zone is found in the water-table lens whereas the overlying vadose zone contains both water and air which can contain soil-derived CO_2 and organic acids (Moore, 2001). The aquifer is also a zone of mixing of meteoric-marine water characterised by increased diagenesis. Phreatic and vadose environment produce particular diagenetic imprint related to either the dissolution of carbonate or the precipitation of blocky equant cement with a meteoric isotopic signature.

4.1.2.2 Marine diagenesis

Marine diagenesis occurs just below the seafloor and includes biological borings by organisms that result in micritization and abiogenic precipitates where the seafloor is regularly flushed by seawater. Marine cements usually consist of isopachous rims and micron-sized equant crystals (micrite) (Tucker & Wright, 1990).

4.1.2.3 Burial diagenesis

Burial stage of diagenesis can result in either the increase or decrease of porosity. Burial environments are characterised by increased temperature (geothermal gradient) and higher pressure (lithostatic and hydrostatic pressure) that results in compaction and fracturing whereas diagenetic fluids are cut off from free exchange with active gases of the atmosphere (O_2 and CO_2).

4.1.3 Stable isotopes

The most abundant stable isotopes of oxygen (^{18}O and ^{16}O) and carbon (^{13}C and ^{12}C) assist in the interpretation of sedimentary and diagenetic conditions (Marshall, 1992; Allan & Matthews, 1982). Isotopic values are reported as the per mil (‰) difference in delta (δ) notation between isotope ratios in the sample and those in the Cretaceous Pee Dee Belemnite (PDB) Formation (South Carolina, USA) which is the international standard that by definition, has $\delta^{18}O$ and $\delta^{13}C = 0‰$ (Moore, 2001). The standard mean ocean water (SMOW) is the water standard defining the isotopic composition of water and can be derived from PDB using the formula:

$$\delta^{18}O_{SMOW} = 1.03\ \delta^{18}O_{PDB} + 30.86$$

4.1.3.1 Oxygen stable isotopes

Two processes affecting the oxygen stable isotope ratio are used to interpret the rock record:

1. Oxygen stable isotopes are used as palaeoclimate indicators. The changes in ocean stable isotope values are recorded in the calcitic tests of deep sea benthic foraminifera. Deep sea water temperature was assumed to be stable and consequently, variations in $^{18}O/^{16}O$ isotopic values of deep seawater reflect the relative increase in sequestration of lighter oxygen isotopes by ice sheets (Shackleton, 1967). However, deep sea temperature has varied through time and this affects isotopic fractionation between ocean water and the oxygen in the crystalline carbonate, e.g., pre-Middle Miocene ocean was *circa* 0.9‰ more negative than the present day (Shackleton & Kennett, 1975). Despite problems related with diagenetic alteration of $\delta^{18}O$ and recrystallization, there is a general consensus that $^{18}O/^{16}O$ isotopic values from the tests of deep sea benthic organisms are a proxy for global ice volume (Abreu & Haddad, 1998). Consequently, deep sea benthic foraminifera provide the most complete stratigraphic record of ice volume and sea-level change, e.g., when $\delta^{18}O$ = *circa* 2.5‰, the permanent ice sheets are about 50% the size of the present day Antarctic ice sheet (Zachos, *et al.*, 2001). Therefore, positive excursions in the oxygen stable isotope record should correspond to falls in sea-level which would result in erosional events on passive margins. Sequence boundaries produced

during maximum regressive events should correlate with increased $\delta^{18}O$ in deep water benthic foraminifera (Abreu & Haddad, 1998). Landmarks in oxygen isotope values include the Eocene-Oligocene boundary marked by an increase of 1‰ which Zachos, *et al.* (1992) attribute to ice-volume enlargement to almost Pleistocene levels (Figure 4.2a).

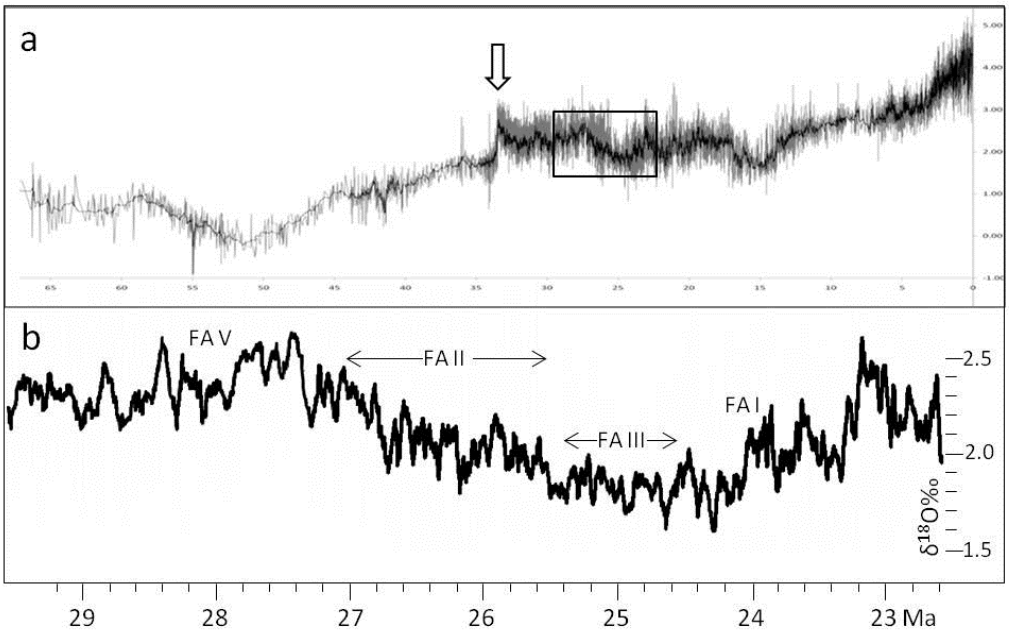

Figure 4.2. (a) The global deep sea oxygen isotope curve from Zachos, *et al.* (2008). Black curve shows that average values. White arrow marks the Eocene-Oligocene boundary at 33.9 Ma. Inset shows the oxygen isotope curve for the Oligocene succession exposed in Malta; (b) Inset expanded and showing facies associations that were predominant over the Malta Platform.

2. The isotopic signal at the local scale may be affected by evaporation of water in restricted basins where it cannot be replenished by influx of ocean water. This produces the preferential fractionation of the lighter isotope in the vapour phase resulting in high $\delta^{18}O$ values in any calcite that precipitates from the remaining water. The nearshore and onshore areas are also affected by the influx of meteoric water that lower $\delta^{18}O$ values (Allan & Matthews, 1982), indicating a sea-level fall that marks subaerial exposure. Variance in isotopic values is great both just below and above subaerial exposure due to a number of factors, e.g., reworking of sediments, so that variance instead of mean values can be a better test for surfaces of exposure (Theiling, *et al.*, 2007).

4.1.3.2 Carbon stable isotopes

The global $^{13}C/^{12}C$ stable isotope values derived from deep sea benthic foraminifera reflect the interaction between the two global carbon reservoirs: The oxidized global carbon reservoir that includes carbon dioxide (pCO_2) gas, HCO_3^{2-} and carbonates, whereas the reduced carbon reservoir comprises organic compounds (CO_2 fixed by photosynthesis), fossil fuels and native carbon (Tucker & Wright, 1990). The exchange between the two global carbon reservoirs and carbon cycling involves carbon fractionation. An increase in organic productivity in oceans reduces the level of $\delta^{12}C$ which is preferentially taken up by photosynthesis and results in more carbon burial. The level of inorganic carbon dissolved in the world's oceans is linked to the rate of organic carbon burial and silicate weathering (that reduces pCO_2) which depends on the silicate exposure area. This is imprinted on the carbon isotopic composition of the ocean, reflected in the level of $\delta^{13}C$ in benthic organisms.

On the local scale, the meteoric diagenesis in limestone results in a negative carbon isotope excursion (0 to -10 ‰) caused by isotopically light soil gas (CO_2) especially under humid conditions, becoming enriched in ^{13}C with increasing depth beneath the subaerial surface (Allan & Matthews, 1982).

4.2 METHODS

Methods used were a combination of thin sections and chemostratigraphy:

1. Over 80 thin sections were examined under transmitted light microscopy to determine cement and porosity. Porosity is classified according to Choquette & Pray (1970) that sub-divides pores into fabric selective pores defined by elements such as grains or crystals, whereas non-fabric-selective porosity cross-cuts the actual fabric of the rock (Figure 4.3).

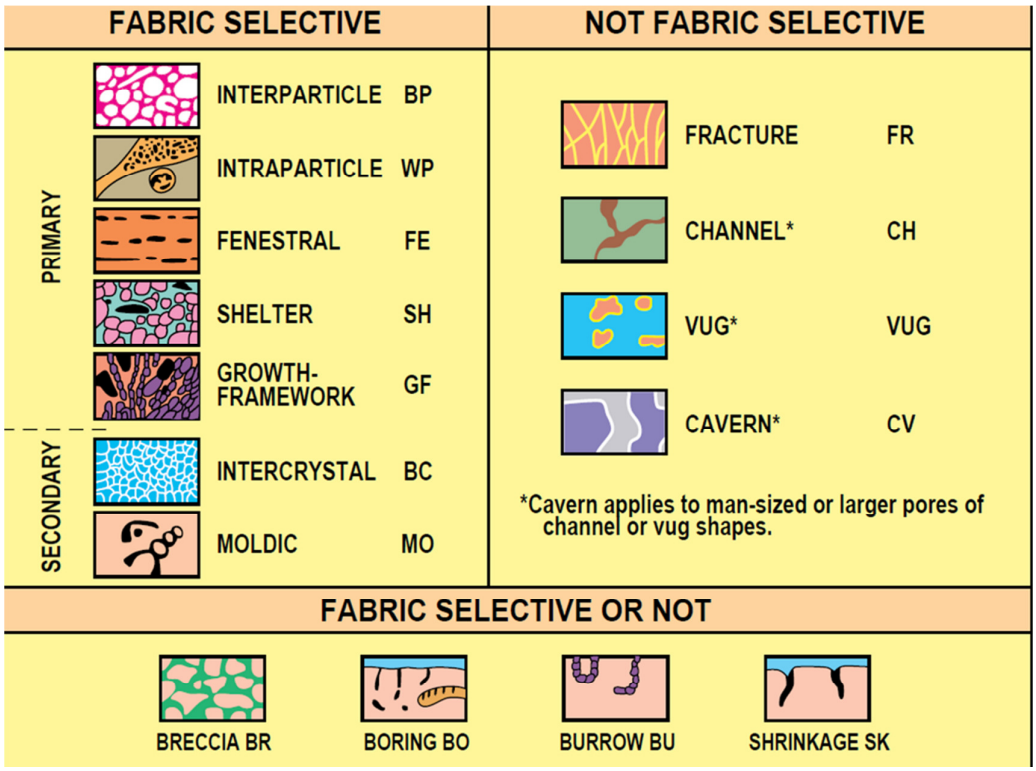

Figure 4.3. Porosity classification by Choquette & Pray (1970). Primary porosity is fabric selective.

2. Oxygen and carbon stable isotope values were derived from bulk rock samples in published (Knoerich & Mutti, 2003) and unpublished (Gatt, 1992) sources.

3. Level of palaeo-oxygenation was assessed by:

   a. Cathodoluminesce microscopy was used to assess the bright cathodoluminescence of sediments produced by manganese reduction associated with slow decay of organic matter in suboxic environment (ten Have & Heijnen, 1985).

   b. Colour of outcrop: the level of palaeo-oxygenation is reflected in the different colours of the facies associations in outcrop which are related to the presence of small amounts of oxidised iron (Fe^{3+}) in the carbonates. Oxic environment produce ferric minerals with a reddish colour.

4.3 DIAGENETIC ENVIRONMENTS IN THE MALTA PLATFORM

The Oligocene limestone exposed in the Maltese Islands was affected by all the major diagenetic processes. The outcrops of the Lower Coralline Limestone Formation are sub-divided by four laterally persistent surfaces of Chattian (CH) age characterised by calcite spar cements (usually found around very shallow marine biotas), early dissolution of metastable grains and covariance of carbon and oxygen negative excursions along these surfaces. Diagenetic characteristics of the formation are shown in (Figure 4.4). In contrast, Eocene limestone and evaporites were affected by dolomitization and large-scale, non-fabric selective dissolution formed by under-saturated meteoric water.

4.3.1 Diagenetic surfaces identified by isotopic values and cement

At locality 1 in Gozo Island, bulk $\delta^{18}O$ range from -0.5‰ to -3.3‰ whereas $\delta^{13}C$ vary between 0.3‰ and -2.5‰ (Knoerich & Mutti, 2006). When isotopic values vary through time, they may reflect the precipitation of $CaCO_3$ under different environments. Meteoric cements show a distinct carbon and sometimes oxygen isotope signature. Cement precipitated by meteoric water is associated with negative $\delta\ ^{13}C$ stable isotope values in the range of -10 to +3 $\delta^{13}C$ as a result of the mixing of isotopically depleted soil gas (-20 $\delta\ ^{13}C$) with meteoric water that carries less depleted CO_3^{2-} ($\delta^{13}C$ = 0 to +5) derived from limestone dissolution (Allan & Matthews, 1982). Farther away from the vadose soil gas reservoir, the $\delta^{13}C$ values increase as the proportion of isotopically heavy carbon derived from the dissolution of limestone increases. Oxygen isotope values in subaerial environments are influenced by isotopically lighter rainwater relative to seawater, although values are strongly latitude dependent and $\delta^{18}O$ may range from -2 to -20‰ (Moore, 2001). However, meridional shift by tectonic drift of the Maltese Islands was <2° latitude throughout the Oligocene.

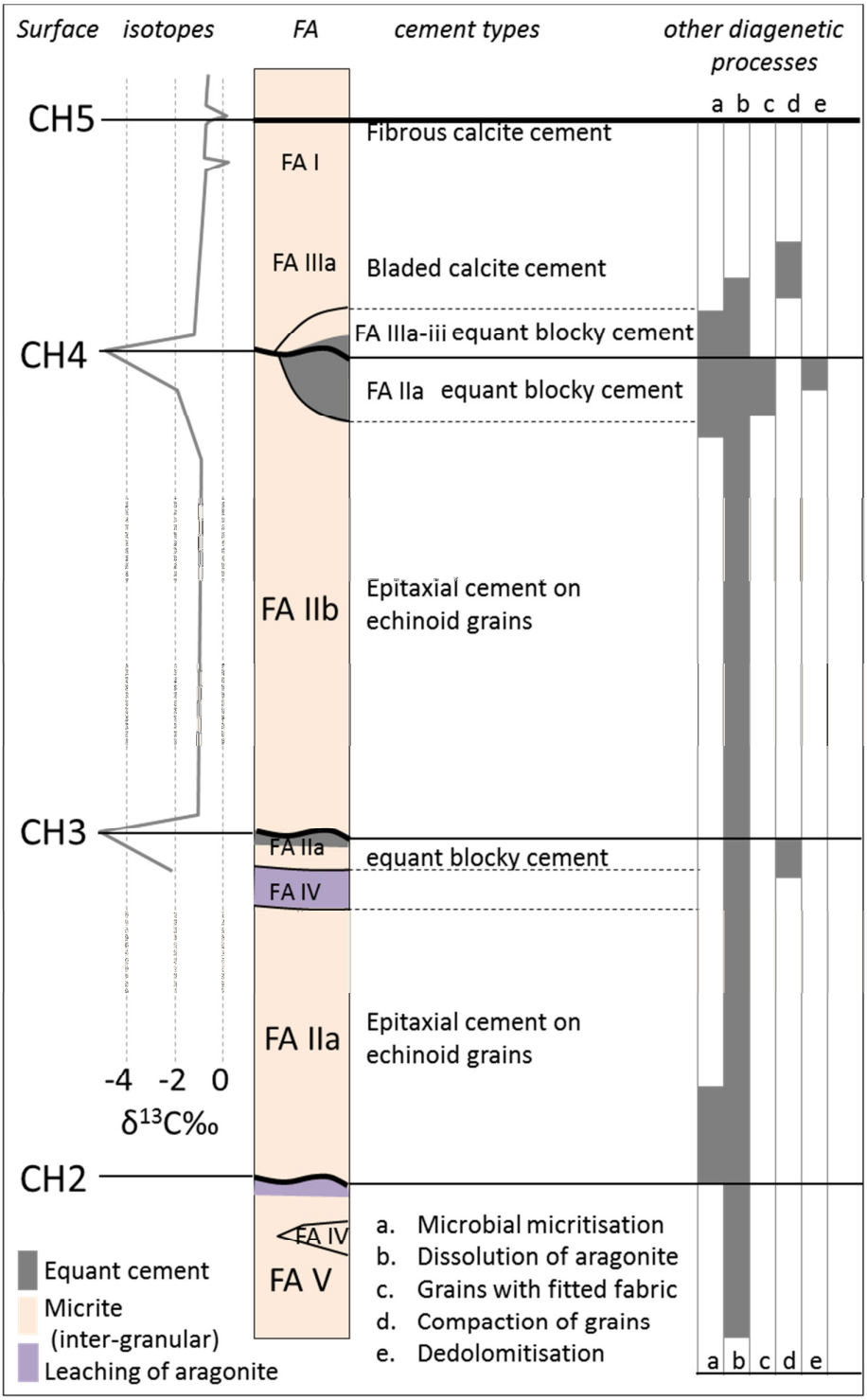

Figure 4.4. Generalised stratigraphy of the Lower Coralline Limestone Formation in outcrop and levels affected by different diagenetic processes. The carbon isotope curve shows the average trend of $\delta^{13}C$ ‰ and main excursions along the log based on Knoerich & Mutti (2006) and Gatt (1992).

Clear blocky calcite cement observed in thin section from along surfaces CH2, CH3 and CH4 suggests the precipitation of calcite within the meteoric lens that is permanently saturated that may extend to several tens of metres below the surface (Tucker & Wright, 1990). Syntaxial overgrowths of echinoid fragments are also common. In both cases, the source of calcite is the dissolution of aragonite in shallow burial conditions. Surface CH5 differs from the other surfaces and is associated with marine fibrous cements along the terminal hardground at the top of the Lower Coralline Limestone. The surface also shows an oxygen isotope excursion to -0.5 ‰ (see Figure 4.6) along the boundary with the overlying Globigerina limestone Formation.

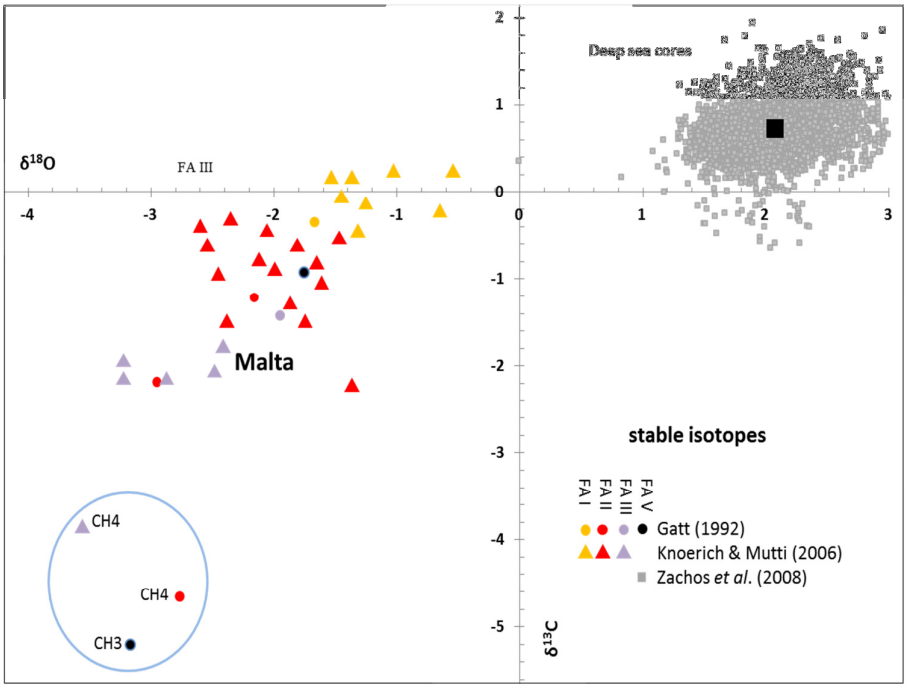

Figure 4.5. Isotope values of bulk rock samples of facies associations I to V from Gatt (1992) for localities 5, 8, 10b, 13 and 14 and from Knoerich & Mutti (2006) for locality 1 compared to global isotope values from deep sea cores (Zachos *et al.*, 2008) for the Chattian (28.4 to 23 Ma). Black square is the average global value. The blue circle comprises samples found along surfaces CH3 and CH4 which are characterised by significant negative $\delta^{13}C$ excursions that reflect the influence of meteoric water and soil gas. The remaining samples show higher isotope values interpreted as influenced by marine diagenesis.

Bulk rock samples from numerous localities show $\delta^{13}C$ and $\delta^{18}O$ values that are higher than samples taken from CH3 and CH4 surfaces (Figure 4.5). Systematic sampling of bulk rock for $\delta^{18}O$ and $\delta^{13}C$ stable isotope values at locality 1 by Knoerich & Mutti (2006) and at locality 14 by Gatt (1992) (results shown in Table 4-

1) confirm that most of the samples have isotope values in the range shown in Figure 4.5, except at the two successive surfaces CH3 and CH4 where isotope excursions of <-3‰ are recorded (Figure 4.6):

1. Surface CH4: A distinct negative isotopic excursion of <-3.3‰ for $\delta^{18}O$ and -4.2‰ for $\delta^{13}C$ in locality 1. The negative isotopic values persist in the succeeding 5 m of cross-bedded LBF packstone and grainstone (FA III).
2. Surface CH 3: A negative isotopic excursion of -2.2‰ and -5.2‰ for $\delta^{13}C$ in localities 1 and 14, respectively. However, the carbon isotopic perturbation is not accompanied by a significant shift in the $\delta^{18}O$ values along this surface.

Facies/surfaces	Height a.s.l.	$\delta^{13}C$‰	$\delta^{18}O$‰	$\delta^{18}O_{SMOW}$*
Facies IIb	37 m	-4.657	-2.766	28
CH3	12 m	-5.2	-3.164	27.599
Facies IIa	5 m	-2.181	-2.952	27.817

Table 4-1. Isotopic values for samples from locality 14 (Gatt, 1992). The CH3 surface at this locality consists of a micritic bed with dense accumulation of *Kuphus*.

Although single samples along vertical stratigraphic horizons may fail to detect an excursion in a geochemical indicator, the negative excursions in $\delta^{13}C$ along surfaces CH4 and CH3 in locality 1 and 14 separated by 40 km suggest a platform-wide isotopic perturbation. Negative $\delta^{13}C$ values result from the input of $\delta^{12}C$-rich carbon from respiration and decay of photosynthesising plants growing on the land surface and contact with isotopically lighter groundwater and soil that could only occur during periods of emergence of the carbonate platform (Allan & Matthews, 1982). The positive covariance of $\delta^{13}C$ and $\delta^{18}O$ values observed in also suggests enrichment of ^{16}O by rainfall and enrichment of ^{12}C as the meteoric water passes through soil. The negative isotopic excursions are interpreted as subaerial surfaces.

The variance in $\delta^{13}C$ values along surface CH4 to ±5 m around this surface is normally associated with sequence boundaries and can be imparted by subaerial sediment reworked with transgressive lags (Theiling, et al., 2007). The increase in geochemical variance supports microfacies data from samples from localities 1 and

10b just above surface CH4 that show coralline algae influenced by subaerial exposure, reworking and mixing with post-exposure LBF (FA III) during the ensuing transgression (discussed in section 4.3.2.2). These subaerial episodes also enhanced porosity by the action of meteoric water that dissolved the aragonitic components consisting mainly of bivalves and corals.

There is a shift to lower $\delta^{18}O$ values along CH4 and in the overlying facies association III which is dominated by LBF. This could reflect the ability of some foraminifera to fractionate oxygen isotopes (Adams, *et al.*, 1990). However, it is likely that the drop in $\delta^{18}O$ values during the deposition of FA III reflects the global fall in $\delta^{18}O$ (Figure 4.2b). Oxygen isotope values in locality 1 begin to rise during the deposition of FA I and the Globigerina Limestone in covariance with the global curve. This shows that despite the influence of local influx of meteoric water and evaporation, the overall trend in oxygen isotope values in Malta follows the average global trend.

The sediments in locality 1 and 14 found in between but not along surface CH2, CH3 and CH4 show a $\delta^{18}O$ isotopic signature with an average range of -3 to -1.5‰. Relative to the three surfaces, these values are higher and closer to the $\delta^{18}O$ in marine cements. The $\delta^{18}O$ of modern marine cements is typically -0.5 to +3‰ (Tucker & Wright, 1990) and generally in equilibrium with that of seawater, where isotopic values may vary with temperature and evaporation due to fractionation affects. Although global Chattian isotope values for marine sediments are much higher than those recorded in Malta which consist mostly of negative values (Figure 4.5), these sediments are interpreted as being influenced by marine diagenesis. The low isotopic values relative to typical global Chattian marine values reflect either a low rate of sea water evaporation (unlikely in the lower mid-latitude Tethys) or the influence of meteoric water that resulted in the influx of isotopically lighter seawater in shallow marine carbonate environments.

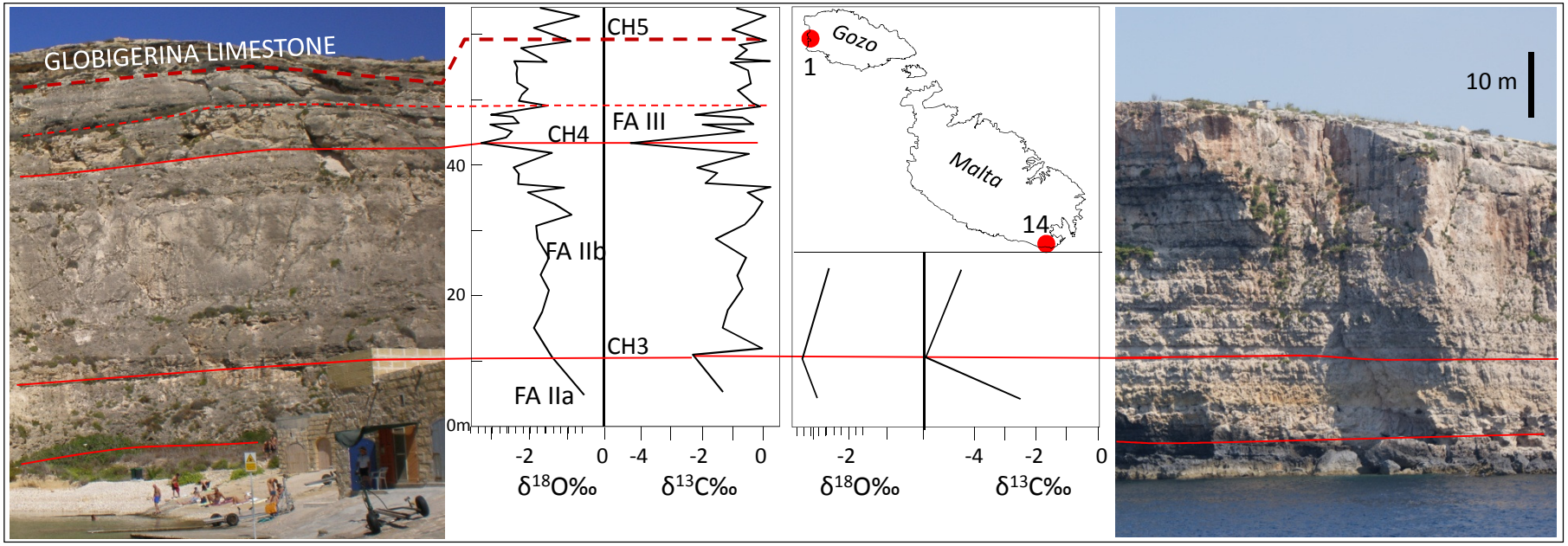

Figure 4.6. Photograph of sampled localities 1 (from Knoerich & Mutti, 2006) and 14 (from Gatt, 1992). The $\delta^{13}C$ minima occur along SbCH3 in locality 1and in locality 14 ($\delta^{13}C‰$ = -5.2).

4.3.2 Diagenesis in facies associations

The late Palaeogene carbonate grains and cements in facies association I to VI have retained a considerable proportion of their original fabric. The type and mineralogy of cement was controlled by the increasing levels of Mg^{2+} during the Palaeogene that favoured the precipitation of HMC calcite and aragonite as the main cement mineralogy (Stanley & Hardie, 1998), although aragonite is not expected to remain preserved. Cements in the Lower Coralline Limestone show well-preserved crystallographic fabrics that suggests original calcitic mineralogy where the transformation to LMC by dissolution precipitation only altered the chemical composition but not the crystal fabric. The preservation of original fabrics permits the recognition of diagenetic environments associated with particular facies.

4.3.2.1 Facies Association I

The bulk of the sediments consist of micrite and the occurrence of planktonic foraminifera suggests environments >50 m deep that remained subtidal. The source of micrite is unknown but the most likely source is shelf mud that was resedimented in deeper outer platform environments. Dewatering of these muds by compaction would lead to significant loss of porosity, usually a reduction to 40% or less (Enos & Sawatsky, 1981). This level of porosity is within the range 30 to 40% porosity in Globigerina Limestone (Wardell-Armstrong, 1996). The topmost sediments of this facies forms the CH5 surface which is very well cemented with fibrous cement at locality 1 (Knoerich & Mutti, 2003) and forms the terminal hardground capping the Lower Coralline Limestone Formation.

4.3.2.2 Facies Association II

The lithology of the coralline red algal biostrome sediments comprises <40% micrite in bulk volume which formed part of the original sediment (lime mud). According to Knoerich & Mutti (2003) the level of calcite cementation in facies association (FA) II is very low (1 to 2%). However, the diagenetic potential of this facies may have been significant. Coralline red algae may contain from 10 to 30% magnesium that is metastable in meteoric environments affected by freshwater. Nevertheless, grains composed of high-magnesium calcite undergo little visible alteration at the light microscope level when converted to low-magnesium calcite (Tucker & Wright,

1990), although the leached Mg^{2+} may favour dolomitization. The following diagenetic processes dominate in Facies Association II:

1. Two processes linked to marine environments are recognised in FA II:

i. Aragonite dissolution: Samples of algal debris packstone from a few metres below the CH3 surface (facies IIa-i) are brightly luminescent when examined under cathodoluminescence microscopy as a result of manganese activation (Figure 4.7a and b). This suggests the accumulation and decay of organic matter which would have increased the level of CO_2. The slightly acidic porewater would cause the very early dissolution of metastable minerals such as aragonite directly on the seafloor.

ii. Sytaxial calcite cement: syntaxial overgrowths over echinoderm fragments are common throughout facies association II (Figure 4.7f). The calcite grows in optical continuity with the echinoid fragment. Knoerich & Mutti (2003) identify two layers of epitaxial cements on echinoid fragments in facies II at locality 1. The first layer is a thin rim (30μm thick), coated with a second, thicker epitaxial cement. Most of the epitaxial cement is clear indicating that microdolomite is absent. The inclusion-free cement suggests a low-Mg precursor (Lohmann & Meyers, 1977) and the dissolution of an aragonitic source. This could have been sourced by the early dissolution of aragonite by the process referred to above in (i). In some cases the epitaxial cement is rounded (Figure 4.7g) which confirms that the early marine syntaxial growth occurred along, or just below the unlithified seabed and was subjected to transport and erosion.

2. Processes linked to meteoric environments:

i. Dolomite crystals have not been observed in outcrop, although rhomb-shaped voids are recognised in thin-section (Figure 4.7c) along the topmost FA II at the interface with FA III (along surface CH 4 in locality 10b) and along some horizons in FA V (locality 5). The shape of these voids suggests the early precipitation of dolomite crystals that were subsequently leached. The formation of dolomite in the meteoric-mixing zone has been rejected (Melim, *et al.*, 2004). Although magnesium can be leached from HMC of red coralline algae, the indirect evidence for dolomite is only found along specific surfaces or in

sediments where coralline red algae are absent (e.g., FA V). It is likely that the process of dolomitization began by the precipitation of calcian dolomite generated by surface evaporative marine conditions that concentrated the source of Mg^{2+}. This protodolomite contains excess calcium and is more soluble than ordered dolomite (Moore, 2001), making it susceptible to subsequent meteoric leaching. Therefore, the formation of dolomite at the top of the rhodolith biostrome (FA II) suggests arid climate and evaporative conditions that favoured the precipitation of dolomite during sea-level fall. Subsequent flushing with meteoric environment along surface CH4 resulted in the leaching of the dolomite. Sediments long this surface in locality 10b also show a fitted fabric that suggests early compaction of grains under the influence of meteoric water that weakened the structure of LBF, making the grains malleable to deformation by overburden pressure.

ii. Meteoric cements: the influence of meteoric water resulted in the precipitation of clear equant blocky calcite spar around algal grains along two surfaces (Figure 4.4): in locality 5, cross-bedded and structureless beds in the uppermost part of facies IIa along the CH3 where coral also occur (Figure 4.7d) and uppermost part of facies IIb along CH4 surface. There is no evidence of any mechanical compaction of grains during the burial of CH3 because sediments were already consolidated by early cementation. The blocky calcite cement that surrounds each grain does not show geopetal fabric typical of vadose environment. The cement is interpreted as having been precipitated in the freshwater phreatic environment when the algal/foraminiferal sands deposited in shallow marine environment (<3 m depth) occasionally emerged during episodes of falling sea-level. Intergranular porosity in these beds tends to be high and can reach 20%.

3. Compaction: Burial in the Lower Coralline Limestone remained relatively shallow and consists of <300 m of Miocene overburden sediments. Three process of compaction are observed:

   i. Algal grains in facies IIa with early isopachous cement that was involved in compaction (Figure 4.7e).
   ii. The oblate to prolate shape and loose packing of geniculate corallines in grain-supported facies IIa resulted in fewer point contacts between the algal

debris grains that concentrated stress at few points. When point contact occurs mid-way along an elongated geniculate algal grain (facies IIa), tension cracks developed prior to lithification (Figure 4.7e).

iii. Evidence of compaction is not common in the rhodolithic sediments (facies IIb) because most of the >2 cm-wide rounded and spherical coated grains (rhodoliths) could slide past each other when compacted by early burial prior to marine lithification. Rare examples of pressure solution occurs at the top of FA II at locality 14 where an echinoid fragment coated by epitaxial cement is lodged into coralline algal grains (Figure 4.7h).

4.3.2.3 Facies Association III

Compaction and cementation are the main diagenetic processes affecting FA III. Diagenetic features vary according to facies:

Facies IIIb: Clear fibrous cement is common around large benthic foraminiferans just above surface CH 4 at locality 10b (Figure 4.8a). The inter-granular porosity between fragmented LBF grains facilitated the flow of seawater and the precipitation of marine calcite cement in environments that were relatively shallow and affected by strong currents. Inter-granular porosity was only partly occluded by cementation so that porosity remains high and ranges between 10 to 30%. Subsequent compaction by burial involved the marine cement that now forms the boundary between grains.

Facies IIIa: Fibrous cement rims grains at locality 3. The cement envelopes foraminiferal fragments as well as micrite fragments which could be intraclasts. This suggests reworking and fragmentation in these condensed beds which has disrupted the integrity of both grains and cements.

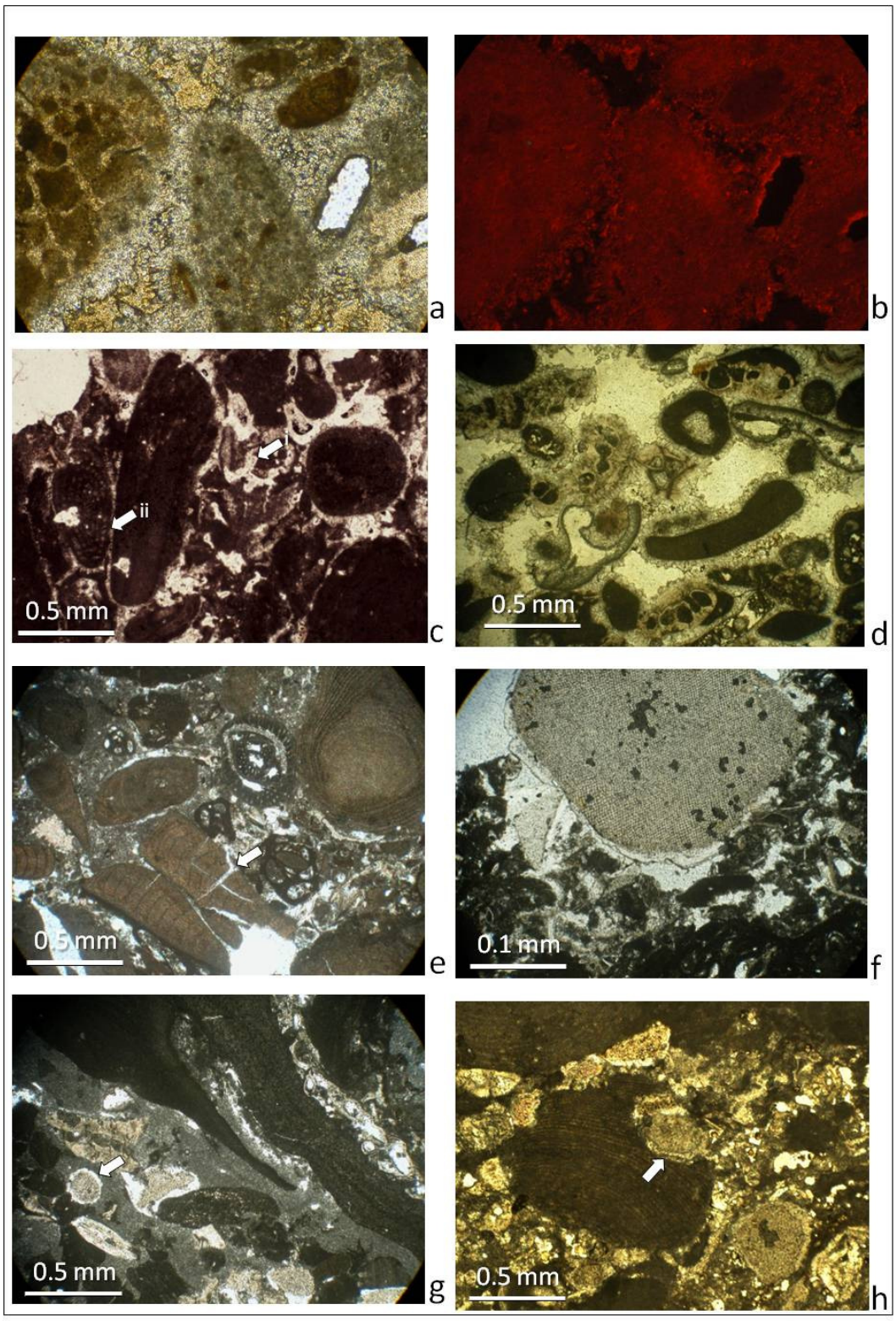

Figure 4.7 (caption next page)

Figure 4.7. Facies association II: (a) Photomicrograph of facies IIa and (b) the same thin section under CL showing bright luminescence especially along late cements around pores; Facies IIa along CH4 surface: (c) Arrow (i) points to rhomb-shaped pores after leached dolomite crystals. Arrow (ii) points to fitted fabric of the foraminferan *Borelis* with other grains that indicates deformation of soft grains affected by meteoric water during compaction. Later bocky equant cement reflect meteoric cementation; (d) Facies IIa along CH3 surface: equant spar cement and dissolution of aragonite grains. Early meteoric cementation prevented compaction during burial; (e) 4 m below CH3 surface: compaction involving early isopachous cement rimming algal grains (arrow). The overburden stress has also resulted in fracturing of grains; (f) syntaxial cement growth on echinoid fragment in facies IIa ; (g) Facies IIb about 7 m above CH3 surface: micrite occupies most of the inter-granular area. Echinoid grains show epitaxial cement which is rounded (arrow); (h) top of facies IIb: compaction has resulted in rare pressure dissolution of algal grains.

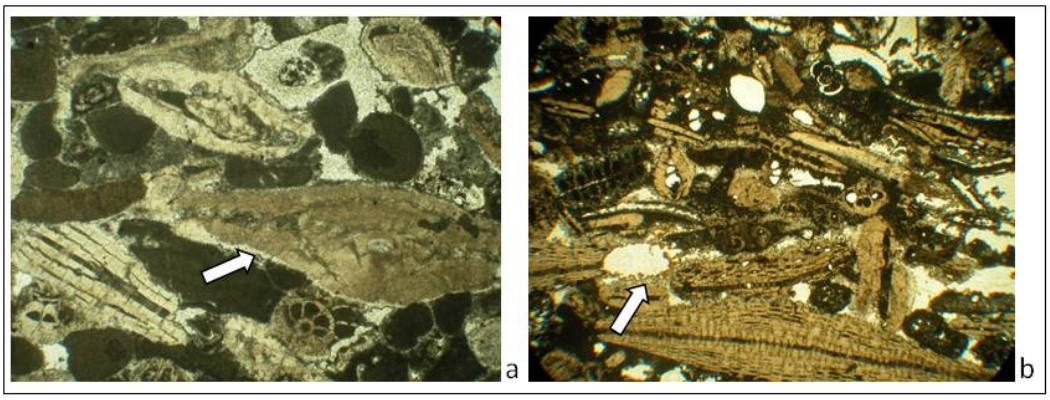

Figure 4.8. FA III. White arrows point to: (a) compaction involving early bladed marine cements. The large foraminfera are 1 mm in diameter; (b) fibrous cement around foraminiferal fragments and intraclasts that include micrite.

4.3.2.4 Facies Association IV

Cenozoic scleractinian corals constructed an aragonitic shell which is metastable and more susceptible to leaching by meteoric water than calcite. All coral in biostromes and patch reefs within the Lower Coralline Limestone has been leached and preserved as moulds. Post-dissolution calcite cement in the coral moulds fills only a small fraction of the void so that the level of preservation of moulds is low and inversely dependent on the grain size of the matrix. Consequently, coral moulds are better preserved in fine-grained sediment or peloidal matrix which is common within the reef framework (Figure 4.9) and is generally thought to result from microbial activity (Moore, 2001).

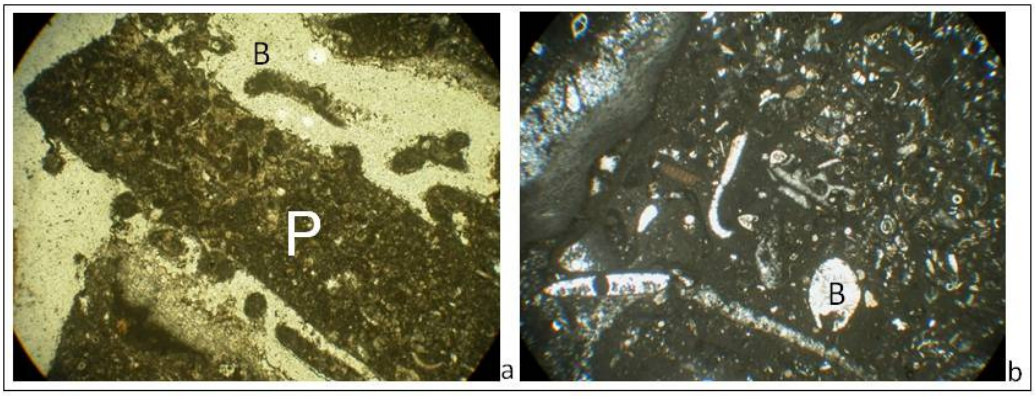

Figure 4.9. Coral framestone/rudstone: (a) lower part of locality 5. Peloids (PL) filling space around coral framework that was later leached and (B) partly cemented with blocky equant calcite; (b) locality 3 showing leached bivalves and coral mould (B) partly filled with equant calcite cement.

4.3.2.5 Facies Association V

The main grains that form FA V are corals, bivalves and benthic foraminifera embedded in a micritic matrix. The characteristic fabrics and textures of these platform interior muds persist to the Late Eocene sediments penetrated by the Naxxar-2 and Aqualta wells, although older sediments are dolomitized and have lost their original fabric. Modern shelf muds consist of elongate needle shape particles with tightly bound water sheaths surrounding the particles (Enos & Sawatsky, 1981). Studies on modern carbonate platform muds show that initial porosity is high but sediments undergo significant dewatering by compaction until a stable grain framework is reached with 35 to 45% porosity after only 100 m of burial. The compacted fabrics result in the obliteration of identifiable marine grasses and vertical "root" tube voids and obliteration of pellets and birdseye or fenestral voids in those sediments where early cementation was lacking (Shinn & Robbin, 1983).

Common diagenetic features seen in the exposed facies Vb include (molluscan) micritic envelopes and mouldic porosity after leaching of coral. Meteoric diagenesis is pervasive and all coral and aragonitic bivalves in FA V is leached and preserved as moulds. Facies association V is similar to the lagoonal carbonates of the Eocene Metlaoui Group in Tunisia that reaches a porosity of 40% as a result of mouldic porosity (Bishop, 1988).

Grains in FA V have been transformed by the following diagenetic processes:

Facies Va: In localities 9 and 14, rounded geniculate algal sand shows intense micritization whereas leached aragonitic grains (bivalves and coral fragments) preserve a micritic envelope cemented by blocky equant spar (Figure 4.10b).

Facies Vb: Most of the deeper sediments consists of micrite that is composed of <62 μm carbonate crystals which could have been precipitated inorganically or organically. The original matrix would have included high-magnesium calcite and aragonitic coral fragments broken down by bioeroders (e.g., crustaceans). The original high magnesium reflects the change from the high calcium sea environment of the Cretaceous to the high Mg/Ca ratio of the Late Palaeogene (Stanley & Hardie, 1998). The Mg content inhibited crystal growth beyond 2-3 μm and resulted in the precipitation of micrite (Figure 4.10c). However, the removal of Mg^{2+} by freshwater flushing (Tucker & Wright, 1990) locally permitted crystals to grow larger by neomorphic aggradation and the replacement by low-Mg calcite. Certain horizons in the upper part of this facies are less mud-rich. Grains are rimmed by bladed calcite cement and inter-granular space by blocky equant cement (Figure 4.10 b, d) which suggests the influx of meteoric water during occasional subaerial exposure of this shallow marine facies.

4.3.2.6 Facies Association VI

This light red to brown facies is accessible along the CH3 surface in localities 5 and 6. In thin section this facies consists of fine-grained sediments with darker-coloured discontinuous seams that bend around grains. The dark bands are interpreted as dissolution seams of insoluble residue (clay and organic matter). Such dissolution seams tend to develop in argillaceous limestone preferentially along thin clay layers (Tucker & Wright, 1990). The seams also resemble wavy organic stringers observed in modern compacted shelf mud (Shinn & Robbin, 1983) although in the case of FA VI, the poorly lithified organic matter is washed away during thin section preparation and now appears as elongate voids within the clay seams (Figure 4.11a). The presence of clays in this facies may have inhibited calcite cementation and limited early lithification. During burial, argillaceous limestone and to a greater

extent marls and shales are susceptible to significant compaction (Goldhammer, 1997). This is consistent with the crushed *Kuphus* tubes seen in thin section that suggest low level of early cementation and significant compaction (Figure 4.11b).

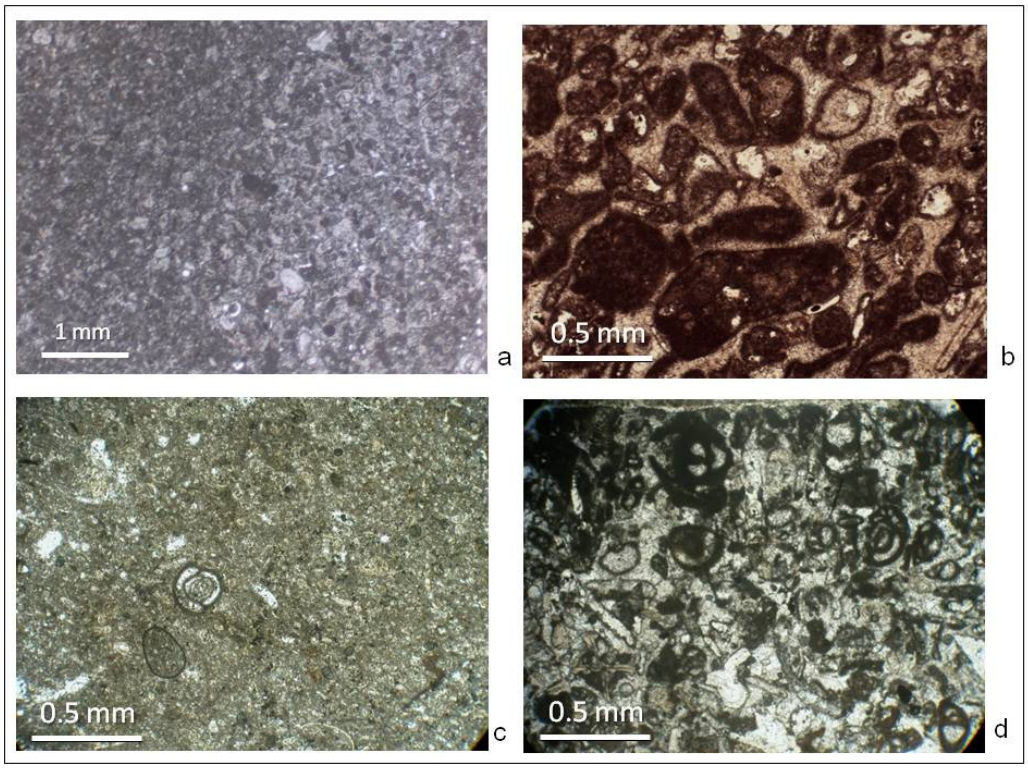

Figure 4.10. (a, b) facies Va at localities 9 and 14: intense micritsation of algal and aragonitic grains which were later leached. The cement is blocky equant spar that rims well-rounded and sorted miliolids and algal grains; (c) Locality 5: facies Vb showing miciritic matrix; (d) Equant blocky cement and micritic envelopes around leached aragonitic fragments that suggests precipitation of calcite from meteoric water.

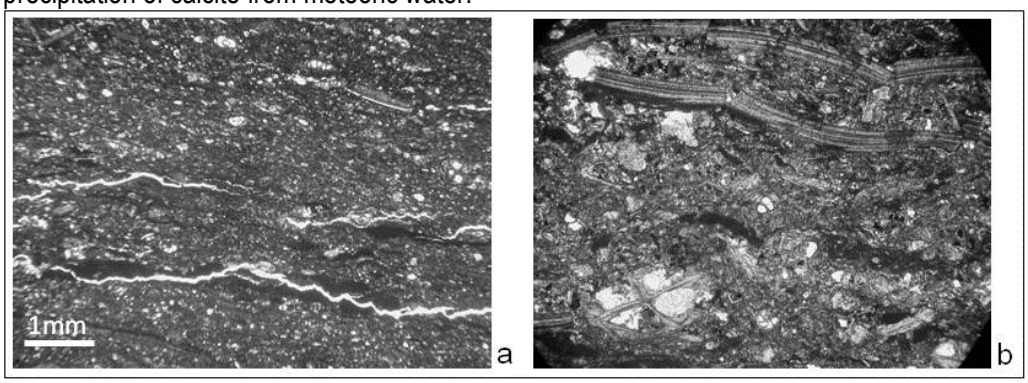

Figure 4.11. Facies VI: (a) Locality 6 showing darker-coloured seams interpreted as clay-rich crossed by elongate voids (white) that could be organic matter lost during thin section preparation; (b) Locality 5 shows crushed circular tube of *Kuphus* that now appears as an elongate ellipse. The direction of stress is normal and applied by overburden (top).

4.3.3 Diagenetic indicators of palaeo-oxygenation

In general, the redox state of most sedimentary rocks can be seen in the colour of the rock. Iron is particularly effective as an indicator of the state of oxidation in the field because oxidation ($Fe^{2+} \rightarrow Fe^{3+}$) results in a change from green to red. Although most of the succession in outcrop is pure calcite, there are small quantities of iron-rich minerals, e.g., Knoerich & Mutti (2006) record >1700 ppm of iron in locality 1. This is within the level of abundance of Fe in calcite cement precipitated from meteoric water (Tucker & Wright, 1990). The occurence of iron with carbonates results in three distinct colours produced by oxidation of iron-rich minerals in the rock:

Iron pyrites and glauconite

Iron pyrite and glauconite are formed under reducing conditions. Pyrite is the most abundant authigenic mineral formed under anoxic marine conditions, although carbonates generally have low pyrite contents (Allison, *et al.*, 1995). Pyrite is recorded from well cuttings at the level of facies IIa in the Zabbar well whereas in outcrop, iron pyrites has been oxidised to produce a pale yellow to orange colour associated with the formation of limonite. Outcrops with a pale yellow colour are seen along the <40 m-thick succession in the lower part of the cliffed coast from locality A to locality D to 14 and localities 5 and 6 which consist of facies IIa sediments. Farther east in locality 14, the pale yellow colour is restricted to *circa* 3 m-thick beds a few metres above present day sea-level within facies IIa (Figure 4.12). The precipitation of iron pyrite in facies IIa is associated with rapid burial in the inner platform during a marine transgression that produces a reducing, poorly oxidised depositional environment. This is consistent with the bright cathodoluminescence of samples from facies IIa (Figure 4.7). At locality 3, one of the facies IIIa bed has an orange colour (Figure 4.12) which can be related to the oxidation of intragranular glauconite observed in thin sections.

Ferric iron minerals

Iron minerals precipitated in oxic conditions impart a reddish colour to sediments due to the presence of ferric iron (Fe^{3+}) and suggest oxidising, subaerial palaeo-environments. The reddish brown colour of FA VI found at the base of the cliffed

coast at locality A points to subaerial conditions that persisted for some time. When limestone weathering is accompanied by pedogenic processes insoluble ferric oxides will begin to concentrate in the soil layer, leaving a residue of iron sesquioxides in soil. The process is analogues to the formation of bright red-coloured ancient terra rossa soils that are commonly found over the present Maltese Islands as a result of intense weathering associated with pedogenic processes during past hot and humid subtropical conditions.

Non-ferrous sediments

Very low concentrations of iron in carbonates result in rock with a bright white colour which is the colour of calcite. The 35 to 50 m of rhodolithic sediments of facies IIb have a bright white colour that can be traced along >30 km of cliffed coast from western Gozo to locality D in Malta. The colour reflects a high level of purity in carbonates associated with the flooding of the carbonate platform when the depositional environment lacked sources of terrigenous material that includes iron.

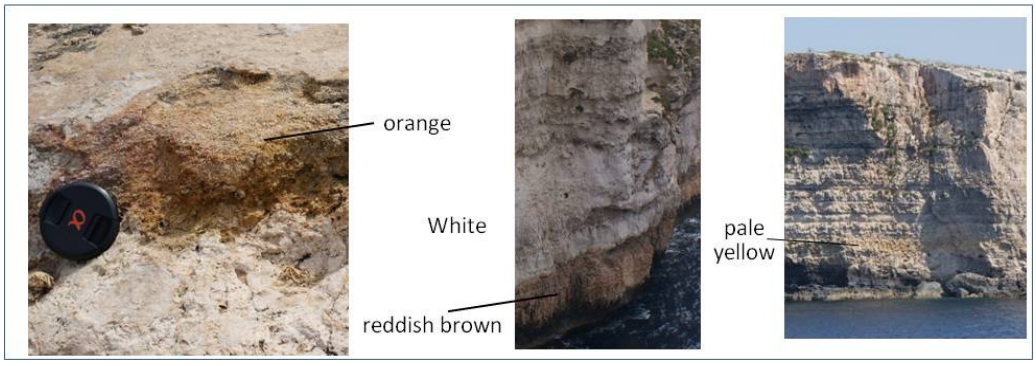

Figure 4.12. Left: Locality 3 showing bed with orange colour that results from the oxidation of pyrites and glauconite. Underlying this bed is facies IIb characterised by bright white carbonates of the rhodalgal biostrome; middle: base of locality A includes a >5 m thick reddish brown beds; right: locality 14 shows an orange-coloured band along facies IIa.

4.3.4 Diagenesis in Mesozoic to early Palaeogene carbonates

Cores of Cretaceous to Eocene sediments from the Aqualta and Naxxar-2 wells consist of dolomite, limestone and some evaporite beds (Figure 4.13). The generally fine-grained sediments and biotas (miliolids and shallow marine LBF) reflect shallow marine platform interior environments that are similar to facies association V seen in outcrop. Late Triassic sediments penetrated by the MTZ well at depth of

4500 to 8000 m also consist of dolomite inter-bedded with evaporite (Debono, *et al.*, 2000). The three main lithologies of the Mesozoic Malta Platform are described:

4.3.4.1 Dolomite

Although present day dolomite precipitation is much less extensive than ancient dolomite found in carbonate platforms, it can serve as an analogue for climatic, eustatic and geological settings. However, ancient dolomites tend to be coarser-grained than dolomite precipitated in modern environments, which suggests re-crystallization (Tucker & Wright, 1990). Four models of dolomitization induced by sea-level changes and climatic controls are proposed Purser, *et al.* (1994):

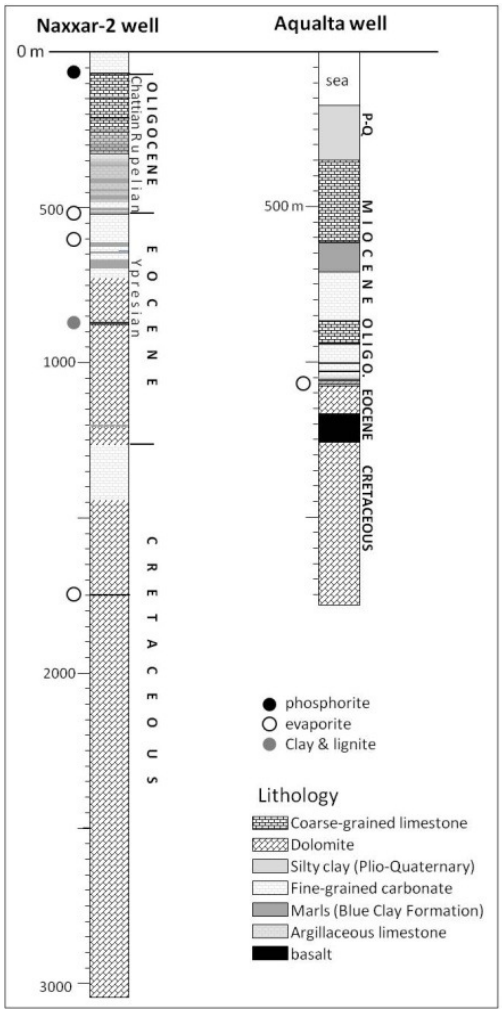

Figure 4.13. Lithology of wells.

1. Reflux dolomitization during sea-level fall under an arid climate associated with high evaporation rate and the precipitation of evaporites in sabkha environments.
2. Mixing-zone-related dolomitization during sea-level fall under a humid climate, although this model has been proved to be unlikely to produce dolomite (Melim, *et al.*, 2004).
3. Seawater dolomitization during sea-level rise or during the lowering of sea level when freshwater flows towards the margin of the platform resulting in the mixing with marine water that favours the precipitation of dolomite.
4. Kohout convection of seawater associated with either a source of geothermal heat that could have come from basaltic sill.

Early diagenetic dolomitization is common in cyclic shallow marine carbonates throughout the Phanerozoic and may be subject to dedolomitization by contact with meteoric water during subaerial episodes. Alternatively, dolomite may preferentially replace micrite during later stages of burial diagenesis as in the case of Eocene Nummulitic carbonates of Tunisia (Beavington-Penney, *et al.*, 2008).

In the Malta Platform, dolomite is often recorded in well cuttings at depths exceeding the range of 700 to 1000 m (Figure 4.13). Well reports describe dolomites that are well-ordered, medium to coarse grained, although crystal size varies and patches of coarse dolomite (0.2 to 0.5 mm) occur in a 'matrix' of fine to medium-grained dolomite. The coarser dolomite may have formed by successive neomorphism of finer-grained dolomite. Dolomite is interpreted as replacement of the original calcite which seems to be mudstone-wackestone limestone with miliolids, although the alteration of limestone to dolomite has destroyed much of the original fabric.

4.3.4.2 Limestone

The upper Eocene beds are not affected by dolomitization and have preserved the original fabrics and grains which include the benthic foraminiferan *Alveolina* that is

associated with shallow marine environments (Geel, 2000). Fenestral porosity is common and reflects the original mudstone fabric of shallow marine settings.

4.3.4.3 Evaporites

The evaporites recorded in Maltese wells consist of gypsum and anhydrite. Gypsum is predominant at depths of <1200 m where temperature is less than 42°C. At greater depths, gypsum will become unstable and begins to transform into anhydrite (Kendall, 1984). The transformation is observed in thin sections of well cuttings at depth of 1600 m from the Naxxar-2 well (Figure 4.14).

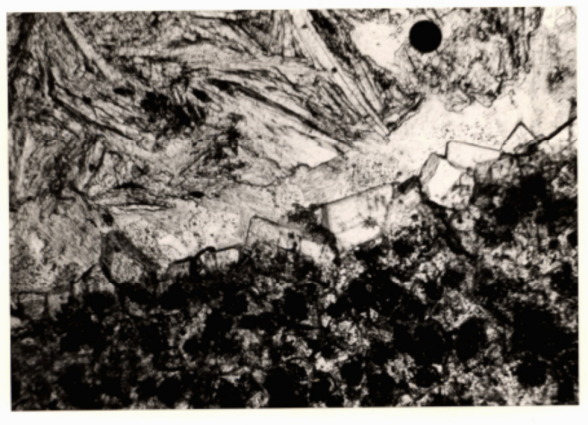

Figure 4.14. Naxxar-2 well (depth 1600 m): photomicrograph showing dolomite, gypsum and fibrous anhydrite.

Associated with the evaporites are breccias and metre-wide cavernous porosity reported in the Naxxar-2 well at about 700 m depth within the Eocene. The breccias may have been produced by collapse of roof-ceiling of caverns. When a cavern's roof-ceiling collapses, the upward migration of voids can penetrate the surface and form circular subsidence hollows (Waltham, *et al.*, 2005). Such structures are described in NE England and attributed to the dissolution of Permian Zechstein gypsum <50 m below the surface (Sargent & Goulty, 2009). In western Gozo several spectacular <300 m-wide circular solution-collapse features trending N-S occur along the coast (Figure 4.15). The density and size of these sinkholes suggests that the subsurface collapsed caverns were considerably large and close to the surface in

western Gozo. The youngest evaporite bed reported in wells is that found along the Eocene-Oligocene boundary (Figure 4.13). This evaporite bed may have been very thick in western Gozo.

Although subsurface caverns can be produced by freshwater water dissolution of limestone to produce karst features, the size, concentration and depth to below present sea-level of the subsidence solution features in western Gozo compared to the rest of the Maltese Islands suggests a more localised and rapid mechanism that involved the dissolution of gypsum by meteoric water. The source of freshwater water can be either the influx of meteoric water or the conversion of gypsum to anhydrite which releases significant amounts of water (Kendall, 1984). However, depths are too shallow for temperature to trigger the latter process in the Maltese Eocene. The influx of meteoric water at such depths requires conduits such as faults that cross some of the circular subsidence features and a significant drop in sea-level, as happened during the Messinian salinity crisis.

Figure 4.15. Circular, <300 m-wide solution collapse features (red circles) along the western coast of Gozo. Some of these circular features have been mostly eroded by the sea; *Left*: One of the solution subsidence features is crossed by a strike-slip fault. The log of locality 1 is based on >60 m of outcrops along the sinkhole wall.

In synthesis, the Early Eocene and Cretaceous dolomite associated with evaporite suggests a sabkha type of environment during a phase of arid climate. However, the replacement of calcite by dolomite suggests pervasive dolomitization which would

require a source of Mg^{2+} ions. Seawater is the likely source of Mg which would suggest some sort of reflux of marine water in the Malta Platform.

4.3.5 Burial stress and diagenesis

The Lower Coralline Limestone Formation is the lowermost of the five Tertiary formations that outcrop in the Maltese Islands and is buried to relatively shallow depths (maximum <230 m). Burial diagenesis is limited to mechanical compaction and consists of the rearrangement of grains and mechanical failure of the grains. Beds were originally thicker before differential compaction although different facies have different average rates of compaction: 1.2 for carbonate sand (e.g., facies IIa), 2.5 for carbonate mud (e.g., facies V) and 3 for marl (Goldhammer, 1997). Outcrops are mostly pure carbonate so the high rate of compaction applicable for marls is rarely relevant except for facies VI and subsurface marly beds in facies V where the subsidiary clay component may have suppressed early calcite cementation. There is little evidence of compaction of individual rhodoliths (facies IIb) that are relatively robust by their nature. However, the rhombohedral packing of rhodoliths with diameters >2 cm could have originally been cubic packing.

Increased compaction with depth reflects the lithostatic pressure gradient *p(z)* that has been estimated by considering the average density of limestone ($\rho_{limestone}$) which is the predominant lithology down to *circa* 700 m, and the density of dolomite ($\rho_{dolomite}$) which becomes common at deeper levels in the Naxxar-2 well. Lithostatic pressure is calculated by the equation:

$$p(z) = p_0 + g \int_0^z \rho(z)\, dz$$

where,

ρ_0 is datum pressure; g is acceleration due to gravity;

$\rho(z)$ is density of overlying rock at depth z

Average density of lithology taken as:

$\rho_{limestone}$ = range: 2100 to 2350 kg/m^3 , average 2200 kg/m^3

$\rho_{dolomite}$ = range: 2350 to 2800 kg/m^3, average 2400 kg/m^3

The effective stress in grains is influenced by the hydrostatic pressure (p) gradient estimated by the equation:

$$p = \rho g z$$

The effective stress (σ') is:

$$\sigma' = \sigma - u$$

where σ is total normal stress and u is pore pressure.

The lithostatic and hydrostatic gradients are presented in Figure 4.16 does not include the effect of cavernous porosity and brecciation on rock density.

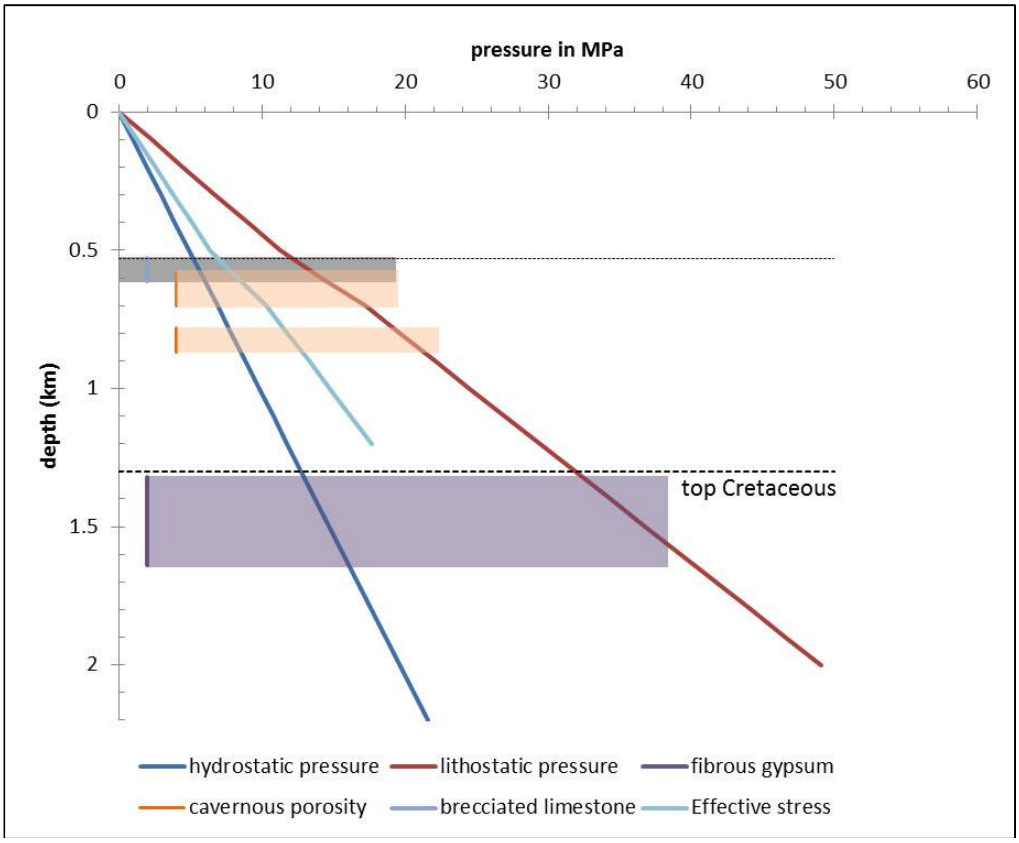

Figure 4.16. Lithostatic and hydrostatic gradients. Base Oligocene is shown by dashed line at *circa* 520 m from surface of Malta.

Burial of the base of the 450 m thick Lower Coralline Limestone at Naxxar-2 well of average density (2.2 kg/m^3) to depth of 650 m (450 m + 200 m overburden) as found in the Maltese Islands will result in lithostatic pressure of 14 MPa and hydrostatic pressure of 5.8 MPa. The effective stress at this level will be 5.2 MPa.

The tested average uniaxial compressive strength (UCS) of the Lower Coralline Limestone is 11.6 MPa for samples within the range of densities of outcrops (Figure 4.17). Therefore, the effective stress of 5.2 MPa is not sufficient to exceed the average uniaxial compressive strength and much less than the triaxial strength of the Lower Coralline Limestone to cause significant fracturing or pressure dissolution. This does not take into account the tectonic stress component which is unknown for Eocene and older rocks. However, the base of the formation at 450 to 200 m includes a gypsum horizon which would be expected to deform under lithostatic stress at that depth. Since the base of the formation is not horizontal, the gypsum bed may deform by gravity.

The effective stress begins to match the UCS of the limestone at depths >0.7 km, although compression in the ground is triaxial so fracturing would begin at even greater depths. However, fracturing in some beds of weaker rock with a UCS below average may be expected at shallower depths (0.6 km) which coincides with the actual depth of breccia recorded in the Naxxar-2 well (Figure 4.16)

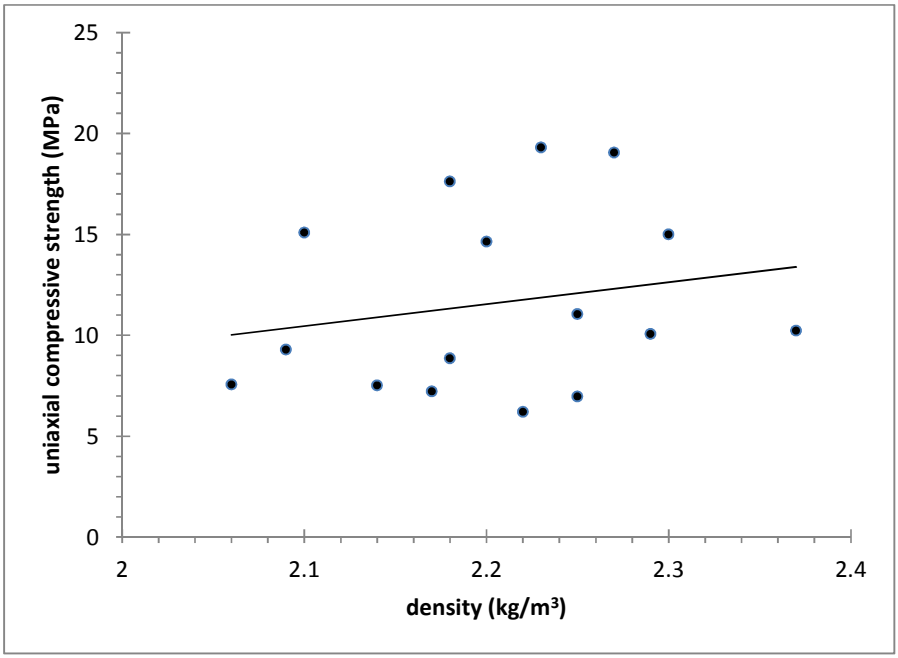

Figure 4.17. Uniaxial compressive strength of Lower Coralline Limestone based on outcrop samples. Data from Wardell-Armstrong (1996). The trend line shows an average uniaxial compressive strength of 10 to 12 MPa. However, the spread of data is relatively large.

4.4. DIAGENETIC HISTORY AND POROSITY DEVELOPMENT

The evolution of porosity in the Lower Coralline Limestone Formation was the result of both original depositional environment and later diagenetic history. Primary porosity (φ) in carbonates ranges from 40 to 70%, although porosity in carbonate reservoirs is commonly between 5 to 15% compared with porosity in siliciclastics that has a range of 15-30% (Choquette & Pray, 1970). Oligocene to Early Miocene outcrops of Malta have a range of porosity between <10 to <40% (Figure 4.18).

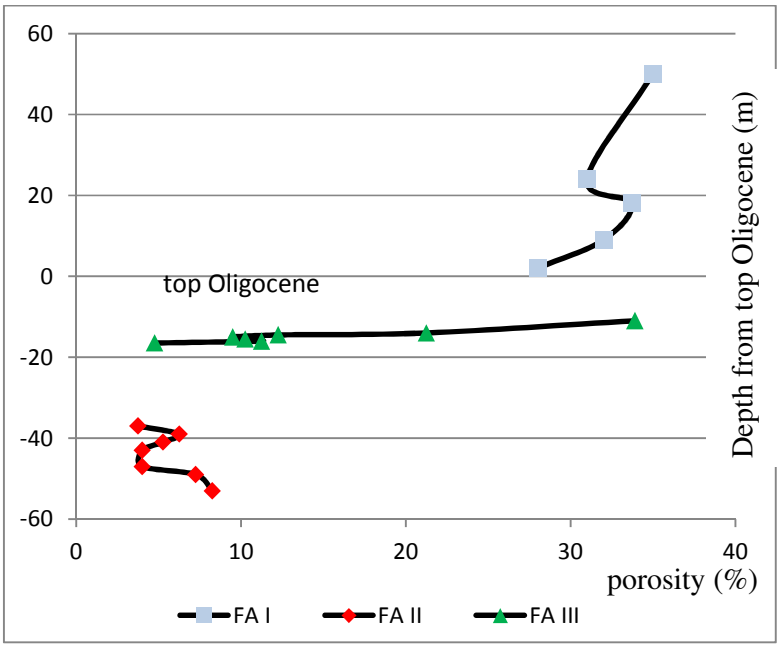

Figure 4.18. Range of porosity in different facies in outcrop. FA I includes Miocene Globigerina Limestone Formation (source: Wardell-Armstrong, 1996).

The high level of porosity in the top Oligocene carbonates is attributed to the coarse-grained nature of FA III and its inter-granular porosity (φ = 5 to 35%) although porosity declines significantly in FA II (<10%) where micrite constitutes up to 40% of the rock. Mouldic porosity is important in the finer-grained FA V, which makes up more than half of the thickness of the Lower Coralline Limestone Formation and includes gas shows in one well (see Appendix III-29). When micrite content is >50%, e.g., in FA I and Globigerina limestone, porosity increases to around 30%. In this case, pores are sub-microscopic and occur as micron-sized pores between micrite crystals.

The successive diagenetic and taphonomic phases affecting facies associations are shown in Figure 4.19. Processes that have increased porosity include dissolution of metastable carbonates. Dolomitization is rare in the Late Palaeogene but widespread in the Early Palaeogene and Cretaceous sediments where it involved the preferential replacement of micrite by dolomite. The dolomitization of micrite is also recognised in the Eocene carbonates in offshore southern Tunisia (Beavington-Penney, *et al.*, 2008). Processes that have destroyed porosity include the precipitation of cement by meteoric water and seawater flushing. Some processes have reduced and enhanced porosity, e.g., bioturbation produces opening new voids in the sediment which increase water circulation that results in precipitation of calcite cement.

Taphonomic	*Vadose meteoric*	*Phreatic meteoric*	*Marine*	*Shallow burial*
bioturbation			**V**	
hydrodynamic sorting			**III,** IIa, E	
Diagenetic feature				
dissolution	IV	**IV**		**E**
dolomitization		top II	**Vb**, Vc	**E**
dedolomitization	top II			
equant cement		IIa, III, V		
epitaxial cement		**II**, III		
microbial micritisation			IIa	
fibrous/bladed cement			III	
compaction				(II), III, **VI**

Figure 4.19. Paragenetic sequence of the diagenetic features observed in the facies associations I to VI of the Lower Coralline Limestone Formation and Eocene (E). Bold letters indicates processes widespread within the facies. Green shading indicates processes that increase porosity, red shading indicates processes destroying porosity and blue indicates processes that do not affect porosity.

Porosity decreases dramatically to a range between 5 to 15% in Eocene and Cretaceous carbonates (Figure 4.20). The qualitative evaluation of the range of porosity is poor to fair for Cretaceous to Eocene carbonates and poor to very good for the Lower Coralline Limestone and Globigerina Limestone. Both the Naxxar-2 and Aqualta wells show a decline in average porosity to 7-8% at depths >500 m. There could be several reasons for poor porosity with depth:

i. Compaction by burial: the effective stress increases with depth and may begin to exceed uniaxial and triaxial compressive strength resulting in compaction and porosity reduction. However, the occurrence of cavernous porosity suggests that compaction was not effective in forcing the collapse of caverns.

ii. Increase of fines: an increase in micrite will reduce porosity. The proximity of Eocene to Cretaceous porosity to the range of porosity of facies II suggests relatively high micrite content, comparable to that of facies V.

iii. Dolomitization: the partial dolomitization of micritic sediments can result in a drop in porosity. (Murray, 1960) demonstrates that porosity drops when the percentage of dolomite is <50% and increases when dolomite exceeds 50% and dolomite rhombs begin to act as a framework that prevents compaction.

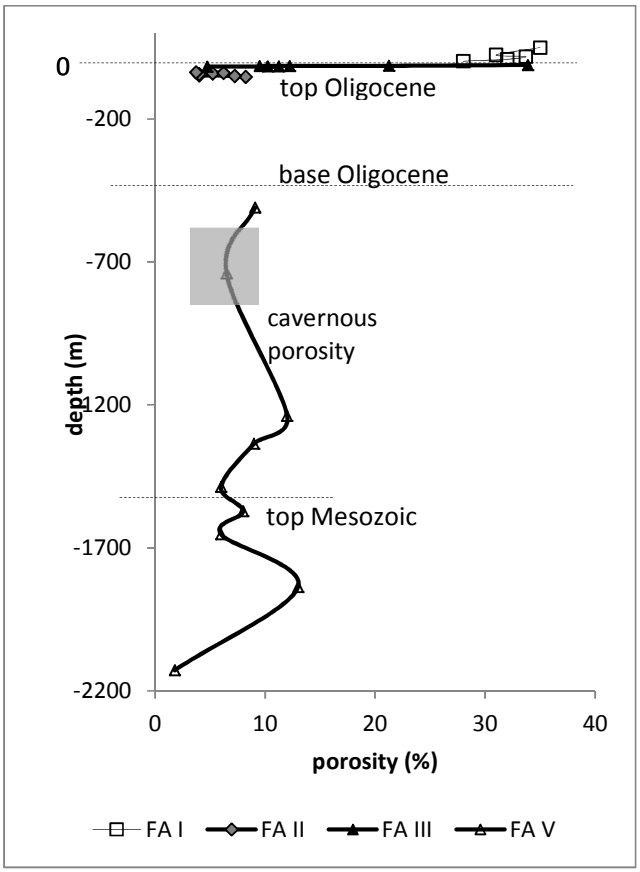

Figure 4.20. Comparison of outcrop and subsurface porosity in the Malta Platform. The 0 m level marks the top Oligocene exposed in Malta whereas FA I includes the Globigerina Limestone.

Shallow burial and the preservation of carbonate grain and cement fabrics despite the change from metastable carbonate minerals to low magnesium calcite permits a number of conclusions on the diagenetic history of the Malta Platform. Diagenetic features recorded along the Oligocene succession suggest recurrent episodes of subaerial exposure followed by flooding of the carbonate platform. These episodes can be related to glacio-eustatic sea-level change that is discussed in detail in the next chapter. Environmental changes related to climate change are also evident in the shift from carbonate/evaporite sediments of the Cretaceous to the Eocene period to carbonates affected by meteoric water and pedogenic processes during the Oligocene. This pattern suggests a change from arid to humid climate that increased the imprint of meteoric diagenesis in Oligocene carbonates.

4.5. SUMMARY

The Malta Platform carbonates underwent diagenetic processes that took place on the seafloor, in meteoric environment and shallow burial. These processes have controlled fabrics and porosity development. Chattian outcrops include four bedding surfaces that recur every few tens of metres and are distinguished by particular diagenetic features. The lower three surfaces show evidence of intense leaching of aragonitic grains, micritic envelopes and were cemented by equant blocky calcite and are marked by negative excursions of the stable isotopes of carbon and oxygen. These fabrics and chemical signals suggest that surfaces were influenced by meteoric water and pedogenic processes during subaerial episodes. The top surface is distinct because it remained subtidal and forms the terminal hardground of the Lower Coralline Limestone Formation. The hardground consists of fibrous calcite cement precipitated along a current-swept seafloor. The rest of the outcrops were affected by marine diagenetic processes that include early epitaxial cement around echinoids and bladed calcite cement rimming grains or micritic matrix. Eocene to Cretaceous sediment shows pervasive dolomitization and horizons of cavernous porosity after gypsum dissolution. Palaeogene cements and stable isotopes indicate changes in diagenetic environments through time that can be linked to fluctuating sea-levels and climate change.

Chapter 5: part 1

Stratigraphy of the Malta Platform:

Sequence stratigraphy

5.1 INTRODUCTION 142

5.2 METHODS AND DATASETS 142

5.3 INTRODUCTION TO SEQUENCE STRATIGRAPHY 143

5.4 PALAEOGENE Cyclostratigraphy and sequence development in Malta 148

5.4.2 Major stratigraphic surfaces 148

5.4.3 Sediment packages 152

5.5 PALAEOGENE Depositional Sequences 156

5.5.2 Depositional Sequences 1a and 1b 158

5.5.3 Depositional Sequence 2 160

5.5.4 Depositional Sequence 3 160

5.5.5 Depositional Sequence 4 166

5.5.6 Depositional Sequence 5 179

5.5.7 Depositional Sequence 6 192

5.1 INTRODUCTION

The first part of this chapter focuses on the application of sequence stratigraphy to the Palaeogene sediments of the Malta Platform whereas the second part of the chapter places sequences within a chronostratigraphic framework based on the geological time scale of Gradstein *et al.* (2004). The detailed logs of the localities in outcrop are shown in Appendix II which includes a correlation chart of the logged sections. The Palaeogene consists of the >0.3 to 1.7 km of subsurface Eocene carbonates, marls and evaporites, and the 0.2 to 0.45 km thick Oligocene Lower Coralline Limestone Formation of which the top <120 m is exposed in the Maltese Islands. Pedley (1978) sub-divided the Lower Coralline Limestone Formation into four Members. However, this classification does not adequately reflect the stratigraphy of the formation and is not based on the study of the entire succession in outcrop (Gatt, 2010) and excludes sediments below present day sea-level. This chapter provides a comprehensive stratigraphy of the Lower Coralline Limestone Formation based on a sequence stratigraphic approach for the entire formation.

The objectives of this chapter are, (1) to identify major unconformity surfaces, (2) to construct a high resolution sequence stratigraphic framework at the third- to fourth-order scale for the Oligocene succession of the Malta Platform.

5.2 METHODS AND DATASETS

Data for Eocene stratigraphical packages are derived from two well reports of the offshore Aqualta and onshore Naxxar-2 wells whereas the Oligocene Lower Coralline Limestone Formation is described in detail on the basis of three data sources: (a) eighteen measured sections from 15 localities in Malta and Gozo (see Appendix II), (b) cores, well cuttings and wireline logs from three deep wells, Aqualta, Naxxar-2, Zabbar wells (see Appendix III-29 for cored sections) and (c) photomontage of seven inaccessible localities labelled A to G along the southern cliff coast of Malta (see Appendix IV) and the inaccessible cliff coast of western Gozo (H) in which bedding planes, sedimentary structures and unconformities along

the bounding surfaces are traced for several kilometres. The method used for the stratigraphical analysis of the Maltese Oligocene rock record is based on the identification of major unconformity surfaces that are correlated using facies data and the photomontage of the southern cliff coast of Malta. The sequence stratigraphic framework is applied by:

i. Sub-dividing sediments into depositional units separated by major unconformity surfaces identified by:
    a. Dramatic facies change along erosional surfaces that persist for several kilometres.
    b. Carbon and oxygen isotopic excursions marking the unconformity surface.
    c. Particular diagenetic characteristics along the unconformity surface.

5.3 INTRODUCTION TO SEQUENCE STRATIGRAPHY

Sequence stratigraphy experienced a major period of development when it began to be used as a tool for seismic stratigraphy (Mitchum & Van Wagoner, 1991). It was a concept originally applied to siliciclastic depositional systems (Haq *et al.*, 1987) but was later used to analyse carbonate depositional systems with the caveat that unlike siliciclastic systems, carbonates are produced *in situ* (Handford & Loucks, 1993). Carbonate depositional sequences result from the interplay of two controls:

i. Sedimentation rate: Environmental conditions and changing physico-chemical parameters, e.g., nutrient level that controls the type and quantity of carbonate produced and the degree of exposure to wind/marine currents controls the rate of accumulation of sediments. Sediment production and accumulation can vary from 10^1 to 10^5 mm/kyr in ancient to modern carbonate platforms (Schlager, 1981).
ii. Accommodation space: On gently subsiding passive margins long-term accommodation space is controlled by the subsidence rate as well as vertical tectonic movement that may create or reduce local accommodation space. In the short term, changes in sea-level control the stratal stacking patterns.

Sea-level change is a fundamental control in both carbonate and siliciclastic sequence stratigraphy. Eustasy occurs at several orders of cyclicity (Goldhammer et al., 1990) and produces distinct sediment packages separated by unconformity surfaces that represent a hiatus, the most important being the sequence boundary. First-order cycles are approximately 200 to 300 Ma long. They are produced by changes in ocean-basin volume related to tectonic plate reorganisation of the Wilson Cycle (Table 5-1).Table 5-1Second-order cycles have an average duration of 9-10 Ma and form the *supersequence* (Haq *et al.* 1987) that represents changes in basin evolution related to rates of uplift or subsidence. A supersequence may consist of a set of five to seven *sequences* formed by third-order sea-level cycles that generally develop on a time scale of 0.5 to 5 Ma (Weber *et al.*, 1995; Hunt & Tucker, 1992). Superimposed on third-order cycles are fourth-order cycles that produce *parasequence sets* defined as a bundle of genetically related *parasequences*.

Many studies show that the higher frequency sea-level cycles (3^{th} to 5^{th} order) are produced by glacio-eustasy as a result of changes in volume of global ice (Goldhammer *et al.*, 1990) and that the amplitude of these sea-level cycles increases during ice-house periods and diminishes during greenhouse conditions (Read, 1998). Glacio-eustasy is linked to the astronomical theory that suggests a relationship between sea-level and changes in the Earth's orbit which influences seasonal and latitudinal distribution of incoming solar radiation.

Order	Duration	Sequence stratigraphic unit
First-order	>50 Ma	Megasequence
Second-order	5-20 Ma	Supersequence
Third-order	0.5-5 Ma	Sequence
Fourth-order	0.1-0.5 Ma	Parasequence set
	0.01-0.1 Ma	Parasequence
Fifth-order	<0.01 Ma	Small scale sequence

Table 5-1. Sequence stratigraphic units produced by orders of sea-level cycles (based on Weber *et al.*, 1995).

Milankovitch (1930) suggested that seasonal variation in irradiation intensity over the past 600,000 years, especially the intensity of radiation received at high latitudes during the summer was critical to the growth and decay of ice sheets. Milankovitch rhythms of 400, 100, 40 and 19 to 23 kyr duration result from three orbital forcing mechanisms (De Boer & Smith, 1994) (Figure 5.1):

1. *Eccentricity of the Earth's orbit around the Sun*: The Earth's orbit has varied from almost circular to maximum eccentricity. Eccentricity has a period of *circa* 100,000 years with superimposed long-term variations of *circa* 400,000 years.
2. *Obliquity*: Changes in axial tilt have a mean period of 41,000 years and modulate seasonality especially in high latitudes.
3. *Precession*: the Earth wobbles on its axis due to lunar and solar attraction on the Earth's equatorial bulge so that the Earth's axis moves around a circular path and completes a revolution every 23,000 years.

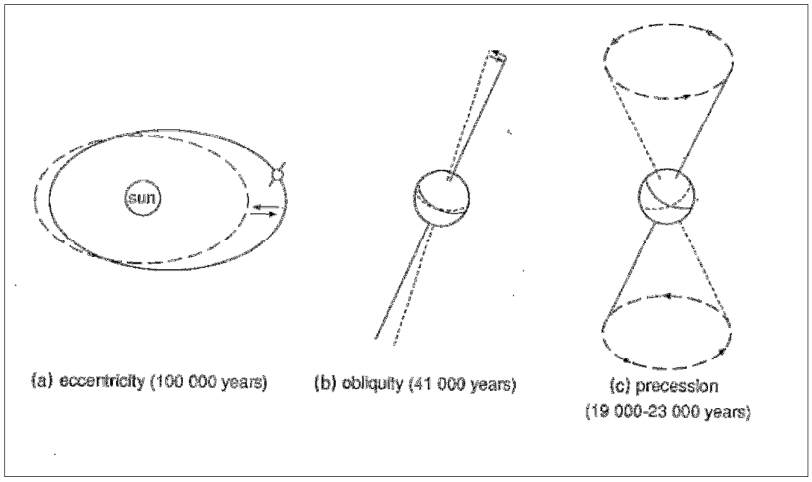

Figure 5.1. Astronomical variables and their average periodicity that affect the Earth's climate (from De Boer & Smith, 1994).

The orbitally-controlled variations in solar insolation have controlled sea-level cycles through time by the waxing and waning of ice-sheets. The third-order and higher frequency sea-level cycles produce three types of sediment packages bounded by stratal surfaces of increasing hierarchal importance (Catuneanu *et al.*, 2009):

1. *Depositional sequences* are bounded by major unconformities and correlative conformities that represent sequence boundaries. The position of the sequence boundary along the sea-level curve differs in the sequence stratigraphic models in use (Catuneanu *et al.*, 2009), e.g., the models proposed by Van Wagoner *et al*, (1988) and Hunt & Tucker (1992) consider the sequence boundary to be the result of the end of base-level fall of a sea-level cycle that produces a subaerial unconformity and its marine correlative conformity, whereas Galloway (1989) proposed a model where genetic depositional sequences are bounded by maximum flooding surfaces.

2. The *systems tract* is defined as "a linkage of contemporaneous depositional systems, forming the subdivision of a sequence" (Posamentier *et al.*, 1988). A systems tract may consist of one or more parasequence sets (PS) depending on the rate of subsidence. The parasequence sets can be progradational, aggradational or retrogradational (Mitchum & Van Wagoner, 1991) (Figure 5.2) and reflect highstand, lowstand and transgressive phases of the sea-level cycle identified in sequence stratigraphic analysis (Van Wagoner *et al.*, 1988). The lowstand systems tract is sub-divided into two parts in some studies, e.g., Hunt & Tucker (1992) that predict four systems tracts.

3. The *parasequence* is a succession of relatively conformable and genetically related beds that form the 'building blocks' of the sequence stratigraphic framework (Van Wagoner *et al.*, 1988). These mostly shallowing-upward successions are the result of the interplay of sea-level rise and carbonate production:

    i. Each parasequence comprises one sea-level cycle ending by a marine flooding surface *sensu* Van Wagoner (1985), although this may not necessarily always be the case (see Spence & Tucker, 1997). Shallowing-upward parasequences are common in the inner to mid-platform environments, implying either falling sea-level or sediment aggradation within each parasequence. Effectively, the parasequence reflects real

changes in depositional environments produced by cyclic shifts along the sea-level curve whereas higher order sequences reflect trends in sea-level change (Catuneanu *et al.*, 2009).

ii. Thickness of each parasequence is related to the rate of production and accumulation of carbonates within the created accommodation space. Carbonate production and accumulation depends on the main carbonate producers and on conditions for the inorganic precipitation of lime mud as well as current activity (Osleger, 1991).

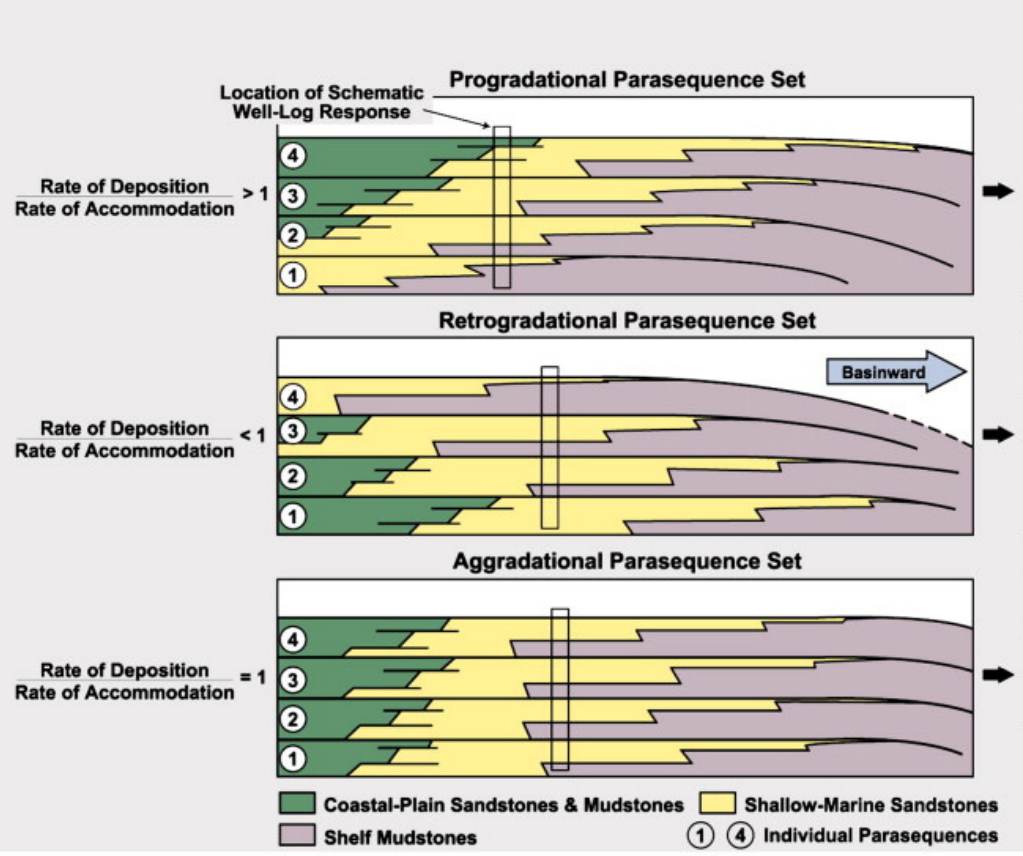

Figure 5.2. Geometries of parasequence sets (Mitchum & Van Wagoner, 1991).

5.4 PALAEOGENE CYCLOSTRATIGRAPHY AND SEQUENCE DEVELOPMENT IN MALTA

In this section the major unconformity surfaces and sediment packages that form depositional sequences in Malta are identified.

5.4.2 Major stratigraphic surfaces

Stratigraphic packages in Eocene sediments and the Oligocene Lower Coralline Limestone Formation are within the range of time associated with third-order and higher frequency cycles. These sediment packages are bound by a number of surfaces that have varying degrees of importance and geographical extent. Four surfaces are recognised in outcrop:

1. *Sequence boundaries*

In this thesis, the sequence boundary is defined as the unconformity surface produced by the maximum drop in sea-level along the sea-level curve that produces a down-platform shift in facies, according to the nomenclature of Hunt & Tucker (1992) and Van Wagoner *et al.* (1988). This choice has practical and economic perspectives since carbonate reservoir rocks are commonly found below sequence boundaries, that is beneath a stratigraphic unconformity produced by subaerial exposure of a shallow marine carbonate platform. Sequence boundaries in carbonate platforms may show the following characteristics discribed by Read (1995):

i. Development of palaeosols, calcrete or increased clay content that reflects pedogenic material in the shallow subtidal environment. However, lowstand deposits along sequence boundaries over carbonate platforms may be thin and poorly developed, although palaeosol/clay deposits may produce a distinct signature on gamma ray logs. These subaerial unconformities are frequent and abrupt in the Lower Coralline Limestone and preferred to other bounding surfaces such as the maximum flooding surface.

ii. Diagenetic cement associated with shifts from marine to meteoric environments which could suggest a sequence boundary.

iii. Negative oxygen and carbon isotope excursions produced by the influence of meteoric water may reflect a sequence boundary.

iv. Dramatic change in carbonate facies and colour between sediments above and below sequence boundary.

The synthesis of facies analysis, diagenetic studies of thin-section (see chapter 4) and major erosional surfaces terminating shallowing upward successions in the Lower Coralline Limestone outcrops reveal four successive major unconformity surfaces with the above characteristics. Consequently, these surfaces are defined as sequence boundaries. The labelling of each sequence boundary (Sb) is based on its age and relative position in the succession, e.g., most of the formation in outcrop is of Chattian (CH) age so that successive sequence boundaries are labelled SbCH1 to SbCH5 (Table 5-2).

Well cuttings from sediments below present sea-level penetrated by the Aqualta well show four horizons with *Microcodium* which is associated with the development of calcrete (Klappa, 1978) whereas the lowermost horizon of the Lower Coralline Limestone Formation consists of gypsum in the Aqualta and Zabbar wells (Figure 5.3). These horizons represent subaerial episodes produced by maximum regressive events and are recognised as three sequence boundaries of Rupelian (RU) age. However, sequence boundaries may not always be subaerial, e.g., the topmost sequence boundary (SbCH5) that separates the Lower Coralline Limestone Formation from the overlying Globigerina Limestone Formation developed as a marine hardground during a fall is sea-level identified by Gruszczynski *et al.* (2008).

Sequence boundaries SbCH2, SbCH3 and SbCH4 in outcrop mark dramatic lithofacies and colour changes and are cemented by blocky equant calcite spar. This type of cement is associated with meteoric water influx (see chapter 4) that suggests an episode of subaerial exposure along these surfaces relative to the other subtidal surfaces (Table 5-3). This is supported by micritic envelopes formed by micritisation of aragonite grains followed by meteoric dissolution of metastable aragonite. Sequence boundary SbCH5 shows no evidence of subaerial exposure and was followed by the drowning of the carbonate platform.

Depositional sequence		Sequence boundary (base of sequence)	
Glob. Lmst.		SbCH5/C_0 bed	Chattian
6		SbCH4	
5		SbCH3	
4		SbCH2	
3		SbCH1	
subsurface	2	SbRU3	Rupelian
	1b	SbRU2	
	1a	SbRU1	

Table 5-2. Depositional sequences of the Lower Coralline Limestone Formation.

Sequence boundary	Lithofacies changes	Isotopic change	Calcite cement	Colour change
SbCH5	Phosphorite	n/a	marine	brown
	FA I, FA III		hardground	Pale yellow
SbCH4	FA III	$\delta^{13}C$: -4.2‰ $\delta^{18}O$: -3.2‰	meteoric	orange-red
	FA II	$\delta^{13}C$: -0.5‰ $\delta^{18}O$: -1.4‰	marine	bright white
SbCH3	FA II	$\delta^{13}C$: -2.2 to -5.2‰ $\delta^{18}O$:no change	marine	white
	FA II, FA IV	$\delta^{13}C$: -1.2 $\delta^{18}O$: -2.9‰	meteoric	reddish brown
SbCH2	FA II, FA IV	n/a	micritisation of grains	pale yellow
	FA V, VI, VII	n/a	n/a	reddish brown

Table 5-3. The four major sequence boundaries in outcrop are marked by a thick line. The changes indicated occur within <2 m above or below the sequence boundary.

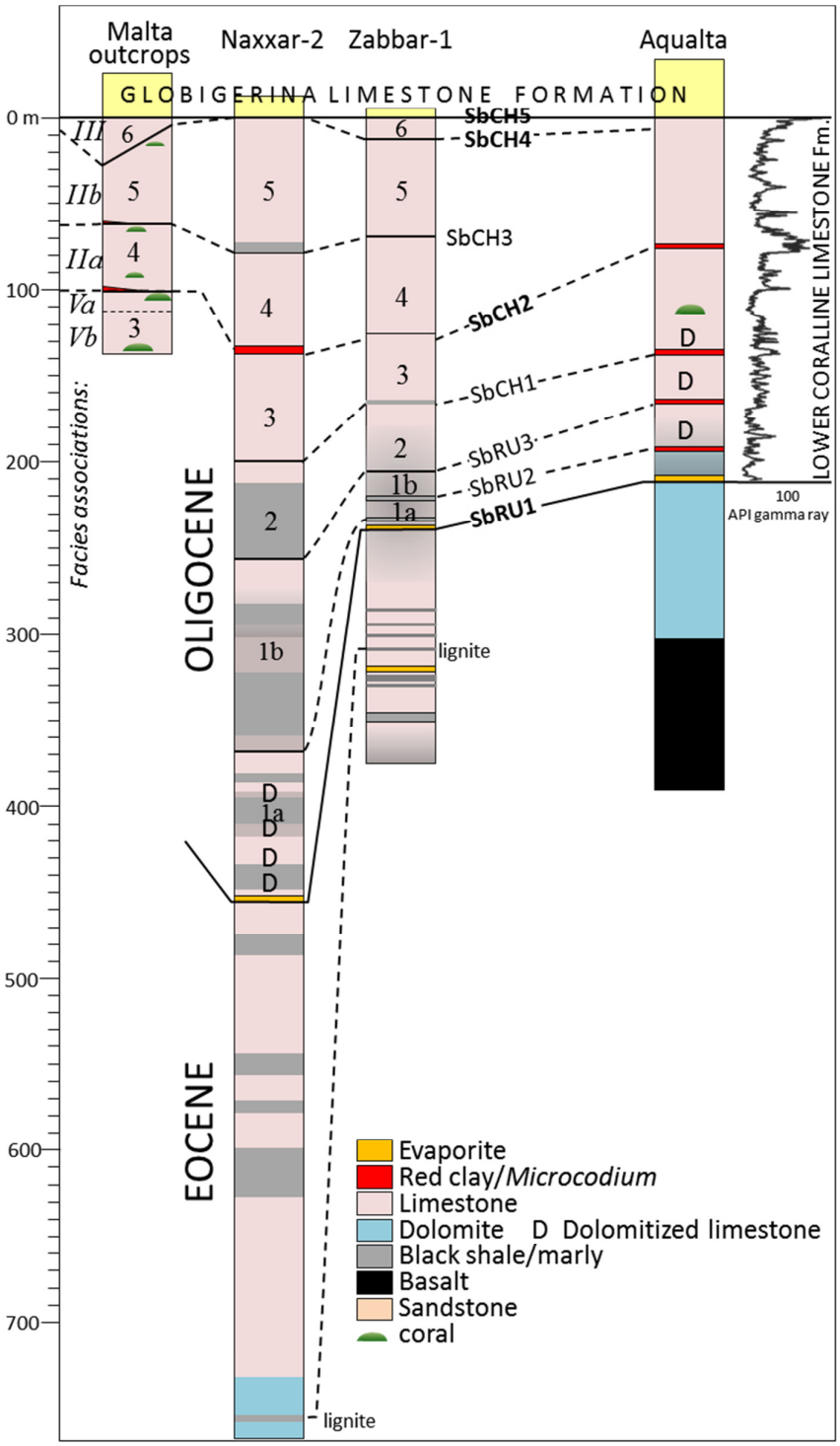

Figure 5.3. Correlation of well logs to outcrops facies associations. Surfaces with *Microcodium* in the Aqualta well indicate subaerial conditions considered as sequence boundaries that are correlated throughout the wells.

2. *Maximum flooding surfaces* (MFS)

Surfaces are characterised by a landward shift of facies belt and sediment starvation that results in some re-working. Although the MFS is considered as a sequence boundary by Galloway (1989), its importance in the Chattian oucrops of the Maltese Islands is secondary. The reason is that unlike carbonate platforms on epeiric shelves, e.g., Arabia (Sharland *et al.*, 2001), and continent-fringing carbonate platforms, e.g., Tunisia (Venin *et al.*, 2003) characterised by increased clay content or oil-prone shale along the MFS, the shallow marine carbonates of Malta were isolated from continenal siliciclastcs during the flooding of the carbonate platform.

Hardground surfaces (H)

Hardgrounds are well cemented surfaces that are bored by *Lithophaga* and associated with overlying glauconitic sediments. These surfaces reflect temporary sediment starvation associated with shallowing events over palaeohighs and upper platform slope.

3. *Ravinement surfaces*:

These surfaces are marked by an erosion that has removed a significant amount of sediment and may be characterised by gutter casts to large (>10 m) undulating erosional surfaces. This surface indicates a marine flooding event that affects proximal areas.

5.4.3 Sediment packages

Unconformity surfaces sub-divide the Lower Coralline Limestone Formation into a structured hierarchical order of sediment packages (Table 5-4). Seven depositional sequences named S1a to S6 with an average thickness of 35 to 40 m in outcrop. The sequence boundaries form distinct erosional surfaces that can be traced for >40 km along the mostly inaccessible southern cliff coast of Malta (Figure 5.4) and western Gozo and can be recognised in the offshore Aqualta well as gamma ray peaks (Figure 5.3). Unconformity surfaces of parasequences (<2.5 to 7 m thick) are also recognised in field studies (Figure 5.4). Two parasequences (P) named P-1 and P-2 are nested in every parasequence set (PS) whereas two parasequence sets labelled PS-A, PS-B with a thickness that ranges from 2.5 to 10 m make up a systems tract. Two parasequence sets make up each of the three or four systems tract within the depositional sequence.

Depositional Sequence	Systems tract	Parasequence set	parasequence	Facies VI	V	IV	III	IIa	IIb	I	Platform setting inner	mid-	outer
S6	HST	PS-B	*P-2*										
			P-1										
		PS-A	*P-2*										
			P-1										
	TST	*PS-B*	*P-2*										
			P-1										
		PS-A	*P-2*										
			P-1										
S5	LST	PS-B	*P-2*										
			P-1										
		PS-A	*P-2*										
			P-1										
	HST	PS-B	*P-2*										
			P-1										
		PS-A	*P-2*										
			P-1										
	TST	PS-B	*P-2*										
			P-1										
		PS-A	*P-2*										
			P-1										
	LSPWST												
S4	FRWST	PS-B	*P-2*										
			P-1										
		PS-A	*P-2*										
			P-1										
	HST	*PS-B*	*P-2*										
			P-1										
		PS-A	*P-2*										
			P-1										
	TST	PS-B	*P-2*										
			P-1										
		PS-A	*P-2*										
			P-1										
S3	LST	PS-B	*P-2*										
			P-1										
		PS-A	*P-2*										
			P-1										
	HST	*PS-B*	*P-2*										
			P-1										
		PS-A	*P-2*										
			P-1										
	TST	subsurface											
S2													
S1b													
S1a													

Table 5-4. Hierarchy of sequences and depositional environments based on Naxxar-2 well (subsurface S1 to S3) and outcrops (S3 to S6). Parasequence sets in grey lettering indicate uncertain stratigraphy.

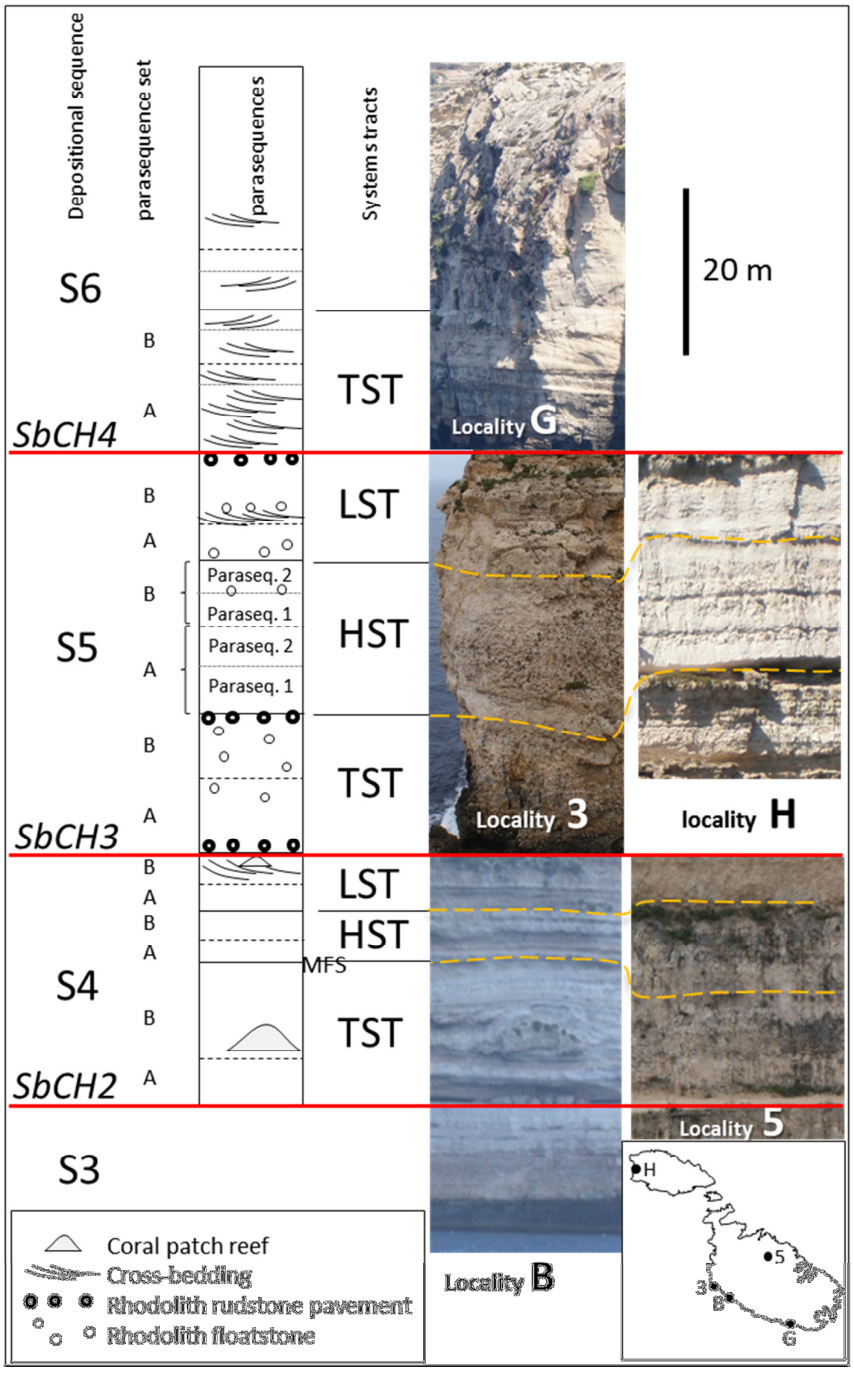

Figure 5.4. Composite log based on photographs and logs of localities B to 5, 3 to H and G. The succession is sub-divided into low to high frequency sequences. Photographs of the entire sections of the localities are in Appendix V.

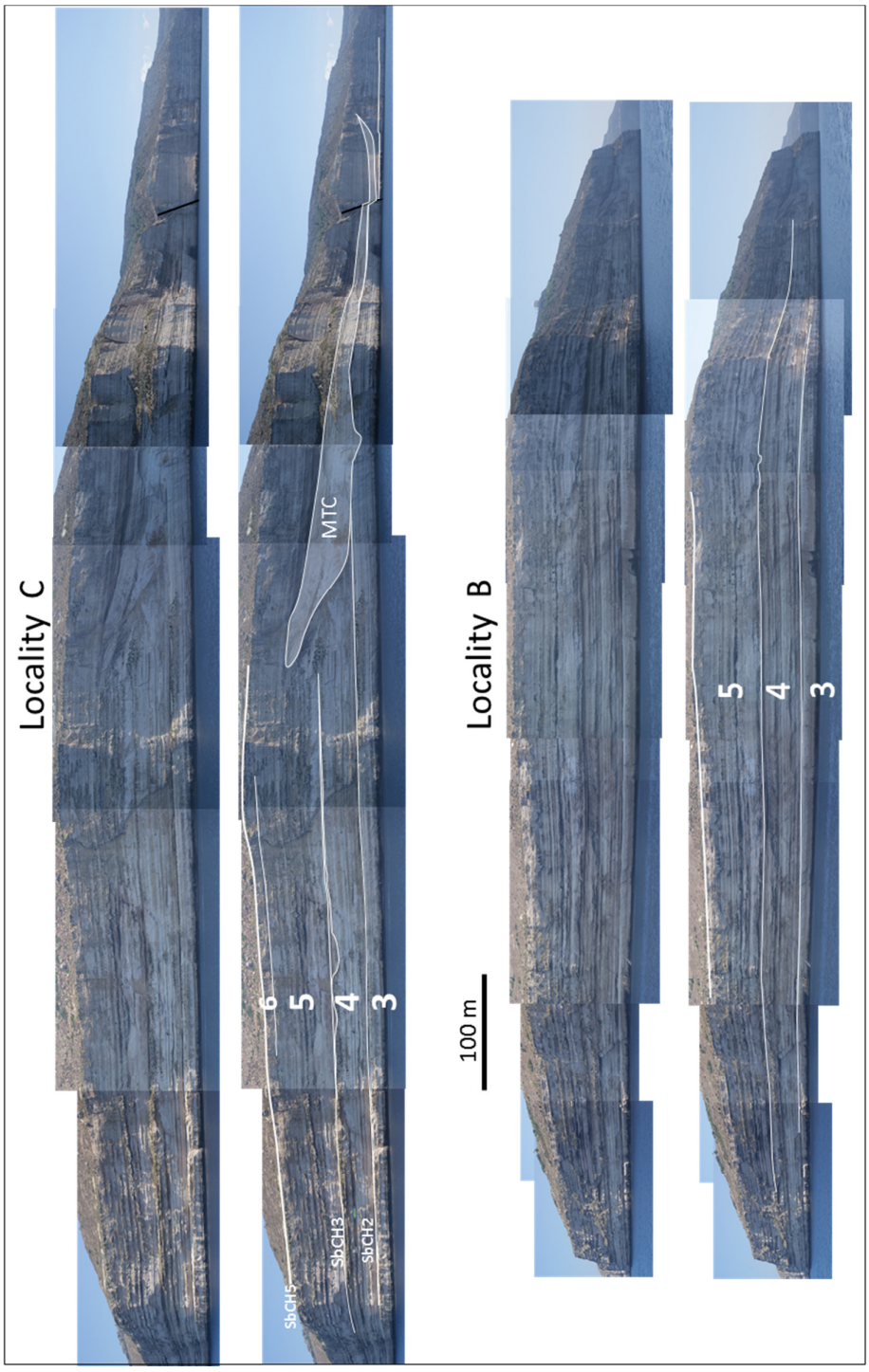

Figure 5.5. Uninterpreted and interpreted cliff section along the southern coast of Malta. The white lines are sequence boundaries that form erosional surfaces marking dramatic changes in facies: Cycle S3 consists of miliolids and is terminated by an extensive surface that is differentially eroded along the cliff; cycle S4 consists of coral patch reefs and geniculate algal sand (FA IIa and IV); cycle S5 comprises the rhodalgal biostome (FA IIb) whereas cycle S6 consists of LBF (FA III). The photomontage can be viewed in Appendix IV.

5.5 PALAEOGENE DEPOSITIONAL SEQUENCES

Eocene

The Naxxar-2 well penetrates >1 km of sediments below the Oligocene basal sequence boundary SbRU1 that are Palaeogene (Figure 5.3). The original biotas of much of the Eocene sediments have been altered by dolomitization and include clay beds with lignite. The Eocene sediments of the Aqualta well are *circa* 200 m thick and consist of fine-grained dolomite with miliolids. The top <200 m of Eocene carbonates in the Naxxar-2 and Zabbar wells are mostly limestone with large benthic foraminifera inter-bedded with marl beds, that terminate with an evaporite bed (SbRU1). Applying a sequence stratigraphic approach is difficult because of the lack of data. Eocene clay beds in the region have been associated with the transgressive Souar Formation recorded in Tunisia (see Table 2-2) and offshore wells along the outer margin of the southwest Malta Platform (Bishop & Debono, 1996). However, the marls beds recorded in the Naxxar-2 and Zabbar wells sometimes include lignite and are likely to represent shallowing events associated with land-derived vegetation. Seismic imaging of this succession provides more information that is discussed in chapter 6.

Oligocene

The thickness of the seven depositional sequences (cycles S1 to S6) and that of parasequence sets varies considerably depending on the rate of change in accommodation space and the rate of accumulation varies across the Maltese Islands which have been sub-divided into four geographical sectors (Table 5-5). Each depositional sequence is described and interpreted in detail starting from the oldest sequence. Four mass transport events have also been identified in S4 and S5.

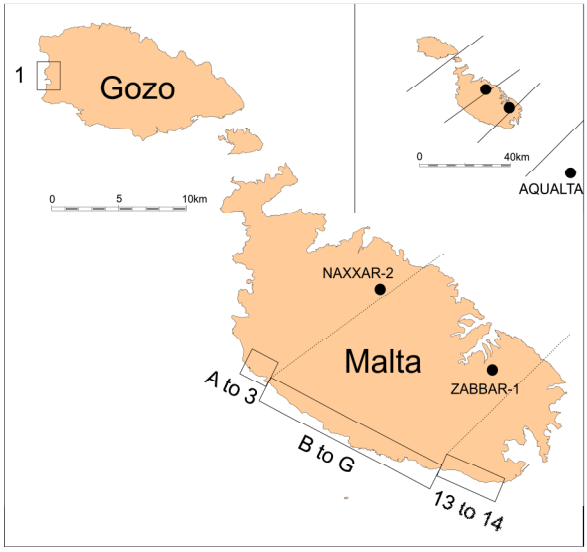

Outcrops:

1	3 to A	B to G	13 to 14	
		Depositional Sequence 6		
7	<3	5 -30	<4	
		Depositional Sequence 5		
35	<35	45 - 60 (max. at C)	40 - 60 (max. at 13)	
		Depositional Sequence 4		
25	<15	25 - 35	15 - 20	
		Depositional Sequence 3		
>10	>15	>20	>7	
	Locality 5: 30	*Below sea-level*		
Wells:	**Naxxar-2**	**Zabbar**		**Aqualta**
		Depositional Seq. 3		
	60	40		60
		Depositional Sequence 2		
	70	30		25
		Depositional Sequences 1b		
	110	20		25
		Depos. Seq. 1a		
	90	15		15

Table 5-5. Thickness (in metres) of depositional sequences across the Malta Platform according to sectors shown in the above map.

5.5.2 Depositional Sequences 1a and 1b

The depositional sequences are entirely subsurface and identified from well cuttings and core data in deep onshore wells (Naxxar and Zabbar wells) and the offshore Aqualta well. These are the most clay-rich sequences in the Lower Coralline Limestone Formation (Table 5-6).

	Depositional Sequence 1a,b		
wells	*Naxxar-2*	*Zabbar*	*Aqualta*
1b	110	20	25
1a	90	15	15

Table 5-6. Thickness of depositional sequences 1a and 1b.

Sequence boundaries: The lower sequence boundary SbRU1 consists of a gypsum bed (FA VII) that is recorded in the Aqualta and Zabbar wells and grades laterally to breccia and gypsum in the Naxxar-2 well. The deposition of evaporites over the underlying shallow marine Eocene carbonates suggests subaerial conditions that mark a drop in sea-level which exposed the Malta Platform during a period of arid climate. In the Tethyan region, the basal Oligocene forms an unconformity capped with evaporites that are found in western Egypt and Cyrenaica and marks the beginning of the Oligo-Miocene tectonostratigraphic sequence (Gerdes *et al.*, 2010). However, the top bounding surfaces of the two sequences (SbRU2, SbRU3) are marked by *Microcodium* and by peaks in the gamma ray logs recorded in Aqualta well (Figure 5.6). *Microcodium* in well cuttings is indicative of calcrete produced by subaerial exposure (Klappa, 1978). The change in nature of the sequence boundaries from SbRU1 to the succeeding sequence boundaries characterised by palaeosols reflects a shift from an arid to a semi-arid climate over the Central Mediterranean.

Sequence 1a

The lower part of the sequence consists of marl/argillaceous limestone in all three wells (Table 5-6) with basal black shale beds above the gypsum bed (SbRU1). The

microbiota commonly includes the foraminiferan *Bolivina* which is associated with low oxygen environments (Murray, 1995) as well as planktonic Globigerinids that are associated with outer platform environments. This suggests that the argillaceous limestone and shale were deposited during the transgressive phase of the cycle when the subaerial platform environments with evaporites were drowned. This resulted in open marine conditions and basin sedimentation especially in the Naxxar-2 well. The succeeding highstand is characterised by increasing amounts of limestone that were later dolomitised. The top of the sequence is marked by *Microcodium* in the Aqualta well.

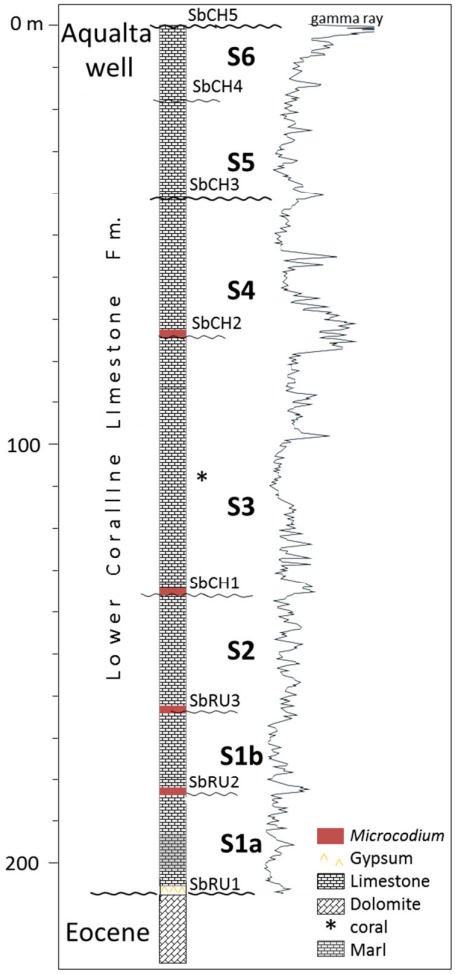

Figure 5.6. Generalised lithological log of Aqualta well and gamma ray log. *Microcodium* horizons mark the sequence boundaries.

Sequence 1b

The transgressive phase resulted in the flooding of the underlying carbonates and the deposition of marls. Sediments and foraminiferal assemblage is similar to sequence 1a. The sequence ends with the deposition of limestone during the regressive phase.

5.5.3 Depositional Sequence 2

This depositional sequence is entirely subsurface and accessed by cores. It comprises miliolids in a micritic matrix becoming marly in the Zabbar and Naxxar-2 wells (Table 5-7). The sequence is transitional between the underlying marl with carbonates of sequences 1a and 1b to the pure carbonates of S3 in outcrop. The presence of miliolids suggests a shallow marine, low energy environment. The sequence boundary SbCH1 is found below present sea-level and just below the base of the quarry in locality 5. The hiatus is marked in Aqualta well by *Microcodium* but is less well-defined in the other wells.

	Depositional Sequence 2		
wells	*Naxxar-2*	*Zabbar*	*Aqualta*
Thickness (m)	70	30	25

Table 5-7. Thickness of depositional sequence 2.

5.5.4 Depositional Sequence 3

The lower half of the quarry at locality 5 consists of *circa* 30 m of predominantly micritic carbonates with miliolids, corals and molluscs of FA V (Figure 5.7). The sequence also outcrops along the base of the southern cliff coast of western Gozo (lowermost beds in locality 1) and the base of the cliff coast of southern Malta (localities B to E). The base of this sequence is not in outcrop, although in onshore wells the S3 is 30 to 60 m thick (Table 5-8).

	Depositional Sequence 3			
Locality	1 *(W. Gozo)*	3 to A	B to G	13 to 14
Thickness (m)	>10	>15	>20	>7
	Below sea-level	*Locality* 5: >30	*below sea-level*	
		Naxxar-2: 60	Zabbar well: 30	

Table 5-8. Thickness of depositional sequence 3.

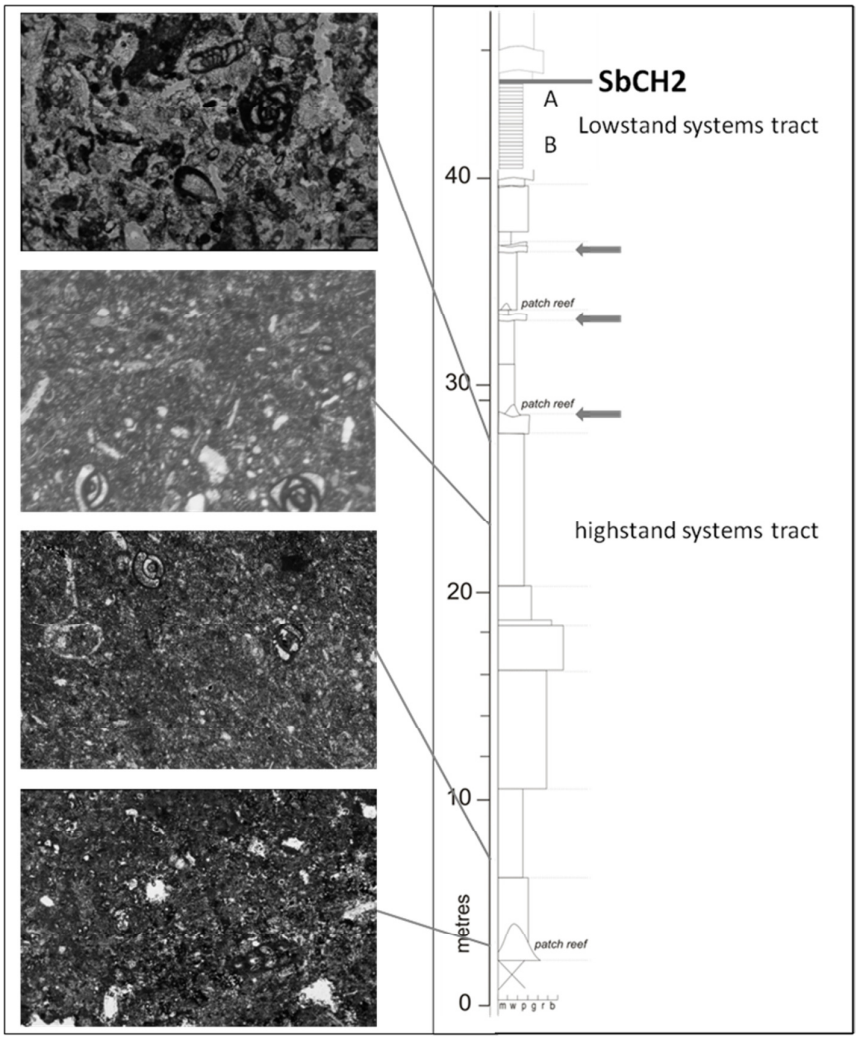

Figure 5.7. Photomicrographs and stratigraphy of cycle S3 at locality 5: highstand systems tract sediments are dominated by micrite and miliolids interrupted by beds of coarse-grained coral rudstones (horizontal arrows), whereas the lower part of the section is rich in coral rudstone and framestone. Lowstand systems tract parasequence sets A and B terminate the sequence that is bounded at the top by SbCH2.

5.5.4.i S3: *Sequence boundary SbCH2*

In all sections and wells, SbCH2 is always overlain by coralline algal debris and miliolids whereas outcrops beneath this boundary are thinly bedded and dominated by micrite and miliolids (FA V). Subtidal sediments below SbCH2 are cemented by blocky equant cement that suggests the influence of meteoric water. This boundary is recognised in the following localities (Figure 5. 8):

i. In Aqualta well the SbCH2 is marked by a gamma ray peak whereas well cuttings include *Microcodium* (Figure 5.6).
ii. The base of the sea cliff between localities 3 and A consists of reddish, thinly-bedded sediments exposed <10 m above sea-level (facies VIa) (Figure 5. 8). These beds correlate to core data from onshore Naxxar and Zabbar wells that include a *circa* 6 m thick clayey limestone unit at a depth of 126 m below the top of the Lower Coralline Limestone Formation and just below present day sea-level.
iii. Along the length of *circa* 20 km long inaccessible southern cliff coast of Malta where it forms a distinct decicentimetre-thick, deeply eroded groove along the cliff. The strong differential erosion suggests weak and poorly consolidated rock that may be clay-rich.
iv. At the base of the cliff coast in western Gozo the topmost of FA V includes thin pale red bed of miliolid packstone that reflects shallow marine conditions along SbCH2 (Figure 5. 8). The colour suggests the influence of palaeosol development (FA VI) and subaerial exposure associated with maximum regressive surface.

5.5.4.ii S3: *Lowstand systems tract*

This unit is only accessible above sea-level at localities 5 and 9 and is inaccessible along the southern cliff coast of Malta and western Gozo. About 10 m of subtidal sediments form two parasequence sets separated by a coral biostrome (Figure 5.9):

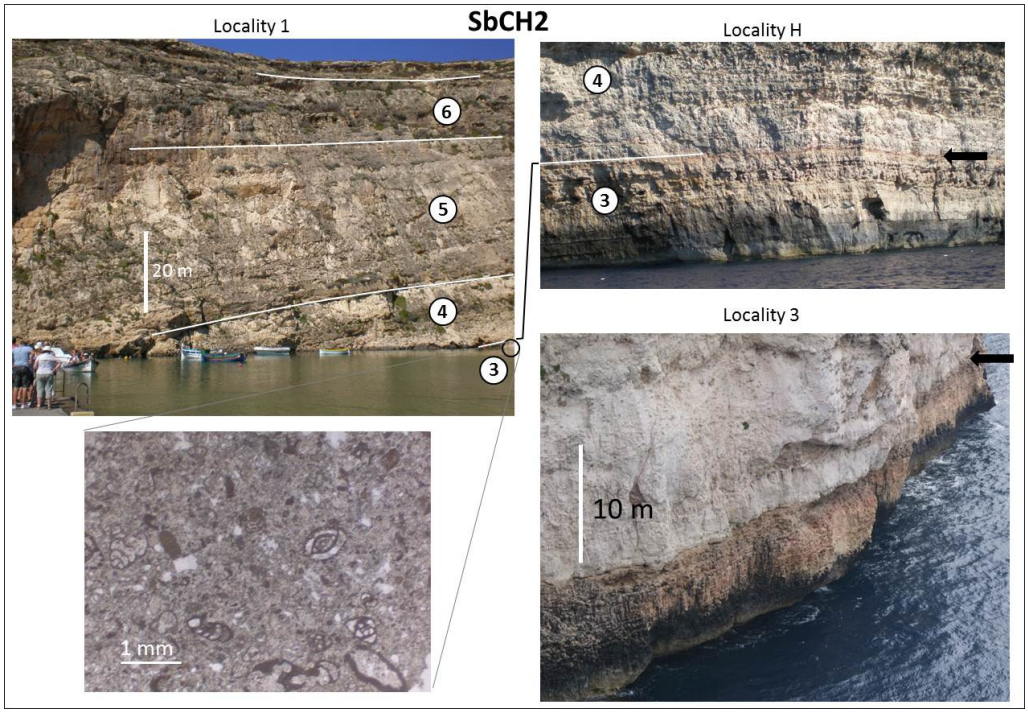

Figure 5. 8. Outcrops of SbCH2 forming the interface between S3 and S4 in Gozo and Malta: Gozo; the base of locality 1 consists of miliolid packstone (photomicrograph) in a thin reddish bed that marks SbCH2 (black arrow) at the inaccessible locality H on the other side of the same cliff. Malta (locality 3); reddish sediments are exposed at the base of the inaccessible cliff coast.

Parasequence set B (PS-B)

At locality 9, *circa* 5 m of pale yellow medium to thin beds (<30 cm) bounded by sharp planar surfaces. In thin section, sediments consist of well-sorted, fine-grained packstones to grainstones of geniculate algal debris, well-rounded bioclasts of crustose algae and miliolids in an equant blocky spar (facies Va). This thinly bedded unit is bounded at the base by a metre-thick tabular coral biostrome and at the top by sequence boundary SbCH2 which marks a dramatic change to coralline red algal sediments.

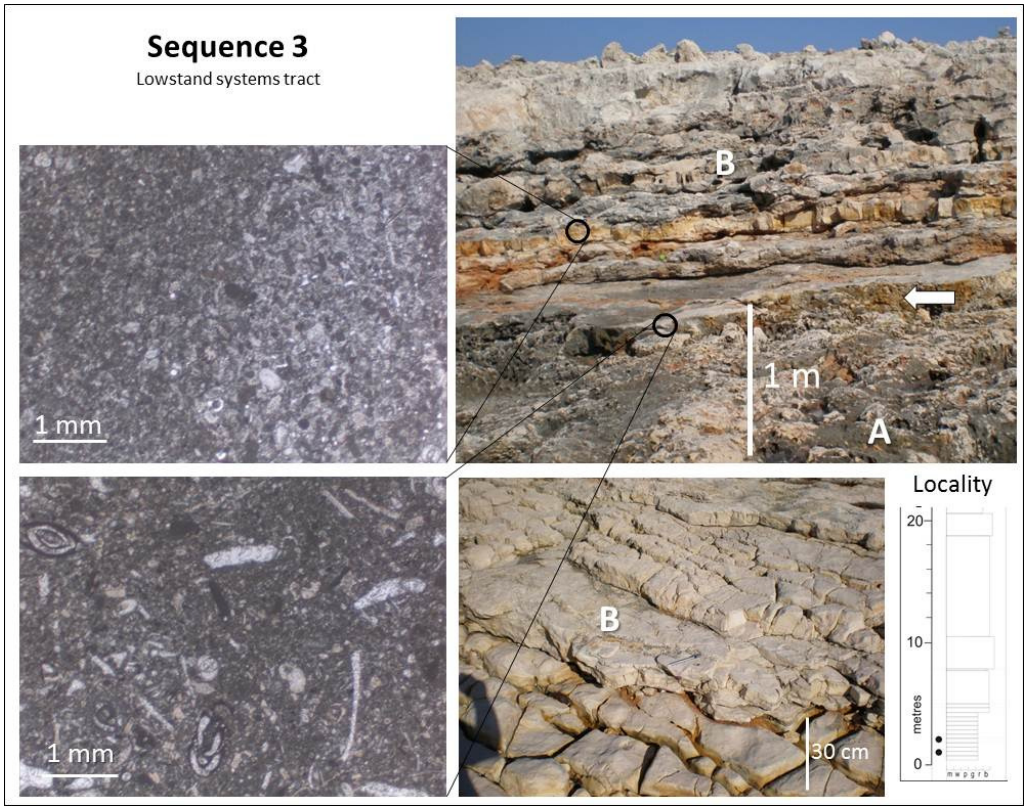

Figure 5.9. Outcrops, log and photomicrographs of top of sequence 3 at locality 9. Sediments are characterised by thin bedding (base of log) and fine-grained, well-rounded geniculate algae and miliolids of FA Vc (upper photomicrograph) cemented by blocky equant calcite crystals. White arrow shows tabular coral biostrome (lower photomicrograph of thin section) separating parasequence set A from B.

Parasequence set A (PS-A)

Found below the coral biostrome although mostly inaccessible in localities 5 and 9. Beds are thin and similar to parasequence set B.

5.5.4.iii S3: *Transgressive and Highstand systems tract (S3HST2)*

The two systems tract are only exposed in outcrop at locality 5 and recorded below sea-level at the Naxxar-2 and Zabbar wells. Sediments consist of >40% micrite with grains consisting of miliolids although coral is common in the lower 20 m and forms coral rudstone and framestone. Vertical facies changes are indistinct in these massive, micrite-rich beds (facies Vb) which include tests of burrowing animals,

e.g., well-preserved crab tests and siphonal tubes of *Kuphus.* Parasequence sets cannot be recognised whereas parasequences are poorly defined and do not show a distinct shallowing upward trend. The fine-grained sediments are occasionally interrupted by <1.5 m thick coarse-grained beds that thin out towards the north and become more frequent up the succession. These beds are characterised by a minor basal erosive and undulating surface succeeded by coral rudstone rich in benthic and epiphytic foraminifera, gastropods and articulated bivalves and capped by a thin mudstone bed.

5.5.4.iv S3: *Interpretation*

The dominance of micrite with miliolids (facies Vb) in depositional sequence 3 suggests a low energy, lagoon-type of environment of the innermost platform. High sediment production during the highstand of sea-level kept the seabed close to sea-level (<5 m deep) although the common occurrence of coral in the lower sediments indicates more open and slightly deeper environments associated with end of the transgression over SbCH1, which is in the subsurface. The mostly acyclic and massive lithology in sequence 3 is similar to the thick Eocene lagoonal deposits in Oman described by Beavington-Penney *et al.* (2006) attributed to be the result of bioturbation. This suggests that these carbonates were intensely bio-retextured by burrowing organisms such as bivalves and crustaceans that are common in micritic sediments stabilised by seagrass. Modern seagrasses are known ecosystem engineers and when seagrass density is high in relatively exposed areas they will cause mudification (the increase of the mud and organic matter fraction in van Katwijk *et al.*, 2010). The accumulation of fine sediment by this mechanism may not show clear bedding surfaces except when interrupted by occasional storm activity that rips through sea-grass meadows and creates new surfaces that are colonised by coral. Such surfaces colonised by coral patch reefs are observed in depositional sequence 3 and are associated with storm beds with a shelly basal lag that fines-upwards into a micritic bed produced by the settling of lime mud. Bioclasts in the storm bed suggest that the provenance of the skeletal material was from the lagoon itself.

The uppermost part of the sequence forms the lowstand systems tract which shows a gradual increase in red algal debris that culminates in subaerial episodes along SbCH2 affected by reddish clay. The development of palaeosol is confirmed by the occurrence of *Microcodium* in the Aqualta well. The increase in geniculate algal sand suggests a change to less restricted environments that could result from migration to the innermost platform of the sandbody barrier protecting the lagoon. The thin bedding suggests a drop in accommodation space caused by a fall in relative sea-level. Each bed represents a parasequence that was truncated immediately above the flooding surfaces so that only the lower subtidal <30 cm is preserved whereas the regressive phase was entirely eroded during subaerial exposure. The well-sorted, rounded, fine-grained geniculate algal sand and miliolids that show reworking are lithified by blocky equant cement that suggests the influence of meteoric water during subaerial episodes. The two parasequence sets A and B are separated by a coral biostrome that reflects a flooding surface during the beginning of parasequence set B when water depth could have deepened to <15 m, which is the typical depth favourable to coral growth (Schlager, 1981).

5.5.5 Depositional Sequence 4

Depositional sequence 4 is recorded in part or completely at localities 1, 3, 5, 6 and 14. All localities are characterised by an increase in coralline red algae relative to depositional sequence 3. The correlation of sections in sequence 4 from west to east (locality 3 to 14 shown in Figure 5.10) also shows significant lateral changes in facies and depositional sequence thickness (Table 5-9). The base of this sequence is marked by a sharp planar surface (SbCH2) that truncates the underlying reddish peritidal (FA VI) sediments at localities 3 to A (Figure 5.8). Three systems tracts are recognised from top to bottom: lowstand, highstand and transgressive systems tracts. The base of S4 is accessible in localities 5 and 14, although samples were also derived from ta' Kandja water gallery located <5 km inland that runs parallel to the cliffs. The lowstand systems tract consists of planar cross-bedding that dips by 2° towards the west between localities A and E (7 km distance) where its top is truncated by SbCH3 along the southern cliff coast of Malta (Figure 5.13).

	Depositional Sequence 4			
Locality	1 *(W. Gozo)*	3 to A	B to G	13 to 14
Thickness (m)	25	<15	25 - 35	15 - 20

Table 5-9. Thickness of depositional sequence 4.

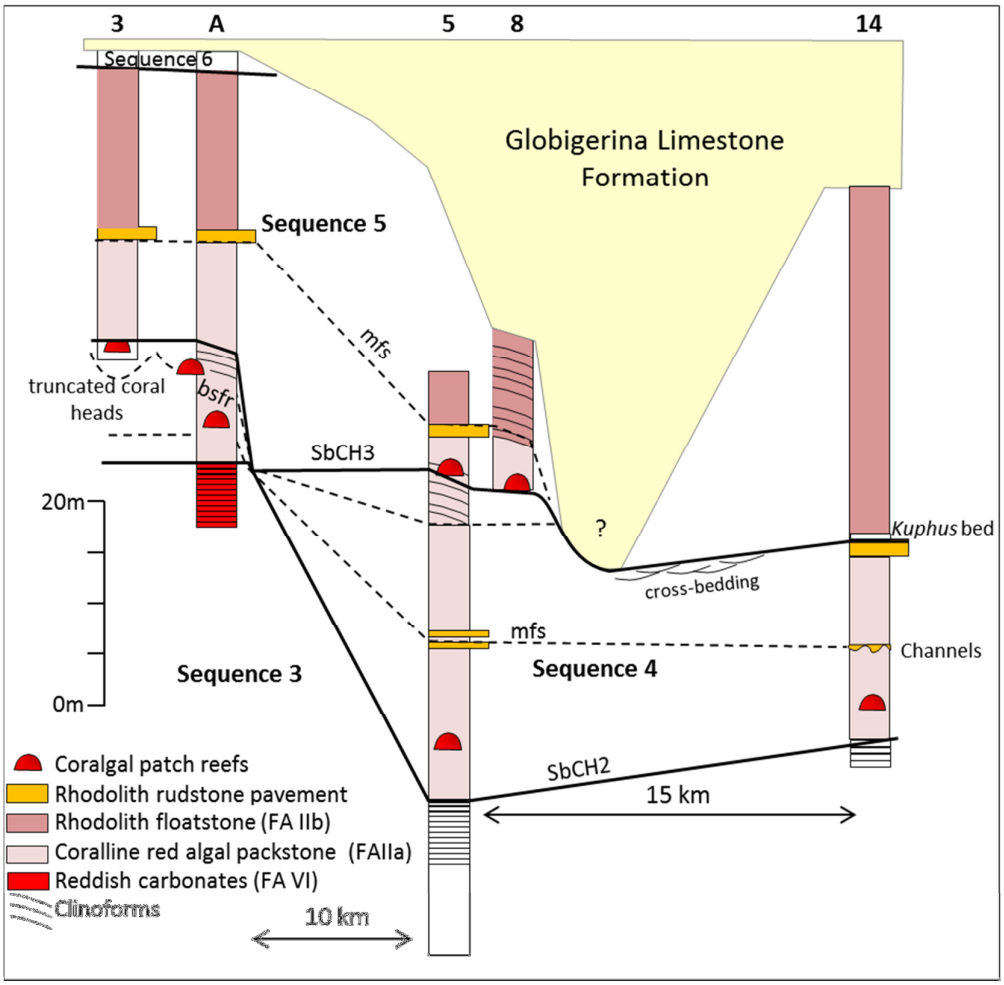

Figure 5.10. Sequence boundaries SbCH2 and SbCH3 along a west-east transect showing thinning of cycle S4 around locality A and thickening east of locality A. In locality 3 coral heads are truncated by SbCH3 whereas in more distal areas the decrease in sedimentation along the maximum flooding surface (mfs) permitted the development of rhodoliths that were reworked into pebbles at locality 5.

5.5.5.i S4: *Sequence boundary SbCH3*

Two types of beds characterise the sequence boundary:

Bed 1: a discontinuous bed that is <1 m thick consisting of foraminiferal and red algal grainstone, showing cross-bedding at locality 5. In thin section the grains are seen to be cemented by coarse calcite crystals that suggest the influence of meteoric water (Figure 5. 11). Cementation occurred before significant burial or compaction so that pore spaces remain preserved although diminished by the cement. The sequence boundary forms an abrupt erosional surface that truncates the top part of several metre-thick large low-angle cross-beds observed along the inaccessible southern cliff coast of Malta (Figure 5.13).

Bed 2: forms a continuous, distinct pale red to yellow laminar micrite with some clay (FA VI). The sediments preserved in localities 5 and 6 initially developed in the deeper topographical parts of the underlying surface relief and gradually levelled the surface, later aggrading as a planar surfaces that trapped intertidal debris and subtidal intraclasts deposited by storms (Figures 5.11 and 5.12).

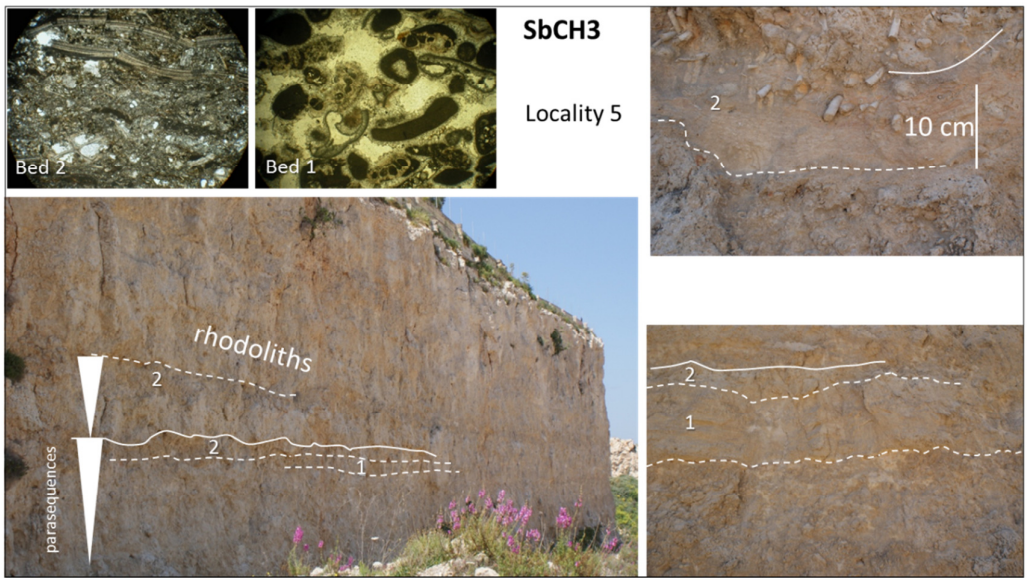

Figure 5. 11. Locality 5. Sequence boundary SbCH3 (solid line) and beds 1 and 2 in outcrop and thin section. Close up of bed 2 shows laminar fine-grained sediments burrowed by *Kuphus* of which the siphonal tube is preserved.

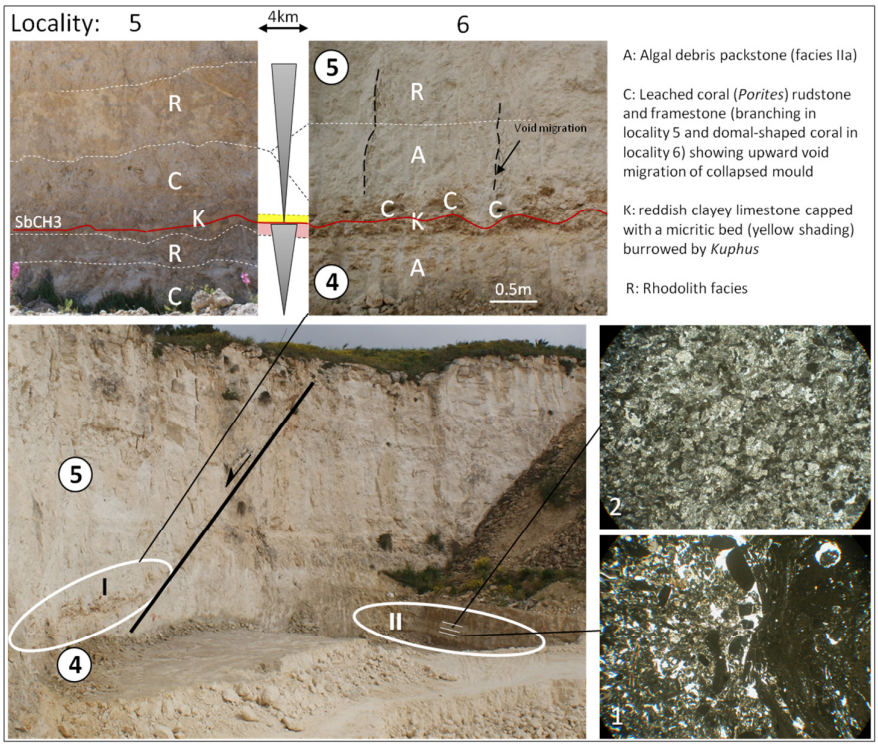

Figure 5.12. Locality 6: (top) SbCH3 (red line) at localities 5 and 6; bottom, I: peritidal cycle capped with facies VIa; II: maximum flooding surface comprising rhodolith pavements (photomicrograph 1) interbedded with thin beds of intensely reworked bioclasts (photomicrograph 2).

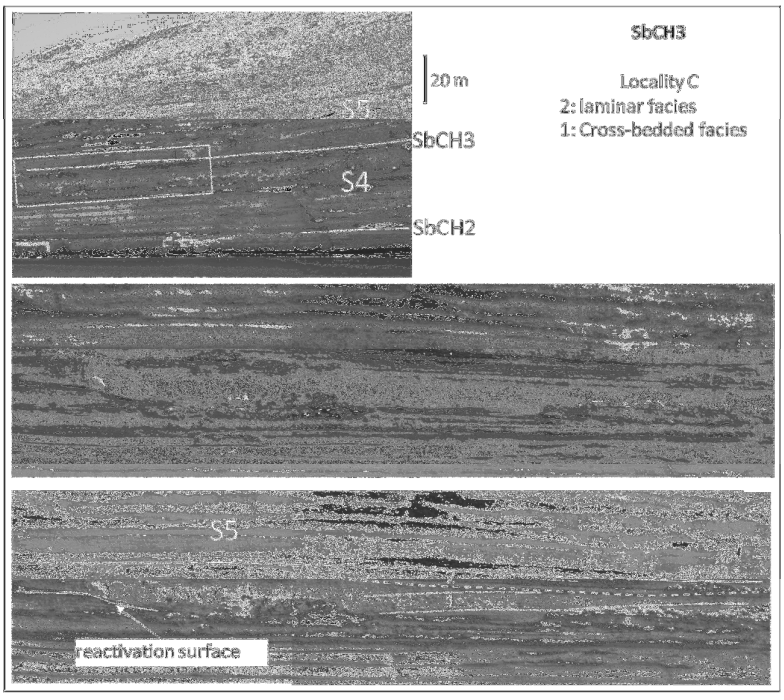

Figure 5.13. Photograph of cliff coast showing cross bedding truncated by SbCH3.

5.5.5.ii S4: *Lowstand systems tract*

This unit outcrops at localities 5 and 6 and just above sea-level at locality 3. Correlative cross-bedded sediments can be observed along the southern cliff coast of Malta over a stretch of 4 km between localities B and C (Figure 5.13) and in western Gozo. The sediments mark a regressive phase characterised by (1) forced regressive wedge showing downlap geometry along the inner platform and (2) mass failure resulting in debris flows.

Forced regressive wedge: consist of <4.8 to 6.5 m thick package of low angle clinoform bedding at locality A (Figure 5.14) that extends in cross-section to <200 m whereas at locality 5 the wedge extends to locality 6 over a distance of <5 km perpendicular to strike. It cannot be ascertained whether this was a single sedimentary wedge trending NE-SW for >10 km or a number of juxtaposed fan-like constructions emanating from a palaeohigh in west Malta and donwlapping to a bathymetric low in central Malta. The regressive wedge is seen in cross-section along the inaccessible cliff outcrop at locality A, where clinoform beds downlap towards the east over the basal surface of forced regression (BSFR) *sensu* Hunt & Tucker (1992) shown in Figure 5.14. The regressive wedge fills the concave space created by erosion along the BSFR that culminates in a slope that is *circa* 25˚ steep. The inclination of the clinoforms is *circa* 20˚. Only one package of clinoforms is preserved along the constructed slope in locality A which is more erosional than accretionary *sensu* Schlager & Camber (1986). The top bounding SbCH3 truncates the constructed slope until its merges with the underlying SbCH2.

At locality 5 the regressive wedge is seen along a quarry face cut oblique to the wedge profile showing a low angle dip towards the north (Figure 5.14). Two parasequence sets are identified, comprising four shallowing upward successions that consist of a triplet (coral floatstone, rhodolith floatstone, bed 1 cross-bedded sediments and/or bed 2 micritic laminates). A similar succession but without bed 2 is described by Brandano *et al.* (2008) <1 km southwest of locality 5:

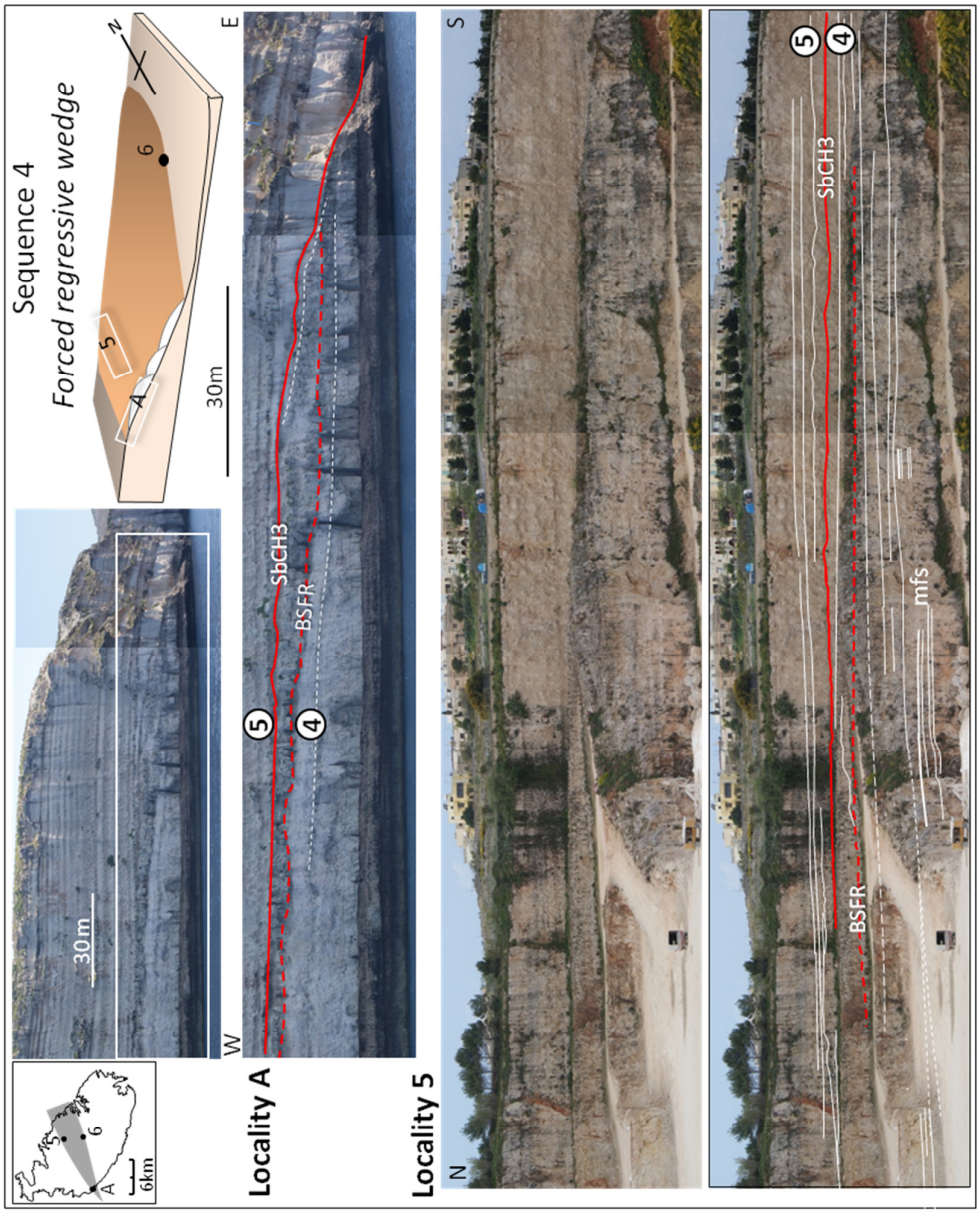

Figure 5.14. Forced regressive wedge systems tract (FRWST) seen in cross-section long profile: locality A section seen along dip of the *circa* 60 m-long sedimentary wedge that downlaps over the basal surface of forced regression (BSFR) shown by a dashed red line whereas its top sediments are truncated by SbCH3 (solid red line); Locality 5 the FRWST is seen along strike, dipping into the page and to the north. Location map (top left) shows that the lateral extent of the FRWST increases northwards and extends to locality 6.

Parasequence set A:

This lower sedimentary triplet consists of a basal bed of coral floatstone or algal grain packstone succeeded by rhodolith floatstone, terminated by undulating lamina of argillaceous carbonate that is seen to be laminar in thin section (Figure 5.15).

Parasequence set B:

The sedimentary triplet includes sub-divisions starting from the top:

1. The regressive phase consists of three beds some of which may be missing in some areas:

i. A thin (<10 cm) lime mud bed at locality 5 increasing to <1 m at locality 14 that is intensely burrowed by the bivalve *Kuphus* which constructed a <30 cm long calcitic siphonal tube within the muddy sediments. The siphonal tubes start at the surface of a <10 cm thick micrite bed and very often penetrate into the underlying pale orange laminar micrite, indicating that the latter had remained soft sediment. This structureless white mudstone with *Miliolids* was deposited at the very initial flooding stage marking the succeeding cycle. This muddy, restricted subtidal environment became a preferred niche habitat for the burrowing bivalve *Kuphus*. The top calcified siphonal tubes of this bivalve were displaced and fragmented by increasingly transgressive conditions (Figure 5. 11) in localities 5 and 6, whereas in locality 14, a dense accumulation of *Kuphus* is preserved in life position along a <1 m thick bed overlying a rhodolith rudstone bed.

ii. Bed of continuous, pale red to yellow laminar micrite (bed 2) with some clay (facies VIa) showing variable width but is always <30 cm-thick in locality 5, where these laminar micritic beds become progressively thicker with each succeeding parasequence. The laminar micrite drapes an irregular surface and is truncated by an abrupt undular surface marking an erosional surface which marks the initial phase of flooding that brought an influx of subtidal lime mud that has a distinct off-white colour. In locality 6 (central Malta), only one pale red to yellow laminar micrite bed is preserved which suggests that this area was at the margin of the regressive wedge, marking the parasequence formed at the lowest point of the sea-level curve. This bed is missing in locality 14.

iii. Sporadic, *circa* 1 m-thick lenses of cross-bedded grainstone (bed 1) dominated by imperforate foraminiferans. These subtidal high-energy bioclastic sand dunes were lithified by equant calcite cement which suggests meteoric influence during subaerial exposure. This cross-bedded facies forms a continuous, <10 m thick unit along the cliff coast of southern Malta that are laterally equivalent to the regressive wedge at the western localities A and 5. Large low-angle cross-bedding is seen along nearly 2 km of inaccessible sea cliffs east of locality A, through B to west of locality C. At locality B, 8 m of distinct reddish-brown coloured planar to low angle cross-bedding prograde westwards. Reactivation surfaces cut through the cross-bedded units shown in Figure 5.13.

iv. The cross-bedding formed under moderate to high energy hydrodynamic conditions during the lowstand of sea-level that formed the regressive wedge although sediments in the shallower western area were mostly eroded.

2. Rhodolith floatstone beds consist of well-rounded rhodoliths (diameter <5 cm) in a matrix of coarse algal debris. At locality 6, the rhodolith bed is replaced by algal debris.

3. The transgressive phase consists of *circa* 1 m-thick coral biostrome formed of thickets of branching *Porites* that form a biostrome (FA IVa). At the more distal locality 6, branching *Porites* are replaced by dome-shaped coral which requires less light and consequently could colonise slightly deeper water (Hallock & Schlager, 1986).

Within the lowstand systems tract a number of mass transport events (MT) consisting of decimetre-wide scoop-shaped scars only a few metres deep observed along the cliff coast at locality C (see photograph in Appendix IV-22) at two successive levels: (i) MT-1 is found a few metres below SbCH3; (ii) MT-2 is along SbCH3. The depletion zones are infilled by reddish-brown sediment and MT-1 includes remnant boulders of the translational domain.

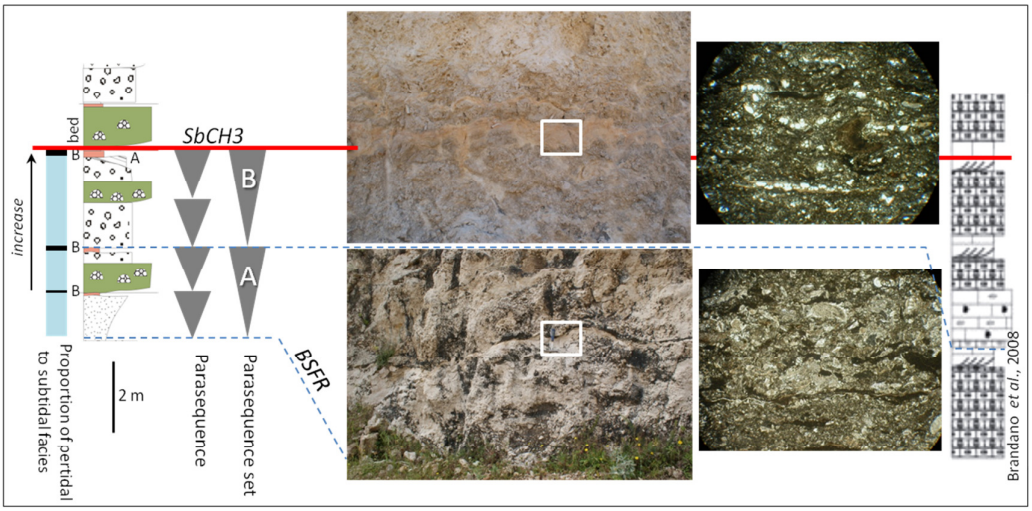

Figure 5.15. Locality 5: parasequence sets A and B. White rectangle marks hammer for scale and the location of sample of photomicrographs. The cycles at locality 5 are correlated to outcrops about 1 km away described by Brandano *et al.* (2008).

5.5.5.ii S4: *Highstand systems tract*

Outcrops are accessible at localities 1, 5, 6 and 14 and the stratigraphy can be viewed along the inaccessible parts of the southern cliff coast of Malta. This unit varies considerably in thickness from <7 m over eastern Gozo and western Malta to 25 m over central Malta. Sediments consist of reworked and fragmented geniculate algal debris with occasional rhodoliths and rare LBF (Figure 5.16). Parasequences and parasequence sets are not clearly defined. At localities 5 and 6, the highstand tract succeeds thin (*circa* 10 cm) pavements of dense rhodolith rudstone beds comprising <2 cm large, very rounded reworked rhodoliths that alternates with thin beds of highly fragmented small foraminifera (unidentified) packstone (Figure 5.12). Farther east at locality 14, loosely packed rhodoliths with open framework structures fill channel-like features (Figure 5.17). The occurrence of rhodoliths within a predominantly algal debris succession in western and eastern localities at the base of the highstand systems tract suggests a drop in sedimentation associated with the maximum flooding event that permitted slow-growing rhodoliths to survive without burial. The highstand systems tract terminates with a metre-thick rhodolith rudstone bed at locality 14 that suggests shallowing and concentration of rhodoliths.

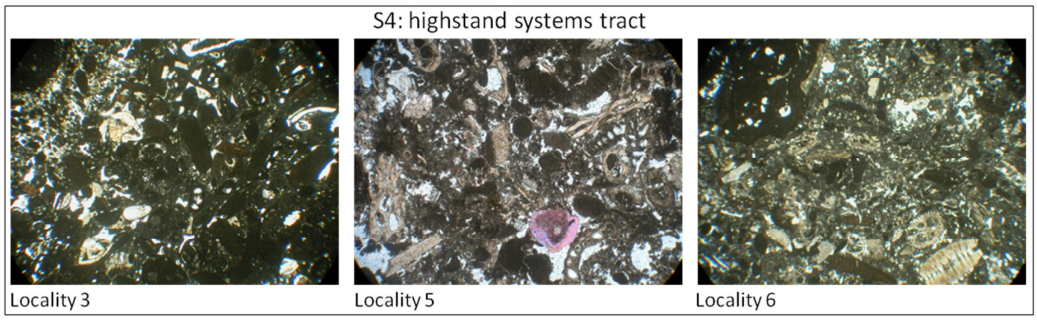

Figure 5.16. S4 highstand systems tract sediments showing fragmented LBF and red coralline algae.

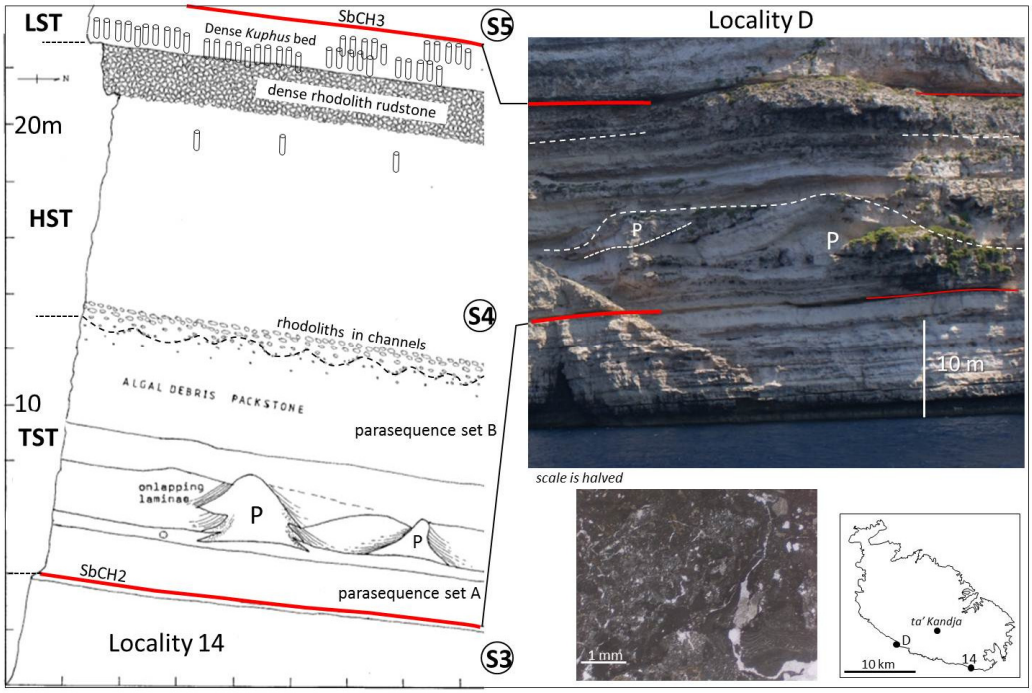

Figure 5.17. Patch reefs and S3 and S4: Locality 14; Section along N-S valley perpendicular to cliff coast. Red line marks the sequence boundaries, dashed line is the maximum flooding surface. The transgressive systems tract of sequence 4 consists of parasequence sets A and B separated by coral patch reefs (P) that are draped by algal debris. The sequence ends with wackestone densely burrowed by *Kuphus*; Locality D. sequence boundaries SbCH2 and SbCH3 form deep grooves in the cliff face. Dome-shaped structures (P) are interpreted to be coralgal patch reefs. These structures occur sporadically at this level all along the 20 km long southern cliff coast of Malta. Photomicrograph of sample taken *circa* 80 m below surface at ta' Kandja water gallery at the level of the lower part of sequence 4. Coral framestone and geniculate algal debris are observed within the gallery.

5.5.5.iii S4*: Transgressive systems tract*

The basal part of this system tract forms a ravinement surface that cuts into the underlying sequence boundary SbCH2 and the reddish-brown sediments at the base of locality A to 3 (Figure 5. 8 and Figure 5.14). The ubiquitous flooding along sequence boundary SbCH2 brought an influx of coralline algal debris (FA IIa). Sediments consist of geniculate coralline algae, fragmented or rounded crustose coralline algae and miliolids which suggest that water depths remained <20 m deep (see Appendix III-23).

Parasequence set A

Parasequences consists mostly of the transgressive phase. Sediments are composed of algal debris beds that show intense micritisation at locality 14 which suggests deposition within the euphotic zone. Gutter casts and coral floatstone are common along bedding. The succession terminates with a coral rudstone/framestone bed at locality 14 and ta' Kandja in central Malta (Figure 5.17).

Parasequence set B

The basal part of the parasequence set consists of coral patch reefs that colonised the coral rudstone bed of parasequence set A. The size of the patch reefs increases eastwards along central Malta: in locality B the patch reefs have a base that is <7 m-wide, whereas at locality D the base is >10 m wide. The level of patch reefs terminates about 15 m above the base of sequence 4 in locality D but is <10 m above base in the western sections (localities B to C). At locality D, stacked coral patch reefs suggest that the corals were trying to keep up with the rapid deepening but were unable to keep up. The drowning of the coral patch reefs is ubiquitous and the patch reefs are draped by algal debris. Laminar algal debris beds are seen onlapping and draping over the coralgal patch reefs at localities 14 and D.

5.5.5.iv S4: *Interpretation*

Sequence 4 begins with the rapid flooding of the carbonate platform that created accommodation space for the development of sporadic metre-wide coralgal patch reefs. The rate of vertical growth of the coral patch reefs could not keep up with sea-level rise and resulted in the drowning and termination of coral growth. This may reflect a change in environmental conditions that was unfavourable to coral growth. The increase in depth culminated in the maximum flooding of the platform which consists mainly of algal sands formed of disarticulated geniculate coralline algae and thin rhodolith pavements in all studied sections. The occurrence of rhodoliths suggests a drop in the sedimentation rate associated with deepening (Figure 5.18).

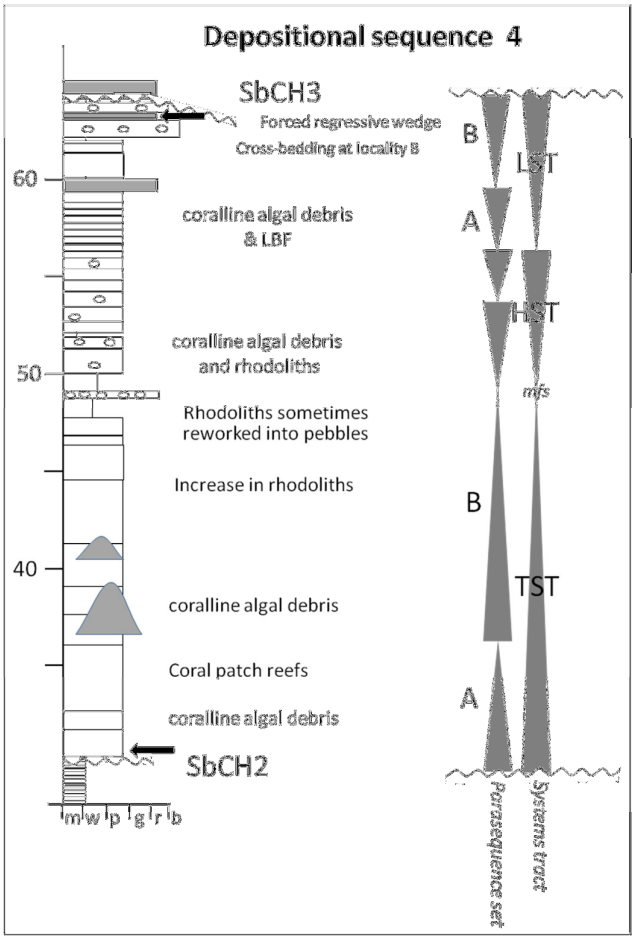

Figure 5.18. Generalised stratigraphy of depositional sequence 4.

The recovery of the sedimentation rate during the highstand of sea-level resulted in relatively thick packages of algal debris until sea-level began to fall during the lowstand systems tract. The subtidal-peritidal triplets in the regressive wedge developed in response to falling sea-level. During the initial flooding stage of the parasequences, open marine conditions favoured coralline red algae and coral biotas. Pre-Miocene coral did not build up to sea-level and remained in relatively deeper conditions, possibly within the oligophotic zone (Pomar & Hallock, 2007). During the regressive stage of parasequences conditions became progressively restricted and lagoon-like (*Kuphus* beds) until disturbed by an influx of reddish (terrigenous) sediments (bed 2) especially towards the shallower western localities. The increase in the thickness of peritidal facies (FA VI) relative to subtidal facies further up parasequence set B at locality 5 suggests a steady drop in relative sea-level that culminated in subaerial exposure and truncation of the regressive wedge along SbCH3. However, the preservation of the regressive wedge during a period of falling sea-level indicates that sufficient accommodation space was available for the aggradation of the prograding peritidal carbonate cycles. This accommodation space was created along the east-facing palaeoslope at localities A and 5 (Figure 5.14). The lowstand of sea-level along the relatively deeper environments of central Malta was characterised by banks of low angle cross-bedded sediments. The migratory sand sheets along the current-swept seabed may have obtained their reddish colour by the influx of eroded reddish inner platform peritidal and terrigenous sediments farther west (FA VI). The bank and the parasequence at locality 6 may represent sedimentation close to the lowest point of the sea along the sea-level curve that culminated in the maximum regressive surface (SbCH3).

Falls in sea-level may trigger failure in unconsolidated carbonates due to reduced pore water pressure (Spence & Tucker, 1997). The scars along SbCH3 in locality C (MT-2 in Appendix IV-22) indicate slope instability during the maximum regressive event. The succeeding transgression formed a ravinement surface that truncated the regressive wedge in the west, the cross-bedded units in central Malta and the much of the peritidal cycles at locality 14 in eastern Malta (Figure 5.19).

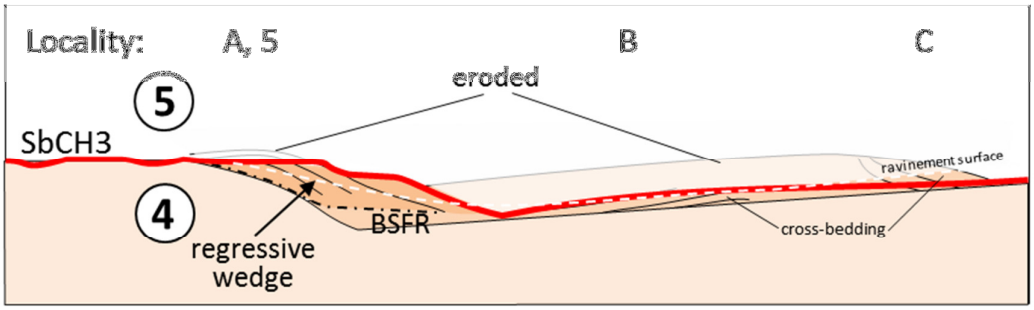

Figure 5.19. Cartoon showing transgressive and lowstand (regressive) systems tracts in sequence 5. The regressive wedge (localities A and 5) prograded along a palaeoslope whereas a moderate energy shoal developed in central Malta (localities B and C). The ravinement surface during the initial transgression in the depositional sequence 5 cycle removed part of the lowstand sediments across Malta.

5.5.6 Depositional Sequence 5

The depositional sequence forms up to 50% of outcrops of the Lower Coralline Limestone in many localities (Table 5-10) and consists of three systems tracts: trangressive, highstand and lowstand systems tracts (Figure 5.20). The last two are characterised by diverse stratal geometries with distinct geographical distribution and mass transport events:

1. Horizontal planar beds: throughout localities 1 to 3 (Gozo and western Malta) stratal geometries consist of horizontal planar beds that form a <40 m thick biostrome of coralline algae with abundant rhodoliths (FA IIb) (Figure 5.21). In eastern Malta, bedding is also horizontal and the rhodolith limestone aggraded to 50 m around locality 13, thinning eastward to 40 m at locality 14. The base of the sequence forms an erosional disconformity with the underlying sequence 4.

2. Large clinoform beds: Three clinoforms packages that extend over several kilometres are found in western, central and eastern Malta.

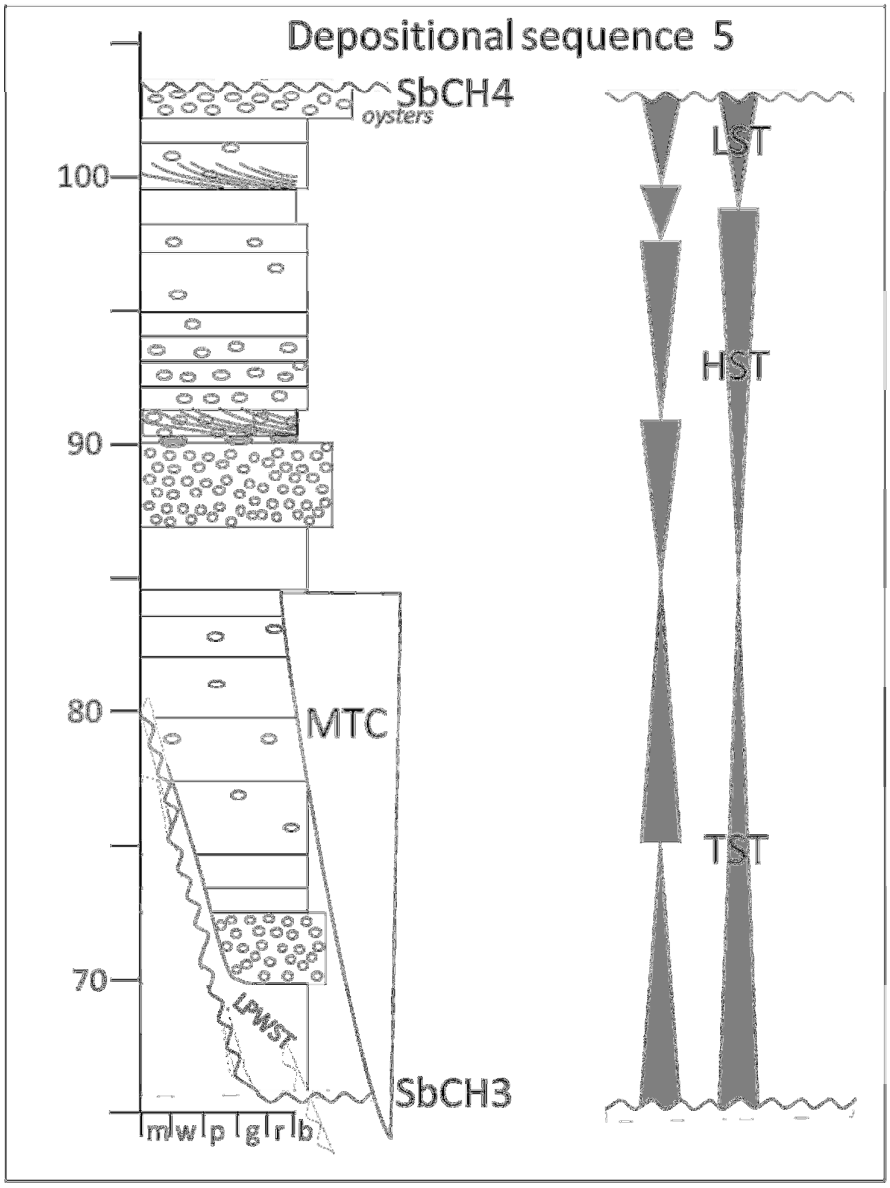

Figure 5.20. Generalised stratigraphic log of depositional sequence 5.

	Depositional Sequence 5			
Locality	1 *(W. Gozo)*	3 to A *(W. Malta)*	B to G *(central Malta)*	13 to 14 *(east Malta)*
Thickness (m)	<20	45	45 – 60 (max. at C)	40 – 60 (max. at 13)

Table 5-10. Thickness of depositional sequence 5.

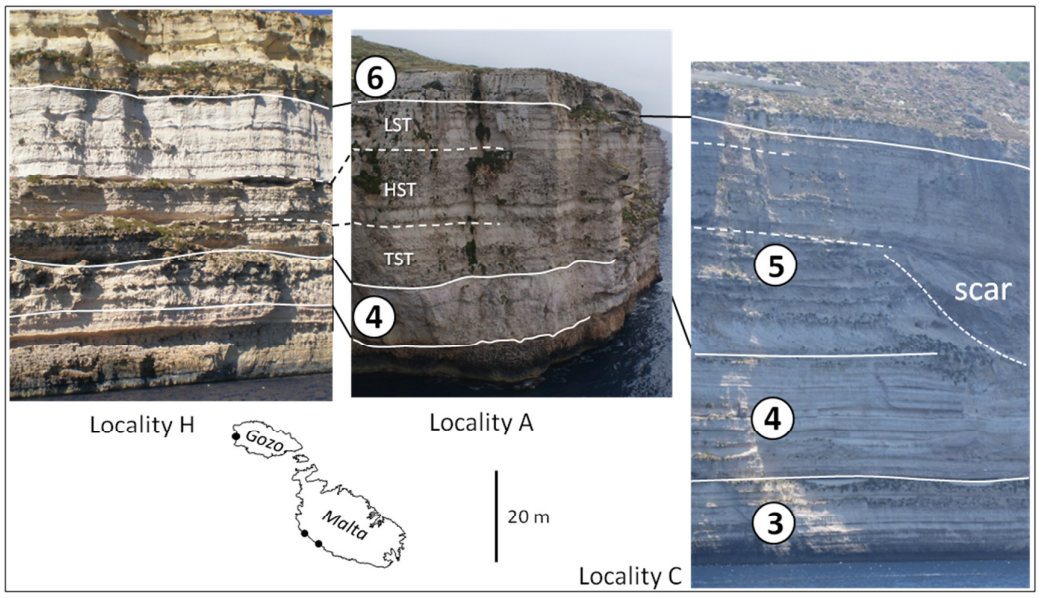

Figure 5.21. Sequence 5: Locality A forms the planar topsets showing horizontal bedding whereas locality C forms part of low-angle sigmoid clinoforms dipping west. The scar along the cliff face was produced by a mass transport complex (MT-3 in Appendix IV-22).

5.5.6.i S5: *Sequence boundary SbCH4*

The major erosional surface along SbCH4 can be recognised along the southern cliff coast of Malta where it forms a horizontal planar surface in the west (localities 9 through 3 to C) whereas in the central to eastern sections (localities D to G) the surface of the sequence boundary is eroded by 10 m-wide and metre-deep scours cut into the underlying sediment. In all logged localities the sequence boundary truncates the topmost rhodolith rudstone bed of the rhodalgal biostrome and is overlain by cross-bedded sediments (FA III) of depositional sequence 6. The planar surface in west Malta shows early cementation along hardgrounds and subsequent corrosion by migrating sand dunes that flattened the surface (Figure 5.22). Evidence of subaerial exposure along SbCH4 is supported by negative isotopic excursions of carbon and oxygen values of >2‰ at locality 1 (Knoerich & Mutti, 2006) and blocky calcite cement and dedolomitization that suggest precipitation and leaching from meteoric water (described in chapter 4).

Figure 5.22. SbCH4 (dashed white line) in locality 9. Rhodolith rudstone pavement along the top of sequence 5 was eroded to a flat surface by corrasion from overlying migrating cross-bedded sediment of sequence 6.

5.5.6.ii S5: *Lowstand systems tract*

The <10 m thick, well-bedded sediment package consists of rhodoliths and fragments of crustose coralline algae, foraminiferans (mainly *Operculina*) and geniculate coralline algae. The increase in geniculate coralline algae and LBF up the succession, interrupted by distinct cross-bedding suggests shallowing upward cycles. Two parasequence sets A and B are recognised in western Gozo (localities 1 and H) and western Malta (localities 3 and A) separated by a bed showing low to high angle cross-bedding. Each parasequence set consists of two parasequences that show faint cross-bedding (Figure 5.23) terminated by an erosional surface. The first appearance of corals along the top part of sequence 5 at locality 13 indicates a gradual change from mesophotic to euphotic conditions which stimulated carbonate productivity. The systems tract terminates with a ubiquitous rhodolith rudstone pavement that is encrusted by oysters at locality 2. The thickness of bedding in the lowstand systems tract thins upward at locality A (Figure 5.24) until sediments are truncated by SbCH4 as seen in Figure 5.22 at locality 9.

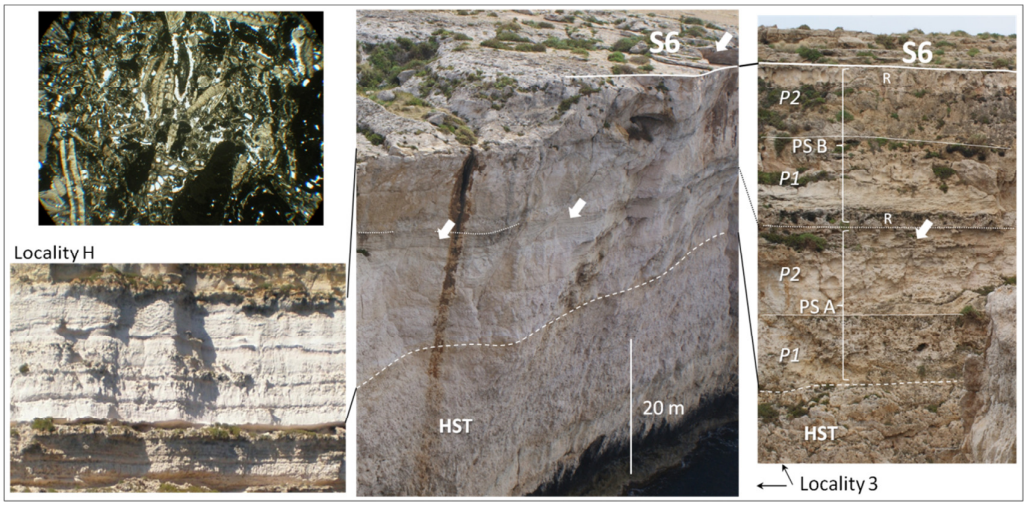

Figure 5.23. Sequence 5; Lowstand systems tract at locality 3 and H above the highstand systems tract (HST) and overlain by sequence 6 (S6). A cross-bedded unit (white arrow) separating parasequence sets PSA A and PS B. Each parasequence set comprises two parasequences (*P1* and *P2*). Rhodolith rudstone pavement (R) is found above or below cross-bedded intervals. Photomicrograph shows abundant *Operculina* (>35% of the rock) in the top parasequence of PS-B.

5.5.6.iii S5: *Highstand systems tract*

Bedding is mostly planar and horizontal. At locality H, differential erosion has exposed bedding produced by high frequency cycles within parasequences. The thickness of this systems tract varies from <15 m in western Gozo to >20 m at locality C. Large clinoforms dipping <5 to 20° are identified at localities 3 and 8. Two parasequence sets are described from outcrops at localities 3 and H:

Parasequence set A

Consists mostly of rhodolith floatstone beds interbedded with rhodolith rudstone pavements. Coralline algal genera include *Sporolithon* whereas <10% volume of accessory grains consists of *Operculina* and *Amphistegina*.

Parasequence set B

Sediments show a decrease in the frequency of rhodoliths and an increase in geniculate algae along beds that become thinner further up the parasequence set. The rhodolith floatstone beds show some faint cross-bedding at locality 3. Distinct packages bounded by erosional surfaces forming parasequences can be recognised along the cliff coast of western Gozo and southern Malta.

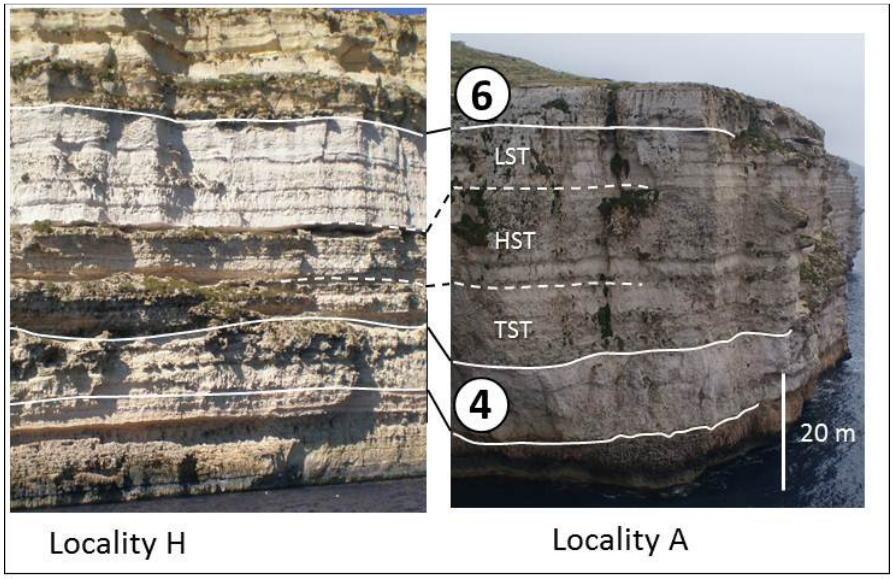

Figure 5.24. Horizontal topsets that thicken from locality H to A although the lowstand sediments are truncated and relatively thinner.

S5: Clinoform bedding:

i. Complex sigmoid-oblique clinoforms: these clinoforms are exposed in three areas and consist of planar topsets that become inclined eastwards:

a. At locality 5 planar topsets consist of rhodolith floatstone and rudstone beds. The topsets offlap eastwards to form *circa* 50 m-thick clinoforms with foresets dipping by <20˚ over >2 km (Figure 5.25). The top 15 m of the clinoforms are exposed at locality 8 and consist of well-rounded and highly spherical rhodoliths. Some of the foresets are interbedded with <1 m thick bed of algal debris that tapers down the foresets. The algal debris and rhodoliths are interpreted to have been transported from the topset area and rhodoliths became very rounded as they rolled down along the top of the foresets. Foresets were affected by upwelling caused by storms or westerly currents that caused reversal in the direction of cross-bedding and created herring bone cross-bedding (Figure 5.25).

b. At locality 3 planar topsets of the rhodolith biostrome become gently inclined towards the east at locality A (Figure 5.26).

c. In eastern Malta, the area immediately east of locality 14 consists of clinoforms beds that dip by 5˚ towards the east. The beds become slightly more expanded downdip.

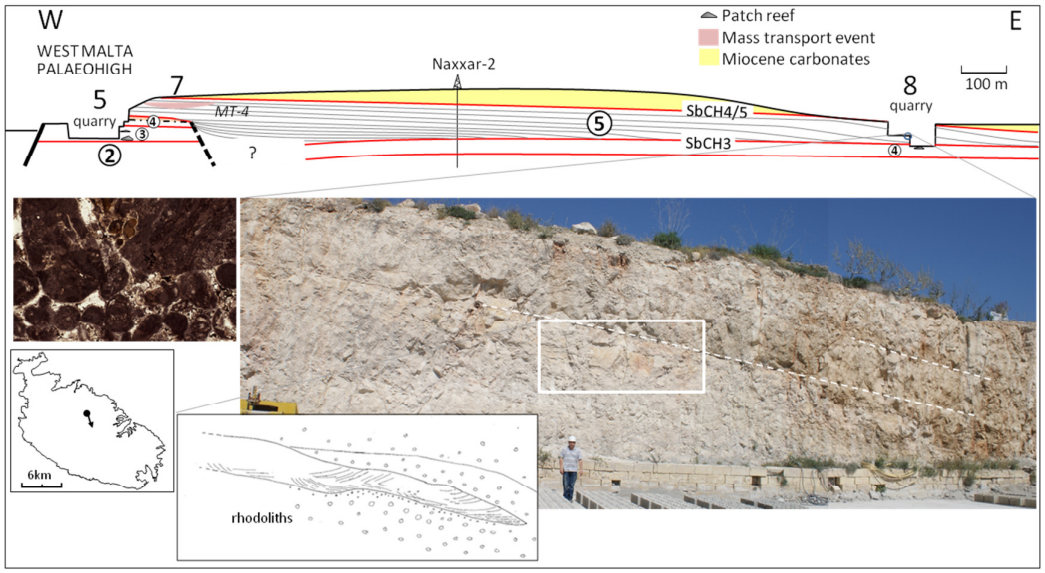

Figure 5.25. Cross-section from the planar topsets at locality 5 to eastward prograding large clinoforms at the Naxxar quarry (locality 8). Inset shows field diagram of grainstone bed showing herring bone cross-bedding interbedded in the rhodolith floatstone. Photomicrograph of sample from cross-bedded unit shows rounded algal grains, *Borelis* and intraclasts. Location map shows direction of clinoform progradation.

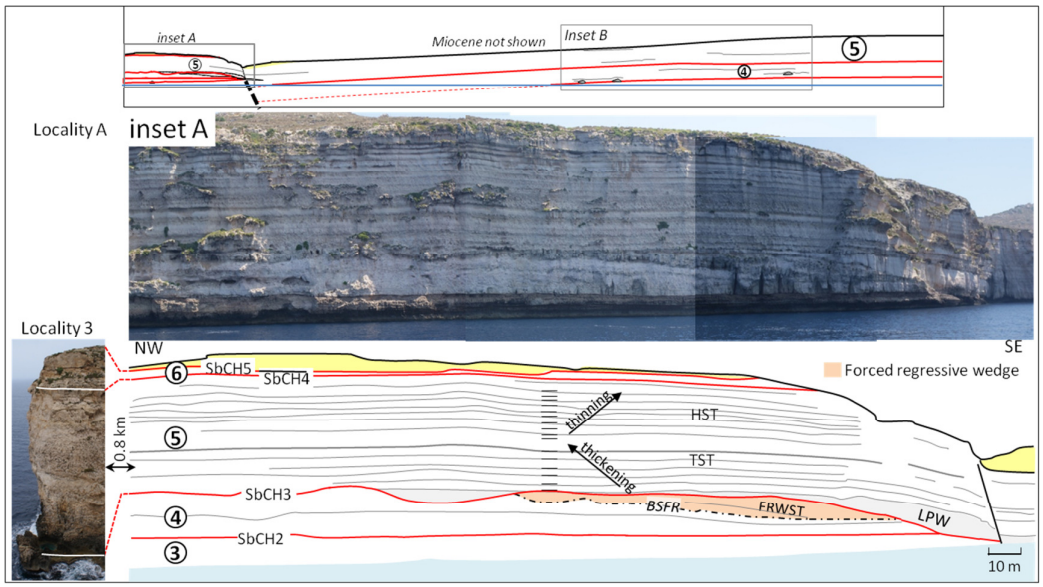

Figure 5.26. Cliff coast of SW Malta: (inset A) uninterpreted and interpreted section at locality A (correlated to accessible locality 3). Sequence boundaries marked by solid red line. The top of sequence 4 was exposed to subaerial erosion which resulted in undulating erosive sequence boundary SbCH3 that truncates coral heads at locality 3 and merges with SbCH2 in the eastern part of locality A. The bedding in the highstand systems tract thins upwards, culminating in an exposure surface marked by SbCH4. (See also Appendix V-27)

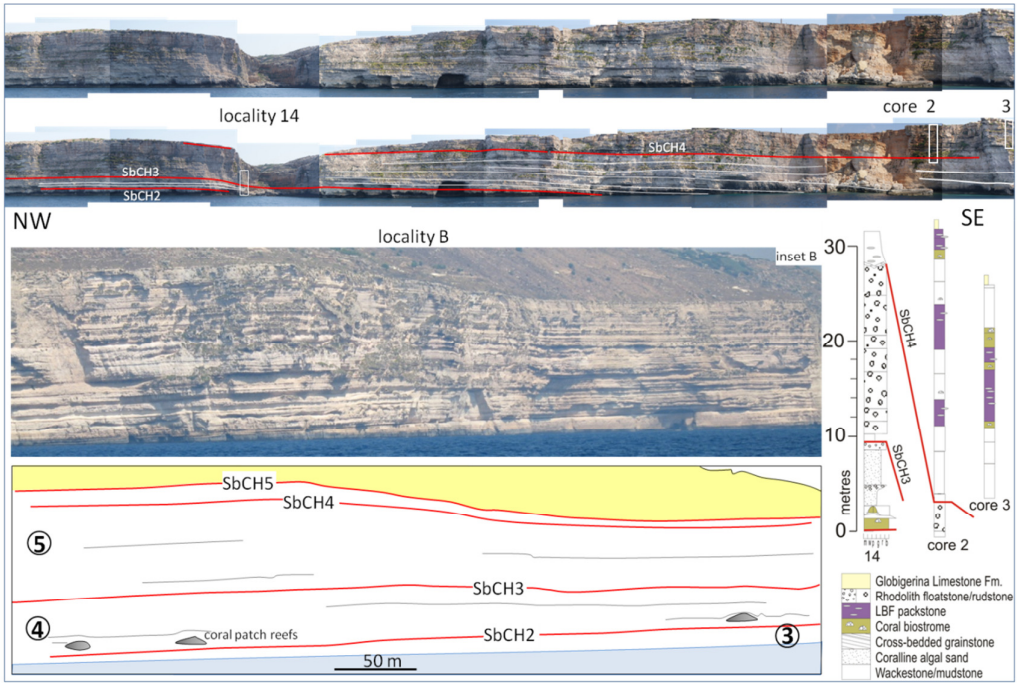

Figure 5.27. Uninterpreted cliff coast around locality 14. The interpreted coast shows sigmoidal clinoforms that dip eastward. Cores 2 and 3 show eastward thickening of depositional sequence 6; Locality B cliff coast (inset B in Figure 5.26) is interpreted on the basis of sequence boundaries (solid red line) and bioconstructions identified by the sediments that drape over coral patch reefs.

ii. Sigmoid clinoform bedding: In the central Malta (localities B to D) the algal biostrome forms planar bedding that dips by <3˚ toward the west, in the opposite direction of the large clinoform foresets in the west (Figure 5.27)

S5: Mass transport events

At locality 7, cycle S5 is scarred by a mass transport event (MT-4) that produced a <300 x 25 m basal shear surface striking N-S within the highstand systems tract with the direction of bulk material movement towards the east (

Figure 5.28). Along the same or slightly lower stratigraphical level, three vertically stacked mass transport events produced the 700 x 30 m mass transport complex (MT-3) at locality C. Outcrops of mass failures consist of only the depleted zones that were later filled with well-bedded sediments. The mass transport event caused lateral compaction and small reverse thrusting along the western margin of MT-3 at locality C, indicating that the sediments were not fully consolidated. The poorly

consolidated condition would have made the sediments susceptible to mass movement.

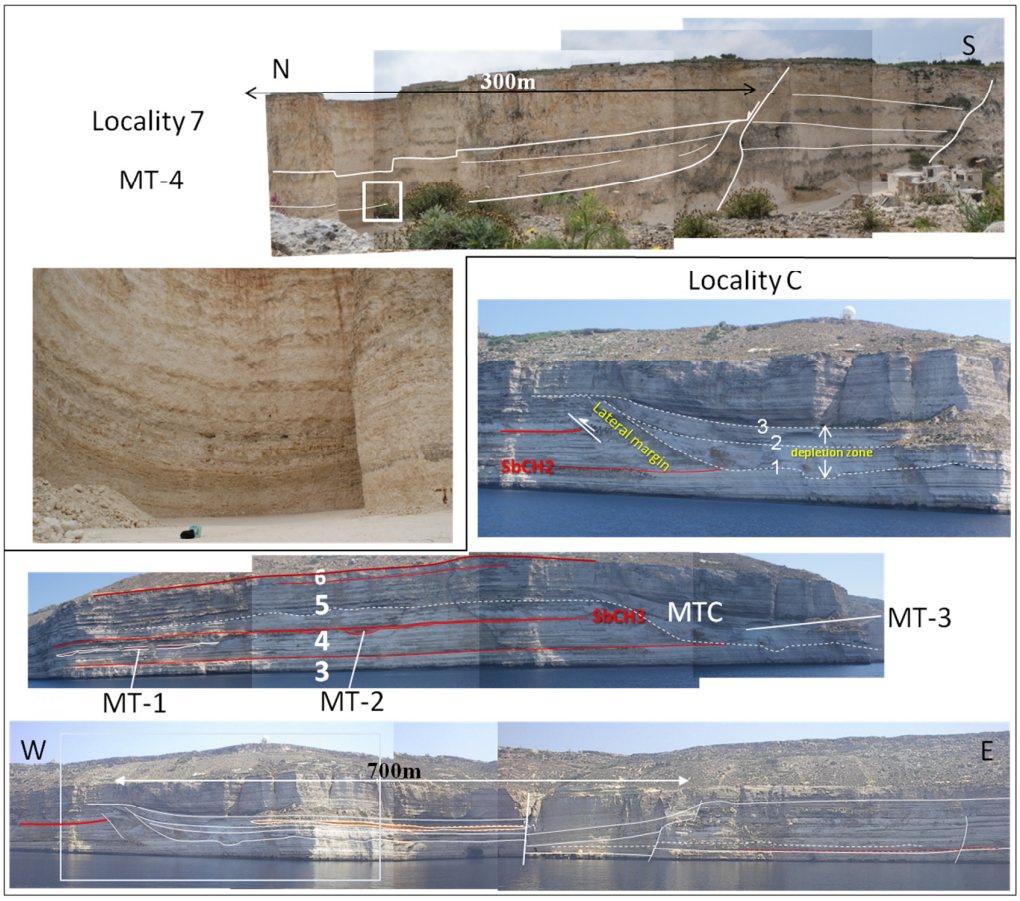

Figure 5.28. Mass transport (MT) events at localities 7 and C: MT-1 and MT-2 occur along or just below SbCH3 whereas the larger mass transport complex MT-3 begins mid-way up sequence 5 and cuts down to sequence 3. The depletion zone shows three scars suggesting repeated failures. The lateral margin shows compressive deformation of sediments and small reverse faults created during failure events. At locality 7, MT-4 also cuts mid-way sequence 5. Bedded sediments fill the depleted zone (inset).

5.5.6.iv S5: *Transgressive systems tract*

Outcrops are exposed along the southern cliff coast of Malta where beds thicken up the succession (Figure 5.26), culminating in the maximum flooding surface capped by a ubiquitous rhodolith rudstone bed. The unit is partly accessible at locality 5 where SbCH3 marks the change from the peritidal cycles at the top of sequence 4 to entirely subtidal sediments. The beds are dominated by rhodoliths that may constitute from 10 to 50% of the rock. Bedding varies from large undulating surfaces at locality H to planar surfaces in locality 5. At locality 5, two parasequence sets are recognised (Figure 5.29):

Parasequence set A

The lower parasequence begins with a 1 m-thick rhodolith floatstone and terminates with a shoaling phase consisting of a 1 m-thick dense rhodolith rudstone pavement. The parasequence set consists mostly of thickly-bedded rhodolith floatstone and terminates with a thin (<5 cm) micritic bed with fragmented LBF. The increase in micrite suggests marine deepening to below the storm wave base and possibly below the photic zone where coralline algae cannot survive. The fragmented LBF shows evidence of transportation from shallower areas.

Parasequence set B

Sediments are similar to parasequence set A and PS-B terminates with a thin micritic bed that represents the maximum flooding surface. In thin section, the rhodolith floatstone bed succeeding the flooding surface shows encrusting coralline algae and echinoid bioclasts with poikilotopic cement that is rounded. This suggests increased current activity and reworking of grains that were already cemented. At the locality 6, sediments consist of large (<10 cm diameter) densely packed rhodolith floatstone that increase in size midway up the section. This represents a deepening that resulted in a drop in sedimentation that allowed the rhodoliths to grow to large sizes.

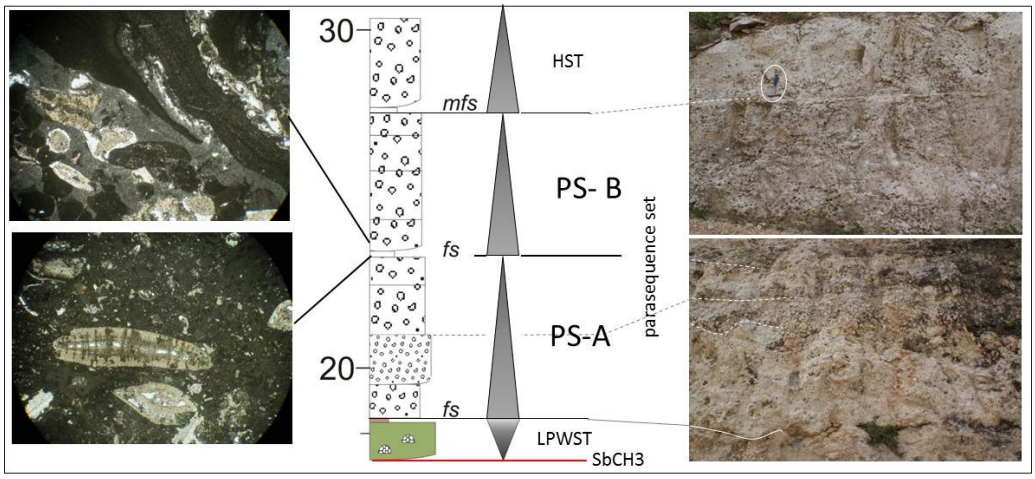

Figure 5.29. Locality 5: transgressive systems tract comprising two parasequence sets A and B formed mostly of rhodolith floatstone and a lower rhodolith rudstone bed. Photomicrographs: (top) shows encrusting coralline red algae and echinoid fragments showing rounded poikilotopic cement; (bottom) mainly micritic with transported and fragmented LBF.

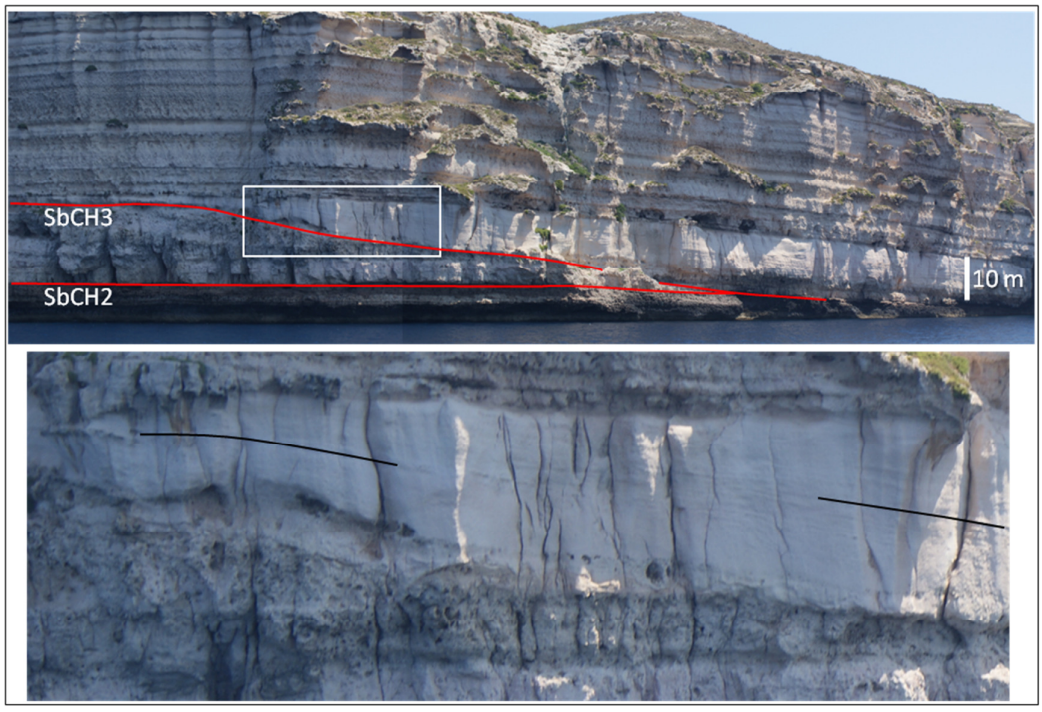

Figure 5.30. Locality A: the lowstand prograding wedge (LPWST) onlaps over SbCH3 and fills the accommodation space created by truncation along the sequence boundary.

5.5.6.v S5: *Lowstand prograding wedge systems tract (LPWST)*

The gradual rise in sea-level following maximum regression resulted in the deposition of a LPWST over SbCH3 exposed at the inaccessible locality A that when seen from some distance appears to be relatively fine-grained and characterised by a bright white-colour (Figure 5.30). The <10 m-thick sedimentary wedge tapers westwards and consists of thin beds of bright white sediments that onlap and downlap over the sequence boundary until it terminates along the palaeo-slope. The base is marked by gutter casts along an erosional surface. At locality 5 the LPWST consists of a metre-thick coral biostrome (Figure 5.29).

5.5.6.vi S5: *Interpretation*

Depositional sequence 5 is the thickest sequence in outcrop. It was produced by aggradation of the coralline algal biostrome (FA IIb) and its progradation east of localities 3 and 5 toward an area which was a bathymetric low. The buildup was controlled by antecedent bathymetry and westerly currents that transported rhodoliths along the palaeoslopes from the main carbonate factories located over western Malta and eastern Malta within the photic zone. The initial increase in accommodation space during the transgressive phase brought mesophotic conditions over the platform and thickening of beds as accommodation space increased.

At the start of sea-level fall, carbonate production was stimulated by increased light along the seabed although the photic level was still low but sufficient for coralline red algae. The carbonate factory over the flat platform top became more productive during the highstand phase of sea-level which resulted in highstand shedding of rhodoliths *sensu* Schlager *et al.* (1994) that produced large clinoforms at different localities. The clinoform bedding in Malta show diverse geometries and direction of progradation as a result of their position with respect to the westerly current flow and the palaeohighs from where the sediment was shed. The direction of the clinoforms relative to the horizontal toplaps suggests that sediment was shed from two distinct linear palaeohighs in western and eastern Malta trending NE-SW (Figure 5.31):

i. Western Malta Palaeohigh (WMP) consists of horizontal topset bedding exposed in localities 3, 5 and 7 that offlap eastwards by highstand shedding of rhodoliths. The clinoforms resulted in a relatively steep constructed palaeoslope along the windward margin affected by westerly-directed currents. Instability along the margin resulted in failure and mass transport at locality 7.

ii. Eastern Malta Palaeohigh (EMP) is characterised by a relatively narrow topset section around locality 13 and low angle clinoform foresets shed off the carbonate factory towards the west over *circa* 10 km between localities E and B. Dispersal by currents leeward of the EMP could not keep up with excess carbonate production and triggered mass failure in the algal biostrome at locality C. The direction of the mass transport events suggests that the depocentre was located in present day offshore north Malta. Sediments were also shed towards the east of EMP along the windward side of the palaeohigh.

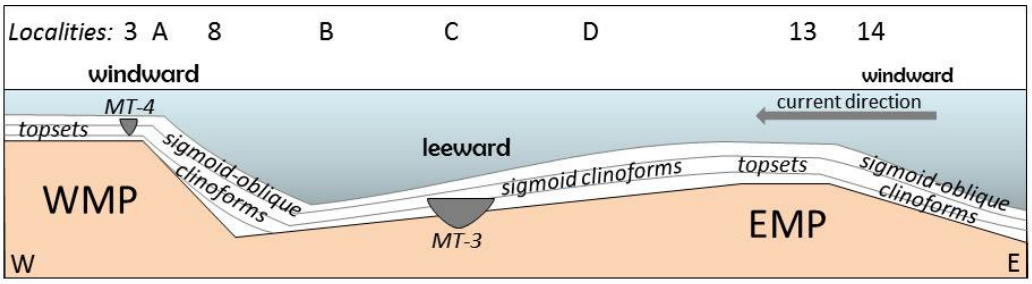

Figure 5.31. West-east model showing the different types of clinoforms bedding and their relation to topsets over the western (WMP) and eastern (EMP) palaeohighs.

The ensuing lowstand of sea-level is characterised by abundant *Operculina*. The thin, plate-like morphology of the tests suggests depths within the lower part of the photic zone (Bassi *et al.*, 2007). Further fall in sea-level exposed the seabed above the FWWB which resulted in transport-controlled processes and the shifting of sediments that produced cross-bedded units. Shoaling produced repetitive subaerial exposure culminating in SbCH4 that eventually switched-off carbonate production along the rhodalgal biostrome, terminating sequence 5.

5.5.7 Depositional Sequence 6

Sequence 6 consists of a succession of mostly cross-bedded sediments of facies association III found in eastern (localities 12, 10b, F and G), western Malta (localities 3, A and 9) and western coast of Gozo (Davies, 1976) that pass upward to more micrite-rich carbonates without distinct sedimentary structures (Figure 5.32). The depositional sequence shows significant geographical variations in thickness and facies and is missing between localities A and B (Table 5-11). This sequence occurs on the two palaeohighs:

The WMP: the tabular LBF shoal facies is <5m thick between localities A and 3 and at locality 9 (FA IIIb). This facies association is missing along the large clinoform beds at locality 8.

The EMP: the LBF sediments become expanded between localities 10 and G and reach a maximum thickness of 30 m but are missing along a ravinement surface at locality 13 where corals are common. Beds of very large *Lepidocyclina* (FA IIIc) accumulated over the NE of Malta in localities 14 and 15 and locality 4a in western Malta.

	Depositional Sequence 6			
Locality	1 *(W. Gozo)*	3 to A *(W. Malta)*	B to G *(central Malta)*	13 to 14 *(east Malta)*
Thickness	7	0 - <3	5 - 30	<10

Table 5-11. Thickness of depositional sequence 6.

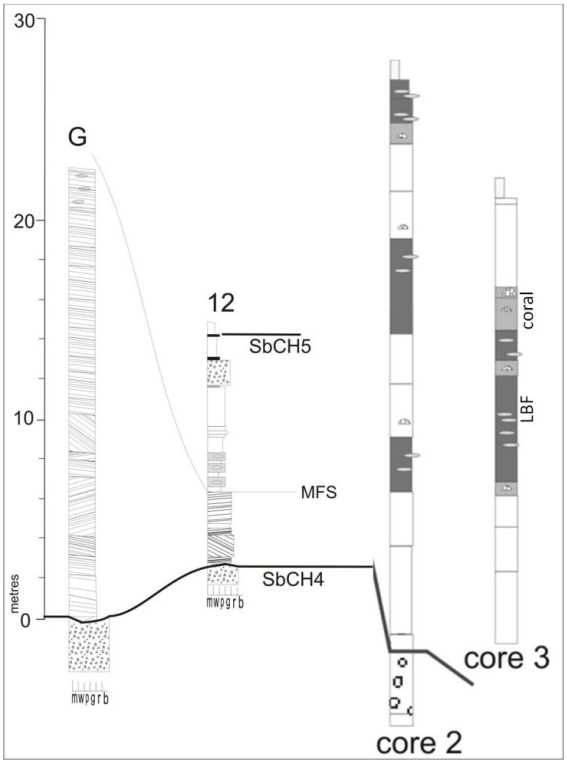

Figure 5.32. Logs of inaccessible locality G (drawn from a distance), the accessible locality 12 and two cores in eastern Malta.

5.5.7.i S6: *Sequence boundary SbCH5*

The top of S6 consists of a hardground along SbCH5 capped by a pectenid pavement and encrusted with oysters. The surface is also capped by sporadic phosphorites at localities 4, 11 and 12. The early cementation reflects an increase in current activity followed by the deposition of allochthonous phosphorite that includes phosphatised moulds of solitary coral which fill neptunian dykes that cut into the hardground at locality 11. The increased current velocity that favours hardground formation over palaeohighs reflects a fall in sea-level which would have also increased current flow from nutrient-rich basinal areas. Increased organic productivity and nutrient levels under low oxygen conditions would stimulate the precipitation of phosphorite. However, conditions always remained subtidal along the sequence boundary throughout the carbonate platform, effectively marking the beginning of carbonate platform drowning.

5.5.7.ii S6: *Highstand systems tract*

In eastern localities 12 and 15, two beds successive with facies IIIc and facies I may represent parasequences. Each cycle comprises a transgressive phase that consists of wackestone to mudstone that is abruptly succeeded by regressive packstone beds with dense accumulations of *Lepidocyclina* (*Eulepidina*) *dilatata* that reach a diameter of 90 mm. The *Lepidocyclina* are either stacked concordant to bedding or in edgewise position (see Figure 3.12 in chapter 3).

5.5.7.iii S6: *Trangressive systems tract*

The bulk of this sequence comprises large cross-bedded units of LBF (FA III) in localities 1 and G to 12 whereas coral biostromes (FA IV) occur in locality 13. The metre-thick sets of cross-bedding are separated by first-order planar bounding planes. The sets extend over 5 km between locality 10 b to G. The foresets are mostly dipping westwards in the direction of the main current flow and less frequently in the opposite direction. Where this systems tract reaches its maximum thickness at locality G, about 10 sets of crossbeds can be identified. Each set represents the preserved transgressive to highstand phase whereas the regressive phase is missing and marked by a sharp erosional surface. It is suggested that this is a succession of high frequency transgressive cycles, each truncating the underlying cross-beds. Parasequence sets are not clearly defined in outcrop but may reflect the gradual thickening of stacked cross-bedded parasequences. At least two parasequence sets are recognised on this basis:

Parasequence set A

At locality G the lower parasequence set is *circa* 16 m thick. The base consists of *circa* 2 m thick cross-bedded units that increase in thickness to *circa* 5 m farther up.

Parasequence set B

The second parasequence set also begins with 2 m thick beds that increase in thickness farther up the succession until sediments become richer in micrite reflecting a drop in energy levels.

Sediments over the WMP have a different fabric from those of the EMP. The WMP is capped by <5 m of beds of highly fragmented LBF with intra-granular glauconite (facies IIIa) separated by bored hardgrounds described in chapter 3.

5.5.7.iv S6: *Lowstand systems tract*

Lowstand sediments are mostly found east of locality 14 at cores 2 and 3 (Figure 5.27). The <30 m thick sediments consist of *Lepidocyclina* beds interbedded with coral and micritic beds. At the accessible locality 15, about 10 m of thick packstone beds consist of up to 90% *Lepidocylcina* that terminate with faintly cross-bedded sediments which represent the ensuing transgressive systems tract. The lowstand systems tract deposits are missing or consist of a hardground in most localities west of localities 14 and 15 except for a thin, <3 m-wide lenticular bed of foraminiferal packstone with large echinoid spines that outcrops along a palaeobathymetric depression at locality 12 between the underlying rhodolith rudstone bed (Sequence 5) and the overlying cross-bedded sediments (Figure 5.33). The micritic texture of this bed suggests a muddy depositional environment similar to a 'lagoon'.

5.5.7.v S6: *Interpretation*

Sediments reflect shifts along the sea-level curve beginning with a lowstand of sea-level (SbCH4). Cores from boreholes east of locality 14 show coral biostromes inter-fingering with thick beds of LBF. The thickening of lowstand sediments east of the EMP and their absence over the EMP suggests a forced regressive wedge (Figure 5.34

During the ensuing transgression, most lowstand deposits over the EMP and WMP were eroded. The absence of lowstand systems tract in most of localities is interpreted to reflect widespread erosion over the EMP and WMP from the

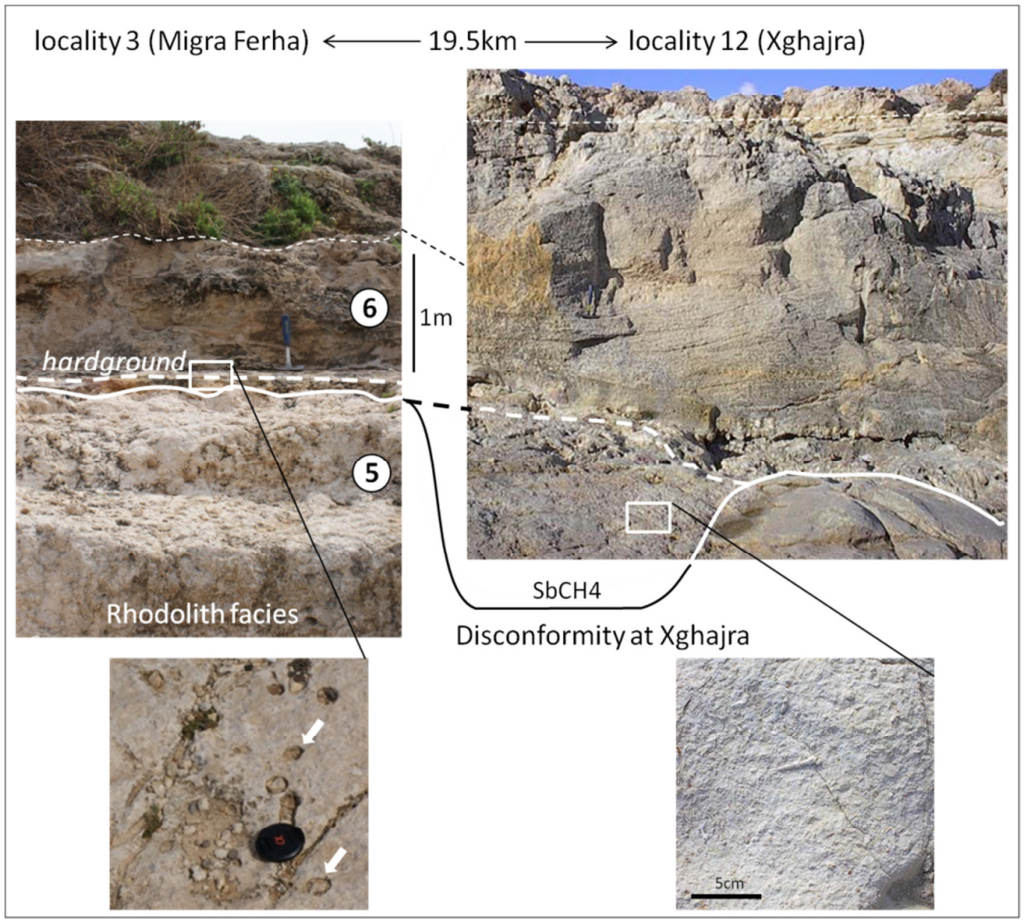

Figure 5.33. The transgressive systems tract sediments. At locality 12 a small part of the lowstand systems tract is preserved.

shoreward-migrating ravinement surface during the ensuing marine transgression. The transgression deposited cross-bedded shoals that migrated over the Malta Platform that removed lowstand deposits by corrasion over the palaeohighs. The transgressive sediments show condensation over the WMP which was the bathymetric high in the area of the Maltese Islands. The shallower environments in localities 13 to 14 (EMP) were colonised by corals and included algal sands and large gastropods suggesting agitated backreef environments. The solitary 'reefal' buildup in southeast Malta was flanked to the west and east by *Lepidocyclina* shoals. The thickness of the LBF shoal sediments corresponds to the palaeobathymetry and the effect of current dispersal of highly hydrodynamic LBF: thicker, expanded accumulations (facies IIIb) occur where accommodation space was largest and

leeward of EMP, whereas the condensed facies IIIa was deposited where accommodation space was least over the WMP (figure 5.34).

Nevertheless, high rates of dispersal resulted in accumulation rates that did not match sea-level rise. The maximum flooding of the platform was accompanied by an increase in fine-grained sediments and decrease of LBF further up the shoal which reflecting the drowning of the bank. The deposition of mainly micritic sediments of facies I is interrupted by cyclic beds of large *Lepidocyclina* during the highstand of sea-level. The large size of the LBF suggests deposition close to the SWB at depths of >40 m. The fall in sea-level during the highstand systems tract was not sufficient to bring the carbonate platform within depths of maximum carbonate production of <15 m (Bosscher & Schlager, 1993) and as a result, the carbonate platform began to drown. However, the drop in sea-level produced a terminal hardground that was capped by a pectinid pavement and sporadic phosphorites along SbCH5.

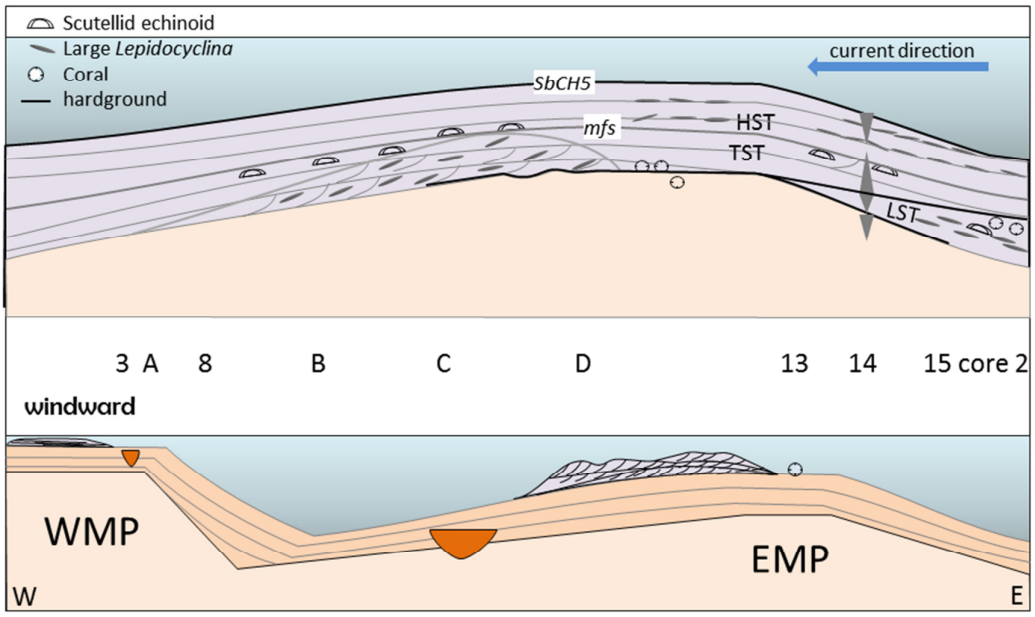

Figure 5.34. Depositional model of sequence 6. Inset shows the Eastern Malta Palaeohigh.

Chapter 5: part 2

Stratigraphy of the Malta Platform:

Chronostratigraphy and the sea-level curve

5.6 INTRODUCTION 199
5.7 BIOSTRATIGRAPHICAL FRAMEWORK 199
5.7.2 Eocene 204
5.7.3 Oligocene 205
5.8 STRONTIUM ISOTOPE DATING 206
5.9 ASTROCHRONOLOGY 208
5.10 DISCUSSION 211
5.10.2 Third-order sea-level cycles 211
5.10.3 Fourth-order sea-level cycles 215
5.10.4 Fifth-order sea-level cycles 216
5.10.5 Sea-level cycles and controls on sedimentary cycles 217
5.10.6 Constructing the relative sea-level curve 220
5.10.7 Correlation to regional sequence boundaries 226
5.10.8 Malta Platform sequences and global third-order cycles 228
5.11 SUMMARY 230

5.6 INTRODUCTION

The chronostratigraphy of the Palaeogene of the Malta Platform is constructed on a number of dating methods that are independent of each other. The scope of chronology is to make correlations to other areas and to global events. The objectives of this part of the chapter are to date and calibrate to the timescale of the International Commission on Stratigraphy (Gradstein *et al.*, 2004) by using the following methods: (1) to date the Palaeogene carbonates of Malta by using large benthic foraminifera, (2) to date the same succession using strontium isotope dating, (3) to fine-tune dating by applying astrochronology based on the hypothesis that astronomical forcing controlled cyclostratigraphy in the Lower Coralline Limestone, and (4) to construct a sea-level curve that can be compared to sea-level curves from other regions.

5.7 BIOSTRATIGRAPHICAL FRAMEWORK

The occurrence of marker large benthic foraminifera in the Palaeogene of the Malta Platform allows comparisons to the Oligo-Miocene shallow marine benthic foraminiferal biozonation (SBZ) of Cahuzac & Poignant (1997) for southern Europe and the SBZ of the Eocene to Palaeocene (Serra-Kiel *et al.*, 1998). Previous work has dated the outcrops of the Lower Coralline Limestone as Chattian by using LBF (Felix, 1973), whereas Eocene sediments have been dated by Bismuth & Bonnefous (1981) as Late Eocene and equivalent to the Halk el Menzel Formation in Tunisia, although such dating is debatable. In this study, the Palaeogene sediments and the depositional sequences described in the first part of this chapter are dated using SBZ biozones. However, the LBF biostratigraphy used in well reports of deep wells drilled over the Malta Platform by BP and Total (see Appendix I-2) rely on biostratigraphic schemes from other regions (e.g., southeast Asia) that pre-date the SBZ biozones for southern Europe of Cahuzac & Poignant (1997) making them relatively inadequate for the Mediterranean. The dating in these well reports has been reinterpreted using the SBZ biozones for southern Europe so as to have a standardised biostratigraphy for both outcrops and subsurface data.

The facies associations show particular benthic foraminiferal assemblages as shown in Table 5-1. The LBF assemblage in Naxxar-2 well is compared to outcrop in Figure 5.35. Detailed biostratigraphy in four localities is shown in Figure 5.36 (see also appendix III) whereas data from Aqualta well is re-interpreted in terms of the SBZ biozones and compared to Maltese outcrops (Figure 5.37).

FA	Sequence	Benthic foraminiferal assemblages
III	6	Top sediments of the formation dominated by high diversity in the genera of LBF of the suborder Rotaliina which have a hyaline, perforate and lamellar wall structure. Lepidocyclinids abundant in some beds. Giant forms have flattened discoidal test adapted to deeper water.
IIb	5	Dominated by coralline red algae (rhodoliths) and low genera diversity LBF, mainly *Operculina* that have flattened discoidal tests and *Amphistegina.*
IIa	4	The main grain type is algal sand that comprises a mix of Miliolina (*Quinqueloculina* and *Austrotrillina*) and Rotaliina. The latter are less abundant and include *Amphistegina,* Lepidocyclinids (rare) and *Miogypsinoides complanatus* (rare).
IV, V	3	Dominated by rounded tests adapted to shallow water of Miliolina comprising superfamilies Soritoidea (e.g., *Peneroplis* and *Praerhapydionina*) and Milioloidea (e.g., *Quinqueloculina* and *Austrotrillina*) which are composed of porcelaneous, calcitic and imperforate walls. The matrix is mainly micrite. Felix (1973) identifies this unit in outcrop as the *Autrotrillina-Praerhapydionina* assemblage

Table 5-12. Main foraniniferal assemblages in depositional sequences that crop out.

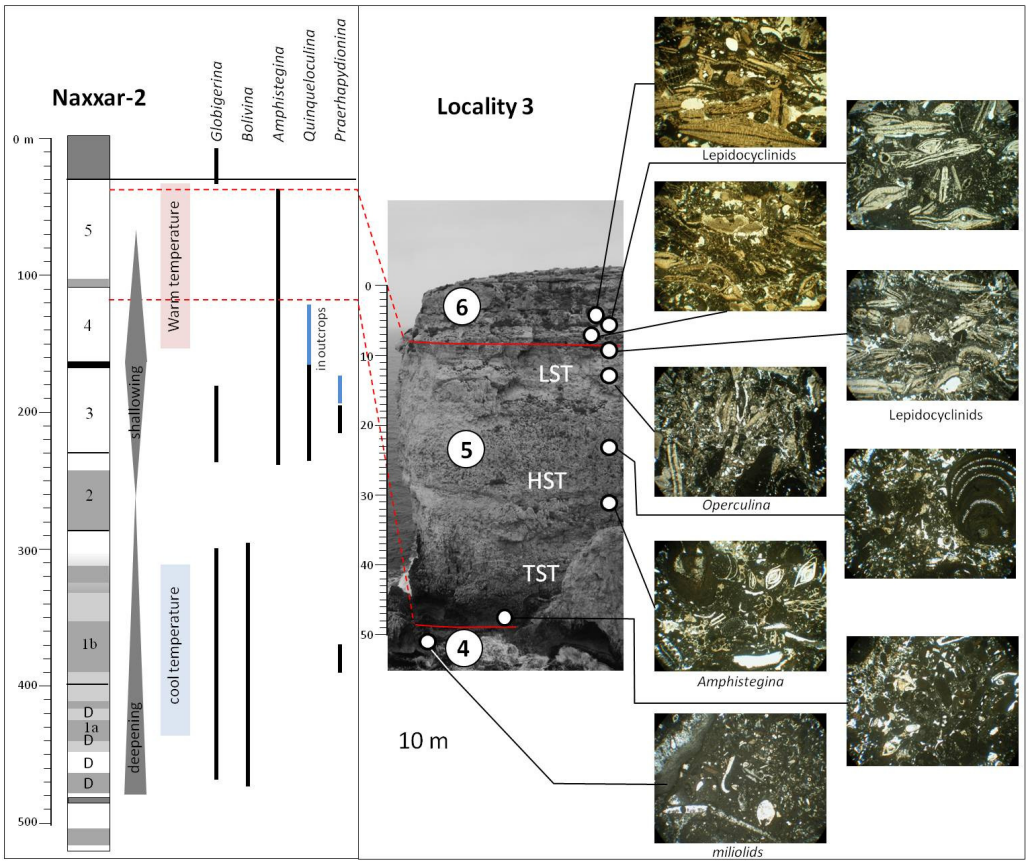

Figure 5.35. Schematic log the Lower Coralline Limestone Formation in Naxxar-2 well. Vertical black bars show extent of foraminiferans in outcrops only (blue line) and in the Naxxar-2 well (black line); Comparison to sequences 4 to 6 at locality 3. Photomicrographs show predominant foraminifera. In some beds foraminifera are rare or abundant but highly fragmented and cannot be identified (see Appendix III-24 and 25).

Benthic foraminifera reflect environmental conditions during the Palaeogene, especially temperature, photic level and nutrient level. The Eocene was a warm period during which Nummulitids and Alveolinids were abundant in oligotrophic conditions. However, no true Alveolinidae survived into the Oligocene whereas the Nummulite assemblages became impoverished by the Late Eocene (Brasier, 1995a). The Early Oligocene appears to have been relatively cooler (Figure 5.35) with reduced oligotrophic-adapted benthic foraminifera (Hallock *et al.*, 1991) whereas the Late Oligocene is marked by warmer temperatures and the occurrence of Amphistegina and later the flourishing of Lepidocyclinids (Buxton & Pedley, 1989).

The Eocene and Oligocene Epochs are dated using the LBF that occur in wells and outcrops. No Palaeocene samples were retrieved from wells.

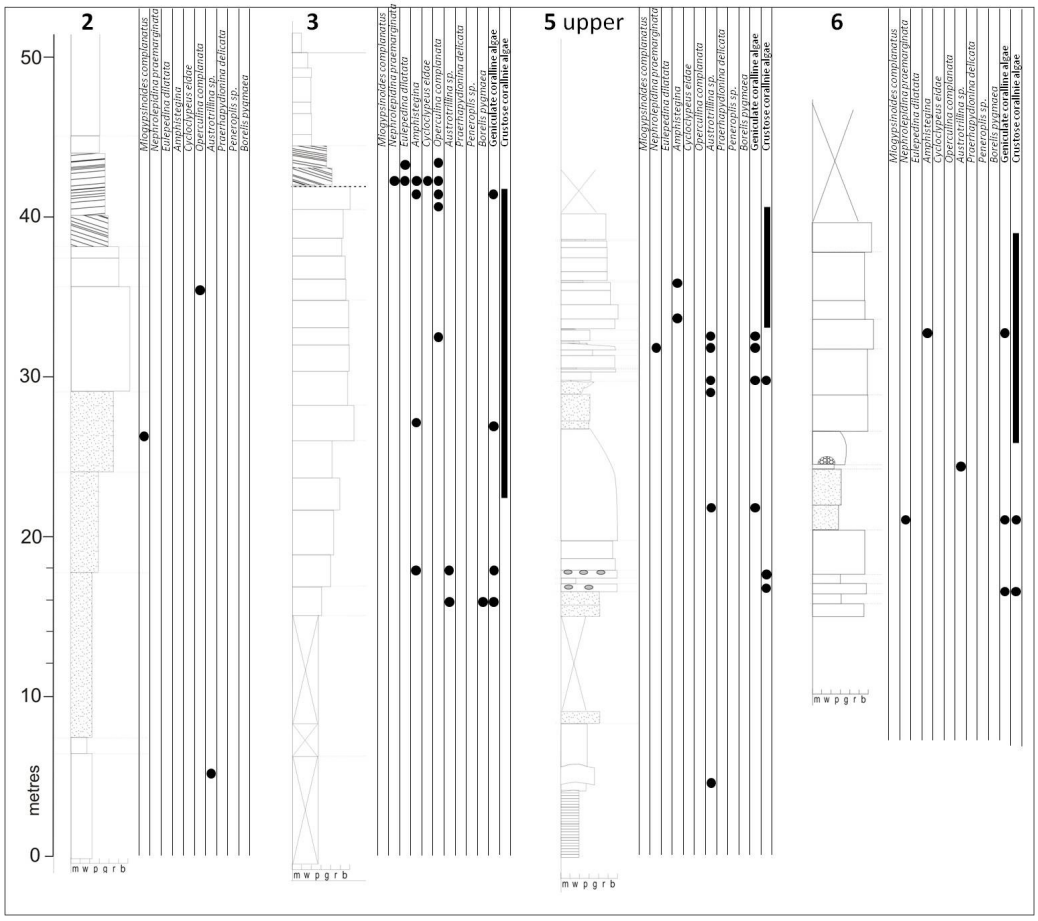

Figure 5.36. Data based on thin sections and hand specimens: Coralline algal forms and LBF in localities 2, 3, 5 and 6. Vertical bars show extent of rhodoliths in the sections. A larger diagram can be viewed in Appendix III-20 and 21.

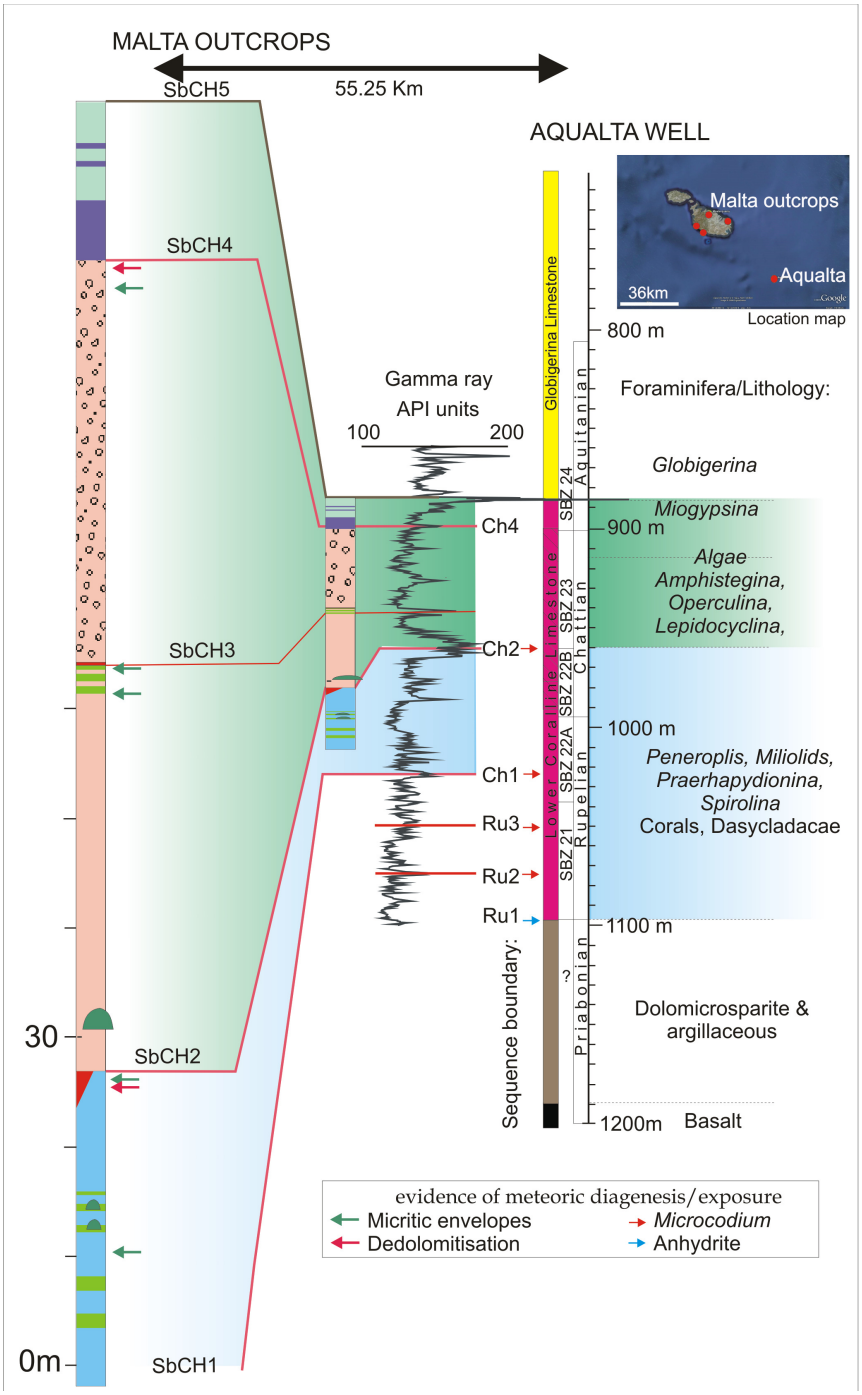

Figure 5.37. Generalised stratigraphic log of the Lower Coralline Limestone Formation in outcrop that reaches *circa* 120 m in thickness (expanded log on left) correlated to the Aqualta well and its biotas recorded from well cuttings. Sequence boundaries are marked by gamma ray peaks and *Microcodium* in Aqualta well and micritic envelopes, anhydrite/gypsum and rare dedolomitization in outcrops.

5.7.2 Eocene

In the Naxxar-2 well, the occurrence of *Alveolina oblonga* in the undolomitised part of the succession below SbRU1 places these sediments within SBZ 10 and 11 of Serra-Kiel *et al.* (1998), dated Early Eocene (Ypresian). The succeeding SBZ 13 to 20 (14 Ma duration) are missing over the Malta Platform (Figure 5.38), implying an erosive depositional hiatus during the Late Eocene during which time gypsum was deposited. This means that the Maltese equivalent to the Late Eocene Halk el Menzel Formation is relatively thin and entirely subsurface in Malta, in contrast to what is suggested by Bismuth & Bonnefous (1981).

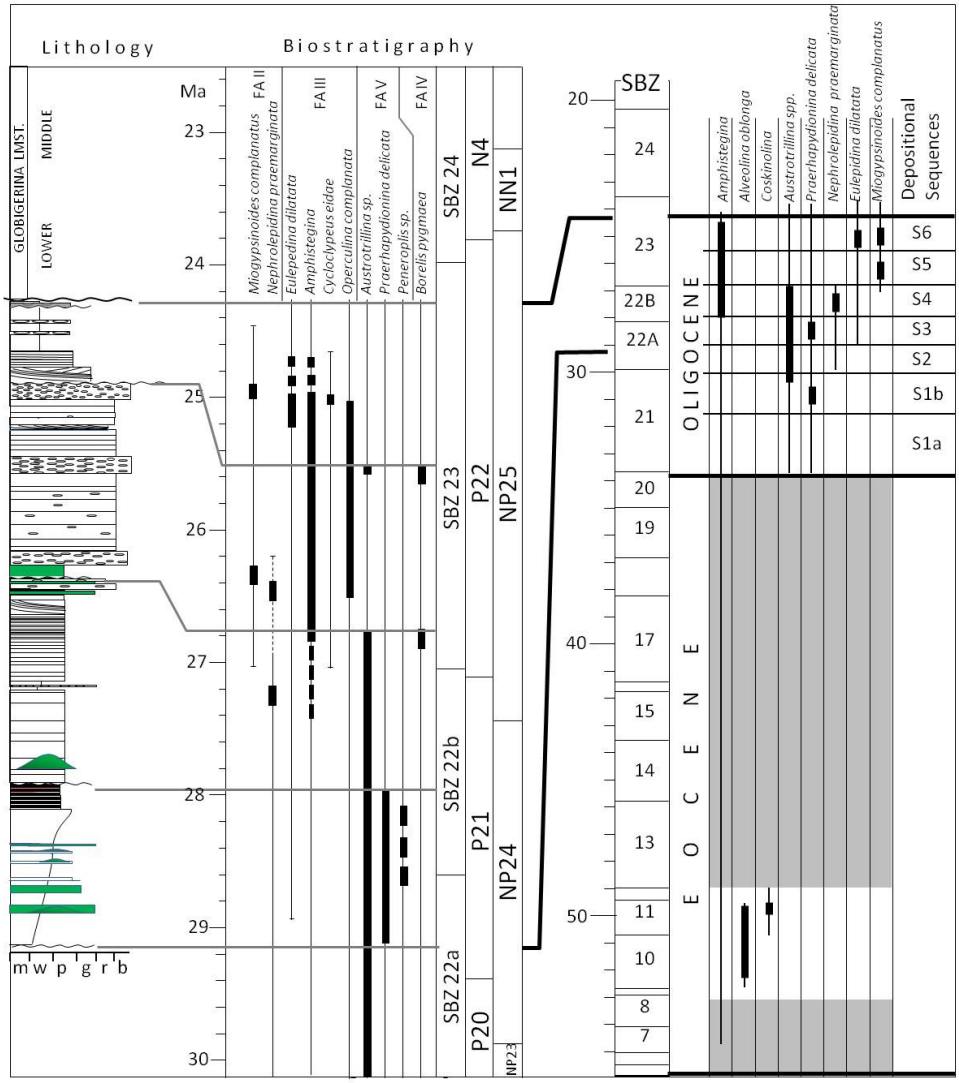

Figure 5.38 (caption on next page)

Figure 5.38. Previous page Left: Generalised log of Lower Coralline Limestone Formation in outcrop from depositional sequence 3 to 6. Grey horizontal lines represent major erosional/hiatal surface along sequence boundaries, the lowest is the subsurface SbCH1; Right: Thin black lines show extent of biozone for each foraminiferan based on LBF biozones SBZ22 to SBZ 23 of Cahuzac & Poignant (1997). Superimposed are thick black vertical lines that show chronostratigraphic occurrence of LBF in the Maltese Islands relative to composite log and major erosional surfaces. Right: summary of Oligocene and Eocene biozonation and occurrence of LBF in outcrops and wells. The grey shading shows missing biozones interpreted as depositional hiatus.

5.7.3 Oligocene

The limestone succession in outcrop is dated on the following biomarker LBF that have relatively restricted biozones through time (Figure 5.38):

i. *Nephrolepidina praemarginata*: identified in thin section in sequence 4 at locality 6 a couple of metres below SbCH3 (Figure 5.39) and also reported by Felix (1973) at localities 2 and 12 where it is subordinate to *Lepidocyclina eulepidina*. *Lepidocyclina nephrolepidina* corresponds to SBZ 22B starting at 30 Ma.

ii. *Miogypsinoides complanatus*: First appearance is reported by Felix (1973) in eastern Gozo (locality 2) in sequence 5 at a level <10 m below cross-bedded facies IIIb. *Miogypsinoides complanatus* marks the start of benthic foraminiferal biozone SBZ 23 dated 27 Ma.

iii. *Miogypsina*: The base of SBZ 24 is defined by the appearance of this foraminiferal marker that coincides with the beginning of the Aquitanian Stage. In Lower Coralline Limestone outcrops *Miogypsina* is not recorded but it is found in the topmost 20 m of the formation in the offshore Aqualta well (Figure 5.37).

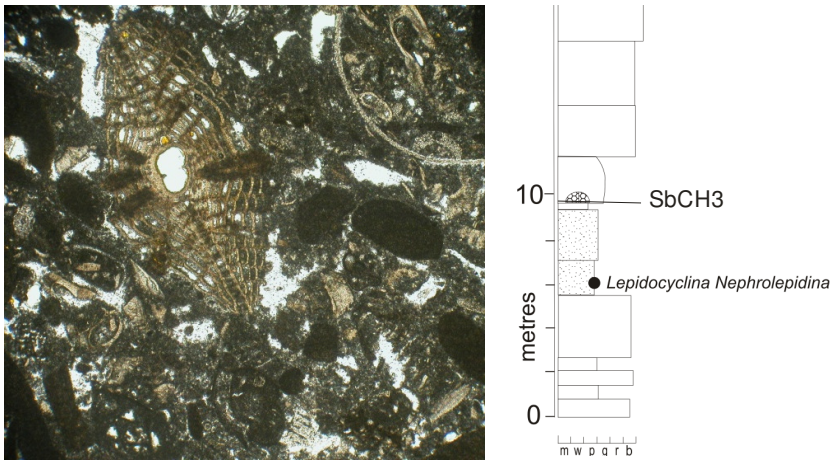

Figure 5.39. Photomicrograph shows *Lepidocyclina Nephrolepidina* that shows evidence of some transportation. The log of locality 6 shows stratigraphic position of sample (see Appendix II for entire log).

5.8 STRONTIUM ISOTOPE DATING

Continental weathering and oceanic hydrothermal processes deliver $^{87}Sr/^{86}Sr$ to seawater depending on global tectonics. As a result, the level of radiogenic strontium varies through time (Burke, *et al.*, 1982). The strontium present in limestone should reflect the temporal variation of strontium in seawater as shown in Figure 5.40 and can be used to date carbonates.

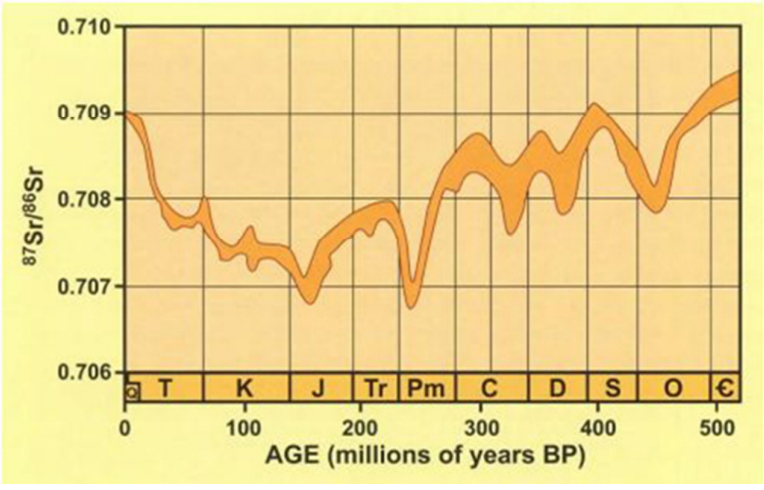

Figure 5.40. $^{87}Sr/^{86}Sr$ isotopes ratios of marine carbonates through time (from Burke *et al.*, 1982).

Published bulk rock samples tested for $^{87}Sr/^{86}Sr$ isotopes of the Lower Coralline Limestone include the following: a level mid-way up depositional sequence 5 at locality 1 and about ten metres below SbCH4 is dated by Knoerich & Mutti (2006) as 25.5 ± 0.7 Ma. The base of the overlying Globigerina Limestone Formation found 27.7 m farther up the same section is dated 24.4 ± 0.7 Ma (Knoerich & Mutti, 2006). About 1 m below this sample point is the hardground (SbCH5) terminating the Lower Coralline Limestone which is sometimes capped with the C_0 phosphate bed farther east (Figure 5.41). The succeeding >130m of hemipelagic carbonates and clay that drape the Lower Coralline Limestone over the entire Malta Platform include the Early to Mid-Miocene Globigerina Limestone formation which is sub-divided into three Members, each separated by a significant depositional hiatus that is capped by the two ubiquitous <1 m-thick phosphate-rich beds (C_1 and C_2 beds).

The C_1 phosphate bed is dated using strontium isotopes as *circa* 23.37 Ma (Föllmi *et al*., 2008). In addition to published strontium dating, a sample from the base of locality 5 (Figure 5.7) was tested for $^{87}Sr/^{86}Sr$ and found to be 0.708098±0.000013 (2σ). The sample is dated 28.6±0.6 Ma using the strontium curve of Miller *et al.* (1988) derived from DSDP site 522 in the South Atlantic, calibrated to the geomagnetic polarity time scale.

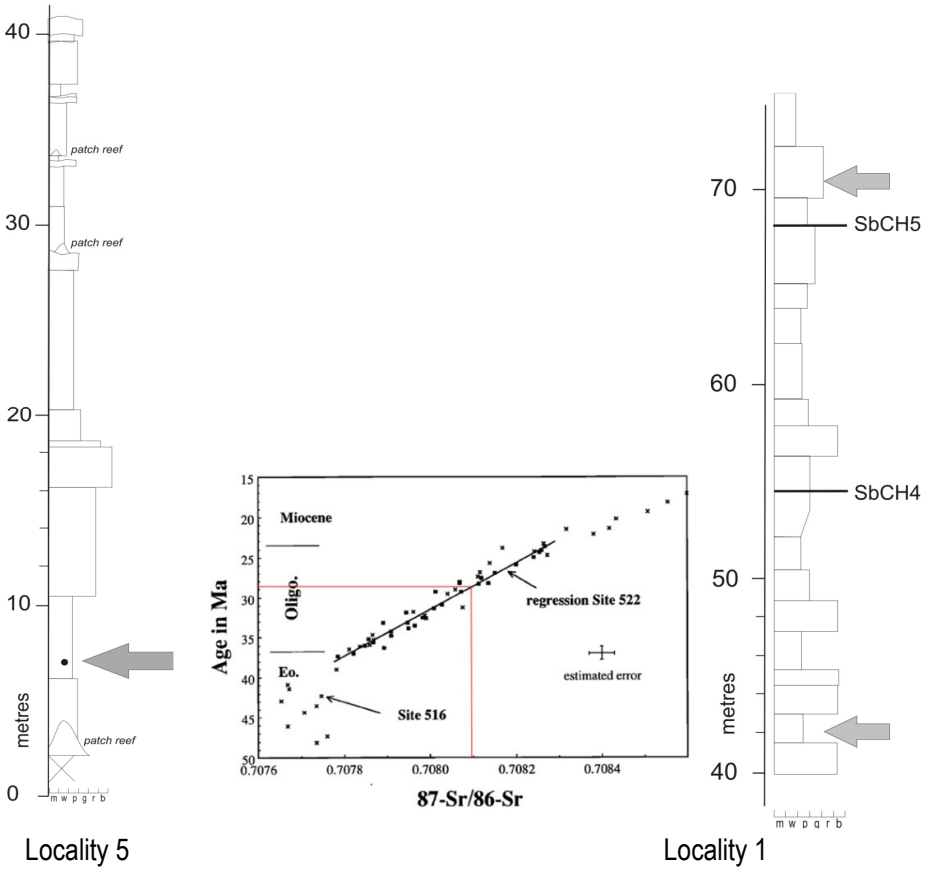

Figure 5.41. Locality 5: Arrow shows point sampled for strontium isotope value (*circa* 50 m below SbCH2); locality 1: points sampled for strontium isotopes by Knoerich & Mutti (2006). Regression from site 522 (Miller *et al.*,1988). Red line shows dating of sample from locality 5 using this regression.

5.9 ASTROCHRONOLOGY

Age calibration using astronomical time scale is now recognised by the International Commission on Stratigraphy as a method for dating rock successions and is used to identify a Global Standard Section and Point (GSSP) at the beginning of the Serravallian based on astronomical calibration of the Blue Clay Formation in western Malta (Hilgen *et al.*, 2008).

Astronomical forcing on global climate results in cyclicity in carbonates. However, controls on carbonate cyclicity can be random or non-random (Read, 1989):

1. Random cyclicity; Drummond & Wilkinson (1993) argue that asymmetric, repetitive shallow-water carbonate lithofacies, often interpreted as evidence of glacio-eustatic cyclicity (Goldhammer *et al.*, 1990; Mitchum & Van Wagoner, 1991), are indistinguishable from random thickness associations and could reflect differential compaction or changing rates of platform subsidence rather than eustatic controls.

2. Non-random cyclicity results from global sea-level change produced by the locking of water in the polar ice caps that produces Milankovitch-type sea-level fluctuations (Miller *et al.*, 2005). Many carbonate successions show cyclic and hierarchical stacking of sedimentary packages that have been interpreted as reflecting climatic oscillations related to Milankovitch cyclicity (Fischer, 1964; Goldhammer *et al.*, 1990; Mitchum & Van Wagoner, 1991) controlled by the Earth's orbital cycles.

The following considerations suggest that cyclicity seen in the field was non-random and reflects platform-wide sea-level changes:

- The successive sequence boundaries representing subearial episodes occur at a regular frequency of *circa* 30 to 40 m.
- The lateral persistence of peritidal cycles along the top sediments of sequence 4 is >4 km (localities 5 to 6) and extend to the Aqualta well (Figure 5.37).
- The lateral persistence of the rhodolithic facies with similar bed thickness in sequence 5 between locality 1 and 3 is >24 km.

The cyclicity seen in outcrops reflecting global glacio-eustatic sea-level fluctuations is compared to the following astronomical cycles of Laskar *et al.* (2004) and Pälike *et al.* (2006) in Figure 5.42:

i. The Oligocene deep sea oxygen and carbon stable isotope record is considered to reflect orbital controls, namely long cycle obliquity and long cycle eccentricity (Pälike *et al.*, 2006). Obliquity minima amplitude events (angle of obliquity around 23˚) reduce summer insolation in high latitudes, favouring the expansion of global ice-sheet during the Oligocene. Bandpass filtering of $\delta\ ^{18}O$ and $\delta\ ^{13}C$

isotope values from deep sea cores of Oligocene sediments has extracted a number of obliquity cycles separated by nodes of minimum obliquity that recur at a periodicity of 1.2 Ma. Four of these cycles are here named A, B, C and D.

ii. Glacio-eustatic fall is also linked to phase relation of glacial lowstands to 1.2 Ma obliquity minima and 405 kyr eccentricty minma. The 405 ky-long cycles are numbered cycles 61 to 72 (Figure 5.42).

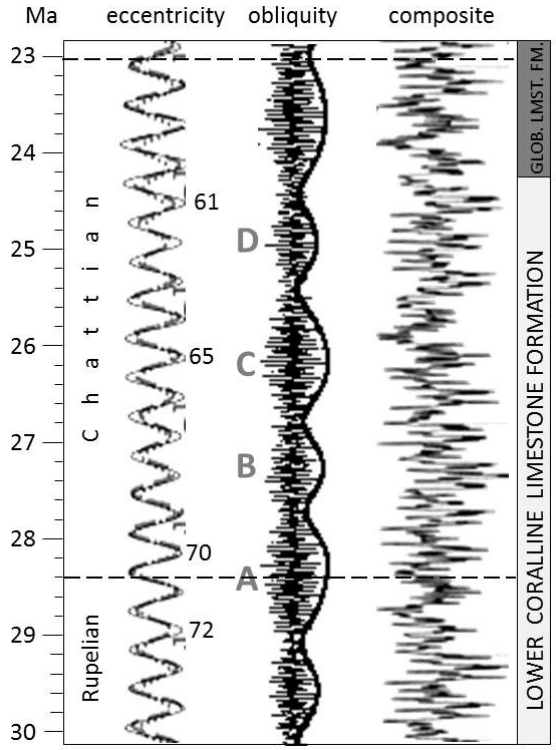

Figure 5.42. Long-term obliquity cycles based on Laskar, *et al.* (2004) labelled A to D and long eccentricty cycles (Pälike *et al.*, 2006) numbered 61 to 72 compared to Oligo-Miocene formations of Malta.

When these cycles coincide with long eccentricity minima they become the main driving force in glacio-eustasy in Cenozoic icehouse sequences that correspond to oxygen isotope events (Boulila *et al.*, 2011). On the basis of the long obliquity and long eccentricity cycles some Oligocene glacial events have been dated as 29.16, 27.91, 26.76 Ma (Wade & Pälike, 2004).

5.10 DISCUSSION

Glacio-eustatic control on sea-level became important during the mid-Cenozoic development of the Antarctic ice sheet. Ice-sheet growth is considered to have started by the earliest Oligocene (Zachos & Kump, 2005) and is associated with the beginning of long-term eustatic sea-level fall. The relatively moderate amplitude third-order sea-level cycles of <40 m during the Oligocene is typical of the transitional climate between the Cretaceous greenhouse and the Quaternary ice-house global conditions (Read, 1998) and is particularly suited for the study of the relationship between sedimentation and eustacy (Kominz & Pekar, 2001), if the effect of tectonism can be distinguished from eustatic control. The following sea-level cycles are discussed:

5.10.2 Third-order sea-level cycles

There is a growing corpus of evidence on Oligo-Miocene depositional sequences in the Mediterranean, northern Europe and the Pacific that points to controls by global third-order sea-level cycles related to obliquity forcing with a long periodicity of 1.2 Ma modulated by 405 kyr eccentricity cycles (e.g., Wade & Pälike, 2004; Pälike, *et al.*, 2006 and Abels, *et al.*, 2007), which began in the Late Eocene (Boulila, *et al.*, 2011) and persisted into the Late Neogene (Lourens & Hilgen, 1997).

The orbital cycles identified by Laskar, *et al.* (2004) are applied to the Maltese succession on the reasonable assumption that sequence boundaries in Malta reflect glacial events along the third-order sea-level cycle. This permits astronomical tuning of the Maltese carbonates. However, glacio-eustatic cyclcity in shallow marine carbonate platform environments is also affected by erosion and other processes that result in an incomplete stratigraphic record and reworking which complicates the recognition of cyclicity.

For astronomical tuning of cyclic sedimentary cycles, a characterisitc curve and at least one reliable age calibration point have to be present according to Abels *et al.* (2007). Dated obliquity minima cycles A to D that represent glacial events of Wade & Pälike, (2004) are compared to the occurrence of sequence boundaries, LBF

biostratigraphy and strontium isotope dating of Maltese carbonates, all calibrated to the geological timescales of Gradstein *et al.*, 2004) in Figure 5.43. This correlation forms the basis for the following third-order cycles:

- Obliquity cycle D (24.4 to 25.4 Ma): During this cycle the deep sea oxygen isotope record reached a minimum averaging 1.9‰ (Zachos *et al.*, 2008). This implies higher sea-level which can be linked to the rapid marine transgression during the deposition of sequence 6 over the Malta Platform followed by platform drowning. The terminal sediments of the Lower Coralline Limestone are capped by sequence boundary SbCH5 that comprises a hardground and sporadic phosphorite sediments (C_0 bed). The base of the overlying Lower Globigerina Limestone is dated 24.4 Ma (Knoerich & Mutti, 2006). Therefore, the terminal hardground is interpreted to coincide with the obliquity minima at around 24.3 Ma. Associated with this drop in sea-level is the deposition of the C_0 phosphorite bed in Malta (Gruszczynski *et al.*, 2008).

- Obliquity cycle C (25.4 to 26.76 Ma): The end of this cycle at 25.4 Ma coincides with SbCH4 during which the Malta Platform underwent significant erosion as a result of subaerial exposure. Strontium isotope dating in locality 1 (Knoerich & Mutti, 2006) is from the end of this cycle. The base of obliquity cycle C corresponds to sequence boundary SbCH3. In locality 2, this sequence boundary is found a few metres below the first appearance of the benthic foraminifera *Miogypsinoides complanatus* (Felix, 1973) that marks the start of the benthic foraminiferal biozone SBZ 23 dated 27 Ma by Cahuzac and Poignant (1997). The beginning of this biozone closely coincides with the beginning of obliquity cycle C and the deposition of sequence 5.

- Obliquity cycle B (26.76 to 27.91 Ma): The biostratigraphical extent of *Nephrolepidina praermarginata* (sequence 4) is within this obliquity cycle found in outcrops at locality 6. Obliquity cycle B ends with low amplitude obliquity coinciding with minimum eccentricity (near circular orbit). This would result in a substantial growth of the Antarctic ice sheet reflected in the global oxygen isotope maxima at 26.75 Ma and a drop in sea-level which produced the

extensive erosional surface and pedogenesis seen in outcrop and wells along sequence boundary SbCH3. The marine regression produced a deep erosional surface that cut down into sequence 4 at locality A and produced the forced regressive wedge ending sequence 4 at locality 5.

- Obliquity cycle A (27.91 to 29.16 Ma): the end of the cycle coincides with sequence boundary SbCH2 that is recorded as becoming subaerial at localities 1, 9 and 14. In deep onshore wells, this boundary is marked by clay deposits and reddish sediments at locality A. This sequence boundary is just above the Rupelian-Chattian boundary. Strontium isotope dating of 28.6 Ma from the base of locality 5 is within this cycle.

Figure 5.43. *(figure on next page*) Chronostratigraphic chart. Columns show: (A) Sequence stratigraphy. (B) Lithology. Colour of facies association based on Appendix II (left-hand side shows localities that are the source of data) and strontium isotope curve. (C) biostratigraphy: range of LBF (thin lines) from Cahuzac & Poignant, 1977 and stratigraphical occurrence in Maltese Islands (thick lines). LBF biozones of Cahuzac & Poignant (1997), planktonic foraminiferal biozones of Blow (1969) and Berggren *et al.* (1995). (D) Obliquity cycles (in degrees) from Laskar *et al.* (2004). (E) Relative sea-level curve based on outcrops in Maltese Islands (see Figure 5.) compared to depositional hiatuses (shaded grey) in NE America (Pekar, *et al.*, 2001) and isotopic events (Miller *et al.*, 1991).

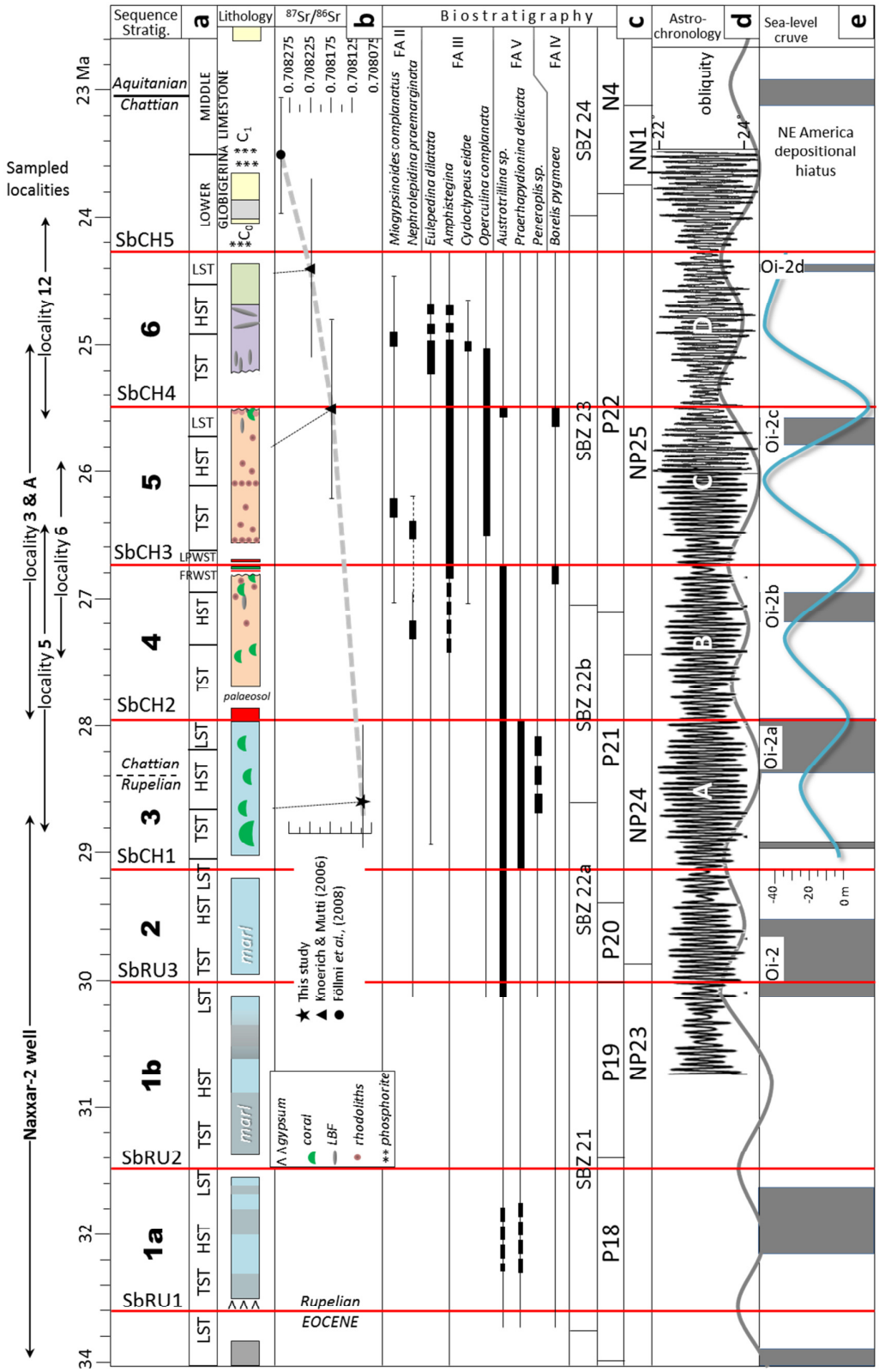

Figure 5.43 (*caption on previous page*)

5.10.3 Fourth-order sea-level cycles

Higher frequency cycles can be extracted within the third-order cycle. Subdividing the third-order cycle time interval of the sequence (1.2 Ma duration) by the number of parasequence sets (two in each systems tract) yields the length of half a fourth-order sea-level cycle in the long eccentricity (405 ka) orbital cycle within the Milankovitch frequency band. Eccentricity maxima produces greater summer insolation in one of the poles which results in partial melting of the ice cap and a sea-level rise, with the converse happening during eccentricity minima.

Higher frequency sea-level cycles resulting from long eccentricity (405 kyr) forcing were well-established by the early Oligocene (Pälike *et al.*, 2006). Numerous studies have proposed that parasequences are produced by low amplitude, higher frequency sea-level cycles produced by 400 ka and 100 ka eccentricity cycles of the Earth's orbit (Read, 1998; Osleger, 1991; Husinec and Read, 2007). However, eccentricity cycles reflect the degree of ellipticity of the Earth's orbit around the Sun (eccentricity) that has a small effect on total yearly radiative heating and consequently on sea-level. As a result, eccentricity only becomes important when combined with precession which controls the timing of seasons relative to the perihelion which significantly affects the total radiative heating. Although precessional cycles form fundamental units in the stratigraphy they are unreliable due to incompleteness, irregular thickness or missing units. The preference for eccentricity-based parasequences is due to their regularity which results in clearly identifiable shallowing upward successions seen in the field. The time series analysis of oxygen and carbon isotope values of deep sea cores suggests a strong eccentricity cycle over precession (Pälike *et al.*, 2006). This is the result of the much more regular eccentricity variations compared to the precession cycle which varies by a factor of two (14-28 ka) (De Boer & Smith, 1994).

The first half of the fourth-order 405 kyr sea-level cycle is transgressive (200 kyr duration), whereas the second half is the regressive parasequence set that terminates in minimum eccentricity (near circular orbit). The following 405 kyr eccentricity cycles are recognised in each depositional sequence:

Sequence 6: The time interval between SbCH4 and 1 m above SbCH5 (the base of the Globigerina limestone Formation dated 24.4 Ma by strontium isotope dating (Knoerich & Mutti, 2006)) are separated by a time interval of 1.1 Ma. If the time interval for the deposition of S6 cycle is subdivided equally by 405 kyr, then three eccentricity cycles would almost fit. These correspond to the three systems tracts predicted in a depositional sequence.

Sequence 5: The time interval between sequence boundaries SbCH3 and SbCH4 is *circa* 1.2 Ma and comprises three long eccentricity cycles when sub-divided by 405 kyr. These would correspond to the three systems tracts identified in outcrop: The lower two parasequence sets form the transgressive system tract, the two middle parasequence sets are the highstand and the top two parasequence sets form the lowstand systems tract.

Sequence 4: deposited between SbCH2 and SbCH3 over an astronomically estimated time interval of *circa* 1.2 Ma which comprises three 400 kyr cycles. Each 405 kyr cycle forms a systems tract.

Sequence 3: the longer obliquity cycles dominated over the weak eccentricity cycles during this period of time (Laskar *et al.*, 2004). This may also explain the absence of well-defined parasequences and systems tracts originating from eccentricity cycles, as well as bioturbation that destroyed bedding.

5.10.4 Fifth-order sea-level cycles

The shallowing upwards parasequence sets comprise smaller-scale (*circa* 2 m thick) fundamental shallowing-upward units. These are interpreted as parasequences that reflect short eccentricity (100 kyr) cycles. Each 405 kyr cycle comprises four successive 100 kyr parasequences that are most distinguishable in the lowstand systems tract when obliquity minima results in the stronger imprint of eccentricity forcing, e.g., the lowstand systems tract at locality 5 is interpreted as a 405 kyr long eccentricity cycle comprising two parasequence sets (200 kyr duration) with two

nested parasequences with a duration of 100 kyr each (Figure 5.44). These successive parasequences show an increase in the proportion of peritidal facies (facies VIa) relative to subtidal coral and coralline algae facies farther up the cycle terminated by the sequence boundary SbCH3. This suggests progressive shallowing up the systems tract culminating in maximum regression along the sequence boundary.

5.10.5 Sea-level cycles and controls on sedimentary cycles

The thickness of depositional sequences is an approximation of change in accommodation space caused by sea-level change over the short term. Figure 5.45 is a bar graph showing the thickness of depositional sequences 3 to 6 at four localities. There is a common trend especially during the deposition of sequence 5 which shows significant thickening across all localities. This suggests a platform-wide increase in accommodation space caused by glacio-eustatic rise. However, sequence thickness on its own may not reflect actual sea-level change because other factors may affect the rate of carbonate accumulation. For example, sequences produced by higher frequency cycles (parasequences) are the result of either predominantly allocyclic or autocyclic controls.

Figure 5.44. (*figure on next page*) Stratigraphy of localities 5 and 14 showing depositional sequences 3, 4 and 5. Locality 5: The forced regressive wedge systems tract (FRWST) consists of two parasequence sets deposited during a long eccentricity cycle (405 kyr) comprising four 100 kyr cycles that produced parasequences; Locality 14.The lower part of sequence 4 (S4) includes patch reefs draped by laminae of algal packstone. Farther up, the drop in sedimentation along the maximum flooding surface resulted channels cutting the seabed that were later filled with rhodoliths. Sequence 4 shallows upward, terminating with a bed of *Kuphus*.

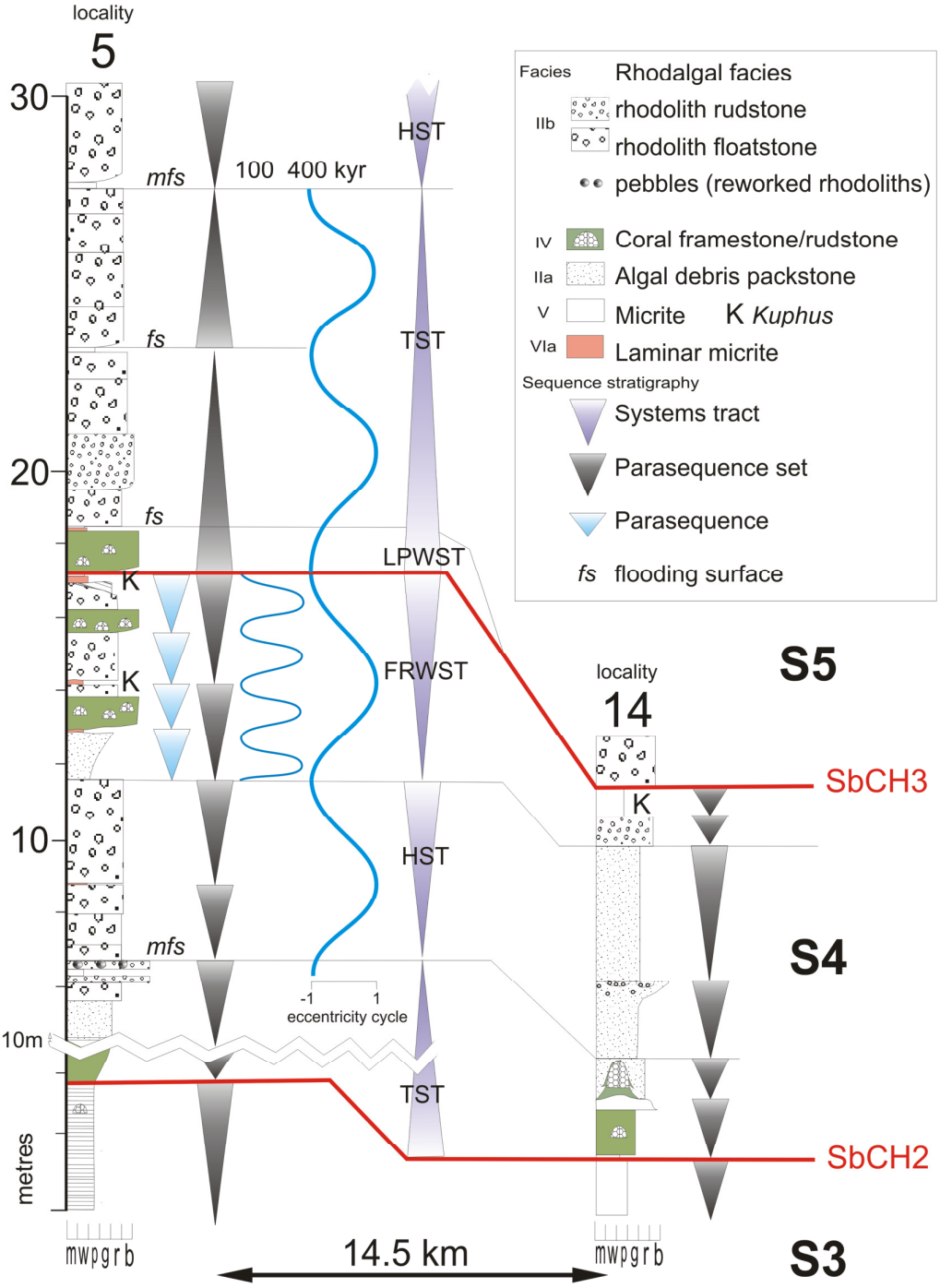

Figure 5.44 (*caption on previous page*)

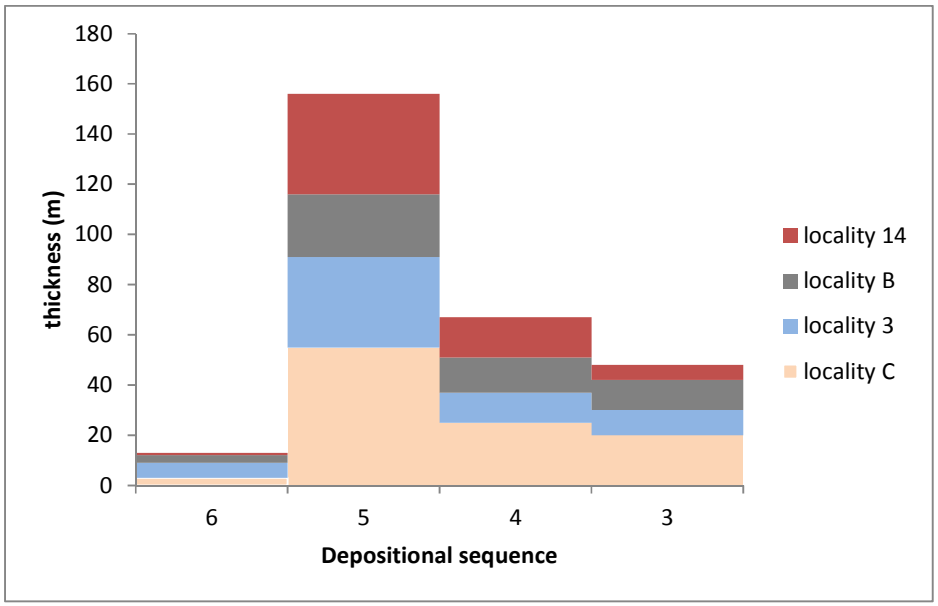

Figure 5.45. Bar graph showing thickness of sequences 3 to 6 at four localities, Sequence 5 is thickest in all localities and represents a significant increase in accommodation space.

Allocyclic and autocyclic controls produce shallowing upward cycles that are either entirely subtidal or peritidal depending on the accumulation rate (Osleger, 1991). Autocyclic processes result in sediment accumulation that does not reach the water surface. This condition precludes the effective use of Fischer plots (Drummond & Wilkinson, 1993).

Each sequence in outcrop shows characteristic facies evolution that reflects allocyclic or autocylic controls and different levels of completeness of the facies succession that are reflected in the change in relative sea-level curve (δR) in m/Ma which comprises two variables that make up the formula:

$$\delta R = \delta A - \delta S$$

where, δA is the rate of change in accommodation space (m/Ma) resulting from glacio-eustasy and, δS is the rate of sedimentation (modulated by rate of accumulation).

When the carbonate platform is exposed to subaerial conditions, δS = 0 and δA reaches its minimum level, this would be the maximum regressive surface along the carbonate platform. The maximum flooding surface (mfs) may not represent the highest point of δA but represents the deepest marine phase along the platform as a result of a high δA and low δS.

The relative sea-level curve reflects the phase disparity in sediment production (δS) and the increase in accommodation as a result of glacio-eustatic sea-level rise (δA) and the overall subsidence rate. This difference results in variable types of sequences which are here referred to by the terminology of Kendall & Schlager (1981) and Hillgartner & Strasser (2003) as shown in Table 5-13. The curves for δA and δS are extrapolated as shown in Figure 5.46 basing on the type of sequence that determines the rate of δA relative to δS through a single third-order sea-level cycle. The relative sea-level curve is modulated by the rate of tectonic subsidence (see Chapter 6).

In synthesis, the depositional sequences that remained mostly subtidal such as sequence 5 could aggrade to reach their maximum thickness whereas sequences 3 and 4 were controlled by allocyclic processes and remained relatively thin as a result of frequent subaerial exposure that resulted in non-deposition and erosion. The different sedimentological processes explain the differences in the thickness of sequences shown in Figure 5.45.

5.10.6 Constructing the relative sea-level curve

In view of allocyclic and autocyclic controls, an attempt is made to reconstruct the third-order sea-level curve for depositional sequences in the Lower Coralline Limestone based on the following methods and parameters:

1. In the sequence stratigraphic concept, the depositional sequence represents a full sea-level cycle beginning and ending with a fall in sea-level (Van Wagoner *et al.*, 1988). When the duration of deposition of the sequence is known then the order of the sea-level cycle can be identified (Figure 5.47a).

2. Diagenetic changes that are a product of meteoric, marine or burial environments reflect position of surface relative to sea-level (discussed in chapter 4).

3. Beds were originally thicker before differential compaction. Different facies have different rates of compaction of 1.2 for carbonate sand, 2.5 for carbonate mud and 3 for marl (Goldhammer, 1997). However, outcrops are mostly purely carbonate and there is little evidence of compaction in the boundstone beds that consists of rhodoliths (facies IIb).

4. Estimation of subsidence rate based on the depositional setting of carbonate platform (discussed in Chapter 6).

5. Certain carbonate-secreting organisms are palaeobathymetric indicators, e.g., coral (Perrin, *et al.*, 1995; Schlager, 1981), geniculate calcareous algae (Wray, 1977) and benthic foraminifera (Geel, 2000). The dominant biotas in a sequence would indicate whether the sequence was deposited at depths that were relatively shallower or deeper than the overlying or preceding sequence (Figure 5.47b).

sequence	Max. thickness	Controls on sedimentation by third-order sea-level cycles		Controls on sedimentation by fourth-order sea-level cycles	
6	30 m	Give-up δS< δA	Drowning type of sequence characterised by the LBF carbonate factory that could not keep up with rising sea-level. Sequence is 'thickness incomplete' and is entirely subtidal reflecting the deepening part of the cycle.	allocyclic/ autocyclic	These are base-cut out cycles which represent only a fraction of the accommodation space created during the eustatic cycle under conditions of high dispersal of hydrodynamic LBF.
5	60 m	Catch-up δS ≤ δA	Significant deepening (40 m) during which the rhodalgal biostrome aggraded. The accumulation rate initially lags behind the creation of accommodation resulting in a sediment-starved conditions characterised by the accumulation of rhodoliths over the Malta Platform. During the highstand, carbonate production begins to outpace the sea-level rise (δS>δA) and begins to fill accommodation space by highstand shedding into bathymetric lows (clinoforms). The lowstand is characterised by erosion and subaerial diagenetic overprint.	autocyclic	The decreased ice-volume had diminished the magnitude of Milankovitch sea-level changes which resulted in poorly-defined parasequences. Sedimentation was controlled mainly by storm and wave reworking and redistribution that maintained the seabed below 10 m and outside the zone of optimal carbonate productivity.
4	35 m	Catch-down	Characterised by maximum lag time of sediment accumulation relative to the accommodation rate. The time lag is reflected in the abrupt change in facies between S3 (FA V) and S4 (FA II). During the initial part of the cycle only the fast growing patch reefs were able to match sea-level rise while the rest of the platform (and eventually the patch reefs themselves) drowns. Towards the end of the cycle, sedimentation overtakes the falling sea-level. The result is foreshortened cycles that show 'forced' progradation (Forced Regressive Wedge Systems Tract) and finally truncation of the cycles, creating a 'facies-incomplete' cycle *sensu* (Hillgartner & Strasser, 2003).	allocyclic	The basal transgressive systems tract consists of two parasequence sets showing coral patch reefs growing mid-way up this systems tract until they drowned. The highstand phase consists of thin horizontal beds of algal debris whereas the lowstand systems tract includes cross-bedded algal debris FA IIa and the peritidal FA VI. Sufficient ice-volume generated high amplitude Milankovitch-scale sea-level cycles reflected in well-defined peritidal parasequences in the forced regressive wedge.
3	30 m	Keep-up δS=δA	Sequence is in dynamic equilibrium between accommodation rate and sedimentation rate, resulting in continuously shallow marine conditions. Sedimentation is mostly aggradational, although there is little evidence of cyclicity except for exposure surfaces that separate cycles .	acyclic	Aggraded under 'keep-up' conditions although affected by thorough bio-retexturing by burrowing organisms and roots of seagrass.

Table 5-2. Controls on sedimentary cycles

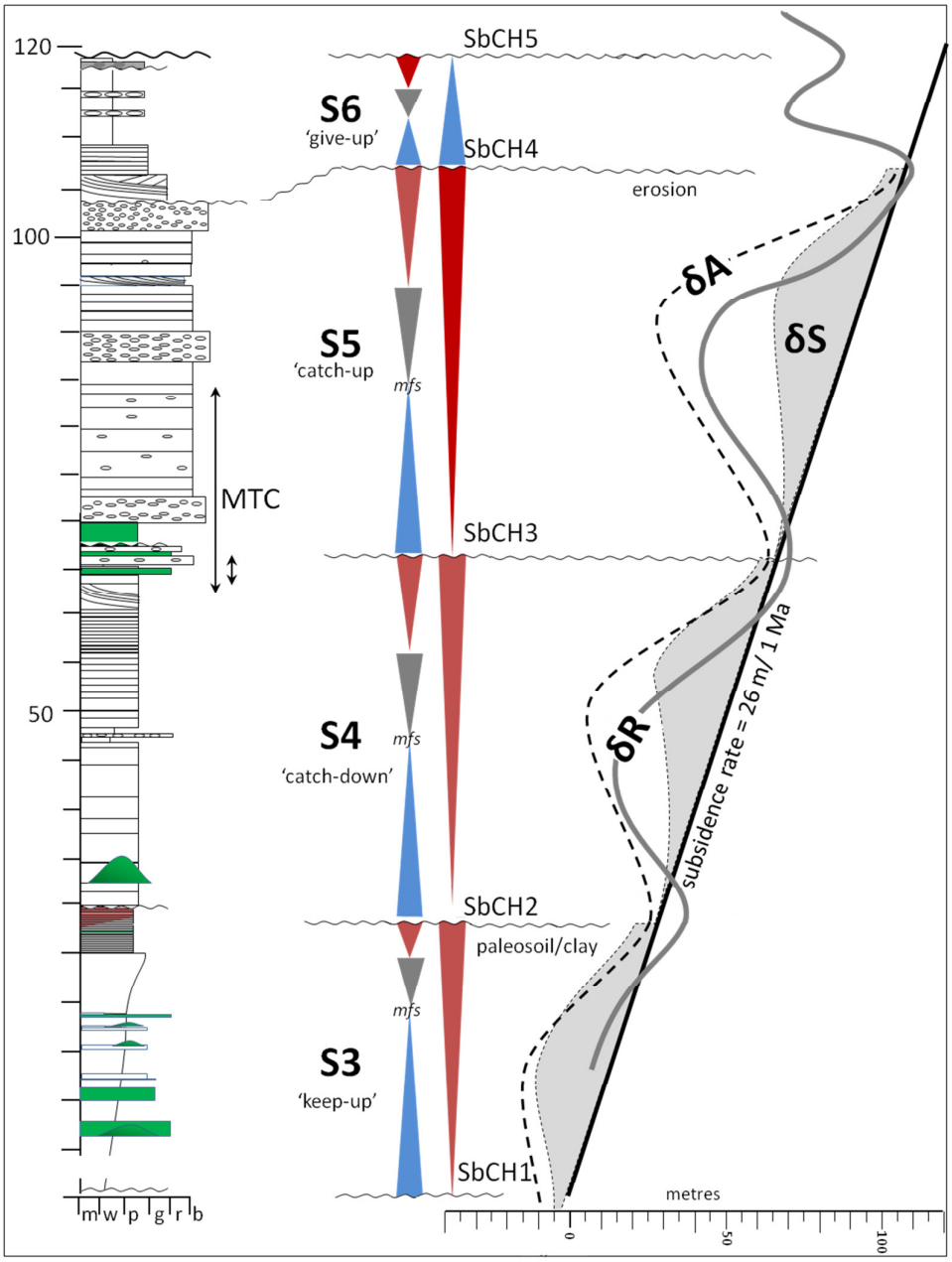

Figure 5.46. The third-order sea-level curve based on the four sequences in outcrop. Descriptive terms for sequences are from Hillgartner & Strasser (2003).The subsidence rate (discussed in Chapter 6) forms the basis for the increase in accommodation rate whereas the superimposed glacio-eustatic changes are reflected in facies changes. The thick grey line is the relative sea-level (based on Figure 5.48) whereas the dashed lines represent the presumed sea-level and sedimentation (accumulation) rates. The two extrapolated curves reflect the type of sequence and the difference between the two curves is equal to the relative sea-level curve.

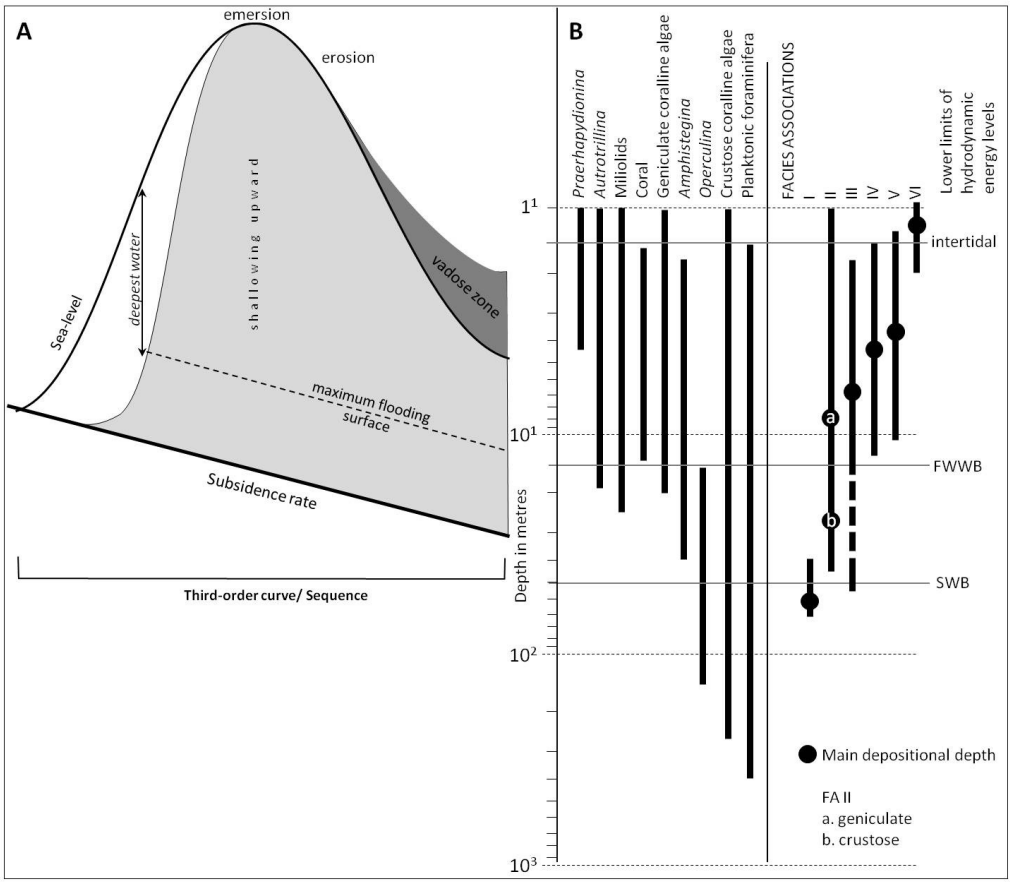

Figure 5.47. A. Sea-level cycle and sedimentation (grey shading) over a third-order sea-level cycle (partly based on Hillgartner & Strasser, 2003); B. Depositional depth of carbonate organisms in the Malta Platform.

Using palaeodepth data from biota (Figure 5.47) the third-order sea-level curve is constructed in Figure 5.48.

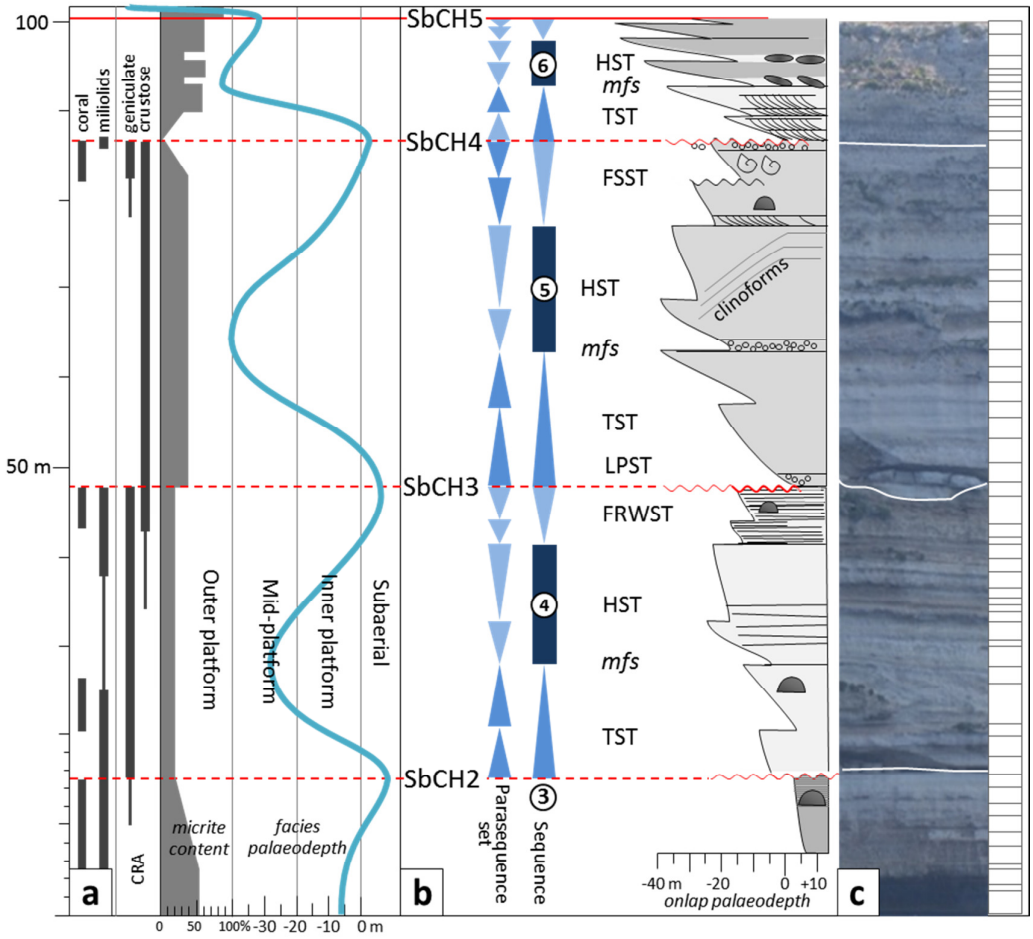

Figure 5.48. Third-order relative sea-level curve for Malta. (a) The curve is based on the extent of palaeodepth indicator organisms and micrite content with associated carbonate platform depositional environment; (b) composite log and sequences; (c) photo section of bedding in locality B.

5.10.7 Correlation to regional sequence boundaries

A number of studies have suggested that eustatic marine flooding or regressive events are synchronous worldwide (Vail, *et al.*, 1977; Haq, *et al.*, 1987; Sharland, *et al.*, 2001; Gerdes, *et al.*, 2010). This would imply that major unconformities over the Malta Platform produced by third-order sea-level changes would correlate to unconformities in the Central Mediterranean. This is especially relevant to the Oligocene when superimposed on the global eustatic oscillations in the range of 10 to <54 m is the long-term eustatic fall of 30 m (Pekar, *et al.*, 2002). At the scale of the glacio-eustatic amplitude, the Malta Platform and other carbonate platforms located on passive margins would be exposed to subaerial conditions that would interrupt the sedimentary cycles, making them correlatable on a global scale. Regional correlation of the seven Oligocene depositional sequences of the Malta Platform and their sequence boundaries is here tentatively correlated to localities in the Central Mediterranean (Figure 5.49) by comparing them to the following:

i. The offshore succession of the Lampedusa Platform penetrated by the Ricco Sud 1 well where the entire Neogene and part of the Oligocene has been eroded.

ii. Offshore succession of the Apulia Platform penetrated by the Giove 1 well (data from the official website of the Italian Government) where the lower Oligocene and early Chattian are dominated by coral growth (Bosellini, 2006).

iii. The Oligocene mixed carbonate-siliciclastic Arida and Diba Formations in the Sirt Basin of northern Libya where seven depositional sequences were identified (Gruenwald, 2001). The Oligocene maximum flooding event is associated with shale deposits at the top of the Arida Formation in Libya. This flooding event may correlate with the transgressive event succeeding sequence boundary SbCH2 over the Malta Platform that resulted in the facies shift from the restricted shallow marine sequences 1 to 3 (FA V) to sequences 4 to 6 where facies are dominated by coralline algae and LBF (FA II and FA III) that reflect open marine conditions.

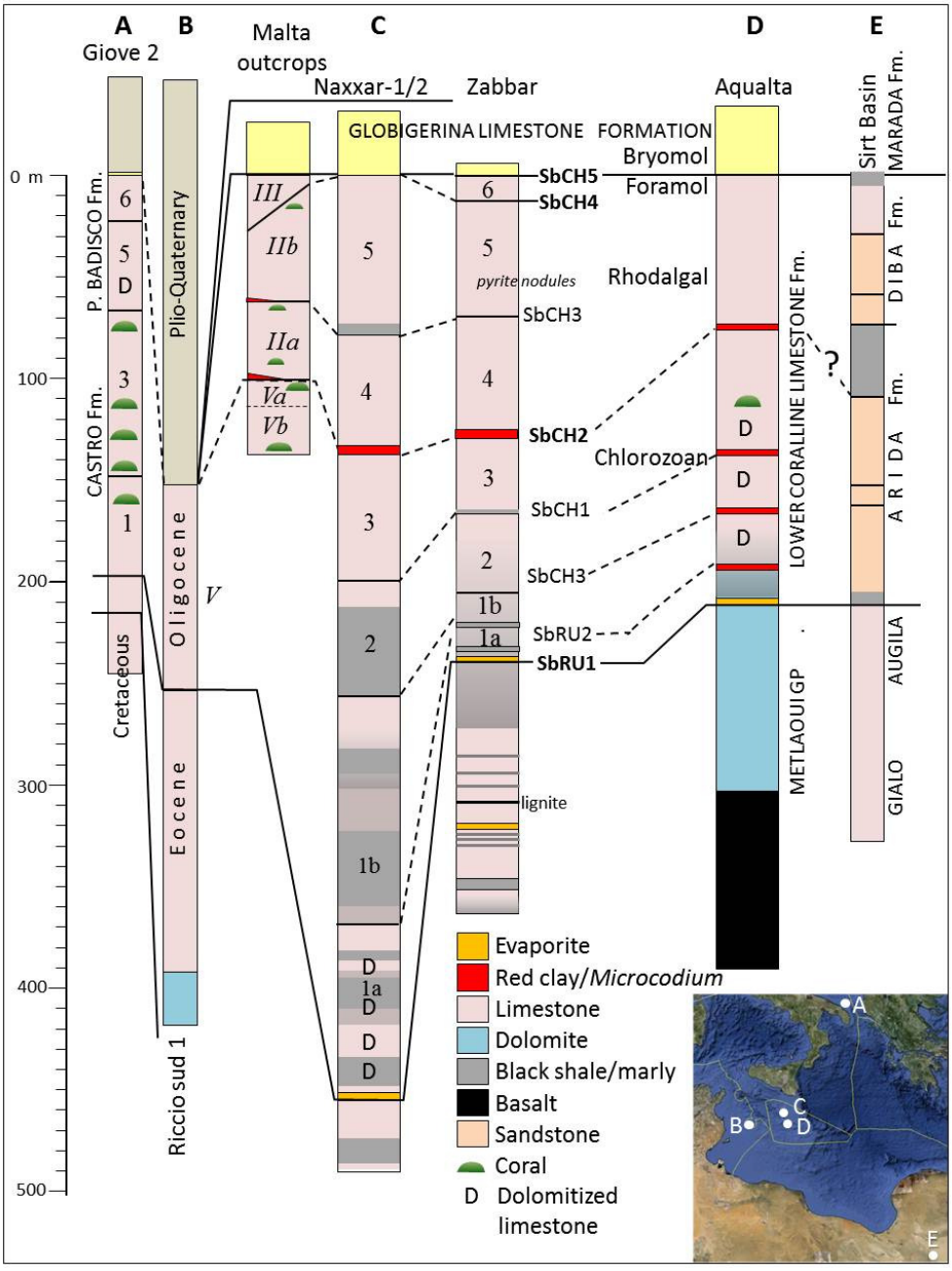

Figure 5.49. Correlation chart of outcrops and wells in Italy (A, B), Malta (C, D) and Libya (E).

5.10.8 Malta Platform sequences and global third-order cycles

Although the major uncertainty is the age assignment of sequence boundaries, it is significant that the number of Chattian sequences in the Malta Platform matches the number of Chattian third-order cycles on the global sea-level chart of Haq, *et al.*, (1987) in supercycle TB1 (Figure 5.50). Nonetheless, there is scepticism about the validity of globally correlatable suite of third-order eustatic cycles (Miall, 1992).

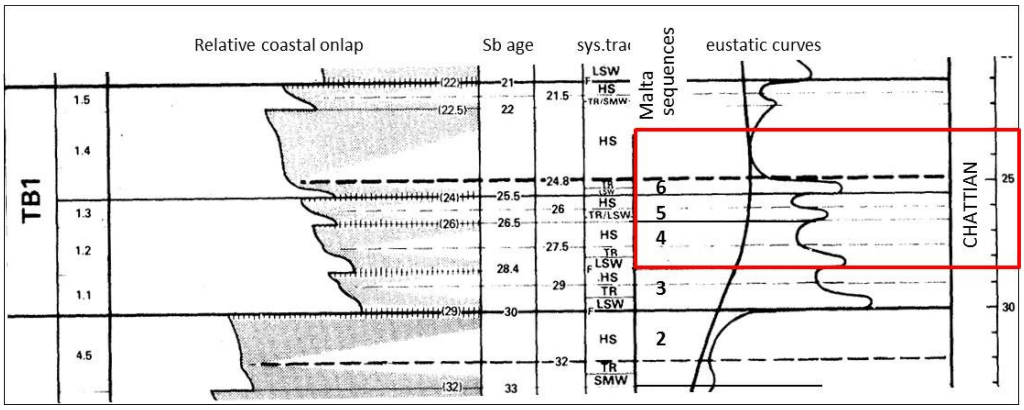

Figure 5.50. Part of global chart of coastal onlap and eustatic curves of Haq *et al.* (1987). The number of Chattian cycles in TB1 (in red rectangle) corresponds to the number of Chattian sequences in the Malta Platform. The age of SbCH4 is identical to the sequence boundary in the Haq curve.

The tentative dating of third-order sea-level curve and sequence boundaries of the Malta Platform makes it possible to compare the Maltese Oligocene sea-level curve to that of the well-documented North Atlantic American passive margin sediments in New Jersey (Pekar *et al.*, 2002; Kominz & Pekar, 2001) and the sequence boundaries therein that correlate with sequence boundaries in the Bahamas and northwest Europe, suggesting global eustatic control (Miller, et al., 2005). Comparing the two sea-level curves (Figure 5.51) shows a offset in the timing of the maximum regressive surfaces (sequence boundaries) over the Malta Platform that become increasingly younger relative to the correlative sequence boundaries along the NE coast of America. This difference could be due to inaccuracy in biostratigraphic dating or different tectonic history of the two platforms.

Passive margin subsidence of the Malta Platform would be expected to be more rapid relative to that of North America because the latter is located at a greater distance (*circa* 3000 km) to the mid-Atlantic rift zone relative to the Malta Platform and its presumed oceanic rift zone (*circa* 220 km from Malta) in the Ionian Basin (Catalano, *et al.*, 2001). The SbCH5 is inconsistent with the dating of the correlative sequence boundary in North America where the relative sea-level curve shows shallowing. This could be the result of early drowning of the Malta Platform and termination of the Lower Coralline Limestone.

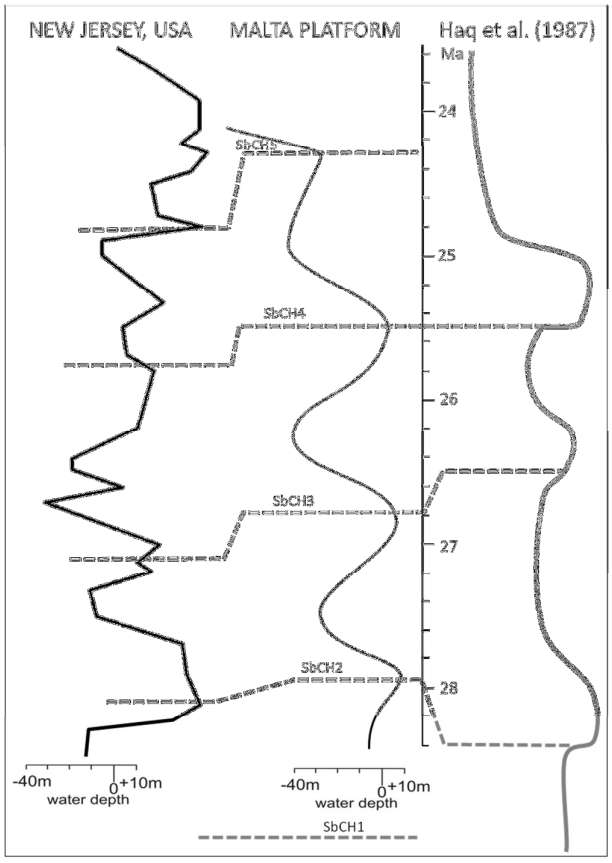

Figure 5.51. Comparison of sea-level curves for Malta (this thesis), NE America (Pekar, *et al.*, 2002) and the global curve (Haq, *et al.*, 1987). Dashed lines represent sequence boundaries that have been tentatively correlated between Malta, North America and the global sea-level curve. The sequence boundaries in the Malta Platform become increasingly younger with time relative to North American sequence boundaries.

5.11 SUMMARY

In the first part of the chapter the Oligocene Lower Coralline Limestone Formation is sub-divided into seven depositional sequences each terminated by maximum regressive events that represent sequence boundaries. The upper four sequences are exposed in the Maltese Islands. Each sequence was deposited during a third-order sea-level cycle and comprises three or four systems tracts each composed of two parasequence sets. Changes in the rate of carbonate production and accumulation reflect the type of main carbonate producers as well as inflections along third-order sea-level cycles. The changes in relative sea-level produced large-scale geometries which include low-angle regressive wedges followed by extensive clinoforms produced by highstand shedding.

In the second part of the chapter the depositional sequences are dated using large benthic foraminiferal biozones and strontium isotope dating. Dating of sequence boundaries is fine-tuned using the predominant astronomical cyclic forcing produced by long-term obliquity with 1.2 Ma periodicity that is linked to third-order sea-level cycles marked by glaciation and maximum regression, whereas higher frequency long eccentricity cycles (405 kyr) produced the transgressive and regressive parasequence sets that each comprises two nested 100 kyr parasequences. The sequences developed by allocyclic forcing although autocyclic influence affected the thickness and level of completeness of the cyclic stratigraphy.

Chapter 6

Tectonostratigraphic development of the Malta Platform

6.1 INTRODUCTION 232

6.2 METHODS and MATERIALS 235

6.3 Regional tectonostratigraphy 236

6.4 SEISMIC STRATIGRAPHY OF THE MALTA PLATFORM 242

6.4.1 Seismic facies of megasequence II 252

6.4.2 Seismic facies and outcrops of megasequence III 253

6.5 GEOTECTONIC SUBDIVISION OF THE MALTA PLATFORM 255

6.5.2 Platform interior zone 256

6.5.3 Central Malta Platform Basin (CMPB) 279

6.5.4 Escarpment zone 288

6.6 DISCUSSION 300

6.6.2 Stratigraphy 300

6.6.3 Tectonics 301

6.7 SUMMARY 306

6.1 INTRODUCTION

This chapter introduces seismic data that is tied to well data and outcrop. Although the focus of this study the Palaeogene carbonates, it is evident that Palaeogene sedimentation over the Malta Platform was impacted by earlier structural controls (Pedley, 1990) which are poorly understood. This chapter integrates sedimentation and tectonics of the Meso-Cenozoic in order to model the evolution of the Malta Platform.

The tectonostratigraphic development of carbonate platforms is controlled by two factors: (1) the high productivity of carbonate ecosystems within the photic zone (0 to 15 m) (Bosscher & Schlager, 1993). As a result, carbonate platforms aggrade to shallow water depths over large areas (Read, 1985) making them distinct from siliciclastics systems (Handford & Loucks, 1993) and, (2) basin evolution which may pass through tectonic phases of activity, quiescence and reactivation and inversion depending on regional kinematics. Basin architecture and tectonic setting can be used as a basis for the classification of carbonate platforms, e.g., Read (1985) and Bosence (2005). The interaction of tectonic, eustatic, sedimentary and climatic processes is reflected in the geometry and constituent biotas of carbonate sequences and parasequences in outcrop as well as seismic reflectors.

Seismic imaging of reflectors along a carbonate platform is caused by significant changes in acoustic impedance, which is the product of sediment sonic velocity (V_p and V_s) and density (ρ). The analysis of geometrical relationships of reflections is the basis of seismic stratigraphy and sequence stratigraphy (Vail *et al.*, 1977; Eberli *et al.*, 2004). Three main surfaces are recognised in the sequence stratigraphic model, e.g., Van Wagoner *et al.* (1988):

i. Maximum regressive surface, considered to be the sequence boundary (Sb) in this study, that can result in subaerial episodes that produce palaeosols, red beds, evaporites and features related to their dissolution (Read, 1995). These

type 1 erosional unconformities produce strong acoustic impedance and a strong seismic reflector.

ii. Maximum flooding surface (MFS) that may consist of clay that transgresses the carbonate platform slope environment. The change from carbonate to clay will produce a strong seismic reflection.

iii. Transgressive surface produced by marine transgression that brings a change in lithology across this surface.

However, pore types also have a strong control on sonic velocity. As a result, there is little correlation between acoustic properties and age or burial depth in pure carbonates, although a strong relationship exists between porosity, depositional lithology, post-depositional (diagenetic) processes and sonic velocity (Anselmetti & Eberli, 1993). Changes in carbonate depositional lithology and post-depositional processes (e.g., cementation or dissolution) can result in reflectors although these do not represent a time line *sensu* the sequence stratigraphic model.

Seismic sequence geometries reflect architecture of the basin fill with the architecture resulting from an interplay between accommodation (A) and sedimentation and growth (G), where A is the sum of the rates of subsidence (by crustal cooling, sediment loading and compaction) and eustasy, whereas G is the rate the platform produces sediment and builds wave-resistant structures. The growth potential varies on location along the platform, namely along the platform rim (G_r) or platform interior (G_p). Variations in A and G result in either maximum regressive or maximum transgressive surfaces that bound sediment packages (depositional sequences) which can be recognised in outcrop and seismic data (Handford & Loucks, 1993). The geometries of these sediment packages are summarised by Schlager (1992) and in Figure 6.1.

In cases where the carbonate sedimentation and growth rate is greater than the creation of accommodation space ($A < G$), or during highstand of sea-level when carbonate production generally reaches its peak, the carbonate platform will aggrade and prograde, triggering slope instability which produces calciturbidites. When the $A < 0$, the drop in sea-level results in the reduction of the area of the carbonate factory

whereas current activity increases along the shelf and interrupts continuous sedimentation. These conditions will result in the development of subtidal hardgrounds accompanied by meteoric diagenesis along the subaerial part of the platform interior. Sea-level fall forces the downward shift of the carbonate factory that builds lowstand terraces produced by the forced regressive wedge (Hunt & Tucker, 1992). Sea-level fall may cause overpressure as fluid drains slowly from sediments that may trigger slope instability that produces megabreccias (Spence & Tucker, 1997).

The objectives of this chapter are to (a) relate seismic facies to depositional environments within a tectonostratigraphic setting, (b) describe seismic facies and geometries of the Malta Platform and, (c) describe the subsidence history of the Malta Platform and compare it to regional carbonate platforms.

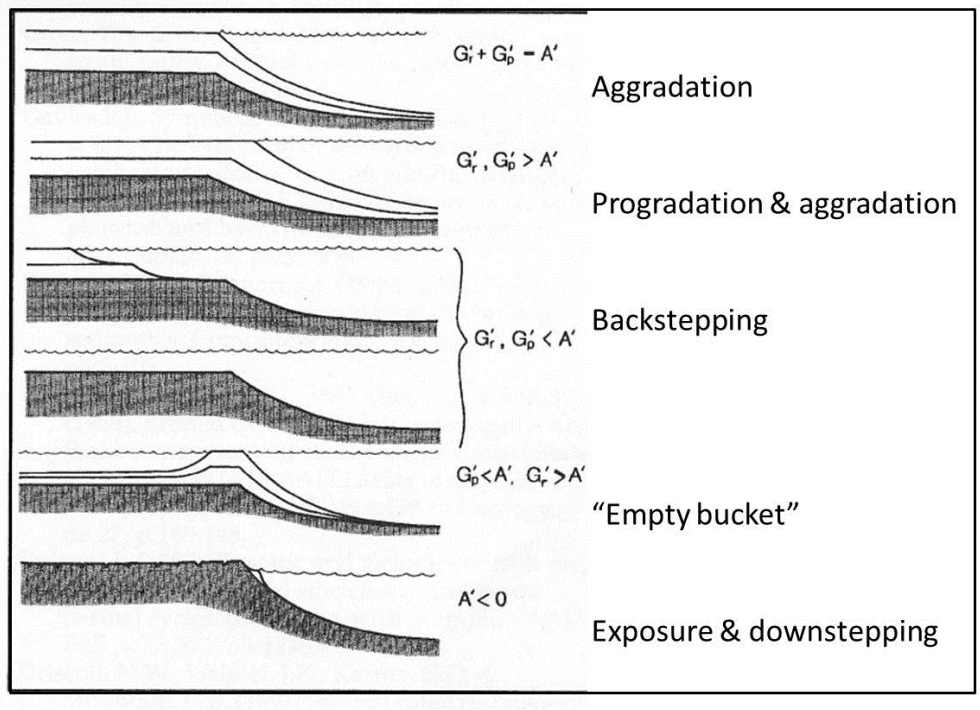

Figure 6.1. Basic geometries in carbonates generated by the interplay of the rate of change in accommodation (A') and the rate of carbonate growth (G'). Growth rate of platform rim is G_r' and growth rate of platform interior is G_p' (from Schlager, 1992)

6.2 METHODS AND MATERIALS

Data from outcrops in the *circa* 50 km long Maltese Islands discussed in chapters 3, 4 and 5 is correlated to the presently submerged areas of the >200 km-wide Malta Platform recognised in seismic at the megasequence scale (>10^3 m thick). The following data sources were available for this study:

i. Seismic data: 2-D seismic grids of the Central Mediterranean carried out by TGS-NOPEC Geophysical Company in 2000-2001. The seismic survey was shot using a 2800 cubic inch tuned Bolt array with a shot point interval of 37.5 m on board the MV *Zephyr*. A 6000 m long streamer, 480 recording channels, at a sample interval of 2 ms and a group interval of 12.5 m. Two datasets are available for this study (Figure 6.2);
   a. Malta Sicily Channel (MSC01) dataset that consists of 5350 km of mostly NW-SE lines shot around the Maltese Islands.
   b. Malta Medina Bank (MB01) dataset that consists of a 3075 km grid of N-S and W-E lines shot to the southeast of Malta. The NW-trending seismic line 303 crosses both datasets.

ii. Stratigraphic well data from the onshore Naxxar-2 and offshore Aqualta exploration wells provided by BP and Total respectively. The lithology of the wells is tied to seismic reflectors. The biostratigraphy presented in the well reports has been re-interpreted in this study in the context of more recent biozonation scheme based on benthic foraminiferans.

iii. Measured sections in the Maltese Islands and a photomontage of the 20 km long southern cliffed coast of Malta were used to determine lateral variations in the thickness of depositional sequences. The nearly continuous outcrop stratigraphy and bedding surfaces in section represent time-lines that are comparable to a seismic horizon, although showing higher resolution.

iv. Field evidence of faulting during the Oligocene.

Many of the seismic lines show intense Plio-Quaternary faults, some with throws greater than 1 km. These faults disrupt the geometry and continuity of Palaeogene reflectors that are the target sequences of this study. Consequently, a 280 km NW-SE seismic transect (line 303 composed of linked seismic lines) and several E-W trending seismic lines (Figure 6.2) that show minimal Plio-Quaternary faulting was selected to assess the tectonostratigraphic development of the Palaeogene Malta Platform.

6.3 REGIONAL TECTONOSTRATIGRAPHY

As discussed in chapter 2, the Malta Platform Mesozoic carbonates aggraded over the sinking passive margin of the North African Plate along the Pelagian Block (Jongsma *et al.*, 1985) that is thought to have rifted from the Apulian Block, creating the Ionian oceanic crust (Catalano *et al.*, 2001) (Figure 6.3). Published burial history diagram based on backstripping (Figure 6.4) shows that the Malta Platform was subsiding at an average rate of 26 m per 1 Ma from the Jurassic/Cretaceous to Palaeogene. The rate of subsidence is more rapid than movements from nearby carbonate platforms.

By the Late Cretaceous, plate movement switched to continental convergence (Dewey *et al.*, 1973). Basin inversion started to affect North Africa and the Middle East (Bosworth *et al.*, 2008), although according to the burial history diagram of Jongsma *et al.* (1985), the Malta Platform continued to experience passive margin subsidence (Figure 6.4). However, the Early Cenozoic is marked by a long Palaeocene depositional hiatus in Tunisia attributed to uplift (Jorry *et al.*, 2003) whereas on the Malta Platform much of the Late Cretaceous, the entire Palaeocene and the Eocene shallow benthic foraminiferal zones (SBZ) 1 to 8 (based on Serra-Kiel *et al.*, 1998) are absent in Aqualta well (Figure 6.5). Palaeocene sediments are thought to occur in deep intra-platform graben of the Malta Platform (Lipparini *et al.*, 2009). The missing SBZ reflect a long gap in sedimentation. This period also coincides with uplift in the Panormide Platform according to Zarcone & DiStefano (2008) which suggests a regional phase of uplift (Figure 6.4).

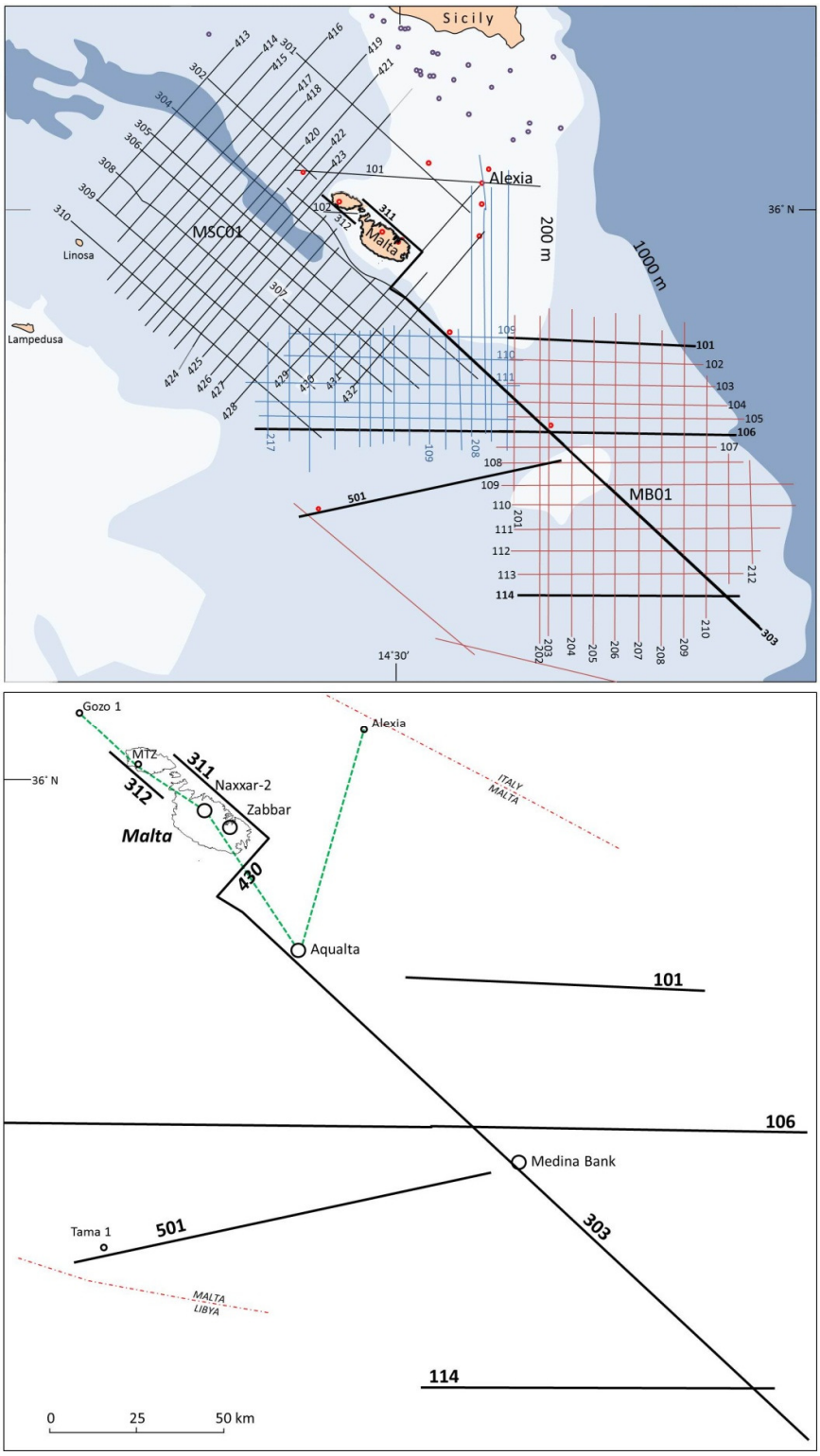

Figure 6.2. MSC01 and MB01 grids (TGS-Nopec, 2003). Seismic lines referred to in text are marked as bold black lines. Wells marked as circles. Dashed green line shows section through wells in Figure 6.9.

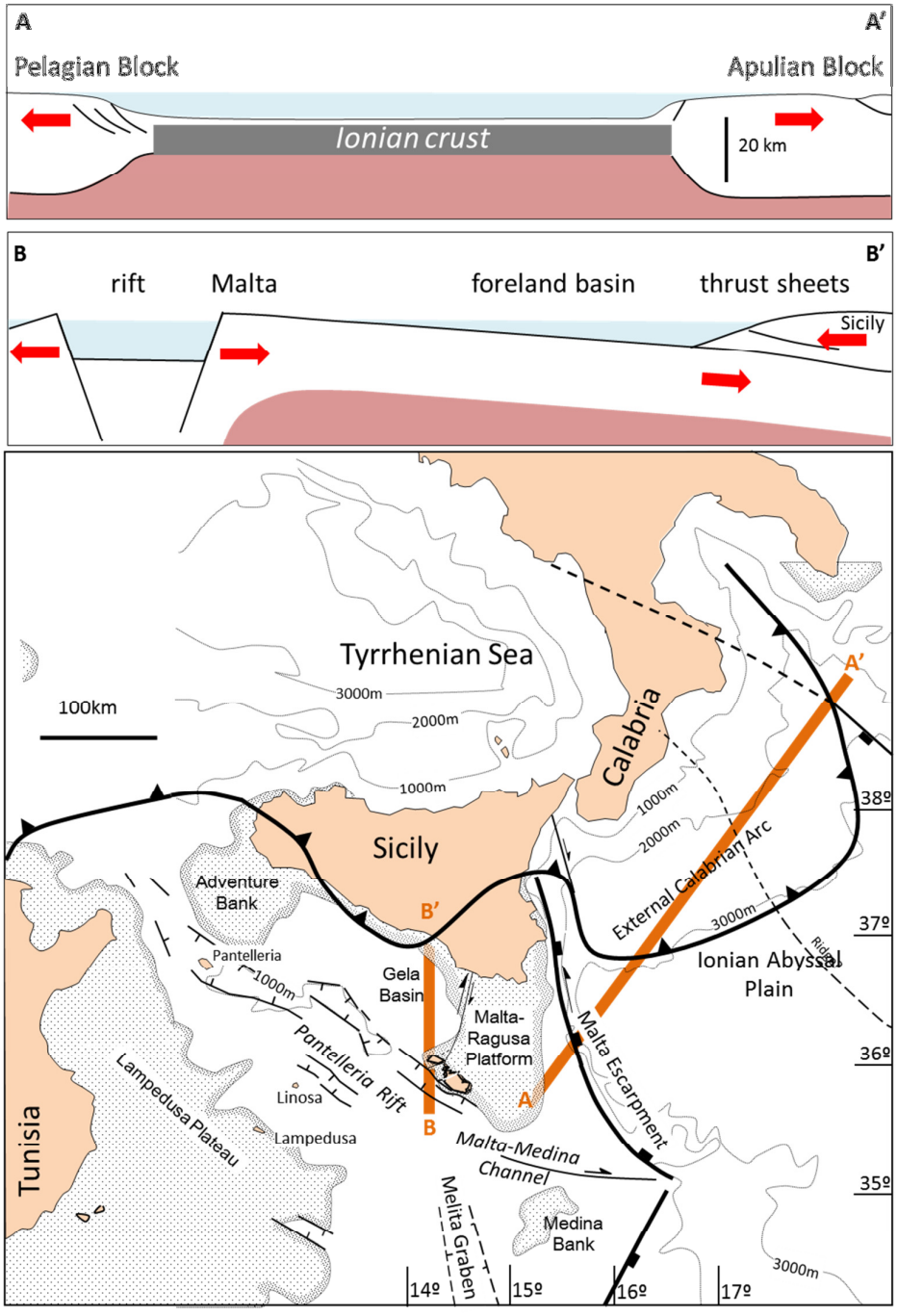

Figure 6.3. Generalised cross-sections across two geotectonic settings: A. Rifting and development of passive margin along Pelagian Block (Malta Platform) beginning during the Mesozoic based on Catalano *et al.* (2001); B. Underthrusting and development of foreland basin by loading of orogenic wedge thrust sheets since the Oligocene. Slab-pull resulted in rifting south of Malta during the Plio-Quaternary.

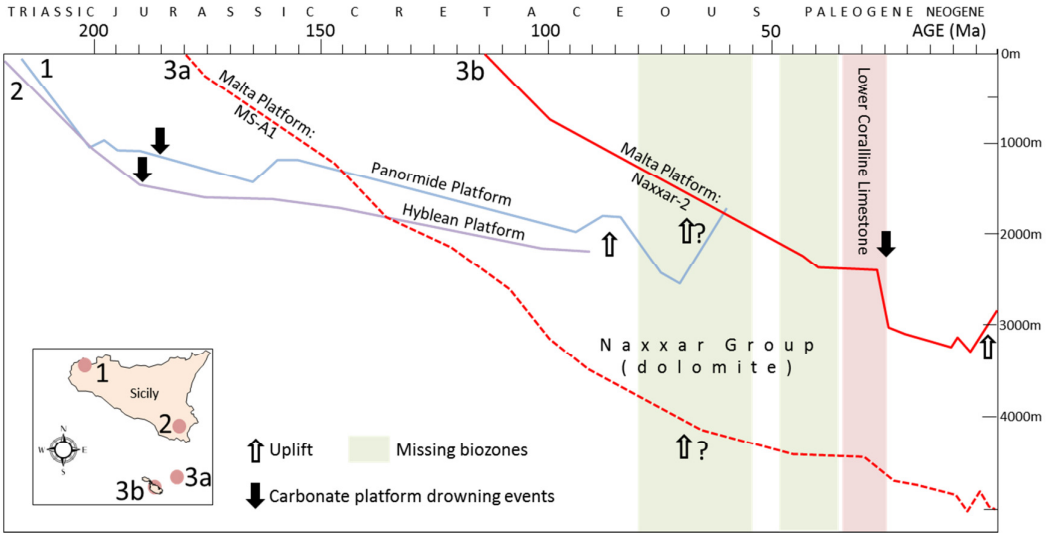

Figure 6.4. Burial history diagram based on well data from three carbonate platforms: The two sites on the Malta Platform (red curves) are based on Jongsma *et al.* (1985) and the Hyblean and Panormide platforms (blue curve) are based on Zarcone & DiStefano (2008). The average rate of subsidence at Naxxar well (3b) lasting from the mid-Cretaceous to mid-Palaeogene is 0.026 mmyr $^{-1}$. The grey shading shows missing biozones in the Malta platform based on Figure 6.5. The (?) indicates possible uplift in the Malta Platform during missing benthic foraminiferal biozones which are not shown in the burial history diagram of Jongsma *et al.* (1985).

In the Naxxar-2 well (Figure 6.6), the undolomitised section of the Early Eocene (Ypresian) is recognised on the basis of foraminiferal biozones. The succeeding SBZ 13 to 20 (14 Ma duration) are missing over the Malta Platform (Figure 6.5), implying an erosive depositional hiatus spanning most of the Late Eocene with limited episodes of deposition of carbonates and evaporites. The depositional hiatus spans the lower part of the Late Eocene to the Oligocene and is recorded over Lampedusa Island to western Sicily (Antonelli *et al.*, 1988). This hiatus terminates along the Malta Platform by an evaporite bed recognised in onshore and offshore Maltese wells that corresponds to the regional evaporites along the Eocene-Oligocene boundary unconformity in western Egypt/Cyrenaica (Gerdes *et al.*, 2010).

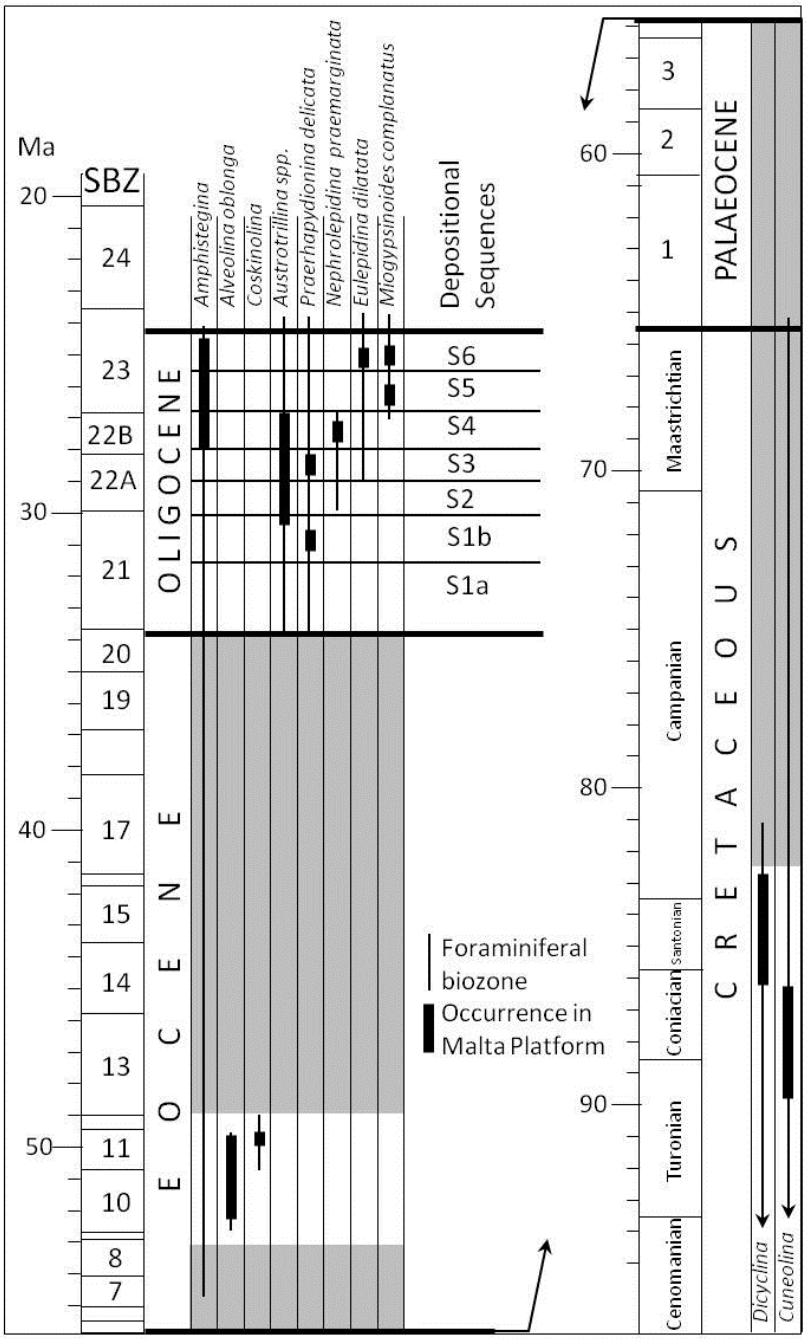

Figure 6.5. Foraminiferal data from the Naxxar-2 well, Aqualta well and outcrops. Foraminiferal Shallow Benthic Zones (SBZ 3 to 24) are from Serra-Kiel *et al.* (1998) and Cahuzac & Poignant (1997). Cretaceous biozonation is based on BouDagher-Fadel (2008). Thick vertical lines show occurrence in the stratigraphy of the Malta Platform whereas the thin vertical lines show range of foraminiferal biozone. The grey shading marks the absence of benthic foraminiferans interpreted to be the result of non-deposition, erosion or evaporite deposition.

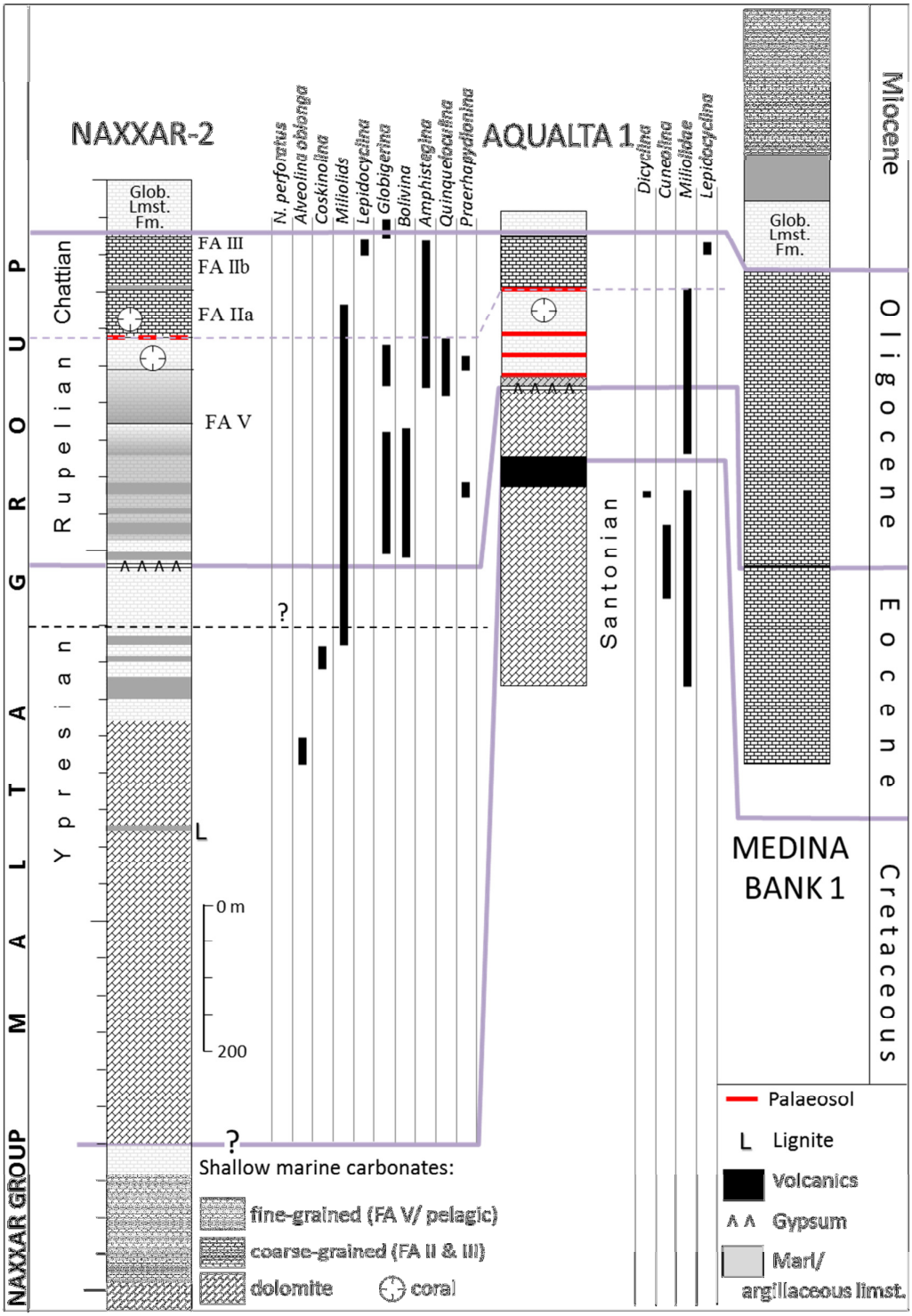

Figure 6.6. Lithology and formation names based on outcrops and well logs. Palaeosols identified by either *Microcodium* or clay in wells.

The burial history diagram shows slower subsidence during the Oligocene, but the trend resumed during the Miocene when transcurrent motions affected the Tethys basins (Gerdes *et al.*, 2010). The Malta Platform drowned and was overwhelmed with Early Miocene pelagic sediments of the Globigerina Limestone Formation.

By the Late Miocene, the collision of North Africa with the Calabrian Arc produced foreland basins along southern Sicily (Figure 6.3B). The underthrusted African slab produced slab-pull tension along the Sicily Channel that resulted in extension and opening of the NW-SE trending Pantelleria Rift (Argnani, 1990). Dart *et al.* (1993) suggest that Miocene faults trending NW and NE in the Maltese Islands are the result of N-S regional extension produced by this slab-pull mechanism. Ridge-push mechanism is associated with the uplifted Plio-Quaternary graben shoulders along the margins of the Pantelleria Rift. Part of the uplifted rift margin became subaerial and produced the north to northeast dipping Maltese Islands (Illies, 1981). The Late Miocene to Recent syntectonic stratigraphic evolution of the Maltese Islands is well-documented (e.g., Reuther & Eisbacher, 1985; Grasso *et al.*, 1986; Pratt, 1990; Gardiner *et al.*, 1995). However, pre-Miocene tectonism affecting the Malta Platform is less well known and is the focus of this chapter.

6.4 SEISMIC STRATIGRAPHY OF THE MALTA PLATFORM

In this study, the sediments of the Malta Platform are sub-divided into four megasequences found along three geotectonic zones: (1) platform interior zone, (2) Central Malta Platform Basin (CMPB) and (3) escarpment zone (Figure 6.7). Each zone shows distinct structural styles and sedimentological characteristics related to the mechanisms that created accommodation space. The lithology of the platform interior zone is better known from outcrops and exploration wells whereas the CMPB and the escarpment zone have been penetrated by only one well. However, some inferences on these geotectonic zones can be made on lithology from seismic imaging and dredged sea-bed samples.

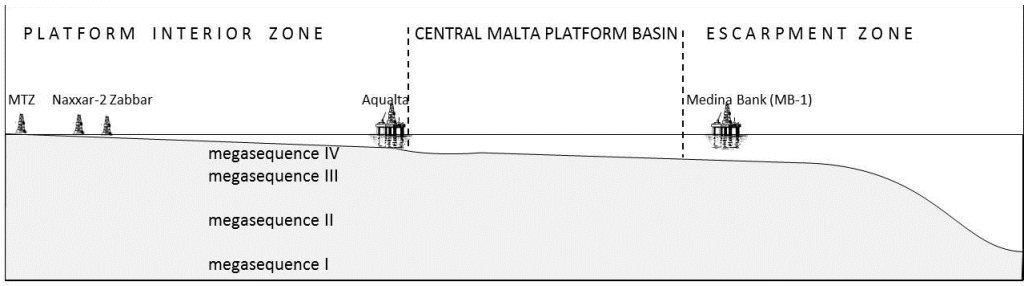

Figure 6.7. Stratigraphy and tectonics of the Malta Platform: Four megasequences, three geotectonic zones and the location of wells.

Seismic sections

The NW-SE and W-E seismic cross-sections shown in
Figure 6.2 were less affected by Plio-Quaternary faulting that dissects and deforms Palaeogene tectonostratigraphy in other areas of the Malta Platform. However, a number of bathymetric features are recognised in the NW-SE seismic line (line 303) shown in Figure 6.8 and summarised as follows:

1. Malta-Ragusa Plateau (here called the Malta Plateau): present day bathymetric high <200 m deep that includes the Maltese Islands and extends to SE Sicily (see Figure 2.2).
2. Malta Graben: a submerged Plio-Quaternary trough at >0.3 to 1 km water depth, infilled by >1 km thick graben fill (Dart *et al.*, 1993) formed by faults with >1 km throw.
3. Malta-Medina Channel: a >300 m deep channel produced by an W-E trending right-lateral transform fault since the Late Miocene (Messinian) that separates the Malta Plateau and the Medina Bank (Figure 6.3). Crustal thickness is about 20 km and Bouguer anomalies of 50-100 mgal suggest crustal thinning (Jongsma *et al.*, 1987).
4. Medina Bank: consists of three *en echelon* major bathymetric highs <200 m deep formed in post-Messinian time (Jongsma *et al.*, 1987).
5. Medina Escarpment: the southern continuation of the Malta Escarpment showing a dramatic increase in water depth to >2000 m. The Malta Escarpment is interpreted as one of the conjugate passive continental margins that confine the remnant of the Mesozoic oceanic crust (Ionian Basin)

(Catalano *et al.*, 2001) with a crustal thickness of 9 km covered with 7 km of sediments

6. Sirte Rise: the offshore Sirt Basin consists of tilted fault blocks buried below <6 km of post-rift sediments.

Seismic stratigraphy

Depositional sequences in the Lower Coralline Limestone Formation outcrops are *circa* 30 to 40 m thick (discussed in chapter 5) which may not be within the resolution of available seismic sections. The main seismic reflectors identified in the NW-SE seismic section (Figure 6.8) occur at two-way travel time (TWT) intervals of about 0.2 to >1 s. In carbonate rock, these TWT represent actual thickness of 1 to >5 km. In sequence stratigraphic terminology, kilometre-thick sediment packages correspond to megasequences deposited during >50 Ma-long first-order cycles (Weber *et al.*, 1995). In this thesis, Mesozoic to Recent tectonostratigraphic packages are grouped into megasequences I to IV, separated by platform-wide unconformities identified by three reflectors named: T-reflector, K-reflector and M-reflector (Figure 6.9), e.g., The Late Cretaceous hiatus identified by missing SBZ discussed in section 6.3 (page 236) forms the K-reflector. The megasequences are compared to the tectonostratigraphic sequences of Gerdes *et al.* (2010) in Table 6-1.

Megasequence IV:

Comprises partly lithified Pliocene carbonates to unconsolidated Recent marls that can be >1 km thick within graben but become very thin over the bathymetric high formed by the Malta-Ragusa Plateau (Gatt, 2007). The base is associated with the major sea-level drawdown in the Mediterranean known as the 'Messinian salinity crisis' (Ryan, 1978). The thick evaporites succeeding the carbonates produced the 'M'-reflector although this may be absent along parts of the Malta Platform (Figure 6.9) or buried under thick sediments in deep Plio-Quaternary graben, e.g., Malta Graben (Jongsma *et al.*, 1985).

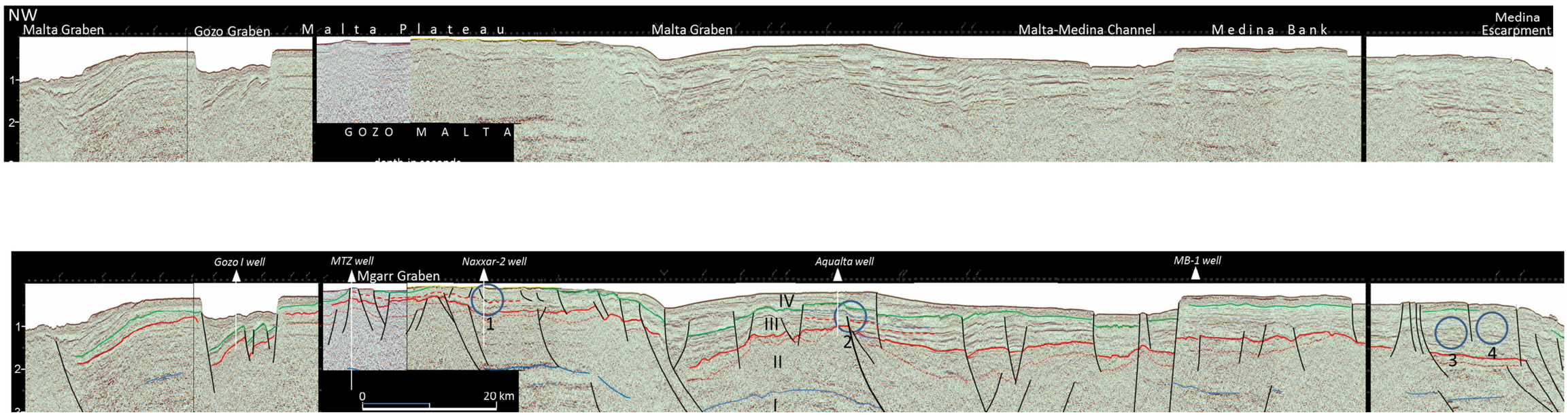

Figure 6.1. Seismic cross-section of Malta Platform (lines 303, 430 and 311. Interpreted section: blue line (T reflector) marks the top of the Triassic megasequence IV, red line (K-reflector) is the top of the Cretaceous of megasequence II, the thick dashed red line is the base Oligocene. The green line is the M-reflector that marks the top of the Tertiary megasequence III above which is the Plio-Quaternary megasequence I. Blue circles indicate main prograding complexes in megasequence III (Palaeogene to Miocene). Depth in seconds two-way time. Detailed sections shown in Fig. 6.11 (circle 1), Fig 6.30 (circle 2) and Figs. 6.36 (circles 3 and 4).

<table>
<tr><th>Megasequences</th><th>TSP[1]</th><th>Period/Epoch</th><th colspan="4">Stratigraphic Groups/Formations</th></tr>
<tr><td rowspan="2">IV</td><td rowspan="2">11</td><td>Quaternary</td><td colspan="4"></td></tr>
<tr><td>Pliocene</td><td colspan="4"></td></tr>
<tr><td rowspan="5">III</td><td rowspan="3">10</td><td rowspan="2">Miocene</td><td colspan="4">M- reflector</td></tr>
<tr><td rowspan="4">MALTA GROUP</td><td colspan="2">Upper Coralline Lmst. Fm.</td><td rowspan="4"></td></tr>
<tr><td colspan="2">Blue Clay Fm.</td></tr>
<tr><td colspan="2">Globigerina Lmst. Fm.</td></tr>
<tr><td>Oligocene</td><td colspan="2">Lower Coralline Lmst. Fm.</td><td>A</td></tr>
<tr><td rowspan="3">9</td><td rowspan="2">Eocene</td><td colspan="2">Halk el Menzel Fm</td><td rowspan="2">B</td></tr>
<tr><td>METLAOUI GP.</td><td>Ain Merhotta Fm.
El Garia Fm.
Bou Dabbous Fm.</td><td>C</td></tr>
<tr><td>Palaeocene</td><td colspan="2">El Haria Fm.</td><td>P</td></tr>
<tr><td rowspan="5">II</td><td>8</td><td rowspan="3">CRETACEOUS</td><td colspan="4">K- reflector</td></tr>
<tr><td>7</td><td colspan="3">NAXXAR GROUP</td><td rowspan="4">E</td></tr>
<tr><td>6</td><td colspan="3"></td></tr>
<tr><td>5</td><td rowspan="2">JURASSIC</td><td colspan="3">HURD BANK GROUP</td></tr>
<tr><td>4, 3, (2)</td><td colspan="3"></td></tr>
<tr><td>I</td><td>2</td><td>TRIASSIC</td><td colspan="4">T- reflector</td></tr>
</table>

Table 6-1. General stratigraphy of the Malta Platform sub-divided into 4 megasequences.. Formations names recorded in Tunisia used for naming Early Palaeogene subsurface successions in the Malta Platform are enclosed by thick black line. Italics show the named reflectors, shaded areas are the main reflectors. [1]Tectonostratigraphic sequences of Gerdes *et al.* (2010).

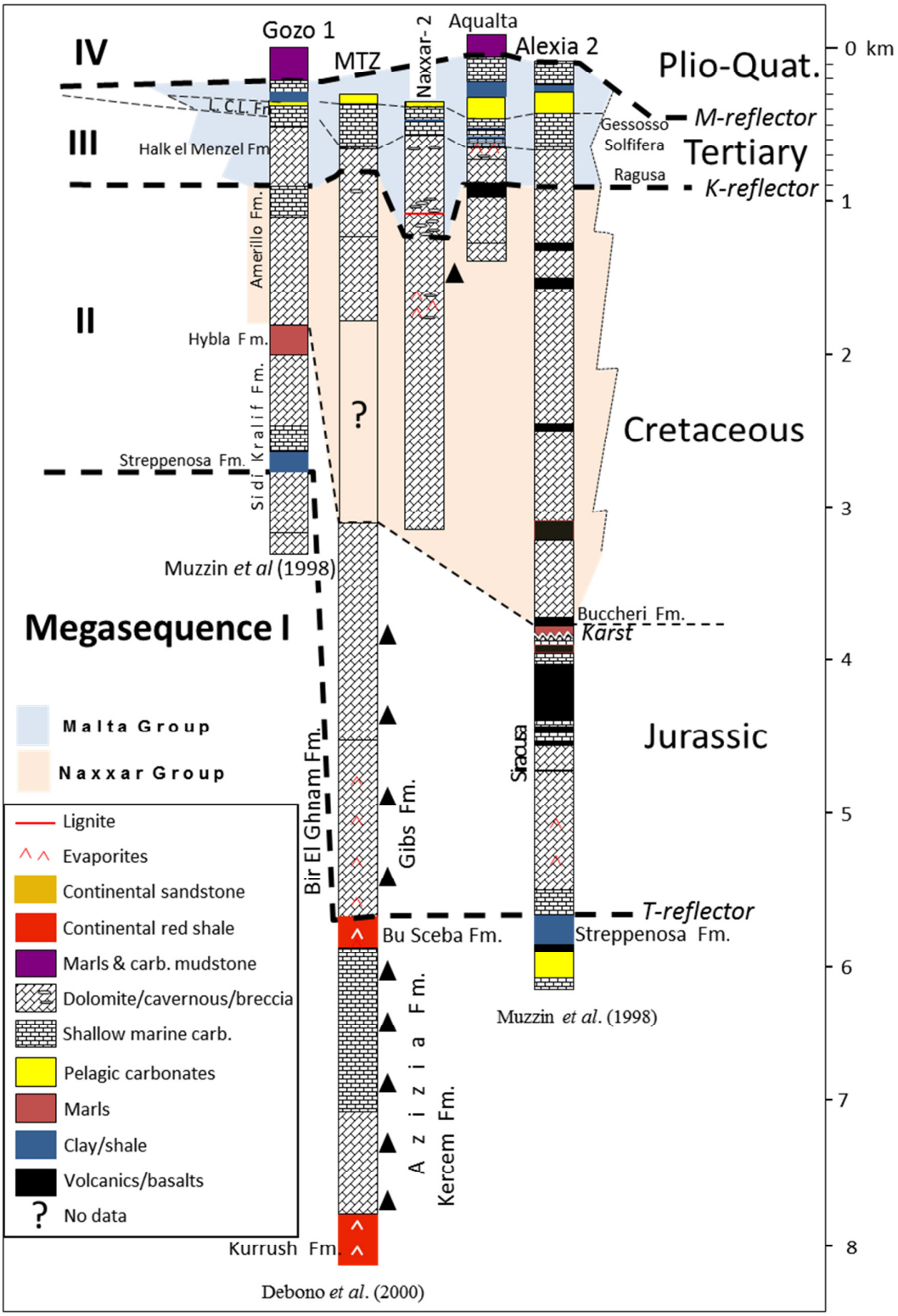

Figure 6.9. Logs of wells that penetrate megasequences I to IV. Thick dashed line is the megasequence boundary which is an unconformity surface and seismic reflector. Well data based on logs from BP (Naxxar-2 well), Total (Aqualta well) and ENI for Gozo-1, Alexia 2 and MTZ (Madonna taz-Zejt) wells (Muzzin *et al*., 1998). Location of wells shown in Figure 6.2B.

Megasequence III:

Consists of Palaeocene to top Miocene sediments (<1 km thick) of the Malta Group. The top M-reflector is associated with the Messinian sea-level lowstand. The base of megasequence III is associated with 25 Ma gap of missing foraminiferal biozones over the Malta Platform (Figure 6.5) corresponding to a hardground surface in Tunisia over a 14 Ma-long depositional hiatus separating the Cretaceous from the Early Eocene (Jorry, 2004). The absence of Palaeocene sediments in exploration wells over the Malta Platform (Muzzin *et al.*, 1998) suggests that this hiatus extended over the Central Mediterranean where it forms a strong reflector.

The sonic velocity of lithologies of megasequence III in the Malta Platform was tested by Harrison (1955) using rock samples perpendicular to bedding. However, these tests are based on cores which were dewatered and not under the lithostatic and hydrostatic pressure at depth. Seismic velocity data derived from *in situ* measurements based on density of lithology and its thickness in the Aqualta well provide more realistic sonic velocity values and are used to construct the synthetic seismic. The sonic velocities of lithology in the Aqualta well are applied to the Naxxar-2 well. On this basis the two-way travel time for the stratigraphy of the Aqualta well and Naxxar-2 well (
Table 6-2) are derived using the formula:

$$\text{Two-way travel time (TWT)} = (d/v) \times 2$$

d: thickness of sediment package (m)
v: sonic velocity (m/s)

The synthetic seismogram is calibrated with the offshore seismic line 311 located *circa* 6 km to the northeast of the Naxxar-2 well and seismic line 303 that coincides with the location of the Aqualta well (Figure 6.2).

Formation	velocity m/s	Aqualta thickness	TWT	Naxxar-2 thickness	TWT ms
water	1481	180	0.243079	50*	0.067
Plio-Quaternary	1600	175	0.21875	20	0.025
Upper Coralline	2700	270	0.2	n/a	0
Blue Clay	2000	100	0.1	n/a	0
Globigerina limestone	3400	160	0.094118	60	0.0352
Lower Coralline Limestone	3400	210	0.123529	450	0.264706
Upper Eocene limestone	3400	90	0.052941	200	0.117647
dolomite/Metlaoui Gp./basalt	4900	90	0.036735	200	0.0816
Top Cretaceous dol./lmst.	4900			350	0.1428
Base Cretaceous dolomite	4900	520	0.212	1800	0.734694
Total depth		1795	1.281152	3130	1.468647

Table 6-2. The TWT depth of formations listed in Table 6-1 (n/a indicates missing strata). * some adjustments are made because seismic line is located at 50 m water depth whereas Naxxar-2 well is onshore.

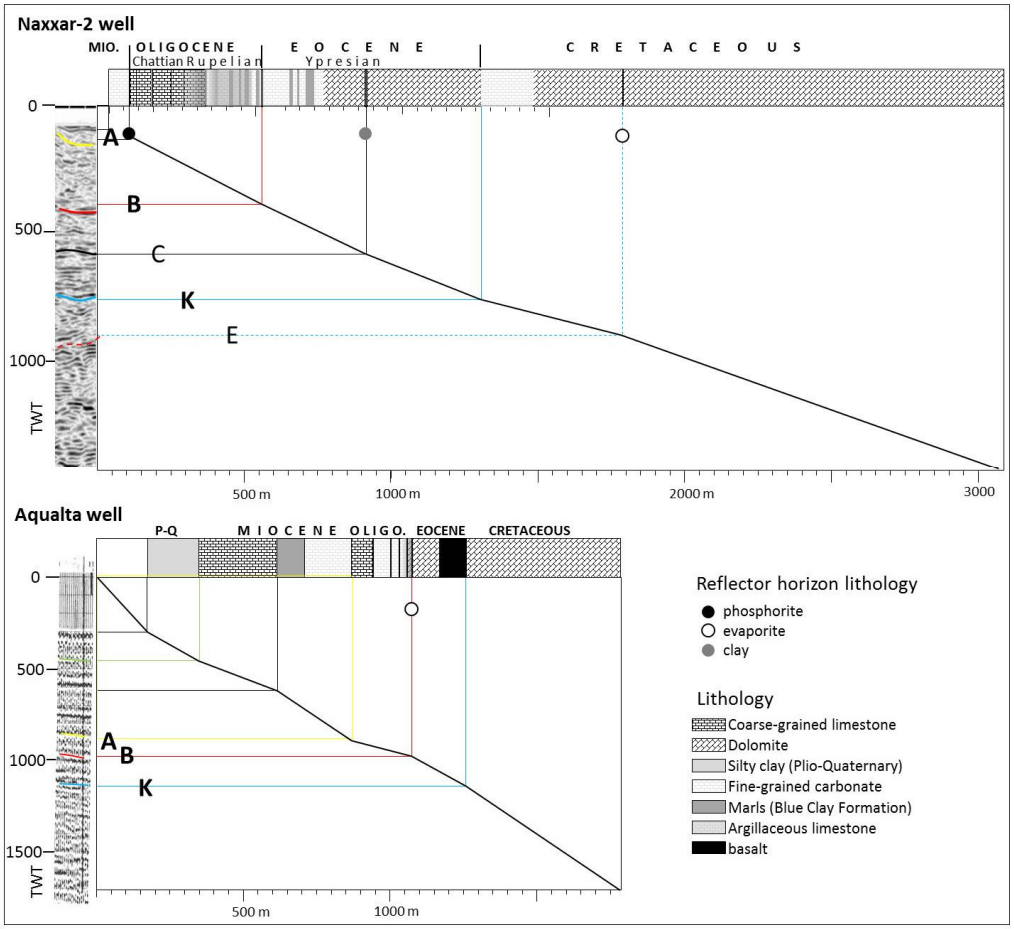

Figure 6.10. Calibration between Naxxar-2 well* and seismic line MSC01 311 and calibration of the Aqualta well to seismic line 303 based on Table 6-2.

Megasequence III is imaged with four continuous high amplitude reflectors (Table 6-1) that are calibrated to onshore well data (Figure 6.10):

Reflector A: Forms the boundary between the Lower Coralline Limestone Formation and the Globigerina Limestone Formation (base Miocene boundary) and includes an extensive hardground capped by a sporadic phosphorite bed in exposed sections (Gatt, 2005) which increase acoustic impedance that strengthens the reflector.

Reflector B: Forms the base Lower Coralline Limestone Formation that consists of gypsum or breccia horizon (SbRU1) that separates the Oligocene from the Eocene. The acoustic impedance between the limestone and evaporite produces this strong reflector.

Reflector C: Corresponds to the Early Eocene (Ypresian) shale bed (lignite in one bed) inter-bedded with carbonates that are penetrated by the Zabbar and Naxxar-2 wells. These are interpreted to be equivalent to the shales of the Bou Dabbous Formation. The thin beds of shale result in a strong reflector because of high acoustic impedance with the surrounding carbonates.

Reflector P: This high amplitude reflector is only imaged in seismic in specific parts of the carbonate platform along some intra-platform basins. In other areas the P-reflector is merged with the underlying K-reflector. This is interpreted to be of Palaeocene age and marks the top boundary of the El Haria shales that is widespread in Tunisia (Bishop, 1975) creating a strong acoustic impedance with the Eocene carbonates above it.

Megasequence II:

Comprises Cretaceous dolomites (<2.5 km thick) of the Naxxar Group (Figure 6.9) to the base Jurassic sediments (Hurd Bank Group) that correspond to TSP 6, 7 and 8 of Gerdes *et al.* (2010). In the seismic section shown in Figure 6.8, Jurassic sediments cannot be distinguished from Cretaceous dolomites in seismic imaging which may indicate relatively a homogeneous dolomitized platform interior lithology throughout the Late Mesozoic except in areas intruded by basaltic sills. However, in the more structured areas of offshore Sicily to northeast offshore Malta (Alexia-2

well) at the margin of the Malta Platform, the two Periods are separated by a karstic horizon and the Buccheri Shale developed along horsts and graben (Figure 6.9).

Reflector K: The top of megasequence II is imaged by the strong K-reflector that separates the overlying Tertiary continuous reflectors from the underlying discontinuous to chaotic Cretaceous seismic facies with local high amplitude horizons. This boundary is marked by a hiatal surface (Figure 6.5) that produces a strong reflector especially when it represents a subaerial episode or marine hardground. Reflectors below this horizon are generally more discontinuous than reflectors above it.

Reflector E: Corresponds to an evaporite horizon penetrated by the Naxxar-2 well (Figure 6.10) which is inter-bedded with carbonates.

Megasequence I:

The top of this megasequence is penetrated by only one well, the MTZ well in onshore western Gozo where a >100 m thick shale bed occurs at a depth of 6048 m. The shale bed is bounded above and below by >1.5 km of carbonates (Figure 6.9). The lithological change would result in acoustic impedance that creates a strong reflector. The time (TWT) equivalent of the shale bed is here estimated by taking the depth of the base of Naxxar-2 well (3100 m equivalent to 1.46 s in TWT) and adding 2948 m to the level of the depth of the shale bed using travel time of 4900 ms (see Figure 6.9).

$$1.46 \text{ ms} + (2928 \text{ m} / 4900 \text{ ms}) = 2 \text{ s}$$

The estimated TWT depth of 2 s of the shale bed coincides with a high amplitude reflector imaged in seismic, although the reflector is not continuous across the Malta Platform (Figure 6.8). Although no palaeontological element is identified in publications on the MTZ well to indicate an age with certainty, the shale is described as continental red beds of North African provenance and interpreted as correlating with the Triassic (Rhaetian) Bu Sceba Formation in North Africa by Debono *et al.* (2000). Consequently, the 2 s depth reflector is tentatively considered to be the top Triassic horizon, here named the T-reflector and equivalent to the shale bed. The dating is supported by a strong reflector in the Alexia-2 well identified at TWT depth

between 2 s to 2.5 s which is correlated to the top Triassic boundary (Muzzin *et al.*, 1998). Parallel to, and *circa* 0.4 ms TWT below the T-reflector in line 303 is another strong reflector that corresponds to the second shale bed recorded in the MTZ well about 1500 m below the top Triassic shale.

6.4.1 Seismic facies of megasequence II

The seismic character of megasequence II is highly variable but can be categorised as having two laterally alternating seismic facies showing strong (S) and weak (W) reflectors identified at TWT depths >0.7 s in (Figure 6.11):

Seismic facies S: High amplitude, continuous to discontinuous reflectors. The high acoustic impedance between two different lithologies produces high amplitude strong reflectors. The Cretaceous dolomite succession of megasequence II penetrated by Naxxar-2 and Zabbar wells (located close to seismic line 311 shown in Figure 6.2) consists of shallow marine fauna (e.g., Alveolinids) and in the Naxxar-2 well shows cavernous porosity after the dissolution of gypsum (Figure 6.9). The occurrence of gypsum or cavernous horizons would produce strong acoustic impedance.

Seismic facies W: Discontinuous to hummocky reflectors found in parts of megasequence II alternating with seismic facies S. The seismic facies extends below central Malta and has not been penetrated by deep wells. However, the lower acoustic impedance and discontinuous reflectors may indicate relatively homogenous density of beds. This type of seismic facies in a carbonate platform setting is interpreted as characteristic of platform interior sediments composed of dolomites and limestone. The reflectors of this seismic facies in megasequence II tend to be weak because interlayered limestone and dolomites have low density variations which generate low acoustic impedance (Eberli *et al.*, 2004).

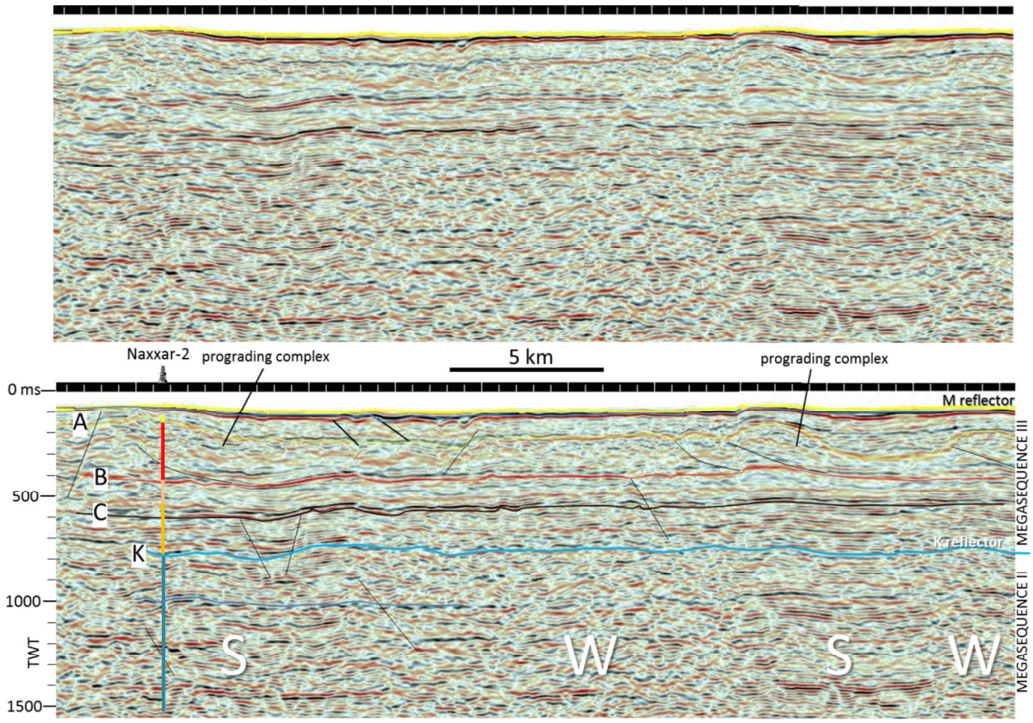

Figure 6.11. Top: uninterpreted seismic line 311. Bottom: Seismic interpretation of megasequence II and III (megasequence IV is missing). Areas marked W show discontinuous to hummocky reflectors whereas areas marked S show weak to strong continuous reflectors. Coloured reflectors mark base Miocene (A - yellow), base Oligocene (B - red), Eocene equivalent to Bou Dabbous Formation (C - black), top Cretaceous (K - blue). Vertical coloured line indicates approximate location of Naxxar-2 well. The stratigraphy is based on synthetic seismogram comprising Miocene (yellow), Oligocene Lower Coralline Limestone Formation (red), Eocene (orange) and Cretaceous (blue) sections.

6.4.2 Seismic facies and outcrops of megasequence III

Megasequence III (reflectors K to A in Figure 6.11) is the main focus of this chapter. The complex tectonostratigraphic development of megasequence III in the Malta Plateau can be partly assessed from seismic imaging and from outcrop. The Early to mid-Palaeogene non-carbonate horizons interbedded with limestones include gypsum and shale which produce strong acoustic impedance and high amplitude reflectors (B and C-reflectors, respectively). Evaporites do not occur in the upper part of the Tertiary (Oligo-Miocene) megasequence III that consists of stacked shallowing-upward parasequences of carbonate skeletal grains (depositional sequences 4 to 6). Acoustic impedance contrasts would be low in this lithology except along palaeosol horizons (facies VI) where these have not been eroded.

The continuous reflectors in megasequence III show three geometries that correspond to the three geotectonic zones (see Figure 6.13):

1. *Horizontal reflectors*: Large areas of the seismic sections over the Malta Plateau consist of horizontal to slightly wavy continuous to discontinuous reflectors down to two-way travel time depth of 0.7 s around the Maltese Islands (unless disturbed by Plio-Quaternary faulting) as seen in Figure 6.11. The continuous horizontal reflectors can be traced over large areas and can be used as time-lines for correlating sections. Horizontal reflectors are produced by deposition of carbonates and platform aggradation during the creation of accommodation space as a result of sea-level fluctuations, e.g., Goldhammer *et al.* (1990).

2. *Steeply inclined reflectors*: These strong and continuous reflectors juxtaposed to platform chaotic reflectors mark the slope environment which is characterised by a declivity of >40°. The platform escarpment is produced by the combination of aggradational growth and erosion (Eberli *et al.*, 2004). Large escarpments are recognised in the Great Bahama Bank where near vertical platform margins are onlapped by highstand clinoforms (Ginsburg *et al.*, 1991). In the central Mediterranean, the Malta Escarpment forms a sharp break in slope (Scandone *et al.*, 1981) that separates the Malta Platform from the Ionian Basin crust.

3. *Sigmoid-shaped reflectors*: Four localities marked by circles in Figure 6.8 show clinoforms which downlap basinward. Details shown in Fig. 6.11 (circle 1), Fig 6.30 (circle 2) and Figs. 6.36 (circles 3 and 4). These are interpreted as large prograding complexes that developed along the platform margin. Some smaller complexes fill antecedent bathymetric lows along the platform interior created by Cretaceous to early Palaeogene faulting. The rate of sediment production over the palaeohighs would have to exceed the available accommodation space in order to generate a succession of downlap or offlap patterns. In shelf break settings, both highstand and lowstand systems tracts produce large clinoform bedding (Figure 6.12). Two methods may distinguish the systems tracts: (a) Eberli & Ginsburg (1989) proposed that a rise in sea-level leads to the

development of individual sigmoids whereas a fall in sea-level separates successive sigmoids and, (b) Highstand and lowstand prograding complexes can be distinguished on seismic data by differences in the type of reflectors (Belopolsky & Droxler, 2004):

i. Strong-amplitude reflector package (SARP): high amplitude reflectors formed by forced regressive wedges in the lower part of sequence. Sediments tend to be coarse-grained and fines winnowed.
ii. Weak-amplitude reflector package (WARP): produced during highstands of sea-level in the upper part of sequence. High carbonate productivity generally results in more fine-grained sediments (Schlager *et al.*, 1994) that produce weak-amplitude reflectors (Figure 6.12).

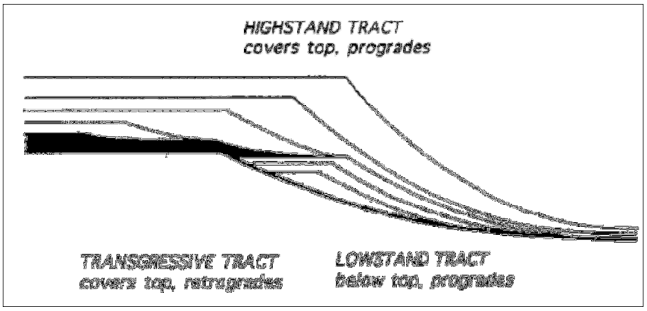

Figure 6.12. Lowstand and highstand systems tracts of rimmed shelf carbonate platforms (from Schlager *et al.*, 1994).

6.5 GEOTECTONIC SUBDIVISION OF THE MALTA PLATFORM

Reflector geometries and thickness of megasequence III are the basis for the sub-division of the Cenozoic Malta Platform although parts of the platform were subsequently disturbed by Plio-Quaternary faulting. Superimposed on passive margin subsidence and sedimentation (Figure 6.4) are local tectonic mechanisms that created additional accommodation space along three Palaeogene geotectonic zones (Figure 6.13) over an area extending from the Maltese Islands to the margin of the Ionian Basin and Sirte Rise in the east:

1. Platform interior zone: extends from the Maltese Islands to the Aqualta well area over >100 km. This area forms the platform interior characterised by continuous to discontinuous horizontal reflectors in megasequence III whereas megasequence IV thins out as a result of erosion or is missing.
2. Central Malta Platform Basin (CMPB): immediately east of the Aqualta well is a >50 km-wide zone characterised by low angle reflectors and expanded sediments towards the depocentre of the basin.
3. Escarpment zone: forms a relatively narrow cusp-shaped zone along the eastern margin of the Malta Platform that is trending NW to SE in the north (Malta Escarpment) and changes direction to NE to SW (Medina Escarpment) in the south. The escarpment zone consists of a narrow ridge (<20 km) bounded by a stepped margin showing steeply inclined reflectors. The escarpment is draped by kilometre thick sediment package of horizontal and sigmoid-shaped reflectors of megasequence III in the south but is thinly covered by sediments along the Malta Escarpment.

6.5.2 Platform interior zone

This geotectonic region is the only one in the Malta Platform that is subaerial along the Maltese Islands. The area is characterised by a relatively thin megasequence III (<1500 m) from the Maltese Islands to Aqualta well, thinning considerably west of Malta. The available subsurface data is limited to wells located on the platform interior zone (Appendix I and Figure 6.2) listed in Table 6-3 according to basin setting. Outcrop and cores from shallow boreholes (Wardell Armstrong, 1996) show that the Palaeogene tectonostratigraphy of the Maltese Islands comprises localised thickness variations at the level of depositional sequences to formations. These variations suggest the development of a number of small basins within the platform interior zone which is consistent with seismic data that shows subtle structural highs and lows.

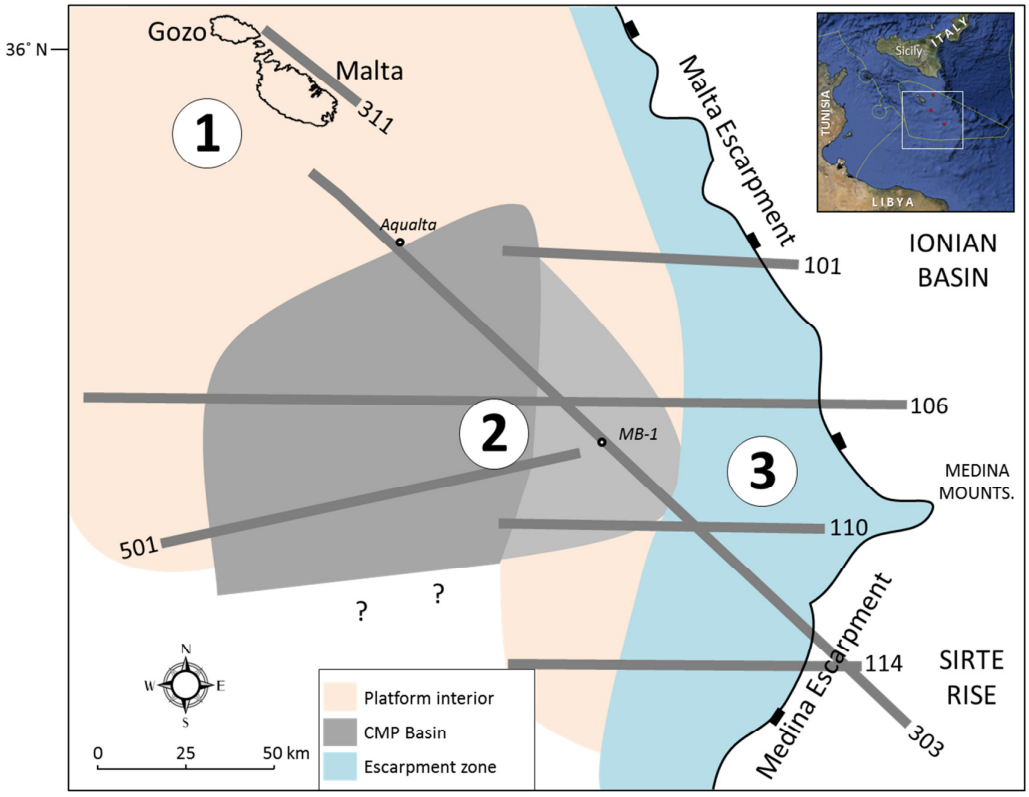

Figure 6.13. Geotectonic sub-divisions of the Malta Platform: 1. Platform interior; 2. Central Malta Platform Basin (darker shading marks deeper area); 3. Malta-Medina Escarpment. Thick grey lines show location of main seismic lines that section the Malta Platform.

Well	Palaeogene basin setting	Thickness of Palaeogene (m)	
		Oligocene	*Eocene*
MTZ (Gozo)	structural high	N/A	N/A
Aqualta	structural high	200	100
Zabbar-1	structural high	240	
Medina Bank-1	basin edge	400	300
Naxxar-2	basin depocentre	450	>1000

Table 6-3. List of wells located on the platform interior. Thickness of sediments reflects setting of well along basins.

6.5.2.1 Cenozoic basins and structures

Reflectors in seismic lines parallel to the NW-SE trending coast of the Maltese Islands are mostly horizontal (unless disturbed by Plio-Quaternary tectonics). Reflectors A to C show some declivity and upwarping in the western and eastern ends of Malta (Figure 6.11) where <10 km-wide prograding complexes within the top <0.2 km are recorded in outcrops at localities A to 8. The progradation resulted from the development of basins that began during the Palaeogene and continued to the Miocene. The basins developed by tectonic activity whereas basin architecture was controlled by glacio-eustatic sea-level. The following basins and structures of the Palaeogene, Miocene and Plio-Quaternary are described:

A. Palaeogene structures:

The facies and sequences are discussed in chapters 3 and 5 respectively, and summarised in Table 6-4. A number of sections are correlated along sequence boundaries and show lateral thickness variations from west to east (Figure 6.14). The stratigraphic correlation chart in Appendix II gives more detailed stratigraphy. The logs in Appendix II-4 are hung from the C_1 phosphorite bed that caps the lower member of the Globigerina Limestone. The thickness of the lower Globigerina Limestone is derived from field outcrops (logs in Appendix II), published data, e.g., Pedley *et al.* (1978) and core data (Wardell Armstrong, 1996). Depocentres were filled by pelagic carbonates so that the C_1 bed is presumed to have been a flat surface.

Age	Sequence	Facies Association
CHATTIAN	6	III
	5	II
	4	II/VI
RUPELIAN	3	V/VI
	2	V
	1b	V
	1a	V/VII

Table 6-4. Summary of depositional sequences and facies of the Lower Coralline Limestone Formation (details in chapter 5).

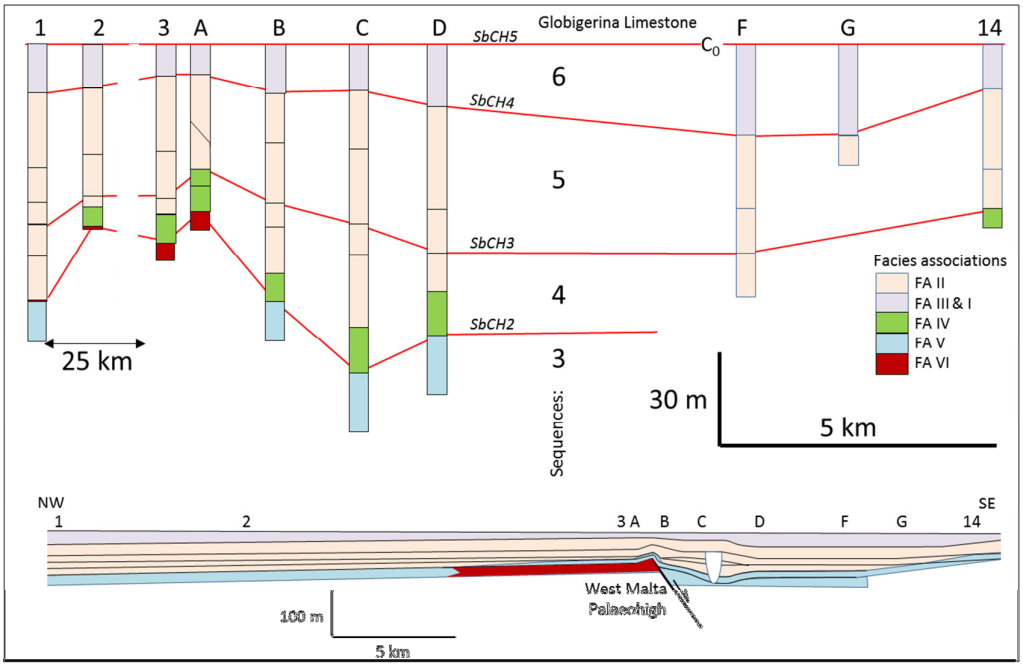

Figure 6.14. Sequence thickness from west to east.

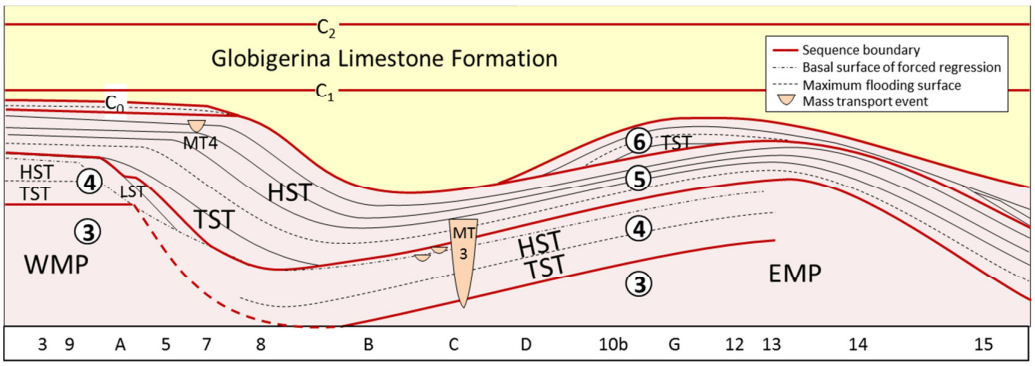

Figure 6.15. Sequence stratigraphic model for the Lower Coralline Limestone Formation.

The correlation chart shows the thinning of the Lower Member of the Globigerina Limestone over Oligocene bathymetric highs where condensed sediments (FA IIIa) are recorded in the Lower Coralline Limestone Formation. These lateral variations in thickness are the basis of the sequence stratigraphic model that shows the overall geometries of sediment packages (Figure 6.15). Two Oligocene bathymetric highs are identified, the Western Malta Palaeohigh (WMP) and the Eastern Malta Palaeohigh (EMP). Inclined sediment packages offlap the bathymetric highs during

two phases during third-order sea-level change: the lowstand regressive wedge (LST of depositional sequence 4) and the much larger highstand prograding and aggrading wedge (HST of depositional sequence 5). The size of the two wedges is consistent with expected rates of carbonate sedimentation which are high during the highstand of sea-level and restricted during the lowstand of sea-level when large parts of the platform are exposed (Schlager *et al.*, 1994).

The NW-SE trending seismic lines 311 and 312 located a few kilometres offshore of the Maltese Islands (Figure 6.16) suggest the development of a number of basins separated by structural highs. The occurrence of facies association VI with associated palaeosols along West Malta Palaeohigh (WMP) confirms periodic emergence consistent with thinning of depositional sequences over western Malta. In seismic, the WMP culminates over the island of Comino and eastern Gozo, here named the Comino Palaeohigh (CP). The CP affected sedimentation into the Miocene and caused the thinning of the Globigerina Limestone and Blue Clay formations recorded in previous works (Pedley *et al.*, 1978; Pedley *et al.*, 1991). Another structural high forms a narrow NE-SW unnamed lineament penetrated by the onshore MTZ well (location map Figure 6.2), which is here named the West Gozo Palaeohigh (WGP). The exposed steep western margin of WGP shows large circular solution subsidence features caused by the dissolution of gypsum (discussed in chapter 4).

Three basins developed throughout the Cenozoic alongside the Comino Palaeohigh which here are named the Naxxar Basin, Mgarr Basin and Marsaxlokk Basin (Figure 6.16). There is little Palaeogene outcrop and well data from the Mgarr Basin located between the islands of Comino and Gozo that can be used to describe this basin. The geometry and extent of the adjacent Naxxar and Marsaxlokk basins can be deduced from well data and the southern cliffed coast of Malta that exposes a NW-SE cross-section along the carbonate platform and shows variations in thickness of depositional sequences. The available database and outcrops limits inferences on tectonostratigraphic development to where the following is observed along the NW-SE strike:

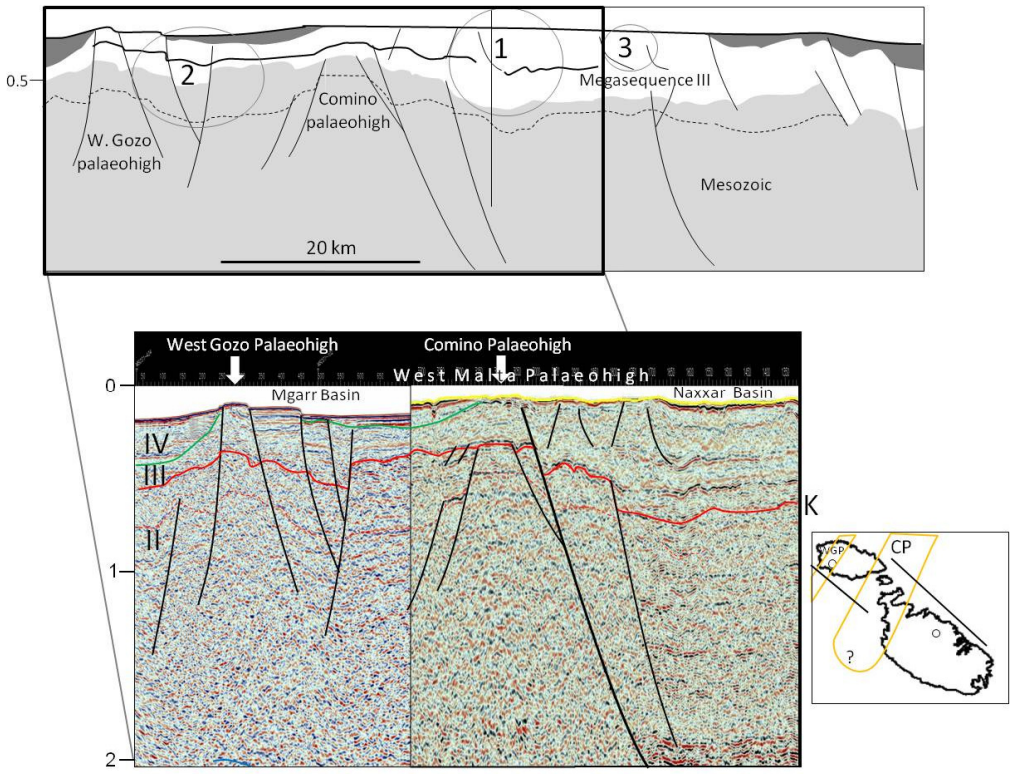

Figure 6.16. Seismic lines 311 and 312 combined. Top: Interpreted seismic section. Megasequence III (shaded white) is sub-divided by a thick black line marking the base of the Oligocene. The circles show the three Cenozoic basins adjacent to the Comino Palaeohigh: 1. Naxxar Basin, 2. Mgarr Basin and 3. Marsaxlokk Basin; Bottom: inset shows seismic cross-section from Gozo to North Malta along the seismic line parallel to Maltese Islands (in map). The white arrows mark the West Gozo Palaeohigh (WGP) and the Comino Palaeohigh (CP).

1. Increased accommodation space: *circa* 450 m of Oligocene carbonates penetrated by the Naxxar-2 well shows the thickening of subsurface Rupelian sediments (sequences 1 to 3) over the western part of the Naxxar Basin relative to the 250 m thick Oligocene sediments over eastern Malta (Zabbar-1 well) found along the western rim of the adjacent Marsaxlokk Basin (Figure 6.17).

2. In outcrop, the Naxxar Basin is characterised by the rapid increase in thickness of about 40 m of the Chattian sediments in locality B to D relative to localities 3 to A (Western Malta Palaeohigh). The increase consists of <15 m to 35 m and 45 to <60 m in sequences 4 and 5, respectively (Figure 6.17). This suggests synsedimentary thickening over central Malta was greater than over western Malta. The thickness of Chattian sediments in the Zabbar-1 well (sequences 4 to 6 are 130 m thick) rimming the Marsaxlokk Basin is only 10 m less than the

Chattian sediments penetrated by the Naxxar-2 well which suggests less accommodation space at the eastern margin of the basin relative to the deeper part of the Naxxar Basin where the Naxxar-2 well is located.

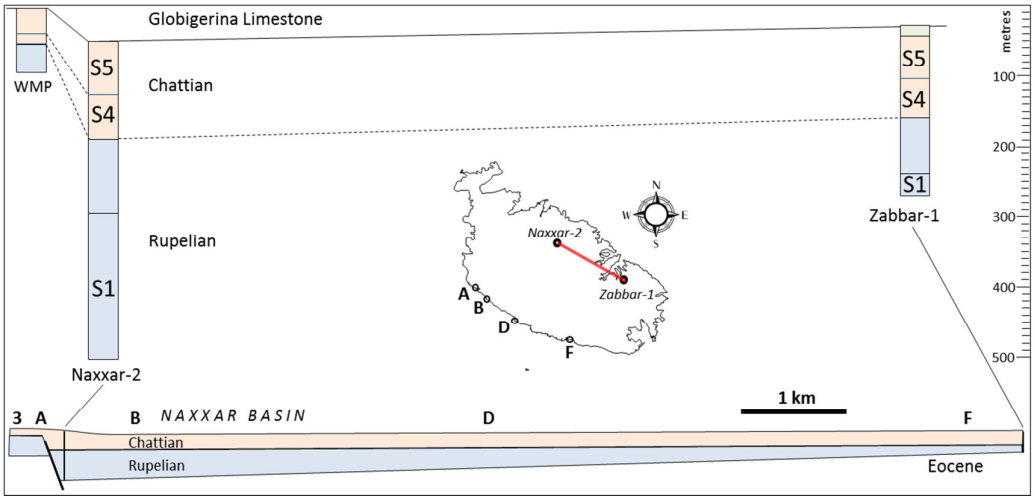

Figure 6.17. Stratigraphic logs showing thickness of Oligocene sediments and thickness of sequences 1 (S1), 4 (S4) and 5 (S5). The cross-section is from Naxxar-2 well to Zabbar-1 well along the Naxxar Basin (drawn to scale). The West Malta Palaeohigh (WMP) is on the left from where clinoforms offlap towards the basin, partly seen in locality 8. Marsaxlokk Basin is east of Zabbar-1.

3. Angle of dip (θ) of bedding: along the southern cliffed coast of Malta bedding consistently dips 2° W from locality D to locality B (Naxxar Basin) whereas east of Zabbar-1 well between localities 13 and 14 (Marsaxlokk Basin) the bedding dips >2° E in the opposite direction (Figure 6.18). The dip of bedding is not post-depositional because coral patch reef growth along depositional sequence 4 was controlled by differential palaeobathymetry along the Naxxar Basin. The southern cliffed coast of Malta shows early drowning of small coral patch reefs along the base of the sequence at locality B (see Appendix V-30) whereas larger patch reefs found at higher levels farther east at locality D (see Appendix V-32) had drowned subsequently. This suggests that the western part (locality B) of the Naxxar Basin was deeper or deepened more rapidly relative to the eastern part (locality D) which is consistent with the cross-section in Figure 6.17. Locality F found between the Naxxar and Marsaxlokk basins shows quasi horizontal bedding (θ = 0°). The dips along basins are the result of synsedimentary tilting during the Oligocene which is reflected in thickening along dip of the succeeding Miocene sediments.

4. Large clinoforms: clinoforms that prograde into areas with greater accommodation space usually mark the rim of the basin. The accretion of sequence 5 was accompanied by eastward prograding clinoforms at locality 8 whereas the forced regressive wedge in sequence 4 occurs at the base of locality A which is also along the western rim of the Naxxar Basin. The underfilled palaeolow between localities A and B became the depocentre for these eastward prograding clinoforms. Mass transport events at locality 7 also translated eastwards towards the Naxxar Basin in central Malta. The seismic line parallel to the northern coast of Malta and the horizons interpreted in Figure 6.11 shows an inclined A-reflector marking the Oligo-Miocene interface which corresponds to the top foresets of the large clinoform bedding exposed at locality 8. The features in these localities are all situated along a NE-SW trending lineament that expresses an Oligocene break in slope between the West Malta Palaeohigh (WMP) and the Naxxar Basin over central Malta (Figure 6.18).

5. Erosional surfaces: erosional surfaces are more pronounced and frequent in western Malta (localities 3 to A) outside the Naxxar Basin and in localities G and 13 along the rim of the Marsaxlokk Basin. The fall in sea-level associated with sequence boundary SbCH3 resulted in extensive erosion and removal of several metres of sediment from depositional sequence 4 along locality A. In addition, the thinning of sediments over locality A is reflected in the condensed sediments of depositional sequence 6 at locality 3. In localities 10b and G thick cross-bedded sediments (sequence 6) are truncated by several sharp erosional boundaries.

Although outcrops show evidence of basins and palaeohighs, Oligocene to early Miocene faulted margins are not explicit in Maltese outcrops. The most prominent palaeobathymetric high along the platform interior is around Aqualta well where the Palaeogene is thinnest (Table 6-3).

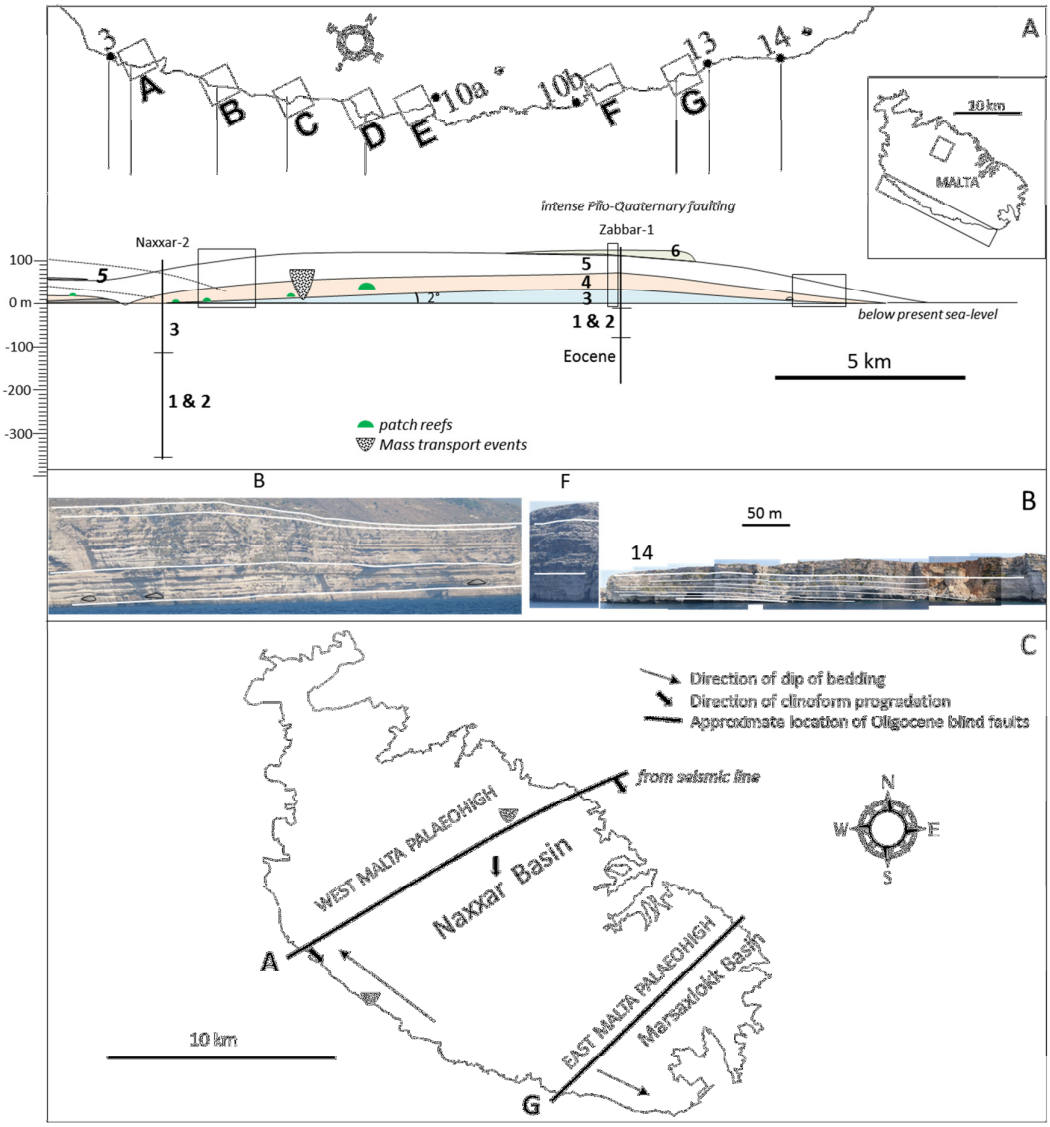

Figure 6.18. A. Schematic cross-section of the Maltese Islands along southern cliffed coast from NW to SE showing depositional sequences 1 to 6. The dashed lines show clinoforms at locality 5 to 8 farther north. The area between localities F and G is intensely faulted by Plio-Quaternary faults and has been tentatively reconstructed prior to such faulting; B. Photographs of cliffed coast of localities B (see Appendix IV-23), F and 14 (see Appendix Iv-24). Location marked by rectangles across cross-section; C. Map showing directions of dips influenced by breaks in slope (thick black lines) along A and G.

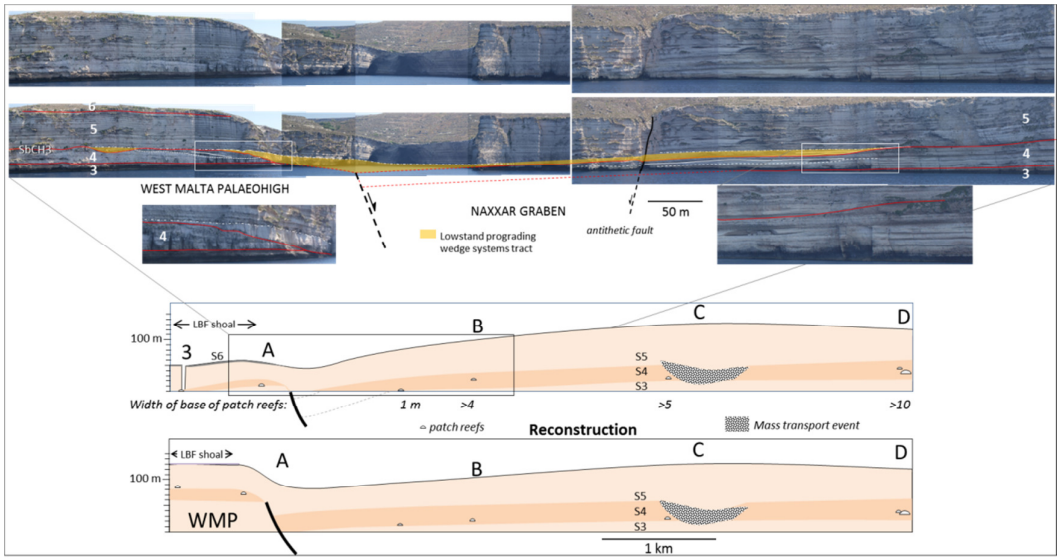

Figure 6. 19. Locality A to B: Uninterpreted section of cliffed coast. Below is the interpreted section showing depositional sequences 3 to 6 and the extent of the lowstand prograding wedge that fills the accommodation space created by the blind normal fault and erosion along footwall crest. An antithetic fault is exposed in locality B. Reconstructed section after removal of effects of Plio-Quaternary tectonism that resulted in subsidence of locality A.

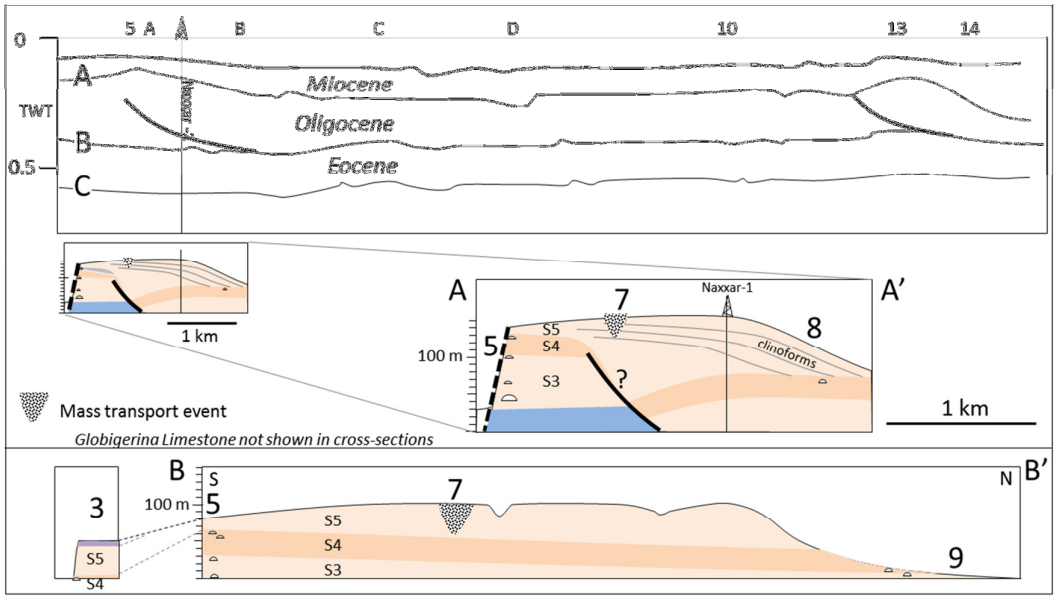

Figure 6.20. Interpreted section based on Figure 6.11 (map of cross sections in Figure 6.21). Cross-section A-A' of the area around the Naxxar-2 well compared to the inclined Oligo-Miocene boundary seen in seismic. Clinoforms observed in outcrop. The Naxxar-2 well is located onshore about 6 km perpendicular to the seismic line; B-B' cross-section runs NE-SW through localities 9, 7 and 5. Locality 3 situated about 10 km SW of locality 5 is included to show the post-depositional anticline around localities 5 and 7 and the syntectonic thinning of sequences towards the west (locality 3) along the margin of the WMP.

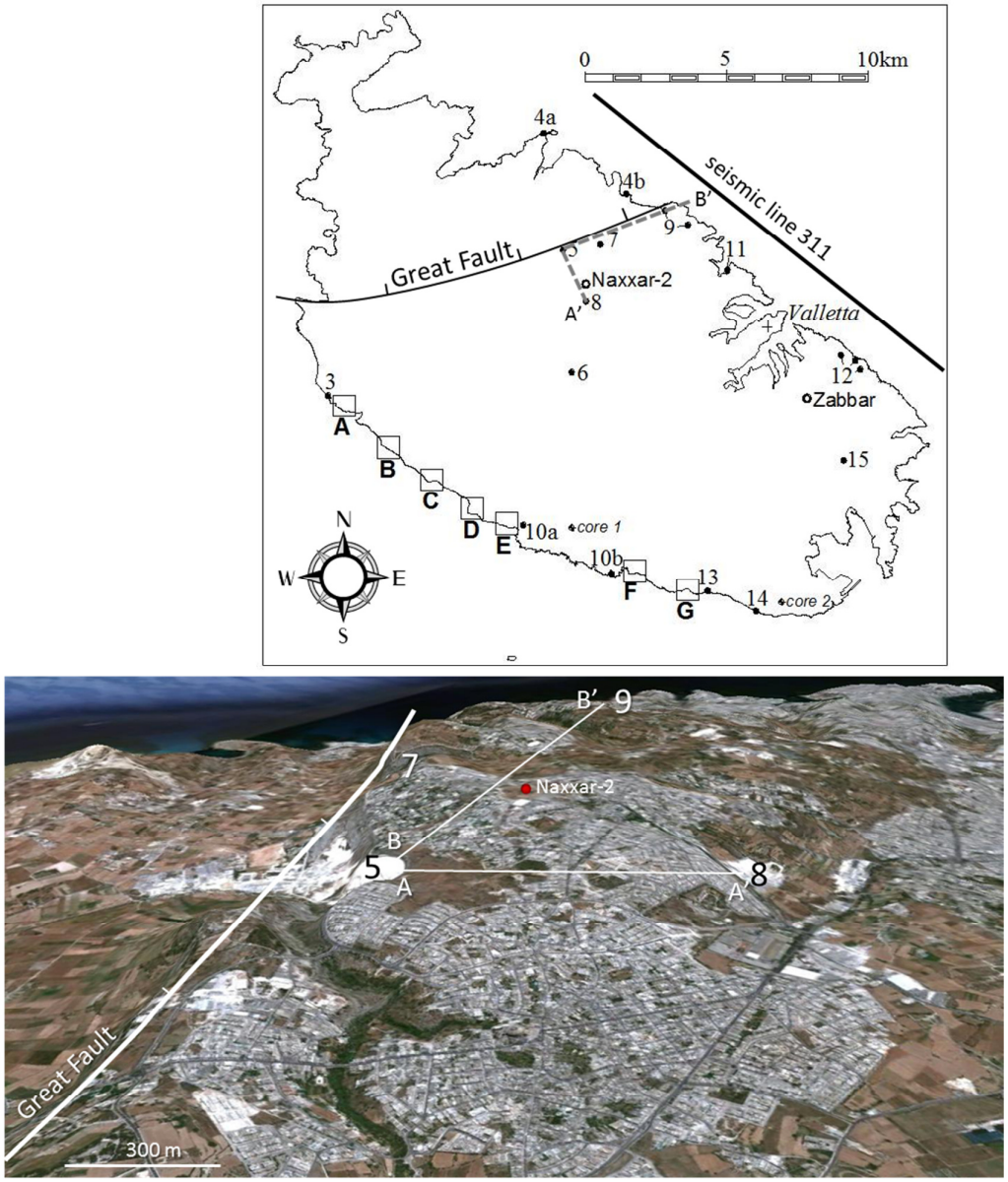

Figure 6.21. Location map of cross-sections and seismic line in Figure 6.20 and aerial photograph of north central Malta with vertical exaggeration. The topography is dome-shaped between localities 5 and 8. The dome is truncated to the west by the Plio-Quaternary Great Fault.

B. Miocene structures

Several authors (e.g., Pedley *et al.*, 1978; Rose *et al.*, 1992) have recognised the increase in thickness of the Lower Member of the Globigerina Limestone Formation over central Malta, named the Valletta Basin. The geometry and lateral thickness variations of this hemipelagic unit is defined more accurately in this study on the basis of outcrop data and cores (Wardell Armstrong, 1996) (Figure 6.22). The Lower Globigerina Limestone is >100 m thick over Valletta but thins to <5 m over the Western Malta Palaeohigh.

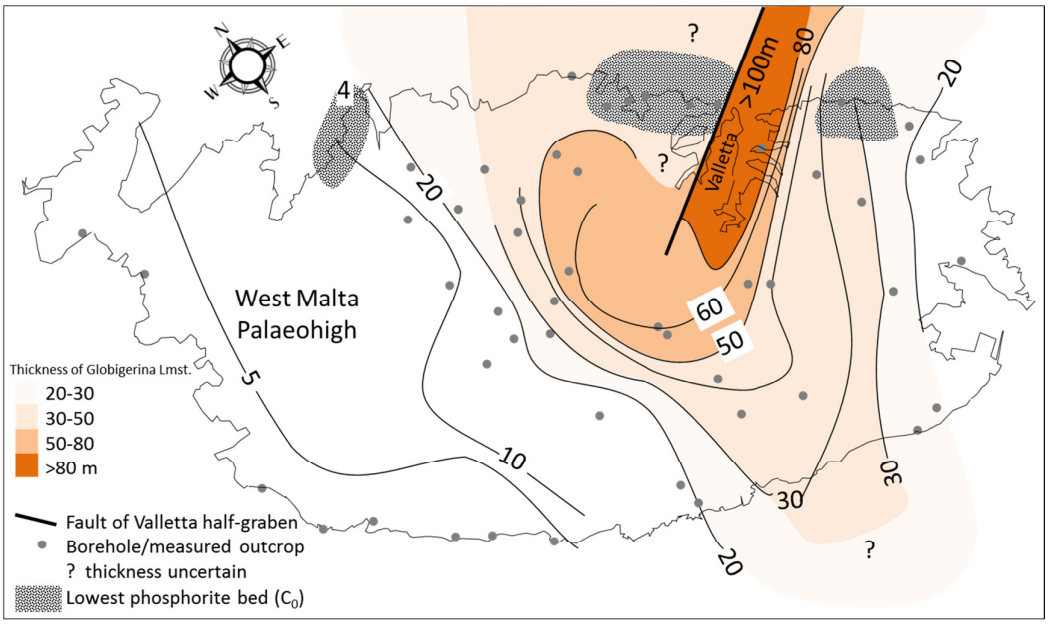

Figure 6.22. Isopach map (isopachs in metres) of the Lower Member of the Globigerina Limestone Formation based on borehole data and outcrops. The depocentre of the Valletta half-graben is shaded grey. Three localities (4, 11 and 12) are capped with phosphorite of the C_0 bed.

The intervening palaeohighs along SbCH5 were affected by phosphogenesis (C_0 phosphorite bed), followed by platform drowning. Three palaeohighs over which Early Miocene hemipelagic sedimentation is thinner are recognised;

i. Western Malta Palaeohigh (WMP) where the Lower Member of the Globigerina Limestone thins to <5 m west of locality 3. The WMP extends over the previously described palaeohighs of the 'Rabat Axis' (Pedley, 1987) and the Comino Straits High (Pedley, 1978). The Lower Coralline Limestone Formation along this area is sporadically capped by the C_0 phosphorite bed, e.g., locality 4a.

ii. At locality 11 and farther east along the coast, the cross-bedded large benthic foraminiferal grainstone to packstone beds of depositional sequence 6 are dissected by <2 m-deep neptunian dykes (Gatt, 2005). The neptunian dykes formed after early cementation along SbCH5 followed by NW-SE extension that produced the presently submerged fault off the northern coast of Valletta. The vertical dykes along the footwall crest of the Valletta half-graben were later filled with <30 cm thick floatstone to rudstone bed of *Pecten* and phosphatised solitary coral (C_0 phosphorite bed). The hardground along SbCH5 is interpreted to have formed by exposure to strong currents along the tectonically uplifted footwall crest of the Valletta Graben. The fault-controlled NE trending Valletta half-graben shows bedding along its eastern margin dipping NW towards the depocentre found along the present-day Valletta peninsula (Figure 6.23).

iii. The Eastern Palaeohigh (EMP) along the area between the Valletta Basin and the Marsaxlokk Basin exposed along locality 12. The EMP is an anticline draped with hemipelagic beds dipping in opposite directions towards the two half-graben. The palaeohigh includes some phosphorite capping the Lower Coralline Limestone whereas the overlying Globigerina Limestone Formation described by Pedley (1990) shows thinning and non-deposition during the Late Miocene.

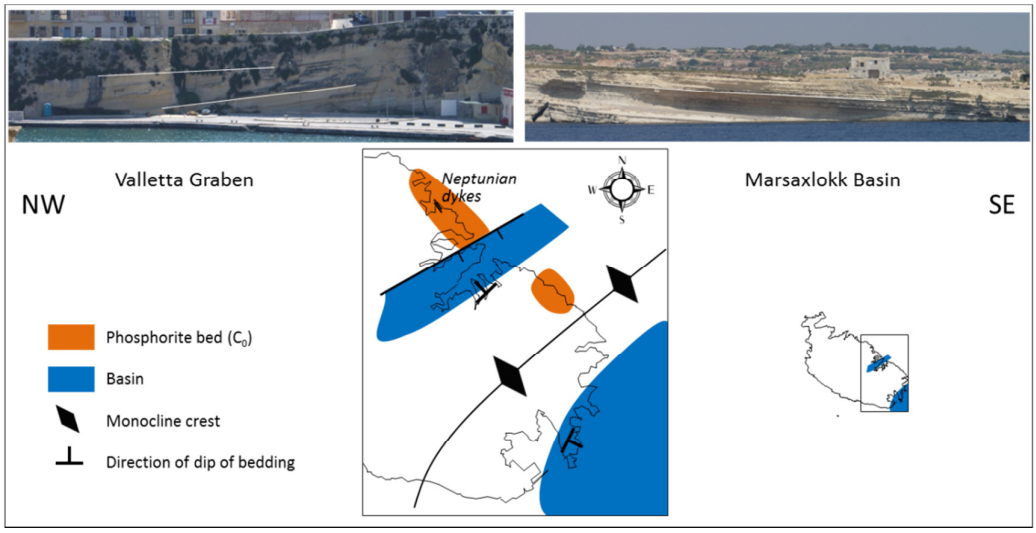

Figure 6.23. The map of southern Malta shows the location of dipping beds shown in the photographs above. The beds dip towards the Valletta half-graben and Marsaxlokk basin. The intervening areas are affected by a fault with neptunian dykes and an anticline. Both areas accumulated phosphorites.

C. Plio-Quaternary and neotectonic structures

Extensional strain active from the Oligocene reached its peak activity during the Plio-Quaternary when foreland extension produced the >300 km long NW-SE trending graben of the Pantelleria Rift south of Malta (Jongsma *et al.*, 1985) discussed in chapter 2. Another set of Plio-Quaternary normal faults exposed in Malta are NE trending and include the Great Fault (Illies, 1981). The NE-SW trending faults with displacements of >10 m reflect NW-SE extension of approximately 3.3% in graben (Putz-Perrier & Sanderson, 2010).

6.5.2.2 Interpretation of Cenozoic structures

Palaeogene to Neogene bathymetric highs (e.g., the WMP and EMP) alternating with bathymetric lows (e.g., Naxxar and Marsaxlokk basins) may reflect structures developed within faulted extensional regimes. Moreover, the increase in accommodation space that produced the doubling in thickness of Oligocene sediments over central Malta (Naxxar-2 well) relative to western and eastern Malta (Zabbar-1 well) suggests fault-controlled syntectonic sedimentation during graben

development. However, Oligocene faults are not seen in outcrop which suggests that faulting preceded the deposition of the Chattian lithology exposed in Malta.

Various models can be invoked to explain the formation of graben by faulted margins in extensional basins with associated syntectonic sedimentation (Schlische, 1991; Gibbs, 1984; Burchette, 1988). In some of these models the faulted margins are characterised by uplift along the footwall, which may be uplifted above sea-level and then subsides below sea-level (Barr, 1987). However, few of the published models consider a fault trace that propagated upward from depth without forming a surface break (i.e., blind, planar normal faults). Blind faults have an approximately elliptical tip line with systematically decreasing throw from a maximum near the centre to zero at the tip (Nicol *et al.*, 1996).

It is suggested that Oligocene blind faults controlled the prograding clinoform bedding and dip of bedding in the Naxxar Basin that produced the following features:

1. Monoclinal warps: monoclines may develop above the footwall block produced by the blind fault as a result of fold propagation folding and differential compaction. The deposition of sequences 4 and 5 was along a monocline that resulted in aggradational footwall-derived fans along the NW-SE monocline strike which produced clinoform bedding in locality 8 (Figure 5.25). The fault tip is close to locality A where estimated break in slope along the monocline is <20 m but increased towards the central part of the fault in the direction of localities 7 and 8 where the height difference between the topsets and foresets of the large clinoforms is >40 m. The outcrops can be related to seismic images of line 311 (Figure 6.11) which show reflectors inclined in the same direction as the exposed clinoforms.

2. The palaeobathymetric differential caused by differentiated hanging-wall subsidence produced the westward dip of bedding in the Naxxar Basin and resulted in the early drowning of small coral patch reefs along the base of sequence 4 at locality B (close to the faulted margin) whereas larger patch reefs found at higher levels farther east at locality D had drowned later. This

suggests that coral patch reefs in the Naxxar Graben could not keep up with sea-level rise combined with subsidence of the downthrown block and consequently drowned. Syntectonic deepening would have reduced carbonate production as the depth of seabed exceeded the euphotic zone characterised by maximum carbonate sedimentation.

6.5.2.3 Syntectonic depositional model for Cenozoic sediments

A tentative geotectonic model for the Naxxar and Marsaxlokk basins is proposed partly based on the domino fault block model of Schlische (1991) that consists of slightly rotated fault blocks that form half graben within an extensional regime (Figure 6.24). In such models, footwall uplift would result in greater erosion and thinning of sediments (Barr, 1987). This is consistent with the subaerial unconformity produced by the merging of SbCH2 and SBCH3 at locality A along the monocline above the footwall crest. The faults do not propagate to the surface and only involved the Rupelian depositional sequences 1 to 3, although the duration of activation of the western and eastern fault was not the same.

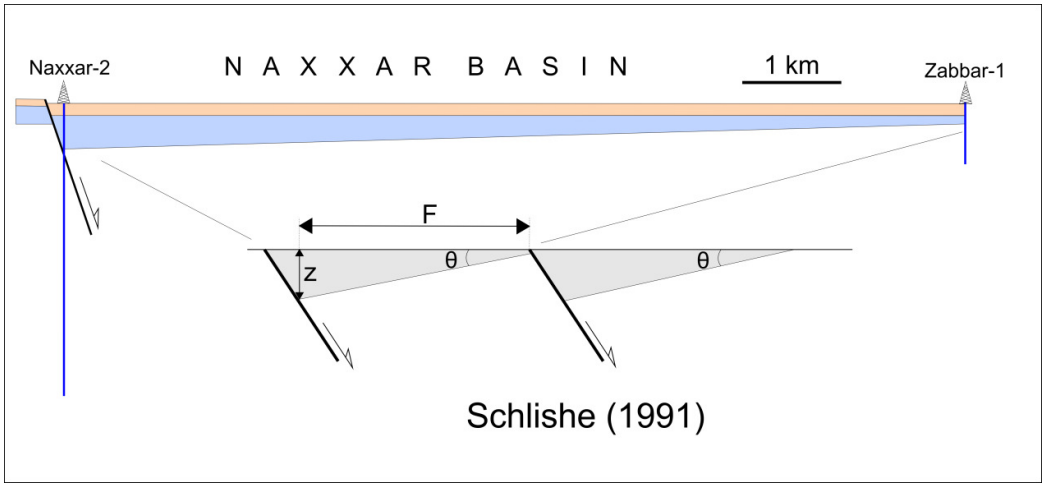

Figure 6.24. The Naxxar half-graben described in Figure 6.17 related to the model by Schlische (1991) for domino fault blocks with half-graben creation.

The angle of dip of bedding ($\theta = 2°$ in Figure 6.18) along the length (F) of the Naxxar half-graben from Naxxar-2 well to Zabbar-1 well (F = *circa* 9 km) can be used to estimate the depth of accommodation space (z) created by the rotation along the domino fault block during extension (Figure 6.24) using trigonometry:

$$z = \tan \theta \times F$$

This gives a thickness of 314 m which is nearly equivalent to the actual thickness of Rupelian sediments in the Naxxar-2 well (320 m). The significant thickness variations of the Rupelian relative to the Chattian sediments seen in Figure 6.17 reflect NW-SE trending extension during the Rupelian followed by relative tectonic quiescence during the Chattian when sediment thickness almost equalised between Naxxar-2 and Zabbar-1 wells.

The controls on carbonate sedimentation in an extensional regime characterised by half-graben topography have been described by Burchette & Wright (1992) in two models of carbonate sedimentation based on active and quiescent tectonic phases whereas Gerdes *et al.* (2010) propose structured and unstructured antecedent topography formed during synrift and post-rift settings, respectively (Figure 6.25).

During active faulting the hangingwall is inclined towards the fault along with the divergent syn-rift fill. A monocline with clinoforms develops along the footwall crest of the faulted margin. During the quiescent phase, the under-filled half-graben is draped by a wedge from the footwall crest that thins towards the depocentre of the half-graben. The geometry of Oligocene outcrops of Malta may consist of a combination of both tectonic phases along domino-style fault blocks that step downwards along older faults towards the east.

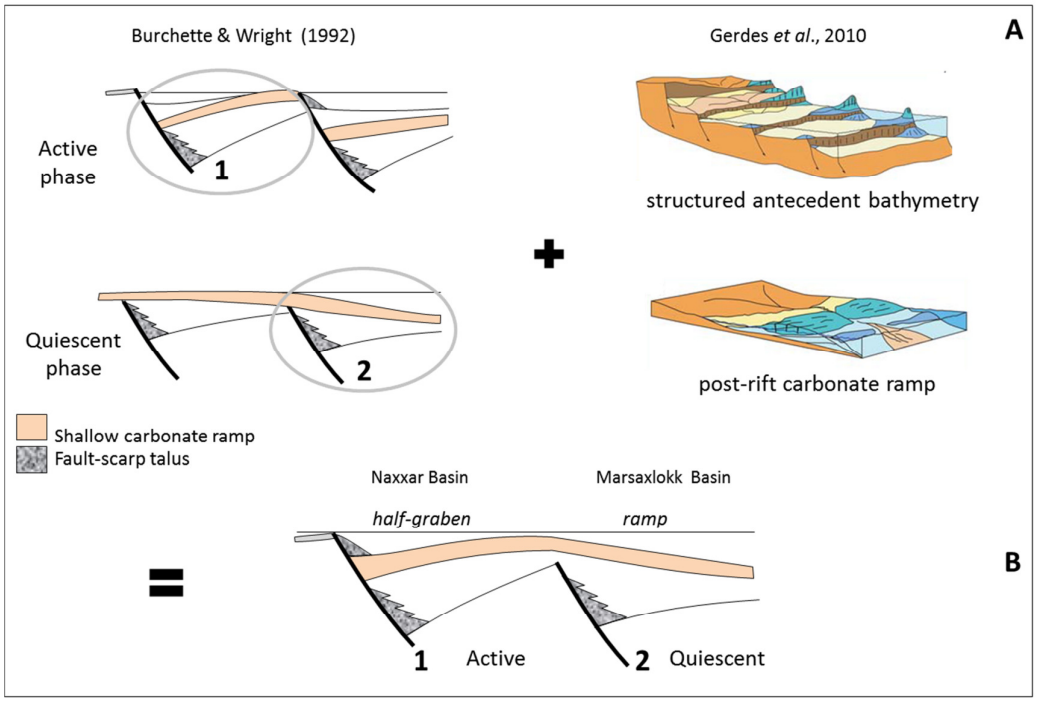

Figure 6.25. A. Models of development of carbonate sequences along antecedent topography; B. combination of the two models proposed in this study to explain Oligocene syntectonic sedimentation.

It is suggested that the Naxxar and Marsaxlokk basins developed differently under the same extensional regime (Figure 6.25):

Naxxar Basin: Sequence 3 that outcrops just above sea-level has a near horizontal dip between localities 3 and A along the WMP but shows a 2˚ dip towards the fault along central Malta (Figure 6. 19). The thickness of Rupelian sediments in the Naxxar-2 is triple that of Zabbar-1 well which suggests that the fault controlling the half-graben remained active till the deposition of sequence 3 (Rupelian). The end of fault movement during the Chattian is supported by the lack of field evidence of fault propagation into Early Chattian sediments (sequences 4 to 6) and the nearly homogeneous thickness of Chattian sediments in both the Zabbar-1 well rimming the eastern margin of the Naxxar Basin and the Naxxar-2 well in the deeper part of the basin. This suggests <40 m differential accommodation space in the Naxxar Basin relative to the WMP during the Chattian which was partly filled by prograding large clinoforms seen in localities A and 8.

Marsaxlokk Basin: The eastward dip of sequences 3 to 6 in the direction of the Marsaxlokk half-graben depocentre suggests that the blind fault controlling the half-graben had switched-off before the deposition of sequence 3 and consequently its upper end was positioned at a lower level relative to the Naxxar fault. Early tectonic quiescence in the Marsaxlokk Basin resulted in slow subsidence which permitted the early filling of the hanging-wall accommodation space. The structured bathymetry was draped by the sequences seen in outcrop (Figure 6.18B). However, the area above the buried footwall crest along the western rim of the Marsaxlokk Basin remained relatively shallow and hosted the high-energy shoal (sequence 6), albeit at greater depth relative to the condensed shoal at locality 3 over the WMP.

Valletta Basin: The NW-SE extension that created the domino-style fault blocks persisted into the end Oligocene and Miocene and produced subsidence over central Malta associated with the development of the Valletta half-graben (Figure 6.22). A Miocene normal fault, <1 km east of locality 11 produced thickening of the lower member of the Globigerina Limestone over Valletta in the hanging-wall block whereas neptunian dykes developed along the crest of the footwall in locality 11.

Figure 6.26 (next page). A. Composite model from Burchette & Wright (1992) showing active (1) and quiescent (2) half-graben faults. Labelled features are observed in the field and are consistent with the model; B. Oligocene depositional sequences 1 to 6. Above sequence 3 exposed along southern cliff coast of Malta whereas subsurface penetrated by wells. The Naxxar half-graben thickens to 450 m next to the West Malta Palaeohigh, double the thickness penetrated by the Zabbar-1 well. The half-graben geometry of the Naxxar Basin favoured mass transport events along palaeohighs; C. Cross-section along northern Malta from Mosta High to Valletta and Marsaxlokk Basin including the Miocene Valletta half-graben.

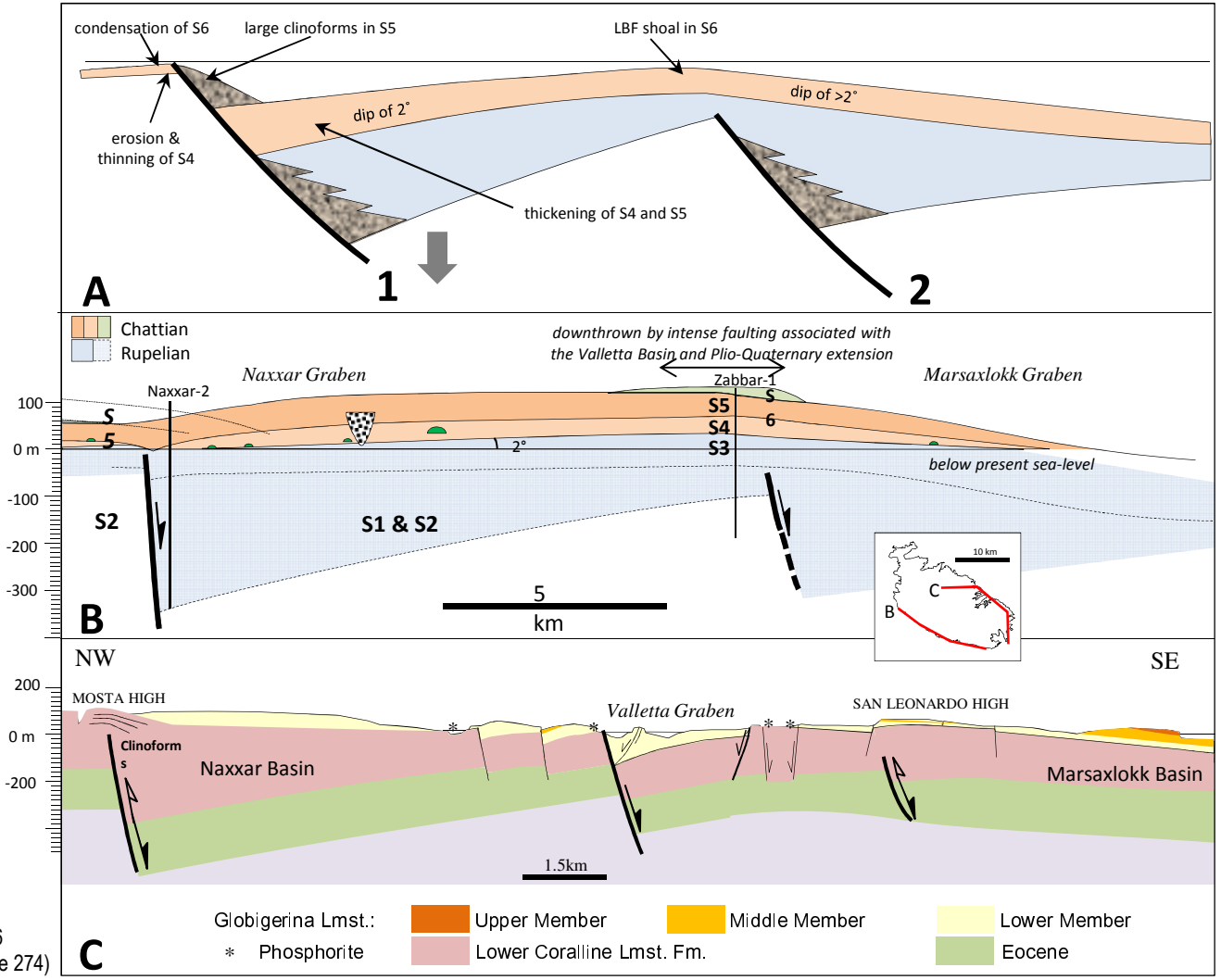

Figure 6.26
(Caption on page 274)

6.5.2.4 Evolution of Oligocene to Miocene and neotectonic structures

Oligocene: Extensional stress in the Rupelian sediments was resolved by brittle failure and normal faulting that produced the Naxxar and Marsaxlokk basins. However, the overlying Chattian sequences 4 to 6 are characterised by monoclines over blind faults that reflects differential compaction or possibly ductile behaviour under stress caused by blind fault reactivation during the Chattian (Figure 6.27). The absence of faults propagating to the surface reflects the different rheological behaviour of Rupelian and Chattian sediments. The depositional environment of the Chattian sequences is characterised by unstable substrates that consisted of mobile algal debris and rhodoliths that hindered early cementation. This is reflected in the low level of cementation (1-2%) (Knoerich & Mutti, 2003) in facies association II that makes up much of much of the Chattian sediments (depositional sequences 4 and 5). However, when FA III sediments were subjected to extension along the footwall crest of the Valletta Graben at locality 11, shallow neptunian dykes that reflect brittle behaviour were produced (Figure 6.23). In contrast to FA II, the muddy substrates of the Rupelian facies association V (sequences 1 to 3) were stabilised by seagrass and irrigated by burrowing animals that may have induced extensive and early cementation in this fine-grained facies which resulted in the brittle nature of the rock.

Miocene to Plio-Quaternary: The high strain zones recognised by Putz-Perrier & Sanderson (2010) as associated with Plio-Quaternary faulting (Figure 6.27A) remarkably coincide with the location of Oligocene blind faults (Figure 6.18C) that controlled the Naxxar and Marsaxlokk half-graben as well as Miocene fault that produced the Valletta half-graben (Figure 6.27). It is suggested that the Late Miocene to Plio-Quaternary faults could have preferentially developed above these pre-existing Oligocene to mid-Miocene faulted zones of weakness.

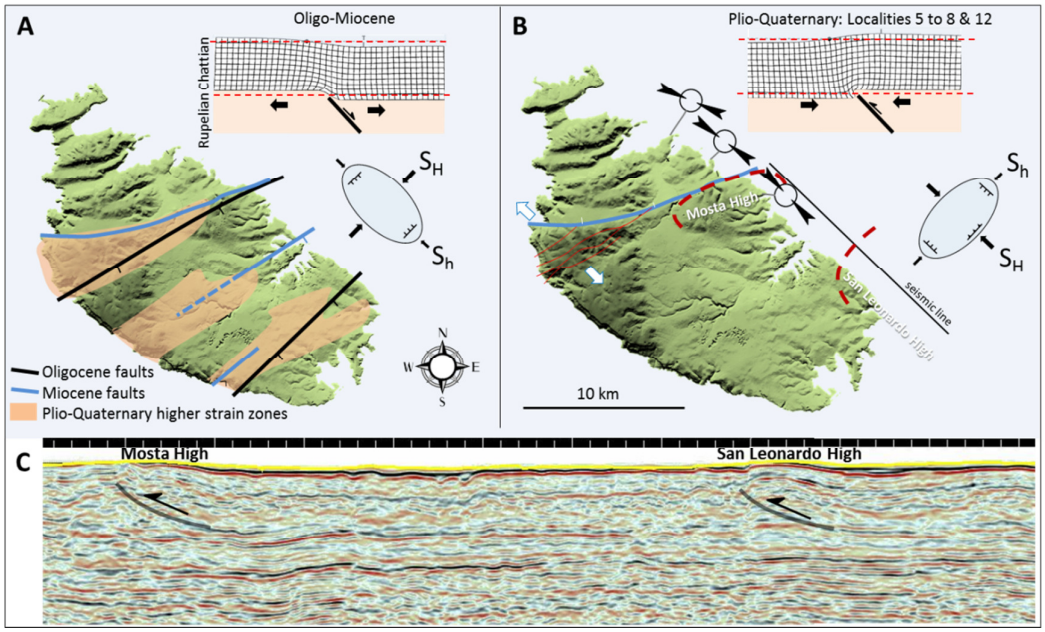

Figure 6.27. Deformation of sediments and formation of monoclines above reverse and normal faults based on experimental and mathematical models where the rigid base (Rupelian) is either converging or diverging (Patton, 1995) represened by the compressional stress ellipse: A. Higher extensional strain zones in Miocene rocks characterised by intense faulting (based on Putz-Perrier & Sanderson, 2010). The strain zones coincide with the Oligocene and Miocene break in slope and blind faults (thick black and blue lines) related to the formation of the Naxxar, Marsaxlokk and Valletta basins; B. Topographic map showing two domes along the northern coast of Malta (Mosta High and San Leonardo High). Present stress field in northern Malta based on overcoring confirms NW compression whereas Plio-Quaternary faulting in western Malta confirms extension (direction shown by white arrows); C. The two domes extend offshore and are imaged in seismic as compressional deformations along reverse faults.

Recent: The present stress field shows NW compression, determined by *in situ* tests along the northern coast of Malta (Grasso *et al.*, 1986). Along the same coast, hitherto two unexplained <7 km-wide dome-shaped topographic highs occur in the region of localities 5 to 8 and close to locality 12 (Mosta and San Leonardo highs, respectively). The San Leonardo High is reported to be an area of erosion by Pedley (1990). The dome-shaped structures are >30 m above present sea-level (cross-section B-B' in Figure 6.20) and are also recognised as bathymetric highs in the offshore seismic section (Figure 6.27).

The dome-shaped structures coincide with the location of monoclines that drape over the Rupelian faults in western and eastern Malta, which suggests that these topographical features were produced by the uplift of part of the monoclines. This is supported by the exposure of the thickest section (>30 m) of sequence 3 at locality 5 whereas the same depositional sequence in other areas of the Maltese Islands is <10 m above present sea-level.

Three hypotheses are considered to explain the dome-shaped structures:

i. The switch from Oligo-Miocene to Plio-Quaternary extensional regime to Recent compression has reactivated the Rupelian NE-SW trending blind faults and produced fault-propagation folds. Patton (1995) uses numerical modelling to describe two types of fault-propagation folds caused by blind faults showing either reverse thrusting or hanging-wall subsidence as shown in Figure 6.27. The morphology of the two folds closely corresponds to those observed in outcrop and seismic line shown in Figure 6.27C for northern Malta where reactivation by reverse faulting created the dome-shaped structures. In southern Malta along the cliffed coast, fault reactivation was either less intense or marked by the continuation of extension.
ii. Strike-slip movement along the Oligocene faults generated transtension and transpression which created areas of extension and subsidence, e.g., localities A to 3 along the southern cliffed coast of Malta (Figure 6.27), and areas of compression, e.g., Mosta High. The strike-slip movement is consistent with the regional movements affected by foreland tectonics (Reuther *et al.*, 1993; Argnani, 1990) described in chapter 2.
iii. Compression over the Mosta High coupled with extension along western Malta may reflect the anti-clockwise rotation of the island of Malta. This is consistent with the hypothesis of Gardiner *et al.* (1995) that considers that Malta Plateau as segmented into micro blocks moving in different directions.

These tentative hypotheses both suggest Recent tectonic reactivation by inversion of earlier structures. The overall result was the erosion of megasequence IV along and around the Maltese Islands.

6.5.3 Central Malta Platform Basin (CMPB)

The thickening of megasequence III immediately east of Aqualta well is the result of the here named quasi asymmetrical Central Malta Platform Basin (CMPB). The CMPB is a *circa* 70 km-wide, NNE-trending zone of basin subsidence (Figure 6.28) that affected the Mesozoic T- and K-reflectors, as well as the Cenozoic B- and C-reflectors (megasequences I to III). Basin development initiated during the Mesozoic and continued into the Cenozoic. The closest well to the CMBP basin rim is Aqualta well and there are no wells penetrating the deeper part of the basin except for the Medina Bank well located along the eastern basin margin. The basin is here sub-divided into the basin margin and depocentre setting with reflectors shown in Table 6-5.

Reflector	*Age*	*Stratigraphic unit*	*Basin rim*	*depocentre*
A	Base Miocene	Globigerina Lmst. Fm.	<150 ms	
B	Base Oligocene	Lower Coralline Lmst. Fm.	150-200	400
C	Mid-Eocene	Metlaoui Group	merged reflectors	800
P	Top Palaeocene	El Haria Fm.		200
K	Top Cretaceous	Naxxar & Hurd Bank Groups	~1500	>1500 ms TWT
T	Top Triassic	Dolomia Principale		

Table 6-5. Reflectors along the CMPB. The thickness of formations is in milliseconds TWT.

The lack of available seismic data to the west and south makes it difficult to accurately define the entire extent of the basin. Nevertheless, the available seismic data shows that the basin depocentre in this V-shaped basin trends NE to NNE where about <5 km of Late Cretaceous to Miocene (megasequence III) sediments accumulated. High-amplitude continuous reflectors expand towards the basin depocentre and pinch out towards the east and west (Figure 6.29). Reflectors below the K-reflector are not well-defined and mostly discontinuous.

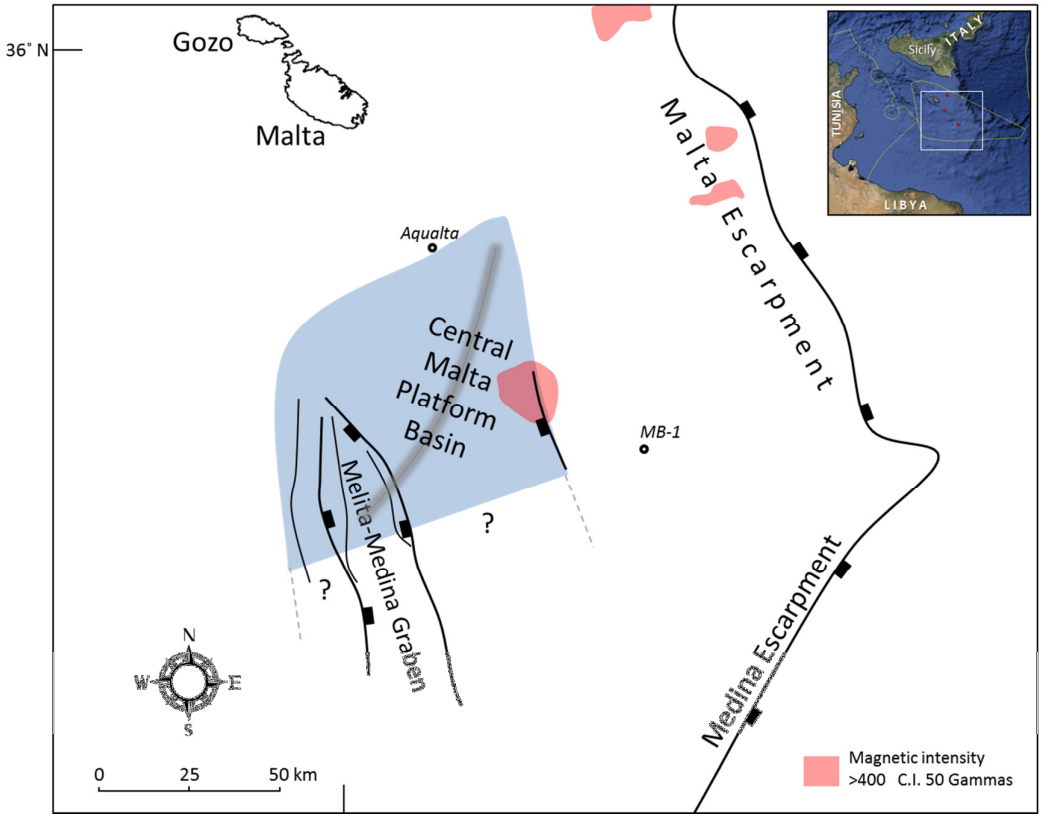

Figure 6.28. The grey area marks the basin margin and the thick dark line shows the trend of the basin depocentre. The extent and position of the Melita-Medina Graben is from Lipparini *et al.* (2009). The dark grey shows areas of high magnetic intensity (from Pedley *et al*., 1993).

Figure 6.29 (*next page*). Location of seismic sections shown in Figure 6.13. The Central Malta Platform Basin (CMPB) adjacent to the escarpment zone on the right: (a) NW-SE seismic line 303. Inset of basin western margin is shown in Figure 6.30; (b) Uninterpreted and interpreted west-east seismic line 106. Inset of basin depocentre is shown in Figure 6.31. Inset on right shows area of fluid escape.

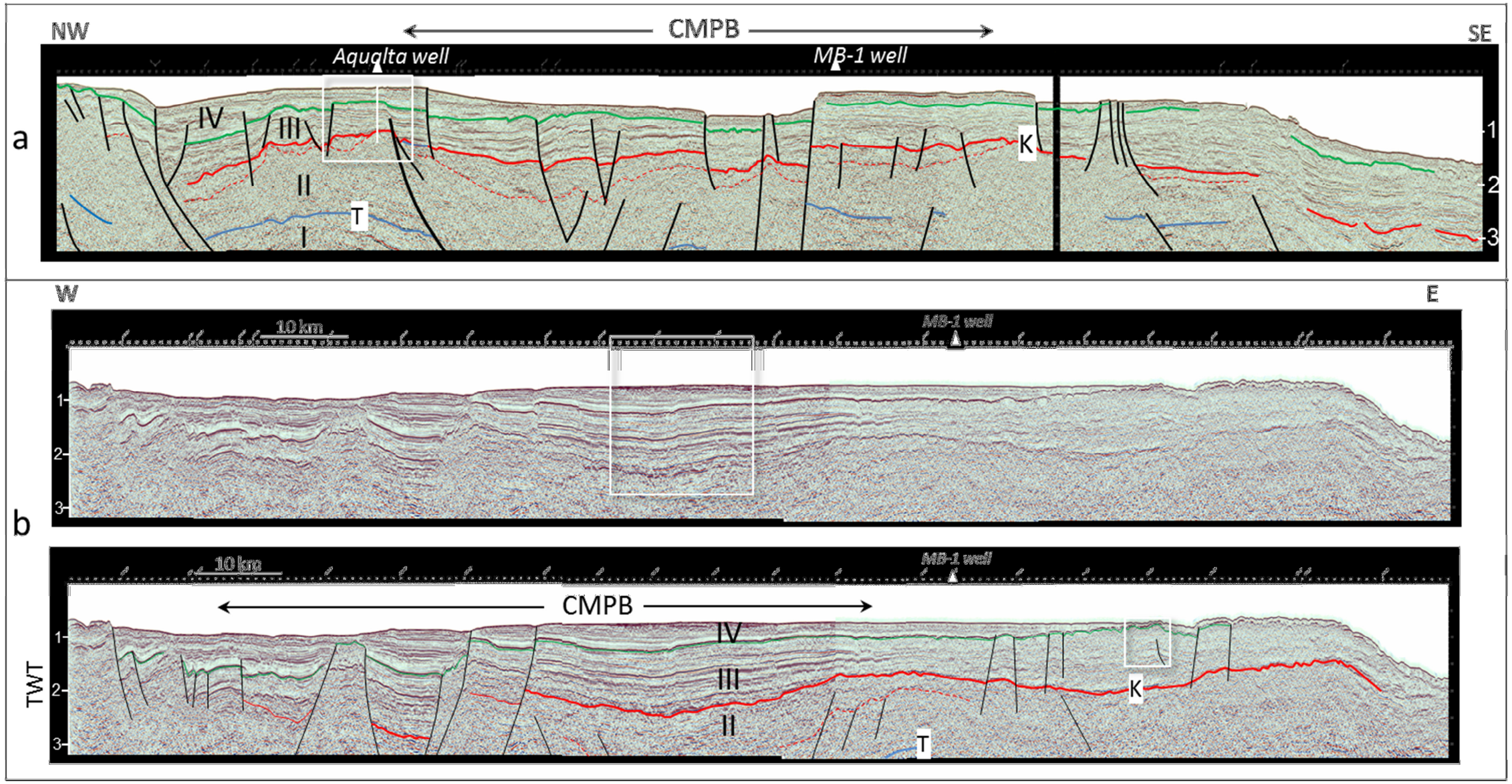

Figure 6.29
(*caption on previous page*)

6.5.3.1 Basin margin

The western margin of the CMBP is penetrated by the Aqualta well (Figure 6.29). Seismic sections along the margin of the CMPB and through the Aqualta well show high amplitude continuous Palaeogene reflectors (C-reflector) vertically offset by a fault that bounds the CMPB. Overlying reflectors are inclined because they drape over the faulted margin (Figure 6.30). Magnetic intensity data shows magnetic highs along parts of the Malta Escarpment that are interpreted by Pedley *et al.* (1993) as the result of Cretaceous volcanic sediments associated with rifting (Figure 6.28). Significantly, a magnetic high also occurs along the eastern margin of the CMPB which is here interpreted as being of magmatic origin. This is consistent with the Cretaceous basaltic sill penetrated by the Aqualta well.

Data on sediments of the CMPB is limited to the Aqualta well located on the here named Aqualta Palaeohigh along the rim of the basin. This palaeohigh forms part of the platform interior zone. The top Cretaceous (K-reflector) is found at 975 ms according to well reports and forms a stratigraphic closure penetrated by the Aqualta well. Eocene sediments thin over the Aqualta Palaeohigh and expand farther west over the dissected Malta Plateau and over the CMPB in the east. The C-reflector onlaps the palaeohigh flanks and merges with the K-reflector over the palaeohigh where a mound-shaped structures (Figure 6.30). Two sets of mounds are recognised:

i. Small mounds 1 and 2 on the faulted western margin of the Aqualta Palaeohigh that backstep to higher levels until terminated by the C-reflector. The backstepping suggests a marine transgressive episode culminating in the Ypresian C-reflector equivalent to clays and shales in onshore Maltese wells.
ii. A large mound (3) with semi-transparent reflectors on the eastern faulted margin where the C-reflector is merged with the K-reflector along the highest point of the structural high. The mound developed above the C-reflector which is the maximum flooding surface and aggraded during the ensuing highstand of sea-level until carbonate sedimentation was terminated by exposure and the deposition of evaporites along the B-reflector (basal Oligocene SbRU1 evaporite bed).

Reflectors on the palaeohigh are horizontal and onlap the more elevated mound from where basin-directed reflectors offlap towards the east. The Aqualta well is located leeward of mound 3 and penetrates Eocene fine-grained dolomite with shallow marine biota (miliolids) typical of backshoal or backreef environment (platform interior). The lithology and the seismic profile suggests an 'empty bucket' geometry (Figure 6.1) where growth potential of the platform rim exceeds that of the platform interior (Schlager, 1993). The older mounds 1 and 2 found between reflectors K and C are located farther west. Miocene sediments (above reflector A) drape over the faulted margin and over a mound-shaped structure between the B-reflector (base Oligocene) and C-reflector (Early Eocene).

6.5.3.2 Basin depocentre

The continuous B, C and K reflectors recognised along the basin margin (Aqualta well) extend to the central part of the CMPB with few disruptions of reflectors (Figure 6.31). An additional strong reflector, the P-reflector, occurs between reflectors C and K within the basin and marks the top of a sediment package that thickens towards the depocentre of the basin over the Cretaceous. This is interpreted to be of Palaeocene age and correlates with the Palaeocene sediment package recognised by Lipparini *et al.* (2009) along the base of the NNW-trending Melita-Medina Graben located in the southern part of the CMPB (Figure 6.28).

Figure 6.30 (*next page*) The western margin of the CMPB penetrated by the Aqualta well along seismic line 303 (see Fig. 6.2 for location). Areas shaded red are interpreted as Eocene carbonate reefs that may extend to the Oligocene. The log to the right shows Eocene and Oligocene sediments that form reflectors A, B and K and depositional sequences S1 to S6.

Figure 6.31. Inset from Figure 6.29b of seismic line 106. Reflectors B, C, P and K are labelled along the Central Malta Platform Basin depocentre showing sediment packages that pinchout and reflectors that onlap along the margin of palaeohighs adjacent to the basin (black arrows). White rectangles show columnar disturbances related to vertical fluid migration.

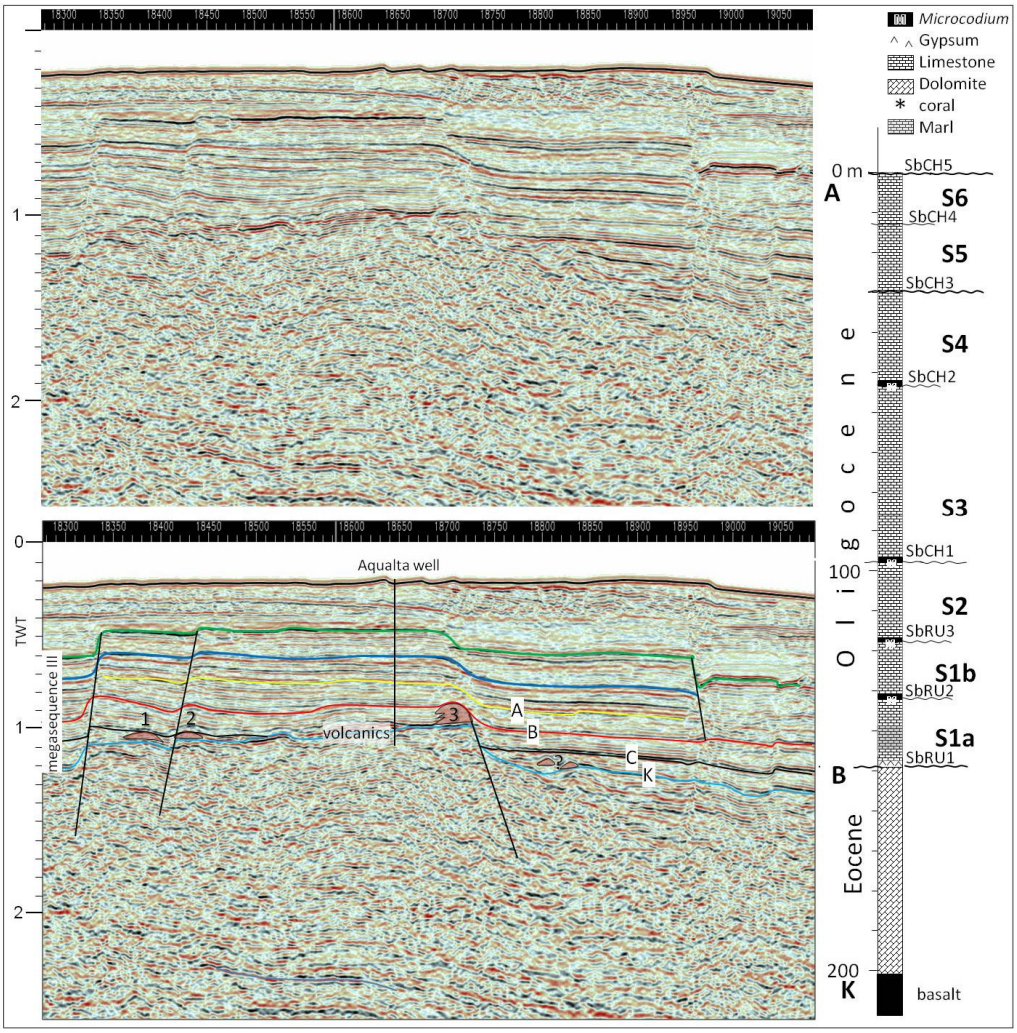

Figure 6.30 (caption on previous page)

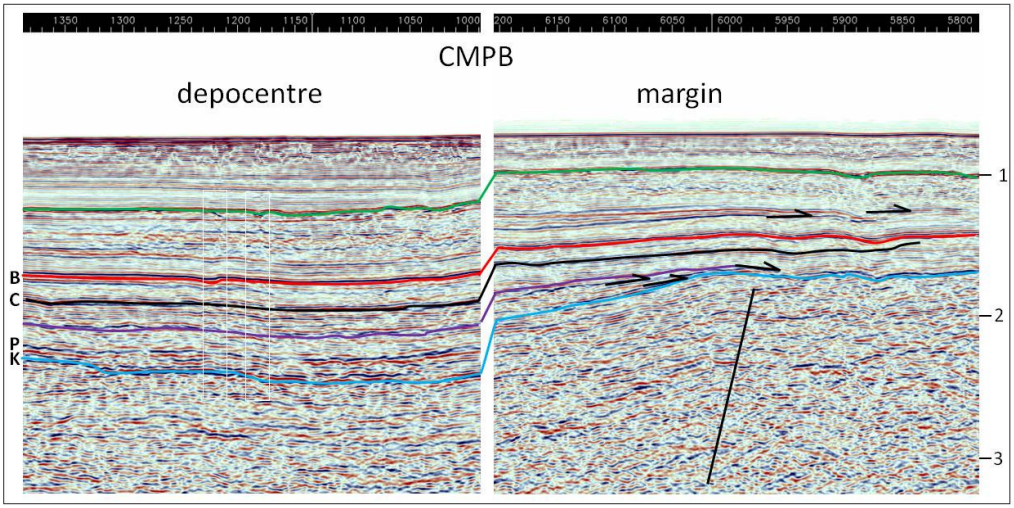

Figure 6.31 (caption on previous page)

6.5.3.3 Interpretation

The architecture of the CMPB represents a polyphase evolution of an intracratonic rift basin *sensu* Kingston *et al.* (1983). The initial graben formation (Stage 1) involved faulting of the E- and T-reflectors which are steeply inclined at towards the basin centre (Figure 6.29 and Figure 6.32). Top Triassic sediments are penetrated by the MTZ well in Gozo Island and include continental red beds and shallow marine carbonates (Debono *et al.*, 2000) that formed part of an extensive shallow marine Tethyan carbonate platform. The same kind of sediments recorded in Gozo may have extended to the Mesozoic graben in CMPB area. Although the Late Triassic/Early Jurassic age of the T-reflector is uncertain, it is consistent with the geodynamics of the Tethyan area at that time, characterised by Early Jurassic block faulting and rifting that destroyed many of the shallow-water sites (Bernoulli & Jenkyns, 1974). The extension resulted in a basin-swell morphology produced by irregular subsidence of the different blocks which are seismically imaged along the T-reflector (Figure 6.32).

Brittle extension of the lithosphere was especially controlled by master faults that remained active throughout the Cretaceous. The development of these fracture zones is associated with basaltic intrusions penetrated by the Aqualta well along the Upper Cretaceous. This was followed by deposition of predominantly marine sediments of megasequences III and II that invaded the partly filled graben. Sediments above the K-reflector do not show progradation along steep fault-controlled margins but passively fill the accommodation space that increases towards the basin centre (Figure 6.31). This suggests that the basin began to sag by thermal relaxation following ductile extension whereas the movement of basement block had ended (Stage 2). However, unlike many present-day divergent continental margins, the CMPB does not show oceanward tilting. This is consistent with the intra-platform setting of the basin.

During the basin sag phase the rate of subsidence diminishes and sedimentation is controlled by glacio-eustatic cycles producing depositional sequences similar to those found in the Maltese Islands. Cenozoic depositional sequences pinchout

towards the eastern margin located above the master faults (Figure 6.31). This suggests truncation during sea-level fall that exposed the basin margin to erosion and peneplanation of the margin. The columnar disturbances imaged in seismic close to the basin depocentre suggest vertical fluid escape features where sediment accumulation is thickest.

Basin margin: The master fault along the western basin margin extends to the base Palaeogene. The basin margin penetrated by the Aqualta well area formed the Aqualta Palaeohigh where palaeosols horizons along sequence boundaries are frequent and the accumulated Palaeogene sediments are thinnest relative to other offshore and onshore wells (Table 6-3). The evidence suggests that the Aqualta Palaeohigh formed the uplifted footwall crest and regional bathymetric high of the platform interior zone.

Three mound-like structures developed along this regional high (Figure 6.30). The shape of the carbonate mounds suggests the development of a reef on the basin rim along the faulted shelf break. Ancient reefs developed along a spectrum ranging from trapping and binding of sediments (mud mounds) to the production of rigid, massive cemented skeletal framework (Longman, 1981). Tethyan coral reef framework structures were on the decline during the Early Eocene (Kiessling *et al.*, 1999) and were replaced by non-framework *Nummulites* that built banks. Loucks *et al.* (1998) have argued that nummulitic accumulations have negligible relief. However, the aggradational morphology of mound 3 suggests an element of rigid framework which may preclude a nummulitic bank. The 'reef' protected the fine-grained carbonates encountered in the backreef area penetrated by the Aqualta well.

The eastern faulted margin of the Aqualta Palaeohigh was distinct from other structural highs because footwall crest uplift was greater relative to other faulted margins of the Malta Plateau, e.g., West Malta Palaeohigh. A number of factors support this interpretation:

- Unequivocal evidence of subaerial exposure along the Aqualta Palaeohigh that produced palaeosol horizons along sequence boundaries (SbRU2, SbRU3, SbCH1, SbCH2) recognised by the occurrence of *Microcodium* in well cuttings (Figure 6.30).
- In contrast, sediments produced by these subaerial episodes were mostly eroded by the ensuing transgression over the Maltese Islands. Nevertheless, the meteoric and pedogenic diagenetic zone is preserved within subtidal limestones of Malta (see Chapters 4 and 5).
- The occurrence of *Miogypsina* (biozone SBZ 24) in the top 20 m of the Lower Coralline Limestone (see chapter 5, part 2) of the shallow marine carbonates at the Aqualta Palaeohigh. This places the uppermost part of the Lower Coralline Limestone Formation in the Aqualta well within the beginning of the Aquitanian (SBZ 24), whereas the same boundary in the Maltese Islands is within the end Chattian (SBZ 23). This proves that the Aqualta Palaeohigh drowned after the Maltese Islands.

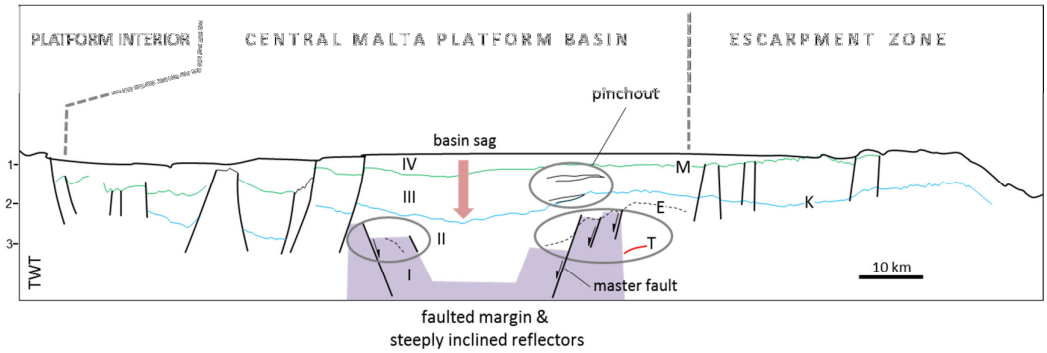

Figure 6.32. Interpretation of seismic line 106 that crosses the Central Malta Platform Basin and escarpment zone (seismic line shown in Figure 6.29). The area shaded grey represents the block-faulted margin of the graben involving megasequences I and II during stage 1 of basin formation. The large grey arrow shows region of maximum sag during stage 2 subsidence of megasequence II, III and IV. The depositional sequences in megasequence III pinchout as a result of sea-level fall and erosion along the basin margin.

6.5.4 Escarpment zone

The eastern margin of the Malta Platform consists of:

i. The here named Malta Ridge which consists of buried narrow horst structures bounded by the CMPB on the west and escarpment on the east. The Malta Ridge is characterised by chaotic to discontinuous reflectors and the thinning of sediments above it.

ii. The NW-SE trending Malta Escarpment and the NE-SW trending Medina Escarpment. The escarpments converge at the W-E trending Medina Mountains that mark the southern boundary of the Ionian crust (Figure 6.33).

The submerged escarpments show large vertical offset which increases northwards towards offshore SE Sicily where the Malta Escarpment is bounded by the Ionian Basin which is presumed to be oceanic crust (Finetti, 1982; Catalano *et al.*, 2001). In contrast, the Medina Escarpment is bound on the east by continental lithosphere of the Sirte Rise.

Both escarpments show large fault-controlled terraces that step basinwards. The faults have been active since the Mesozoic and have listric geometry. However, the slope angle along the Medina Escarpment and the Malta Escarpment differ considerably as a result of the different depositional processes operating along the two escarpments. A middle section around the Medina Mountains is transitional.

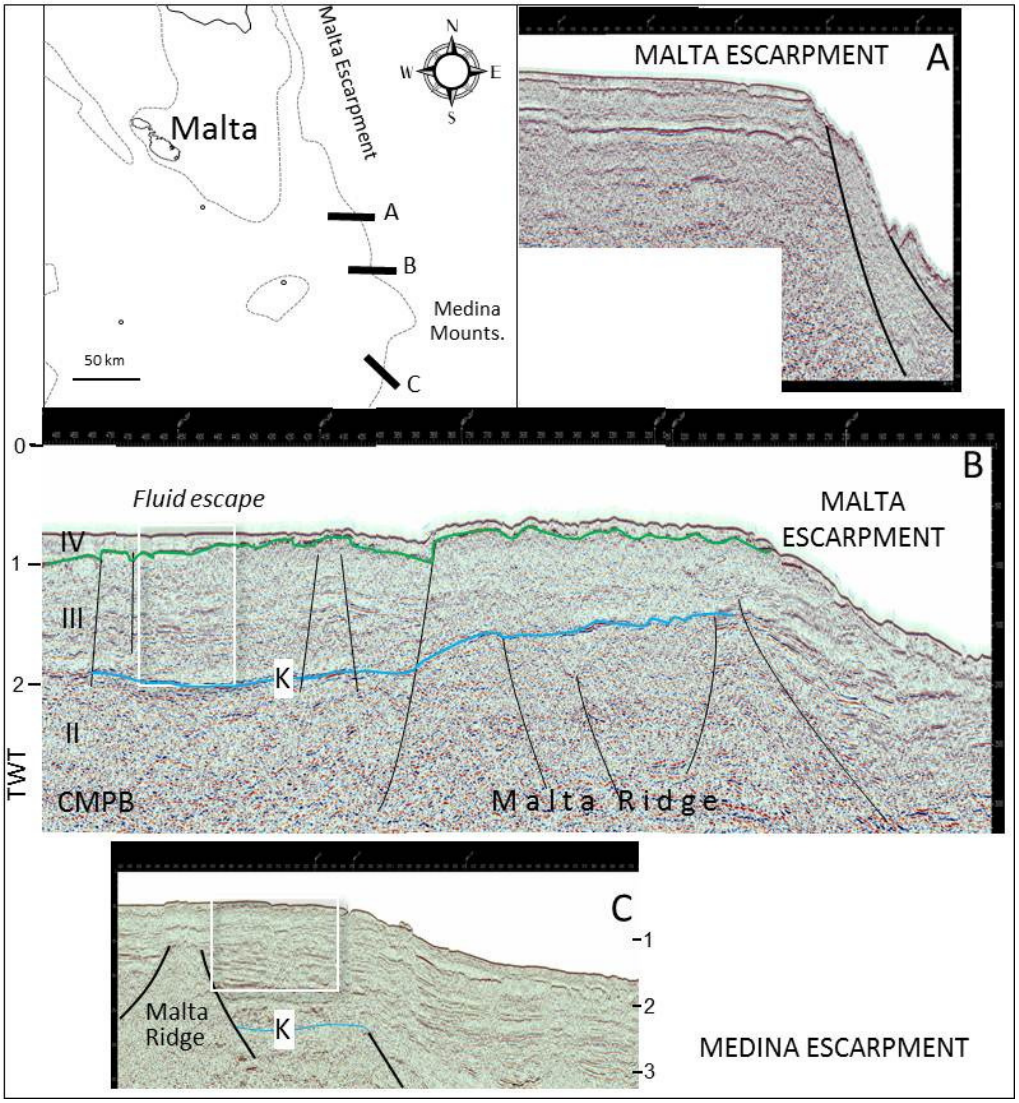

Figure 6.33. Comparison of the Malta and Medina escarpments. (A. seismic line 101, B. Seismic line 106, C. seismic line 303). In line B, the Malta ridge is bounded by the CMPB on the west and the Malta Escarpment on the east.

6.5.4.1 Malta Escarpment

The large listric faults produced the narrow terracing characterised by high walls that forms the present bathymetry (section A in Figure 6.33). The topography suggests the combination of aggradation and erosion that produces slope declivity of >40° (Eberli *et al.*, 2004). Excess sediment produced along the Malta Platform is by-passed directly to the basin where toe-of slope deformation is reported in offshore eastern Sicily (Finetti, 1982). A small basin sub-parallel to the CMPB developed within the escarpment zone that resulted in the thickening of megasequence III (Figure 6.33). The basin is the source of fluid escape structures.

Sediments

Sediments dredged along the Malta Escarpment are described by Scandone *et al.* (1981) could include transported material although some may be *in situ* which permits comparison to well data and outcrops over the Malta Platform. Sediments comprise Triassic shallow marine platform carbonates which are similar to Triassic sediments penetrated by the MTZ well in Gozo, whereas Jurassic shallow marine carbonates show red hemipelagic infills. Cretaceous carbonates are rich in planktonic foraminifera which suggest deeper water conditions relative to the onshore Malta area, although basalts were also encountered just as in the Aqualta well. The succeeding Eocene shallow marine carbonates (coral, miliolids) mark shallowing along the escarpment area which is associated with the Late Eocene in the rest of the Malta Platform. Oligocene sediments are similar to the Chattian sediments in Malta and include the LBF *Lepidocyclina, Amphistegina* and *Operculina*.

Plio-Quaternary sediments along the escarpment are mostly marly, although in the area of the Medina Mountains (section B in Figure 6.33), megasequence IV thins out towards the escarpment. The thinning of megasequence IV reflects erosion during a period of uplift.

6.5.4.2 Fluid flow systems

The basinal area adjacent to the west side of the Malta Ridge shows disrupted reflectors that suggest upward fluid flow through the lithology (Figure 6.33B). The seabed between Malta and Sicily is known to have numerous active mud volcanoes and gassy seeps from the seabed (Savini *et al.*, 2009). Mud volcanoes are associated with mud diapirism rather than trapped petroleum as in the case of gassy seeps. In the mechanically brittle Cretaceous to Palaeogene sediments of the Malta Platform, rupturing can occur as a result of hydrofracturing and tectonic fracturing. When pressure in the sediment pore fluid (P_f) exceeds the minimum principal stress (σ_3) and the tensile stress of the overburden (T), a hydrofracture will form as determined by the expression (Jolly & Lonergan, 2002):

$$P_f > \sigma_3 + T$$

A vertical fracture will develop when the minimum principal stress is horizontal and the maximum principal stress is vertical, as in the case of a sedimentary basin without imposed tectonic stress. Fluid pressure may also be resolved along existing fractures and faults.

Columnar-shaped disturbed reflectors are features associated with fluid escape pipes that terminate along the seabed as pockmarks (Judd & Hovland, 1992). The area west of the Malta Ridge shows such evidence of vertical fracturing. In megasequence III, reflectors are up-bended whereas the surface of the megasequence consists of sporadic depressions (Figure 6.34). Velocity pull-down is also recognised at the top and within megasequence III.

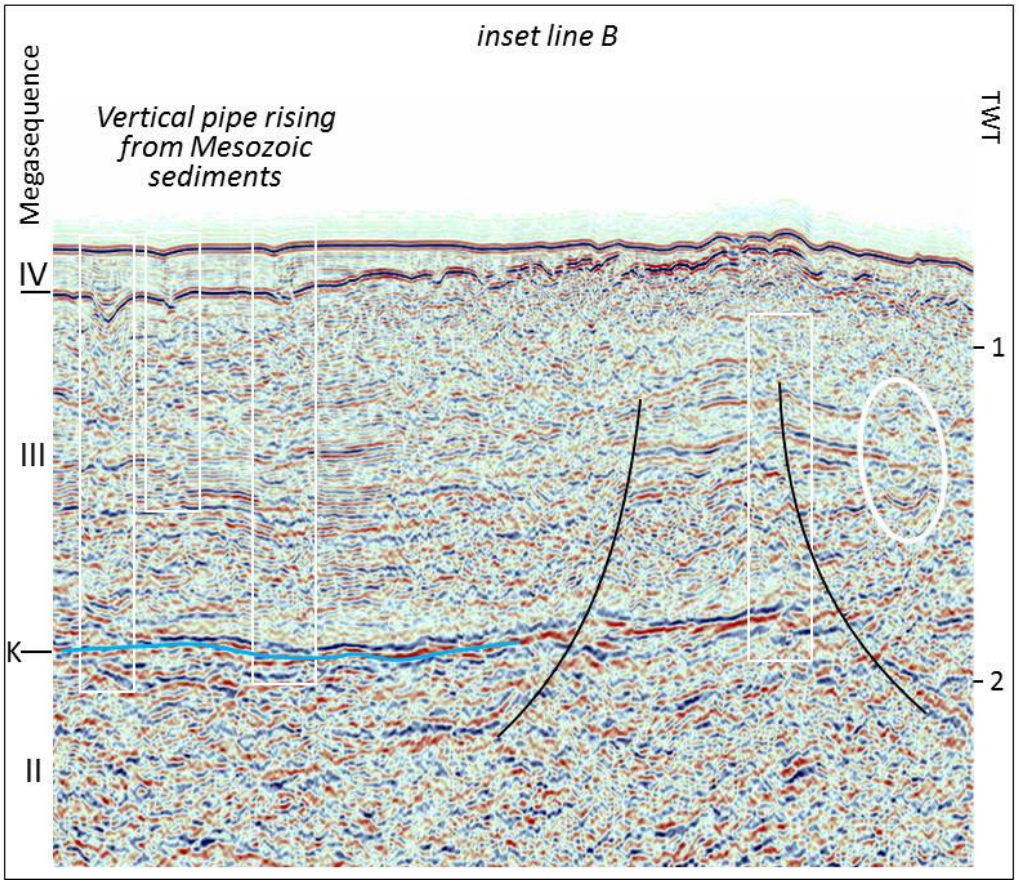

Figure 6.34. Inset of Figure 6.33B. Megasequence IV thins out towards the Malta Escarpment. Rectangles show fluid escape pipes recognised by acoustic disturbance that emerges from the K-reflector forming the basin along the escarpment zone. The circle shows areas of velocity pull-down associated with lower density of gas.

6.5.4.3 Medina Escarpment

The escarpment is characterised by two seismic facies: (i) chaotic and discontinuous reflectors of the Malta Ridge horsts and, (ii) inclined, continuous high amplitude reflectors along the terraced escarpment (

Figure 6.35). The first facies is analogous to platform interior seismic facies found in other carbonate platforms, e.g., the chaotic seismic facies imaged in the interior part of the Mesozoic sediments of the Great Bahama Bank (Walles, 1993) and the Mesozoic Maiella platform, central Italy (Eberli *et al.*, 2004). The second facies forms the prograding platform sediments.

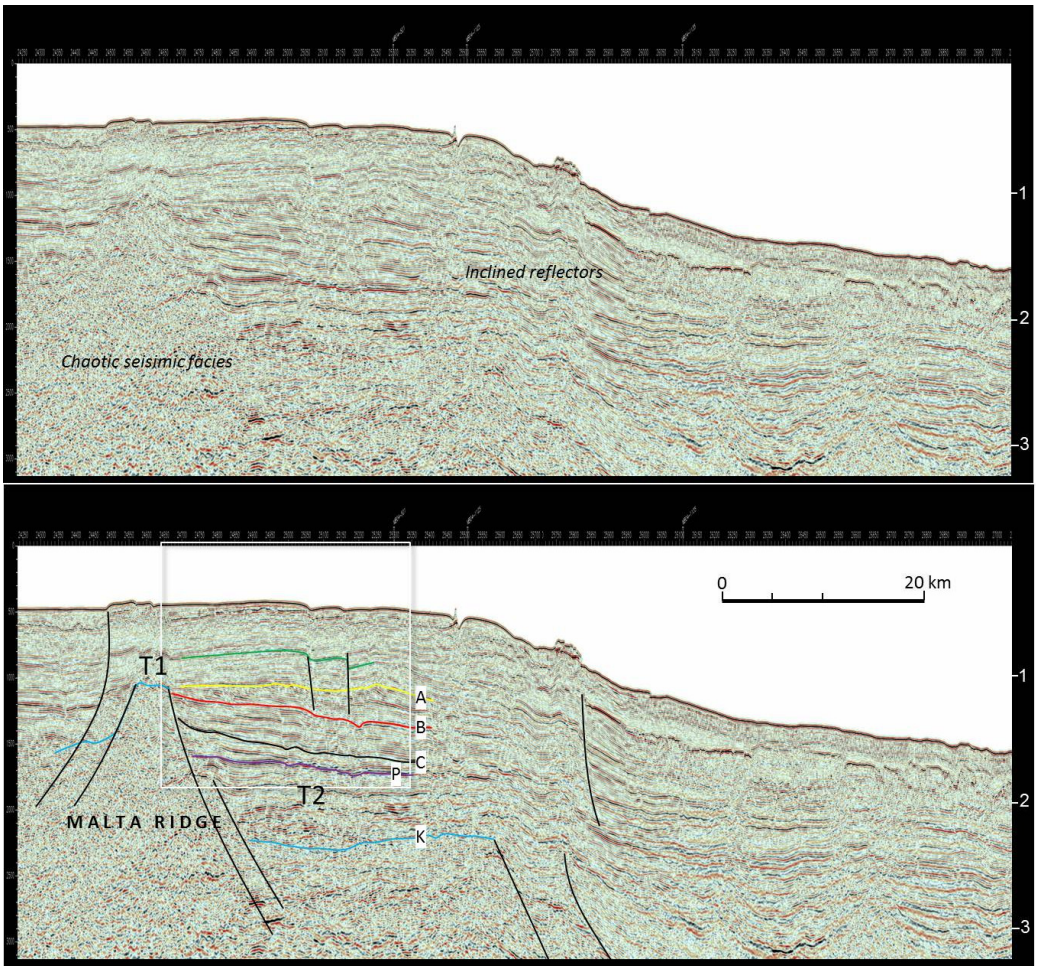

Figure 6.35. Terraces 1 and 2 (T1, T2) buried under megasequence IV and III along line 303. In the uninterpreted lines above The Malta Ridge is characterised by chaotic reflectors whereas the escarpment shows inclined reflectors. Downlapping high amplitude reflectors fill a wedge-shaped space created by the rotation of the downthrown blocks forming terrace 2 (T2).

Sediments have draped the faulted escarpment and reduced its declivity to an angle of <40° (inset of section C in Figure 6.33). Although there are no wells along the escarpment zone that can confirm the stratigraphy, the reflectors are tentatively correlated to those at the Aqualta well on the basis of geometry and the nature of seismic facies.

The chaotic and steeply inclined seismic facies are separated by large listric faults that produce three fault-controlled terraces (terrace 1, 2 and 3) buried by aggrading and prograding complexes (
Figure 6.35):

Terrace 1 (T1)

Forms the structural high of the Malta Ridge bounded at the top by the K-reflector. The horst consists of chaotic seismic facies of megasequence II and is draped by Miocene (top part of megasequence III) and Plio-Quaternary sediments of megasequence IV.

Terrace 2 (T2)

The rotation of the terrace produced considerable accommodation space that is filled by prograding complexes with mirror image geometry that consists of:

i. The wedge-shaped sediment packages between A- and B-reflectors that thicken towards the basin. Sedimentation was controlled by three third-order cycles of sea-level comprising systems tracts labelled a to f (Figure 6.36).

ii. Sediments between reflectors C and B reflectors that onlap on the footwall block (Malta Ridge).

iii. Wedge-shaped sediment package between reflectors P and C that thickens towards the footwall block. The wedge comprises downlapping reflectors that fill accommodation space partly created by anti-clockwise rotation of the downthrown block along the listric fault.

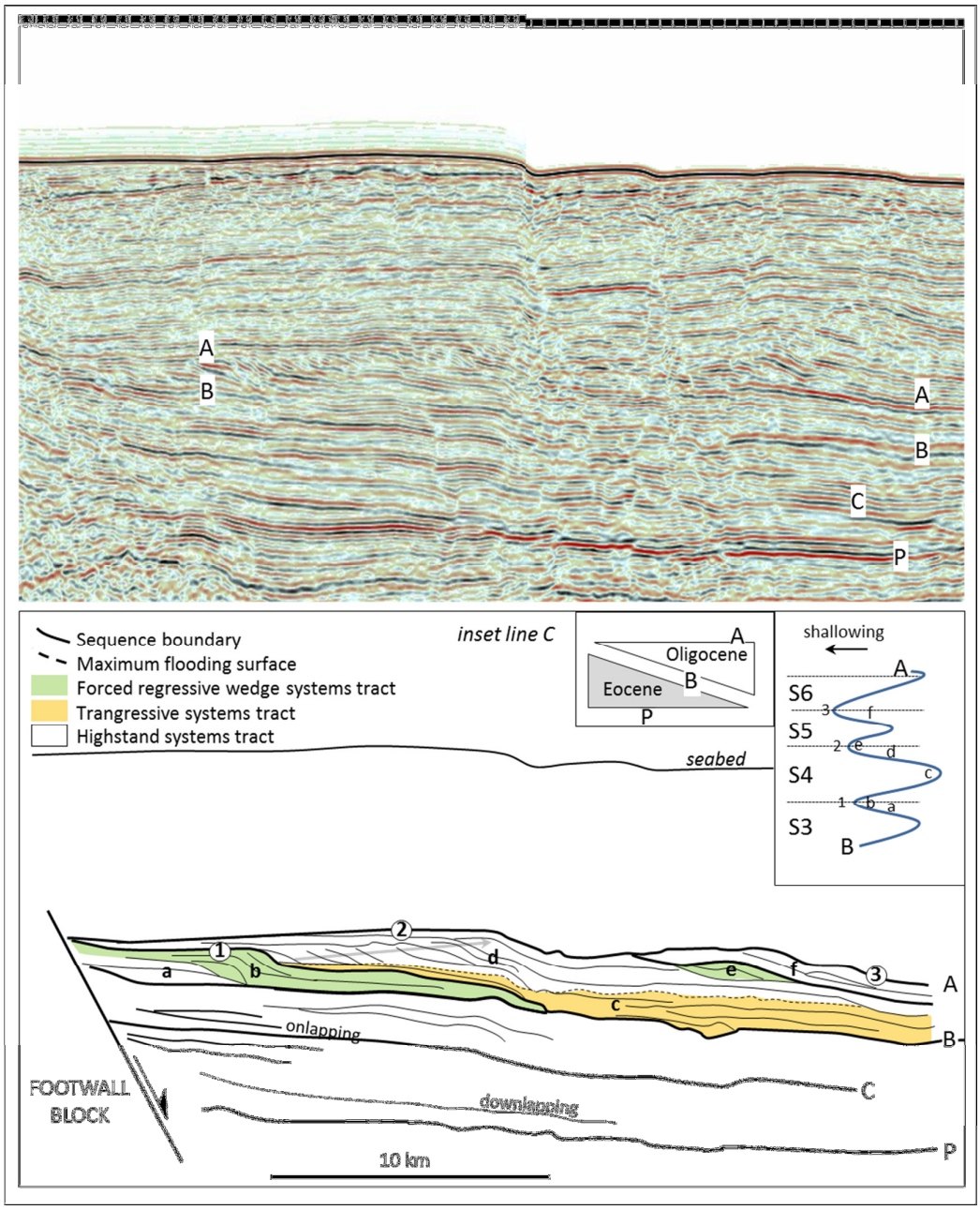

Figure 6.36. Uninterpreted seismic line from inset in
Figure 6.35 showing sedimentation along terrace 2. The interpreted section shows the systems tracts a to f that make up the three sequences prograding from the faulted margin. The grey arrow shows progradation and aggradation along the highstand systems tract of sequence B terminating in sequence boundary 2. Top right is the relative sea-level curve extracted from the systems tract and their thickness in seismic.

The Oligocene sediments between the A- and B-reflectors (Figure 6.36) consist of three sequences that are described in more detail:

- Sequence 1 (systems tracts a and b): the initial fall in sea-level produced low angle reflectors that onlap the faulted margin. The sediments may represent highstand shedding and erosion of the adjacent footwall block (Malta Ridge) and sediment by-passing to the under-filled downthrown block. These are succeeded by a strong-amplitude reflector package (SARP *sensu* Belopolsky & Droxler, 2004) showing inclined reflectors (systems tract b) that are interpreted as a forced regressive wedge building off the faulted margin as sea-level fall reached its lowest level. Increased erosion of the footwall crest augmented the amount of sediment transported which built a coarser-grained regressive wedge that produced strong amplitude reflectors. The sediment package is terminated by the sequence boundary 1 that may have been subaerial and produced the peneplanation of sediments towards the faulted margin.

- Sequence 2 (systems tracts c and d): the sequence boundary is draped by a thin package of sediments that thickens basinwards (c in Figure 6.36) where it fills channel-like features. This represents the marine transgression that may have had a long duration and resulted in the thick succession of near horizontal reflectors which culminate in the maximum flooding surface. The succeeding highstand systems tract consists of clinoforms along a sigmoid-oblique prograding complex that produced relatively weak amplitude reflector package (WARP). The inclined reflectors prograde and aggrade over *circa* 9 km and are draped by high amplitude horizontal reflectors. The highstand is terminated by a fall in sea-level that produced a relatively small forced regressive wedge (systems tract e) culminating in the second sequence boundary. The sea-level fall resulted in further erosion leading to peneplanation of the highstand systems tract d towards the west. This suggests peritidal or subaerial depositional environments along sequence boundary 2.

- Sequence 3 (systems tract f): The absence or sub-seismic thickness of the transgressive systems tract suggests a rapid rise in sea-level and maximum flooding. The ensuing highstand system tract produced prograding clinoforms truncated by the third sequence boundary during sea-level fall along sequence boundary 3.

Terrace 3

The terrace is entirely buried by sediments. It is recognised by the abrupt change in the juxtaposed seismic facies: chaotic to discontinuous reflectors of the Malta Ridge and steeply inclined reflectors that fill the buried escarpment. The steep reflectors onlap along the faulted margin of the escarpment and form a wedge of sediments similar to that found along the modern Bahamas Platform margin, which is interpreted to be the highstand systems tract. The overlying sediments of megasequence III and IV drape over terraces 2 and 3 and continue laterally to the basin.

6.5.4.4 Interpretation

The escarpment zone forms the transition from the Malta carbonate platform to the Ionian Basin. The escarpment zone also defines the changes in the mode of growth of the carbonate platform. Carbonate aggradation over a platform may change to progradation along a turnaround surface (Eberli *et al.*, 2004). In the Medina Escarpment, the buried escarpment shows geometries associated with four phases of aggradation or progradation shown in Figure 6.37 as vertical white arrows indicating aggradation (except phase D which is characterised by progradation):

i. Platform aggradation phase A: the Mesozoic carbonate platform aggrades and forms a steep erosive escarpment. Mound-shaped structures along the crest of the escarpment which are tentatively interpreted as Cretaceous reefs. Sediments onlap along the steep escarpment and reefs.

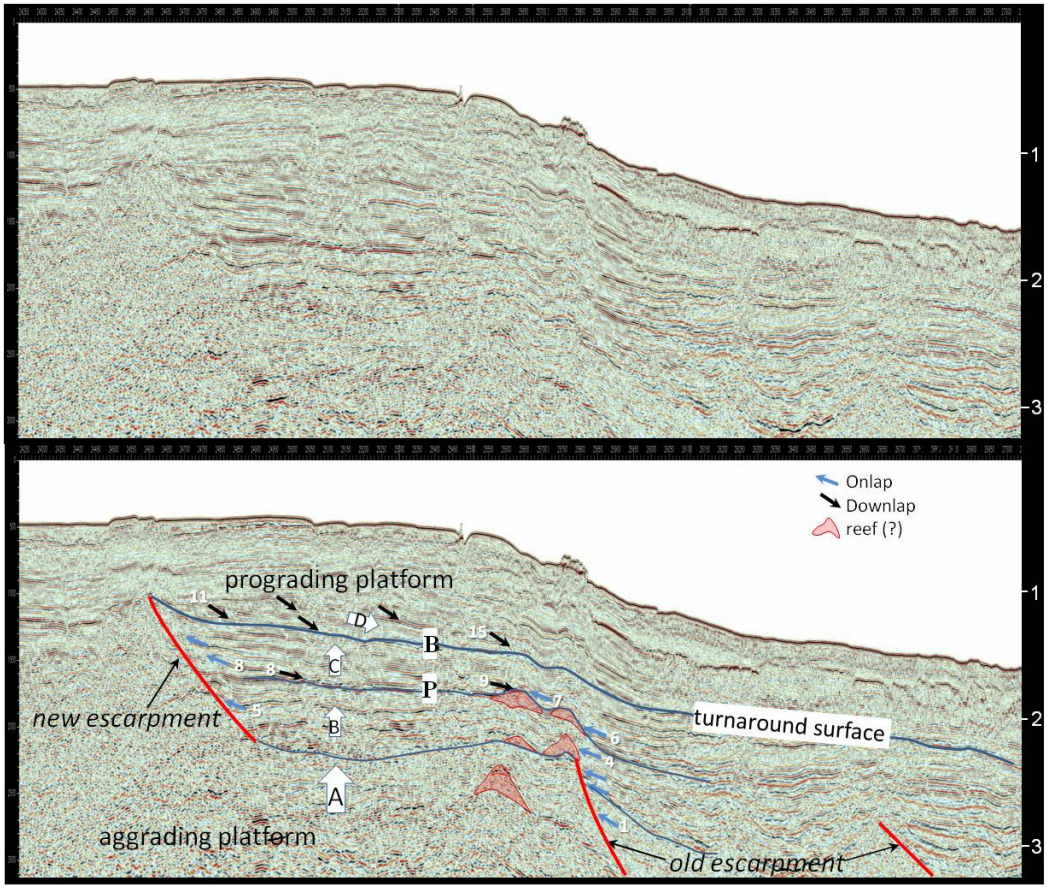

Figure 6.37. Eastern end of seismic line 303 along the Medina Escarpment. The thick blue line shows the turnaround surface (Eocene-Oligocene boundary) from platform aggradation to platform progradation. The thin blue lines are the P- and B-reflectors. The thick white arrows show aggradation/progradation phases A to D. The onlap/downlaps are sequentially numbered 1 to 15.

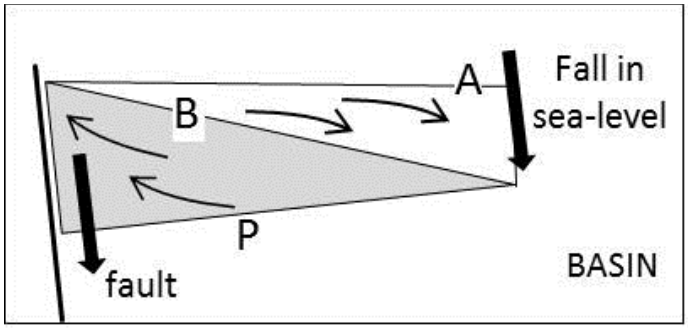

Figure 6.38. Change in geometry of Phases C and D along terrace 2. Arrows show onlap during Palaeocene-Eocene aggradation and downlap during Oligocene progradation. The turnaround surface is the B-reflector. Phase C (grey triangle) shows accommodation space created by faulting whereas in phase D accommodation space is reduced by falling sea-level resulting in basinward progradation.

ii. Platform aggradation phase B: Sediments begin to aggrade over terrace 2 as a result of increase in accommodation space by hanging wall subsidence during marine transgression associated with the P- and C-reflectors (Palaeocene and Eocene flooding events). Reflectors onlap the upper part of the old escarpment and reefal structure. The development of a listric fault further inland results in the backstepping of the escarpment. The 'new' escarpment is onlapped by Late Cretaceous to early Palaeocene sediments which are missing along the platform interior zone. The top of this aggrading sediment package develops reef structures along the crest of the old escarpment. The top of sediment package B is bounded by the high amplitude P-reflector. The reef-like structures are buried along the P-reflector which represents the Late Palaeocene transgression.

iii. Platform aggradation phase C: This corresponds to the Palaeocene to Eocene global sea-level rise. Reflectors onlap the reef structures and backstep inland to the new escarpment. Steeply-inclined reflectors that onlap the escarpment also form low angle downlaps on the hanging wall.

iv. Platform aggradation and progradation phase D: The turnaround from aggradation to progradation occurs along the B-reflector (base Oligocene). Steep reflectors begin to downlap on the turnaround surface (see Figure 6.36) and the platform progrades towards the Sirte Rise/Ionian Basin.

The Oligocene sediments that downlap on the turnaround surface indicate long-term falling sea-level. Excess carbonate production and erosion of the shallow marine/subaerial footwall area (Malta Ridge) is shed towards the basin. The prograding sediments are dominated by Sequence 2 which includes highstand sigmoids that prograde over *circa* 9 km (Figure 6.36). The sediments also aggrade which suggests a relatively long period of high carbonate productivity, although the top sediments are truncated and eroded to a flat surface. This suggests an overall fall in sea-level during a phase of relative tectonic quiescence along the (new) escarpment fault. The geometry of the sigmoids is characteristic of high energy systems (Mitchum *et al.*, 1977). The clinoforms are draped by horizontal high amplitude reflectors that suggest flat-lying lagoonal sediments which were a source

of mud added to the coarse-grained bioclastic sediments along the clinoforms. The muddy lithology of the highstand clinoforms (WARP) relative to the winnowed regressive wedge may be responsible for the high amplitude reflectors (SARP) in the latter (Belopolsky & Droxler, 2004).

It is suggested that the three sequences correspond to the three Chattian sequences 4, 5 and 6 described in chapter 5 which preceded the Late Chattian/Early Miocene drowning of the Malta Platform (Figure 6.36). The Chattian depositional sequences 4, 5 and 6 over Malta are dominated by coarse-grained coralline red algae and large benthic foraminiferans. The thickness of the highstand systems tract of sequence 2 along the escarpment zone may correspond to the thick depositional sequence 5 in Malta which is characterised by rhodoliths and clinoform bedding.

6.6 DISCUSSION

6.6.2 Stratigraphy

The thicknesses of the four megasequences imaged in seismic reflect the changing sedimentation patterns over the post-rift African continental margin. The African shelf accumulated carbonates which aggraded to shallow water depths during relatively high global sea-level from the Cretaceous to the Palaeocene/Eocene (Serrane, 1999) (Figure 6.39). At this time, a number of isolated carbonate platforms that remained free of siliciclastics developed over the Pelagian Block in the Central Mediterranean (see chapter 2). This phase is equivalent to the thick megasequence II sediments in the Malta Platform where wells drilled to the east of Malta record *circa* 3000 m of Cretaceous sediments (Figure 6.9).

As sea-level began to fall as a result of the growth of polar ice-sheets from the Oligocene onwards, the African continental margin was invaded by prograding siliciclastic wedges (Serrane, 1999). The switch from Cretaceous aggradation to Oligocene progradation was accompanied by widespread erosion over Africa accompanied by uplift and increased continental terrigenous flux (Clift, 2010). In the isolated Malta Platform, the switch corresponds to the turnaround surface in Figure

6.37 which truncates some earlier reflectors, possibly indicating an erosive surface. This phase of platform progradation is equivalent to megasequence III which is ubiquitously thinner than the underlying megasequence II and shows significant erosion of its upper part in the area of the Maltese Islands.

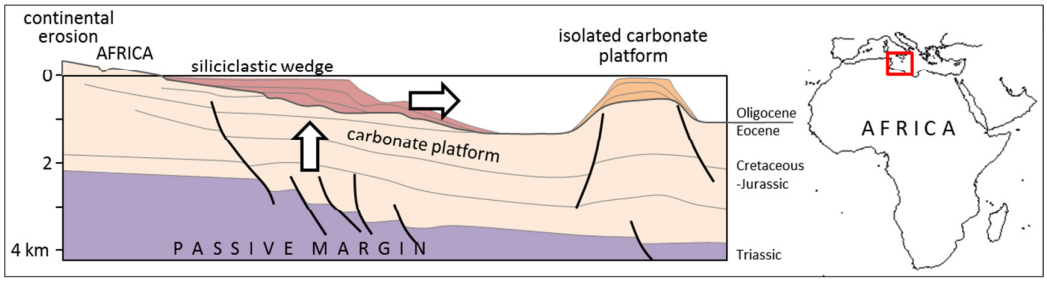

Figure 6.39. Tectonostratigraphic model of the Pelagian Block showing Cretaceous to Eocene aggradation along the African continental margin and isolated Malta Platform followed by the development of an Oligocene siliciclastic wedge as sea-level began to fall.

6.6.3 Tectonics

The Malta Platform developed during rift-induced stretching of the lithosphere that resulted in upwelling mantle to melt, causing igneous intrusions. As the lithosphere migrated away from the zone of mantle upwelling during post-rift stage, cooling begins. This increases the density of the lithosphere which causes subsidence along the passive margin. The rate of continental subsidence and accommodation space diminishes away from the oceanic crust so that passive margins are characterised by the formation of a seaward-thickening prism of post-rift sediments. The overall wedge shape of megasequence III thickens toward the basin and fits in the passive margin subsidence model (Figure 6.40). The rate of post-Jurassic subsidence is within the post rift stage (Figure 6.41).

Mesozoic extension initiated the rifting of the Central Malta Platform Basin and the escarpment zone farther east during the deposition of megasequences I and II. The CMPB became a failed rift whereas the Malta Escarpment continued rifting. The

area between the CMPB and the large listric faults that form the escarpment remained relatively less affected and became the Malta Ridge.

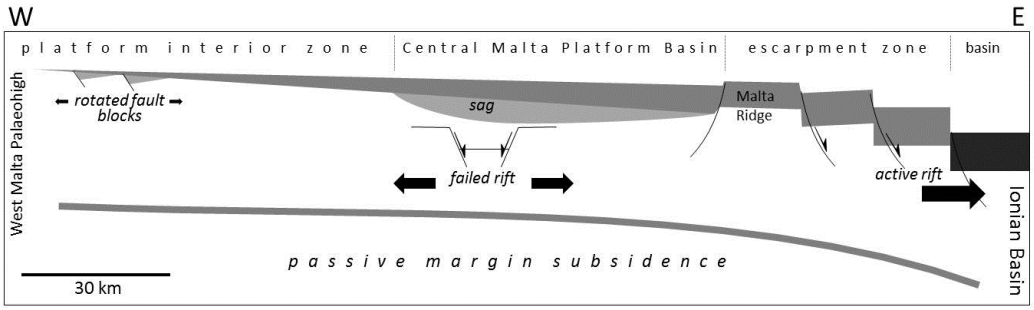

Figure 6.40. Model of megasequence III sediments across a west-east transect of the Malta Platform. The arrows show direction of extension. The dark grey shading shows the wedge-shaped geometry of megasequence III whereas the light grey shows additional thickening caused by local subsidence or faulting.

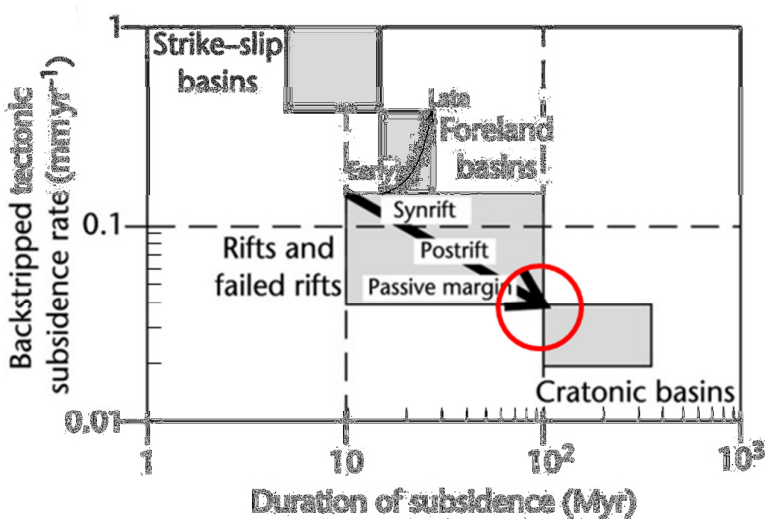

Figure 6.41. Rates of lithospheric subsidence in different tectonic settings (from Allen & Allen, 1990). Red circle shows average rate of subsidence along Malta Platform based on burial history diagrams shown in Figure 6.4. The rate of subsidence lies within the region of post-rift passive margin subsidence.

The degree of crustal thinning by stretching follows the pattern of passive margin subsidence, with minimum stretching in the west and maximum extension in the east towards the rift zone. These elements of local extension produced different structures along the passive margin as follows:

1. Platform interior zone:

Extension produced rotated fault blocks involving an evaporite décollement surface (SbRU1). The palaeobathymetry can be deduced from facies and sediment geometries especially at localities A and 8 (Figure 6.42). The extension is limited to the Cenozoic (megasequence III) and produced the Naxxar and Marsaxlokk basins. The seaways along the intra-platform basins were partly filled with prograding clinoforms. Analogous geometry of prograding carbonates is recognised along the Strait of Andros intra-platform seaway in the Bahamas Platform (Figure 6.43) exposed to westward-directed Trade winds that supply the leeward margin with sediment (Schlager, 1993). As in the Naxxar Basin, the clinoforms on the windward side are steeper and aggrade upward relative to the much wider horizontal extent of clinoforms aggrading along the leeward side of the seaway (Eberli & Ginsburg, 1989).

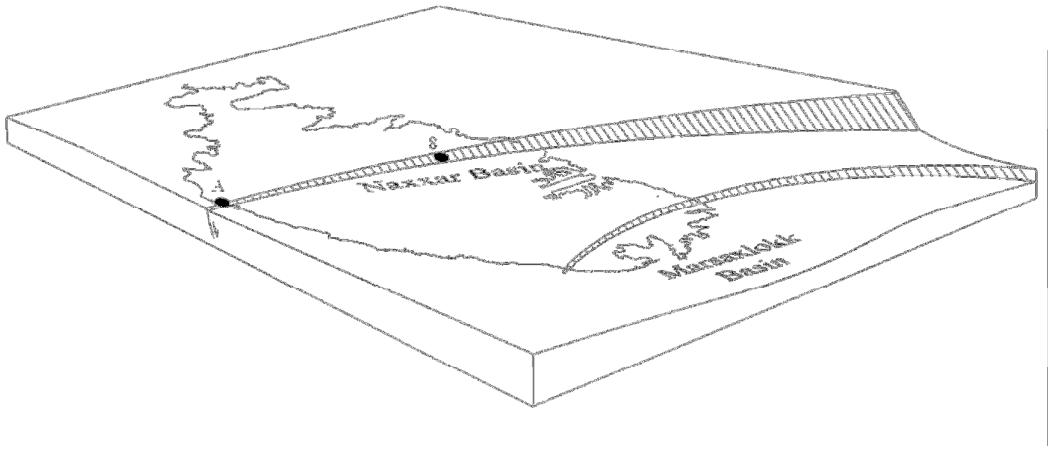

Figure 6.42. The Naxxar and Marsaxlokk basins across Malta formed by buried faults that cross localities A and 8 where clinoform bedding is exposed.

The development of hardgrounds and sediment condensation (facies IIIa) on the windward side of the WMP marks the change from slope accretion during sequence 5 to erosion during sequence 6. However, the dominance of the highly hydrodynamic large benthic foraminiferans in sequence 6 resulted in significant transport and

uneven sediment accumulation rates along the Malta Platform. Large benthic foraminiferans cannot build rigid structures so that thick LBF bioclastic shoals (facies IIIb) only developed on the leeward side of the WMP in western Gozo (locality 1) and EMP in eastern Malta (localities 10 to 12).

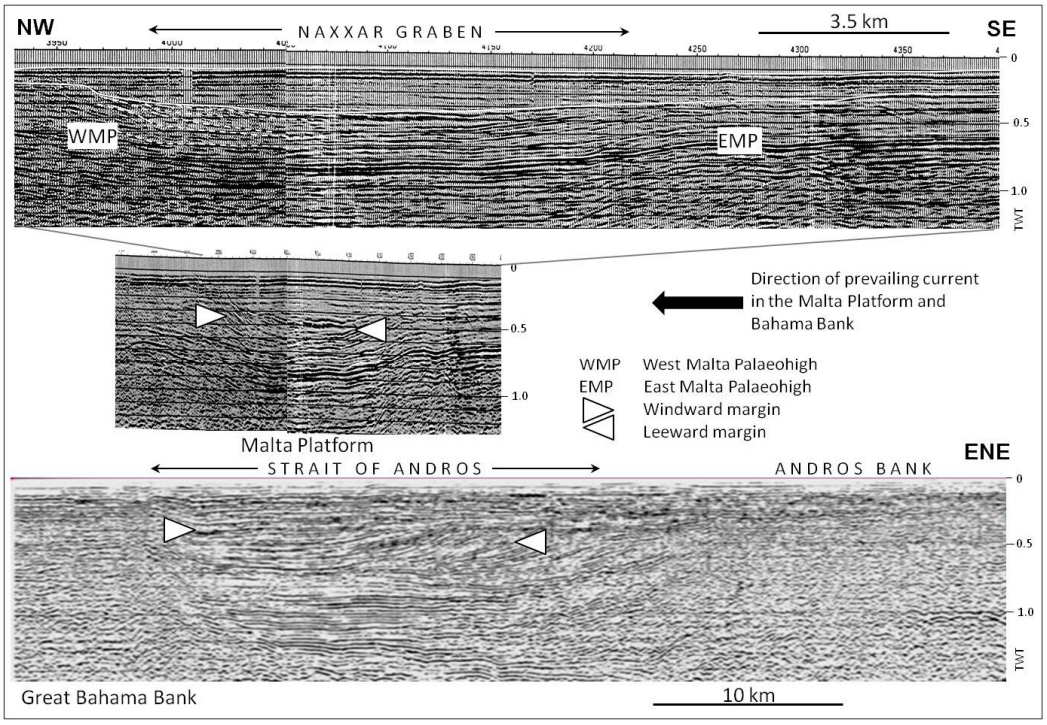

Figure 6.43. Comparison of progradation in the Strait of Andros, Great Bahama Bank (Eberli & Ginsburg, 1989) with progradation in the Naxxar Basin (vintage seismic line parallel to line 311 just offshore of the north coast of Malta). Both seaways have a western windward margin that is steeper whereas most of the seaway is filled by clinoforms prograding from the east.

2. Central Malta Platform Basin zone:

Extension and rifting since the Early Mesozoic resulted in block faulting and basaltic intrusions throughout the Mesozoic. Rifting stopped by the Early Mesozoic and on cooling of the lithosphere this zone began to subside. The sagging created accommodation space and resulted in thickening of megasequence III. This zone represents an early stage of failed rifting within the Malta Platform that was later transferred to the escarpment zone.

3. Escarpment zone:

This zone forms the cusp-shaped eastern margin of the Malta Platform bounding the rift zone that floors the Ionian Basin. The escarpment zone is best preserved in the south (Medina Escarpment) where it consists of the Malta Ridge bounded on the east by *en echelon* kilometre-deep listric faults that control large rotational blocks which step down towards the basin. The faults along the old escarpment are of Mesozoic age and backstep into the platform during the Cenozoic forming the three terraces described in section 6.5.4.ii. The prograding complexes along the eastern escarpments of the Malta Platform (Medina Bank area) have been interpreted by hydrocarbon exploration companies as Nummulitic banks (TGS-NOPEC, 2003). However, these prograding complexes have not been drilled by a well and are characterised by flat tops and steep prograding margins. The high hydrodynamic mobility of *Nummulites* precludes steep constructional margins. The geometry of these seismically imaged sediments is similar to those of sequence 5 seen in Maltese outcrops and imaged in seismic along a line <2 km offshore Malta. The rhodolith biostrome shows constructional slopes that are relatively steep (15°) that prograde from a nearly horizontal aggradational core (Figure 6.44). This suggests that the Chattian tectonic quiescence concomitant with rising sea-level was a phase of ubiquitous progradation over intra-platform seaways and the escarpment zone.

The Malta Escarpment in the north comprises mostly the escarpment. This could reflect ongoing tectonism linked to the subduction of the Ionian crust under the Calabrian Arc which has caused a tear zone that expands northwards. The tear zone may have caused the rapid retreat of the escarpment by backstepping *en echelon* listric faults into the Malta Platform, eliminating the antecedent palaeohighs. The increased number of mass transport events towards offshore eastern Sicily (Finetti, 1982) is consistent with slope instability associated with Plio-Quaternary subduction of the Ionian seafloor towards the north.

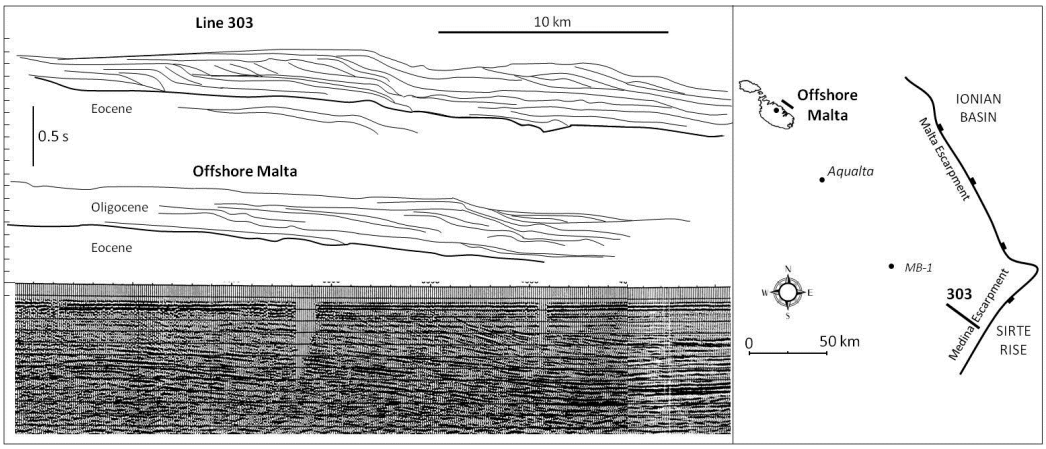

Figure 6.44 Prograding complexes along the escarpment zone (line 303 from Figure 6.36) and interior platform zone (vintage offshore seismic line). Both prograding complexes show a flat top geometry with offlapping clinoforms with similar angle to prograding Chattian sediments in Malta comprising depositional sequences 4, 5 and 6.

6.7 SUMMARY

The Tethyan region is characterised by phased changes in accommodation space through time resulting from the prevalent tectonic and eustatic processes. The processes can be analysed using laterally persistent seismic reflectors that are tied to wells and outcrops. Three high amplitude reflectors sub-divide the Malta Platform carbonates into four megasequences (I to IV) that show variable thickness and geometries. The increase in accommodation space caused by Cretaceous sea-level rise resulted in significant aggradation of megasequence II (*circa* 4 km) succeeded by the thinner megasequence III (1.5-2 km) deposited as global sea-level began to fall during the Oligocene. Superimposed on glacio-eustasy are Mesozoic to the Neogene tectonic controls reflecting the passive margin setting of the Malta Platform that produced three platform geotectonic zones:

(1) the ***platform interior zone*** which is characterised by Palaeogene shallow marine carbonates involved in NW-SE- trending thin-skinned extension along an basal Oligocene evaporite décollement surface that produced rotated fault blocks characterised by small (<10 km wide), *en echelon* shallow intra-platform basins;

(2) the ***Central Malta Platform Basin*** (CMPB) that developed as a 70 km-wide polyphase basin beginning with fault-controlled rifting of the Triassic megasequence I followed by sagging and thickening of megasequences II and III, and,

(3) the cusp-shaped ***escarpment zone*** that formed a ridge bounded by megablocks controlled by kilometre-deep listric faults that produced a terraced profile along the eastern margin of the Malta Platform adjacent to the 4 km deep Ionian Basin. In the south the terraces are draped by a thick cover of sediments that produced a gentler slope in the direction of the Sirte Rise.

Chapter 7

Environmental controls on Palaeogene carbonate sedimentation

7.1 PREAMBLE 309
7.1.1 Global ice volume, sea-level and oxygen isotopes 309
7.2.2 Global climate belts 310
7.1.3 Carbonate ecosystems 313
7.2 CLIMATIC CONTROLS ON FACIES IN PALAEOGENE MEDITERRANEAN SUBTROPICAL CARBONATE PLATFORMS 316

7.1 PREAMBLE

This chapter discusses climate change in low latitudes as a consequence of the growth of polar ice-sheets and links this to changes in carbonate ecosystems in the Malta Platform and the Western Tethys. The first part is a preamble to the paper by Gatt & Gluyas (2012) reproduced here, which discusses climate-sediment inter-relationships.

From the discussions in chapter 3 and 5, a photozoan-heterozoan-photozoan triplet of grain associations can be identified in the Oligocene carbonates of Malta. These changes in carbonate ecosystems reflect shifts in physico-chemical parameters related to temperature, nutrient level, light intensity, sea-level and hydrodynamic energy level and, atmospheric carbon dioxide (pCO_2) which known to control the type of dominant carbonate biota on a regional to global scale (Pomar *et al.*, 2004). The fundamental factor that relates all these physico-chemical variables and their effect on the carbonate rock record is climate.

The objectives of this chapter are to: (1) describe the main variables affecting carbonate ecosystems that include global ice-volume, climatic patterns, temperature and nutrient level, (2) to reconstruct the level of nutrient flux in the marine environment through time on the basis of trophic level reflected in the predominant biotic assemblage: coralline red algae (CRA), large benthic foraminifera (LBF) and corals, on the Malta Platform and relate this to the global isotopic carbon signature, and (3) discuss regional environmental changes based on the hypothesis that carbonate sediments can be used as a proxy for changing climatic conditions in the western Tethys.

7.1.1 Global ice volume, sea-level and oxygen isotopes

Global climate and volume of ice are reflected in glacio-eustasy which is controlled by changes in global insolation (e.g., Milankovitch-type orbital controls) that determines the waxing and waning of ice-sheets (described in chapter 5). These changes control the level of sequestration of lighter oxygen isotopes by the ice-caps that is recorded in changes in the $\delta^{16}O/^{18}O$ ratio of benthic foraminifera from deep

sea cores acquired by the Deep Sea Drilling Programme followed by the Ocean Drilling Program and now the International Ocean Drilling Program, interpreted in a number of studies (Miller *et al.*, 1991; Abreu & Haddad, 1998; Zachos *et al.*, 2008). It can be deduced from changing $\delta^{18}O$ values that the Earth's climate passed through phases of climatic optimum and climatic deterioration (expansion of polar ice-sheets) shown in Figure 7.1.

The growth of large ice-sheets during the transition from a greenhouse into an ice-house world occurred at three major stages: the Eocene/Oligocene boundary, the middle Miocene and the middle Pliocene (Miller *et al.*, 1991; Zachos *et al.*, 2001). The growth of ice-sheets reflects the drop in the level of pCO_2. The level of global pCO_2 since the Eocene has been derived from the carbon isotopic composition of sedimentary alkenones ($\delta^{13}C_{37:2}$) (Pagani *et al.*, 2005).

The first stage of the transition to an ice-house world is marked by the increase in the size of the Antarctic ice-cap since the earliest Oligocene when orbital controls on insolation coincided with a drop in pCO_2. However, the Earth remained unipolar throughout the Oligocene until the beginning of the Miocene when pCO_2 dropped to pre-industrial levels of *circa* 280 p.p.m., triggering the expansion of the Arctic ice-cap (DeConto *et al.*, 2008) which increased further in size after the middle Miocene.

7.2.2 Global climate belts

The location of climatic belts is controlled by the global air circulation pattern which is zoned latitudinally along three cells (Figure 7.2): Hadley cell, Ferrel cell and the Polar cell (Matthews & Perlmutter, 1994). The meridional margins of each cell consist of rising or descending air. The size of the three cells is controlled by the thermal equator or the intertropical convergence zone (ITCZ) that consists of the juxtaposed rising air currents of the two Hadley cells in each hemisphere. When the ITCZ shifts seasonally towards one pole, the three cells in that hemisphere are compressed whereas the cells in the other hemisphere are extended.

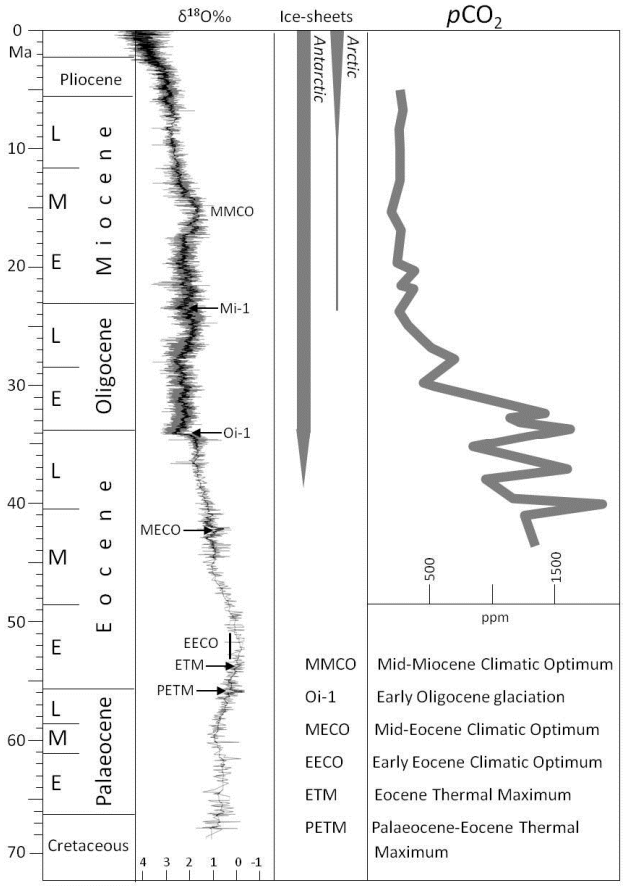

Figure 7.1. Duration of ice-sheets and important climatic events reflected in global oxygen isotopes (Zachos *et al*., 2008). The pCO_2 curve from Pagani *et al*. (2005).

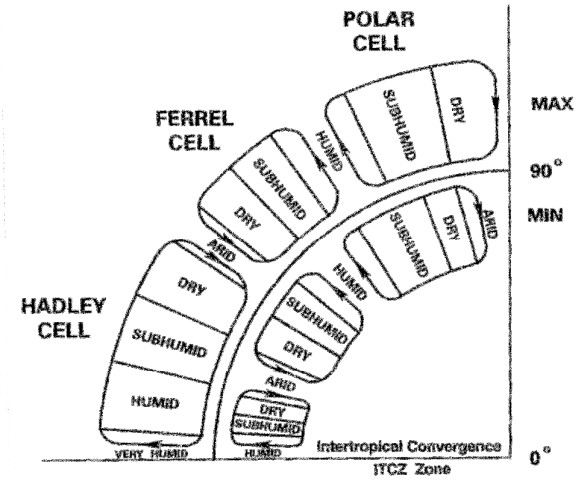

Figure 7.2. Climate belts and how they change in size and meridional position as a result of shifts in the ITCZ (from Matthews & Perlmutter, 1994).

The seasonal shifts in the ITCZ are manifest in the global monsoon that affects all continents except Antarctica. Nevertheless, the ITCZ and the zonal distribution of climate belts can also shift in the long term as a result of astronomical forcing that causes variations in the spatial distribution of solar energy reaching the Earth's surface (De Boer & Smith, 1994). The mechanism for these shifts is linked to the development of a polar ice sheet in one hemisphere that steepens the pressure gradient and results in a significant meridional shift in the position of the Hadley cell away from the hemisphere with high latitude ice (Chiang & Bitz, 2005).

During times when both polar ice-sheets are developed (e.g., Quaternary Era), the meridional shifts in climate belts are restricted to a maximum of 10° in both hemispheres as shown in Figure 7.3. However, a unipolar (Antarctic) ice-sheet world is known to have existed during the Oligocene (DeConto *et al.*, 2008) which would have caused the ITCZ to shift to much higher latitudes within the northern hemisphere (*circa* 30˚N).

Climatic controls in the Maltese Islands are considered to have caused the change from pelagic carbonate (Globigerina Limestone) to the Blue Clay Formation in the Miocene, interpreted by John *et al.* (2003) as reflecting a northward shift of the ITCZ that resulted in more weathering over North Africa and an influx of siliciclastics (clay) over the Malta Platform.

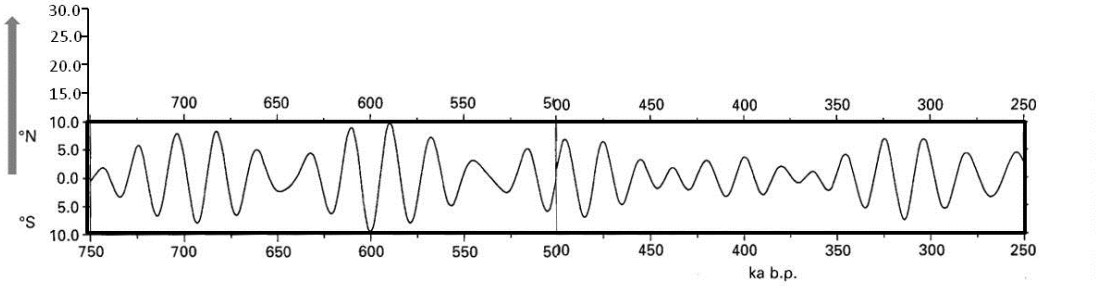

Figure 7.3. Changing position of thermal equator and ITCZ during the bipolar ice-sheet Quaternary (De Boer & Smith, 1994). Grey arrow shows the maximum meridional northward shift of ITCZ during the Oligocene (Fluteau *et al.*, 1999) when a unipolar ice-sheet developed.

7.1.3 Carbonate ecosystems

Climate affects carbonate platform sedimentation as a result of sea-level, temperature and nutrient flux:

1. ***Sea-level and temperature***: Organisms on carbonate platforms are not directly affected by water depth, although it controls:

i. Light intensity and the strength of water currents along the seabed: Three groups of carbonate-producing biota may be distinguished according to their dependence upon light: (a) euphotic (good light) in shallow, wave-agitated areas; (b) oligophotic (poor light) in deeper, commonly non-wave-agitated areas; and (c) photo-independent biota in all water-depth ranges (Pomar *et al.*, 2004).
ii. The type of biotic assemblage: It is generally assumed that cooler temperatures favour rhodalgal, bryomol and foramol assemblages, whereas warm, tropical environments are ideal for the chlorozoan assemblage that includes coral. This is reflected in the negative correlation between sea temperature and corals, that results in the drop in diversity of Miocene coral genera towards higher latitudes of the Mediterranean (Bosellini & Perrin, 2008).

It is well known that in the Pleistocene, siliciclastic sediment supply to basin environments was at its maximum during glacial lowstands and that carbonate production over platforms was in antiphase to this rhythm (Schlager, 1992). During periods of global warming, sea-level rise increases accommodation space over carbonate platforms. Very rapid sea-level rise during marine transgressions (6 to 10 mm/ yr) can result in the drowning of carbonate platforms (e.g., early Holocene platforms), although modern tropical coral reefs respond to moderate sea-level rise (0.5 to 3 mm/yr) by increasing productivity in order to keep up with highstand sea-level rise (Schlager, 1981). During episodes of sea-level fall as a result of global cooling there will be the subaerial exposure of a greater area of the carbonate platform. In addition, a global lowstand of sea-level will rejuvenate fluvial systems that results in an increase in nutrient flux from the continents to the sea. Both of these circumstances result in a reduction of productivity in tropical carbonate ecosystems (Sharland *et al.*, 2001).

2. ***Nutrient level***: The trophic level of ecosystems reflects the level of nutrients in the sea. The mechanisms that affect the level of nutrients in the sea include the regional upwelling of water or the increase of nutrient flux from the continents to the sea as a result of increased rainfall over continental areas. Nutrient level is an important control on benthic assemblages in tropical environments (Hallock & Schlager, 1986) because it affects the level of trophism in the ocean: Autotrophs, e.g., algae extract nutrients from the ocean and use light to photosynthesise food, whereas heterotrophs are consumers of food, e.g., herbivores. The skeletal assemblages of these ecosystems are classified by James (1997) into the photozoan association and heterozoan association. This sub-division is based on trophic requirements of biota that reflects nutrient level as well as sea temperature. The photozoan association includes green algae, hermatypic coral, LBF and rudists. Because of efficient nutrient re-cycling, photozoan organisms thrive in oligotrophic environments within the photic zone. The heterozoan assemblage consists of light-dependent coralline algae and light independent bryozoans, echinoderms and molluscs. Heterozoan organisms are eurythermal and can thrive in low as well as cooler high latitudes in mesotrophic conditions.

Trophic level in carbonate ecosystems is linked to two parameters affected by nutrient level:

i. Light penetration: Increased nutrients will result in a bloom in suspension-feeding organisms and the rapid growth of epiphytic and free-floating macro- and micro-algae that is reflected in increased chlorophyll production (Figure 7.4). In these conditions, the amount of sunlight reaching the seabed is reduced. However, during oligotrophic episodes, the water column is clear and light penetration enhanced (Mutti & Hallock, 2003), which benefits photo-autotrophic organisms such as coral found close to sea-level and LBF in deeper water.
ii. Competition: Mesotrophic conditions favour fleshy algae and other soft-bodied organisms that outpace carbonate producers (Schlager, 1992). However, herbivorous organisms (echinoids, molluscs and gastropods) that graze on fleshy algae can give carbonate-secreting organisms such as coralline red algae a competitive edge by reducing the area of the seabed occupied by soft-bodied algae (Steneck, 1986). In the case of coral reefs, an increase in nutrient level can

result in zooxanthellate organisms being out-competed by fleshy algae and greater destruction of reef framework through bio-erosion (Hallock, 1988).

Global or regional nutrient level has controlled the main type of grain in carbonate ecosystems. High nutrient environments (meso- eutrophic conditions) are unfavourable to carbonate ecosystems which tend to thrive in submarine deserts (oligotrophic conditions) where they efficiently recycle nutrients (Schlager, 1992). As a result, the two skeletal associations are found in distinct geographic areas marked by the 30° latitude in both hemispheres (Figure 7.4). There are exceptions, and a number of areas with heterozoan associations occur within the tropical zone. These areas are affected by large fluvial discharge, water upwelling and aeolian desert dust (Westphal *et al.*, 2010). It is thought that increased land-derived nutrient supply in the oceans was responsible for higher trophic resources (mesotrophic to eutrophic conditions) and the global dominance of rhodalgal lithofacies during the middle Miocene (Halfar & Mutti, 2005).

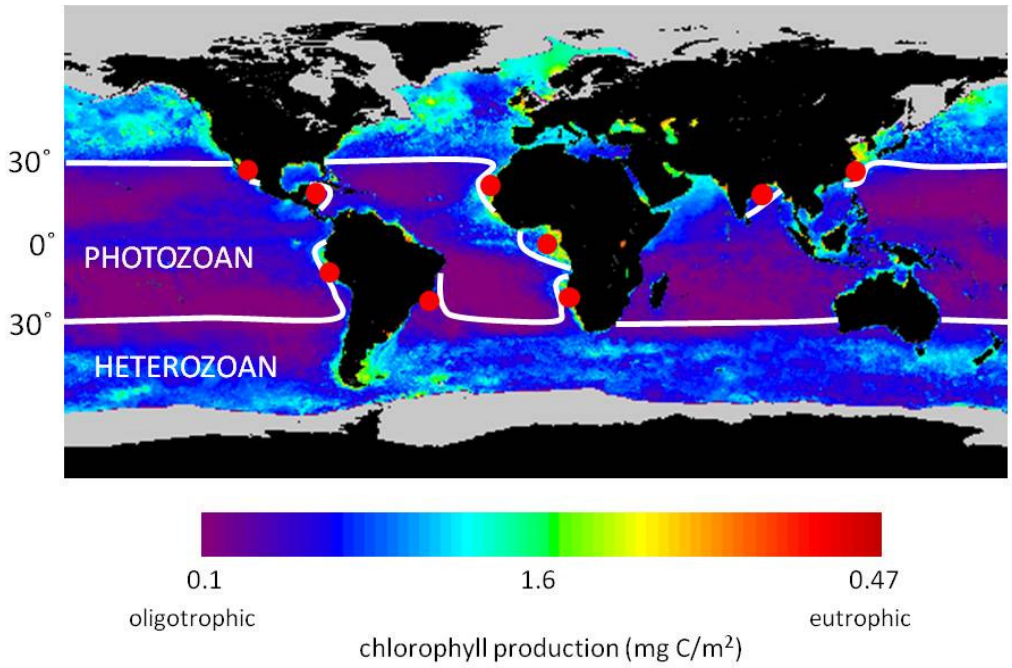

Figure 7.4. World map of summer chlorophyll concentration over 1978 to 1981 (from Rutgers University website) which reflects nutrient level in the sea. Superimposed is the present global distribution of photozoan and heterozoan skeletal associations (based on James, 1997). The modern photozoan assemblage is found in tropical climate belt between 30˚ in both hemispheres although areas marked with red dots indicate exceptions where heterozoan biotas dominate in tropical conditions.

7.2 CLIMATIC CONTROLS ON FACIES IN PALAEOGENE MEDITERRANEAN SUBTROPICAL CARBONATE PLATFORMS

A paper submitted to Petroleum Geoscience in 2011and published in 2012.

Gatt, P.A. & Gluyas J.G. (2012) Climatic controls on facies in Palaeogene Mediterranean subtropical carbonate platforms, *Petroleum Geoscience*, 18(3).

Abstract

Cenozoic carbonate platforms in the central Mediterranean region show distinct vertical changes in carbonate skeletal assemblages and porosity characteristics that reflect shifts in environmental conditions affecting the western Tethys. The Photozoan Association produced by carbonate ecosystems adapted to low nutrient environments and the Heterozoan Association favoured by mesotrophic conditions alternate through time over the Malta Platform and nearby carbonate platforms, although not in phase with trans-Mediterranean Oligocene carbonates. This anomaly reflects the transitional nature of Cenozoic climate as well as continental convergence of the Tethyan margins. Restricted conditions amplified the effect of nutrient flux from North African fluvial systems that was controlled by meridional shifts in the inter-tropical convergence zone (ITCZ) precipitation belt. A model of climate-carbonate interaction is constructed by comparing the global oxygen isotope proxy to ice volume and meridional position of the ITCZ to changes in trophic level of carbonate ecosystems. The results show that the development of Palaeogene Mediterranean photozoan assemblages coincide with periods when the ITCZ had shifted away from North Africa (as is the case presently) whereas the heterozoan assemblages thrived during increased nutrient flux when the precipitation belt was located over the Sahara. The climatic controls resulted in facies characteristics that exert a fundamental influence on porosity in carbonate reservoirs.

Introduction

The characterisation of shallow-water carbonate systems and carbonate reservoirs have traditionally relied on two groups of predictive models: (1) tectonostratigraphic models that give an overview of processes and depositional environments in end-member models of shallow marine carbonate platforms (e.g., Read, 1985; Burchette & Wright, 1992; Bosence, 2005) and, (2) the sequence stratigraphic model *sensu* Van Wagoner *et al.* (1988) which analyses seismic data within a chronostratigraphic framework that reflects sea-level control on the geometry of sediment packages. This approach was later extended to carbonate facies (Handford & Loucks, 1993). Standard facies belts have been associated with both models (Wilson, 1975; Burchette & Wright, 1992), and have been applied to Tethyan Tertiary carbonate platforms (Buxton & Pedley, 1989).

A third model is introduced based on climate change and its effect on regional palaeogeography. The model reduces uncertainty in the exploration for petroleum accumulations by improving our understanding of global climatic controls on vertical and lateral facies changes affecting carbonate reservoir porosity development at the concession scale in the western Tethys. Palaeoclimate change studies have traditionally relied on atmospheric general circulation models, e.g., Fluteau *et al.* (1999) although attempts have been made to link theoretical circulation models to the rock record. Studies on the Neogene by Lyle *et al.* (2002) and John *et al.* (2003) have relied on mineralogy and the extent of siliciclastic sedimentation as proxy for meridional shifts in climate belts. However, publications on climatic controls on Oligocene sedimentation are few, albeit this was a time characterised by marked increase in global continental erosion (Clift, 2010) and the development of a sizeable polar ice-sheet (DeConto *et al.*, 2008). Climate change had especially affected carbonate ecosystems in the restricted western Tethys, although Mediterranean carbonates remain less known than those of the Caribbean (Mutti *et al.*, 2005) and the Indo-Pacific region (Wilson, 2008).

This study relies exclusively on carbonate platform sedimentation in order to infer climatic control on the western Tethys. We hypothesise that a relationship exists

between changes in the trophic level of environmentally-sensitive carbonate platform ecosystems and the global oxygen isotope curve obtained from deep-sea benthic foraminifera (Zachos *et al.*, 2008). The latter is the proxy for Antarctic ice-sheet volume and concomitant meridional shifts of climate belts during the Oligocene, which are confirmed independently by sediments in Antarctic islands (Francis *et al.*, 2009) and global CO_2 levels (Pagani *et al.*, 2005). The verification of the relationship between oxygen isotopes and ecosystem trophic level forms the basis of the climate-sediment interaction model we have constructed based on the intensity of rainfall and erosion over the North African continental landmass and the west Tethyan carbonate grain associations.

The model is tested on the Oligocene carbonates of the Maltese Islands in the Central Mediterranean which provide a relatively continuous stratigraphic record that serves as an analogue for other carbonate facies in the region. The objectives of this study are: (1) to present a climate-sediment interaction model based on the effect of climate on carbonate ecosystems, (2) use the model to reconstruct a high resolution climate record for the Oligocene and (3) discuss climatic controls on carbonate facies, grain size, mineralogy (calcitic-aragonitic) and framework biota that affect overall reservoir porosity.

METHODS AND DATASETS

Published chronostratigraphic studies on Central Mediterranean carbonates listed in Table 7-1 are dated using the large benthic foraminiferal biozones of Cahuzac & Poignant, (1997), supported by strontium isotope dating. These are correlated to the >250 m thick Oligocene Lower Coralline Limestone Formation that is penetrated by wells over the 150 x 100 km Malta Platform. The top <120 m of the formation outcrops in the Maltese Islands. Microfacies analysis based on 80 thin sections are described in terms of the Dunham (1962) classification of carbonate textures. Major unconformity and hiatal surfaces and cycles are recognised in outcrop studies and subsurface data derived from reports on three exploratory wells over the Malta Platform (BP and Total well reports) and well data from the Apulia Platform (Official Italian Government website, 2011) and are interpreted within a sequence stratigraphic framework.

No.	Location	Formation name	*Dominant biota*	inner	mid	outer	Principal references
M	Malta	Lower Coralline Lmst.	*CRA, LBF, coral*	■	■		This study
1	Sirt, Libya	Bu Hashish	*coral, LBF*	■			Hladil *et al.*(1991)
		Umm ad Dahiy	*coral, LBF*	■			Imam & Galmed (2000)
2	SE Sicily	Ragusa	*CRA, LBF*		■	■	Knoerich & Mutti (2006)
3	Apulia, S Italy	Porto Badisco	*CRA, LBF*		■		Brandano *et al.*, (2008)
		Calcare di Castro	*coral*	■			Bosellini & Russo (1992)
4	Maiella, Italy	Bolognano	*Bry,LBF,CRA*		■	■	Vecsei & Sanders (1999); Mutti *et al.*, (1999)
5	Veneto, NE Italy	S Urbano/Casteluccio	*CRA,LBF*	■	■	■	Bassi & Nebelsick (2010)
		Castelgomberto	*coral*	■			Frost (1981)
6	Central Greece	Mesolouri	*coral, LBF*	■		■	Wieland-Schuster *et al.*, (2004)
7	S Spain	Alicante	*coral, LBF, (CRA)*	■			Geel (2000)
8	SW France	Aquitaine (various)	*coral, LBF*	■			Cahuzac & Chaix (1996)
9	Oman	Shuwayr & Warak	*coral, LBF*	■			Reuter *et al.*, (2008)

Table 7-1. Location and name of Oligocene formations referred to in text. Biotas include coralline red algae (CRA), large benthic foraminifera (LBF), bryozoans (Bry) and coral recorded in outcrops from the inner, mid- and outer platform environment.

PALAEOGEOGRAPHY AND PALAEOCLIMATE OF THE PALAEOGENE WESTERN TETHYS

Carbonates in the Mediterranean accumulated in both extensional regimes and compressive foreland settings, e.g., Malta Platform (Jongsma *et al.*, 1985) and Italian Apennines and Alps (Ricci Lucchi, 1986), respectively (Figure 7.5a). The switch from Mesozoic continental divergence of Africa from Adria and Eurasia to convergence since the Late Cretaceous (Dewey *et al.*,1973) resulted in the northward drift of the northern African margin to *circa* 27°N by the end Palaeogene (Schettino & Scotese, 2005), which is well within the limits of subtropical conditions suitable for coral growth during the Oligocene (Kiessling *et al.*, 2000). Increased restriction

of the Tethyan seaway, still connected to global oceans by the western and eastern gateways, culminated in the latter's closure by the Early Miocene (Stille *et al.*, 1996). Despite plate convergence, lithospheric extension persisted throughout the African foreland (Butler *et al.*, 1992) and carbonate platforms rimming the Ionian Basin (Central Mediterranean) continued to accumulate shallow marine carbonates free of continental siliciclastics (Pedley, 1998) (Figure 7.5b). In contrast, some foreland areas were invaded by siliciclastic sand such as the Veneto in northeast Italy (Bassi & Nebelsick, 2010), whereas drowned carbonate platforms like the Maiella platform (Vecsei & Sanders, 1999) and Mesohellenic platforms (Wieland-Schuster *et al.*, 2004) were draped with mud. Similarly, carbonate platforms fringing the North African coast of Libya (Imam & Galmed, 2000) and especially Tunisia were overwhelmed by continental clastics of the Fortuna Formation (Bishop, 1975).

Mediterranean carbonate ecosystems were affected by the decrease in global atmospheric partial pressure of carbon dioxide (pCO_2) (Pagani *et al.*, 2005) and the change from greenhouse to ice-house world. Throughout these changes in the Earth's climate, the distribution of climatically sensitive Cenozoic sediments has been assumed to be related to present-day humid or arid climatic zones that are roughly parallel to latitude (Parrish & Curtis, 1982). However, terrigenous successions within ±5˚ of palaeolatitude 30˚N bisecting the Early Cenozoic sub-tropical (>20˚C) western Tethys (Figure 7.5b) show significant climatic contrasts. Evaporites are observed in the early Eocene Faid Formation in Tunisia (Beavington-Penney *et al.*, 2005) up till the base Oligocene in subsurface Malta (Figure 7.6 and Figure 7.7) and northern Egypt (Rasmussen *et al.*, 1992). These are succeeded by fluvial sediments and silicified wood in the early Oligocene Jebel Qatrani Formation of Fayum in northern Egypt (Brown, 1982) whilst coal is observed in Spain (Cabrera & Saez, 1987) and paleosols over the Oligocene Malta Platform (Figure 7.6), suggesting the shift from arid Eocene to humid Oligocene climate over the same latitudes in the Mediterranean. The global Oligocene climate is also transitional to the cooler Neogene and is characterised by climatic shifts from relatively warm periods alternating with glacial episodes marked by hiatal events (Keller *et al.*, 1987).

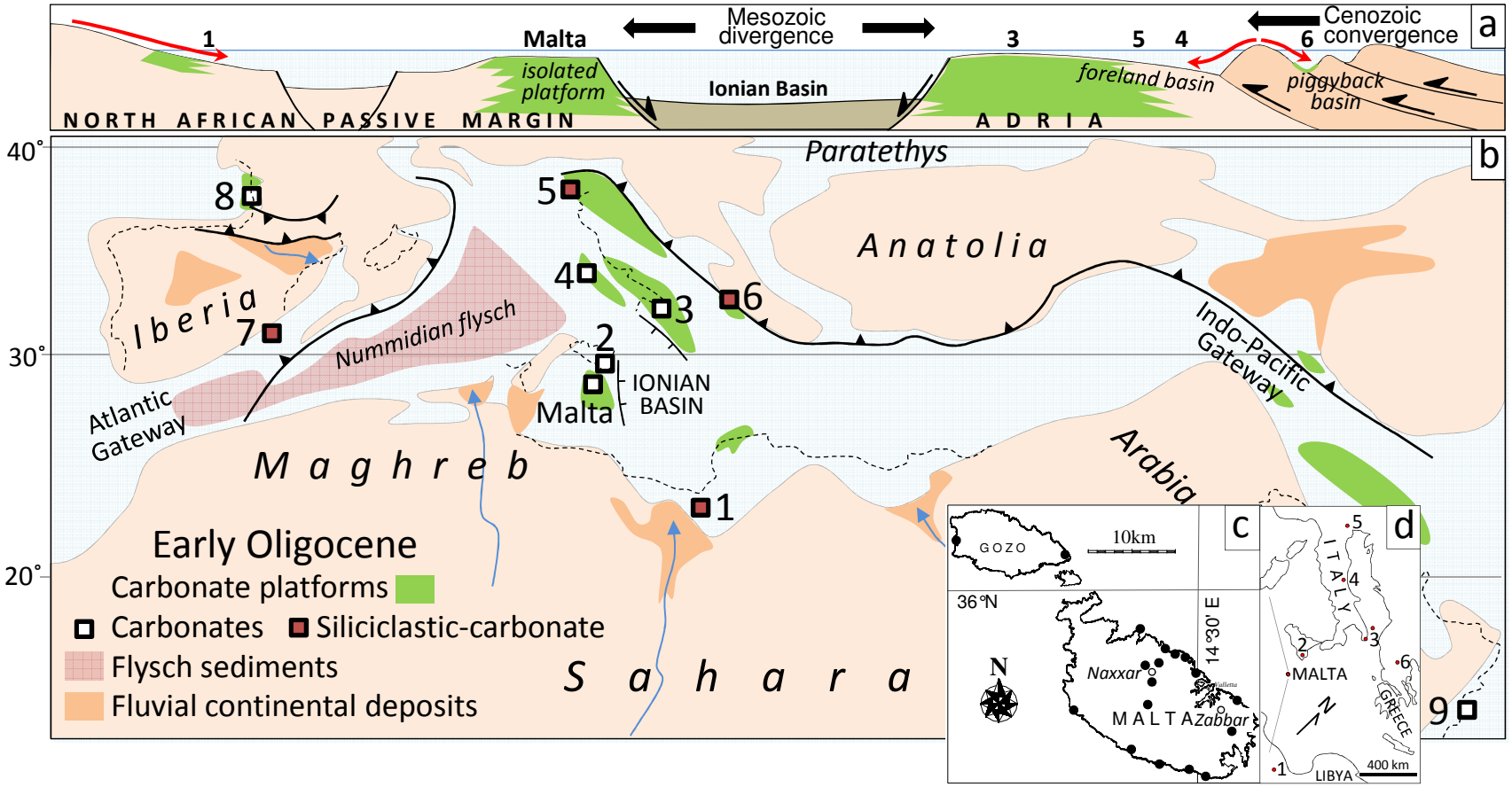

Figure 7.5. a. Simplified schematic SW-NE cross-section showing geotectonic setting of carbonate platforms in the Central Mediterranean. Red arrows show direction of siliciclastic influx in carbonate platforms (green); b. Early Oligocene Palaeogeography of the western Tethys (based on Meulenkamp & Sissingh, 2003). Numbered carbonate platforms are listed in Table 7-1; c. Field localities in the Maltese Islands and named wells; d. Present day location of localities in text.

Three main climatic phases reflected in changes in global $\delta^{18}O$ values (Figure 7.7) are observed during the Oligocene: (1) an early Oligocene stepwise increase in $\delta^{18}O$ values that reflects the development of an unipolar ice-sheet from *circa* 34 Ma (Oi-1 oxygen isotopic event in (Miller *et al.*, 1991) triggered by orbital forcing (Pälike *et al.*, 2006) and a drop in pCO_2 to below the threshold level 2.6 x PAL (preindustrial atmospheric level) for the growth of the Antarctic ice-sheet (DeConto *et al.*, 2008), (2) the lower pCO_2 concentration promoted sensitivity of the climate system to orbital forcing that triggered glacial episodes. Sustained pCO_2 drawdown (Pagani *et al.*, 2005) resulted in, (3) the development of an early sizeable Arctic ice-sheet (Mi-1 isotopic event) during the Oligo-Miocene boundary (~23 Ma).

These successive climatic episodes are expected to leave an imprint in the geological record regardless of geotectonic setting. However, Oligocene sediments in the North African hinterland have been mostly eroded along an extensive regional unconformity over the Sahara (Swezey, 2009), although a relatively complete high resolution stratigraphic record for the Mediterranean is preserved in the subtidal carbonate facies of the isolated Malta Platform which are used to infer links between facies and climate.

OLIGOCENE CARBONATE FACIES OF THE MALTA PLATFORM

The central location of the Malta Platform in the Mediterranean makes it suitably representative of facies associations and their stacking pattern in the region except for the influx of continental siliciclastics affecting continent-fringing carbonate platforms. The Oligocene carbonates comprise the entire Lower Coralline Limestone Formation of Malta were measured, logged and sampled at eighteen localities (Figure 7.5c). The formation is here sub-divided into seven facies associations deposited in environments ranging from the outer to inner platform, defined by the depth of the storm wave base (SWB) and the fair-weather wave base (FWWB) (Burchette & Wright, 1992), respectively. Each facies is classified by constituent grains and grouped into *facies associations* (FA) that reflect the type of carbonate ecosystem and the environmental parameters required for its survival. Nutrient level is a fundamental control on carbonate ecosystems and determines the development

of two carbonate grain associations *sensu* James (1997). The first is the *Photozoan association* characterised by carbonate ecosystems with increased species diversity and larger body size (Brasier, 1995a) that develop in nutrient-deficient (oligotrophic) water. Biotas rely on photosynthesising algal symbionts as a source of energy, e.g., Recent subtropical environments with coral growth (Hallock & Schlager, 1986). The *Heterozoan association* thrives in mesotrophic conditions where predation is the main source of food. Carbonate biotas comprise both light-dependent coralline red algae (CRA) and light-independent herbivorous and filter-feeding organisms (bryozoans, molluscs and echinoids), e.g., Recent CRA in mesotrophic water of Gulf of California (Halfar *et al.*, 2004). The two mutually exclusive ecosystems are recorded in the fossil grain associations of Meso- Cenozoic subtropical carbonate platform limestone (Carannante *et al.*, 1988; Pomar *et al.*, 2004). The facies associations of the Lower Coralline Limestone Formation are described and categorized by the trophic level of their carbonate ecosystem:

Globigerinid micrite facies association: FA I

Planktonic foraminifera, echinoids and bivalves are the main biotic constituents in the hemipelagic to pelagic carbonates and marly sediments that occur at the top of the Oligocene and persist to the early mid-Miocene (Globigerina Limestone Formation with inter-bedded phosphorite). The abundant micrite and the bryomol fauna suggest low energy outer platform sub-photic environments with high nutrient level that induced the precipitation of phosphate and favoured a heterozoan carbonate ecosystem.

Coralline red algal facies association: FA II

Two distinct facies are recognised in Malta: facies IIa consists of medium to coarse-grained sand of disarticulated geniculate red algae with miliolids and sporadic coral patch reefs. Facies IIb consists of crustose CRA (Sporolithoideae, Mesobesoideae and Mastophoroideae) that form thick beds of rhodolith (2 to 5 cm diameter) floatstone in a coarse-grained matrix of algal debris and echinoid bioclasts inter-bedded with rhodolith rudstone beds along a >50 m thick biostrome spread over >40

km. Corallines can be found in both oligotrophic and mesotrophic environments along a broad range of water depth: Geniculate CRA (facies IIa) are known to be abundant in high wave energy habitats from the intertidal zone to a depth of <20 m (Wray, 1977) whereas rhodoliths in modern transparent Mediterranean water are found at depths of 50 to 100 m (Carannante *et al.*, 1988), above the SWB. Nevertheless, facies IIb is analogous to the Chattian proximal mid-ramp rhodolith facies in NE Italy that thrived in a mesotrophic environment (Bassi & Nebelsick, 2010), 2010). The low light level restricted CRA growth to depth of <50 m where currents caused significant winnowing of fines and overturning of rhodoliths. Herbivory by echinoids was important to reduce fouling by fleshy algae (Steneck, 1986) and allowed the development of a heterozoan carbonate ecosystem.

Large benthic foraminifera (LBF) facies association: FA III:

The main rock constituents are dense accumulations of large Rotalid foraminifera (radius 2 to 5 mm) comprising Asterigerinoidea (mainly Lepidocyclinids) with subordinate Nummulitoidea. Cross-bedded grainstone to packstone beds of fragmented to highly fragmented LBF form two <5 km-wide, <30 m thick, NE-SW trending sand bodies in Malta (Pedley, 1987) and Gozo Island (Davies, 1976) that reflect pre-existing structural highs well above the FWWB (<5 m depth). The succeeding sediments (FA IIIb) are mainly micritic wackestone beds interfingered with thick packstone beds of large (5 to 9 cm diameter) discoidal *Lepidocyclina* and subordinate *Amphistegina* showing oblique to edgewise imbrication reflecting bidirectional currents above the SWB. Large benthic foraminifera host algal symbionts that require light to provide nourishment in oligotrophic conditions (Hallock, 1985) and their increased size was in response to the maximisation of light level by algal symbionts (Racey, 2001). Tropical foraminiferal facies with non-framework builders are classified within the Photozoan Association (Wilson & Vecsei, 2005). The clear water column in these environments allowed the large *Lepidocyclina* (facies IIb) to survive at depths of >40 m.

Coral limestone: FA IV

Coral facies are volumetrically small in Malta and form <10 m wide coral patch reefs that grade shoreward to <2 m thick tabular coral biostromes. Corals are sporadic in FA V and restricted to specific horizons within FA IIa above which they failed to keep up with sedimentation and were drowned and draped by algal debris. Poritid corals are common among the 21 coral genera of Atlantic and Indo-Pacific provenance (Chaix & Saint-Martin, 1994) and associated with *Borelis*, the benthic foraminifera found in unvegetated shoal environments (Brasier, 1995a). Corals host light-dependent symbionts that constrain growth within the euphotic zone <15 m depth (Schlager, 1981) and are classified within the photozoan association.

Imperforate foraminiferal wackestone/packstone: FA V

The lower two thirds of the Lower Coralline Limestone Formation is dominated by micrite, miliolid and soritid foraminifera that form thick, massive mudstone to packstone foraminiferal beds that include *Austrotrillina* and *Praerhapydionina* which are associated with shallow to very shallow inner platform environments (Geel, 2000). These are inter-bedded with thin beds of coral rudstone rich in the epiphytic foraminifera *Peneroplis* that suggest seagrass meadows. Subsurface sediments include thick marly sections that alternate with dolomitised limestone. The microbiotas, abundant micrite and lack of sedimentary structures suggest low energy, bioturbated, lagoonal-type of environment stabilised by extensive sea-grass meadows that were occasionally ripped up during storms, favouring coral colonisation. Although lagoonal environments may locally have high nutrient levels due to seagrass decay, the occurrence of coral suggests an overall oligotrophic environment that contributed to a photozoan grain association.

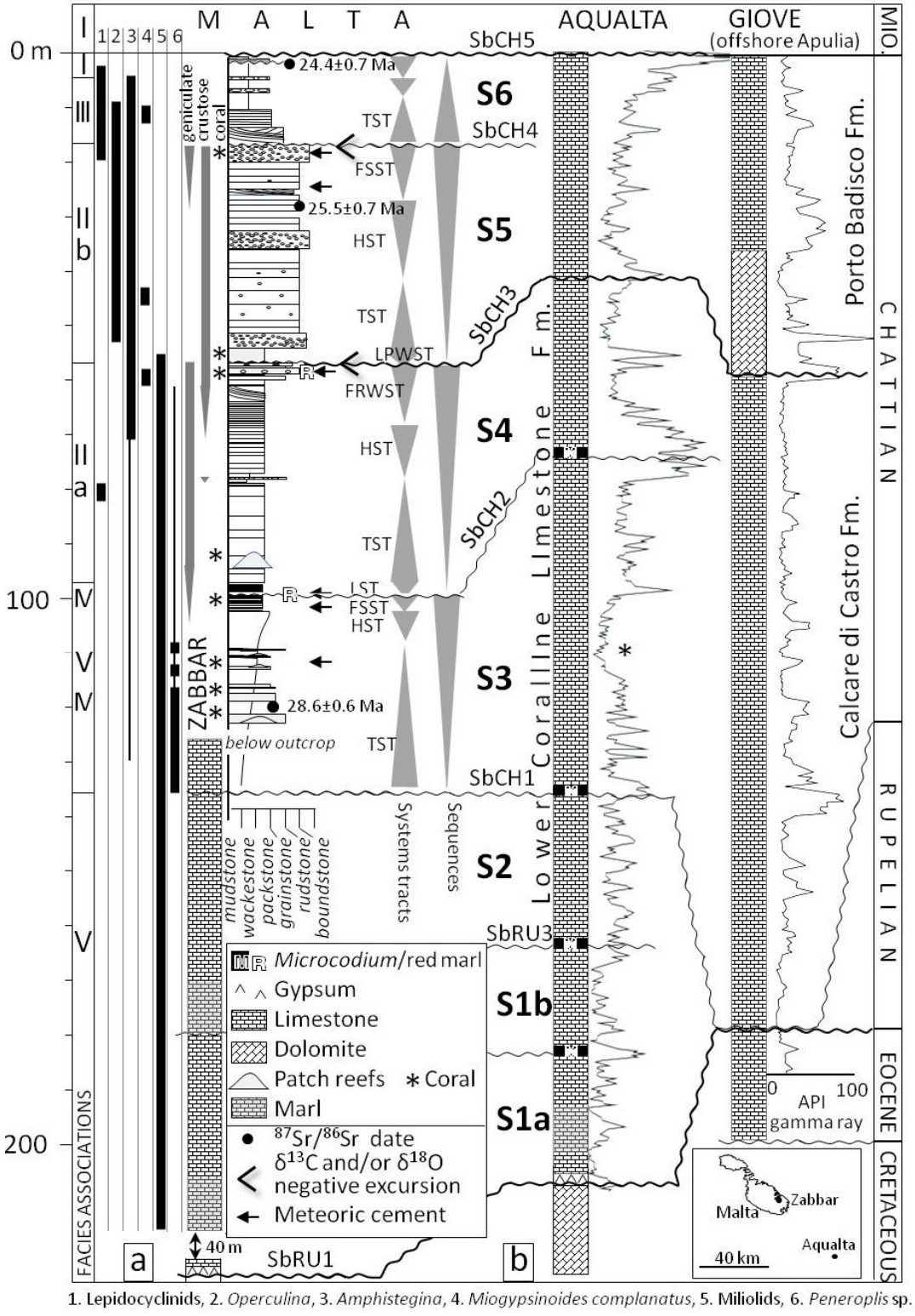

Figure 7.6. Stratigraphic distribution of biotas and correlation of well and outcrop data from Malta and Apulia (S Italy).

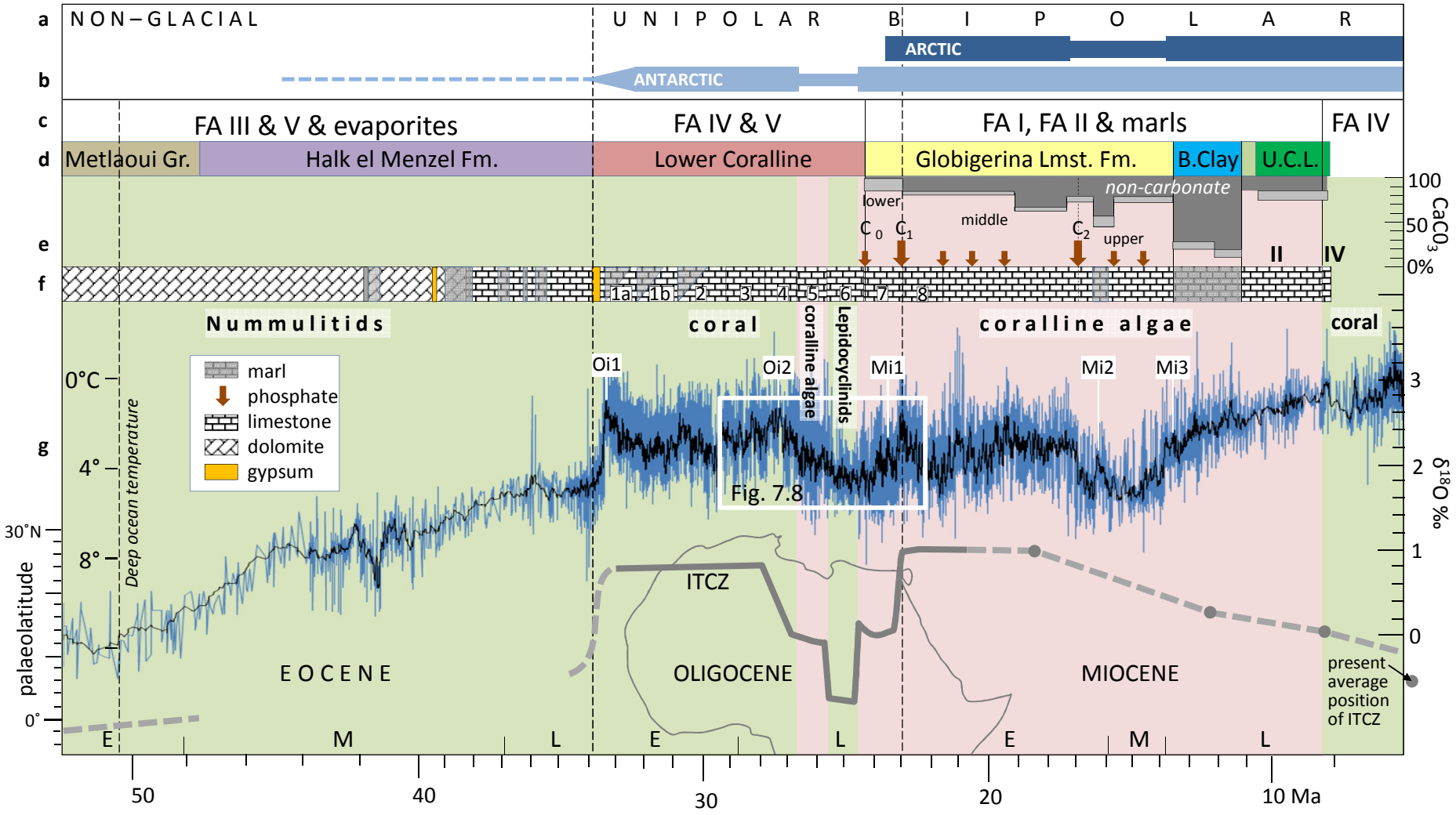

Figure 7.7 (caption on next page)

Figure 7.7. Shifts in carbonate ecosystems from photozoan (green background) to heterozoan (red background); a. Planetary ice-sheets; b. Temporal range of ice-sheet development; c. Facies associations; d. Formation names (Malta Platform); e. Miocene non-carbonate fraction (clay & quartz) in outer Malta Platform based on Wardell Armstrong (1996) and John *et al.*, (2003). Brown arrows mark phosphorite deposition; f. Lithology and sequences of the Lower Coralline Limestone Fm.; g. Global oxygen isotope values (blue curve) and average values (black curve) derived from deep-sea benthic foraminiferans (Zachos *et al.*, 2001) and Miller (1991) $\delta^{18}O$ isotopic events; Palaeolatitude of ITCZ (thick grey line). Oligocene based on this study. Dashed line (Miocene) based on Lyle *et al.* (2002), present position (Flohn,1981).

Peritidal facies association: FA VI

Exploratory subsurface wells record a metre-thick gypsum bed along the Eocene-Oligocene boundary in association with shallow carbonate facies which suggest deposition in sabkha type of environment. Further up, well cuttings include *Microcodium* at four levels of the formation (Figure 7.6) which is associated with caliche horizons indicative of palaeosols (Klappa, 1978). In outcrop, <1 m thick pale red, marly laminar beds inter-finger with beds of facies IV and II, interpreted as peritidal sediments influenced by the influx of reddish clay produced by the subaerial weathering of limestone (terra rossa).

Depositional sequences

The Maltese Oligocene carbonates comprise cyclic sediments with major unconformity surfaces that we interpret within the sequence stratigraphic framework *sensu* Van Wagoner *et al.* (1988) and Hunt & Tucker (1992) which predict four systems tracts in a depostional sequence produced along the sea-level curve. Aggradation in the highstand systems tract (HST) diminishes as the sequences terminate along the falling stage systems tract (FSST) or forced regressive wedge (FRWST) that culminate in maximum regression and erosion along the sequence boundary (Sb) which is recognised in subsurface wells (Figure 7.6) by either evaporite or *Microcodium* horizons (FA VI). In outcrop, the FSST shallow subtidal to peritidal carbonates show early aragonite dissolution and equant blocky calcite cement associated with the influence of meteoric water (Moore, 2001) and carbon ($\delta^{13}C$) and/or oxygen ($\delta^{18}O$) negative isotopic excursions of *circa* -2‰ recorded in published isotope data (Knoerich & Mutti, 2006) and unpublished studies (Gatt, 1992) of bulk rock samples. Negative isotopic excursions are associated with meteoric influence (Allan & Matthews, 1982) and contrast with the prevalently

marine isotopic signature in the rest of the outcrops. The succeeding lowstand prograding wedge systems tract (LPWST) tract is poorly preserved in carbonate platforms or entirely eroded by the ensuing transgressive systems tract (TST).

Studies of high-resolution $\delta^{18}O$ records from the Middle Eocene to Holocene have demonstrated that climate variations are consistent with the quasi-periodic orbital parameters (Wade & Pälike, 2004) and that Oligo-Miocene depositional sequences in gently subsiding settings are thought to reflect global third-order sea-level cycles with a periodicity of *circa* 1.2 Ma ((Abels *et al.*, 2005; Abels *et al.*, 2007; Lourens & Hilgen, 1997). Orbital forcing by cyclic obliquity minima triggered successive glacial events at 29.16, 27.91, 26.76 Ma (Wade & Pälike, 2004) and 25.5 Ma which are here correlated to sequence boundaries in the Malta Platform reflecting subaerial exposure over the Central Mediterranean (Figure 7.6). Astronomical dating is independently verified by LBF biostratigraphy based on the shallow benthic biozones (SBZ) of Cahuzac & Poignant (1997) and published (Föllmi *et al.*, 2008; Knoerich & Mutti, 2006) and unpublished (this thesis) strontium ($^{87}Sr/^{86}Sr$) values that are used to date sediments *sensu* Burke *et al.* (1982). The dated unconformity surfaces and sequences are calibrated to the time-scale of Gradstein *et al.* (2004).

The sequence boundaries sub-divide Maltese outcrops and subsurface sediments into seven depositional sequences (S1a to S6 in Figure 7.6 and Figure 7.9). The three Chattian (CH) sequences bounded by sequence boundaries SbCH2 to 5 matches the number of third-order cycles in the global sea-level chart of Haq *et al.* (1987) within supercycle TB1 (Figure 7.8). The sequences are correlated to carbonate platforms in the Central Mediterranean (Figure 7.9) on the basis of LBF biozones, major erosional surfaces and strontium isotope dating described in published stratigraphical and sedimentological studies (Table 7-1): cycles S3 and S4 in Malta and Central Mediterranean carbonates include the index foraminiferans *Nephrolepidina praemarginata* corresponding to the entire biozone SBZ22 whereas S5 to S6 cycles include *Miogypsinoides complanatus* in Malta (Felix, 1973), Apulia, Libya and Veneto (references in Table 7-1) which marks LBF biozone SBZ23 beginning at 27 Ma. Each depositional sequence is characterised by one or two carbonate facies associations shown in Table 7-2:

Localities recorded (M =Malta)	Depositional Sequence	*Peneroplis*	Miliolids	coral	Geniculate CRA	Crustose CRA	*Miogypsinoides*	*Amphistegina*	*Operculina*	Lepidocyclinids	echinoids	bryozoans	Planktonic foram.	FA
M, 4, 5	S7										●	●	●	I
M, 5	S6			○			○	○	●	●	○	○	○	III
M, 3,4,5	S5				○	●	○	○	○		○	○		II
M,1,2,3,5	S4		●	●	●	○				○	○			II, IV
M, 4, 5	S3	○	●	●										V, IV
M, 5	S2	○	●	○										V
M	S1b S1a		●										○	V
Depositional depth (m)			<10	<15	<20	50	<50		>15	5-40			>50	

Table 7-2. biota (●) dominant, (○) secondary. Range of depositional depth based on Geel (2000).

Figure 7.8. Chart showing climate-controlled Oligocene carbonate sedimentation over the Malta Platform through time and changing climatic conditions over North Africa, nutrient level in the Tethys, relative sea-level over Malta Platform (grey shading shows maximum palaeodepth parameter of biota, dashed line is average trend), facies in Malta outcrops (inverted black triangle indicates strontium isotope dating of stratigraphic level), average global oxygen isotope values (Zachos *et al.*, 2001), pCO_2 level (Pagani *et al.*, 2005), possible meridional position of ITCZ relative to size of Antarctic ice-sheet. Legend to lithological column is in Figure 7.9.

Figure 7.9. Correlation of carbonate platforms in the Central Mediterranean: (a) location map of sites, (b) lithology relative to LBF biozones by Cahuzac & Poignant (1997) showing synchronous changes from photozoan to heterozoan biota (green and red bars). Vertical lines are the sequence boundaries, circled numbers are the depositional sequences 3 to 8 that outcrop in Malta, (c) conceptual depositional model showing vertical changes in ecosystem trophic level in Oligocene Mediterranean carbonate platforms.

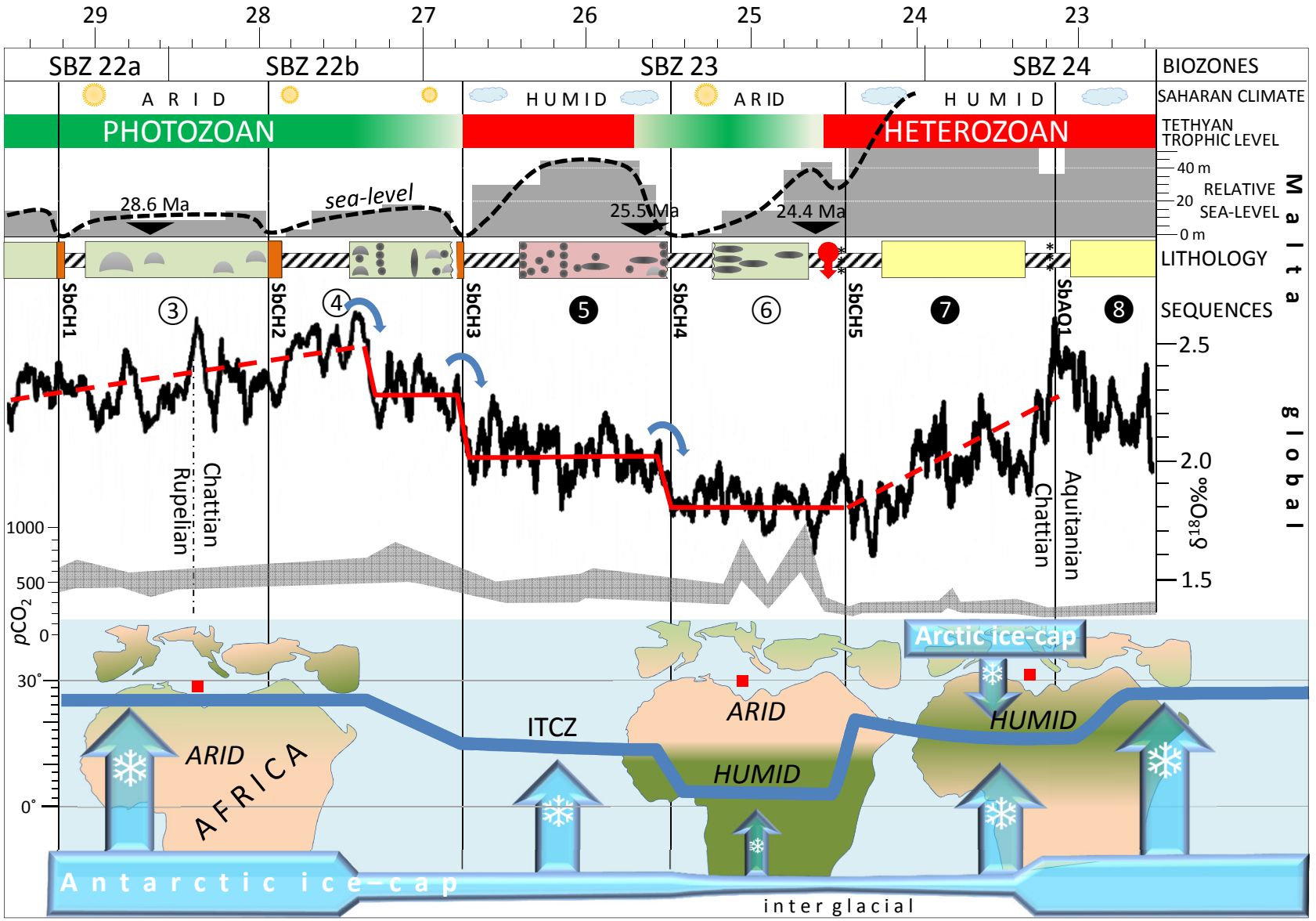

Figure 7.8. (*caption in previous page*)

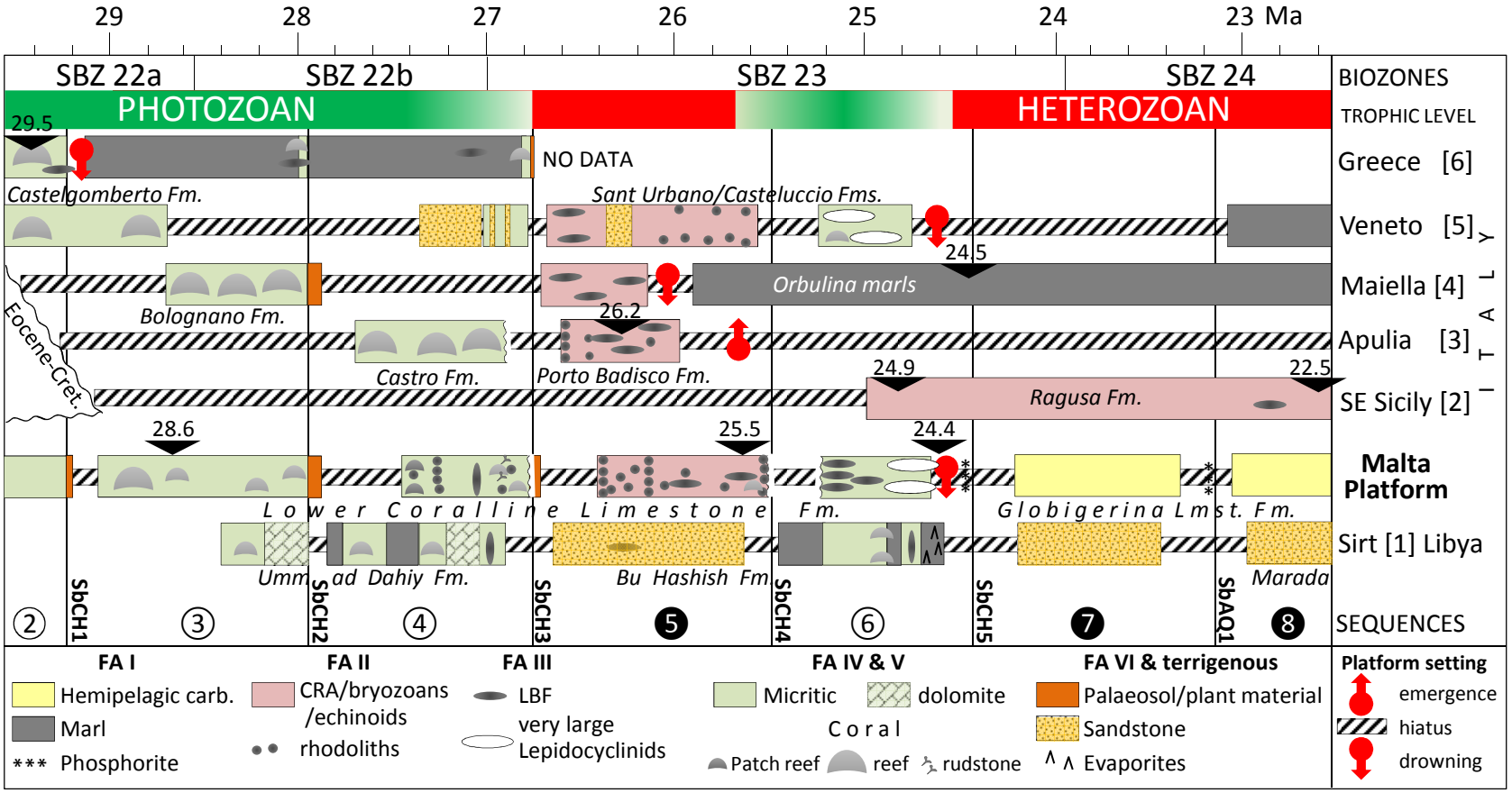

Figure 7.9 (*caption on page 30*)

S1a, S1b and S2: Data from subsurface Malta indicates miliolid wackestone with corals (FA V) whereas outcrops of the Castelgomberto Formation in Veneto (Italy) (Frost, 1981) and Greece (Wieland-Schuster *et al.*, 2004) include coral reef framework (FA IV) and miliolid packstone associated with lagoonal environment. Data from other localities is sparse since due to major depositional hiatuses separating the top Cretaceous from the Eocene/Oligocene in the Central Mediterranean (Jorry *et al.*, 2003; Antonelli *et al.*, 1988).

S3: This is a 'lagoonal' type of environment (FA V and FA IV) characterised by lime mud deposition along >60 km of the Malta Platform. The transgressive and highstand systems tracts include coral buildups whereas the lowstand phase was affected by intense bio-retexturing by burrowing organisms and sea-grass that destroyed sedimentary structures. More extensive coral buildups occur in Maiella. The bounding surfaces recorded in Maltese deep wells (Figure 7.6) reflect subaerial episodes (palaeosol) during the Rupelian (SbCH1) and the lowermost Chattian (SbCH2).

S4*:* In Malta, Apulia and Veneto transgressive sand sheets of geniculate CRA (FA IIa) invaded the lagoon-type of environment during the Rupelian/Chattian boundary global transgression (Coccioni *et al.*, 2008). Coral patch reefs colonised some early surfaces but failed to keep up with sea-level rise and drowned, becoming draped with CRA sand. Maximum flooding produced a horizon of reworked rhodoliths. Moderate coral growth was re-established during the lowstand systems tract in Malta, although the lateral and vertical extent of coral frameworks increases with distance from North Africa and culminates in reefal build-ups in Apulia (Bosellini, 2006). Surfaces with meteoric calcite cement (SbCH3) terminate the sequence in Malta whereas palaeosol are recorded in the Aqualta well.

S5: Extensive transgressive rhodolith pavements formed thick (>20 m) biostromes (facies IIb) that aggraded and prograded in the highstand systems tract in mid-platform environments of the Mediterranean (localities 3 to 5 in Table 7-1 and Malta). Shallower areas proximal to land received an influx of continental siliciclastic sand (localities 1 and 5). The Maiella Platform drowns although slow-

growing rhodoliths with *Operculina* persist in Malta, becoming locally capped by corals and LBF during the lowstand systems tract terminating cycle S5.

S6: the underlying SbCH4 and LST sediments in the Maltese Islands are eroded or modified by transgressive, <30 m-thick high energy LBF shoals comprising *Lepidocyclina* and *Amphistegina* (FA III) that developed leeward of palaeohighs whereas the windward side accumulated condensed (<3 m thick) and highly reworked LBF. Micrite content increases farther up the sequence as environments deepen to >40 m. Thick beds of dense accumulations of very large *Lepidocyclina* (>8 cm diameter) occur in Malta and Veneto (Bassi & Nebelsick, 2010) during sea-level highstand. The lowstand systems tract is entirely subtidal along the drowned Malta Platform (Gatt *et al.*, 2009) although increased current activity results in extensive hardgrounds along SbCH5, later capped by phosphorite (Gatt, 2005).

S7 to S9: the drowned Malta Platform is draped by >150 m of Miocene hemipelagic Globigerina Limestone Formation (FA I), interbedded with two ubiquitous phosphorite beds correlative to sequence boundaries produced by lowstand systems tracts. The shallow water equivalent in SE Sicily comprises CRA and bryozoans (Knoerich & Mutti, 2006).

DISCUSSION

The Lower Coralline Limestone record of the Malta Platform and correlative carbonates in the Central Mediterranean consist of alternating thick (>30 m) packages of photozoan and heterozoan grain associations: sequences 1 to 4 and sequence 6 consist of the Photozoan Association (FA IIa, III, IV and V) whereas sequences 5, 7 and 8 (FA I and IIb) are characterised by the Heterozoan Association. The shift in trophic level in carbonates is recognised throughout the inner to mid-platform environments irrespective of depositional setting, although the heterozoan grain association in carbonate platforms proximal to an orogen may be accompanied by continental quartz sand affecting the inner and mid-platform environment.

Sea-level change and nutrient level

Shifts in trophic level of carbonate ecosystems throughout the Phanerozoic are traditionally considered to be controlled by sea-level change that also determines the prevalence of either siliciclastic or carbonate depositional systems in subtropical epeiric seas, e.g., in the tectonically stable Arabian Plate marine transgressions trapped clastics in shoreline systems which permitted the expansion of photozoan carbonates along the shelf whereas during lowstands of sea-level, the clastic system expanded along the shelf favouring the heterozoan association as well as suppressing overall carbonate production (Sharland *et al.*, 2001). The same inverse relationship between sea-level and nutrient level is recorded in Early to mid-Miocene phosphorite beds of Malta (Globigerina Limestone) produced during eutrophic episodes associated with sea-level falls (Gruszczynski *et al.*, 2008) (Figure 7.7) as well as Quaternary glacial episodes associated with eutrophic conditions (Brasier, 1995b).

However, the inverse relationship breaks down in the western Tethys when sea-level and trophic level began to co-vary during the Oligocene Lower Coralline Limestone. In Malta, the photozoan association (corals) occur around regressive sequence boundaries SbCH3 and SbCH4 whereas during S5 cycle the carbonate platform could not keep up with sea-level rise which resulted in deepening and slow platform aggradation by heterozoan CRA and echinoids. In contrast, Oligocene carbonate ecosystems including those located just outside the Mediterranean in Atlantic France (Cahuzac & Chaix, 1996) and Oman (Reuter, *et al.*, 2008) remained invariably photozoan with coral buildups throughout the Chattian. This implies that the west Tethyan carbonate ecosystems were not tuned to global carbonate ecosystems.

The anomalous trophic level of carbonate ecosystems in the semi-enclosed Mediterranean Sea suggests that nutrient flux was overriding sea-level as the main depositional control. The increase in nutrient flux is caused by two mechanisms: (1) wind-driven currents that trigger upwelling of nutrient-rich deep water along western continental margins and the Equatorial belt (Parrish & Curtis, 1982) and climatic change. However, upwelling in the restricted present day Mediterranean Sea is patchy and <50% the intensity of upwelling along western continental margins

(Bakun & Agostini, 2001). But when the climate over a continent switches from arid to humid so that fluvial sedimentation (mainly quartz sand and clay) and dissolved nutrients (P, NO_3^-, NH^+, Fe) flowing into an adjacent sea can be expected to increase. This can result from the positioning of the tropical rain belt over a continent as happened during the Early Miocene over South Asia when increased rainfall and erosion became an important driver in Himalayan exhumation (Armstrong & Allen, 2011) which increased strontium level in the sea (Richter, *et al.*, 1992).

When the sea adjacent to the continent is restricted or semi-enclosed, nutrient flux becomes concentrated whereas in the oceans (e.g., Atlantic and Pacific) it remains mostly invariable because the soluble nutrient input is dispersed and diluted with distance from fluvial systems. In the case of the western Tethys, the restriction of the seaway favours the intensification of nutrient level whenever nutrient flux from the North African provenance increased. It is proposed that this happened intermittently during the Oligocene whereas the present day oligotrophic conditions over the Central Mediterranean Sea are maintained by low nutrient flux from the Sahara Desert region.

Climate-sediment interaction model

We hypothesise that the mechanism responsible for alternating photozoan (FA III to V) and heterozoan (FA II) ecosystems reflected in the rock record and the eventual demise of shallow marine carbonate ecosystems over the Malta Platform was controlled by meridional shifts in climatic belts over North Africa that produced episodes of either arid or humid climate over the Sahara. Land erosion is one of the ways in which continents and the climate system interact and results in increased nutrient flux to the sea. A climate-driven global pulse of erosion and exhumation across Eurasia, North America and Africa is also known to have started at the beginning of the Oligocene (Clift, 2010) which coincides with the positive shift in global $\delta^{18}O$ isotope values linked to the development of a sizeable Antarctic ice-sheet (Figure 7.7 b,g). Meridional shifts of climate belts over North Africa have been suggested by John *et al.*, (2003) to explain variations in the flux of fine siliciclastics

into the Maltese outer platform carbonate environment during the mid-Miocene (Figure 7.7e). However, increased deposition of clastic fines in basins that coincides with positive oxygen isotope excursions can be explained by lowstand progradation of fluvio-deltaic systems without the need for invoking climate change over North Africa. In this respect, and independently of siliciclastic flux, shallow marine carbonate ecosystems are more reliable and accurate indicators of climate change because they are sensitive to the level of biolimiting soluble nutrients produced by continental weathering. The interaction between the meridional position of climate belts and carbonate ecosystems has for the first time been modelled (Figure 7.10), backtracked to the Oligocene and compared to published works on the Miocene (Figure 7.7).

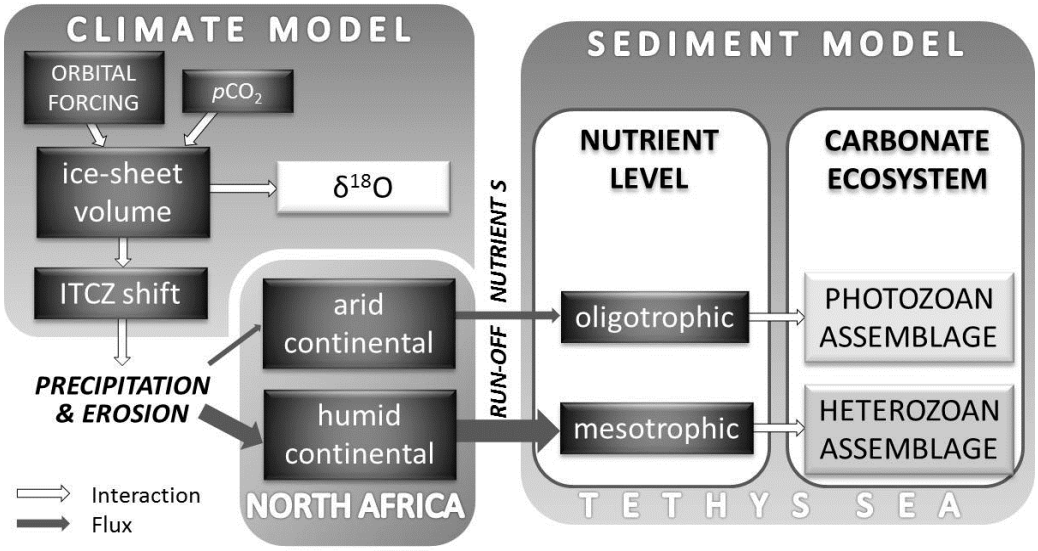

Figure 7.10. Climate-sediment interaction model.

Climate model: The stepwise decrease of global $\delta^{18}O$ by *circa* 0.3‰ reflects consecutive episodes of waning Antarctic ice-sheet during the Late Oligocene (Figures 7.7 and 7.9). These variations in ice-sheet volume controlled the pole-to-equator pressure gradient (Flohn, 1981) that affected the position of climatic belts in low latitude areas including the Inter-tropical Convergence Zone (ITCZ). The ITCZ is the thermal equator where the ascending branch of the Hadley cell forms a belt of intense precipitation. However, the position of the ITCZ is not constant through

time. The atmospheric pressure gradient is known to be steepened by the growth of a polar ice-sheet and results in significant meridional shift in the position of the Hadley cell away from the hemisphere with high latitude ice (Chiang & Bitz, 2005). Therefore, it can be assumed that in a unipolar ice-sheet world, the average position of the ITCZ is directly controlled by the relative size of the Antarctic ice-sheet. The northern shift of the ITCZ precipitation belt during the Oligocene, when the unipolar (Antarctic) ice-sheet had developed, is supported by atmospheric circulation modelling of Fluteau, *et al.* (1999) that demonstrates a palaeolatitude of 22°N for the northern front of the African monsoon, which coincides with the Oligocene North African margin.

Conditions changed during the evolution of bipolar ice-sheets from *circa* 25 Ma to the present as a result of the drop in pCO_2 to 1 x PAL (~280 p.p.m.v.) (DeConto, *et al.*, 2008). The initiation of the Arctic and Greenland ice-sheets is reflected in the positive shift of the oxygen isotopic values by 1.2‰, starting from 24 Ma to its peak at 23.7 Ma (the Mi-1 event) (Zachos, *et al.*, 2001). The development of the Northern Hemisphere ice-sheets during the Miocene had dampened and reversed its northward migration that had started from the early Oligocene. This factor is overlooked by John *et al.*, (2003) when they proposed the northward shift of the ITCZ during the Serravallian, which is in contrast to other studies (Lyle, *et al.*, 2002; Hyeong, *et al.*, 2005) that suggest the shift to increasingly lower latitudes throughout the Miocene to the present average latitude of 6˚N (Flohn, 1981) (figure 7.7).

Sediment model: Changes in carbonate ecosystems were synchronous to the meridional shifts of the ITCZ over the Sahara region of North Africa and triggered by glacial episodes that produced unconformities (sequence boundaries) along shallow marine Malta Platform facies. Increased precipitation over the Sahara resulted in an increase in continental run-off and nutrient flux to the semi-enclosed western Tethys. As a result, mesotrophic conditions favoured heterozoan biotas. The lower productivity of these ecosystems resulted in mostly subtidal rhodolith accumulations and overall deepening conditions. However, when the ITCZ shifted either north or south of the Sahara region, North Africa became relatively arid. The diminished continental run-off and decreased nutrient flux produced oligotrophic

conditions suitable for the growth of photozoan biotas. Carbonates in such favourable environment will aggrade rapidly and would remain close to sea-level until interrupted by subaerial exposure during falls in sea-level.

Climate control on the Cenozoic Mediterranean limestone record

The application of the climate-sediment interaction model results in four successive carbonate factories (shown in the conceptual model in Figure 7.9c) that produced the Tethyan Oligocene limestone record of the Central Mediterranean. The carbonate factories reflect three successive global cryospheric phases with subordinate climatic phases that controlled the meridional position of the ITCZ. Each carbonate factory was characterised by distinct skeletal assemblages and primary porosity with diagenetic potential for secondary porosity:

1. The Paleocene to Early Eocene greenhouse world: high concentrations of pCO_2, warm seas (Pearson, *et al.*, 2001) and $\delta^{18}O$ values below 2‰, suggest an ice-free world. Atmospheric circulation was nearly symmetrical and the ITCZ would be expected to be located close to the equator although Hoffmann, *et al.* (2003) suggest a location a few degrees south of the equator during the Cretaceous. The occurrence of Eocene evaporites in Tunisia and Malta suggests that North Africa experienced mostly arid conditions. Fluvial discharge into the western Tethys would have been moderate to low and oligotrophic conditions were favourable to photozoan biota. However greenhouse temperatures hindered the ability of some organisms to host obligate algal symbionts, namely coral which are susceptible to 'bleaching' by the loss of algal symbiont as a result of increased seawater temperature (Baker, *et al.*, 2004), whereas LBF can withstand higher summer temperatures without symbiont loss (Hallock, 2000).

The main carbonate factory comprised nummulitid shoals/banks. *Nummulites* thrived in the lower mid-latitudes during the warm Eocene whereas corals were pushed polewards to 46°N (Kiessling, 2002) and outside the Mediterranean region. Nummulitid LBF began to diversify and spread to vacant ecological niches following the end Cretaceous global extinctions (BouDagher-Fadel, 2008). From the

early Eocene, banks of *Nummulites* developed in Tunisia, Egypt, Croatia and Italy (Racey, 2001). The LBF banks grade laterally to restricted inner platform micritic facies with gastropods and bivalves where meteoric water dissolution-enhanced secondary porosity reaches 40% in Tunisia (Bishop, 1988). *Nummulites* were transported from inner to mid-platform settings (Beavington-Penney *et al.*, 2005) where secondary porosity was enhanced by preferential dolomitisation of micritic facies (Beavington-Penney *et al.*, 2008).

2. The Oligocene transitional world: marked by the development of a unipolar ice-sheet over Antarctica recorded by the Oi-1 oxygen isotopic event. Glacial episodes fine-tuned the overall Oligocene northward migration of the ITCZ, resulting in three climatic and depositional phases:

i. Rupelian to early Chattian: marked by a steady increase in average $\delta^{18}O$ values from >2‰, to 2.5‰ during sequences 1 to 3 and early part of 4. The high isotopic values reflect a period of Antarctic ice-sheet expansion and glacio-eustatic lowstand of sea-level. We speculate that the waxing of the ice-sheet would have pushed the ITCZ just north of the African continent. Consequently, the Sahara became arid whereas the Mediterranean was relatively humid, as confirmed by the occurrence of *Microcodium* which suggests humid conditions during subaerial episodes over the Maiella Platform (Vecsei & Sanders, 1999), SE Spain (Geel, 2000) and Malta. The influx of nutrients from subaerial parts of carbonate platforms was relatively small and generally depleted of phosphate relative to continental sources of nutrient flux which had decreased as a result of arid conditions over North Africa. Consequently, the Western Tethys became an oligotrophic sea which permitted photozoan biota (FA IV and V) to flourish.

The main carbonate factory comprised scleractinian corals that reached their zenith of generic diversity during the Early Oligocene (Bosellini & Perrin, 2008). Coral frameworks increased in size from isolated to coalescent patch reefs in northern Sirt Basin of Libya (Hladil *et al.*, 1991) and Malta, to large reefal constructions in north central Greece (Wieland-Schuster *et al.*, 2004) and in Italy along palaeoslopes of the Apulian Platform (Bosellini, 2006) and Veneto (Frost, 1981). Secondary porosity is

enhanced by the dissolution of the aragonite of scleractinian corals resulting in heterogeneous vertical and horizontal porosity. Oligocene coral build-ups grade laterally to thick inner platform accumulations of lime mud with imperforate foraminifera reported in Malta (FA V), SE Spain (Geel, 2000) and Apulia (Bosellini & Russo, 1992). The muddy sediments were baffled and stabilised by seagrass meadows encrusted by foraminiferal epibionts preserved in the rock record.

ii. Early to mid-Chattian 27.2 to 25.5 Ma: The successive stepwise decrease to average isotopic levels of 2.3 and 2‰ reflects further waning of the Antarctic ice-sheet. The dramatic decrease in $\delta^{18}O$ is reflected in the flooding of the Malta Platform during the global Early Chattian transgression (Coccioni *et al.*, 2008). Global warming would have caused the migration of the ITCZ to lower latitudes over North Africa resulting in humid conditions in the Sahara region and an increase in nutrient flux recorded by the change to heterozoan biota in sequences 4 and 5. Significantly, the timing of increased siliciclastic fluvial flux accompanied by increased Numidian Flysch in the Western Mediterranean coincided with sea-level highstands (Thomas *et al.*, 2010) whereas the carbonate depositional realm of the Central Mediterranean is marked by the deposition CRA sediments during this transgressive phase. The increased temperature and mesotrophic conditions had severely restricted coral growth and to some extent the LBF, but did not affect the eurythermal CRA.

The main carbonate factory during the mid-Chattian comprised coralline red algae. Widespread CRA sands followed by thick rhodalgal accumulations (FA II) occur over the Malta Platform, Apulia (Brandano *et al.*, 2008) and Central Italy (Mutti *et al.*, 1999). Coarse-grained CRA, echinoid and bryozoans formed cross-bedded high energy shoals along the inner platform in SE Sicily (Knoerich & Mutti, 2006) extending to the mid-platform environment in Malta and Veneto (Bassi & Nebelsick, 2010) as rhodolith floatstone facies where micrite content is <40%. Significantly, modern tropical CRA in mesotrophic conditions are associated with herbivorous echinoids and become the only algal group persisting in zones where herbivory is most intense (Steneck, 1986). Porosity is reduced due to micrite and epitaxial cementation on echinoids clasts. Potential carbonate reservoirs include Porto Badisco

Formation in offshore southern Italy (Figure 7.6), although wells are not yet producing.

iii. Late Chattian 25.5 to 24.6 Ma: A further stepwise decrease in $\delta^{18}O$ values starting from SbCH4 brought the isotopic values (average $\delta^{18}O$ = 1.9‰) down to a level comparable to that of the late Eocene. This episode of global warming coincides with a marked increase in pCO_2 (Figure 7.8) and the deposition of non-glacial sediments dated 26 to 24.5 Ma over diamictite and ice-rafted deposits in islands off the Antarctic Peninsula (Francis *et al.*, 2009). The waning of the Antarctic ice-sheet would have shifted the ITCZ to even lower latitudes close to the equator. The scenario would have been similar to that in the Eocene when North Africa was arid. The drier continental conditions would have reduced nutrient flux to the Mediterranean and brought the resurgence of photozoan biota. However, unlike the Rupelian, the LBF became the dominant biota in the Mediterranean whereas coral growth was very limited at this time, possibly as a result of high pCO_2 (Figure 7.8) which is unfavourable to hypercalcification of scleractinian coral.

The main carbonate factory by the end Chattian consisted of Lepidocyclinid shoals and banks. *Lepidocyclina* accompanied Late Eocene coral reef development in the Caribbean (Frost, 1977) but became the dominant carbonate grain in the Mediterranean at the end of the Oligocene when coral abundance began to decline. Fragmented lepidocyclinids with secondary nummulitids in inner platform settings formed high energy shoals in Malta. Lepidocyclinids appear to have expanded down-ramp from a reefal habitat during the Oligocene (Buxton & Pedley, 1989) and occupied mid- to outer platform setting when water transparency increased during oligotrophic phases. *Lepidocyclina* in these offshore banks thrived up to depths of 60 m (Bosellini *et al.*, 1987) and reached very large sizes (>8 cm diameter) in the upper Chattian sediments of Malta (FA III) and Veneto (Bassi & Nebelsick, 2010) (Figure 7.9). These potential reservoirs are the Oligocene equivalent of the productive Eocene nummulitic carbonate reservoirs in Tunisia and offshore Libya (Racey, 2001) but remain poorly investigated and have not been an exploration target.

3. Early Miocene ice-house world from 24.4 Ma: global cooling triggered the development of a bipolar ice-sheet world. The ITCZ began to migrate northwards as the Antarctic ice-sheet grew larger in the early Miocene, but its northward shift was suppressed by the synchronous development of the Arctic ice-sheet. This constrained the ITCZ over the Sahara and increased continental run-off and nutrient flux reaching the Mediterranean. As conditions became eutrophic, there was a strong regional shift to heterozoan biota.

The main carbonate factory comprised coralline red algae. Species diversity of CRA reached their peak by the early Miocene (Aguirre *et al.*, 2000) and rhodoliths became the global dominant carbonate facies by the mid-Miocene as a result of increased global trophic resources (Halfar & Mutti, 2005). Meso- to eutrophic conditions terminated shallow marine carbonate sedimentation and resulted in the precipitation of phosphorite along the drowned Malta Platform. Other Central Mediterranean platforms continued to be draped with hemipelagic carbonate muds (FA I). By the Early Miocene, corals had declined in the central Mediterranean and were limited to small monogeneric *Porites* coral build-ups in Italy (Brandano & Corda, 2002), diminishing further by the mid-Miocene (Pedley, 1996) when the Malta and Hyblean platforms began to be affected by clay sedimentation (Antonelli *et al.*, 1988).

CONCLUSIONS

Climatically-controlled environmental change in the Mediterranean resulted in significant variations in carbonate reservoir characteristics. Skeletal associations in the Central Mediterranean and global oxygen isotope values tend to change synchronously during the Oligocene and are used to infer meridional shifts in climate belts over North Africa (Figure 7.11). Low levels of precipitation and run-off over the Sahara resulted in the reduction of nutrient level which favoured scleractinian coral reefs with muddy back reef 'lagoons'. These facies alternate with heterozoan coralline red algae during an episode of increased nutrient level associated with humid climate and increased run-off over North Africa. The change in the type of ecosystem can be traced throughout carbonate platforms in the Mediterranean and can serve as a means of correlation. By the end Oligocene, LBF shoals dominated by

Lepidocyclina in Malta and NE Italy were deposited during an episode of dry climatic conditions over North Africa and increased temperature. The climate-based model presented in this study is the basis for regional correlation based on synchronous changes in carbonate ecosystems of the Mediterranean and serves as a predictive tool for carbonate facies and reservoir porosity.

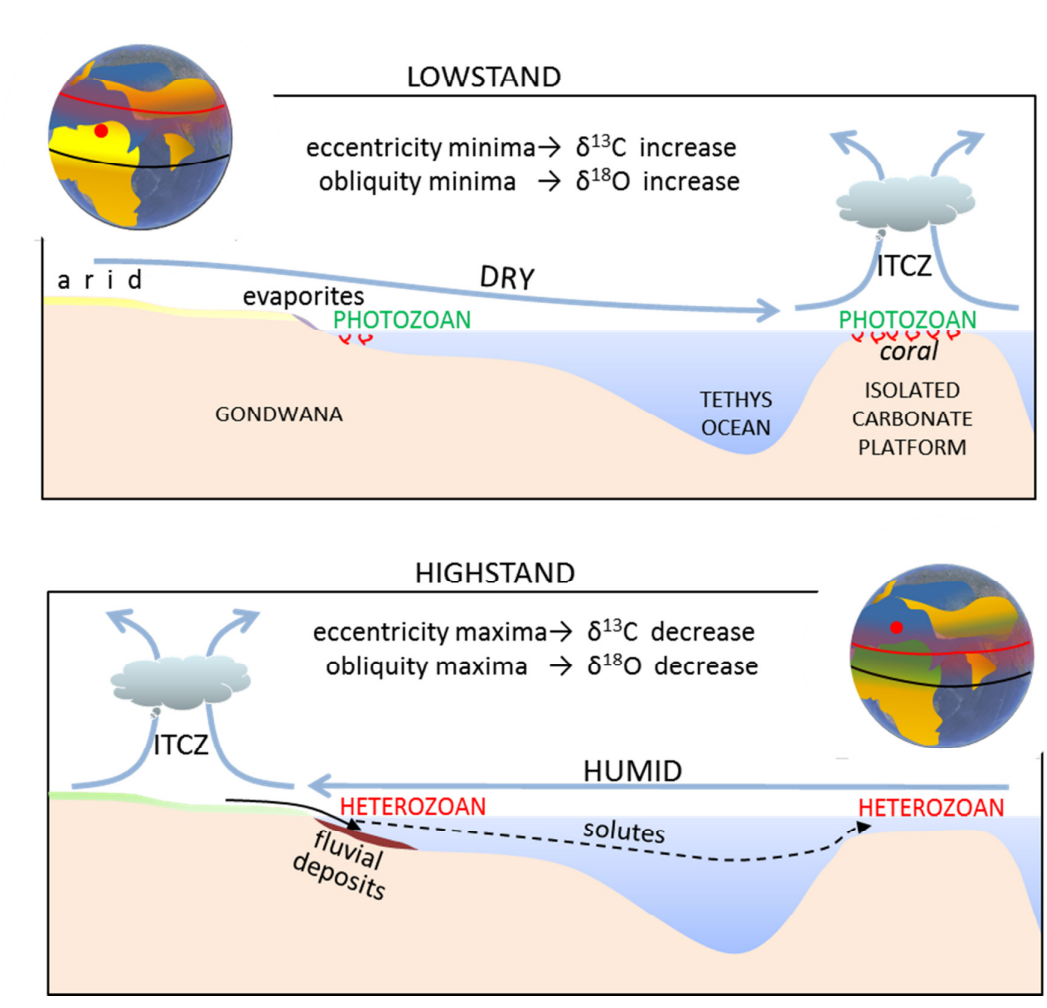

Figure 7.11. Model showing shifts in the ITCZ and its effect on North Africa and an isolated carbonate platform.

Chapter 8

Discussion and Conclusions

8.1 INTRODUCTION 346

8.2 KEY FINDINGS AND THEIR IMPLICATIONS 347

8.2.2 Stratigraphy 349

8.2.3 Carbonate platform model 349

8.2.4 Tectonics 351

8.3 TECTONOSTRATIGRAPHIC PLATFORM EVOLUTION 352

Tectonostratigraphic Phase 1 356

Tectonostratigraphic Phase 2 356

Tectonostratigraphic Phase 3 357

Tectonostratigraphic Phase 4 358

Tectonostratigraphic Phase 5 360

Tectonostratigraphic Phase 6 361

8.4 FUTURE WORK 361

8.5 CONCLUSIONS 362

8.1 INTRODUCTION

This thesis is the first detailed study of the entire Lower Coralline Limestone Formation. It provides many new findings and establishes a new lithostratigraphy for the Oligocene of the Maltese Islands. It also provides insights on the development of the Malta Platform from the Mesozoic to the Palaeogene and the impact of climate on lithology.

Chapters 3, 5 and 7 include discussion sections on research results. This chapter provides a broader discussion inclusive of research results of all preceding chapters placed within a framework embraces tectonostratigraphy, palaeoclimate, carbonate biotas and sequence stratigraphy. This comprehensive approach offers a more realistic understanding of the complex nature of the internal structures and the bioclastic and framework sediments of carbonate platforms which are sensitive to environmental changes at the physical and chemical level.

This final chapter begins with a list of the key findings of this thesis discussed in the respective chapters. The objectives of this chapter are: (1) to discuss the new findings and interpretations and their implications to what is already published on the Malta Platform and, (2) to present the new findings and their interpretations in the context of the tectonostratigraphic development of the Malta Platform.

8.2 KEY FINDINGS AND THEIR IMPLICATIONS

The key findings related to the Palaeogene carbonates of the Malta Platform are summarised in Table 8-1 under four headings discussed in the respective chapters.

	Key findings	chapter
Facies	The 7 carbonate facies associations make up a photozoan-heterozoan-photozoan carbonate grain association triplet that reflects the response of carbonate ecosystems to changing nutrient level, water depth and hydrodynamic energy level.	**3**
Stratigraphy	The Malta Platform aggraded >4 km of carbonates throughout the Mesozoic, terminated by Late Cretaceous to Palaeocene depositional hiatuses, after which Oligocene sediments began to prograde towards the basin/s. Oligocene carbonates are interpreted within a sequence stratigraphic framework that reflect the rhythmic imprint of orbital forcing at the Milankovitch scale along the 1.2 Ma long obliquity cycle and 400 kyr long eccentricity cycle scale.	**4, 5,6**
Tectonics	The syntectonic development of the Malta Platform carbonates was controlled by passive margin subsidence and lithospheric extension. Sedimentation was affected by prolonged depositional hiatuses and differential extension which created 3 geotectonic zones that comprise small (<10 km-wide) basins in the platform interior, a large (>50 km) intra-platform polyphase basin and large listric faults that form the platform escarpment.	**6**
Palaeoclimate	The photozoan-heterozoan-photozoan triplet of grain associations can be correlated across Central Mediterranean carbonate platforms, invoking a regional control. The sedimentary triplet reflects climate change on the North African continent which controlled nutrient flux into the Western Tethys and impacted the trophic level of the carbonate ecosystems. Consequently there is a close association between carbonate ecosystems in the Mediterranean and the waxing and waning of Antarctic polar ice-sheets reflected in stepwise shifts in oxygen isotope ratio for deep sea cores.	**3, 7**

Table 8-1. Key findings of this thesis.

The implications of the new findings are the following:

1. It is suggested that the Malta Platform developed as an isolated platform in a pericratonic setting where siliciclastics are absent. The entire suite of facies associated with isolated platforms is present: marginal escarpment, talus slope and winnowed slope (Read, 1985). Isolated platforms usually evolve along passive margins and undergo faulting that creates intra-platform basins. The carbonate platform aggraded since the Mesozoic and started to prograde during the Oligocene.
2. A major control on sedimentation in isolated platforms is the difference between windward and leeward margins of the isolated platform. Evidence of shallowing of the carbonate platform towards west Malta (windward side) is persistent in a number of facies: the west-facing foresets in the cross-bedded shoal deposits of FA III, reworked and condensed LBF (facies IIIa in localities 3 and 9) accumulated along the Western Malta Palaeohigh (WMP). Similarly, the high energy accumulations of *Scutella* (FA I) in western Malta and eastern Gozo environments suggest relatively shallower environments.
3. Isolated carbonate platforms along sinking passive margins have to keep up with sea-level rise. A reduction in carbonate productivity may result in platform drowning (Schlager, 1981). The decline or termination of the carbonate factory can result from a shift in trophic level of the carbonate ecosystem. The occurrence of phosphorite that caps the topmost Lower Coralline Limestone Formation along the drowning surface suggests conditions that became unfavourable for shallow marine carbonate production resulting in the drowning of the Malta Platform at the end Oligocene.

The implications of the key findings offer new perspectives on what is already published on the Lower Coralline Limestone and the Malta Platform. Some of these findings contrast with conclusions found in previous works and are listed as follows:

8.2.2 Stratigraphy

Previous works have sub-divided the Lower Coralline Limestone Formation into facies-based stratigraphical units (e.g., Pedley, 1978; Pedley, 1978; Bennett, 1980; Pedley, 1993a; Pedley, 1993b). However, these studies do not encompass the entire stratigraphy of both subsurface and outcrops of the Lower Coralline Limestone Formation (Gatt, 2010). Published works exclude any reference to facies association VI whereas facies association IIb is considered to be far thinner than it actually is in outcrop. A new lithostratigraphy of the entire Lower Coralline Limestone Formation is presented here based on a sequence stratigraphic and facies approach discussed in chapters 3 and 5 (Table 8-2).

The prograding complexes along the eastern escarpments of the Malta Platform have been interpreted in hydrocarbon exploration reports as Nummulitic banks (TGS-NOPEC, 2003) and considered as exploration targets similar to the Eocene carbonate reservoirs in Tunisia (Beavington-Penney *et al.*, 2008). However, the geometry of these prograding complexes is similar to prograding clinoforms composed of coralline red algae (rhodoliths) seen in outcrop and nearby seismic lines which are of Oligocene age.

8.2.3 Carbonate platform model

Previous works based on field studies at the scale of the Maltese Islands (<40 km) (e.g., Buxton & Pedley, 1989; Antonelli *et al.*, 1988; Brandano *et al.*, 2009) suggest that the Lower Coralline Limestone Formation was deposited along a carbonate ramp. Carbonate ramps are considered to have a low-gradient slope (<1˚) (Burchette & Wright, 1992). However, the occurrence of condensed carbonates (facies 3a in sequence 6), the two contemporaneous bioclastic shoals (facies III b) located >30 km apart in eastern Malta (localities G to 12) and western Gozo (e.g., locality H) respectively, and significant lateral variations in thickness of sequences 4 and 5 (see chapters 5) is not typical of carbonate ramps facies distribution and long profile.

It is suggested that the carbonate platform in the region of the Maltese Islands had a fault-block-controlled topography *sensu* Bosence (2005) as discussed in chapter 6. The carbonate platform did not develop into a carbonate ramp *sensu* Read (1985) possibly because the termination of shallow marine sedimentation and drowning by the end Oligocene occurred before the long-profile could be filled to a gradient of <1˚.

<table>
<tr><th>Sequence</th><th>Sequence boundaries</th><th>this thesis</th><th>Maximum thickness (metres)</th><th>Facies Associations</th><th>Pedley (1978)</th><th colspan="2">Bennett (1980)</th></tr>
<tr><td></td><td>SbCH5</td><td>Globigerina limestone</td><td colspan="5"></td></tr>
<tr><td rowspan="2">6</td><td rowspan="2">SbCH4</td><td>Mara Mbr.</td><td>10</td><td>I, III</td><td colspan="3">Mara Member</td></tr>
<tr><td>Xlendi Mbr.</td><td>30</td><td>III</td><td colspan="3">Xlendi Member</td></tr>
<tr><td rowspan="2">5</td><td rowspan="2">SbCH3</td><td rowspan="2">Miġra Ferħa[1] Member</td><td rowspan="2">60</td><td rowspan="2">IIb</td><td colspan="3">unnamed/unrecorded</td></tr>
<tr><td></td><td colspan="2">Mosta Bed</td></tr>
<tr><td rowspan="3">4</td><td rowspan="3">SbCH2</td><td>Mosta Mbr.[2]</td><td>6</td><td>II,IV, VI</td><td rowspan="3">Attard Mbr.</td><td colspan="2">Wied Incita Bed</td></tr>
<tr><td rowspan="2">Attard Member</td><td rowspan="2">24</td><td rowspan="2">IIa</td><td rowspan="2">Attard Mbr.</td><td rowspan="2">Wied Babu Bed</td></tr>
<tr><td></td></tr>
<tr><td rowspan="2">3</td><td rowspan="2">SbCH1</td><td rowspan="2">Magħlaq Member</td><td>10</td><td>V, VI</td><td colspan="3">Maghlak Member</td></tr>
<tr><td>30</td><td>V</td><td colspan="3" rowspan="3">unnamed</td></tr>
<tr><td>2</td><td>SbRU3</td><td>Għar Lapsi Member[3]</td><td>80</td><td>V</td></tr>
<tr><td>1b</td><td>SbRU2</td><td rowspan="2">Żabbar Member[3]</td><td rowspan="2">200</td><td rowspan="2">V</td></tr>
<tr><td>1a</td><td>SbRU1</td></tr>
</table>

Table 8-2. New lithostratigraphy of the Lower Coralline Limestone Formation compared with previous stratigraphy (grey: unrecorded). The new members are named after type localities where the depositional sequences are exposed and accessible or based on core data: [1] Miġra Ferħa Member type locality is found in locality 3; [2] Mosta Member type locality is in locality 5; [3] based on core data from three onshore wells.

8.2.4 Tectonics

Dart *et al.* (1993) describe Oligocene strata of the Maltese Islands as having parallel stratal geometry without fault-related thickness changes. This interpretation is inaccurate since depositional sequences in the Lower Coralline Limestone Formation show significant lateral changes in thickness (see chapter 5). In fact, the tectonic movements of the Palaeogene have had a significant effect on Neogene tectonism in the region of the Maltese Islands.

Bishop & Debono (1996) have produced facies maps of the Malta Platform that show a large intra-platform basin located just offshore of eastern Malta since the Mesozoic. However, the main Meso-Cenozoic intra-platform basin (CMPB) is actually located farther east along the eastern margin of the Aqualta well as discussed in chapter 6. A lithofacies map of the Cretaceous has been constructed and compared to previous works which misplaced the actual position of the main basin (figure 8.1).

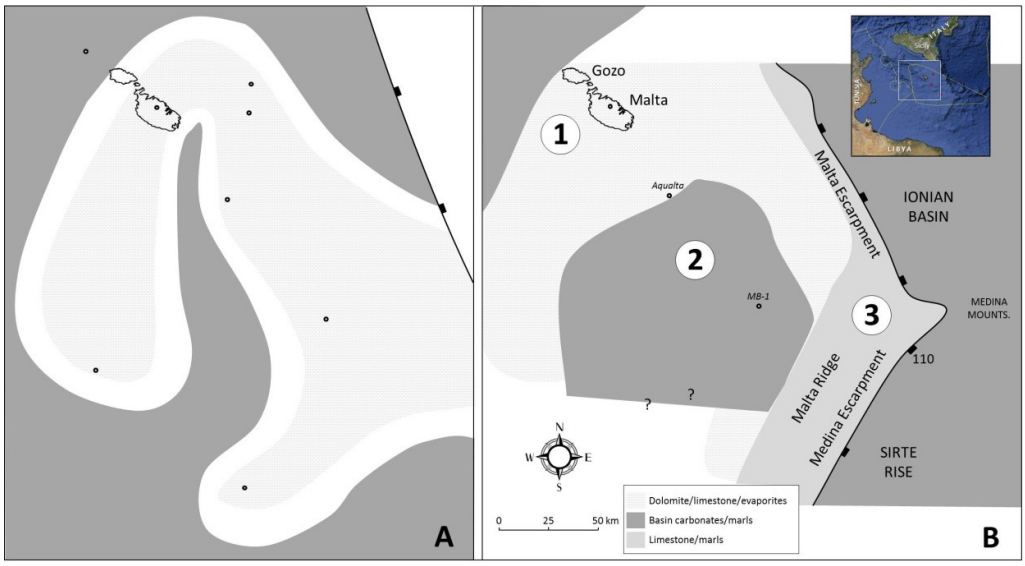

Figure 8.1. Lithofacies maps for the Cretaceous: A. Published lithofacies map of Bishop & Debono (1996) compared to, B. Lithofacies map in this thesis. The position of the basin Central Malta Platform Basin is to the east of Aqualta well in map B and extends farther west south of the well.

8.3 TECTONOSTRATIGRAPHIC PLATFORM EVOLUTION

The findings of the preceding chapters are synthesized and used to construct a simplified model of the Malta Platform in Figure 8.2. The three geotectonic zones observed in the Malta Platform are similar to the structure of the Sirt Rise along the Ionian Basin described by Fiduk (2009). The two areas are compared in Figure 8.3. A number of similarities and contrasts stand out:

- The narrow Malta Ridge is analogous to the buried Cyrenaica Ridge found at the margin of the Sirt Embayment (Sirte Rise).
- Megasequence II in the Malta Platform is twice as thick as the equivalent sediments along the Sirt Rise. This reflects the ability of the Malta Platform carbonates to aggrade and remain close to sea-level during the Cretaceous global highstand of sea-level.
- The platform interior zone is marked by a succession of palaeohighs similar to those found within 200 km offshore the Libyan coast. The highest palaeohigh is the one next to the Sirt Trough which is equivalent to the Aqualta Palaeohigh that is also adjacent to the Central Malta Platform Basin (CMPB).

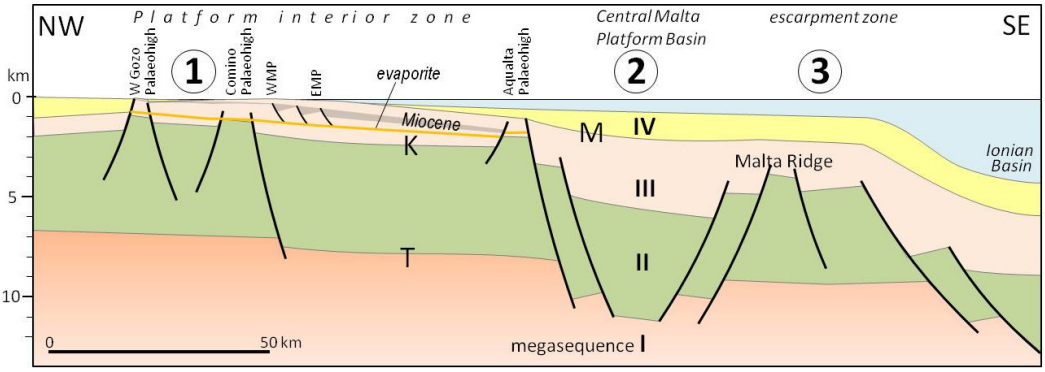

Figure 8.2. Generalized NW to SE cross-section of the Malta Platform showing the three geotectonic zones mapped in Figure 8.1. The T-, K- and M-reflectors subdivide the succession into megasequences: I (Triassic and earlier), II (Jurassic to Palaeocene), III (Eocene to end Miocene) and IV (Plio-Quaternary).

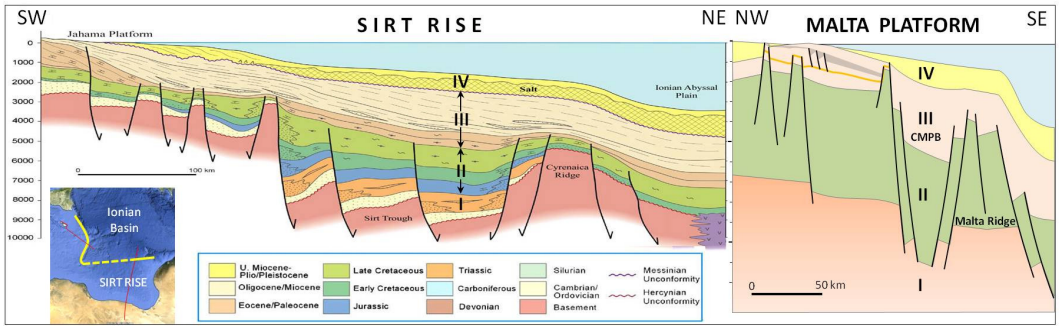

Figure 8.3. Generalised cross-section across the Sirt Rise (from Fiduk, 2009) with megasequences I to IV equivalent to the Malta Platform compared to cross-section of Malta Platform shown in Figure 8.2 (same scale). Map shows cross section lines. Thick yellow line marks the Malta to Cyrenaica Ridge.

The development of the Malta Platform is summarised in six tectonostratigraphic phases represented in a chronostratigraphic chart along with main isotopic and climatic events (Figure 8.4). Each phase comprises a suite of carbonate sediments separated by major drowning surfaces followed by long (>1 Ma) depositional hiatuses, sometimes with several missing large benthic foraminiferal biozones (SBZ) (see chapters 5 and 6). These hiatal surfaces produce strong seismic reflectors (Table 8-3). Each MTSP is characterised by a change in tectonic regime and particular climatic conditions that are reflected in the global oxygen isotope curve.

Mega-sequence	Tectono-stratigraphic phase	Top seismic reflector	General trend of global $\delta^{18}O$ values	Characteristic depositional environment
IV	T6	seabed	rapid increase	hemipelagic carbonates/marl
III	T5	M	increase	hemipelagic carbonates/marl
	T4	A	pos. excursion & stepwise shifts	shallow marine carbonates
	T3	B	increase	long hiatus/marls/carbonates
II	T2	K, P, (C)	decrease	shallow marine carbonates
I	T1	T		shallow marine carb./evaporites

Table 8-3. Stratigraphic subdivisions of the Malta Platform.

Tectonostratigraphic chart of the Malta Platform

Legend

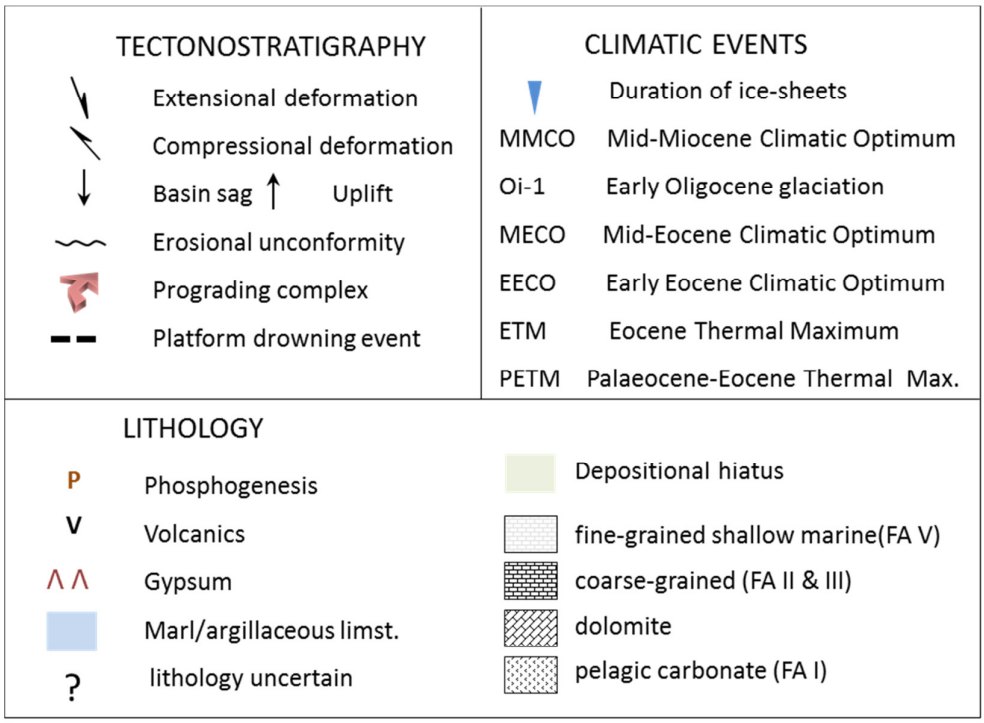

Figure 8.4. Legend to the tectonostratigraphic chart (*next page*) showing stratigraphic development with main tectonic deformations affected the three zones of the Malta Platform. The platform interior stratigraphy and biostratigraphy is derived from outcrops and exploratory wells whereas the escarpment zone lithology is from dredged samples (Scandone *et al.*, 1981). The LBF biozones (SBZ) for the Eocene and Oligocene are shown. The MTSP column comprises the six tectonostratigraphic phases (T1 to T6) of the Malta Platform described in text. The oxygen isotope curve is from Zachos *et al.* (2008).

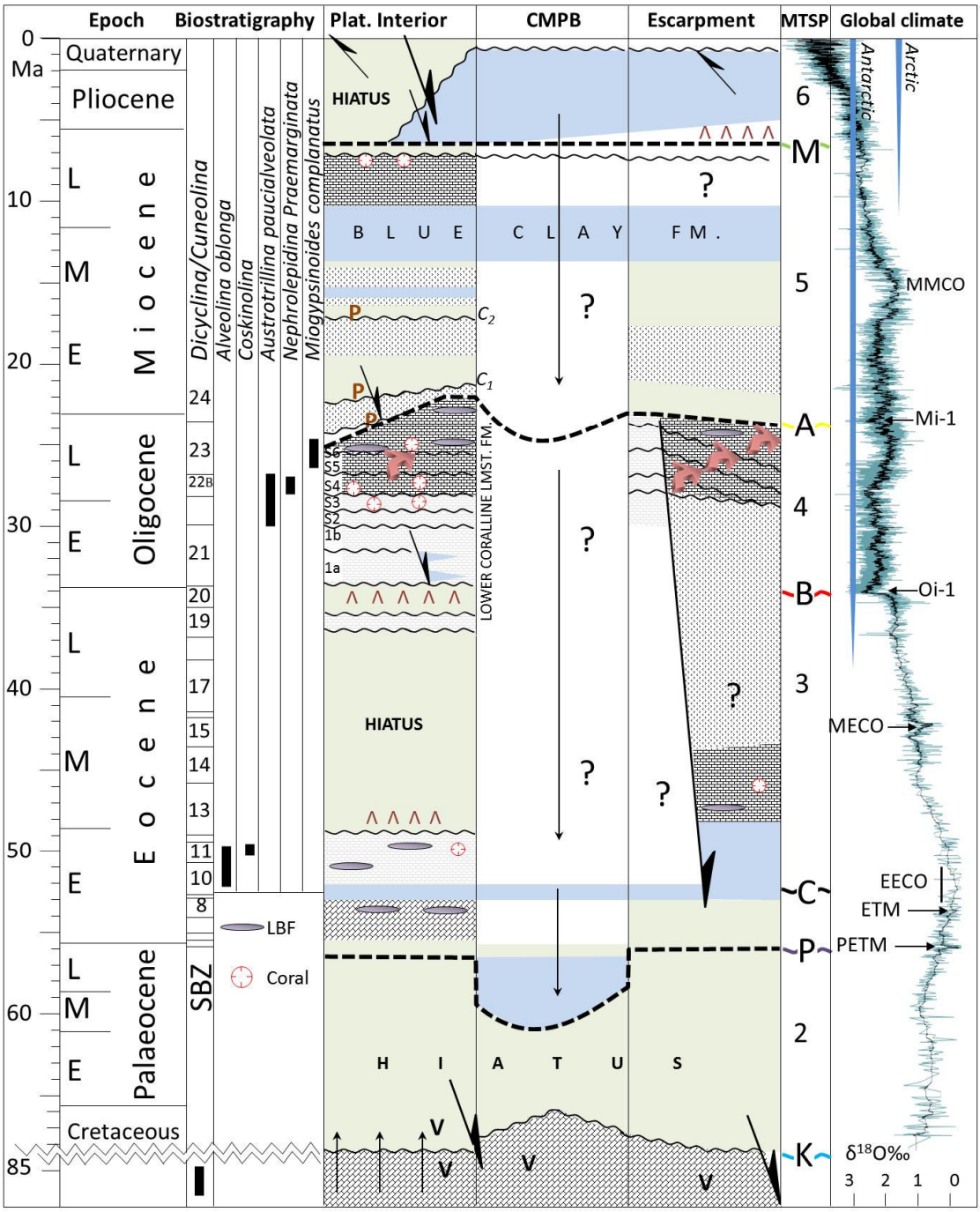

Figure 8.4 (caption and legend on previous page) **Tectonostratigraphic chart of the Malta Platform**

Description of the Malta tectonostratigraphic phases (MTSP):

Tectonostratigraphic Phase	megasequence	age	Top reflector
T1	**I**	Triassic	T-reflector

Malta Platform: Early failed rifting along the Central Malta Platform Basin and rifting along the opening Ionian Basin. The Malta Platform becomes part of the North African passive margin of Gondwana.

Tethys: Regional rifting from Norian to Early Jurassic in the Adria carbonate platform in Italy (Bosellini, 2004) and Ragusa Basin in Sicily which resulted in the accumulation of the Streppenosa Shales (Antonelli *et al.*, 1988).

Tectonostratigraphic Phase	megasequence	age	Top reflector
T2	**II**	Jurassic-Palaeocene	K-reflector

Malta Platform: High rate of shallow marine carbonate aggradation (>4 km) over the Malta Platform as global sea-level rises. Campanian to Palaeocene sediments missing over the platform interior zone although they accumulate in structural lows such as the CMPB and the hanging walls of the faulted escarpment zone. Tectonic uplift is the likely cause for extensive erosion or lack of deposition over the platform interior.

Tethys: Many carbonate platforms begin to drown during the Jurassic (e.g., Panormide and Trapanese platforms). By the Late Cretaceous compressive deformations in the Mediterranean (Guiraud & Bosworth, 1999) cause uplift in Tunisia (Jorry *et al.*, 2003).

Palaeoclimate: The global oxygen isotope curve shows declining values that culminate in the Palaeocene thermal maximum which coincide with the deposition of the El Haria Shales in Tunisia.

Tectonostratigraphic Phase	megasequence	age	Top reflector
T3	**III**	Eocene	B-reflector

Malta Platform: the extensional regime along the passive margin produces horst structures (Comino and West Malta Palaeohigh, West Gozo Palaeohigh and Aqualta Palaeohigh) over the platform interior zone during the Late Cretaceous to Palaeocene depositional hiatus. Palaeogene sediments begin to fill the intervening basins and unevenly drape over the structured surface. Early Eocene clayey sediments are missing or very thin (C-reflector merges with K-reflector) over the horsts which become periodically subaerial, eroded and capped with evaporites. Backstepping reefs along the margins of the Aqualta Palaeohigh suggest late Early Eocene sea-level rise followed by falling sea-level during the beginning of the Mid-Eocene characterised by non-deposition and widespread evaporites in the platform interior zone. In the escarpment zone, Eocene sediments aggrade and onlap an erosional surface along the upper old (Mesozoic) escarpment and then onlap new fault-controlled escarpment walls along the Medina Escarpment.

Tethys: In Tunisia, the nummulite-dominated Metlaoui Group is deposited along a carbonate ramp with the outer ramps accumulating the 50 to 300 m thick Bou Dabbous Formation source rocks (Klett, 2001). These are equivalent to the relatively thin Ypresian clays along the Malta Platform.

Palaeoclimate: The global oxygen isotope values show a rising trend, punctuated by the Mid-Eocene climatic optimum (MECO). Early Eocene (Ypresian) marls and clays suggest marine transgression associated with the Early Eocene thermal maximum (ETM) and climatic optimum (EECO).

Tectonostratigraphic Phase	megasequence	age	Top reflector
T4	**III**	Oligocene	A-reflector

Malta Platform: Sedimentation is controlled by astronomically driven cycles of 1.2 Ma duration marked by glaciations that produced sequence boundaries along the Malta Platform. In the platform interior zone, basinward gravity sliding facilitated by viscous evaporite bed (SbRU1) acted as the décollement surface and produced domino-style fault blocks. The orientation of the <10 km-wide Naxxar and Marsaxlokk half-graben is consistent with the NE maximum regional stress (σ_1) field in the central Mediterranean that resulted in NW-SE extension during the Oligocene (Reuther, 1987). Oligotrophic conditions favoured corals and high rates of accumulation of the widespread acyclic 'lagoonal' carbonates stabilised by sea grass during the Rupelian. The sediments partly filled the structured topography produced during the Eocene hiatus (Figure 8.5). Higher frequency cycles at the long eccentricity level (400 kyr) are especially imprinted in lowstand systems tracts as glacio-eustatic cycles were more pronounced during these periods of relative ice-sheet growth although reduced accommodation space resulted in relatively thinner sequences (S4).

The mid-Chattian deglaciation of the Antarctic ice-sheet resulted in increased humidity over North Africa that increased nutrient flux in the Tethys. Conditions favoured heterozoan biota (FA II) and marked the turnaround from platform aggradation or non-deposition to progradation during sea-level highstands. Progradation was facilitated by platform-wide relative tectonic quiescence. Large clinoform beds prograded into the Naxxar Basin whereas seismic imaging shows prograding complexes along the Medina Escarpment. The moderately unstable substrate (rhodoliths of sequence S5) became more unstable with the deposition of large benthic foraminiferans during the ensuing sequence S6. The LBF signal a return to oligotrophic sea although sea-level rise was not balanced by sediment accumulation and widespread carbonate aggradation because the hydrodynamic LBF are easily dispersed. These conditions resulted in the initial deepening of the carbonate platform and the shift to gigantic LBF.

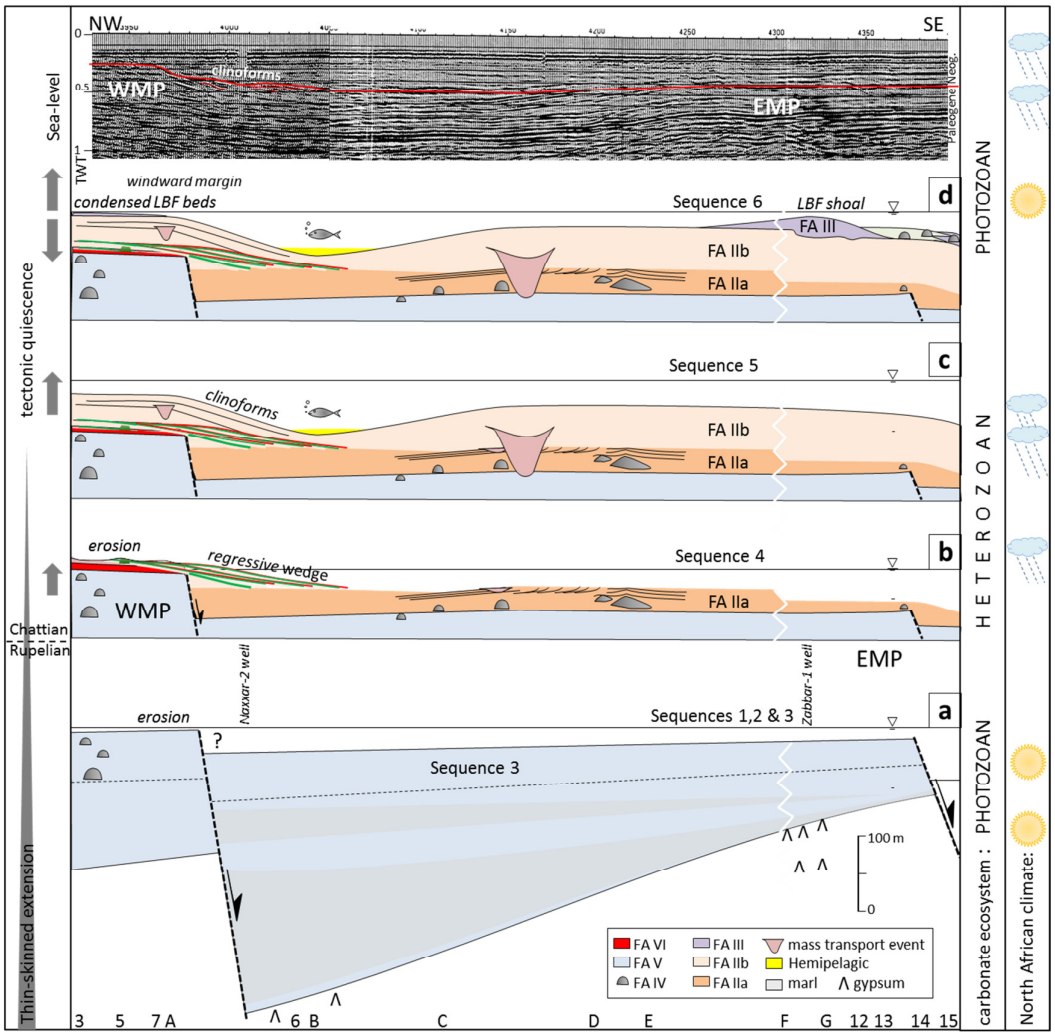

Figure 8.5. Tectonostratigraphic phase T4 in Malta across localities 3 to 15. The model shows facies and geometry of depositional sequences of the Lower Coralline Limestone Formation. The rate of tectonic extension and sea-level change shown on left. Climate change and trophic level on right: (a) Rupelian extension and development of Naxxar half-graben during a phase of high carbonate productivity and keep-up. Depocentre accumulates marl, (b) Early Chattian transgression and deposition of sequence 4, (c) Rhodolith biostrome aggrades as sea-level and nutrient level rises. Clinoforms prograde over blind faults and mass failure occurs along slopes, (d) Fall in nutrient level favours the development of an LBF shoal and bank over Western and Eastern Malta Palaeohigh; The model is compared to a vintage seismic line parallel to the north coast of Malta where sediments were not affected by Plio-Quaternary tectonic inversion of tectonostratigraphic phase T6.

Tethys: The Eocene-Oligocene boundary coincides with evaporite deposition over the Malta Platform (SbRU1) and west Egypt. Plate convergence resulted in more reduction of accommodation space for carbonates whereas siliciclastic supply was on the increase (Gerdes *et al.*, 2010).

Palaeoclimate: The global $\delta^{18}O$ curve is marked by a dramatic positive excursion at the beginning of the Oligocene that reflects the significant growth of the Antarctic ice-sheet (Zachos *et al.*, 2008) The growth of the Antarctic ice-sheet also produced a long-term global fall of 30 m in sea-level (Pekar *et al.*, 2002). The shrinking of the Antarctic ice-sheet beginning around 26.5 to 27 Ma triggered marine transgression that produced a meridional shift of the ITCZ and increased humidity over the Sahara region.

Tectonostratigraphic Phase	megasequence	age	Top reflector
T5	**III**	Miocene	M-reflector

The T5 begins with the precipitation of phosphorites (C_0 bed and A-reflector) over the Lower Coralline Limestone Formation marking a shift to eutrophic conditions in the semi-enclosed Mediterranean. These conditions terminated shallow marine sedimentation which drowned the Malta Platform. The under-filled depocentre of the Naxxar Basin started to be filled with hemipelagic carbonates of the lower member of the Globigerina Limestone Formation (40 m) which thin considerably (<5 m) over the Western and Eastern Malta Palaeohighs. The rapid development of the new Valletta Basin over central Malta (lower member >100 m thick) suggests that NE maximum stress (σ_1) field was rejuvenated throughout the Miocene till the Messinian. Pelagic carbonates are succeeded by marls (Blue Clay Formation) that reflect a regional increase in continental siliciclastics.

Tectonostratigraphic Phase	megasequence	age	Top reflector
T6	**IV**	Plio-Quaternary	seabed

The T6 consists of Plio-Quaternary sediments of megasequence VI. The thickness of these sediments is highly variable, from 0 m to >1 km thick (Gatt, 2007) as a result of tectonic structuring in the Central Mediterranean associated with plate convergence. Continued NW-SE extension produced the well-documented NE-SW trending faults (Illies, 1981; Dart *et al.*, 1993) especially along zones of higher strain over Malta (Putz-Perrier & Sanderson, 2010). The opening of the Plio-Quaternary Pantelleria Rift reflects the changing regional stress patterns (Reuther, 1987) and is associated with a shift in σ_1 to WNW compression after the Tortonian. Compression triggered fault reversal that involving the SbRU1 evaporite (B-reflector) as a décollement surface. Compression resulted in inversion and uplift of part of the Oligocene fault-blocks. Post-inversion erosion exhumed the Lower Coralline Limestone in northern Malta (localities 5, 7, 8 and 9).

8.4 FUTURE WORK

During the investigations for this study a number of aspects that need further study became evident. Some of these aspects include:

- Investigating the larger structural highs that have not been drilled, e.g., the Comino Palaeohigh. These structural highs may act as potential hydrocarbon traps. The Malta Ridge along the Escarpment Zone may also have potential.
- Investigating the role of evaporites in thin-skinned tectonics affecting Oligocene and younger sediments. Evaporites are important seals and their occurrence has important implications for hydrocarbon exploration.
- Investigating the carbonate reservoir potential of the Oligocene *Lepidocyclina* banks which are similar to the productive Eocene *Nummulite* reservoirs.

8.5 CONCLUSIONS

- A new and comprehensive lithostratigraphy of the Lower Coralline Limestone Formation is presented that incorporates sequence stratigraphic sub-divisions (page 350, table 8-2).

- The lithostratigraphy and sequence stratigraphy of the Palaeogene Malta Platform was controlled by 1.2 Ma obliquity cycles and to a lesser extent the 400 kyr long eccentricity cycle forcing. The rhythmic stratigraphy facilitates the correlation of the Maltese carbonates to nearby carbonate platforms and global glacio-eustasy.

- The Malta Platform experienced extension and subsidence along a passive margin setting from the Early Mesozoic to the end Miocene. This extension was resolved by different structural processes with increasing distance from the rift zone: i. deep listric faults that form large escarpments along the margin of the basin; ii. extension followed by sagging that formed a large intra-platform basin and, iii. rotated block faulting that produced small *en echelon* half-grabens located distal from the platform margin. These structures had a fundamental control on sedimentation and sediment geometry.

- The vertical changes in carbonate facies at the scale of depositional sequences (>30 m thick) are abrupt and do not represent lateral shifts in contiguous facies *sensu* Walther's Law, nor do they reflect a carbonate ramp depositional setting as had been previously thought.

- Vertical changes in carbonate facies may reflect climate change over North Africa which resulted in fluctuations in nutrient flux to the semi-enclosed western Tethys that influenced the trophic level of carbonate ecosystems. These changes correspond to the waxing and waning of the Antarctic ice-sheet and concomitant meridional shifts in low latitude climate belts. The change in carbonate ecosystems in carbonate platforms of the Central Mediterranean is synchronous to that of the Malta Platform.

List of Appendices

Appendix I..... 364
Table of outcrop localities and their UTM grid 1
Table of exploratory wells 2
Appendix II..... 366
Key to sedimentary logs 3
Stratigraphic correlation chart 4
Log of locality 1 (part 1) 5
Log of locality 1 (part 2) 6
Log of locality 2 7
Log of locality 3 & A 8
Logs of localities 4 a & b 9
Log of locality 5 (part 1) 10
Log of locality 5 (part 2) 11
Log of locality 6 12
Log of locality 8 13
Log of locality 9 14
Log of locality 10a 15
Logs of localities G & 10b 16
Log of locality 11 17
Log of locality 14 18
Log of locality 15 19
Appendix III 384
Large benthic foraminifera of localities 2 and 3 20
Large benthic foraminifera of localities 5 and 6 21
Coralline morphology 22
Facies Association IIa photomicrographs 23
Facies Association IIIb photomicrographs 24
Facies Association IIIa photomicrographs 25
Facies Association IV photomicrographs 26
Facies Association V photomicrographs 27
Facies Association VI photomicrographs 28
Cored sections and biostratigraphy of wells 29
Appendix IV.....394
Photomontage of cliffed coast of localities C & B 30
Photomontage of cliffed coast of localities A & B 31
Photomontage of localities 10b, 13, 14 32
Appendix V.....397
Photograph of locality 1 33
Photograph of locality 1 (inland sea) 34
Photograph of locality A 35
Photograph of locality A & 3 36
Photograph of locality 5 37
Photograph of locality B 38
Photograph of locality C 39
Photograph of locality D 40
Photograph of locality 13 41
Photograph of locality 14 42

Appendix I - 1

Locality	Locality name	UTM (S33) co-ordinates	Depth of log in metres	Site description
1	Dwejra (Gozo)	272 902	62	inland and coastal cliff
2	Għar Dorf (Gozo)	399 883	79	quarry/core
3	Miġra Ferħa	405 703	51	gorge cut into coastal cliff
4a	Qawra	481 796	4	coastal platform/collapsed cave
4b	Baħar iċ-Ċagħaq	510 775	4	coastal platform
5	Mosta	489 751	70	quarry
6	Attard	492 714	40	quarry
7	Għargħur	502 759	35	quarry
8	Naxxar	497 739	30	quarry
9	Pembroke	533 766 525 771	35	coastal platform
10a	Ix-Xaqqa	473 657	52	quarry and faulted cliff
10b	Wied iż-Żurrieq	504 641	25	valley cut into coastal cliff
11	Sliema	547 750	5	coastal platform
12	Xgħajra	587 720 592 718 594 715	17	coastal platform
13	Wied Moqbol	540 637	20	quarry
14	Wied Żnuber	557 630	32	valley cut into coastal cliff
15	Wied iz-Ziju	588 683	33	quarry
Core 1	Ta' San Niklaw	492 659	80	vertical rock cores (Wardell Armstrong 1996)
Core 2	Ħal Far Airfield	566 633	55.2	

well name	Depth of well in metres	location	Date	company
Naxxar-1 & 2	2998	onshore	1956-1958	D'Arcy - BP
Żabbar	593			
Għar Lapsi (tal-Qanpiena)	274			
MTZ (Madonna taż-Żejt)	8100		1998	ENI
Aqualta	1791	offshore	1971	Total
Medina Bank-1	n/a			ENI

Appendix I - 2

Appendix II

Key to sedimentary logs	3
Stratigraphic correlation chart	4
Log of locality 1 (part 1)	5
Log of locality 1 (part 2)	6
Log of locality 2	7
Log of locality 3 & A	8
Logs of localities 4 a & b	9
Log of locality 5 (part 1)	10
Log of locality 5 (part 2)	11
Log of locality 6	12
Log of locality 8	13
Log of locality 9	14
Log of locality 10a	15
Logs of localities G & 10b	16
Log of locality 11	17
Log of locality 14	18
Log of locality 15	19

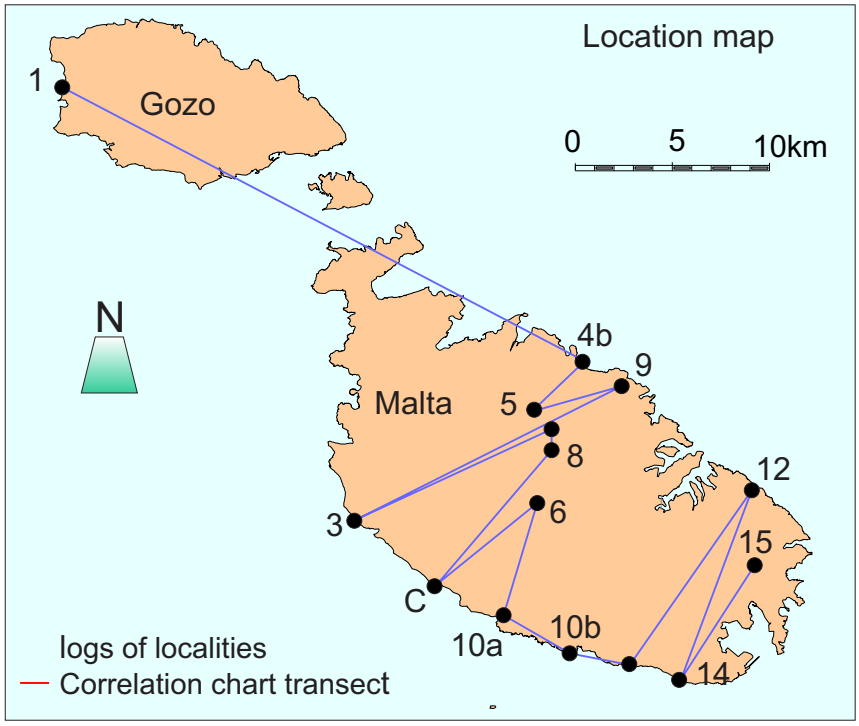

Key to sedimentary logs

Macrofossils

- Coral - solitary
- Coral - compound
- Bivalves
- Bivalves siphonal tube - *Kuphus*
- Gastropods
- Large benthic foraminifera
- Red calcareous algae- disarticulated
- Red calcareous algae- branching
- Red calcareous algae- rhodoliths >5cm <2cm
- Echinoids
- Bryozoans

- Inaccessible
- Sample point
- Algal sand

Facies associations

- VI
- V
- IV
- III
- II
- I

Sedimentary Structures

- SbCH2 Sequence boundary
- Parallel lamination
- Planar cross-bedding
- Trough cross-bedding
- Bioturbation - slight
- Bioturbation - intense
- Undulating bedding
- Onlap of patch reef

Foraminiferal biozones

LBF biozonation (Cahuzac & Poignant, 1997)

SBZ21 SBZ22 SBZ23

- M *Miogypsinoides*
- L *Lepidocyclina*
- O *Operculina*
- S *Spiroclypeus*
- A *Amphistegina*
- H *Heterostegina*
- P *Peneroplis*
- m *Miliolids*
- p *Praerhapydionina*
- a *Austrotrillina*
- b *Borelis*

Stratigraphic correlation chart

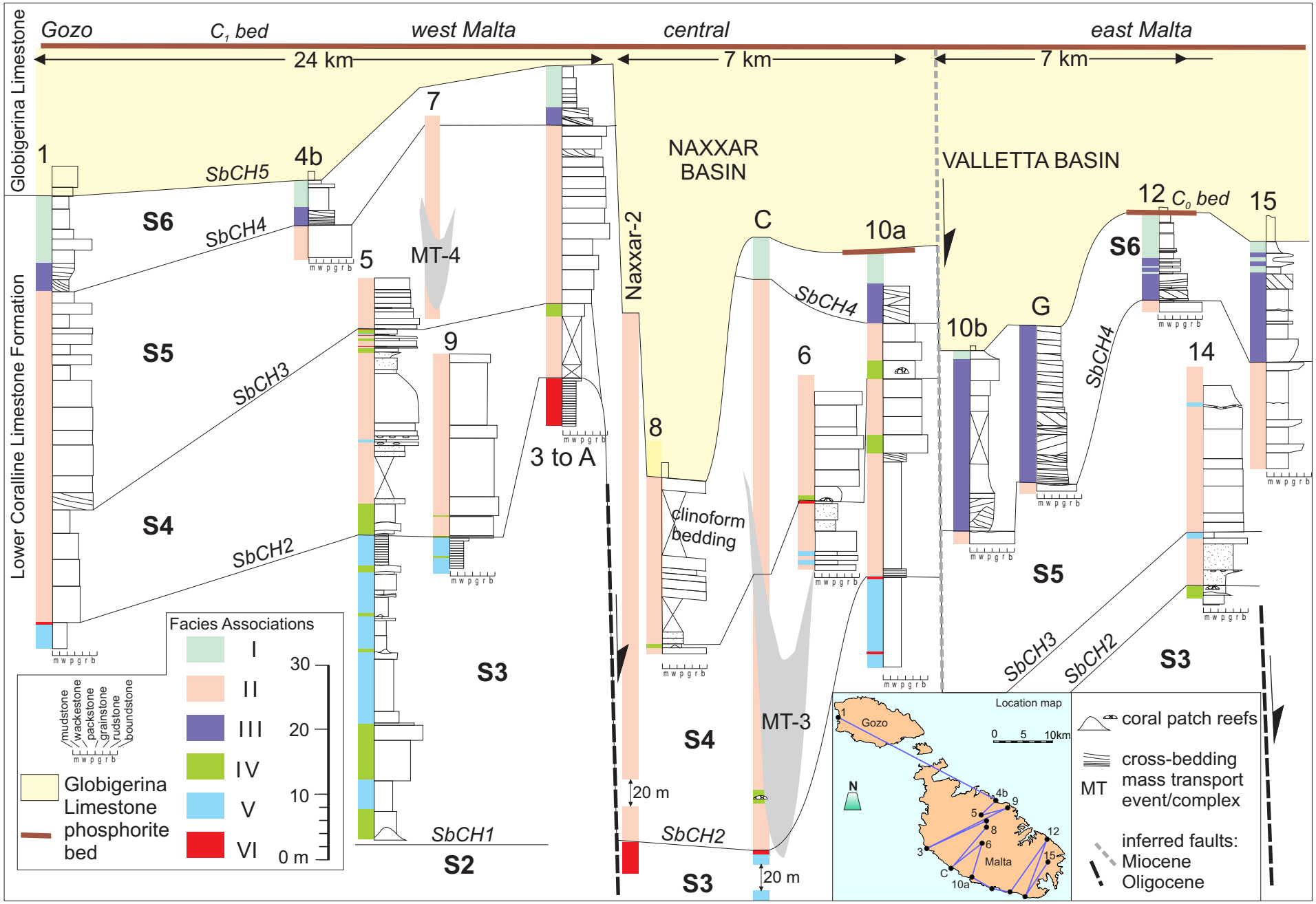

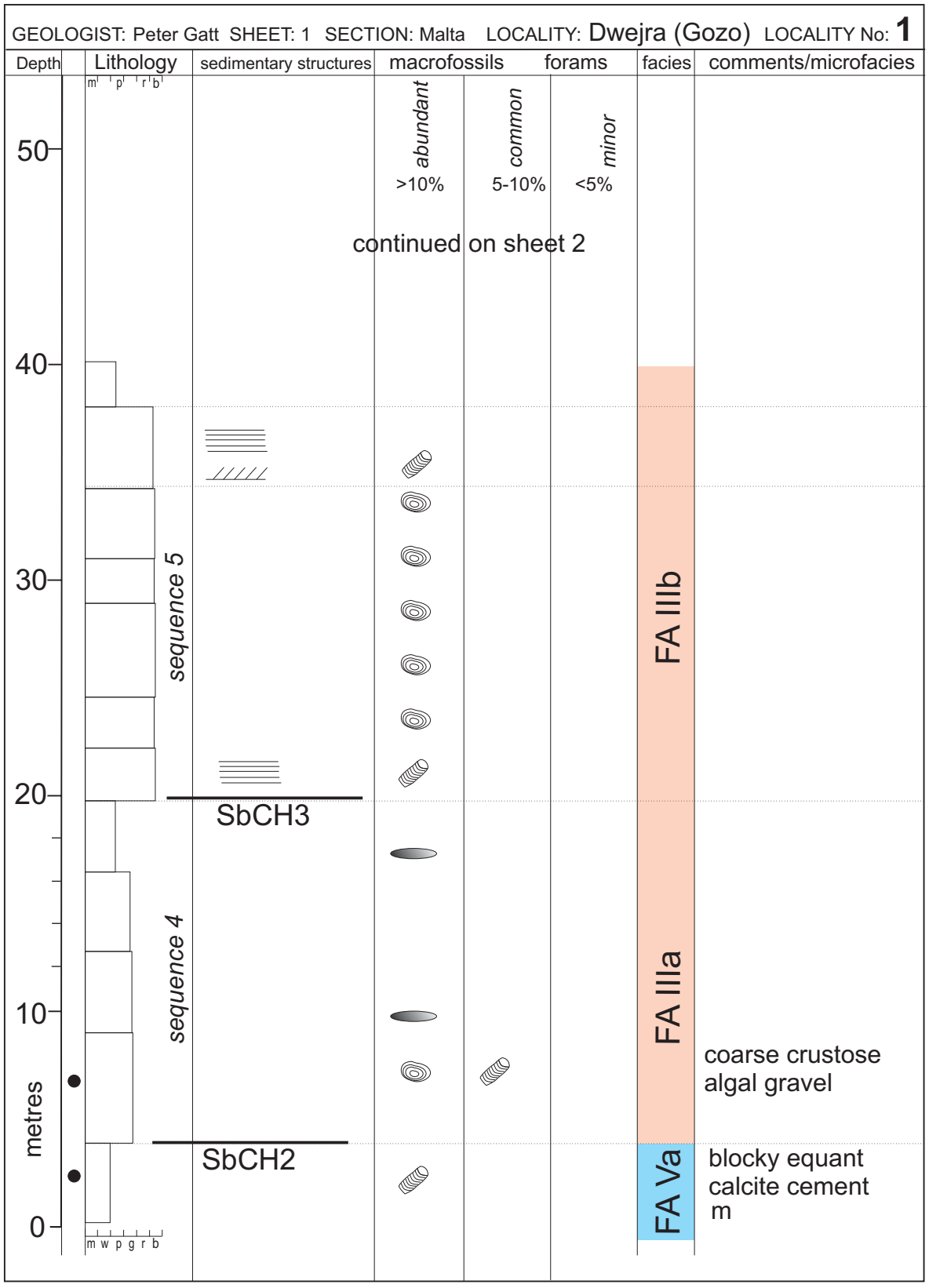
GEOLOGIST: Peter Gatt SHEET: 1 SECTION: Malta LOCALITY: Dwejra (Gozo) LOCALITY No: 1
Depth
Lithology
sedimentary structures
macrofossils
forams
facies
comments/microfacies
abundant
>10%
common
5-10%
minor
<5%
continued on sheet 2
50
40
30
20
10
0
metres
sequence 5
sequence 4
SbCH3
SbCH2
FA IIIb
FA IIIa
FA Va
coarse crustose algal gravel
blocky equant calcite cement
m
m w p g r b

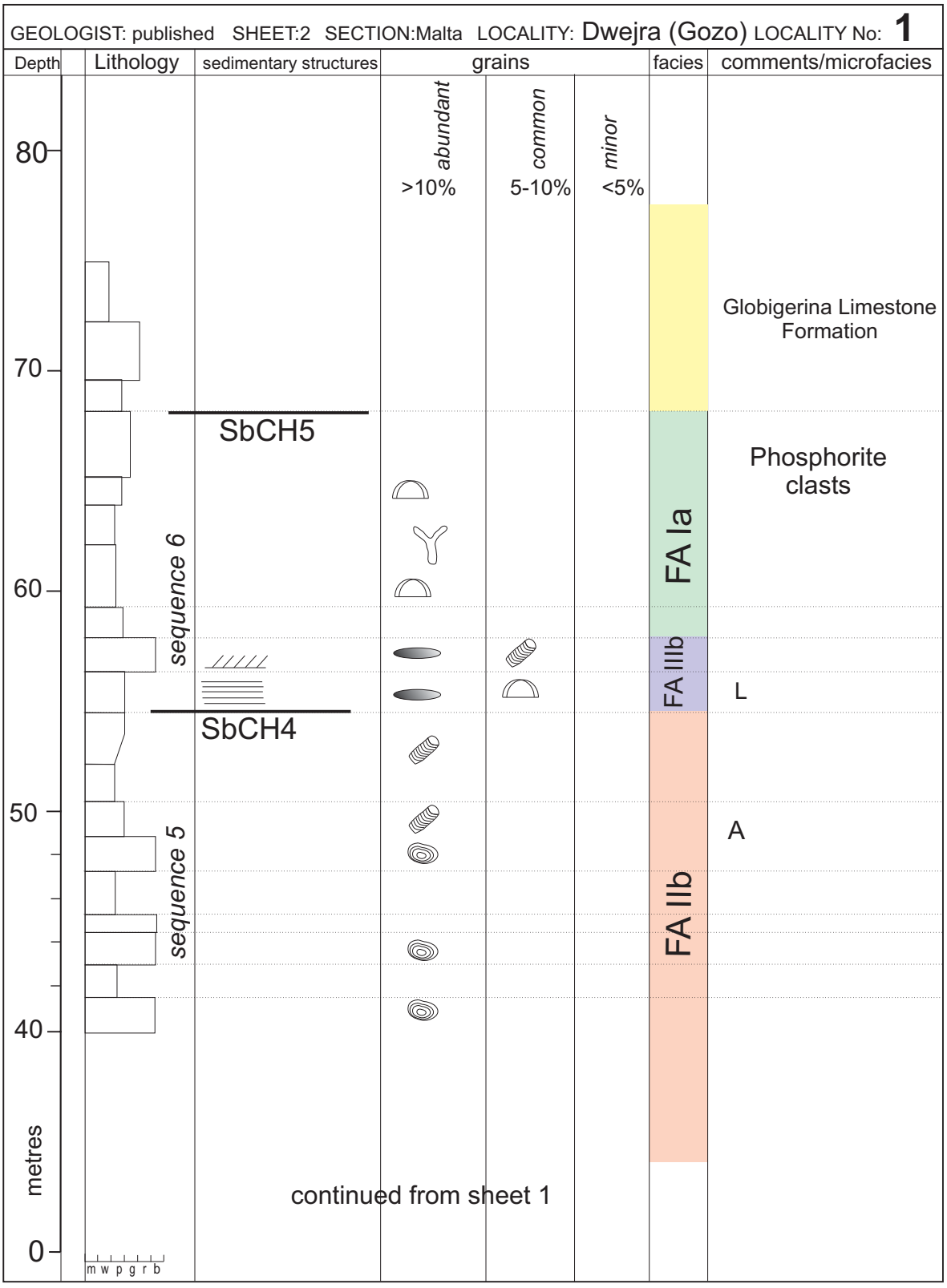
GEOLOGIST: published SHEET:2 SECTION:Malta LOCALITY: Dwejra (Gozo) LOCALITY No: 1
Depth
Lithology
sedimentary structures
grains
facies
comments/microfacies
abundant
>10%
common
5-10%
minor
<5%
80
70
60
50
40
metres
0
m w p g r b
SbCH5
SbCH4
sequence 6
sequence 5
FA Ia
FA IIIb
FA IIb
Globigerina Limestone Formation
Phosphorite clasts
L
A
continued from sheet 1

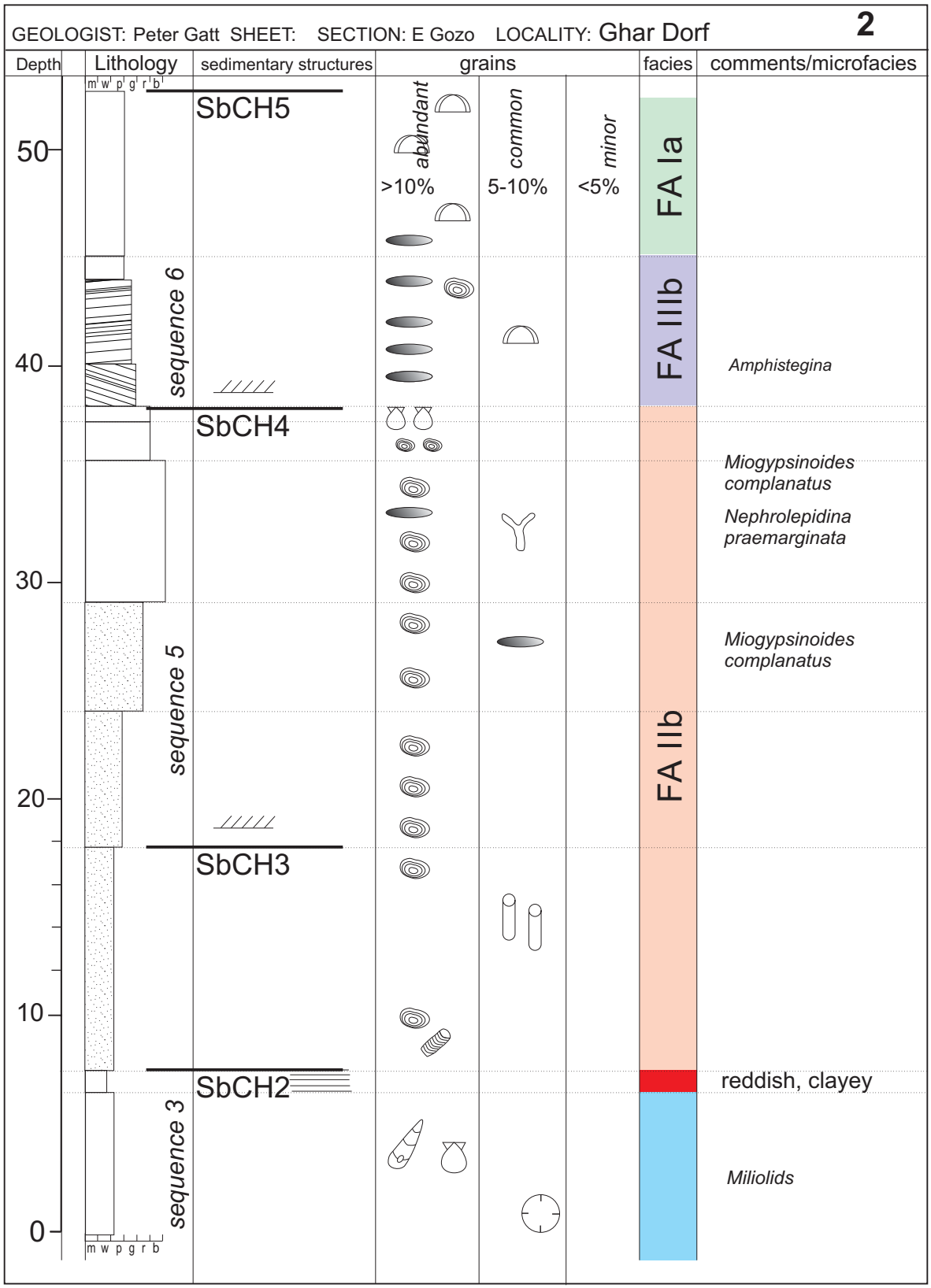
GEOLOGIST: Peter Gatt SHEET: SECTION: E Gozo LOCALITY: Ghar Dorf
2
Depth
Lithology
sedimentary structures
grains
facies
comments/microfacies
m w p g r b
SbCH5
SbCH4
SbCH3
SbCH2
sequence 6
sequence 5
sequence 3
abundant
common
minor
>10%
5-10%
<5%
50
40
30
20
10
0
FA Ia
FA IIIb
FA IIb
Amphistegina
Miogypsinoides complanatus
Nephrolepidina praemarginata
Miogypsinoides complanatus
reddish, clayey
Miliolids

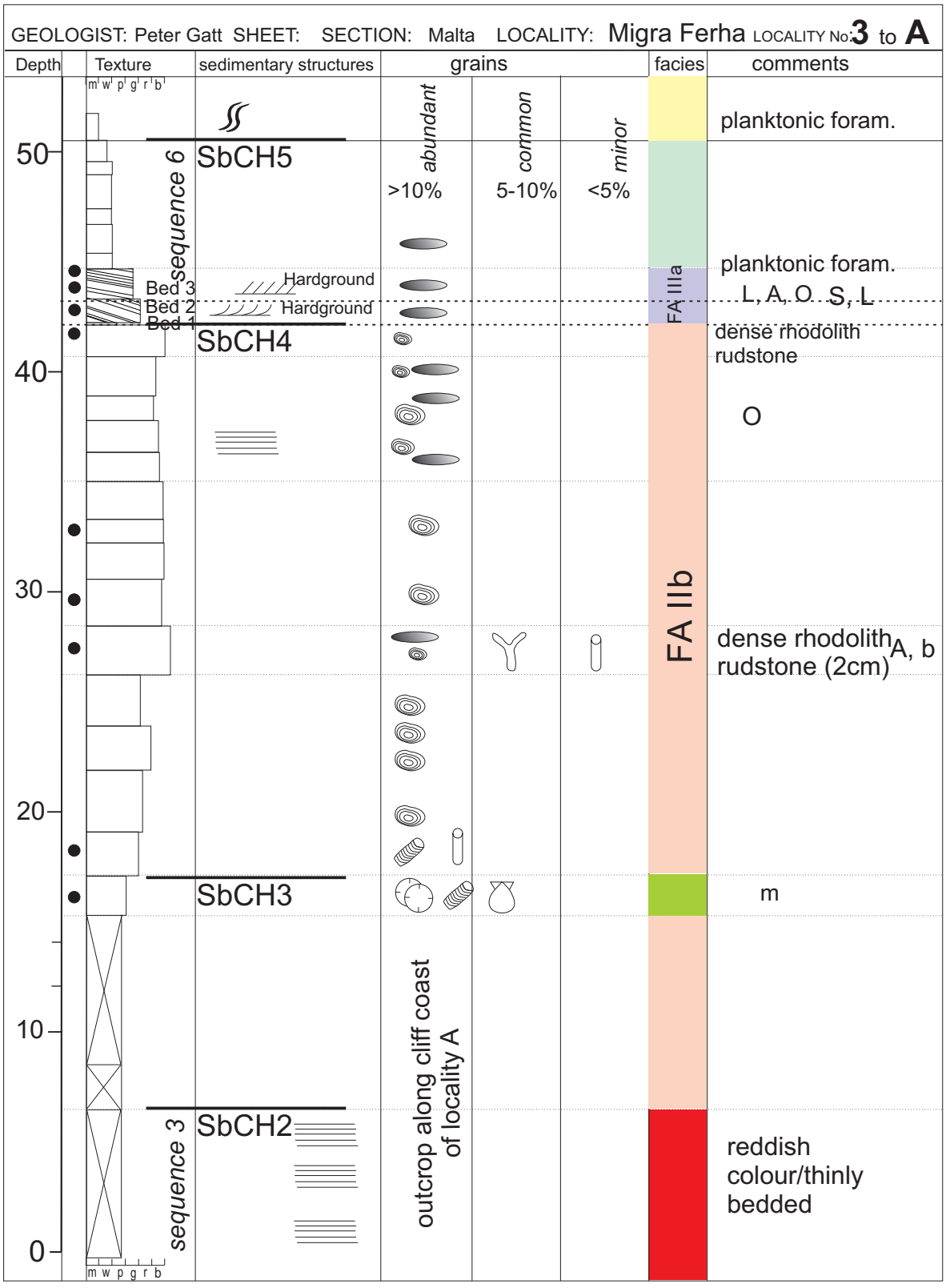
GEOLOGIST: Peter Gatt SHEET: SECTION: Malta LOCALITY: Migra Ferha LOCALITY No: 3 to A
Depth
Texture
sedimentary structures
grains
facies
comments
m w p g r b
abundant
common
minor
>10%
5-10%
<5%
planktonic foram.
sequence 6
SbCH5
Hardground
Bed 3
Bed 2
Hardground
Bed 1
SbCH4
planktonic foram.
L, A, O, S, L
FA IIIa
dense rhodolith rudstone
O
50
40
30
20
10
0
FA IIb
dense rhodolith rudstone (2cm)
A, b
SbCH3
m
outcrop along cliff coast of locality A
sequence 3
SbCH2
reddish colour/thinly bedded

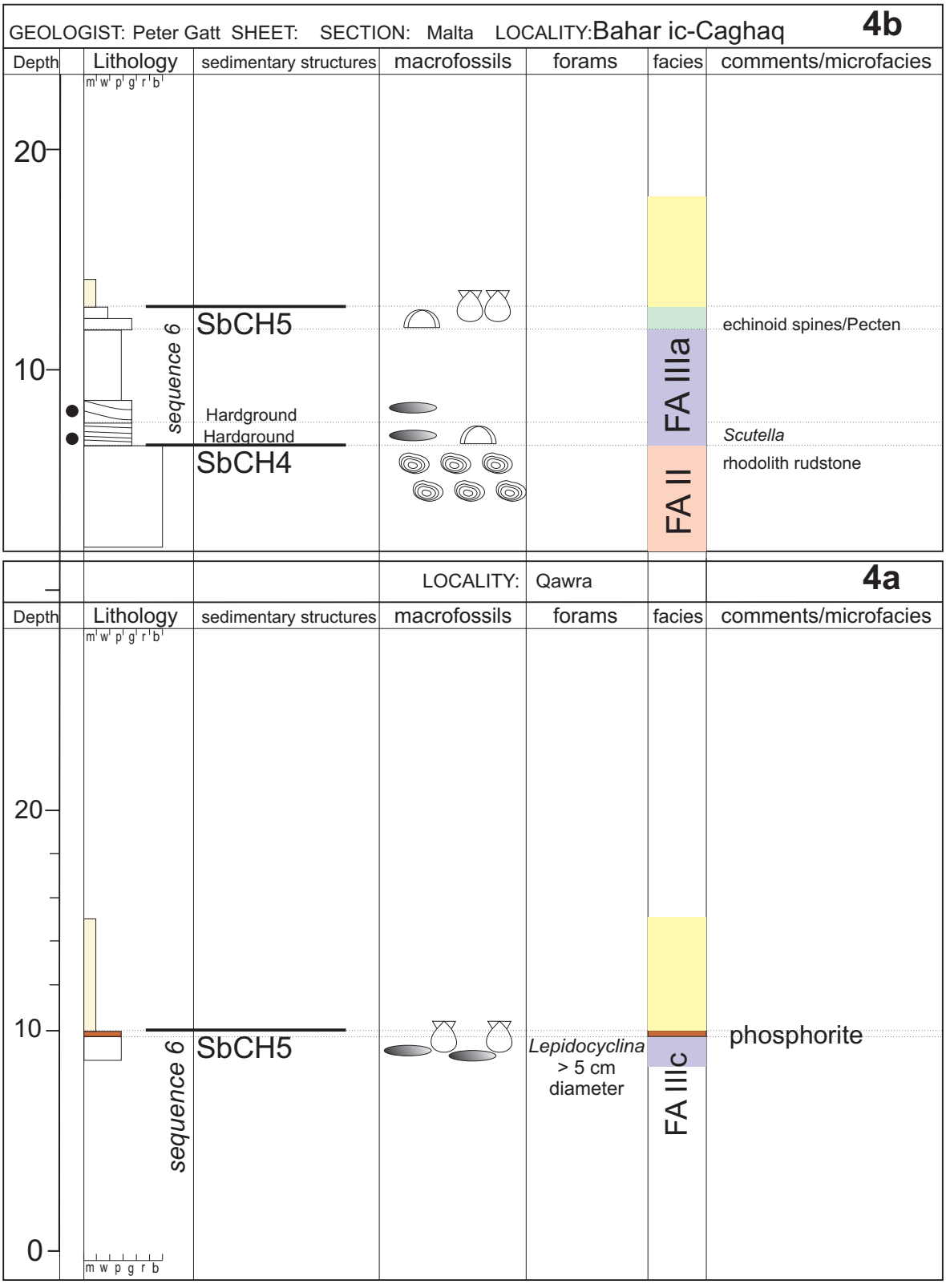
GEOLOGIST: Peter Gatt SHEET: SECTION: Malta LOCALITY: Bahar ic-Caghaq
4b
Depth
Lithology
sedimentary structures
macrofossils
forams
facies
comments/microfacies
m w p g r b
20
10
sequence 6
SbCH5
Hardground
Hardground
SbCH4
FA IIIa
FA II
echinoid spines/Pecten
Scutella
rhodolith rudstone
LOCALITY: Qawra
4a
Depth
Lithology
sedimentary structures
macrofossils
forams
facies
comments/microfacies
m w p g r b
20
10
0
sequence 6
SbCH5
Lepidocyclina
> 5 cm
diameter
FA IIIc
phosphorite
m w p g r b

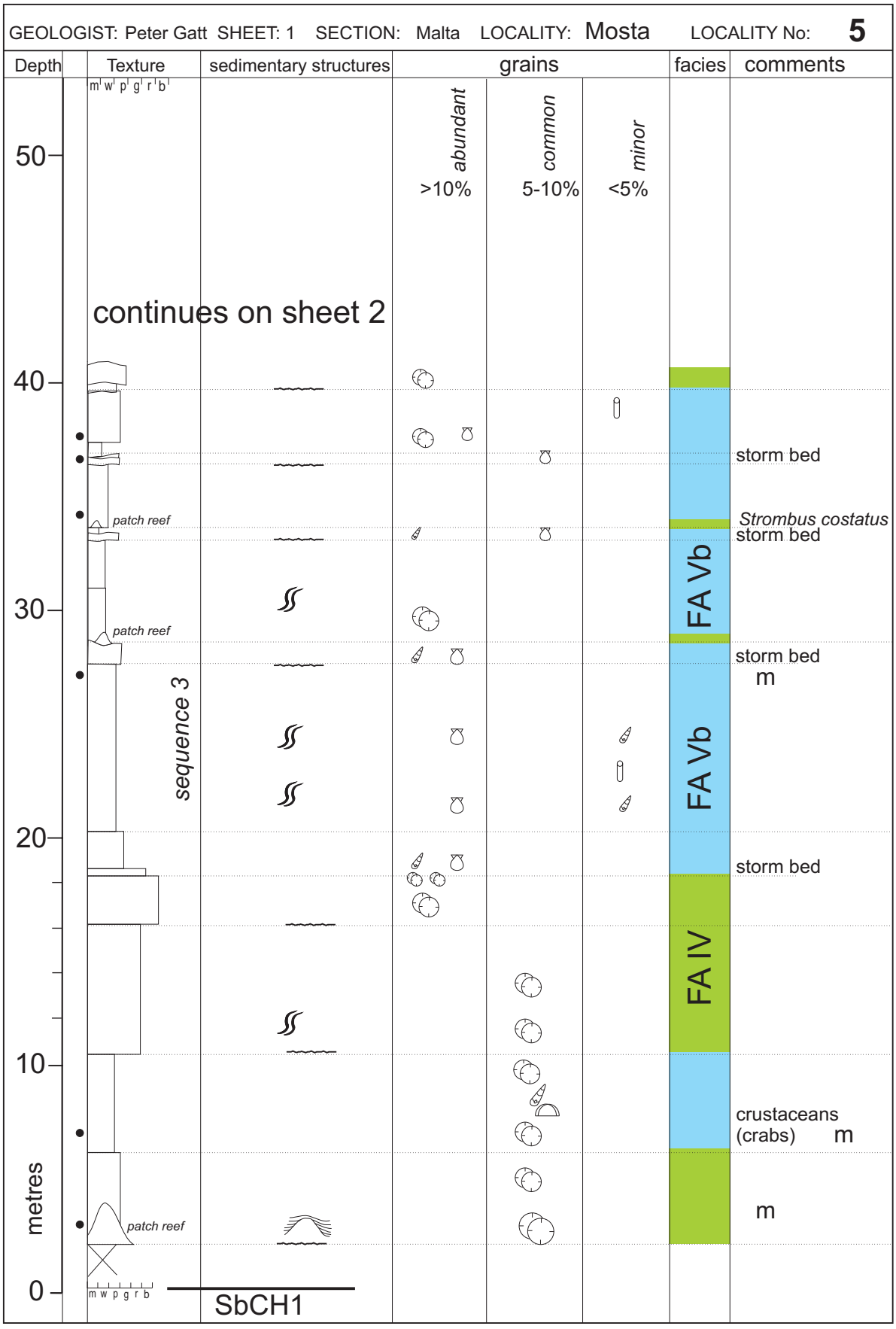
GEOLOGIST: Peter Gatt SHEET: 1 SECTION: Malta LOCALITY: Mosta LOCALITY No: 5
Depth
Texture
sedimentary structures
grains
facies
comments
m w p g r b
abundant
>10%
common
5-10%
minor
<5%
50
40
30
20
10
0
metres
continues on sheet 2
patch reef
patch reef
patch reef
sequence 3
storm bed
Strombus costatus
storm bed
storm bed
m
storm bed
crustaceans
(crabs) m
m
FA Vb
FA Vb
FA IV
SbCH1

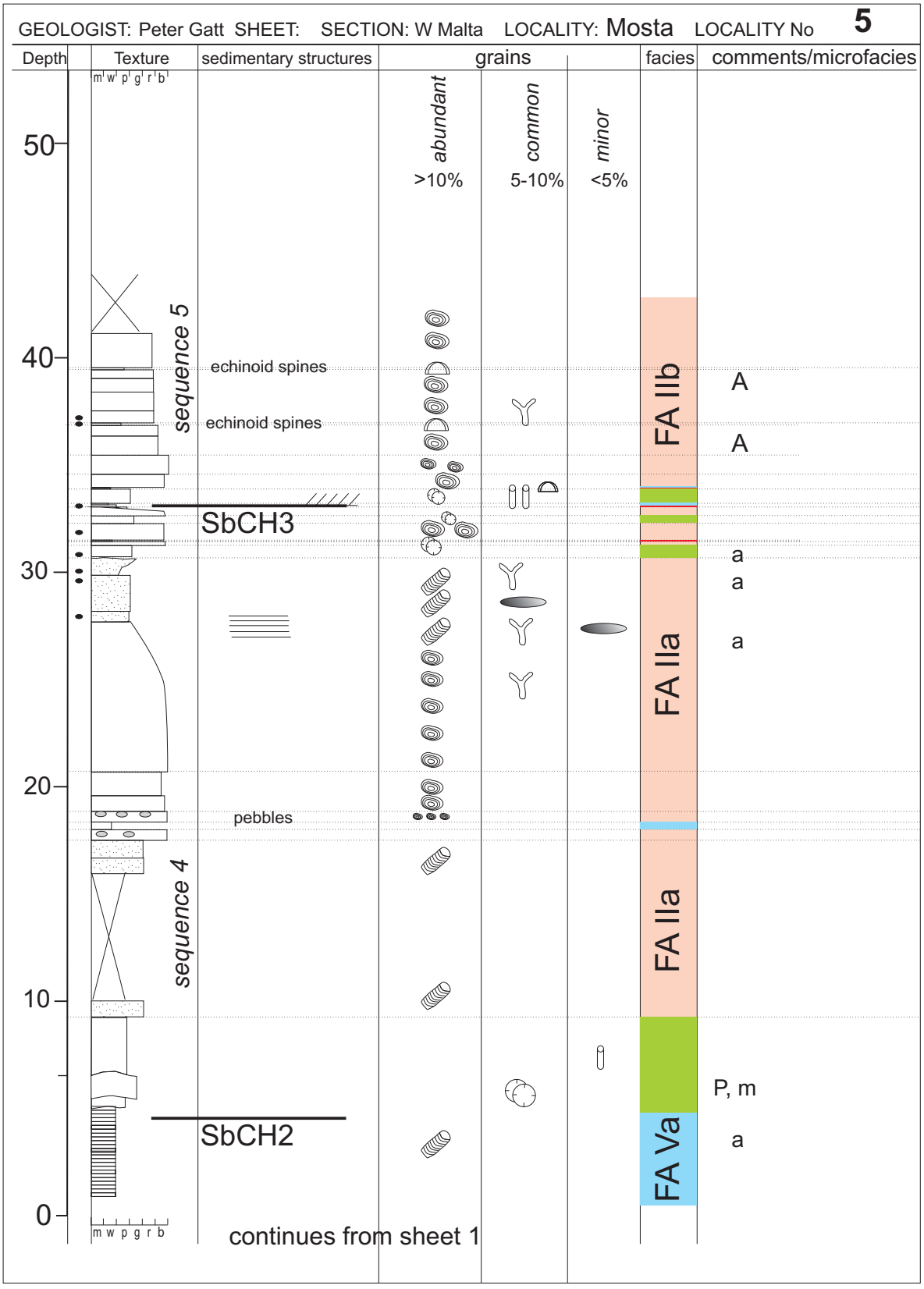
GEOLOGIST: Peter Gatt SHEET: SECTION: W Malta LOCALITY: Mosta LOCALITY No 5
Depth
Texture
sedimentary structures
grains
facies
comments/microfacies
abundant
>10%
common
5-10%
minor
<5%
50
40
30
20
10
0
sequence 5
sequence 4
echinoid spines
echinoid spines
SbCH3
pebbles
SbCH2
continues from sheet 1
FA IIb
FA IIa
FA IIa
FA Va
A
A
a
a
a
P, m
a

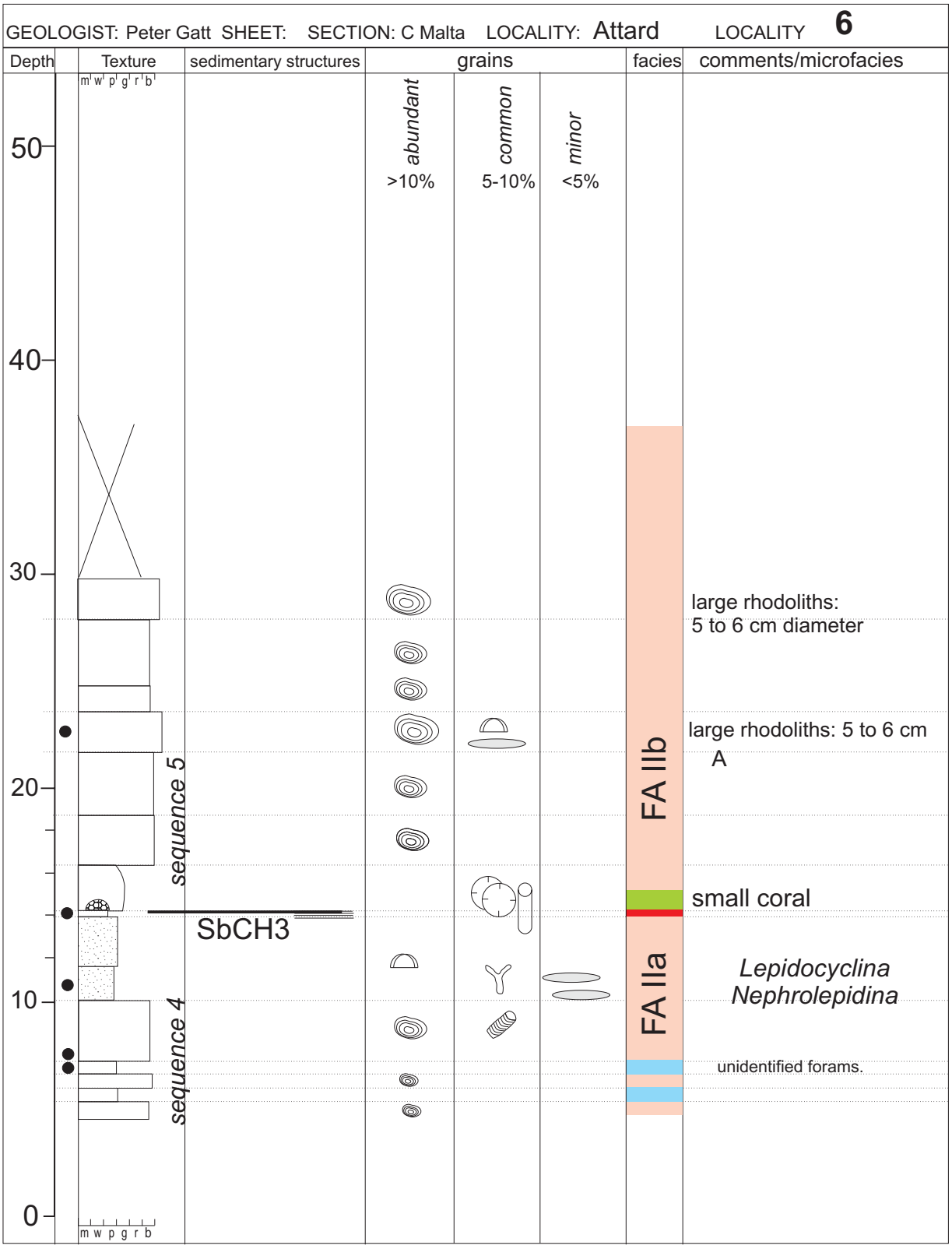
GEOLOGIST: Peter Gatt SHEET: SECTION: C Malta LOCALITY: Attard LOCALITY 6
Depth
Texture
sedimentary structures
grains
facies
comments/microfacies
m w p g r b
abundant
>10%
common
5-10%
minor
<5%
50
40
30
20
10
0
sequence 5
sequence 4
SbCH3
FA IIb
FA IIa
large rhodoliths:
5 to 6 cm diameter
large rhodoliths: 5 to 6 cm
A
small coral
Lepidocyclina
Nephrolepidina
unidentified forams.

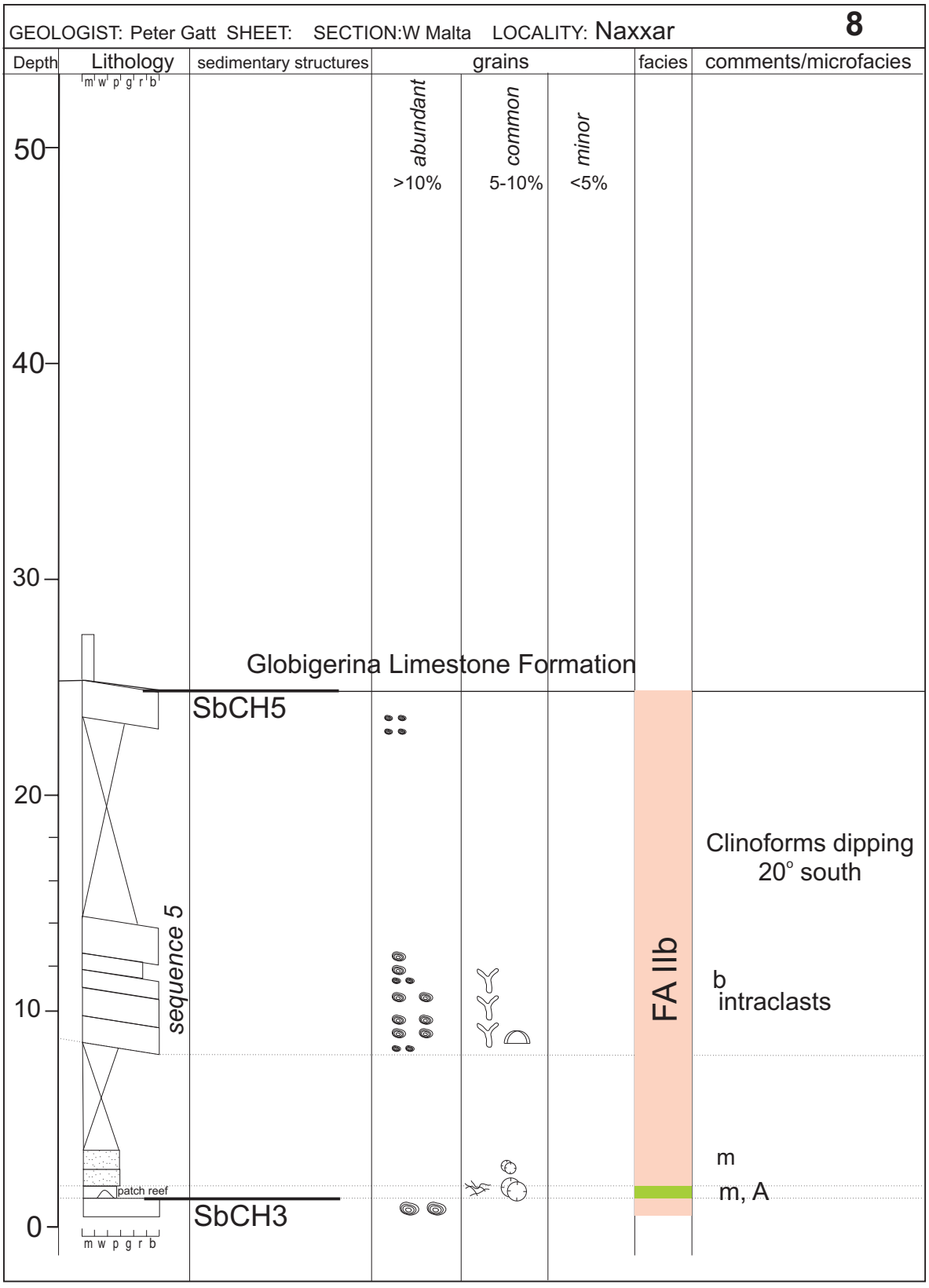
GEOLOGIST: Peter Gatt SHEET: SECTION:W Malta LOCALITY: Naxxar
8
Depth
Lithology
m w p g r b
sedimentary structures
grains
facies
comments/microfacies
abundant
>10%
common
5-10%
minor
<5%
50
40
30
20
10
0
Globigerina Limestone Formation
SbCH5
SbCH3
sequence 5
patch reef
FA IIb
Clinoforms dipping 20° south
b
intraclasts
m
m, A

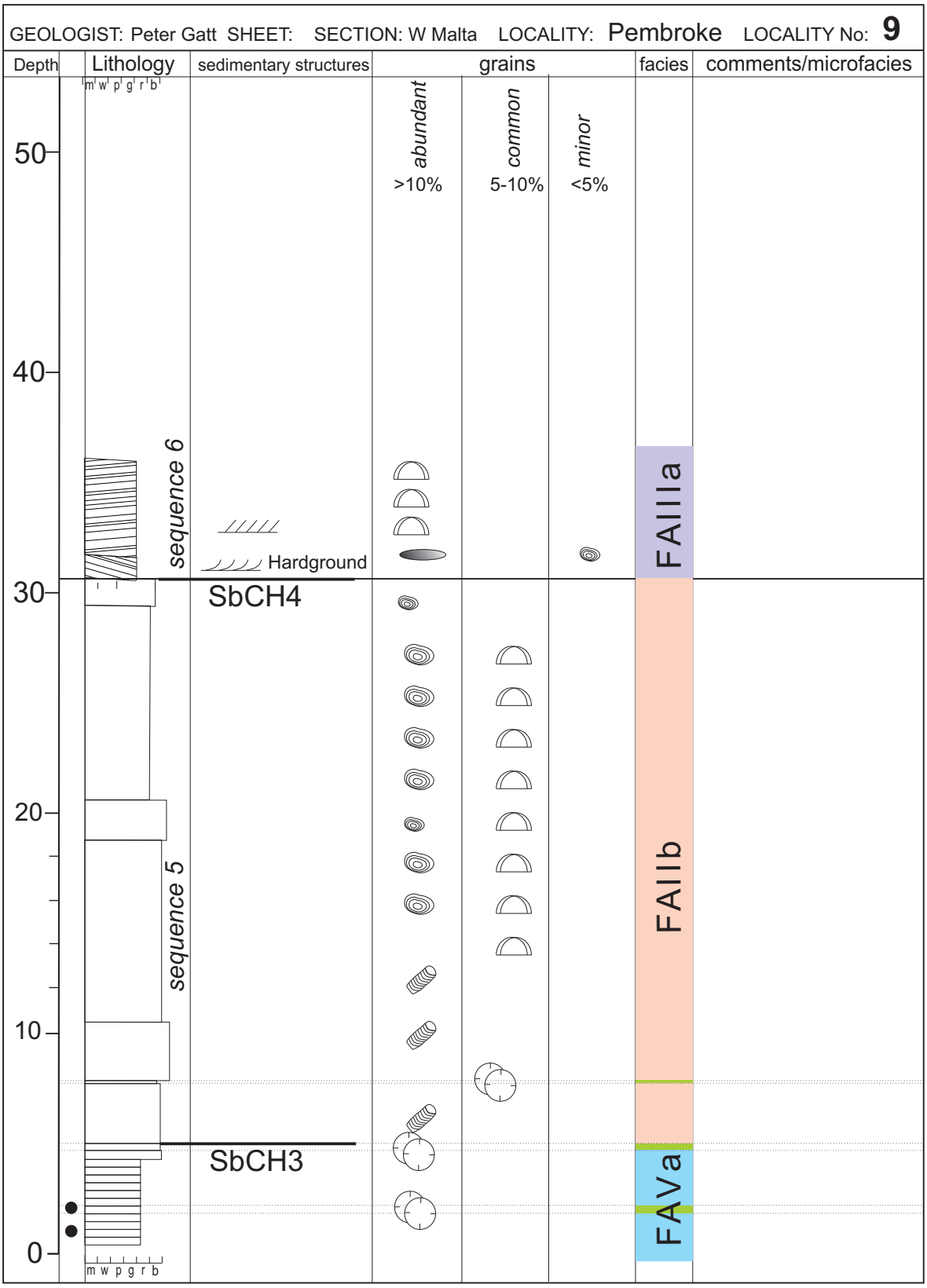
GEOLOGIST: Peter Gatt SHEET: SECTION: W Malta LOCALITY: Pembroke LOCALITY No: 9
Depth
Lithology
sedimentary structures
grains
facies
comments/microfacies
m w p g r b
abundant
>10%
common
5-10%
minor
<5%
50
40
30
20
10
0
sequence 6
sequence 5
Hardground
SbCH4
SbCH3
FAIIIa
FAIIb
FAVa

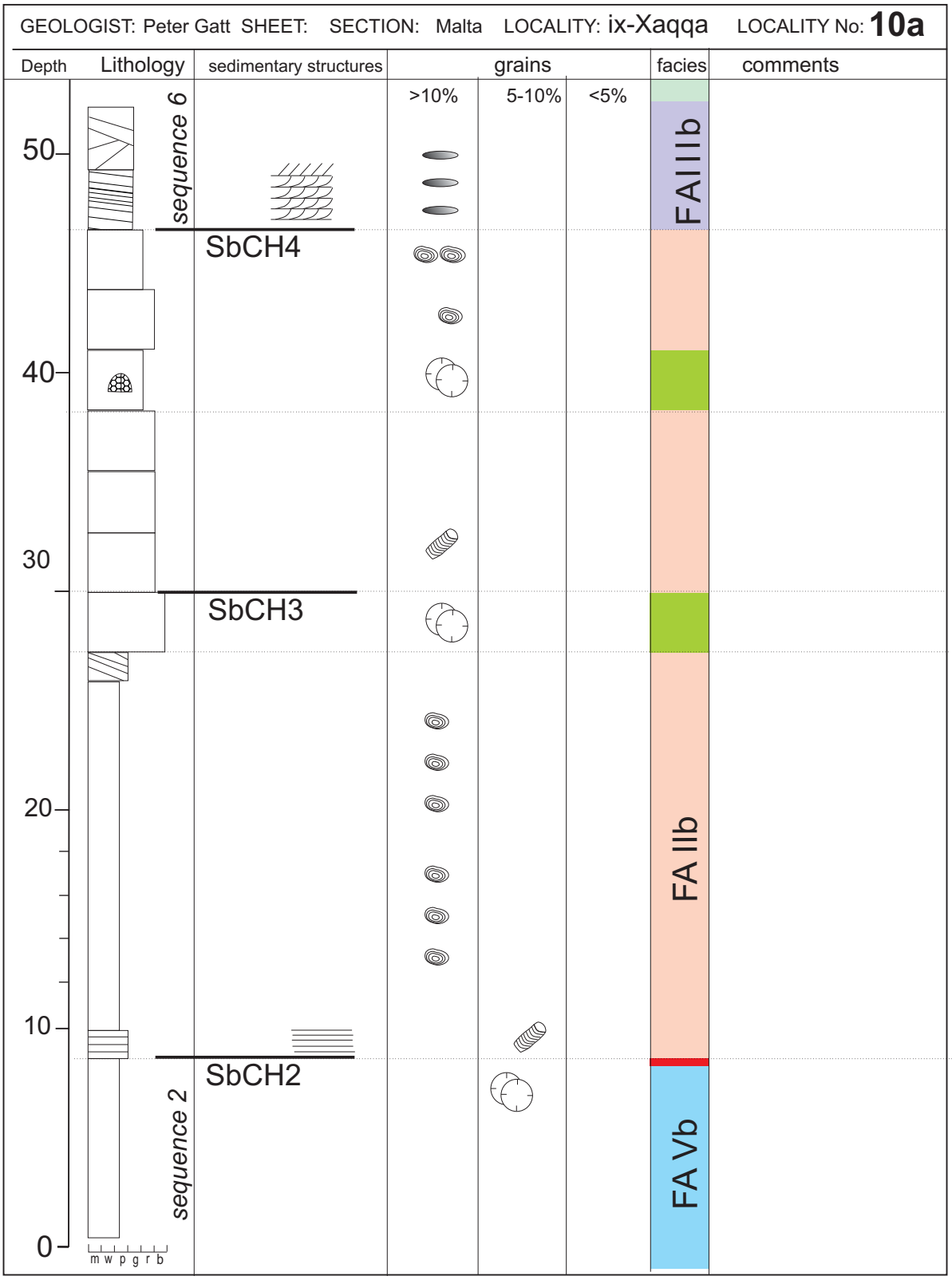
GEOLOGIST: Peter Gatt SHEET: SECTION: Malta LOCALITY: ix-Xaqqa LOCALITY No: 10a
Depth
Lithology
sedimentary structures
grains
>10%
5-10%
<5%
facies
comments
50
40
30
20
10
0
sequence 6
SbCH4
SbCH3
SbCH2
sequence 2
m w p g r b
FA IIIb
FA IIb
FA Vb

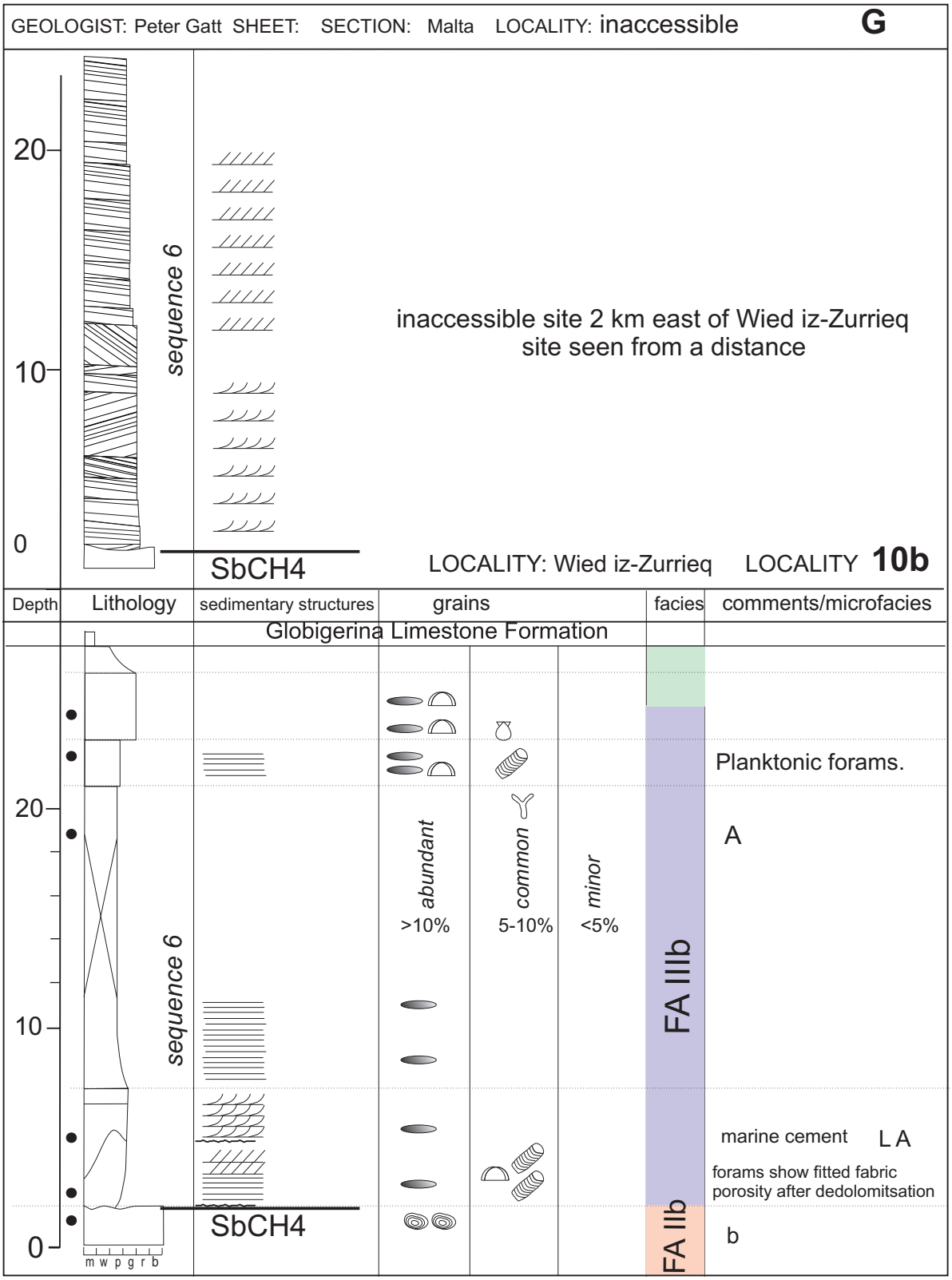
GEOLOGIST: Peter Gatt SHEET: SECTION: Malta LOCALITY: inaccessible
G
20
10
0
sequence 6
SbCH4
inaccessible site 2 km east of Wied iz-Zurrieq
site seen from a distance
LOCALITY: Wied iz-Zurrieq
LOCALITY 10b
Depth
Lithology
sedimentary structures
grains
facies
comments/microfacies
Globigerina Limestone Formation
abundant
>10%
common
5-10%
minor
<5%
FA IIIb
FA IIb
Planktonic forams.
A
marine cement
L A
forams show fitted fabric
porosity after dedolomitsation
b
m w p g r b

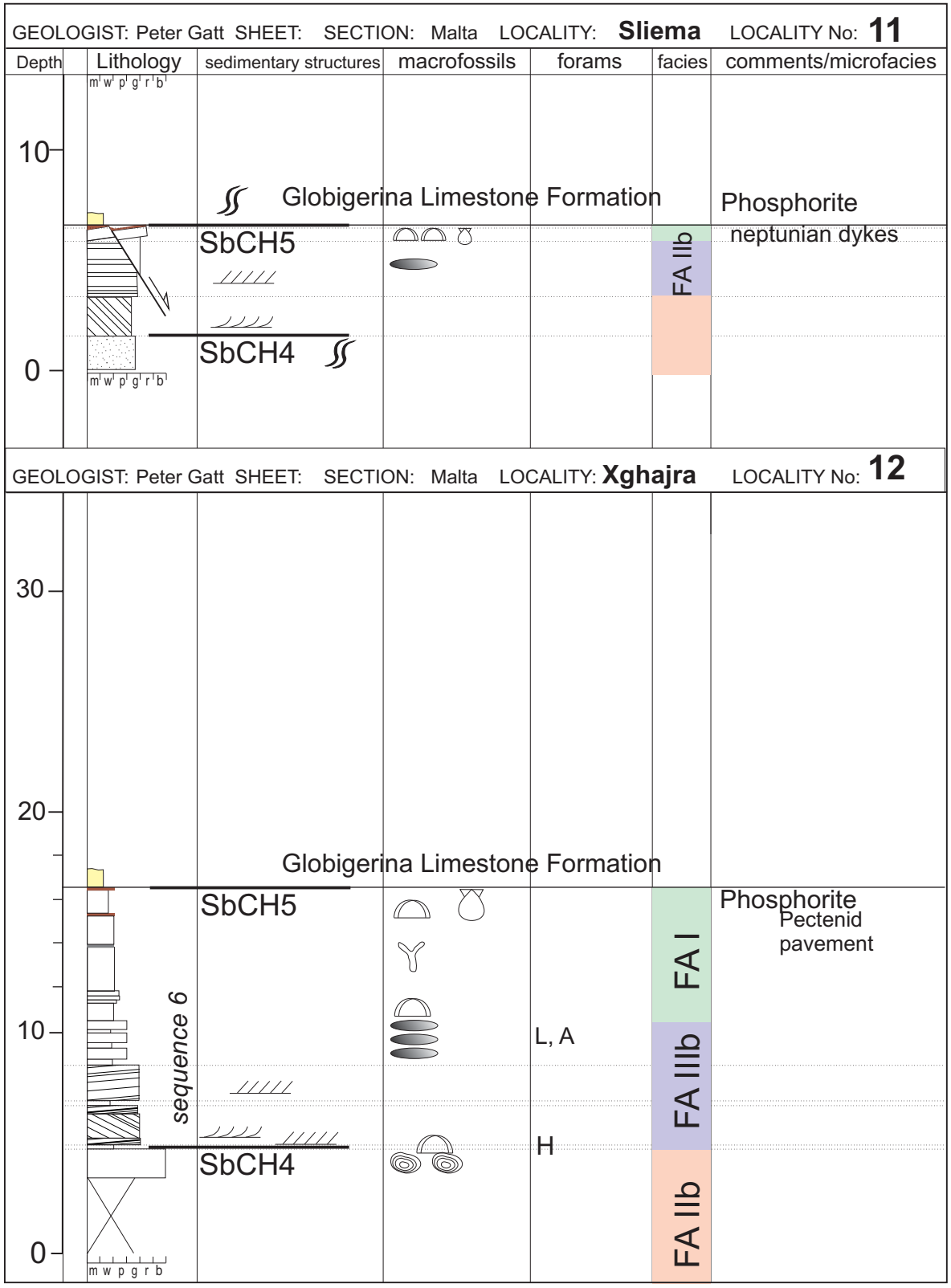
GEOLOGIST: Peter Gatt SHEET: SECTION: Malta LOCALITY: Sliema LOCALITY No: 11
Depth
Lithology
sedimentary structures
macrofossils
forams
facies
comments/microfacies
10
0
Globigerina Limestone Formation
Phosphorite
neptunian dykes
SbCH5
SbCH4
FA IIb
GEOLOGIST: Peter Gatt SHEET: SECTION: Malta LOCALITY: Xghajra LOCALITY No: 12
30
20
10
0
Globigerina Limestone Formation
Phosphorite
Pectenid
pavement
SbCH5
SbCH4
sequence 6
L, A
H
FA I
FA IIIb
FA IIb

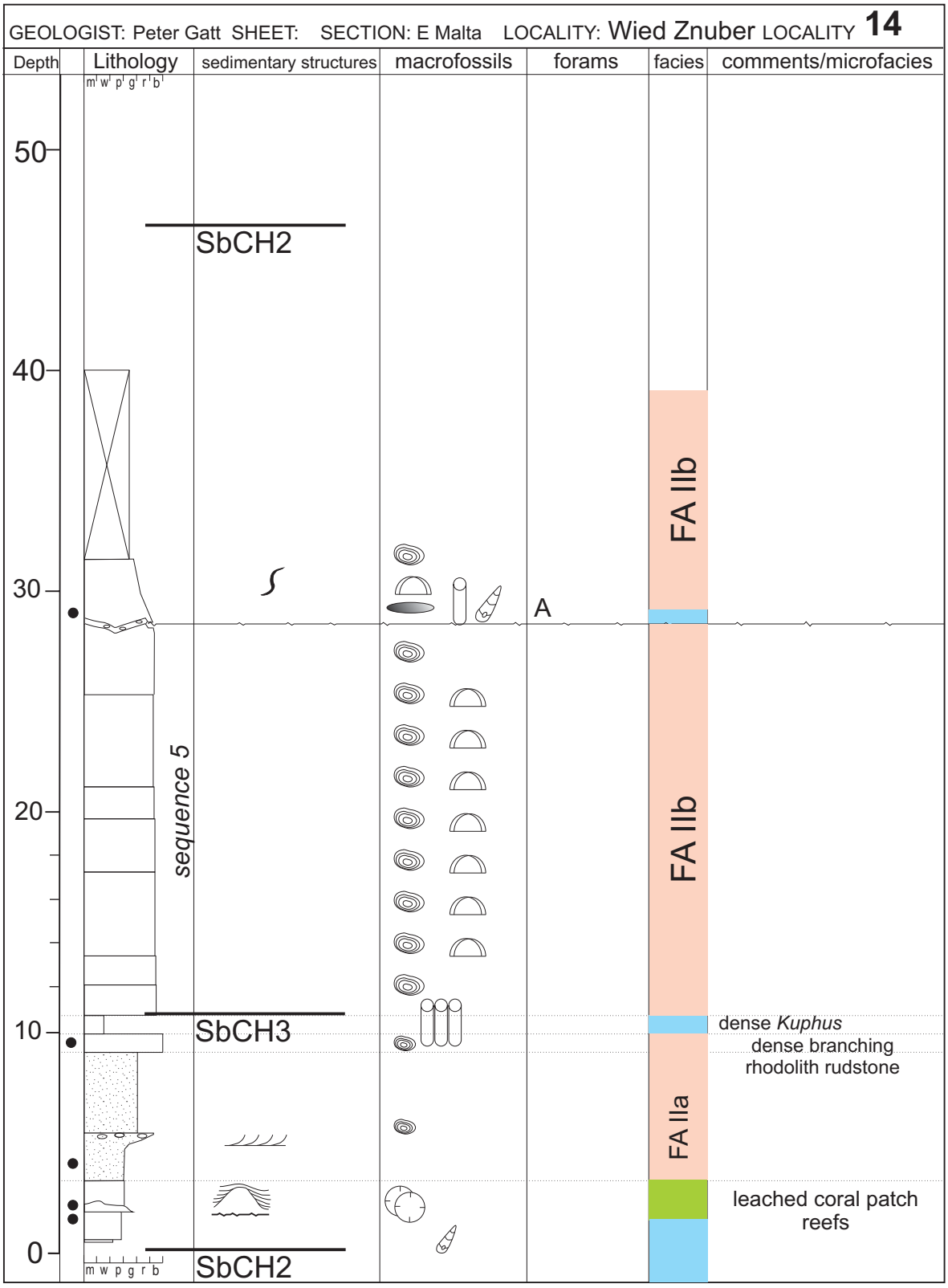
GEOLOGIST: Peter Gatt SHEET: SECTION: E Malta LOCALITY: Wied Znuber LOCALITY 14
Depth
Lithology
m w p g r b
sedimentary structures
macrofossils
forams
facies
comments/microfacies
50
40
30
20
10
0
SbCH2
SbCH3
SbCH2
sequence 5
A
FA IIb
FA IIb
FA IIa
dense Kuphus
dense branching
rhodolith rudstone
leached coral patch
reefs

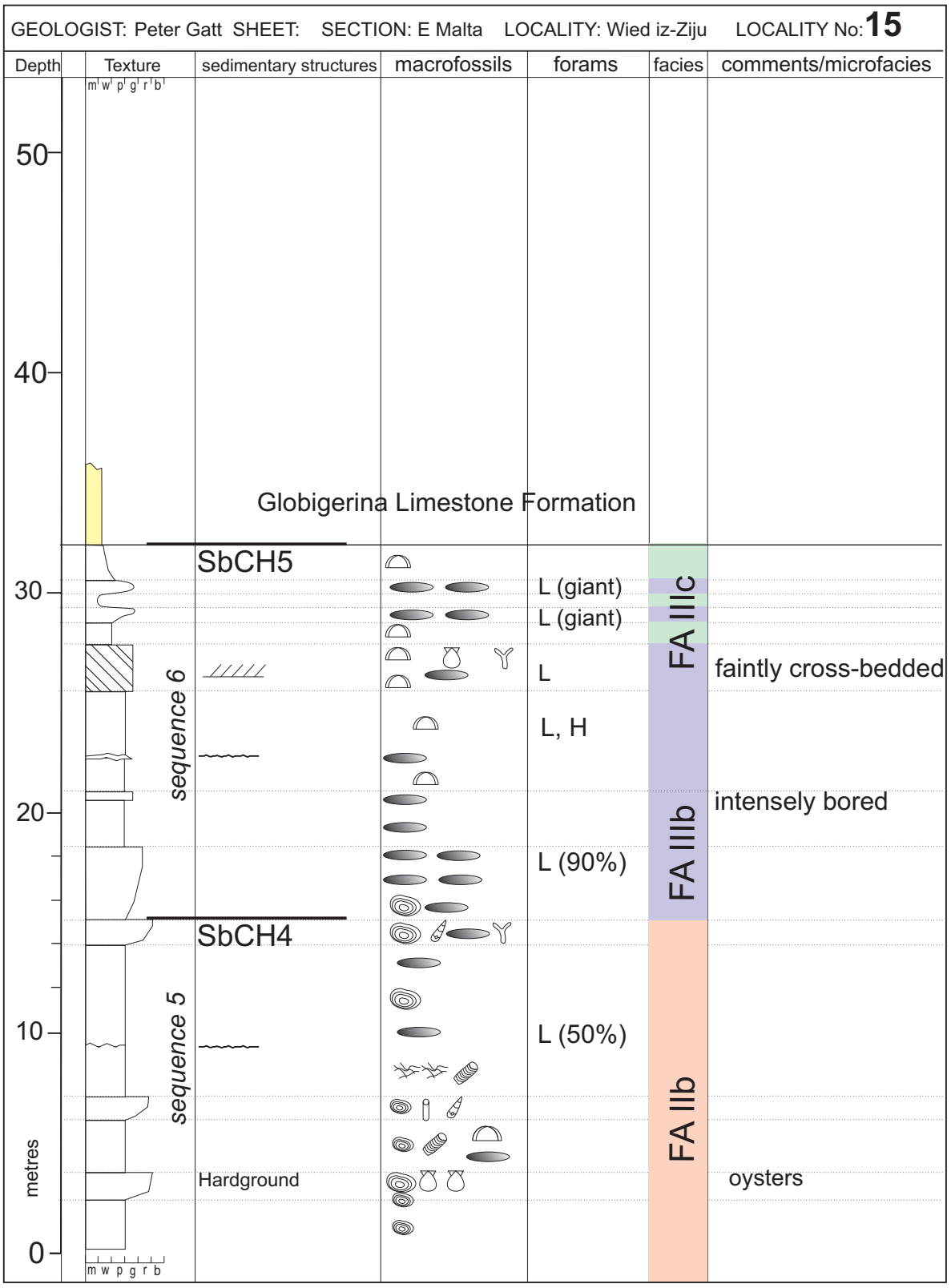
GEOLOGIST: Peter Gatt SHEET: SECTION: E Malta LOCALITY: Wied iz-Ziju LOCALITY No: 15
Depth
Texture
m w p g r b
sedimentary structures
macrofossils
forams
facies
comments/microfacies
50
40
30
20
10
0
metres
Globigerina Limestone Formation
SbCH5
SbCH4
sequence 6
sequence 5
Hardground
L (giant)
L (giant)
L
L, H
L (90%)
L (50%)
FA IIIc
FA IIIb
FA IIb
faintly cross-bedded
intensely bored
oysters

APPENDIX III

Appendix III - 20

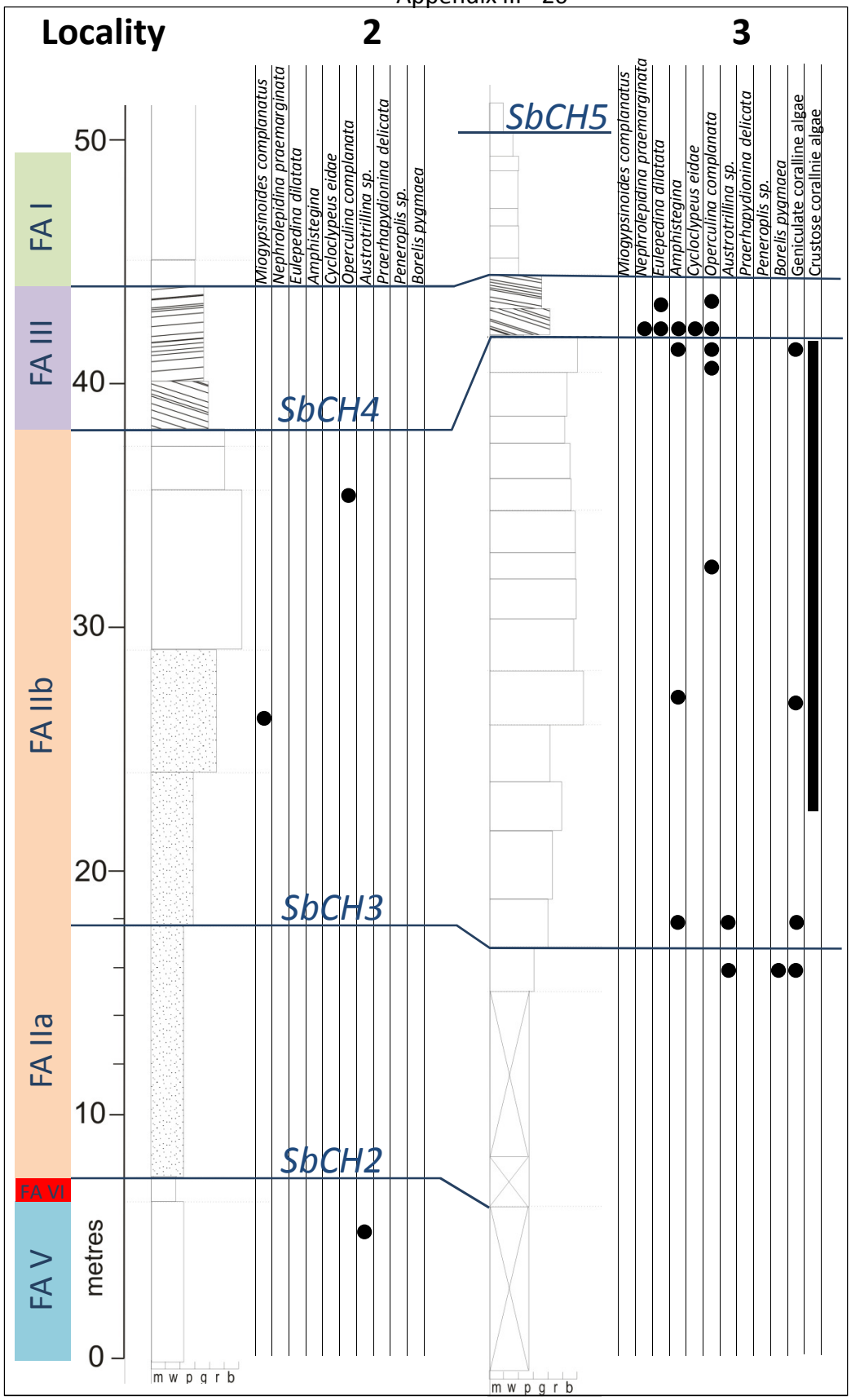

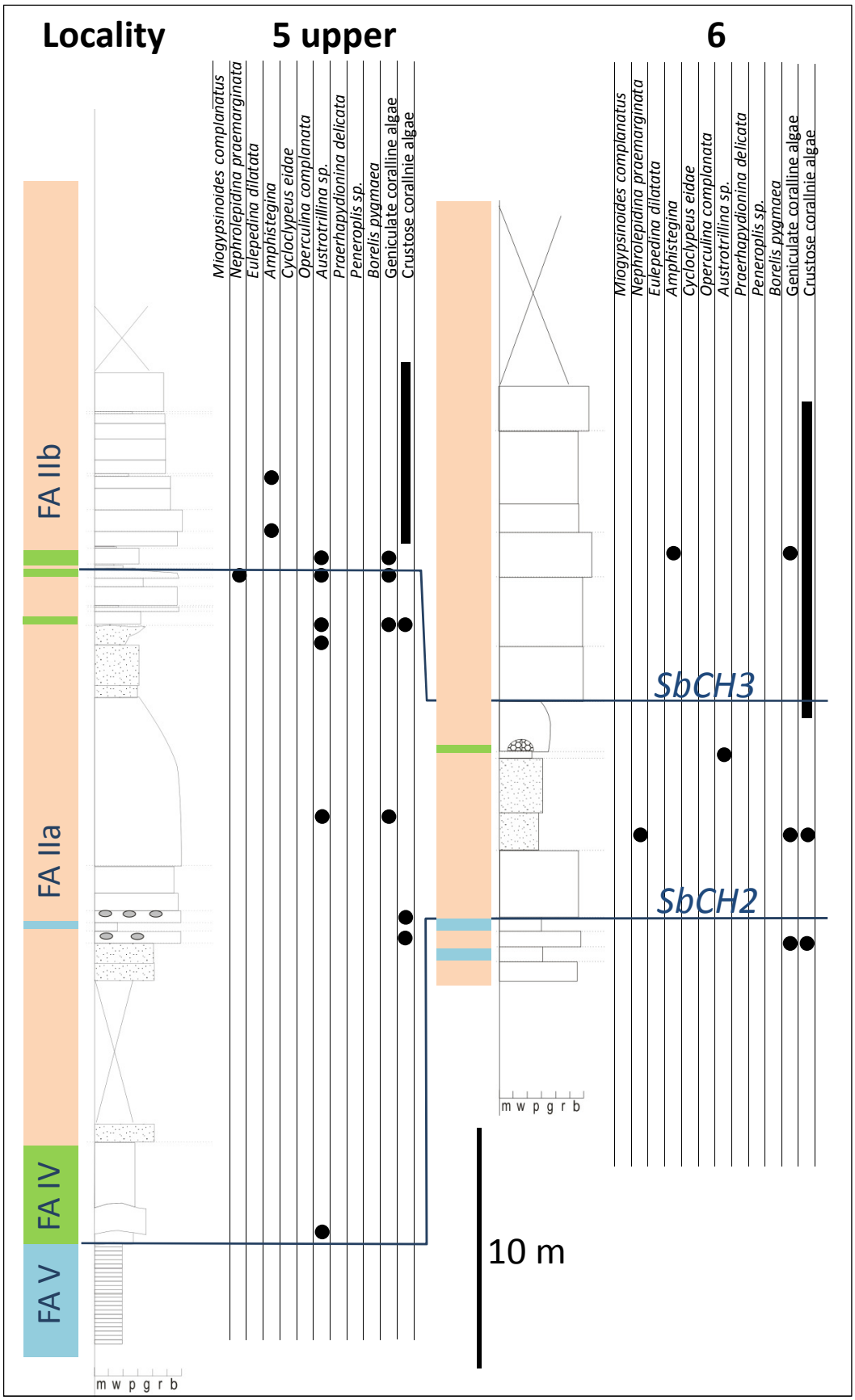
Locality
5 upper
6
Miogypsinoides complanatus
Nephrolepidina praemarginata
Eulepedina dilatata
Amphistegina
Cycloclypeus eidae
Operculina complanata
Austrotrillina sp.
Praerhapydionina delicata
Peneroplis sp.
Borelis pygmaea
Geniculate coralline algae
Crustose corallnie algae
FA IIb
FA IIa
FA IV
FA V
SbCH3
SbCH2
m w p g r b
10 m

Coralline morphology based growth form and taphonomy

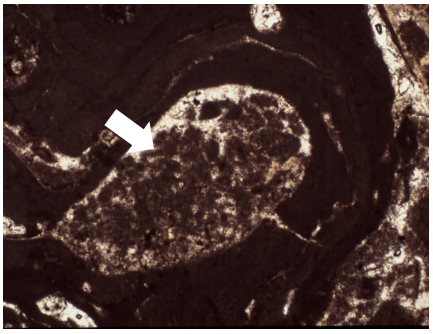

1. Bioerosion

Crustose algae forming a rhodolith showing boring

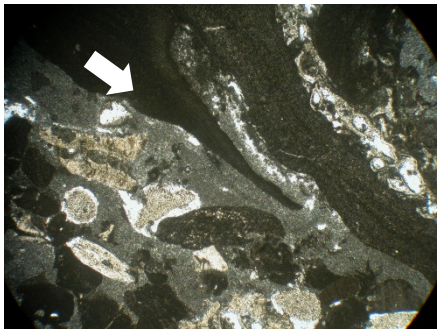

2. Encrustation

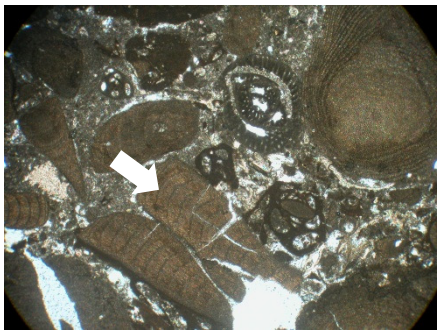

3. Disarticulation

Post mortem disarticulation of geniculate corallines

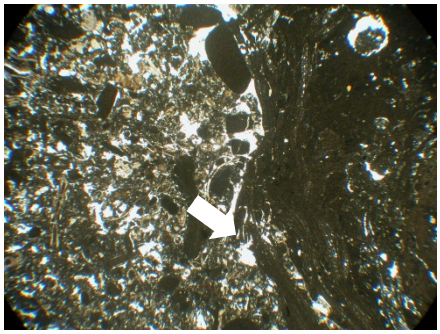

4. Fragmentation

Breakage of protuberances in crustose coralline algae.

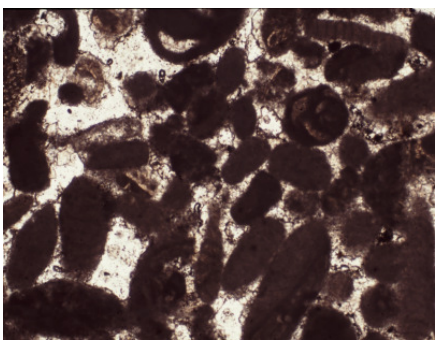

5. Abrasion

Well-rounded Corallines

Facies IIa

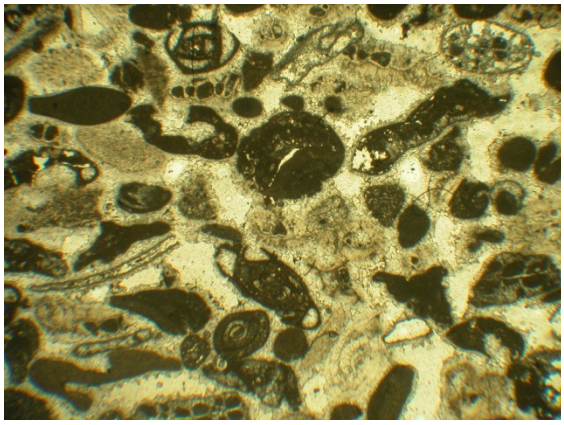

a. Locality 5: cross-bedded grainstone along SbCH3 showing geniculate CRA, miliolids, leached micritic envelopes with equant calcite cement.

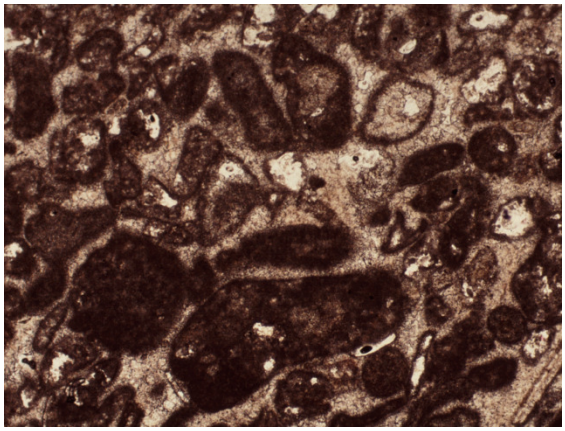

b. Locality 14: <1 m above SbCH2 showing peloids (micritised CRA?) in equant calcite cement.

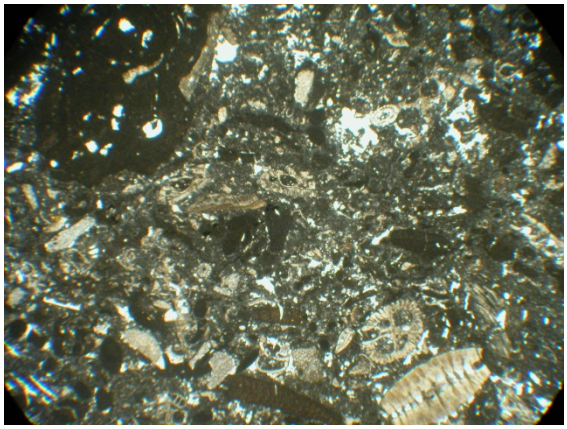

c. Locality 6: packstone 3m below SbCH3 showing geniculate CRA, crustose CRA, echinoid spines and LBF (nummulitid?).

d. Locality 5: packstone with geniculate CRA, crustose CRA and miliolids (*Austrotrillina paucialveolata).*

1 mm

Facies IIb

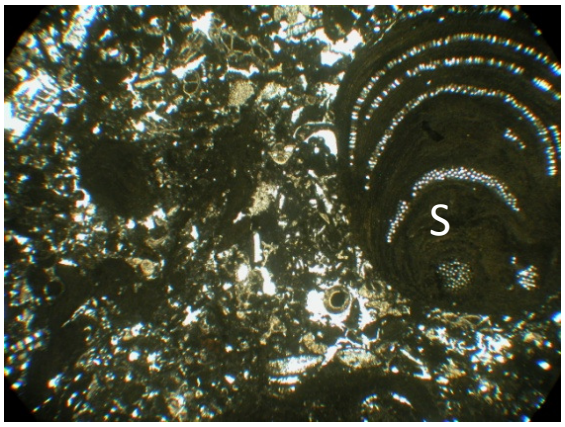

a. Locality 3: Sporolithaceae: *Sporolithon* (S) showing sporangial chambers grouped in *sori*.

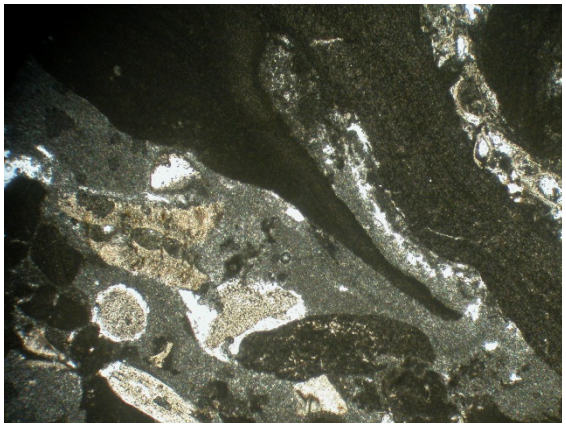

b. Locality 5: Melobesioideae *Lithothamnion*(?) forming a thin crust.

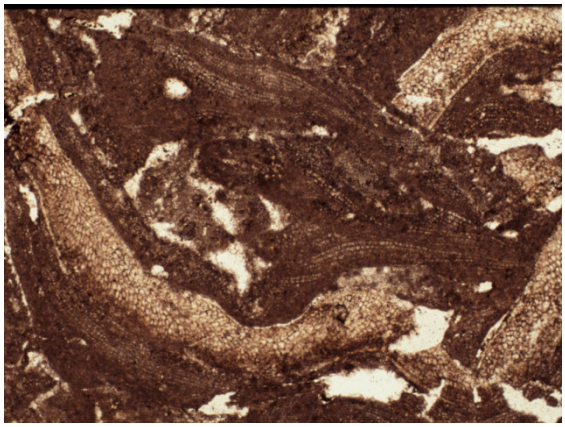

c. Locality 14 Mastophoroideaea: *Neogoniolithon* encrusting a rhodolith.

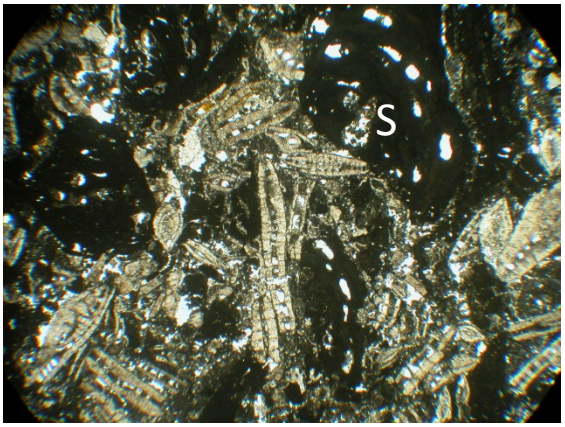

d. Locality 3 Mastophoroideaea: fragmented *Spongites* (S) showing uniporate sporangial conceptacles. The foraminifera are O*perculina.*

1 mm

Facies III

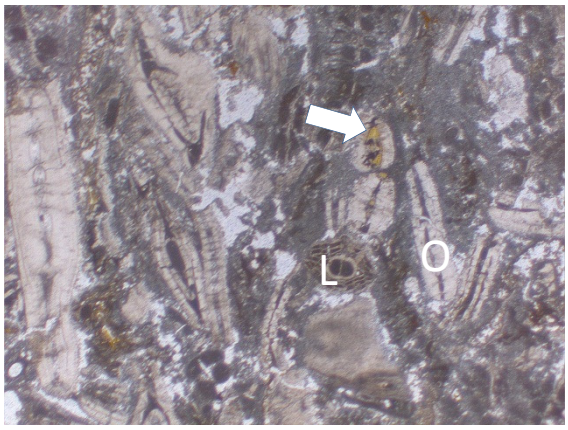

a. FA IIIa. Locality 3 bed 1. Intragranular glauconite

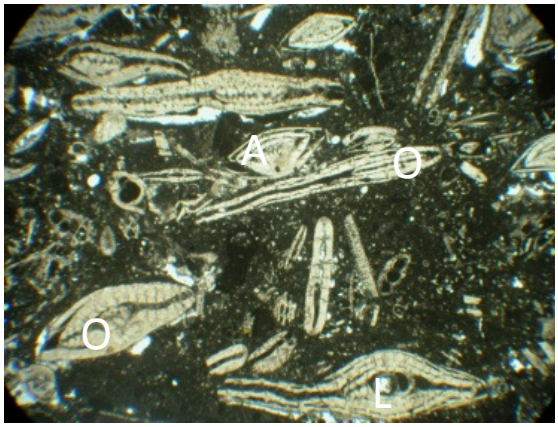

b. FA IIIa. Locality 3 bed 4a.

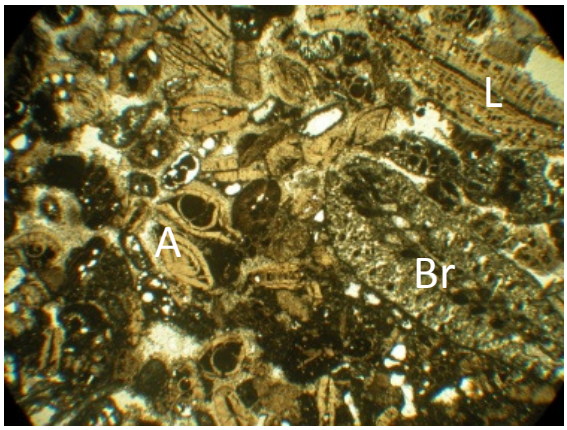

c. FA IIIa. Locality 3, bed 4b

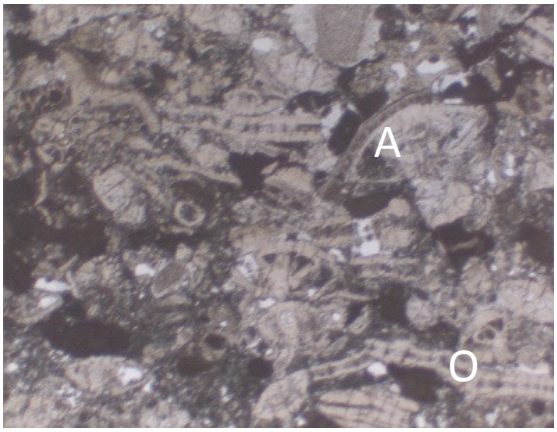

d. FA IIIa. Locality 4b

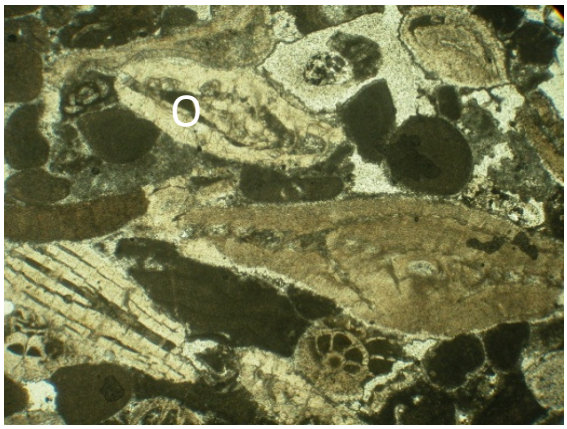

e. Facies IIIb. Locality 10b. LBF with CRA

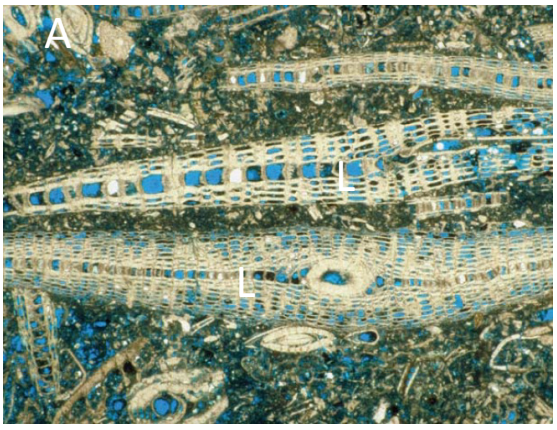

f. FA IIIc.

1 mm

A: *Amphistegina*; O. *Operculina*; L. *Lepidocyclina;* Br: bryozoans

Facies IV

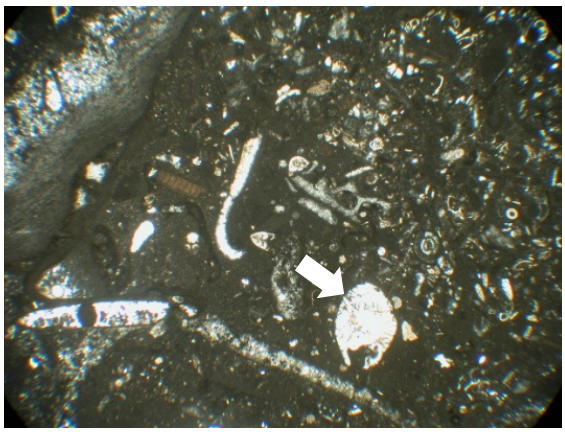

a. Locality 3 (lowermost 2 m).

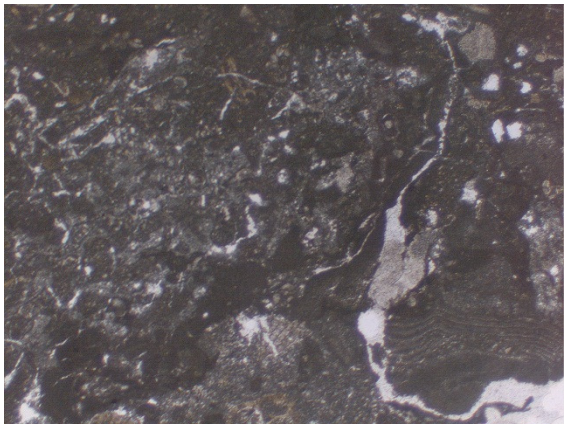

b. Ta' Kandja locality. Matrix surrounding leached coral framestone

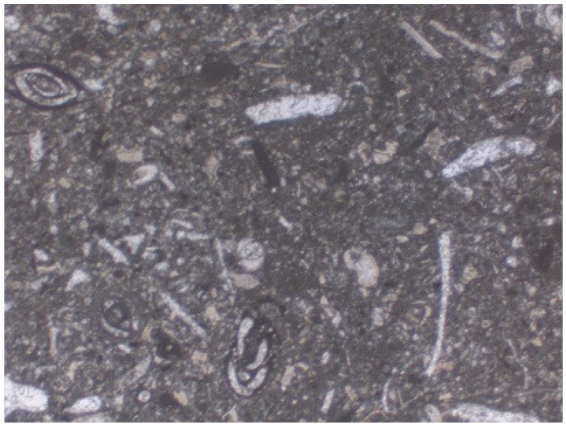

1 mm

c. Locality 9. Miliolid-bivalve packstone matrix around leached coral

Facies V

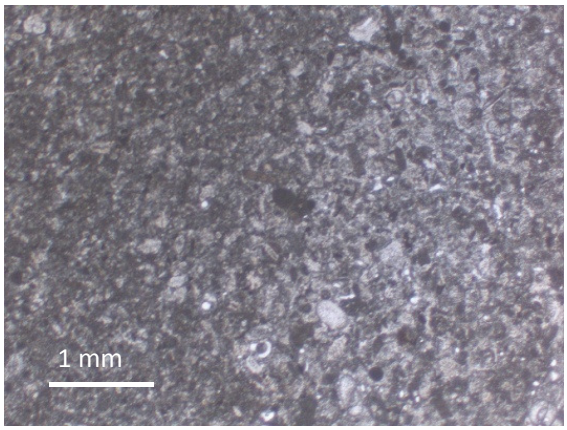

a. Locality 9. fine grained packstone

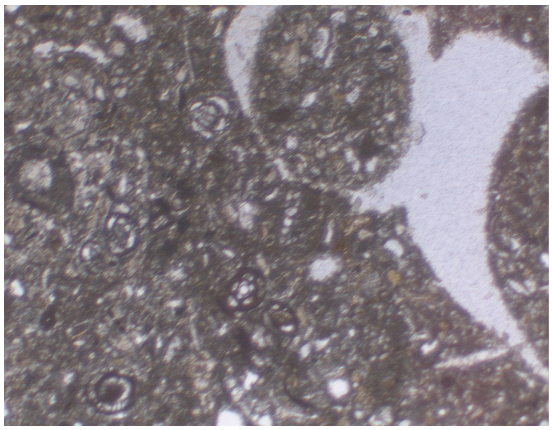

b. Locality 5. packstone with miliolids and leached aragonite macrofossils.

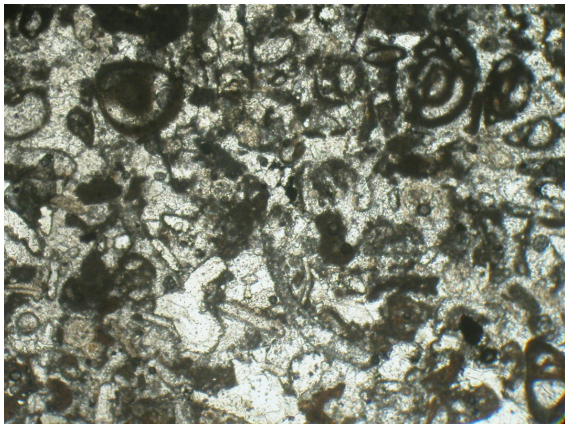

c. Locality 5. Mililolid grainstone and micritic envelopes after leached aragonite grains.

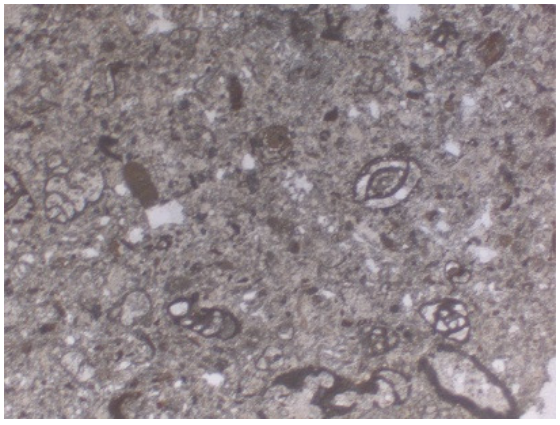

d. Locality 1. Miliolid packstone with rare geniculate coralline algae

Facies VI

a. Locality 5. Crushed *Kuphus* tube in a packstone matrix.

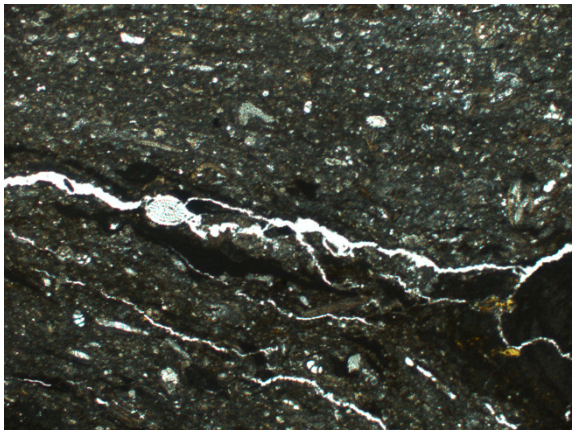

b. Locality 6. Seams of organic matter/clay in a laminated fine-grained marl matrix.

1 mm

Deep wells in the Malta Platform

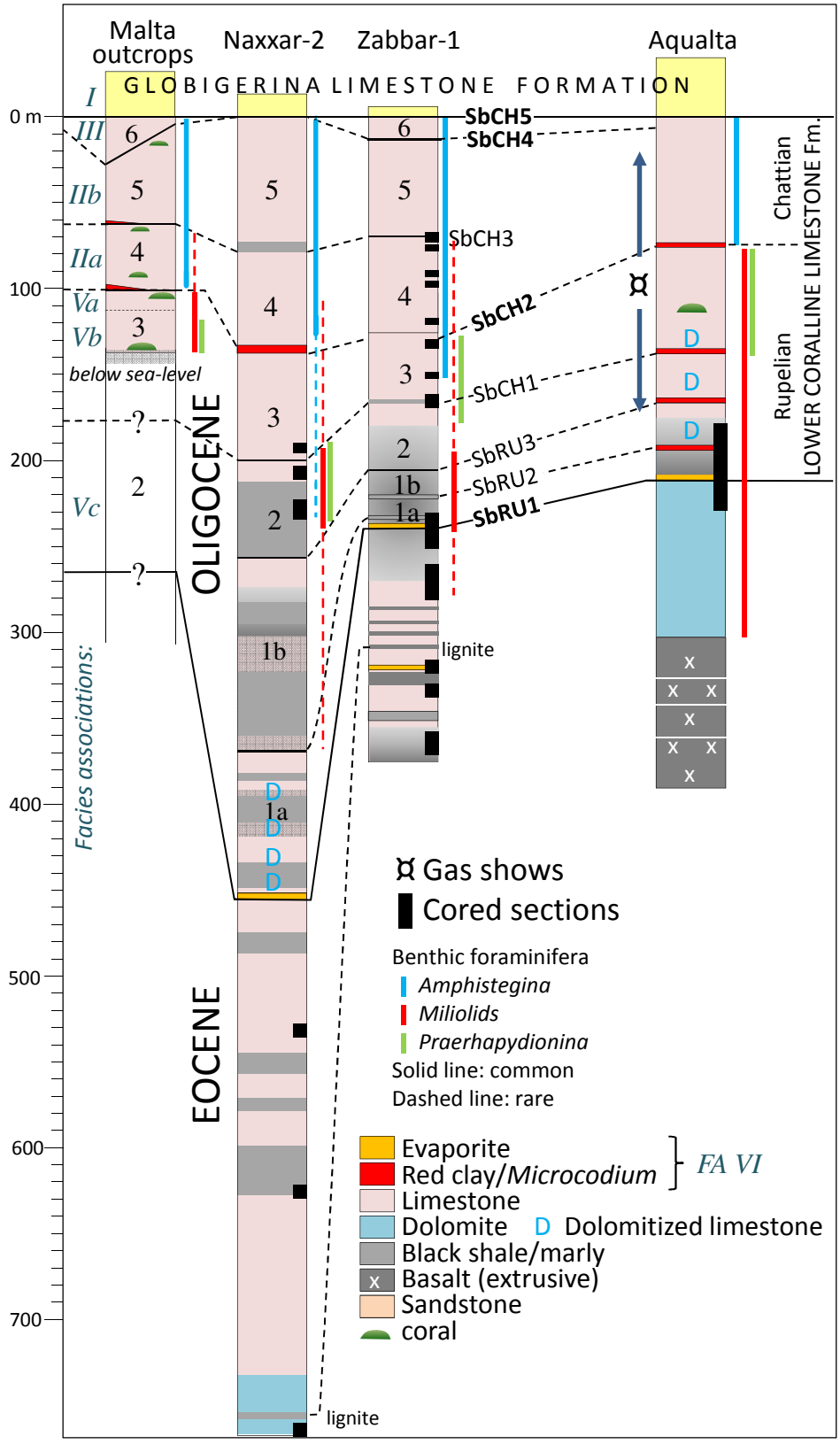

Appendix IV

Photomontage of cliffed coast of localities C & B

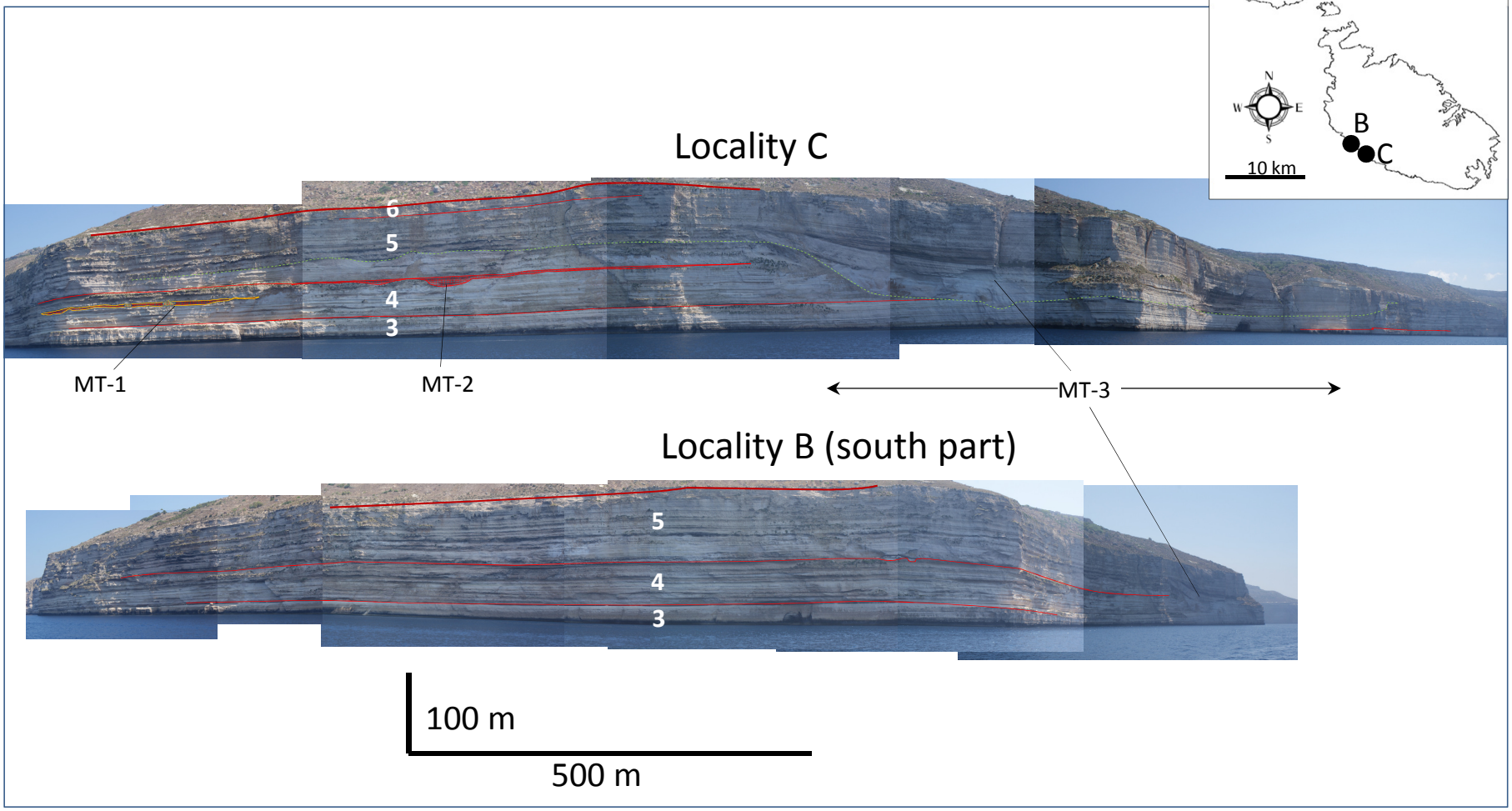

Photomontage of cliffed coast of localities A & B

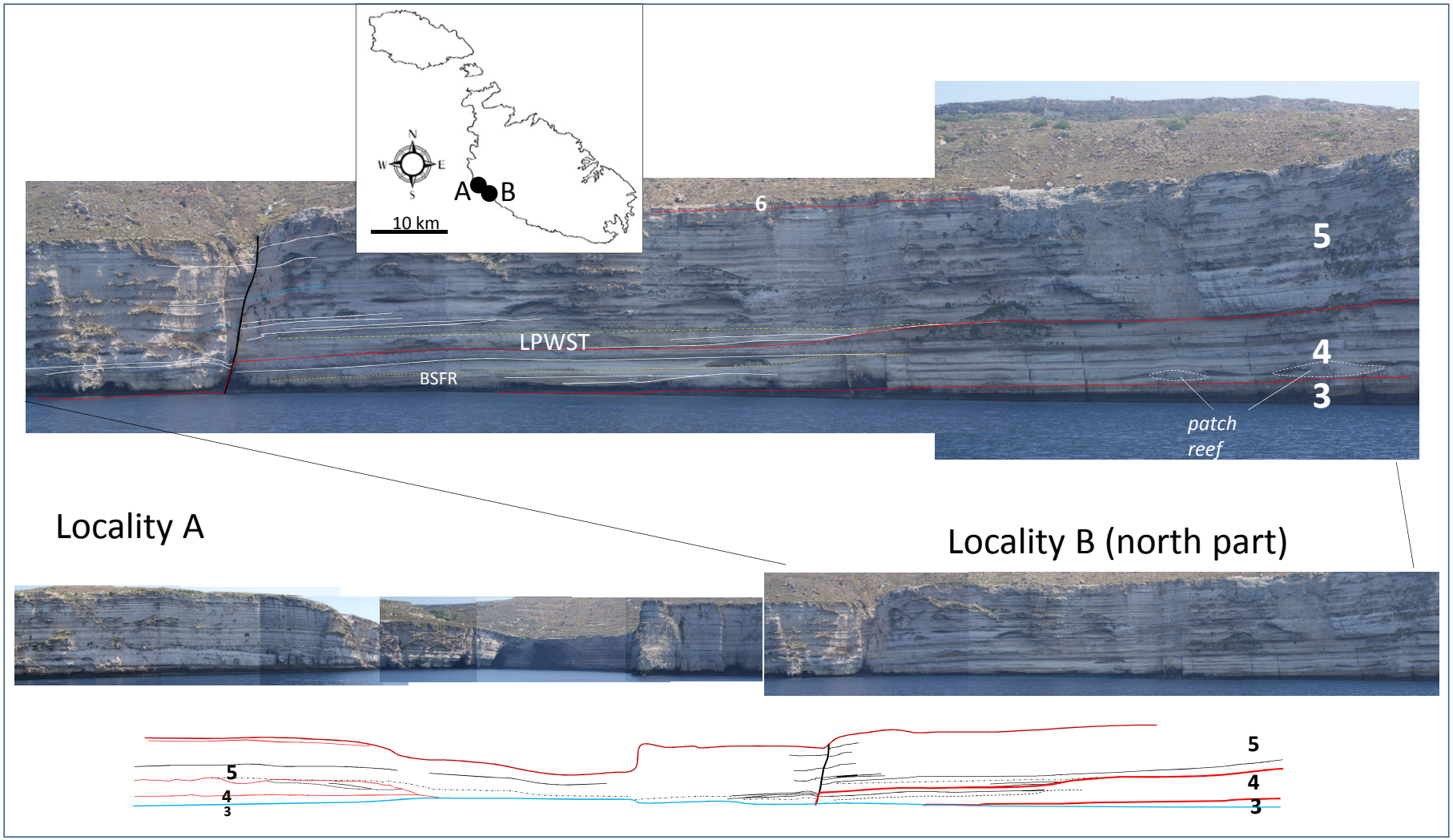

Photomontage of localities 10b, 13, 14

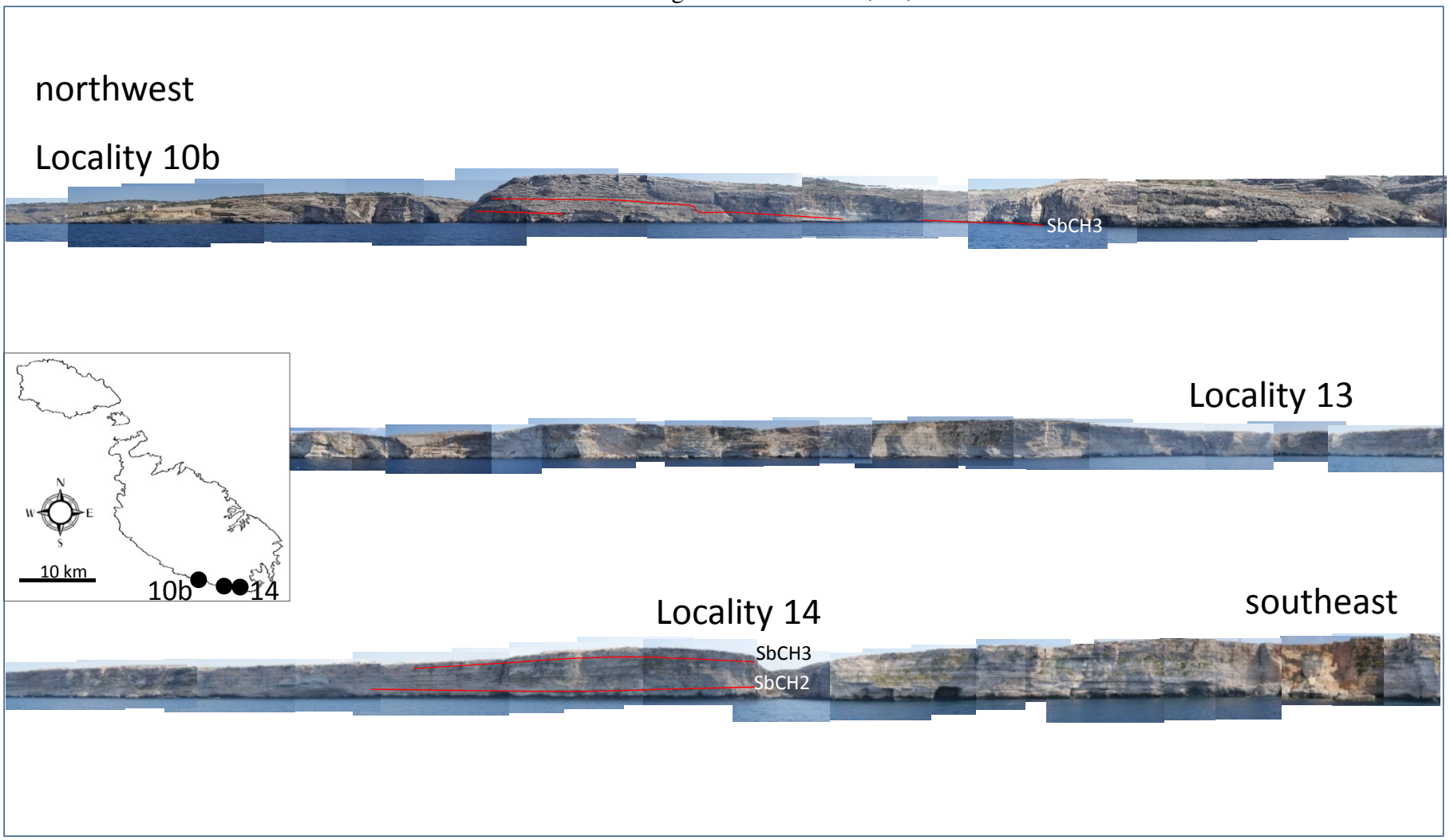

Appendix V

Photograph of locality 1	33
Photograph of locality 1 (inland sea)	34
Photograph of locality A	35
Photograph of locality A & 3	36
Photograph of locality 5	37
Photograph of locality B	38
Photograph of locality C	39
Photograph of locality D	40
Photograph of locality 13	41
Photograph of locality 14	42

Locality H

Dwejra cliffs

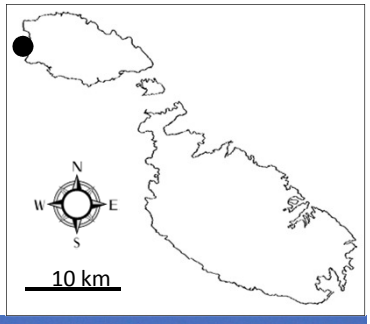

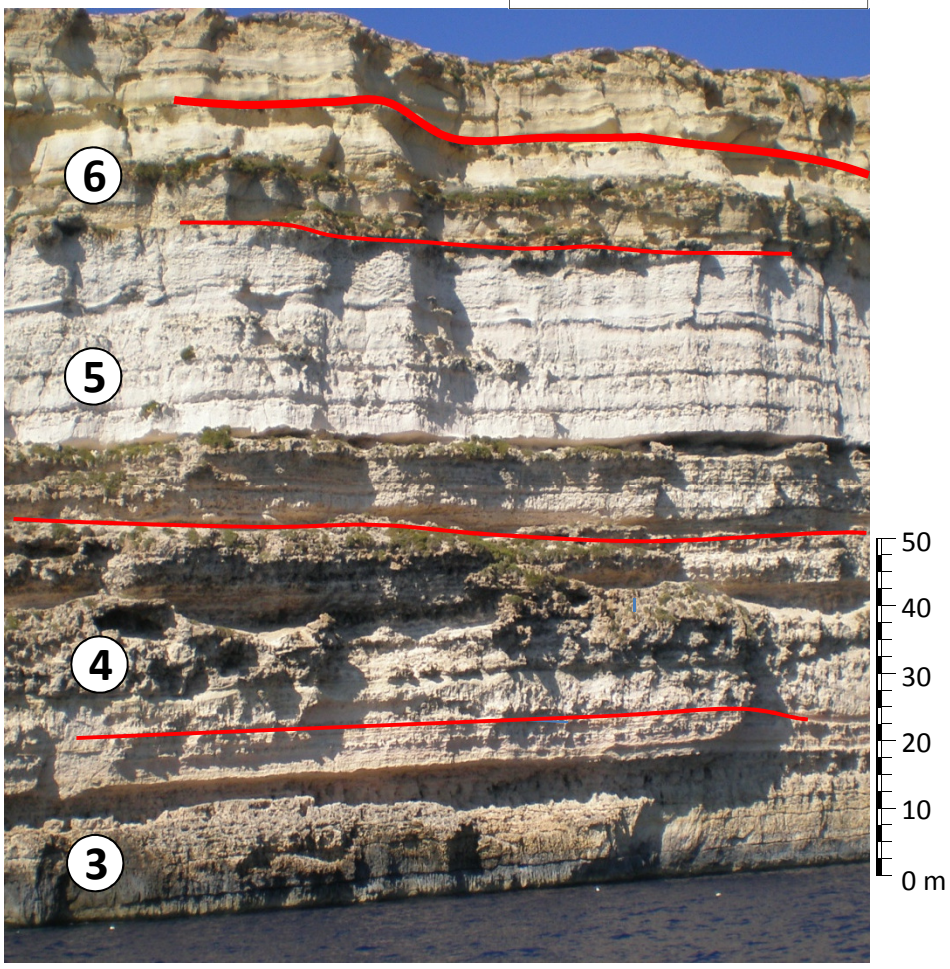

③ *Depositional sequence*

Sequence boundary (SbCH)

Locality 1

Dwejra (Inland Sea)

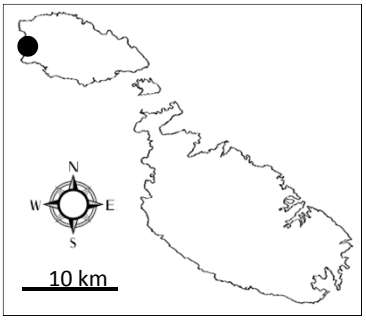

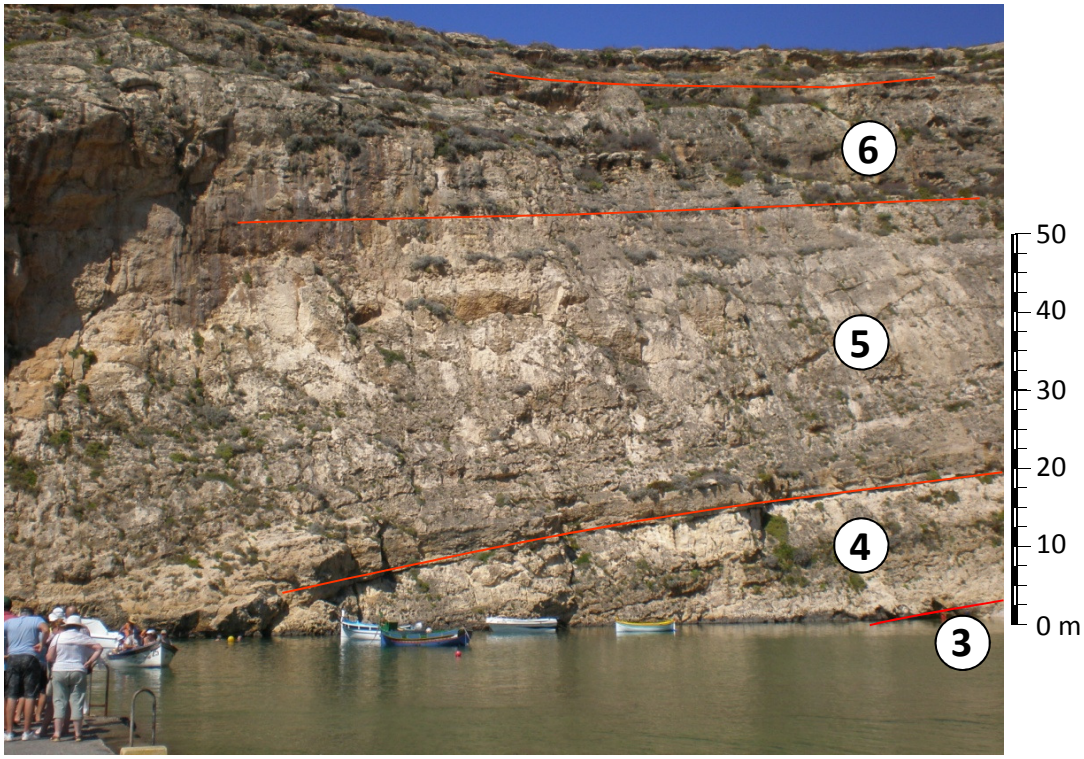

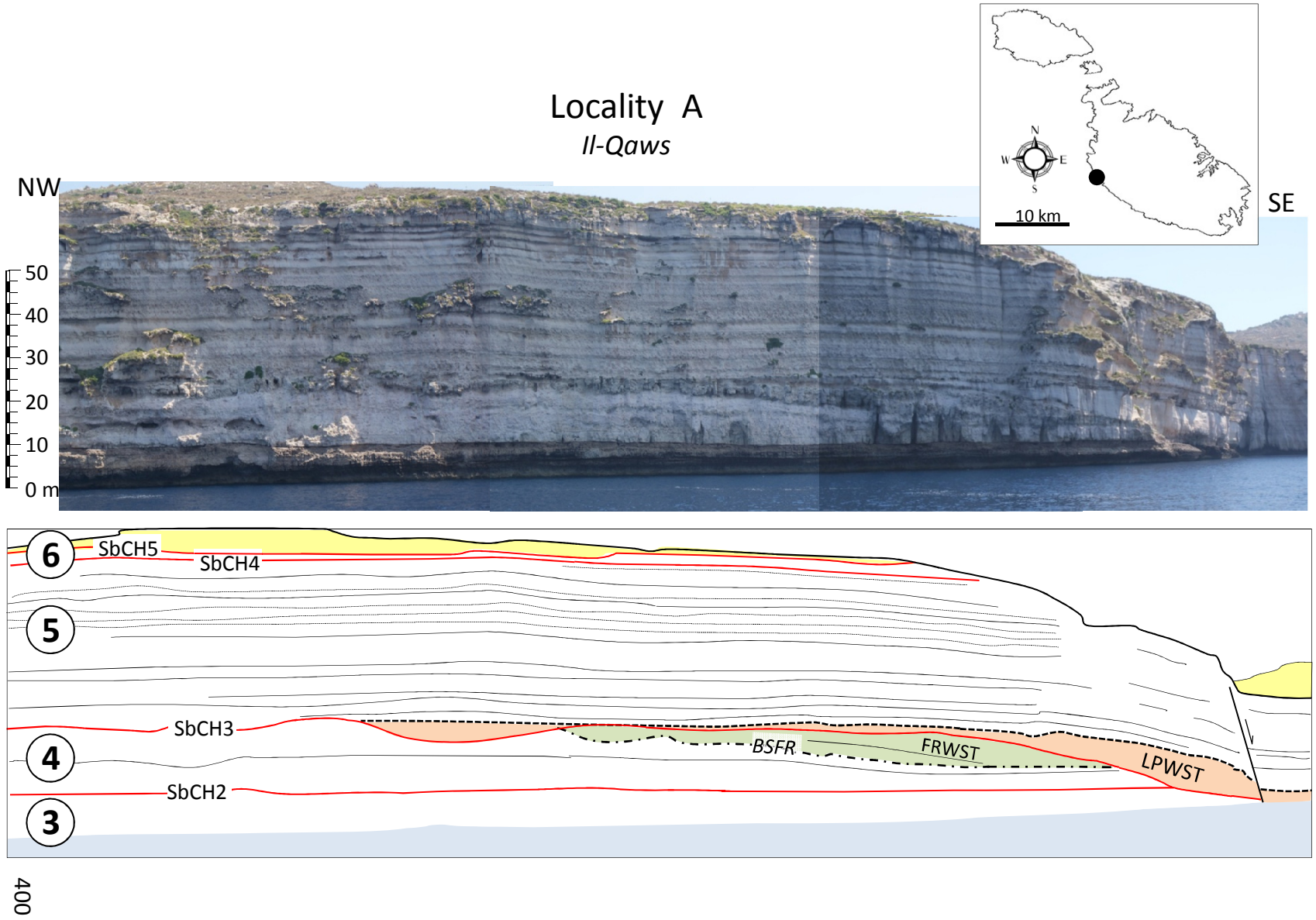
Locality A
Il-Qaws
NW
SE
50
40
30
20
10
0 m
10 km
N
W
E
S
6
5
4
3
SbCH5
SbCH4
SbCH3
SbCH2
BSFR
FRWST
LPWST

400

3

Locality 3 to A

Migra Ferha/Ras id-Dawwara

Locality 5

Mosta Quarry

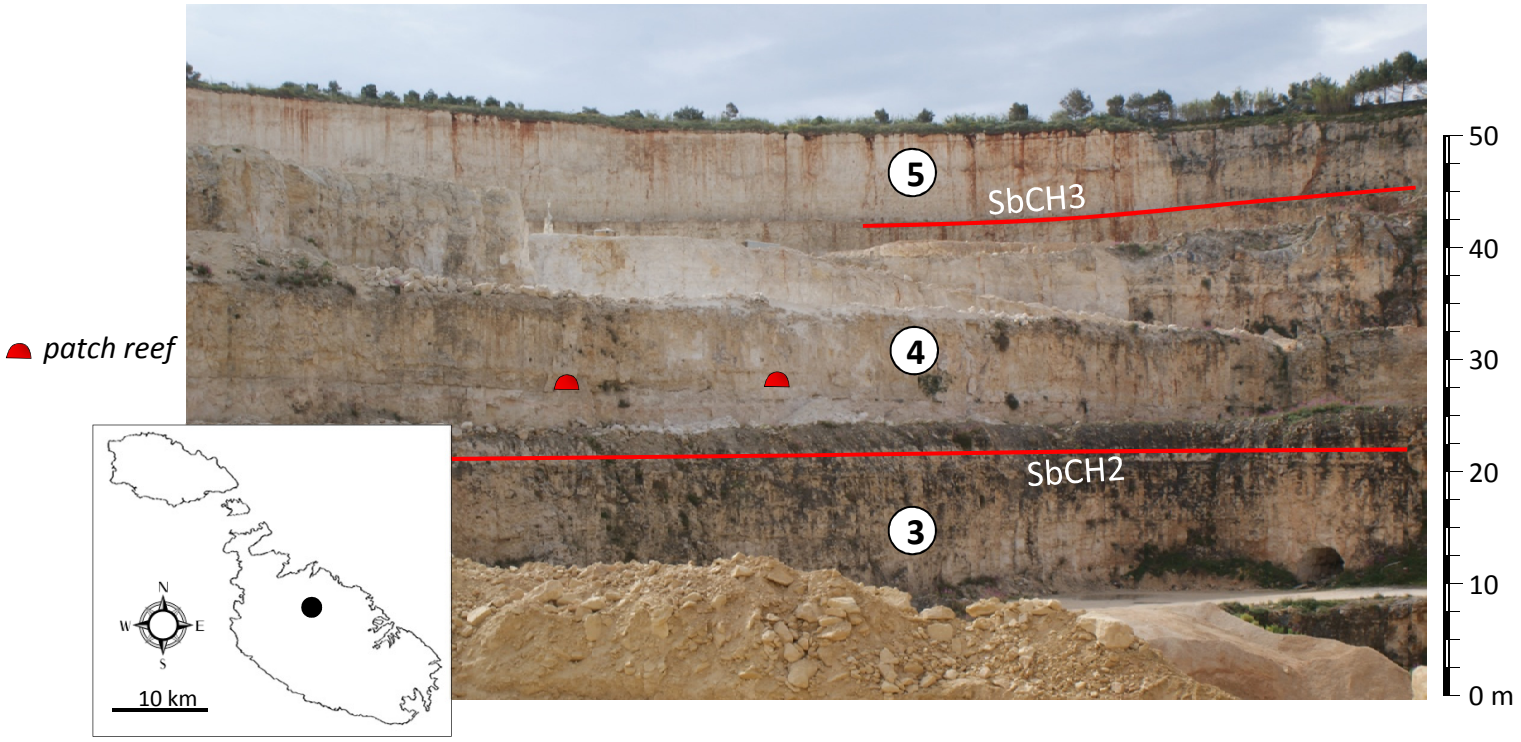

Locality B

Rdum ta' Dun Nazju

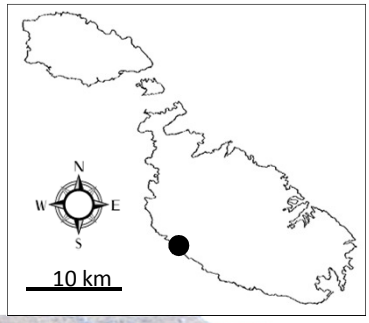

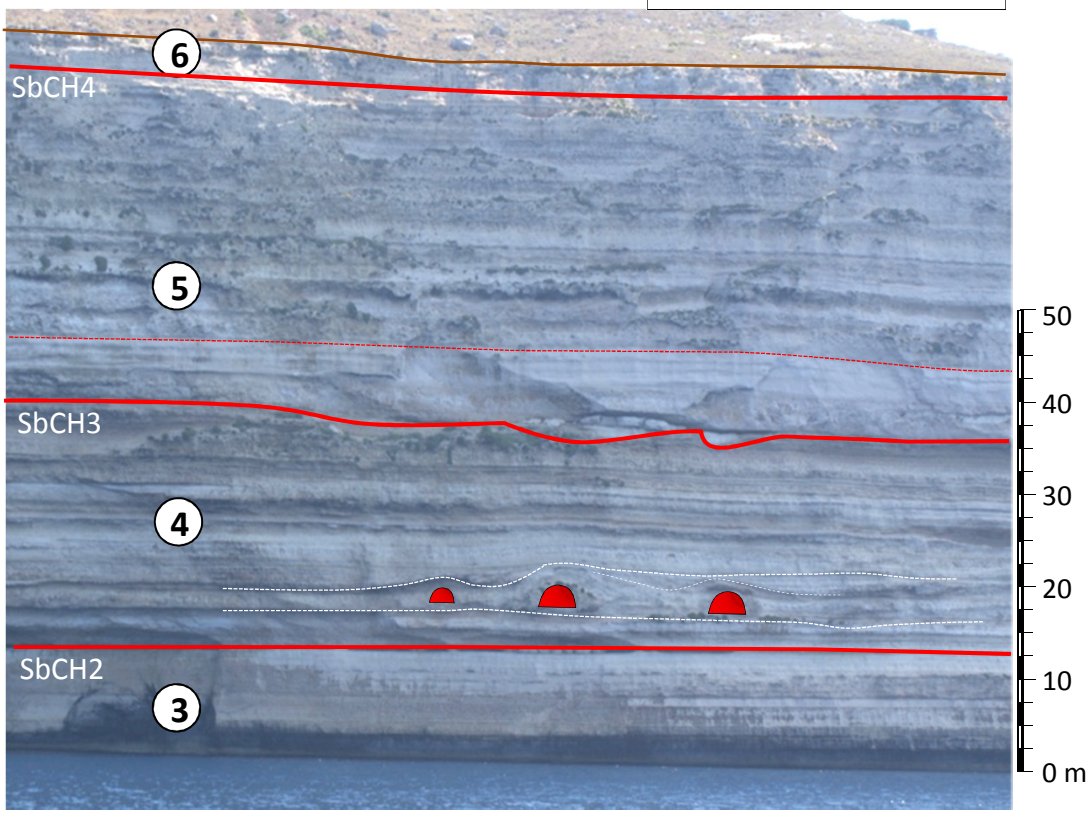

Locality C

Rdum Dikkiena

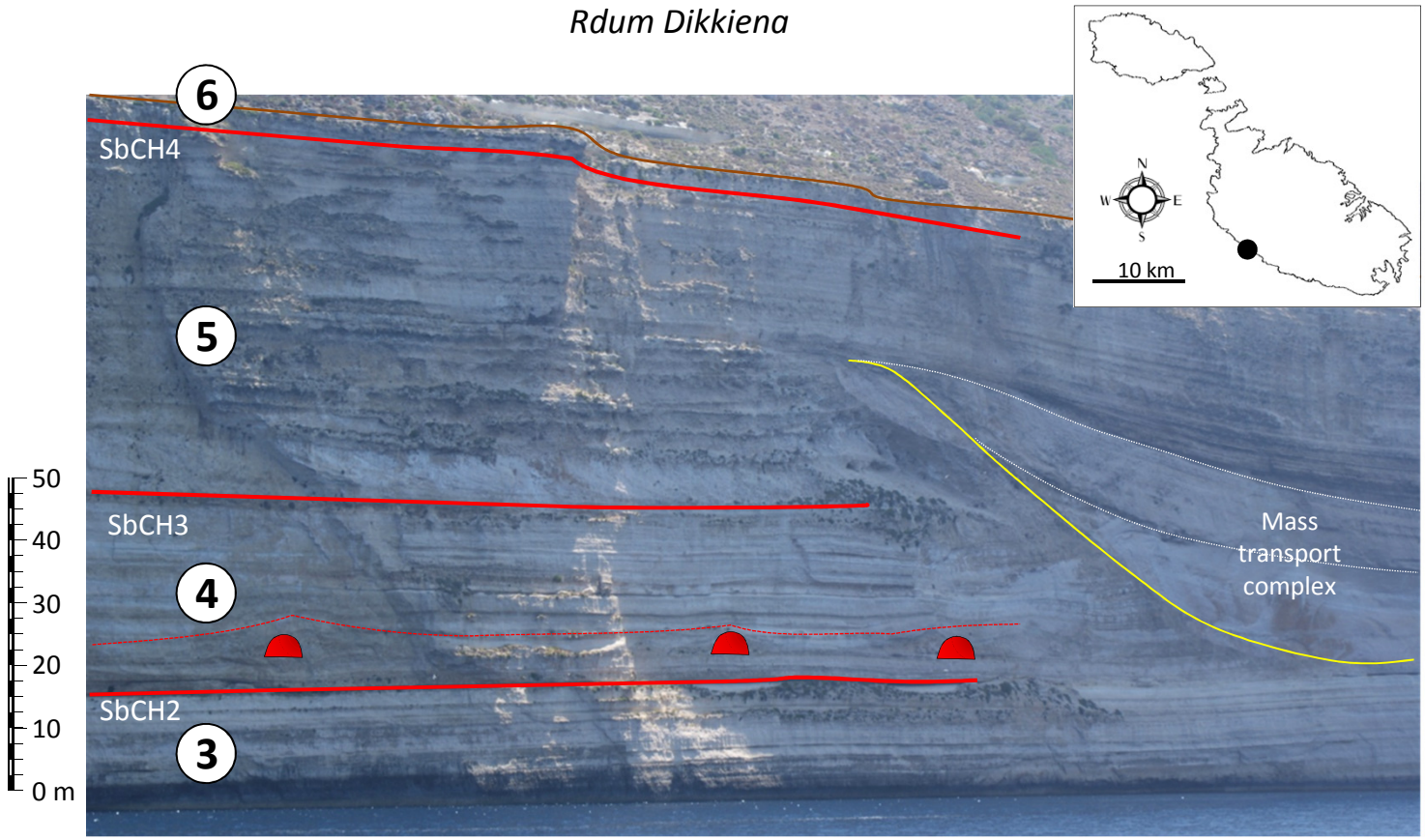

Locality D

Il-Kullana/Migra ilma

Locality 13

Wied Moqbol

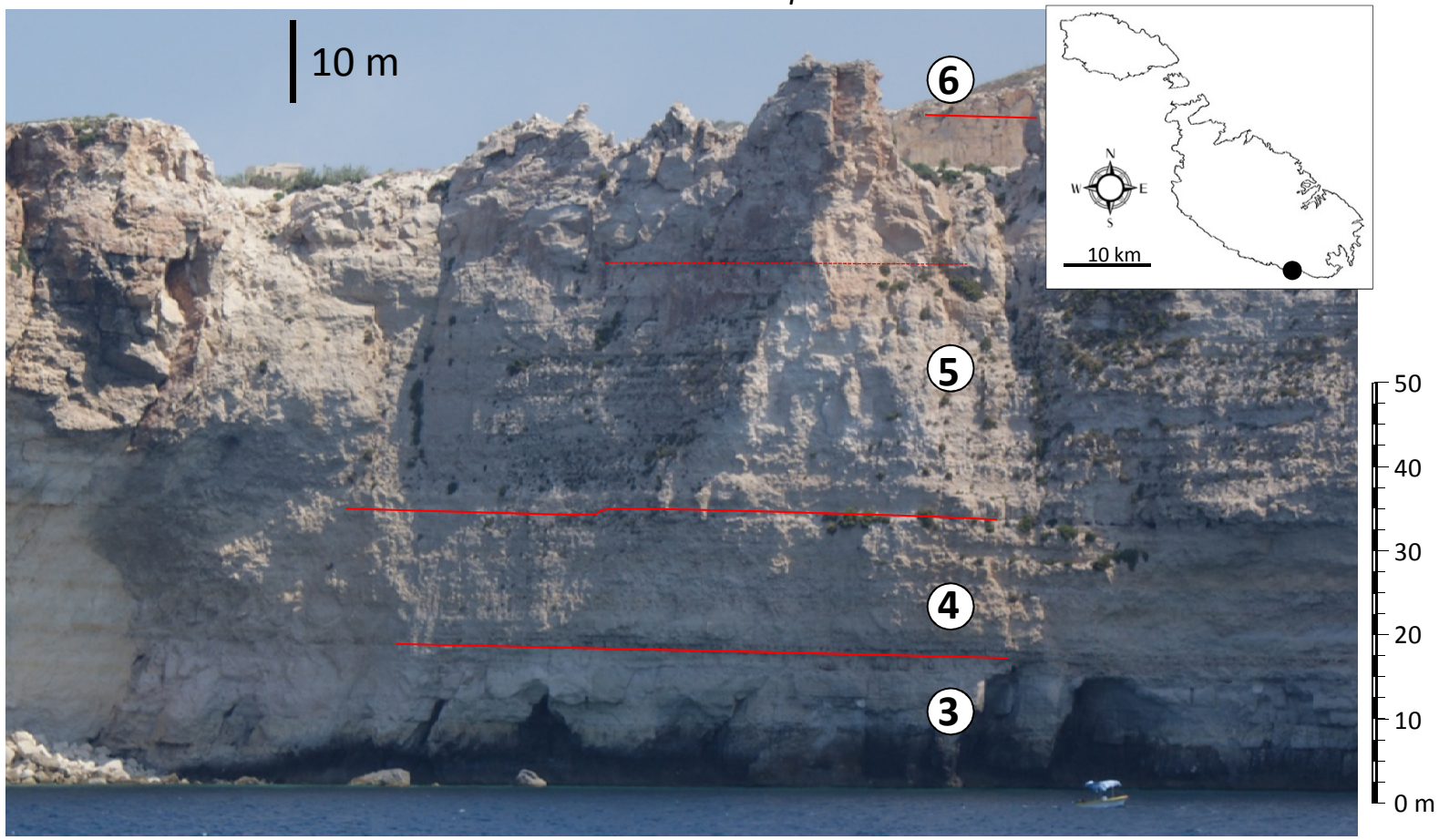

Locality 14

Wied Znuber

REFERENCES

Abels, H., Hilgen, F., Krijgsman, W., Kruk, R., Raffi, I., Turco, E., *et al.*. (2005). Long-period orbital control on middle Miocene global cooling: Integrated stratigraphy and astronomical tuning of the Blue Clay Formation on Malta. *Paleoceanography*, **20**, 1-17.

Abels, H., Van Simaeys, S., Hilgen, F., De Man, E., & Vandenberghe, N. (2007). Obliquity-dominated glacio-eustatic sea level change in the early Oligocene: evidence from the shallow marine siliciclastic Rupelian stratotype (Boom Formation, Belgium). *Terra Nova*, **19**, 65-73.

Abreu, V. S., & Haddad, G. A. (1998). Glacioeustatic fluctuations: The mechanism linking stable isotope events and sequence stratigraphy from thr Early Oligocene to Middle Miocene. *In:* P.-C. Graciansky, J. Hardenbol, T. Jacquin, & P. R. Vail (Eds.), *Mesozoic and Cenozoic Sequence Stratigraphy of European Basins.* Society for Sedimentary Geology (SEPM) Special Publication **60**, 245-259.

Adams, C. G., Lee, D. E., & Rosen, B. R. (1990). Conflicting isotopic and biotic evidence for tropical sea-surface temperatures during the Tertiary. *Palaeogeography, Palaeoclimatology, Palaeoecology*, **77**, 289-313.

Aguirre, J., Riding, R., & Braga, J. (2000). Diversity of coralline red algae: origination and extinction patterns from the Early Cretaceous to the Pleistocene. *Paleobiology*, **26**, 651-667.

Aigner, T. (1985). Biofabrics as dynamic indicators in Nummulite accummulations. *Journal of Sedimentary Research*, **55**, 131-134.

Allan, J., & Matthews, R. (1982). Isotope signatures associated with early meteoric diagenesis. *Sedimentology*, **29**, 797-817.

Allen, P., & Allen, J. (1990). *Basin Analysis.* Blackwell Scientific Publications.

Allison, P., Wignall, P., & Brett, C. (1995). Palaeo-oxygenation: effects and recognition. *In:* D. W. Bosence, & P. Allison (Eds.), *Marine palaeoenvironmental analysis from fossils.* Geological Society Special Publication **83**, 97-112.

Anselmetti, F., & Eberli, G. (1993). Controls on sonic velocity in carbonate rocks. *Pure and Applied Geophysics*, **141**, 287-323.

Antonelli, M., Franciosi, R., Pezzi, G., Querci, A., Ronco, G. P., & Vezzani, F. (1988). Palaeogeographic evolution and structural setting of the northern side of the Sicily Channel. *Memorie della societa geologica italiana*, **41** (5), 141-157.

Armstrong, H., & Allen, M. (2011). Shifts in the Intertropical Convergence Zone, Himalayan exhumation, and late Cenozoic climate. *Geology* **39**, 11-14.

Armstrong, W. (1996). *Minerals Resource Assessment for the Planning Authority of Malta.* Planning Authority, Malta.

Baker, A., Starger, C., McClanahan, T., & Glynn, P. (2004). Corals' adaptive response to climate change. *Nature*, **430**, 741.

Bakun, A., & Agostini, V. (2001). Seasonal patterns of wind-induced upwelling/downwelling in the Mediterranean Sea. *Scientia Marina*, **65**, 243-257.

Barr, D. (1987). Lithospheric stretching, detached normal faulting and footwall uplift. *In:* M. Coward, J. Dewey, & P. Hancock (Eds.), *Continental Extensional Tectonics.* Geological Society, London, Special Publications, **28**, 75-94.

Basilone, L. (2009). Mesozoic tectono-sedimentary evolution of Rocca Busambra in western Sicily. *Facies*, **55**, 115-135.

Bassi, D., & Nebelsick, J. (2010). Components, facies and ramps: Redefining Upper Oligocene shallow water carbonates using coralline red algae and larger foraminifera (Venetian area, NE Italy). *Palaeogeography, Palaeoclimatology, Palaeoecology*, **295**, 258-280.

Bassi, D., Hottinger, L., & Nebelsick, J. (2007). Larger foraminifera from the Upper Oligocene of the Venetian area, northeast Italy. *Palaeontology*, **50**, 845-868.

Bathurst, R. G. (1975). *Carbonate sediments and their diagenesis. Developments in Sedimentology 12.* Elsevier, Amsterdam, 658pp.

Beavington-Penney, S. J. (2004). Analysis of the effects of abrasion on the test of Palaeonummulites venosus: implications for the origin of nummulithoclastic sediments. *Palaios*, **19**, 143-155.

Beavington-Penney, S. J., Wright, V. P., & Racey, A. (2005). Sediment production and dispersal on foraminifera-dominated early Tertiary ramps: the Eocene El Garia Formation, Tunisia. *Sedimentology*, *52*, 537–569.

Beavington-Penney, S., Nadin, P., Wright, V., Clarke, E., McQuilken, J., & Bailey, H. (2008). Reservoir quality variation on an Eocene carbonate ramp, El Garia Formation, offshore Tunisia: Structural control of burial corrosion and dolomitisation. *Sedimentary Geology*, **209**, 42-57.

Beavington-Penney, S., Wright, V., & Racey, A. (2005). Sediment production and dispersal on foraminifera-dominated early Tetiary ramps: the Eocene El Garia Formation, Tunisia. *Sedimentology*, **52**, 537–569.

Beavington-Penney, S., Wright, V., & Racey, A. (2006). The middle Eocene Seeb Formation of Oman: An investigation of acyclicity, stratigraphic completeness,and accummulation rates in shallow marine carbonate settings. *Journal of Sedimentary Research*, **76**, 1137–1161.

Belopolsky, A., & Droxler, A. (2004). Seismic expressions of prograding carbonate bank margins: Middle Miocene, Maldives, Indian Ocean. *In:* G. Eberli, J. Masaferro, & J. Sarg (Eds.), *Seismic imaging of carbonate reservoirs and systems.* AAPG Memoir **81**, 267-290.

Ben Avraham, Z., Lyakhovsky, V., & Grasso, M. (1995). Simulation of collision zone segmentation in the central Mediterranean. *Tectonophysics*, **243**, 57-68.

Ben-Avraham, Z., & Ginsburg, A. (1990). Displaced terranes and crustal evolution of the Levant and the Eastern Mediterranean. *Tectonics*, **9** (4), 613-622.

Ben-Avraham, Z., Woodside, J., Lodolo, E., Gardosh, M., Grasso, M., Camerlenghi, A., *et al.*. (2006). Eastern Mediterranean basin systems. *In:* D. G. Gee, & R. A. Stephenson (Eds.), *European Lithosphere dynamics.* Geological Society of London, Memoir **32**, 263-276.

Bennett, S. (1980). *Palaeoenvironmental studies in Maltese mid-Tertiary carbonates.* Unpublished PhD thesis, University of London.

Berggren, W. A., Kent, D. V., Swisher, C. C., & Aubry, M. P. (1995). A revised Cenozoic Geochronology and Chronostratigraphy. *In:* W. A. Berggren, D. V. Kent, & J. Hardenbol (Eds.), *Geochronology Time Scales and global Stratigraphic Correlations: A Unified Temporal Framework for an Historical Geology.* Society of Economic Paleontologists and Mineralogists Special **54**.

Bernoulli, D., & Jenkyns, H. C. (1974). Alpine, Mediterranean, and Central Atlantic Mesozoic facies in relation to the early evolution of the Tethys. *In: Modern and Ancient geosynclinal sedimentation.* Tulsa, USA: SEPM Special publication, **19**, 129-160.

Bevan, T., Roberts, A., Kusznir, N., & Mohn, G. (2010). Cretaceous or Permo-Triassic opening of S Tethys in the Ionian sea? Support from crustal structure and subsidence analysis of the offshore Sirt Basin, Libya. *New and emerging plays in the Eastern Mediterranean.* Geological Society, London, Conference Abstract, p.29.

Bishop, W. (1975). Geology of Tunisia and adjacent parts of Algeria and Libya. *American Association of Petroleum Geologists Bulletin*, **59** (3), 413-450.

Bishop, W. (1988). Petroleum geology of east-central Tunisia. *American Association of Petroleum Geologists Bulletin*, **9**, 1033-1058.

Bishop, W., & Debono, G. (1996). The hydrocarbon geology of southern offshore Malta and surrounding regions. *Journal of Petroleum Geology*, **19** (2), 129-160.

Bismuth, H., & Bonnefous, J. (1981). The biostratigraphy of carbonate deposits of the middle and upper Eocene in northeatern offshore Tunisia. *Palaeogeography, Palaeoclimatology, Palaeoecology*, **36**, 191-211.

Blow, W. (1969). Late Middle Eocene to Recent planktonic foraminiferal biostratigraphy. *Proceedings of the 1st International conference on Planktonic Microfossils. 1*, pp. 199-422. Geneva: Brill, Leiden.

Bobier, C., Viguier, C., Chaari, A., & Chine, A. (1991). The post-Triassic sedimentary cover of Tunisia: Seismic sequences and structure. *Tectonophysics*, **195**, 371-410.

Bortolotti, V. P. (2005). Tethyan ophiolites and Pangaea break-up. *The Island Arc*, **14**, 442-470.

Bosellini, A. (2002). Dinosaurs "re-write" geodynamics of the Eastern Mediterranean and the palaeogeography of the Apulia Platform. *Earth Sciences Review*, **59**, 211-234.

Bosellini, A. (2004). The western passive margin of Adria and its carbonate platforms. *Special Volume of the Italian Geological Society for the IGC* (pp. 32, 79-92).

Bosellini, A., Russo, A., Arush, M., & Cabdulqadir, M. (1987). The Oligo-Miocene of Eil (NE Somalia): a prograding coral-Lepidocyclina system. *Journal of African Earth Sciences*, **6**, 583-593.

Bosellini, F. (2006). Biotic changes and their control on Oligocene-Miocene reefs: A case study from the Apulia Platform margin (southern Italy). *Palaeogeography, Palaeoclimatology, Palaeoecology*, **241**, 393–409.

Bosellini, F. R., & Perrin, C. (2008). Estimating Mediterranean Oligocene–Miocene sea-surface temperatures: An approach based on coral taxonomic richness. *Palaeogeography, Palaeoclimatology, Palaeoecology*, **258**, 71-88.

Bosellini, F., & Russo, A. (1992). Stratigraphy and Facies of an Oligocene Fringing Reef (Castro Limestone, Salento Peninsula, Southern Italy). *Facies*, **26**, 145-166.

Bosence, D. (2005). A genetic classification of carbonate platforms based on their basinal and tectonic settings in the Cenozoic. *Sedimentary Geology*, **175**, 49-72.

Bosence, D. (1983). Description and classification of rhodoliths (rhodoids, rhodolites). *In:* T. Peryt (Ed.), *Coated grains* (pp. 217-224). Springer-Verlag, Berlin.

Bosence, D. (1983). The Occurence and Ecology of Recent Rhodoliths - A Review. *In:* T. M. Peryt (Ed.), *Coated Grains* (pp. 225-242). Springer-Verlag.

Bosscher, H., & Schlager, W. (1993). Accumulation Rates of Carbonate Platforms. *The Journal of Geology*, **101**, 345-355.

Bosworth, W., El-Hawat, A., Helgeson, D., & Burke, K. (2008). Cyrenaican "shock absorber" and associated inversion strain shadow in the collision zone of northeast Africa. *Geology*, **36**, 695-698.

BouDagher-Fadel, M. (2008). *Evolution and geological significance of larger benthic foraminifera.* Developments in Paleontology and Stratigraphy, 21, Elsevier.

Boulila, S., Galbrun, B., Miller, K., Pekar, S., Browning, J., Laskar, J., *et al.*. (2011). On the origin of Cenozoic and Mesozoic "third-order" eustatic sequences. *Earth-Science Reviews,* **109**, 94-112.

Brandano, M., & Corda, L. (2002). Nutrients, sea level and tectonics: constrains for the facies architecture of a Miocene carbonate ramp in central Italy. *Terra Nova*, **14**, 257–262.

Brandano, M., Bosellini, F., Mateu-Vicens, G., Morsilli, M., & Parente, M. (2008). Rhodalgal lithofacies of the Porto Badisco Calcarenite (upper Chattian, Salento, Apulia, southern Italy). *Geophysical Research Abstracts*, **10**.

Brandano, M., Frezza, V., Tomassetti, L., & Cuffaro, M. (2009). Heterozoan carbonates in oligotrophic tropical waters: The Attard member of the Lower Coralline Limestone Formation (U. Oligocene), Malta. *Palaeogeography, Palaeoclimatology, Palaeoecology*, **274**, 54-63.

Brandano, M., Virgilio, F., Tomassetti, L., Pedley, M., & Matteucci, R. (2008). Facies analysis and palaeoenvironmental interpretation of the Late Oligocene Attard Member (Lower Coralline Limestone Formation), Malta. *Sedimentology*, **56**, 1138-1158.

Brasier, M. (1975). An outline history of seagrass communities. *Palaeontology*, **18**, 681-702.

Brasier, M. (1995a). Fossil indicators of nutrient level. 2: Evolution and extinction in relation to oligotrophy. *In:* D. Bosence, & P. Allison (Eds.), *Marine palaeoenvironmental analysis from fossils.* Geological Society Special Publication, **83**, 113-149.

Brasier, M. (1995b). Fossil indicators of nutrient levels.1: Eutrophication and climate change. *In:* D. Bosence, & P. Allison (Eds.), *Marine palaeoenvironmental analysis from fossils.* Geological Society Special Publication, **83**, 133-132.

Brown, T. (1982). Ichnofossils and rhizoliths of the nearshore fluvial Jebel Qatrani Formation (Oligocene), Fayum Province, Egypt. *Palaeogeography, Palaeoclimatology, Palaeoecology*, **40**, 255-309.

Burchette, T. P., & Wright, V. P. (1992). Carbonate ramp depostional systems. *Sedimentary Geology*, **79**, 3-57.

Burchette, T. (1988). Tectonic control on carbonate platform facies distribution and sequence development: Miocene, Gulf of Suez. *Sedimentary Geology*, **59**, 179-204.

Burke, W., Denison, R., Hetherington, R., Koepnick, R., Nelson, H., & Otto, J. (1982). Variations of seawater $^{87}Sr/^{86}Sr$ through Phanerozoic time. *Geology*, **10**, 516-519.

Burollet, P. F. (1967). General geology of Tunisia. *In: Guidebook to the Geology and History of Tunisia.* Petroleum Exploration Society of Libya, 51-58.

Burollet, P. F., Muginot, J. M., & Sweeney, P. (1978). The geology of the Pelagian Block: The margins and basins of southern Tunisia and Tripolitania. *In:* A. Nairn, W. Kanes, & F. G. Stehli (Eds.), *The Ocean Basins and Margins (4C): The Western Mediterranean.* New York: Plenum Press, 331-359.

Butler, R. H., Grasso, M., & LaManna, F. (1992). Origin and deformation of the Neogene-Recent Maghrebian foredeep at the Gela Nappe, SE Sicily. *Journal of the Geological Society, London*, **149**, 547-556.

Buxton, M. W., & Pedley, H. M. (1989). A standardised model for Tethyan Tertiary carbonate ramps. *Journal of the Geological Soceity, London,* **146***,746-748* .

Cabrera, L., & Saez, A. (1987). Coal deposition in carbonate-rich shallow lacustrine systems: the Calaf and Mequinenza sequences (Oligocene, eastern Ebro Basin, NE Spain). *Journal of the Geological Society, London*, **144**, 451-461.

Cahuzac, B., & Chaix, C. (1996). Structural and faunal evolution of Chattian-Miocene reefs and corals in western France and northeastern Atlantic Ocean. *In:* E. Franseen, M. Esteban, W. Ward, & J.-M. Rouchy (Eds.), *Models for Carbonate Stratigraphy: from Miocene reef complexes of the Mediterranean regions.* Concepts in Sedimentology and Paleontology, SEPM, **5**, 105-127.

Cahuzac, B., & Poignant, A. (1997). Essai de biozonation de l'Oligo-Miocene dans les bassins européens à l'aide des grands formaninfères néritiques. *Bulletin de la Societé géologique de France*, **168***(2)*, 155-169.

Camoin, G. (1993). Turonian and Coniacian Carbonate Platforms from the African Tethyan Margin, Algeria, Tunisia. *In:* J. A. Toni Simo, R. W. Scott, & J.-P. Masse (Eds.), *Cretaceous Carbonate Platforms.* American Association of Petroleum Geologists Memoir **56**, 155-162.

Carannante, G., Esteban, M., Milliman, J. D., & Simone, L. (1988). Carbonate lithofacies as paleolatitude indiactors: problems and limitations. *Sedimentary Geology*, **60**, 333-346.

Carbone, S., Grasso, M., & Pedley, H. M. (1987). The distribution and palaeoenvironment of early Miocene phosphorites of southeast Sicily and their relationships with Maltese phosphorites. *Palaeogeography, Palaeoclimatology, Palaeoecology*, **58**, 35-53.

Carminati, E., & Doglioni, C. (2004). Mediterranean tectonics. *In: Europe: Mediterranean tectonics and neotectonics* (pp. 1-12). Elsevier.

Catalano, R., Di Stefano, P., Nigro, F., & Vitale, F. P. (1993). Sicily mainland and its offshore: A structural comparision. *In:* M. D. Max, & P. Colantoni (Eds.), *Geological Development of the Sicilian-Tunisian Platform.* UNESCO reports in Marine Science, **58**, 19-24.

Catalano, R., DiStefano, P., & Kozur, H. (1991). Permian circumpacific deep-water faunas from the western Tethys (Sicily, Italy), new evidence for the position of the Permian Tethys. *Palaeogeography, Palaeoclimatology, Palaeoecology*, **87**, 75-108.

Catalano, R., Doglioni, C., & Merlini, S. (2001). On the Mesozoic Ionian Basin. *Geophysical Journal international*, **144**, 1-49.

Catuneanu, O., Abreu, V., Bhattacharya, J. P., Blum, M. D., Dalrymple, R. W., Eriksson, P. G., *et al.* (2009). Towards the standardization of sequence stratigraphy. *Earth-Science Reviews*, **92**, 1-33.

Chaix, C., & Saint-Martin, J.-P. (1994). Les associations coralliennes oligo-miocènes de Malte, un résumé de l'histoire paléobiogéographique de la Méditerranée. *In: Interim Colloquium R.C.M.N.S (abstract book),* **12***.* Marseille.

Challis, G. (1979). Miocene echinoid biofacies of the Maltese Islands. *Annales Géol. Pays Hellén. Tome hors série fasc. 1 VIth International Congress on Mediterranean Neogene, Athens.*, (pp. 253-262).

Channell, J., D'Argenio, B., & Horvath, F. (1979). Adria, the African promontory in Mesozoic Mediterranean Paleogeography. *Earth Science Reviews*, **15**, 213-292.

Chiang, J., & Bitz, C. (2005). Influence of high latitude ice cover on the marine Intertropical Convergence Zone. *Climate Dynamics*, **25**, 477-496.

Choquette, P., & Pray, L. (1970). Geologic nomenclature and classification of porosity in sedimentary carbonates. *AAPG Bulletin*, **54**, 207-250.

Clift, P. (2010). Enhanced global continental erosion and exhumation driven by Oligo-Miocene climate change. *Geophysical Research Letters*, **37**, 1-6.

Coccioni, R., Marsili, A., Montanari, A., Bellanca, A., Neri, R., Bice, D., *et al.* (2008). Integrated stratigraphy of the Oligocene pelagic sequence in the Umbria-Marche basin (northeastern Apennines, Italy): A potential Global Stratotype Section and Point (GSSP) for the Rupelian/Chattian boundary. *Geological Society of America Bulletin*, **120**, 487-511.

Corti, G., Cuffaro, M., Doglioni, C., Innocenti, F., & Manetti, P. (2006). Coexisting geodynamic processes in the Sicily Channel. *Geological Society of America*, *Special Paper* **409**, 83–96.

D'Argenio, B., & Alvarez, W. (1980). Stratigraphic evidence for crustal thickness changes on the southern Tehyan margin during the Alpine cycle. *Geological Society of America Bulletin*, **91** (1), 681-689.

D'Argenio, B., & Horvath, F. (1984). Some remarks on the deformation history of Adria, from the Mesozoic to the Tertiary. *Annales Geophysicae*, **2**, 143-146.

Dart, C. J., Bosence, D. W., & McClay, K. R. (1993). Stratigraphy and structure of the Maltese graben system. *Journal of the Geological Society, London*, **150**, 1153-1166.

Davies, C. (1976). Accretion sets in the Lower Coralline Limestone of the Maltese Islands. *Journal of Sedimentary Petrology*, **46***(2)*, 414-417.

De Boer, P., & Smith, D. (1994). Orbital forcing and cyclic sequences. *In:* P. De Boer, & D. Smith (Eds.), *Orbital formcing and cyclic sequences.* International Association of Sedimentologists Special Publication, **19**, 1-14.

Debono, G., Xerri, S., & Bishop, W. F. (2000). Continental, sabkha and open marine Liassic-Triassic sequence offers new exploration plays in Malta. *EAGE conference on geology and petroleum geology*, (pp. 1-4). St Julians, Malta.

DeConto, R. M., Pollard, D., Wilson, P. A., Palike, H., Lear, C. H., & Pagani, M. (2008). Thresholds for Cenozoic bipolar glaciation. *Nature*, **455**, 652-656.

Dercourt, J. (1972). The Canadian cordillera, the Hellenides, and the seafloor spreading theory. *Canadian Journal of Earth Sciences*, **9**, 709.

Dercourt, J., Gaetani, M., Vrielinck, B., Barrier, E., Biju-Duval, B., Brunet, M., *et al.* (2000). *Atlas peri-Tethys palaeogeographical maps.* Paris: Commission de la Carte Geologique du Monde. p. 269.

Dercourt, J., Zonenshain, L., Ricou, L., Kazmin, V., Le Pichon, X., Knipper, A., *et al.* (1986). Geological evolution of the Tethys belt from the Atlantic to the Pamirs since the Lias. *Tectonophysics*, **123**, 241-315.

Dewey, J. F., Helman, M. L., Turco, E., Hutton, D. H., & Knott, S. D. (1989). Kinematics of the western Mediterranean. *In:* M. P. Coward, D. Dietrich, & R. G. Park (Eds.), *Alpine Tectonics.* Geological Society of London Special Publication, **45**, 265-283.

Dewey, J. F., Pitman, W. C., & Bonin, J. (1973). Plate tectonics and the evolution of the Alpine system. *Geological Society of America Bulletin*, **84**, 3137-3180.

Di Stefano, P. (1990). The Triassic of Sicily and southern Apennines. *Bollettino della società geologica italiana*, **109**, 21-37.

Drummond, C., & Wilkinson, B. (1993). On the use of cycle thickness diagrams as records of long-term sea-level change during accummulation of carbonate sequences. *Journal of Geology*, **101**, 687-702.

Dunham, R. J. (1962). Classification of carbonate rocks according to depositional texture. *In:* W. E. Ham (Ed.), *Classification of Carbonate Rocks.* Memoirs of the American Association of Petroleum Geologists, **1**, 108-121.

Eberli, G., & Ginsburg, R. (1989). Cenozoic progradation of northwestern Great Bahama Bank, a record of lateral platform growth and sea-level fluctuation. *In: Controls on carbonate platform and basin development.* SEPM Special Publication **44**, 339-351.

Eberli, G., Anselmetti, F., Betzler, C., Van Konijnenburg, J.-H., & Bernoulli, D. (2004). Carbonate platform to basin transitions on seismic data and in outcrops: Great Bahama Bank and the Maiella Platform margin, Italy. *In:* G. Eberli, J. Masaferro, & J. Sarg (Eds.), *Seismic imaging of carbonate reservoirs and systems.* AAPG Memoir **81**, 207-250.

Eberli, G., Masaferro, J., & Sarg, J. (2004). Seismic imaging of carbonate reservoirs and systems. *In: Seismic imaging of carbonate reservoirs and systems.* AAPG Memoir **81**, 1-9.

Embry, A., & Klovan, J. E. (1971). A late Devonian reef tract on the northeastern Bank Island, Northwest Territories. *Bulletin of Canadian Petroleum Geologists*, **19**, 730-781.

Enos, P., & Sawatsky, L. (1981). Pore networks in Holocene carbonate sediments. *Journal of Sedimentary Petrology*, **51**, 961-986.

Farrugia, P., & Panza, G. F. (1981). Continental character of the lithosphere beneath the Ionian Sea. *In:* R. Cassinis (Ed.), *The Solution of the Inverse Problem in Geophysical Interpretation.* New York: Plenum.

Felix, R. (1973). *Oligo-Miocene stratigraphy of Malta and Gozo.* Wageningen: Veeman.

Fiduk, J. (2009). Evaporites, petroleum exploration, and the Cenozoic evolution of the Libyan shelf margin, central North Africa. *Marine and Petroleum Geology,* **26**, 1513–1527.

Finetti, I. (2004). Innovative CROP seismic highlights on the Mediterranean Region. *In: Special Volume of the Italian Geological Society for the IGC 32* (pp. 131-140). Florence.

Finetti, I. (1982). Structure, stratigraphy and evolution of Central Mediterranean. *Bollettino di Geofisica teorica ed applicata*, **XXIV** (**96**), 247-315.

Fischer, A. (1964). The Lofer cyclotherms of the Alpine Triassic. *Geological Survey of Kansas Bulletin*, **169**, 107-149.

Flohn, H. (1981). A hemispheric circulation asymmetry during late Tertiary. *Geologische Rundschau*, **70**, 725-736.

Fluteau, F., Ramstein, G., & Besse, J. (1999). Simulating the evolution of the Asian and African monsoons during the past 30 Myr using an atmospheric general circulation model. *Journal of Geophysical Research*, **104**, 11,995-12,018.

Föllmi, K. B., de Kaenel, E., Stille, P., John, C. M., Adatte, T., & Steinmann, P. (2005). Phosphogenesis and organic-carbon preservation in the Miocene Monterey Formation at Naples Beach, California - The Monterey hypothesis revisited. *Geological Society of America Bulletin*, **117** (5/6), 589–619.

Föllmi, K. B., Gertsch, B., Renevey, J.-P., De Kaenel, E., & Stille, P. (2008). Stratigraphy and sedimentology of phosphate-rich sediments in Malta and south-eastern Sicily (latest Oligocene to early Late Miocene). *Sedimentology*, **55**, 1029-1051.

Francis, J., Marenesi, S., Levy, R., Hambrey, M., Thorn, V., Mohr, B., *et al.* (2009). From Greenhouse to Icehouse - The Eocene/Oligocene in Antarctica. *In:* F. Florindo, & M. Siegert (Eds.), *Antarctic climate evolution* (pp. 209-368). Elsevier.

Frost, S. H. (1981). Oligocene reef coral biofacies of the Vicentin, northeast Italy. *In:* D. F. Toomey (Ed.), *European fossil reef models.* Society of Economic Palaeontologists and Mineralogists Special Publication, **30**, 483-540.

Galloway, W. (1989). Genentic stratigraphic sequences in basin analysis-1: Architecture and genesis of flooding surface bounded depositional units. *American Association of Petroleum Geologists Bulleti*, **73**, 125-143.

Gardiner, W., Grasso, M., & Sedgeley, D. (1995). Plio-Pleistocene fault movment as evidence for mega-block kinematics within the Hyblean-Malta plateau, Central Mediterranean. *Journal of Geodynamics*, **19** (1), 35-51.

Gatt, P. (2007). Controls on Plio-Quaternary foreland sedimentation in the Region of the Maltese Islands. *Bolletino della societa geologica italiana*, **126** (1), 119-129.

Gatt, P. (2010). Discussion: ‘‘Facies analysis and palaeoenvironmental interpretation of the Late Oligocene Attard Member (Lower Coralline Limestone Formation), Malta’’ by Brandano *et al.* (2009), Sedimentology, **56**, 1138–1158. *Sedimentology*, *57*, 1152–1154.

Gatt, P. (2005). Syntectonic deposition of an Oligo-Miocene phosphorite conglomerate bed in Malta. *Central Mediterranean Naturalist*, **4** (2), 109-118.

Gatt, P. (1992). *The sedimentology of the Lower Coralline Limestone Formation (Oligocene) of the Maltese Islands.* Unpublished MSc dissertation, University of Reading, UK.

Gatt, P., & Gluyas, J. (2012). Climatic controls on facies in Palaeogene Mediterranean subtropical carbonate platforms. *Petroleum Geoscience,* **18** (*in press*).

Gatt, P., Tucker, M., & Davies, R. (2009). Drowning of the Malta carbonate platform: facies and sequence stratigraphy of the Lower Coralline Limestone (U. Oligocene). *In:* V. Pascucci, & S. Andreucci (Ed.), *Sedimentary environments of Mediterranean Islands.* International Association of Sedimentologists Abstracts, p.181, Alghero, Italy.

Geel, T. (2000). Recognition of startigraphic sequences in carbonate platform and slope deposits: empirical models based on microfacies analysis of Paleogene deposits in sotheastern Spain. *Palaeogeography, Palaeoclimatology, Palaeoecology*, **155**, 211-238.

Gerdes, K., Winefield, P., Simmons, M., & Van Oosterhout, C. (2010). The influence of basin architecture and eustacy on the evolution of Tethyan Mesozoic and Cenozoic carbonate sequences. *In:* F. van Buchem, K. Gerdes, & M. Esteban (Eds.). Geological Society, London, Special Publications, **329**, 9-41.

Gibbs, A. (1984). Structural evolution of extensional basin margins. *Journal of the Geological Society, London*, **141**, 609-620.

Ginsburg, R., Harris, R., Eberli, G., & Swart, P. (1991). The growth potential of a bypass margin,Great Bahama Bank. *Journal of Sedimentary Petrology,* **61**, 976-987.

Goldhammer, R. (1997). Compaction and decompaction algorithms for sedimentary carbonates. *Journal of Sedimentary Research*, **67**, 26-35.

Goldhammer, R. K., Dunn, P. A., & Hardie, L. A. (1990). Depostional cycles, composite sea-level changes, cyclic stacking patterns, and the hierarchy of stratigraphic forcing: Examples from Alpine Triassic platform carbonates. *Geological Society of America Bulletin*, **102**, 535-562.

Goldhammer, R., & Elmore, R. (1984). Paleosols capping regressive carbonate cycles in the Pennsylvanian Black Prince Limestone, Arizona. *Journal of Sedimentary Petrology*, **54**, 1124-1137.

Gradstein, F., Ogg, J., Smith, A., & al., e. (2004). *A Geological time scale.* Cmbridge University Press.

Grasso, M., Mazzoldi, G., & Torelli, L. (1993). Structural and stratigraphic framework of the Tunisian Shelf surrounding the Islands of Lampione and Lampedusa (Pelagian sea). *In:* M. D. Max, & P. Colantoni (Ed.), *International Scientific meeting, University of Urbino.* UNESCO reports in marine science, **58**, 65-70.

Grasso, M., Reuther, C.-D., Baumann, H., & Becker, A. (1986). Shallow crustal stress and neotectonic framework of the Malta Platform and the SE Pantelleria Rift (Central Mediterranean). *Geologica Romana*, **25**, 191-210.

Grasso, M., Torelli, L., & Mazzoldi, G. (1999). Cretaceous–Palaeogene sedimentation patterns and structural evolution of the Tunisian shelf, offshore the Pelagian Island (Central Mediterranean). *Tectonophysics*, **315**, 235-250.

Groupe ESCARMED (1982). Donneés nouvelles sûr le marges du bassin Ionien profond (Mediterraneé Orientale). *Rev. Inst. Fr. Petrol.,* **37**, 713-731.

Gruenwald, R. (2001). The hydrocarbon prospectivity of Lower Oligocene deposits in the Maragh Trough, SE Sirt Basin Libya. *Journal of Petroleum Geology*, **24**, 213-231.

Gruszczynski, M., Marshall, J. D., Goldring, R., Coleman, M. L., Małkowski, K., Gaździcka, Semil, J. & Gatt, P. A. (2008). Hiatal surfaces from the Miocene Globigerina Limestone Formation of Malta: Biostratigraphy, sedimentology, trace fossils and early diagenesis. *Palaeogeography, Palaeoclimatology, Palaeoecology*, **270**, 239–251.

Guarnieri, P., Carbone, S., & DiStefano, A. (2002). The Sicilian orogenic belt: a critical tapered wedge? *Bollettino della società geologica italiana*, **121** (7), 221-230.

Guiraud, R., & Bosworth, W. (1999). Phanerozoic geodynamic evolution of northeastern Africa and the northwestern Arabian platform. *Tectonophysics*, **315**, 73-108.

Halfar, J., & Mutti, M. (2005). Global dominance of coralline red-algal facies: A response to Miocene oceanographic events. *Geology*, **33**, 481-484.

Halfar, J., Godinez-Orta, L., Mutti, M., ValdezHolguin, J., & Borges, J. (2004). Nutrient and temperature controls on modern carbonate production: An example from the Gulf of California, Mexico. *Geology*, **32**, 213-216.

Hallock, P. (2000). Larger foraminifera as indicators of coral-reef vitality. *nvironmental Micropaleontology*, **15**, 121-150.

Hallock, P. (1988). The role of nutrient availability in bioerosion: consequences to carbonate buildups. *Palaeogeography, Palaeoclimatology, Palaeoecology*, **63**, 275-291.

Hallock, P. (1985). Why are larger Foraminfera large? *Paleobiology*, **11***(2)*, 195-208.

Hallock, P., & Glenn, E. (1986). Larger Foraminifera: A tool for Paleoenvironmental Analysis of Cenozoic Carbonate Depositional Facies. *Palaios*, **1**, 55-64.

Hallock, P., & Pomar, L. (2008). Cenozoic Photic Reef and Carbonate Ramp Habitats: A New Look Using Paleoceanographic Evidence. *Proceedings of the 11th International Coral Reef Symposium.* Ft. Lauderdale, Florida.

Hallock, P., & Schlager, W. (1986). Nutrient excess and demise of Coral Reefs and Carbonate Platforms. *Palaios*, **1**, 389-398.

Hallock, P., Premoli Silva, I., & Boersma, A. (1991). Similarities between planktonic and larger formainiferal evolutionary trends through the Paleogene paleoceanographic changes. *Palaeogeography, Palaeoclimatology, Palaeoecology*, **83**, 49-64.

Handford, C., & Loucks, R. (1993). Carbonate depositional sequences and systems tracts- Responses of carbonate platforms to relative sea-level changes. *In:* R. Loucks, & J. Sarg (Eds.), *Carbonate sequence stratigraphy.* American Association of Petroleum Geologists Memoir **57**, 3-41.

Haq, B. U., Hardenbol, J., & Vail, P. R. (1987). Chronology of fluctuating sea levels since the Triassic. *Science*, **235**, 1156-1167.

Harrison, J. (1955). An interpretation of gravity anomalies in the eastern Mediterranean. *Philosophical Transactions of the Royal Society of London. Series A, Mathematical and Physical Sciences*, **248**, 283-325.

Hilgen, F., Abels, H., Iaccarino, S., Krijgsman, W., Raffi, I., Sprovieri, R., *et al.* (2008). The global stratotype section and point (GSSP) of the Serravallian stage (Middle Miocene). *Episodes,* **32,** 1-46.

Hillgartner, H., & Strasser, A. (2003). Quantification of high-frequency sea-level fluctuations in shallow-water carbonates: an example from the Berriasian^Valanginian (French Jura). *Palaeogeography, Palaeoclimatology, Palaeoecology,* **200**, 43-63.

Hladil, J., Otava, J., & Galle, A. (1991). Oligocene Carbonate Builups of the Sirt Basin, Libya. *In:* M. Salem, O. Hammuda, & B. Eliagoubi (Eds.), *The Geology of Libya* (pp. 1401-1420). Elsevier.

Hoffmann, P., Wagner, T., & Beckmann, B. (2003). Millennial- to centennial-scale record of African climate variability and organic carbon accumulation in the Coniacian -Santonian eastern tropical Atlantic (Ocean Drilling Program Site 959, off Ivory Coast and Ghana). *Geology*, **31**, 135-138.

Hohenegger, J., Yordanova, E., Yoshikatsu, N., & Tatzreiter, F. (1999). Habitats of larger foraminfera on the upper reef slope of Sesoko Island, Okinawa, Japan. *Marine Micropaleontology*, **36**, 109–168.

Hsü, K. (1971). Origin of the Alps and western Mediterranean. *Nature*, **233**, 44-48.

Hughes, G. (1977). Recent foraminfera from the Honiara Bay area, Solomon Islands. *Journal of Foraminiferal Research*, **7**, 45-57.

Hunt, D., & Tucker, M. E. (1992). Stranded parasequences and forced regressive wedge systems tract; depsotion during base-level fall. *Sedimentary Geology*, **81**, 1-9.

Hyeong, K., Park, S.-H., Min Yoo, C., & Kim, K.-H. (2005). Mineralogical and geochemical compositions of the eolian dust from the northeast equatorial Pacific and their implications on paleolocation of the Intertropical Convergence Zone. *Paleoceanography*, **20**, 1-11.

Illies, J. H. (1981). Graben formation - the Maltese Islands - a case history. *Tectonophysics*, **73**, 151-168.

Imam, M., & Galmed, M. A. (2000). Stratigraphy and microfacies of the Oligocene Sequence at Gabal Bu Husah, Marada oasis, south Sirte Basin Libya. *Facies*, **42**, 93-106.

Italian Government. (2011). *Ministero dello sviluppo economico* website: http://unmig.sviluppoeconomico.gov.it/unmig/pozzi/dettaglio.asp?cod=6236

Jacobs, E., Weissert, H., & Shields, G. (1996). The Monterey event in the Mediterranean: A record from shelf sediments of Malta. *Paleoceanography*, **11**, 717-728.

James, N. (1997). The cool-water carbonate depositional realm. *In:* N. P. James, & J. A. Clarke (Eds.), *Cool-water carbonates.* Society for Sedimentary Geology Special Publication **56**, 1-20.

John, C. M., Mutti, M., & Adatte, T. (2003). Mixed carbonate-siliciclastic record on the North African margin (Malta)—coupling of weathering processes and mid-Miocene climate. *Geological Society of America Bulletin*, **115**, 217-229.

Jolly, R., & Lonergan, L. (2002). Mechanisms and controls on the formation of sand intrusions. *Journal of the Geological Society,* **159**, 605-617.

Jongsma, D., van Hinte, J. E., & Woodside, J. M. (1985). Geologic structure and neotectonics of the North African continental margin south of Sicily. *Marine & Petroleum Geology*, **2**, 156-179.

Jongsma, D., Woodside, J., King, G., & vanHinte, J. (1987). The Medina Wrench: a key to the kinematics of the central and eastern Mediterranean over the past 5 Ma. *Earth and Planetary Science letters*, **82**, 87-106.

Jorry, S. (2004). *The Eocene nummulite carbonates (central Tunisia and NE Libya): sedimentology, depositional environments and application to oil reservoirs.* Unpublished PhD thesis, University of Geneva, Switzerland.

Jorry, S., Davaud, E., & Caline, B. (2003). Controls on the distribution of Nummulite facies: A case study from the Late Ypresian El Garia Formation (Kesra plateau, central Tunisia). *Journal of Petroleum Geology*, **26**, 283-306.

Jorry, S., Hasler, C-A., & Davaud, E. (2006). Hydrodynamic behaviour of Nummulites: implications for depositional models. *Facies*, **52**, 221-235.

Judd, A., & Hovland, M. (1992). The evidence of shallow gas in marine sediments. *Continental Shelf Research*, **12**, 1081-1095.

Keller, G., Herbert, T., Dorsey, R., D'Hondt, S., Johnsson, M., & Chi, W. (1987). Global distribution of late Paleogene hiatuses. *Geology*, **15**, 199-203.

Kendall, A. (1984). Evaporites. *In:* R. Walker (Ed.), *Facies models.* Geoscience Canada Reprint Series, **259**-296.

Kendall, C. G., & Schlager, W. (1981). Carbonates and relatives changes in sea-level. *Marine Geology*, **44**, 181-212.

Kidwell, S., & Bosence, D. (1991). Taphonomy and time-averaging of marine shelly faunas. *In:* P. Allison, & D. Briggs (Eds.), *Taphonomy: releasing the data locked in the fossil record.* (pp. 115-209). Plenum Press, New York.

Kiessling, W. (2002). Secular variations in the Phanerozoic reef ecosystem. *In:* W. Kiessling, E. Flugel, & J. Golonka (Eds.), *Phanerozoic reef patterns.* SEPM Special Publications, Tulsa, **72**, 625-690.

Kiessling, W., Flugel, E., & Golonka, J. (2000). Fluctuations in the carbonate production of Phanerozoic reefs. *In:* E. Insalaco, P. Skelton, & T. Palmer (Eds.), *Carbonate Paltform systems: components and interactions.* Geological Society, London, Special Publications, **178**, 191-215.

Kiessling, W., Flügel, E., & Golonka, J. (1999). Paleoreef Maps: Evaluation of a Comprehensive Database on Phanerozoic Reefs. *AAPG Bulletin*, **83**, 1552-1587.

Kingston, D., Dishroon, C., & Williams, P. (1983). Global basin classification system. *AAPG Bulletin*, **67**, 2175-2193.

Klappa, C. (1978). Biolithogenesis of Microcodium: elucidation. *In:* V. Wright, & M. Tucker (Eds.), *Calcretes.* Blackwell Scientific Publications, Oxford, 115-148.

Klett, T. (2001). *Total petroleum petroleum systems of the Pelagian Province, Tunisia, Libya, Italy and Malta- the bou Dabbous Tertiary and Jurassic-Cretaceous composite.* U.S. Geological Survey Bulletin 2202-D.

Knoerich, A. C., & Mutti, M. (2003). Controls of facies and sediment composition on the diagenetic pathway of shallow-water Heterozoan carbonates: the Oligocene of the Maltese Islands. *International Earth Science Review (Geologische Rundschau)*, **92**, 494-510.

Knoerich, A. C., & Mutti, M. (2006). Missing aragonitic biota and diagenetic evolution of Heterozoan Carbonates: a case study from the Oligo-Miocene of the Central Mediterranean. *Journal of Sedimentary Research*, **76**, 871-888.

Kominz, M. A., & Pekar, S. F. (2001). Oligocene eustasy from two-dimensional sequence stratigraphic backstripping. *Geological Society of America Bulletin*, **113**, 291-304.

Laskar, J., Gastineau, M., Joutel, M., Robutel, P., Levrard, B., & Correia, A. (2004). Long term evolution and chaotic diffusion of the insolation quantities of Mars. *Icarus*, **170**, 343-364.

Laskar, J., Robutel, P., Joutel, F., Gastineau, M., Correia, A., & Levrard, B. (2004). A long-term numerical solution for the insolation of the Earth. *Astronomy and Astrophysics*, **428**, 261-285.

Lawver, L., Dalziel, I., Gahagan, L., Kygar, R., & Herber, B. (2004). *Atlas of plate reconstructions (750 Ma to present day).* University of Texas Institute for Geophysics.

Lees, A., & Buller, A. (1972). Modern temperate-water and warm-water shalef carbonates sediments contrasted. *Marine Geology*, **13**, 67-73.

Lipparini, L., Scrocca, D., Marsili, P., & Morandi, S. (2009). Offshore Malta licence in the Central Mediterranean Sea offers hope of hydrocarbon potential. *First break*, **27**, 105-116.

Lohmann, K., & Meyers, W. (1977). Microdolomite inclusions in cloudy prismatic calcites: A proposed criterion for former high-magnesium calcites. *Journal of Sedimentary Research*, **47**, 1078-1088.

Longman, M. (1981). A process approach to recognising facies of reef compexes. *In:* D. Toomey (Ed.), *Euorpean fossil reef models.* SEPM Special Publication, **30**, 9-40.

Loucks, R., Moody, R., Bellis, J., & Brown, A. (1998). Regional depostional setting and pore network system of the El Garia Formation, offshore Tunisia. *In: Petroleum Geology of North Africa.* Geological Society, London, Spec. Publ. **132**, 355-374.

Lourens, L., & Hilgen, F. (1997). Long-periodic variations in the Earth's obliquity and their relation to third-order eustatic cycles and Late Neogene glaciations. *Quaternary International*, **40**, 43-52.

Lyle, M., Liberty, L., Moore, T. C., & Rea, D. K. (2002). Development of a seismic stratigraphy for the Paleogene sedimentary section, central tropical Pacific Ocean. *In:* M. Lyle, P. A. Wilson, T. R. Janecek, & e. al., *Procedures of the Ocean Drilling Program, Texas,* **199***, 1-21.*

Malinverno, A., & Ryan, W. (1986). Extension in the Tyrrhenian sea and shortening in the Apennines as result of arc migration driven by sinking of the lithoshpere. *Tectonics*, **5** (2), 227-245.

Marshall, J. (1992). Climatic and oceanographic isotopic signals from the carbonate rock record and their preservation. *Geological Magazine*, **129**, 143-160.

Matthews, M., & Perlmutter, M. (1994). Global cyclostratigraphy: an application to the Eocene Green River Basin. *In:* P. De Boer, & D. Smith (Eds.), *Orbital forcing and cyclic sequences.* Spec. Publs. International Association of Sedimentologists, **19**, 459-481.

Mazzei, R. (1985). The Miocene sequence of the Maltese Islands: biostratigraphic and chronostratigraphic references based on nannofossils. *Atti della societa Toscana di Scienze naturali*, **92**, 165-197.

McKenzie, D. (1978). Some remarks on the development of sedimentary basins. *Earth and Planetary Science Letters*, *40*, 25-32.

Melim, L., Swart, P., & Eberli, G. (2004). Mixing-zone diagenesis in the subsurface of Florida and the Bahamas. *Journal of Sedimentary Research*, **76**, 904-913.

Meulenkamp, J., & Sissingh, W. (2003). Tertiary palaeogeography and tectonostratigraphic evolution of the Northern and Southern Peri-Tethys platforms and the intermediate domains of the African^Eurasian convergent plate boundary zone. *Palaeogeography, Palaeoclimatology, Palaeoecology*, **196**, 209-228.

Miall, A. (1992). Exxon global cycle chart: An event for every occasion? *Geology*, **20**, 787-790.

Milankovitch, M. (1930). *In:* W. Koppen, & R. Geiger (Eds.), *Handbuch der Klimatologie.* Borntraeger, Berlin, Vol. **1**, part A.

Miller, K. G., Wright, J., & Fairbanks, R. (1991). Unlocking the Ice House: Oligocene-Miocene Oxygen isotopes, eustasy, and marine erosion. *Journal of Geophysical Research*, **96** (B4), 6829-6848.

Miller, K., Feigenson, M., Kent, D., & Olsson, R. (1988). Upper Eocene to Oligocene isotope standard section, deep sea drilling project site 522. *Paleoceanography*, **3**, 223-233.

Miller, K., Kominz, M., Browning, J., Wright, J., Mountain, G., Katz, M., *et al.* (2005). The Phanerozoic record of global sea-level change. *Science*, **310**, 1293-1298.

Mitchum, R., & Van Wagoner, J. (1991). High-frequency sequences and their stacking patterns: sequence-stratigraphic evidence of high-frequency eustatic cycles. *Sedimentary Geology*, **70**, 131-160.

Mitchum, R., Vail, P., & Sangree, J. (1977). Seismic stratigraphy and global changes in sea-level; Stratigraphic interpretation of seismic reflection patterns in depostional sequences. *In:* C. Payton (Ed.), *Seismic stratigraphy - applications to hydrocarbon exploration.* AAPG Memoir **26**, 117-133.

Moore, C. (2001). *Carbonate Reservoirs: Porosity evolution and diagenesis in a sequence stratigraphic framework* (Vol. Developments in Sedimentology **55**). Elsevier.

Murray, J. (1995). Microfossils indicators of ocean water masses, circulation and climate. *In:* D. J. Bosence, & P. Allison (Eds.), *Marine palaeoenvironmental analysis.* Geological Society Special Publications, **83**, 245-264.

Murray, J. (1890). The Maltese Islands with special reference to their geological structure. *Geographical Magazine*, **6**, 449-488.

Murray, R. (1960). Origin of porosity in carbonate rocks. *Jounral of Sedimentary Petrology*, **30**, 59-84.

Mutti, M., & Hallock, P. (2003). Carbonate systems along nutrient and temperature gradients: some sedimentological and geochemical constraints. *Inernational Journal of Earth Science (Geologische Rundschau)*, **92**, 465–475.

Mutti, M., Bernoulli, D., Spezzaferri, S., & Stille, P. (1999). Lower and middle Miocene carbonate facies in the Central Mediterranean: The impact of paleoceanography on sequence stratigraphy. *In:* P. Harris, A. Saller, J. Simo, & C. Handford (Eds.), *Advances in carbonate sequence stratigraphy: Application to reservoirs, outcrops and models.* Society for Sedimentary Geology Special Publication, **63**, 371-384.

Mutti, M., Droxler, A., & Cunnignham, A. (2005). Evolution of the Northern Nicaragua Rise during the Oligocene-Miocene: drowning by environmental factors. *Sedimentary Geology*, **175**, 237–258.

Muttoni, G., Garzanti, E., Alfonsi, L., Cirilli, S., Germani, D., & Lowrie, W. (2001). Motion of Africa and Adria since the Permian:paleomagnetic and paleoclimatic constraints from northern Libya. *Earth and Planetary Science Letters*, **192**, 159-174.

Muttoni, G., Kent, D., Olsen, P., DiStefano, P., Lowrie, W., Bernasconi, S., *et al.* (2004). Tethyan magnetostratigraphy from Pizzo Mondello (Sicily) and correlation to the Late Triassic Newark astrochronological polarity time scale. *Geological Society of America Bulletin*, **116** (9/10), 1043–1058.

Muzzin, A., Cazzini, F., & Mariani, M. (1998). *North Malta offshore regional study.* Progress meeting 1, ENI.

Nalin, R., Nelson, C., Basso, D., & Massari, F. (2008). Rhodolith-bearing limestones as trangressive marker beds: fossil and modern examples from North Island, New Zealand. *Sedimentology*, **55**, 249-274.

Nebelsick, J., & Bassi, D. (2000). Diversity, growth and taphonomy: key factors controlling the fabric of coralline algae dominated shelf carbonates. *In:* E. Insalaco, P. Skelton, & T. Palmer (Eds.), *Carbonate Platform Systems: components and interactions.* Geological Society, London, Special Publications, **178**, 89-107.

Nebelsick, J., & Kroh, A. (2002). The Stormy Path from Life to Death Assemblages: The Formation and Preservation of Mass Accumulations of fossil Sand Dollars. *Palaios*, **17**, 378-393.

Nelson, C. (1988). An introductory perspective on non-tropical shelf carbonates. *Sedimentary Geology*, **60**, 3-12.

Nicol, A., Waterson, J., Walsh, J., & Childs, C. (1996). The shapes, major axis orientations and displacement patterns of fault surfaces. *Journal of Structural Geology*, **18**, 235-248.

Nicosia, U., Marino, M., Mariotti, N., Muraro, C., & Panigutti, S. (2000). The Upper Cretaceous dinosaur tracksite near Altamura (Bari, southern Italy). *Geologica Romana*, **35**, 231-236.

Osleger, D. (1991). Subtidal carbonate cycles: Implications for allocyclic vs. autocyclic controls. *Geology*, **19**, 917-920.

Pagani, M., Zachos, J. C., Freeman, K. H., Tipple, B., & Boharty, S. (2005). Marked decline in atmospheric carbon dioxide concentrations during the Paleogene. *Science*, **309**, 600-603.

Pälike, H., Norris, R., Herrle, J., Wilson, P., Coxall, H., Lear, C., *et al.* (2006). The Heartbeat of the Oligocene Climate System. *Science*, **314**, 1894-1898.

Panza, G. (1987). The deep structure of the Mediterranean-Alpine region and large shallow earthquakes. *Memorie della società geologica italiana*, **29**, 5-13.

Parrish, J., & Curtis, R. (1982). Atmospheric circulation, upwelling, and organic-rich rocks in the Mesozoic and Cenozoic Era. *Palaeogeography, Palaeoclimatology, Palaeoecology*, **40**, 31-66.

Patacca, E., & Scandone, P. (2004). The Plio-Pleistocene thrust belt-foredeep system in the Southern Apennines and Sicily (Italy). *In: Special Volume of the Italian Geological Society for the IGC.* Societa geologica italiana, Florence, **32**, 93-129.

Patton, T. (1995). Mathematical block-motion model for deformation of a layer above a buried fault of arbitrary dip and sense of slip. *Journal of Structural Geology*, **17**, 1455-1472.

Pearson, P., Ditchfield, P., Singano, J., Harcourt-Brown, K., Nicholas, C., Olsson, R., *et al.* (2001). Warm tropical sea surface temperatures in the Late Cretaceous and Eocene epochs. *Nature*, **413**, 481-487.

Pedley, H. (1993a). *Geological Map of the Island of Malta, 1:25,000 scale, British Geological Survey, Keyworth.*

Pedley, H. (1993b). *Geological Map of the Islands of Gozo and Comino, 1:25,000 scale, British Geological Survey, Keyworth.*

Pedley, H. M. (1978). A new lithostratigraphical and palaeoenvironmental interpretation for the coralline limestone Formation of the Maltese Islands. *Overseas Geological & Mineralogical Resources*, **54**, 1-17.

Pedley, H. M. (1998). A review of sediment distributions and processes in Oligo-Miocene ramps of southern Italy and Malta (Mediterranean divide). *Geological Society Special Publications*, **149**, 163-179.

Pedley, H. M. (1987). Controls on Cenzoic carbonate deposition in the Maltese Islands: Review and reinterpretation. *Memorie della società geologica italiana*, **38**, 81-94.

Pedley, H. M. (1990). Syndepositional tectonics affecting Cenozoic and Mesozoic depostion in Malta and SE Sicily (Central Mediterranean) and their bearing on Mesozoic reservoir development on the N Malta offshore region. *Marine and Petroleum Geology*, **7**, 171-180.

Pedley, H. M., & Grasso, M. (1992). Miocene syntectonic sedimentation along the western margins of the Hyblean-Malta Platform: A guide to plate margin processes in the Central Mediterranean. *Journal of Geodynamics*, **15** (1/2), 19-37.

Pedley, H. M., Grasso, M., & Maniscalco, R. (1998). Lithological assocations and their modification by fabric selective biogenic and early diagenetic processes in outer ramp settings: An example from the Oligocene of SE Sicily, Italy. *Bollettino della societa geologica italiana*, **117**, 133-149.

Pedley, H., Bosence, D., Dart, C., Pratt, S., & Buxton, M. (1991). Field guide to the Cenozoic Platform carbonates of the Maltese Islands. *In:* D. Bosence (Ed.), *13th International association of Sedimentologists congress (field guide 22).* BSRG, University of Cambridge.

Pedley, H., House, M., & Waugh, B. (1976). The geology of Malta and Gozo. *Proc. Geol. Ass.*, **87**, 325-341.

Pedley, H., House, M., & Waugh, B. (1978). The Geology of the Pelagian Block: The Maltese Islands. *In:* A. Nairn, W. Kaines, & F. Stehli (Eds.), *The Ocean Basins and Margins,* **48***, 201-256.* New York: Plenum Press.

Pedley, M., Debono, G., & Yeaman, M. (1993). Mesozoic structuring and volcanics along the Pelagian-Ionian boundary. *In:* M. D. Max, & P. Colantoni (Eds.), *Geological Development of the Sicilian-Tunisian Platform.* UNESCO reports in Marine Science, **58**, 81-86.

Pekar, S. F., Christie-Blick, N., Kominz, M. A., & Miller, K. G. (2002). Calibration between eustatic estimates from backstripping and oxygen isotopic records for the Oligocene. *Geology*, **30**, 903-906.

Pekar, S., Christie-Blick, N., Kominz, M., & Miller, K. (2001). Evaluating the stratigraphic response to eustasy from Oligocene strata in New Jersey. *Geology*, **29**, 55–58.

Perrin, C., Bosence, D., & Rosen, B. (1995). Quantitative approaches to palaeozonation and palaeobathymetry of corals and coralline algae in Cenozoic reefs. *In:* D. Bosence, & P. Allison (Eds.), *Marine Palaeoenvironmental analysis from fossils.* Geological Society Special Publication, **83**, 181-229.

Pomar, L. (2001). Types of Carbonate platforms: a genetic approach. *Basin Research*, **13**, 313-334.

Pomar, L., & Hallock, P. (2007). Changes in coral-reef structure through the Miocene in the Mediterranean province: Adaptive versus environmental influence. *Geology*, **35***(10)*, 899-902.

Pomar, L., Brandano, M., & Westphal, H. (2004). Environmental factors influencing skeletal grain sediment associations: A critical review of Miocene examples from the western Mediterranean. *Sedimentology*, **51**, 627–651.

Posamentier, H. W., Jervey, M. T., & Vail, P. R. (1988). Eustatic constrols on clastic depostion I - conceptual framework. *In:* C. K. Wilgus, B. S. Hastings, C. G. Kendall, H. W. Posamentier, C. A. Ross, & J. C. Van Wagoner (Eds.), *Sea level Cahnges - An integrated Approach.* Society of Economic Paleontologists and Mineralogists (SEPM), **42**. 110-124.

Pratt, S. (1990). *Hardground diagenesis in pelagic carbonates from the Miocene of Malta and the Cretaceous of Southern England.* Unpublished PhD thesis, University of London.

Purser, B., Tucker, M., & Zenger, D. (1994). Problems, progress and future research concerning dolomites and dolomitization. *In:* B. Purser, M. Tucker, & D. Zenger (Eds.), *Dolomites. A volume in honour of Dolomieu.* International Association of Sedimentologists Special Publication, **21**, 3-20.

Putz-Perrier, M., & Sanderson, D. (2010). Distribution of faults and extensional strain in fractured carbonates of the North Malta Graben. *American Association of Petroleum Geologists*, **94**, 435-456.

Racey, A. (2001). A review of Eocene Nummulite accumulations: Structure, fomration and reservoir potential. *Journal of Petroleum Geology*, **24**, 79-100.

Rasmussen, D., Brown, T., & Simons, E. (1992). The Eocene-Oligocene transition in continental Africa. *In:* D. Prothero, & W. Berggren (Eds.), *Eocene-Oligocene climatic and biotic evolution* (pp. 548-566).

Read, J. (1985). Carbonate platform facies models. *American Association of Petroleum Geologists Bulletin*, **69**, 1-21.

Read, J. (1989). Controls on evolution of Cambrian-Ordovician passive margin, U.S. Appalachians. *In: Controls on carbonate platform and basin development.* SEPM Special Publication, **44**, 147-165.

Read, J. F. (1985). Carbonate Platform Facies Models. *American Association of Petroleum Geologists Bulletin*, **69***(1)*, 1-21.

Read, J. F. (1998). Phanerozoic carbonate ramps from greenhouse, transitional and ice-house worlds: clues from field and modelling studies. *In:* P. V. Wright, & T. P. Burchette (Eds.), *Carbonate Ramps.* Geological Society, London, Special Publications, **149**, 107-135.

Read, J. (1995). Overview of carbonate platform sequences, cycle stratigraphy and reservoirs in greenhouse and ice-house worlds. *In:* J. Read, C. Kerans, & L. Weber (Eds.), *Milankovitch sea level changes, cycles and reservoirs on carbonate paltforms in greenhouse and ice-house worlds, SEPM Short Course notes,* **35**. (pp. 1-102).

Reading, H. (1996). *Sedimentary Environments and Facies.* Blackwell Scientific Publications.

Rehfeld, U., & Janssen, A. (1995). Development of phosphatised hardgrounds in the Miocene Globigerina Limestone of the Maltese Archipelago, including a dscription of *Gamopleura melitensis* sp. nov. *Facies*, **33**, 18-21.

Reuter, M., Werner, P., Harzhauser, M., Kroh, A., & Bassi, D. (2008). Termination of the Arabian shelf sea: Stacked cyclic sedimentary patterns and timing (Oligocene/Miocene, Oman). *Sedimentary Geology*, **212**, 12-24.

Reuther, C., & Eisbacher, G. (1985). Pantelleria Rift - Crustal extension in a convergent intraplate setting. *Geologische Rundschau*, **74** (3), 585-597.

Reuther, C.-D. (1987). Extensional tectonics within the Central Medinterranean segment of the Afro-European zone of convergence. *Memorie della societa geologica italiana*, **38**, 69-80.

Reuther, C.-D., Ben-Avraham, Z., & Grasso, M. (1993). Origin and role of major strike-slip transfers during plate collision in the Central Mediterranean. *Terra Nova*, **5**, 249-257.

Richter, F., Rowley, D., & DePaolo, D. (1992). Sr isotope evolution of seawater-The role of tectonics. *Earth and planetary science letters*, **109**, 11-23.

Ride, W., Cogger, H., Dupuis, C., Kraus, O., Minelli, A., Thompson, F., *et al.* (2000). *International Code of Zoological Nomenclature* (4th ed.). The International Trust for Zoological Nomenclature, London.

Rizzo, C. (1932). *Report on the Geology of the Maltese Islands.* Malta Government Printing Office.

Roberston, A. H., & Grasso, M. (1995). Overview of the Late Tertiary-Recent tectonic and palaeo-environmental development of the Mediterranean region. *Terra Nova*, **7**, 114-127.

Ronco, G. P., Palombi, E., & Fossaluzza, S. (1990). The Vega oilfield. A stratigrapihc structural trap in the Iblean foreland. *Memorie della società geologica italiana*, **45**, 777-782.

Rose, E., Pratt, S., & Bennett, S. (1992). Evidence for Sea-level Changes in the Globigerina Limestone Formation (Miocene) of the Maltese Islands. *Paleontologia i Evolucio*, **24**-**25**, 265-276.

Rosenbaum, G., & Lister, G. S. (2004). Neogene and Quaternary rollback evolution of the Tyrrhenian Sea, the Apennines, and the Sicilian Maghrebides. *Tectonics*, **23**, 1-17.

Rosenbaum, G., Lister, G. S., & Duboz, C. (2004). The Mesozoic and Cenozoic motion of Adria (Central Mediterranean): A review of constraints and limitations. *Geodinamica Acta*, **17** (2), 125-139.

Rosenbaum, G., Lister, G., & Duboz, C. (2002). Reconstruction of the tectonic evolution of the western Mediterranean since the Oligocene. *Journal of the Virtual explorer*, **8,** 107-130.

Ryan, W. (1978). Messinian badlands in the sotheastern margin of the Mediterranean Sea. *Marine Geology*, **27**, 349-363.

Salvador, A. (1994). *International Stratigraphic guide.* Boulder, Colorado: International Union of Geological Sciences and the Geological Society of America.

Sargent, C., & Goulty, N. (2009). Seismic reflection survey for investigation of gypsum dissolution and subsidence at Hell Kettles, Darlington, UK. *Quaterly Journal of Engineering Geology and Hydrogeology*, **42**, 31-38.

Sartori, R. (2003). The Tyrrhenian back-arc basin and subduction of the Ioninan lithosphere. *Episodes*, **26** (3), 217-221.

Savini, A., Malinverno, E., Etiope, G., Tessarolo, C., & Corselli, C. (2009). Shallow seep-related seafloor features along the Malta plateau (Sicily channel – Mediterranean Sea): Morphologies and geo-environmental control of their distribution. *Marine and Petroleum Geology,* **26**, 1831-1848.

Scandone, P., Patacca, E., Radoicic, R., Ryan, W. B., Cita, M. B., Rawson, M., *et al.* (1981). Mesozoic and Cenozoic rocks from the Malta Escarpment (Central Mediterranean). *American Association of Petroleum Geologists Bulletin*, **65**, 1299-1319.

Schettino, A., & Scotese, C. R. (2005). Apparent polar wander paths for the major continents (200 Ma to the present day): a palaeomagnetic reference frame for global platetectonic reconstructions. *Geophys. J. Int.*, **163**, 727-759.

Schlager, W. (1993). Accommodation and supply- a dual control on stratigraphic sequences. *Sedimentary Geology*, **86**, 111-136.

Schlager, W. (2003). Benthic carbonate factories of the Phanerozoic. *International Journal of Earth Sciences (Geologische Rundschau)*, **92**, 445–464.

Schlager, W. (1999). Scaling of sedimentation rates and drowning of reefs and carbonate platforms. *Geology*, **27**, 183-186.

Schlager, W. (1992). *Sedimentology and sequence stratigraphy of reefs and carbonate platforms* (Vol. 34). Tulsa, Oklahoma: American Association of Petroleum Geologists.

Schlager, W. (1981). The paradox of drowned reefs and carbonate platforms. *Geological Society of America Bulletin*, **92**, 197-211.

Schlager, W., & Camber, O. (1986). Submarine slope angles, drowning unconformities, and self-erosion of limestone escarpments. *Geology*, **14**, 762-765.

Schlager, W., Reijmer, J., & Droxler, A. (1994). Highstand shedding of carbonate platforms. *Journal of Sedimentary Research*, **B64**, 270-281.

Schlische, R. (1995). Geometry and origin of fault-related folds in extensional settings. *AAPG Bulletin*, **79**, 1661–1678.

Schlische, R. (1991). Half-graben basin filling models: New constraints on continental extensional basin development. *Basin Research*, **3**, 123-141.

Schramm, M. W., & Livraga, G. (1986). Vega field and the potential of Ragusa Basin, offshore Sicily. *In:* M. Halbouty (Ed.), *Future petroleum provinces of the World.* American Association of Petroleum Geologists Memoir **40**, 559-566.

Sciberras, M., Rizzo, M., Mifsud, J., Camilleri, K., Borg, J., Lanfranco, E., *et al.* (2009). Habitat structure and biological characteristics of a maerl bed off the northeastern coast of the Maltese Islands (central Mediterranean). *Marine Biodiversity*, **39**, 251-264.

Sebei, K., He'di Inoubli, M., Boussiga, H., Tlig, S., Alouani, R., & Boujamaoui, M. (2007). Seismic stratigraphy, tectonics and depositional history in the Halk el Menzel region, NE Tunisia. *Journal of African Earth Sciences*, **47**, 2-29.

Serra-Kiel, J., Hottinger, L., Caus, E., Drobne, K., Ferrandez, C., Jauhri, A., *et al.*. (1998). Larger foraminifieral biostratigraphy of the Tethyan Paleocene and Eocene. *Bulletin de la Societé géologique de France*, **169**, 281-299.

Serrane, M. (1999). Early Oligocene stratigraphic turnover on the west Africa continental margin: a signature of Tertiary greenhouse-to-icehouse transition? *Terra Nova*, **11**, 135-140.

Shackleton, N. (1967). Oxygen isotope analysis and Pleistocene temperature re-assessed. *Nature*, **215**, 15-17.

Shackleton, N., & Kennett, J. (1975). Paleotemperature history of the Cenozoic and the initiation of Antarctic glaciation: Oxygen and carbon isotope analyses in DSDP Sites 277, 279 and 281. *In:* J. Kennett, & R. Houtz (Eds.), *Initial reports of the Deep Sea Drilling Project 29.* US Government Printing Office, 743-755.

Sharland, P., Archer, R., Casey, D., Davies, R., Hall, S., Heward, A., *et al.*. (2001). *Arabian plate sequence stratigraphy.* Manama, Bahrain: Gulf PetroLink.

Shinn, E., & Robbin, D. (1983). Mechanical and chemical compaction in fine grained shallow-water limestones. *Journal of Sedimentary Petrology*, **53**, 595-618.

Spence, G., & Tucker, M. (1997). Genesis of limestone megabreccias and their significance in carbonate sequence stratigraphic models: a review. *Sedimentary Geology*, **112**, 163-193.

Stampfli, G. M., & Borel, G. D. (2001). A plate tectonic model for the Paleozoic and Mesozoic constrianed by dynamic plate boundaries and restored oceanic isochrons. *Earth and Planetary Science letters*, **196**, 17-33.

Stampfli, G. M., & Mosar, J. (1999). The making and becoming of Apulia. *Mem.Sci.Geol.*, **51**, 141-154.

Stanley, S. M., & Hardie, L. A. (1998). Secular oscillations in the carbonate mineralogy of reef-building and sediment-producing organisms driven by tectonically forced shifts in seawater chemistry. *Palaeogeography, Palaeoclimatology, Palaeoecology*, **144**, 3-19.

Steneck, R. (1986). The Ecology of Coralline Algal Crusts: Convergent Patterns and Adaptative Strategies. *Annual Review of Ecology and Systematics*, **17**, 273-303.

Stille, P., Steinmann, M., & Riggs, S. (1996). Nd isotope evidence for the evolution of the paleocurrents in the Atlantic and Tethys Oceans during the past 180 Ma. *Earth and Planetary Science Letters*, **144**, 9-19.

Suess, E. (1883). *Das Antlitz der Erde* (Vol. 1a.). Tempsky, Leipzig.

Swezey, C. S. (2009). Cenozoic stratigraphy of the Sahara, Northern Africa. *Journal of African Earth Sciences*, **53**, 89-121.

ten Have, T., & Heijnen, W. (1985). Cathodoluminescence activation and zonation in carbonate rocks: an experimental approach. *Geologie en Mijnbouw*, **64**, 297-310.

TGS-NOPEC. (2003). *Exploration study invitation: Medina Bank, offshore Malta.* Brochure issued for Government of Malta.

Theiling, B., Railsback, L., Holland, S., & Crowe, D. (2007). Heterogeneity in geochemical expression of subaerial exposures in limestone, and its implications for sampling to detect exposure surfaces. *Journal of Sedimentary Research*, **77**, 159–169.

Thomas, M., Bodin, S., Redfern, J., & Irving, D. (2010). A constrained African craton source for the Cenozoic Numidian Flysch: Implications for the palaeogeography of the western Mediterranean basin. *Earth-Science Reviews*, **101**, 1-23.

Toni Simo, J., Scott, R., & Masse, J.-P. (1993). Cretaceous carbonate platforms: an overview. *In:* J. Toni Simo, R. Scott, & J.-P. Masse (Eds.), *Cretaceous carbonate platforms.* AAPG Memoir **56**, 1-14.

Tucker, M. E., & Wright, V. P. (1990). *Carbonate Sedimentology.* Blackwell Scinetific Publications, Oxford.

Vail, P., Mitchum, R., & Thompson, S. (1977). Seismic stratigraphy and global changes of sea level, Part 4: Global cycles of relative changes of sea level. *In: Seismic stratigraphy- Applications to hydrocarbon exploration.* AAPG Memoir **26**, 83-97.

van Katwijk, M., Bos, A., Hermus, D., & Suykerbuyk, W. (2010). Sediment modification by seagrass beds: Muddification and sandification induced by plant cover and environmental conditions. *Estuarine, Coastal and Shelf Science*, **89**, 175-181.

Van Wagoner, J. C. (1985). Reservoir facies distribution as controlled by sea-level change. *Society of Economic Paleontologists and Mineralogists (SEPM). Annual meeting,* **2***, 91* .

Van Wagoner, J., Posamentier, H., Mitchum, R., Vail, P., Sarg, J., Loutit, T., *et al.*. (1988). An overview of sequence stratigraphy and key definitions. *In:* C. Wilgus, B. Hastings, C. Kendall, H. Posamentier, C. Ross, & J. Van wagoner (Eds.), *Sea level changes - An integrated approach.* Society of Economic Paleontologists and Mineralogists (SEPM) Special Publication, **42**, 39-45.

Vecsei, A., & Sanders, D. G. (1999). Facies analysis and sequence stratigraphy of a Miocene warm-temperate carbonate ramp. *Sedimentary Geology*, **123**, 103-127.

Venin, E., van Buchem, F., Joseph, P., Gaumet, F., Sonnenfeld, M., Rebelle, M., *et al.*. (2003). A 3D outcrop analogue model for Ypresian nummulitic carbonate reservoirs: Jebel Ousselat, northern Tunisia. *Petroleum Geoscience*, **9**, 145-161.

Wade, B., & Pälike, H. (2004). Oligocene climate dynamics. *Paleoceanography,* **19**, *PA4019, doi:10.1029/2004PA001042*.

Walles, F. (1993). Tectonic and diagenetically induced seal failure within the south-western Great Bahamas Bank. *Marine and Petroleum Geology*, **10**, 14-28.

Waltham, T., Bell, F., & Culshaw, M. (2005). *Sinkholes and subsidence.* Praxis Publishing Ltd.

Wanless, H. (1981). Fining upwards sedimentary sequences generated in sea grass beds. *Journal of Sedimentary Petrology*, **51**, 445-454.

Wardell-Armstrong. (1996). *Minerals Resource Assessment for the Planning Authority of Malta.* Planning Authority, Malta.

Weber, L., Sarg, J., & Wright, F. (1995). Sequence stratigraphy and reservoir delineation of the Middle Pennsylvanian (Desmoinesian), Paradox Basin and Aneth Field, southwestern USA. *In:* J. Read, C. Kerans, & L. Weber (Eds.), *Milankovitch sea level changes, cycles and reservoirs on carbonate paltforms in greenhouse and ice-house worlds, SEPM Short Course notes,* **35***, 1-81.*

Westphal, H., Halfar, J., & Freiwald, A. (2010). Heterozoan carbonates in subtropical to tropical settings in the present and past. *International Journal of Earth Sciences (Geologische Rundschau)*, *published online DOI 10.1007/s00531-010-0563-9*, 1-17.

Wieland-Schuster, U., Schuster, F., Harzhauser, M., Mandic, O., Kroh, A., Rogl, F., *et al.*. (2004). Stratigraphy and palaeoecology of Oligocene and Early Miocene sedimentary sequences of the Mesohellenic Basin (NW Greece). *Cour. Forsch.-Inst. Senckenberg*, **248**, 1-55.

Wilson, J. (1975). *Carbonate facies in geologic history.* Springer Verlag, New York.

Wilson, M. E., & Bosence, D. W. (1997). Platform-top ramp deposits of the Tonasa Carbonate Platform, Sulawesi, Indonesia. *In:* A. J. Fraser, S. J. Matthews, & R. W. Murphy (Eds.), *Petroleum Geology of Southeast Asia.* Geological Society Special Publication, **126**, 247-279.

Wilson, M. E., & Vecsei, A. (2005). The apparent paradox of abundant foramol facies in low latitudes: their environmental significance and effect on platform development. *Earth-Science Reviews*, **69**, 133-168.

Wilson, M. (2008). Global and regional influences on equatorial shallow-marine carbonates during the Cenozoic. *Palaeogeography, Palaeoclimatology, Palaeoecology*, **265**, 262-274.

Wilson, S., Blake, C., Berges, J., & Maggs, C. (2004). Environmental tolerances of free-living coralline algae (maerl): implications for European marine conservation. *Biological Conservation*, **120**, 283-293.

Winnock, E. (1981). Structure du bloc pélagien. *In:* F. Wezel (Ed.), *Sedimentary Basins of Mediterranean margins.* Bologna, 445-464.

Wray, J. (1977). *Calcareous algae.* Elsevier.

Wright, V., Platt, N., & Wimbledon, W. (1978). Biogenic laminar calcretes: evidence of calcified root-mat horizons in paleosols. *In:* V. Wright, & M. Tucker (Eds.), *Calcretes.* Blackwell Scientific Publications, 243-260.

Zachos, J. C., Gerald, R. D., & Zeebe, R. E. (2008). An early Cenozoic perspective on greenhouse warming and carbon-cycle dynamics. *Nature*, **451***/17*, 279-283.

Zachos, J., & Kump, L. (2005). Carbon cycle feedbacks and the initiation of Antarctic glaciation in the earliest Oligocene. *Global and Planetary Change*, **47**, 51-66.

Zachos, J., Breza, J., & Wise, S. (1992). Early Oligocene ice-sheet expansion on Antarctica: sedimentological and isotopic evidence from Kerguelen Plateau. *Geology*, **20**, 569-573.

Zachos, J., Dickens, G., & Zeebe, R. (2008). An early Cenozoic perspective on greenhouse warming and carbon-cycle dynamics. *Nature*, **451**, 279-283.

Zachos, J., Pagani, M., Sloan, L., Thomas, E., & Billups, K. (2001). Aberrations in Global Climate 65 Ma to Present. *Science*, **292**, 686-693.

Zachos, J., Shackleton, N., Revenaugh, J., Palike, H., & Flower, B. (2001). Climate Response to Orbital forcing across the Oligo-Miocene boundary. *Science*, **292**, 4-8.

Zammit-Maempel, G. (1993). *Kuphus melitensis*, a new Teredinid bivalve from the Late Oligocene Lower Coralline Limestone of Malta. *Contributions to Tertiary and Quaternary Geology*, **30**, 155-175.

Zarcone, G., & DiStefano, P. (2008). Mesozoic discontinuities in the Panormide Carbonate Platform: constraints on the palaeogeography of the central Mediterranean. *Rend. online Societa Geologica Italiana,* **2** *(2008), Note Brevi*, *2*, 191-194.

Ziegler, P. (1992). Plate tectonics, plate moving mechanisms and rifting. *Tectonophysics*, **215**, 9-34.